

- Sneyers, B., Novotny, D. W., and Lipo, T. A. (1985). Field-weakening in buried permanent magnet a.c. motor drives. *IEEE Transactions on Industry Applications* IA-21, 398–404.
- Stronach, A. F., Vas, P., and Neuroth, M. (1997). Implementation of intelligent self-organising controllers in DSP-controlled electromechanical drives. *Proceedings of the IEE, Pt. D* 144, 324–30.
- Takeda, Y., Morimoto, S., Hirasa, T., and Fuchi, K. (1988). Most suitable control method for permanent magnet synchronous motors. In *Proceedings of the International Conference on Electrical Machines, Pisa*, pp. 53–8.
- Tso, S. K. and Wai, L. K. (1987). A novel implementation of high-performance synchronous motor drives. *BICEM*, pp. 667–70.
- Vagati, A., Fratta, A., Franceschini, G., and Rosso, P. (1996). AC motors for high-performance drives: a design-based comparison. *IEEE Transactions on Ind. Application*, IA-32, 1211–19.
- Vagati, A. (1994). The synchronous reluctance solution: a new alternative in a.c. drives. *IECON, Bologna*.
- Vas, P. (1992). *Electrical machines and drives: a space-vector theory approach*. Oxford University Press.
- Vas, P. (1993). *Parameter estimation, condition monitoring, and diagnosis of electrical machines*. Oxford University Press.
- Vas, P. and Drury, W. (1994). Vector-controlled drives. *PCIM, Nürnberg*, pp. 213–28.
- Vas, P. and Drury, W. (1996). Future trends and developments in electric machines and drives (in Italian). *Energia Elettrica* 73, 11–21.
- Vas, P., Alaküla, M., Brown, J. E., and Hallenius, K. E. (1988). Field-oriented control of saturated a.c. machines. *3rd International Conference on Power Electronics and Variable-speed drives*, pp. 283–6. IEE, London.
- Vauhkonen, V. and Mård, M. (1987). Compensated field-oriented control of cycloconverter-fed synchronous motors in rolling-mill drives. In *Proceedings of Beijing International Conference on Electrical Machines, Beijing*, pp. 679–82.
- Wu, R. and Semon, G. R. (1990). A permanent magnet motor drive without a shaft sensor. *IEEE IAS Meeting*, pp. 553–8.

## 4 Vector and direct torque control of induction machines

Induction machines have been used for over a hundred years. Because of their simplicity, ruggedness, reliability, efficiency, low cost, compactness, and economical and volume manufacturing advantages, induction machines with a squirrel-cage rotor are the most widely used machines at fixed speed. This is especially the case at lower power levels, where on the rotor there is a squirrel-cage winding, which is manufactured by die-casting. However, recent developments in the field of variable-speed drives have made possible the large-scale application of variable-speed induction motor drives.

Although the induction machine is superior to the d.c. machine with respect to size, weight, rotor inertia, efficiency, maximum speed, reliability, cost, etc., because of its highly non-linear dynamic structure with strong dynamic interactions, it requires more complex control schemes than, say, a separately excited d.c. machine. The general dynamic model of the induction machine can be represented by a sixth-order state-space equation, where the inputs to the stator are voltage and frequency and the outputs can be rotor speed, rotor position, electromagnetic torque, stator or rotor flux linkages, magnetizing flux linkage, stator or rotor currents, magnetizing current or a combination of these. Furthermore, the cost of a.c. power converters is higher for the variable-speed induction motor drive than for the converters which can supply d.c. machines. Until recently the cost of the introduction of the variable-speed induction motor has been prohibitive and the complexity of control has made its development difficult and acceptance reluctant. However, the rapid developments in the field of power electronics, whereby better and more powerful semiconductor devices are available (with higher switching speeds, high conducting currents and very high blocking voltages, which can be turned on and off, etc.) and where the power devices and circuits are packaged into modular form, and the existence of powerful and inexpensive microprocessors, which allow the complex control functions of the a.c. drive to be performed by utilizing software instead of expensive hardware, mean that a.c. drives employing induction machines can be considered as economical alternatives to adjustable-speed d.c. drives.

Some of the other functional advantages of the application of microprocessors or digital techniques are:

- Cost reduction in control electronics;
- Improved reliability due to the reduction of the number of components;
- Standard universal hardware is required and the only changes are to the software, which is very flexible and can be easily modified;
- Digital transmission requires a minimal amount of cabling and is very tolerant to noise; it eliminates drift and electromagnetic interference problems;

- Very high accuracy, excellent repeatability, linearity, and stability with different setting ranges;
- Centralized operator communications, monitoring, and diagnostics. The diagnostics programs monitor the operation of the system. Some parts of the programs monitor the various semiconductor devices (this is continuously performed), current/voltage transducers, supply voltages, speed/rotor angle detectors, serial data communication, etc.;
- Complex, high-speed arithmetic and capability of decision making.

Some of the service and diagnostic features of the application of microprocessors or digital circuits are:

- Only a few standard modules are required without any special adjustments;
- There is the possibility of plug-in memory modules for user programs, parameters and modifications to functions, etc.;
- Powerful system software for on-line measurements, control parameter setting (e.g. current-control parameter setting, speed-control parameter setting, etc.), and testing;
- Automatic location of hardware faults with the help of system and user software.

It is expected that the present trends in technology will result in cost reduction and performance improvement of a.c. drives and will thus lead to an even more widespread application of these drives. The MOS bipolar power devices, which include the Insulated Gate Bipolar Transistor (IGBT), and the MOS-Controlled Thyristor (MCT), can be turned on and off with a MOS gate and have such excellent characteristics that it is expected that in future they will revolutionize power converters.

The method of vector control described in earlier sections for synchronous machines can be extended to induction machines (see also Section 1.2.1.2). However, whilst in the electrically excited synchronous machine and the permanent-magnet synchronous machine, the space angle between the field winding and the direct axis of the stator and the space angle between the magnet flux and stator direct axis can be directly measured, for the induction machine the space angle of the rotor flux-linkage space phasor with respect to the direct axis of the stator is not a directly measurable quantity. Furthermore, in the case of the converter-fed induction machine, as well as supplying active power, the converter must supply reactive power for magnetization, since there is no external excitation as in the case of the synchronous machine. Thus both excitation (reactive) and torque-producing (active) currents must simultaneously exist in the stator windings of the induction machine.

The methods discussed in this chapter can be applied to induction machines with quadrature-phase stator windings ('two-phase' machine) or to induction machines with three-phase stator windings. The induction machine can have either a wound rotor (slip-ring machine) or a rotor with squirrel-cage winding,

and it is possible to implement vector control on both types of induction machines. The squirrel cage can be of the double-cage or the single-cage type.

The mechanism of electromagnetic torque production in smooth-air-gap machines has been described in Section 2.1.6 and various forms of the expressions for the electromagnetic torque have been given in Section 2.1.8. It has been shown that in special reference frames fixed to the magnetizing flux-linkage, the stator flux-linkage, or the rotor flux-linkage space phasor, the expression for the electromagnetic torque of the smooth-air-gap machine is similar to the expression for the torque of the separately excited d.c. machine. This suggests that torque control of the induction machine can be performed by the decoupled control of the flux- and torque-producing components of the stator currents, which is similar to controlling the field and armature currents in the separately excited d.c. machine. However, it should be noted that in the squirrel-cage induction machine it is not possible to monitor the rotor currents directly. The stator currents of the induction machine can be separated into the flux- and torque-producing components by utilizing the transformations described in Section 2.1.8, whilst in the d.c. machine, as a result of the decoupled orthogonal field and armature axes, it is straightforward to achieve independent control of the flux and torque. It follows from Section 2.1.8 that the implementation of vector control (stator flux-oriented control, rotor flux-oriented control, or magnetizing flux-oriented control) requires information on the modulus and space angle (position) of the stator-flux, rotor-flux, or magnetizing-flux space phasors respectively. The control can be performed in a reference frame fixed to the stator-flux, rotor-flux, or magnetizing-flux space phasor respectively, and the direct- and quadrature-axis stator currents are obtained in the corresponding reference frame. These stator currents are similar to the field and armature currents of the separately excited d.c. machine.

In the case of induction machines rotor-flux-oriented control is usually employed, although it is possible to implement stator-flux- and also magnetizing-flux-oriented control, as described below. With rotor-flux-oriented control there are two main implementations to obtain the modulus and space angle of the rotor flux-linkage space phasor. When the so-called direct rotor-flux-oriented control is used (flux-feedback control), these quantities are directly measured (by using Hall-effect sensors, search coils, or tapped stator windings of the machine, etc.) or they are calculated from a so-called flux model. However, in one specific form of the so-called indirect rotor-flux-oriented control (flux-feedforward control), the modulus and space angle of the rotor flux-linkage space phasor are obtained by utilizing the monitored stator currents and the rotor speed. The space angle of the rotor flux-linkage space phasor is then obtained as the sum of the monitored rotor angle ( $\theta_r$ ) and the computed reference value of the slip angle ( $\theta_{s1}$ ), where the latter quantity gives the position of the rotor flux-linkage space phasor relative to the direct axis of the rotor, as shown below. However, it will also be shown in this chapter that the slip angle ( $\theta_{s1}$ ) can be calculated from the reference values of the torque- and flux-producing stator currents and strongly depends on the rotor parameters (rotor time constant, which is equal to the ratio of the rotor inductance to the rotor resistance) of the machine under consideration, and when

inaccurate parameters are used it is not possible to achieve correct field orientation. The rotor time constant can change as a result of saturation, variation of the temperature, and effects of current displacement. Thus it is preferable to implement schemes which incorporate some form of on-line parameter adaption. In practice, despite its parameter sensitivity and the fact that it requires the use of shaft encoders, which are expensive, the indirect method has gained more widespread application, since it does not require flux sensors or a flux model.

It should be noted that with stator-flux-oriented control or magnetizing-flux-oriented control there can also be two main different implementations, direct and indirect, and they will be discussed later in this section.

Direct torque control (DTC) of induction machines is similar to that described for synchronous machines in Section 3.3 (see also Section 1.2). In the present chapter various direct-torque-control schemes will be described for voltage-source inverter-fed induction motors and also for a current-source inverter-fed induction motors.

Induction machines represent an alternative to synchronous machines in high-performance servo-drive applications. Although both the permanent-magnet synchronous machine and the induction machine are suitable for this type of application, for the selection of the appropriate machine, the following points have to be considered:

- Induction machines are more difficult to control.
- If field weakening is excluded, the drive containing the induction machine requires an inverter with higher rating (in the PM synchronous machine there are no rotor losses, and if there is field weakening, the machine is overexcited and draws large stator currents resulting in large stator losses).
- Because of the rotor losses, an induction machine normally requires forced cooling (a PM synchronous machine has no rotor losses and natural cooling can be sufficient).
- For the same torque produced, the efficiency (which has direct effects on the size of the machine) for the induction machine is lower (a PM synchronous machine has high efficiency because there are no rotor losses).
- An induction machine can be designed for higher flux densities (in a PM synchronous machine this is restricted by the magnets).
- An induction machine is cheaper (in a PM synchronous machine the price of the required magnets is still high).
- In the case of the drive containing the induction machine, field-weakening (constant-power mode) is easily achieved over a wide speed range (in a PM synchronous machine this is not the case).
- The drive with the induction machine requires the application of a more complicated microcomputer. (The microcomputer can be simpler for the permanent-magnet synchronous machine, since it does not require the application of a signal processor; or the machine can even be designed without any microprocessor.)

Vector control can be applied to an induction machine supplied by a voltage-source inverter or by a current-source inverter or by a cycloconverter. It is simpler to implement the control when controlled-current operation is achieved. The vector-controlled induction machine can achieve four-quadrant operation with high dynamic response. In the following sections, first the rotor-flux-oriented control of induction machines is discussed in detail and, as they are very similar, this will be followed by shorter discussions of the stator-flux-oriented and magnetizing-flux-oriented control techniques. Various 'sensorless' control schemes are also described. However, the direct torque control of VSI-fed induction motors will also be discussed in great detail. For this purpose different DTC schemes will be described. This will then be followed by the DTC of CSI-fed induction motors.

## 4.1 Rotor-flux-oriented control of induction machines

In this part of the chapter the rotor-flux-oriented control of induction machines is discussed for the case when the machine is supplied by impressed stator voltages, impressed stator currents, or impressed rotor currents. Both direct and indirect methods are discussed.

### 4.1.1 CONTROL OF AN INDUCTION MACHINE SUPPLIED BY A VOLTAGE-SOURCE INVERTER

#### 4.1.1.1 General introduction

It is assumed that the induction machine is supplied by a pulse-width modulated (PWM) voltage-source thyristor inverter, whose switching frequency is low, usually in the range of 100 Hz–1 kHz. Such converters are used up to ratings of several 100 kW and one of the main applications is the high-dynamic-performance position-controlled servo drive. At lower power levels, inverters containing transistors are used where the switching frequency is high. At higher power levels, converters employing thyristors and gate turn-off thyristors are used.

Because of the low switching frequency, it is not possible to achieve fast closed-loop current control of the stator currents with, for example, sinusoidal stator current references in the steady state. In this drive the stator currents can contain time harmonics with large amplitudes. Since the stator currents cannot be assumed to be impressed by fast control loops, it is necessary to utilize the stator voltage equations as well, once the equation of the stator reference voltages are established. However, it will be shown in Section 4.1.2 that a significant simplification arises in the equations and thus in the drive control system if the induction machine can be considered to be supplied by current sources. This is the case for an induction machine supplied by a voltage-source transistor inverter with fast current control (used at lower power levels at a high switching frequency, usually above 15 kHz), for a cycloconverter-fed induction machine (used for high-power,

low-speed applications), where the stator currents are approximately sinusoidal and where the stator currents can be controlled by individual current control loops, or for an induction machine supplied by, say, a current-source thyristor inverter.

#### 4.1.1.2 Stator voltage equations in the rotor-flux-oriented reference frame

In this section the stator voltage equations are derived and formulated in the reference frame fixed to the rotor-flux linkage space phasor. There are many ways to obtain the stator voltage equations in this reference frame. However, a straightforward method is followed here, whereby the space-phasor forms of the voltage equations formulated in the general reference frame (see Section 2.1.7) are used directly. The rotor-current space phasor is deliberately expressed in terms of the so-called rotor magnetizing-current space phasor and thus the resulting voltage equations will contain the modulus and space angle of the rotor magnetizing-current space phasor (or rotor flux-linkage space phasor), which are necessary to implement vector control.

It has been shown in Section 2.1.8, eqn (2.1-195), that the so-called rotor magnetizing-current space phasor in the rotor-flux-oriented reference frame ( $\bar{I}_{mr}$ ) is obtained by dividing the rotor flux-linkage space phasor established in this reference frame ( $\bar{\psi}_{r\psi r}$ ) by the magnetizing inductance ( $L_m$ ). Thus under linear magnetic conditions (where the magnetizing inductance is constant),  $\bar{I}_{mr}$  and  $\bar{\psi}_{r\psi r}$  are proportional. For convenience, eqn (2.1-195) is repeated here, and this also gives the relationship between the rotor magnetizing space phasor to the stator and rotor current space phasors:

$$\bar{I}_{mr} = \frac{\bar{\psi}_{r\psi r}}{L_m} = \bar{I}_{s\psi r} + (1 + \sigma_r) \bar{I}_{r\psi r}, \quad (4.1-1)$$

where  $\sigma_r$  is the rotor leakage factor (it is the ratio of the rotor leakage inductance to the magnetizing inductance, as shown in Section 2.1.8).

By considering eqns (2.1-148) and (2.1-150), which give the stator space-phasor voltage and stator flux-linkage space phasor equations in the general reference frame respectively, and by assuming linear magnetic conditions (i.e.  $L_m = \text{constant}$  and the leakage inductances are also constant), the following stator voltage equation is obtained in the reference frame fixed to the rotor flux-linkage space phasor, which rotates at the speed  $\omega_{mr}$  (this speed is defined in eqn (2.1-188) as the first time-derivative of the space angle  $\rho_r$ , which is the space angle of the rotor magnetizing-current space phasor with respect to the direct axis of the stationary reference frame):

$$\bar{u}_{s\psi r} = R_s \bar{I}_{s\psi r} + L_s \frac{d\bar{I}_{s\psi r}}{dt} + L_m \frac{d\bar{I}_{r\psi r}}{dt} + j\omega_{mr} L_s \bar{I}_{s\psi r} + j\omega_{mr} L_m \bar{I}_{r\psi r}. \quad (4.1-2)$$

It follows from eqn (2.1-189) that in the special rotor-flux-oriented ( $x, y$ ) reference frame, the space phasor of the stator currents can be expressed in terms

of the space phasor of the stator currents established in the stationary reference frame ( $\bar{i}_s$ ) as

$$\bar{I}_{s\psi r} = i_{sx} + j i_{sy} = \bar{i}_s e^{-j\rho_r} = (i_{sD} + j i_{sQ}) e^{-j\rho_r} \quad (4.1-3)$$

and a similar expression can be obtained for the stator-voltage space phasor, since the stator quantities in the same reference frame must be transformed by the same transformation,

$$\bar{u}_{s\psi r} = \bar{u}_s e^{-j\rho_r} = u_{sx} + j u_{sy} = (u_{sD} + j u_{sQ}) e^{-j\rho_r}. \quad (4.1-4)$$

From eqn (4.1-1) and the fact that as a result of the special selection of the reference frame the rotor magnetizing-current space phasor is coaxial with the direct-axis and thus  $\bar{I}_{mr} = |\bar{I}_{mr}|$ , the rotor-current space phasor in the special reference frame is obtained in terms of the stator-current and rotor magnetizing-current space phasors as

$$\bar{I}_{r\psi r} = \frac{|\bar{I}_{mr}| - \bar{I}_{s\psi r}}{1 + \sigma_r}. \quad (4.1-5)$$

Substitution of eqn (4.1-5) into eqn (4.1-2) yields the following differential equation for the stator currents, if both sides of the equation are divided by the stator resistance  $R_s$  and if it is expressed in the form required by a time-delay element:

$$T'_s \frac{d\bar{I}_{s\psi r}}{dt} + \bar{I}_{s\psi r} = \frac{\bar{u}_{s\psi r}}{R_s} - j\omega_{mr} T'_s \bar{I}_{s\psi r} - (T_s - T'_s) \left( j\omega_{mr} |\bar{I}_{mr}| + \frac{d|\bar{I}_{mr}|}{dt} \right). \quad (4.1-6)$$

$T'_s$  is the stator transient time constant of the machine,  $T'_s = L'_s/R_s$ , where  $L'_s$  is the stator transient inductance,  $L'_s = (L_s - L_m^2/L_r)$ , and can be expressed in terms of the total leakage factor  $\sigma$  and the stator inductance as  $L'_s = \sigma L_s$ . Thus it is possible to define  $\sigma$  as  $1 - L_m^2/(L_s L_r)$ .  $T_s$  is the stator time constant,  $T_s = L_s/R_s$ , and thus it is also possible to express  $T'_s$  as  $\sigma T_s$ . It follows that the term  $(T_s - T'_s)$  can be expressed in terms of the total leakage factor and the stator time constant as  $(1 - \sigma)T_s$ .

By resolving eqn (4.1-6) into its real ( $x$ ) and imaginary axis ( $y$ ) components, the following two-axis differential equations are obtained for the stator currents:

$$T'_s \frac{di_{sx}}{dt} + i_{sx} = \frac{u_{sx}}{R_s} + \omega_{mr} T'_s i_{sy} - (T_s - T'_s) \frac{d|\bar{I}_{mr}|}{dt} \quad (4.1-7)$$

$$T'_s \frac{di_{sy}}{dt} + i_{sy} = \frac{u_{sy}}{R_s} - \omega_{mr} T'_s i_{sx} - (T_s - T'_s) \omega_{mr} |\bar{I}_{mr}|. \quad (4.1-8)$$

The relationship between the stationary-axis voltage ( $u_{sD}, u_{sQ}$ ) and stator current components ( $i_{sD}, i_{sQ}$ ) and the corresponding voltage ( $u_{sx}, u_{sy}$ ) and current ( $i_{sx}, i_{sy}$ ) components can be obtained by utilizing the transformations defined by eqns (4.1-3) and (4.1-4) respectively. It follows from eqns (4.1-7) and (4.1-8) that with respect to the stator currents  $i_{sx}$  and  $i_{sy}$ , the induction machine behaves as a

first-order time-delay element, whose time constant is equal to the stator transient time constant of the machine, and its gain is equal to the inverse of the stator resistance. However, it can be seen that there is an unwanted coupling between the stator circuits on the two axes. For the purposes of rotor-flux-oriented-control, it is the direct-axis stator current  $i_{sx}$  (rotor flux-producing component) and the quadrature-axis stator current  $i_{sy}$  (torque-producing component) which must be independently controlled. However, since the voltage equations are coupled, and the coupling term in  $u_{sx}$  also depends on  $i_{sy}$  and the coupling term in  $u_{sy}$  also depends on  $i_{sx}$ ,  $i_{sx}$ , and  $i_{sy}$  cannot be considered as decoupled control variables for the rotor flux and electromagnetic torque. The stator currents  $i_{sx}$  and  $i_{sy}$  can only be independently controlled (decoupled control) if the stator voltage equations [eqns (4.1-7) and (4.1-8)] are decoupled and the stator current components  $i_{sx}$  and  $i_{sy}$  are indirectly controlled by controlling the terminal voltages of the induction machine. Various implementations of the necessary decoupling circuit will be described in the next section.

#### 4.1.1.3 Decoupling circuits in the rotor-flux-oriented reference frame

In this section the decoupling circuits valid for the case of an ideal drive are derived first and then the derivation is given of the necessary decoupling circuits if there is an inverter time delay.

*Decoupling circuits of an ideal drive:* From eqns (4.1-7) and (4.1-8) there is in the direct-axis voltage equation a rotational voltage coupling term  $\omega_{mr} L'_s i_{sy}$ , and thus the quadrature-axis stator current  $i_{sy}$  affects the direct-axis stator voltage  $u_{sx}$ . Similarly, in the quadrature-axis voltage equation there is a rotational voltage coupling term  $-\omega_{mr} L'_s i_{sx} - (L_s - L'_s) \omega_{mr} |\bar{I}_{mrl}|$  and thus the direct-axis stator current  $i_{sx}$  affects the quadrature-axis voltage  $u_{sy}$ . However, by assuming an ideal drive (which has no extra time delays apart from the natural ones, i.e. there is no inverter dead time, no delay due to signal processing, etc., and for which the parameters are those used in the equations) and by assuming constant rotor-flux operation ( $|\bar{I}_{mrl}| = \text{const.}$ ), it follows from eqns (4.1-7) and (4.1-8) that the stator current components can be independently controlled if the decoupling rotational voltage components,

$$u_{dx} = -\omega_{mr} L'_s i_{sy} \quad (4.1-9)$$

$$u_{dy} = \omega_{mr} L'_s i_{sx} + (L_s - L'_s) \omega_{mr} |\bar{I}_{mrl}|, \quad (4.1-10)$$

are added to the outputs ( $\hat{u}_{sx}$ ,  $\hat{u}_{sy}$ ) of the current controllers which control  $i_{sx}$  and  $i_{sy}$  respectively. This can be proved by considering that  $\hat{u}_{sx} + \hat{u}_{dx}$  yields the direct-axis terminal voltage component, and the voltage on the output of the direct-axis current controller is

$$\hat{u}_{sx} = R_s i_{sx} + L'_s \frac{di_{sx}}{dt}. \quad (4.1-11)$$

Similarly,  $\hat{u}_{sy} + u_{dy}$  gives the quadrature-axis stator voltage component and the voltage on the output of the quadrature-axis current controller is

$$\hat{u}_{sy} = R_s i_{sy} + L'_s \frac{di_{sy}}{dt}. \quad (4.1-12)$$

Thus  $\hat{u}_{sx}$  and  $\hat{u}_{sy}$  directly control the stator currents  $i_{sx}$  and  $i_{sy}$  through a simple time delay element with the stator transient time constant  $T'_s$ . The required decoupling circuit is shown in Fig. 4.1, where the decoupling voltages  $u_{dx}$  and  $u_{dy}$  are obtained from  $i_{sx}$ ,  $i_{sy}$ ,  $|\bar{I}_{mrl}|$ , and  $\omega_{mr}$  by using eqns (4.1-9) and (4.1-10) respectively.

In the decoupling circuit described above the inputs are the stator currents  $i_{sx}$  and  $i_{sy}$ , the rotor magnetizing current  $|\bar{I}_{mrl}|$ , and the angular speed of the rotor flux-linkage space phasor,  $\omega_{mr}$ . The current components  $i_{sx}$  and  $i_{sy}$  can be obtained from the measured three-phase stator currents by utilizing the transformations described by eqn (4.1-3), and  $|\bar{I}_{mrl}|$  and  $\omega_{mr}$  can be obtained by utilizing a so-called flux-model, which can be obtained by considering the rotor voltage equations, as shown in the following section. However, it is also possible to have an implementation of the decoupling circuit where the stator currents are not utilized as input quantities, but instead, the output voltages of the stator current controllers ( $\hat{u}_{sx}$ ,  $\hat{u}_{sy}$ ) are used. For this purpose eqns (4.1-11) and (4.1-12) are utilized and the stator currents  $i_{sx}$ ,  $i_{sy}$  are expressed in terms of the output voltages of the current controllers. When these are substituted into eqns (4.1-9) and (4.1-10), the following expressions are obtained for the decoupling voltage components:

$$u_{dx} = -\omega_{mr} \frac{T'_s}{1+T'_s p} \hat{u}_{sy} \quad (4.1-13)$$

$$u_{dy} = -\omega_{mr} \left[ (L_s - L'_s) |\bar{I}_{mrl}| + \frac{T'_s}{1+T'_s p} \hat{u}_{sx} \right], \quad (4.1-14)$$

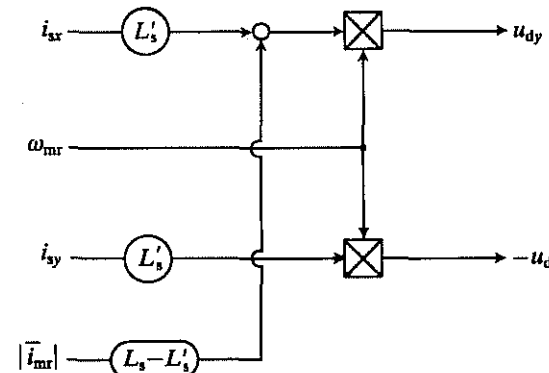


Fig. 4.1. Decoupling circuit to obtain decoupling voltages  $u_{dx}$ ,  $u_{dy}$  (if  $|\bar{I}_{mrl}| = \text{constant}$ ). Inputs are  $i_{sx}$ ,  $i_{sy}$ ,  $\omega_{mr}$ ,  $|\bar{I}_{mrl}|$ .

where  $p = d/dt$  and it should be noted that these equations are valid if the rotor flux is constant. The decoupling circuit corresponding to eqns (4.1-13) and (4.1-14) is shown in Fig. 4.2, where the two blocks contain a lag element with time constant  $T'_s$  and gain  $T'_s p$ .

It can be seen that the decoupling circuit shown in Fig. 4.2 also utilizes the stator resistance of the induction machine in addition to the machine parameters which have been used in the implementation shown in Fig. 4.1. The direct-axis reference value of the inverter voltage (in the rotor-flux-oriented reference frame) is again obtained as the sum of the direct-axis voltage obtained from the decoupling circuit and the direct-axis voltage which is present on the output of the direct-axis stator current controller. Similarly, the quadrature-axis reference value of the inverter voltage (in the rotor-flux-oriented reference frame) is obtained as the sum of the quadrature-axis voltage obtained from the decoupling circuit and the quadrature-axis voltage which is present on the output of the quadrature-axis stator current controller. To obtain the three-phase stator voltage references of the inverter, these have to be transformed into the two-axis stator voltage components by the application of the transformation  $e^{j\theta_r}$  [see eqn (4.1-4)] and this transformation is followed by the two-phase to three-phase transformation.

*Decoupling circuits considering the effect of the inverter time delay:* It has been assumed above that the drive is ideal. However, the main difference between a real drive and an idealized drive is that in the real drive there are dead-time

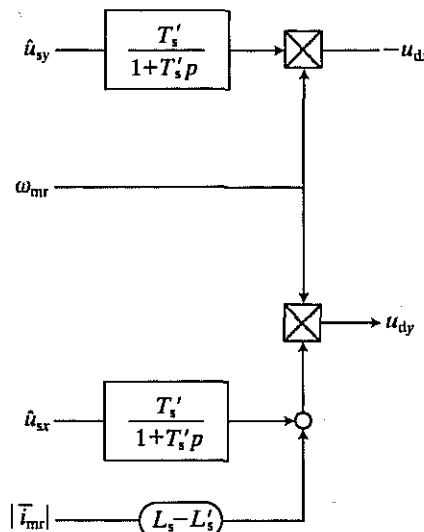


Fig. 4.2. Decoupling circuit to obtain decoupling voltages  $u_{dx}$ ,  $u_{dy}$  (if  $|I_{mr}| = \text{constant}$ ). Inputs are  $\dot{u}_{sy}$ ,  $\omega_{mr}$ ,  $|I_{mr}|$ .

components due to the delay of the inverter, signal processing (if a microcomputer or microprocessor is employed), etc. These have to be taken account of, since they cause unwanted coupling terms and it is therefore not possible to perform the required decoupling of the stator circuits using the circuit described above. The unwanted coupling can cause instabilities, etc. and make the vector control scheme totally inoperative. It is now shown how the decoupling circuits have to be modified in order to take account of these effects.

For simplicity it is assumed that the total dead time  $T$  is concentrated at the end of the signal process, between the control circuits and the machine, i.e. in the inverter. The lag effect of the inverter is described by a first-order delay element, thus in the stationary reference frame

$$T \frac{d\bar{u}_s}{dt} + \bar{u}_s = \bar{u}_{sref} \quad (4.1-15)$$

holds, where  $\bar{u}_s$  is the space phasor of the stator voltages in the reference frame fixed to the stator and  $\bar{u}_{sref}$  is its reference value. By using eqn (4.1-4), it is possible to transform eqn (4.1-15) into the rotor-flux-oriented reference frame. Thus the inverter can be described by the following first-order differential equation in the rotor-flux-oriented reference frame:

$$T \frac{d\bar{u}_{s\psi r}}{dt} + j\omega_{mr} T \bar{u}_{s\psi r} + \bar{u}_{s\psi r} = \bar{u}_{s\psi rref} \quad (4.1-16)$$

resolution of which into direct- and quadrature-axis components yields

$$T \frac{du_{sx}}{dt} + u_{sx} = \omega_{mr} T u_{sy} + u_{sxref} \quad (4.1-17)$$

$$T \frac{du_{sy}}{dt} + u_{sy} = -\omega_{mr} T u_{sx} + u_{syref}. \quad (4.1-18)$$

Thus it can be seen that the two equations are coupled; in the direct-axis equation there is an unwanted coupling  $\omega_{mr} T u_{sy}$  and in the quadrature-axis  $-\omega_{mr} T u_{sx}$ . When the delay time is zero, the coupling disappears as expected. If the machine is operated in the field-weakening range (above base speed), it follows from eqns (4.1-17) and (4.1-18) that the undesirable decoupling terms will be the largest during field weakening. In the constant-flux range (below base speed), the effect of the delay time can be neglected. Equations (4.1-17) and (4.1-18) can be implemented by the circuit shown in Fig. 4.3.

Thus it is possible to obtain a combined decoupling circuit of the machine and inverter system, which is a series connection of a decoupling circuit of the machine (as described in Fig. 4.1 or Fig. 4.2) and the decoupling circuit of the inverter as shown in Fig. 4.3. If, for example, the decoupling circuit of the machine used is the one shown in Fig. 4.1, the combined decoupling circuit takes the form shown in Fig. 4.4.

However, it is not possible to decouple the machine and the drive system completely when this method is used, since the machine and the inverter represent

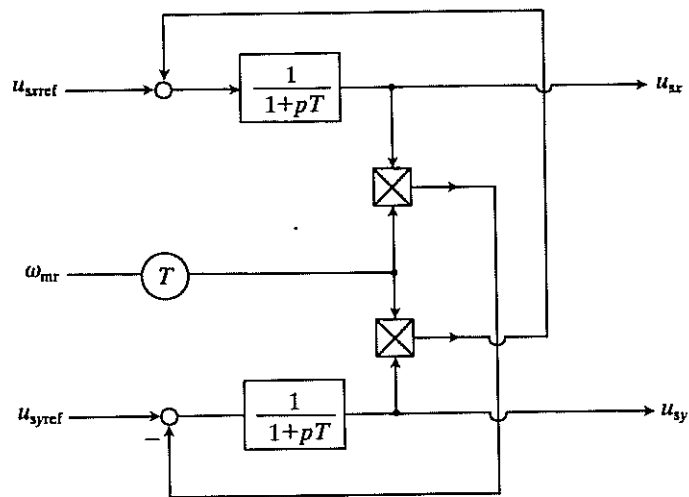


Fig. 4.3. Circuit for inverter in rotor-flux-oriented reference frame.

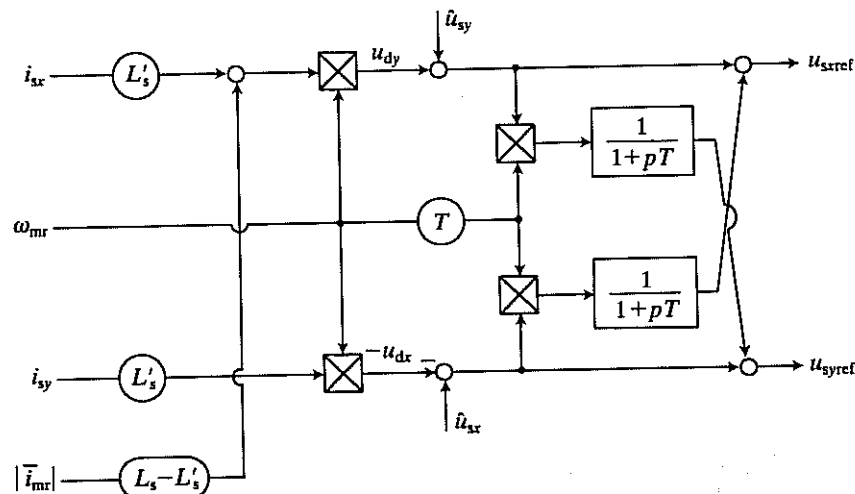


Fig. 4.4. Series connection of the decoupling circuits of the machine and inverter.

a total system, which cannot be decoupled by considering the machine and the inverter individually. However, by combining the equations of the machine with the equations of the inverter, it is possible to obtain a full decoupling circuit for the machine-inverter drive system as a whole. This will now be discussed.

For simplicity  $|\bar{i}_{mr}| = \text{constant}$  is assumed, but similar considerations hold when this assumption is not made. Thus substitution of the expression for  $u_{sx}$ , which can be obtained by considering eqn (4.1-7), into eqn (4.1-17) yields the following

expression for the direct-axis stator voltage reference:

$$\begin{aligned} u_{sxref} &= [R_s + (L'_s + TR_s)p + TL'_s p^2]i_{sx} - \omega_{mr}(L'_s + TR_s + 2TL'_s p)i_{sy} \\ &\quad - \omega_{mr}^2 [TL'_s i_{sx} + T(L_s - L'_s)|\bar{i}_{mr}|] - TL'_s i_{sy}(p\omega_{mr}) \\ &= \hat{u}_{sx} + \hat{u}_{dx}, \end{aligned} \quad (4.1-19)$$

where  $p = d/dt$ . Similarly, substitution for  $u_{sy}$  [given by eqn (4.1-8) into eqn (4.1-18)] gives

$$\begin{aligned} u_{syref} &= [R_s + (L'_s + TR_s)p + TL'_s p^2]i_{sy} + \omega_{mr}(L'_s + TR_s + 2TL'_s p)i_{sx} \\ &\quad + \omega_{mr}^2 TL'_s i_{sy} + [TL'_s i_{sx} + T(L_s - L'_s)|\bar{i}_{mr}|](p\omega_{mr}) \\ &= \hat{u}_{sy} + \hat{u}_{dy} \end{aligned} \quad (4.1-20)$$

for the quadrature-axis stator voltage reference. If  $T = 0$ ,  $u_{dx}$ , and  $u_{dy}$  in eqns (4.1-19) and (4.1-20) take the forms of eqns (4.1-9) and (4.1-10) respectively, which is an expected result. However, when  $T$  is not zero, the required full decoupling circuit corresponding to the full inverter-machine system is shown in Fig. 4.5 and this has been obtained by considering eqns (4.1-19) and (4.1-20).

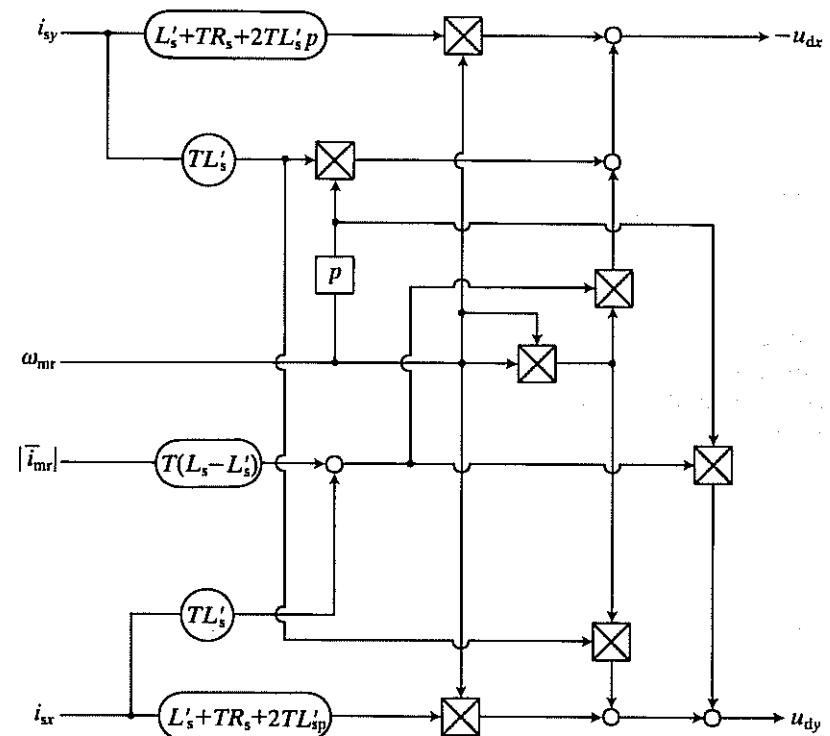


Fig. 4.5. Full decoupling circuit considering the inverter-machine system.

Although the circuit shown in Fig. 4.5 is much more complex than the one shown in Fig. 4.4, when this is used in the implementation of the vector-controlled drive, the drive will operate correctly for any value of the total dead time  $T$ .

In this and following sections various flux models are described, which yield the modulus and speed (or phase angle) of the rotor flux (or rotor magnetizing current) space phasor.

#### 4.1.1.4 Flux models

##### 4.1.1.4.1 Rotor voltage equations for the rotor flux model in the rotor-flux-oriented reference frame

The rotor voltage equations expressed in the rotor-flux-oriented reference frame can be used to obtain the modulus and phase angle of the rotor-flux space phasor or they can be used to obtain the modulus of the so-called rotor magnetizing current  $|\bar{i}_{\text{mr}}|$  and its speed  $\omega_{\text{mr}}$ . This flux model is derived in the present section.

By considering eqn (2.1-149), which gives the rotor voltage equation in the space-phasor form established in the general reference frame, the rotor voltage equation of the induction machine in the special rotor-flux-oriented reference frame will take the following form:

$$0 = R_r \bar{i}_{r\psi_r} + \frac{d\bar{\psi}_{r\psi_r}}{dt} + j(\omega_{\text{mr}} - \omega_r) \bar{\psi}_{r\psi_r}, \quad (4.1-21)$$

where  $\bar{\psi}_{r\psi_r}$  is the rotor flux-linkage space phasor in the rotor-flux-oriented reference frame and has been defined in eqns (2.1-190) and (2.1-193). Alternatively, it follows from eqn (4.1-1) that, because in the special reference frame  $\bar{i}_{\text{mr}} = |\bar{i}_{\text{mr}}|$ ,

$$\bar{\psi}_{r\psi_r} = L_m |\bar{i}_{\text{mr}}|, \quad (4.1-22)$$

which gives a linear relationship if the magnetizing inductance is assumed to be constant. Substitution of eqn (4.1-22) into eqn (4.1-21) yields the following rotor voltage differential equation if the effects of main flux saturation are neglected ( $L_m = \text{constant}$ ):

$$0 = R_r \bar{i}_{r\psi_r} + L_m \frac{d|\bar{i}_{\text{mr}}|}{dt} + j(\omega_{\text{mr}} - \omega_r) L_m |\bar{i}_{\text{mr}}|. \quad (4.1-23)$$

By substituting eqn (4.1-5) into eqn (4.1-23) and dividing by  $R_r$ , which is the rotor resistance, finally the following equation is obtained, which is deliberately put into the form which is similar to the differential equation describing a time-delay element:

$$T_r \frac{d|\bar{i}_{\text{mr}}|}{dt} + |\bar{i}_{\text{mr}}| = \bar{i}_{s\psi_r} - j(\omega_{\text{mr}} - \omega_r) T_r |\bar{i}_{\text{mr}}|. \quad (4.1-24)$$

By resolving into real- and imaginary-axis components, the following extremely simple equations are obtained which describe the flux model in the rotor-flux-oriented reference frame:

$$T_r \frac{d|\bar{i}_{\text{mr}}|}{dt} + |\bar{i}_{\text{mr}}| = i_{sx} \quad (4.1-25)$$

$$\omega_{\text{mr}} = \omega_r + \frac{i_{sy}}{T_r |\bar{i}_{\text{mr}}|}. \quad (4.1-26)$$

In eqn (4.1-26) the term  $i_{sy}/(T_r |\bar{i}_{\text{mr}}|)$  represents the angular rotor frequency (angular slip frequency of the rotor flux)  $\omega_{sl}$ , and it follows that the angular speed of the rotor flux is equal to the sum of the angular rotor speed and the angular slip frequency of the rotor flux. If  $|\bar{i}_{\text{mr}}|$  is constant, it follows from eqn (4.1-25) that  $|\bar{i}_{\text{mr}}| = i_{sx}$ , which is in accordance with Section 2.1.8. The modulus of the rotor flux-linkage space phasor can be kept at a desired level by controlling the direct-axis stator current  $i_{sx}$ , as seen from eqn (4.1-25), but if there is no field weakening (below base speed) the electromagnetic torque is determined by the quadrature-axis stator current  $i_{sy}$ , in accordance with eqn (2.1-197).

Figure 4.6 shows the flux models of the induction machine in the rotor-oriented reference frame, based on eqns (4.1-25) and (4.1-26). The implementation shown in Fig. 4.6(a) utilizes the monitored values of the stator currents ( $i_{sA}, i_{sB}, i_{sC}$ ), the monitored value of the rotor speed ( $\omega_r$ ), and the rotor time constant ( $T_r$ ). The three stator currents are monitored and transformed into their two-axis components by the application of the three-phase to two-phase transformation. In the absence of zero-sequence currents, it is sufficient to monitor only two stator currents. The direct- and quadrature-axis stator currents, which are formulated in the stationary reference frame fixed to the stator ( $i_{sD}, i_{sQ}$ ), are then transformed into the two-axis stator current components in the rotor-flux-oriented reference frame ( $i_{sx}, i_{sy}$ ), by utilizing the transformation given in eqn (4.1-3). The current component  $i_{sx}$  serves as an input to a first-order time-delay element with gain 1 and time constant  $T_r$ , the output of which is the modulus of the rotor magnetizing current. This is proportional to the modulus of the rotor magnetizing flux-linkage space phasor and the proportionality factor is equal to the magnetizing inductance of the machine (which has been assumed to be constant). The quadrature-axis stator current  $i_{sy}$  is divided by  $T_r |\bar{i}_{\text{mr}}|$ , thus yielding the angular slip frequency of the rotor flux, and when the rotor speed is added to this, finally  $\omega_{\text{mr}}$  is obtained. Integration of  $\omega_{\text{mr}}$  yields the angle  $\rho_r$ , which defines the position of the rotor-flux space phasor with respect to the real axis of the stationary reference frame. This angle is used in the transformation block  $e^{-j\rho_r}$ .

However, it is possible to have a similar flux model where, instead of using the monitored values of the rotor speed, the monitored values of the rotor angle ( $\theta_r$ ) are utilized. This is shown in Fig. 4.6(b). It can be seen that the outputs of this flux-model are again  $|\bar{i}_{\text{mr}}|$ ,  $\rho_r$ , and  $|\bar{\psi}_r|$ , but not the speed of the rotor flux-linkage space phasor  $\omega_{\text{mr}}$ .

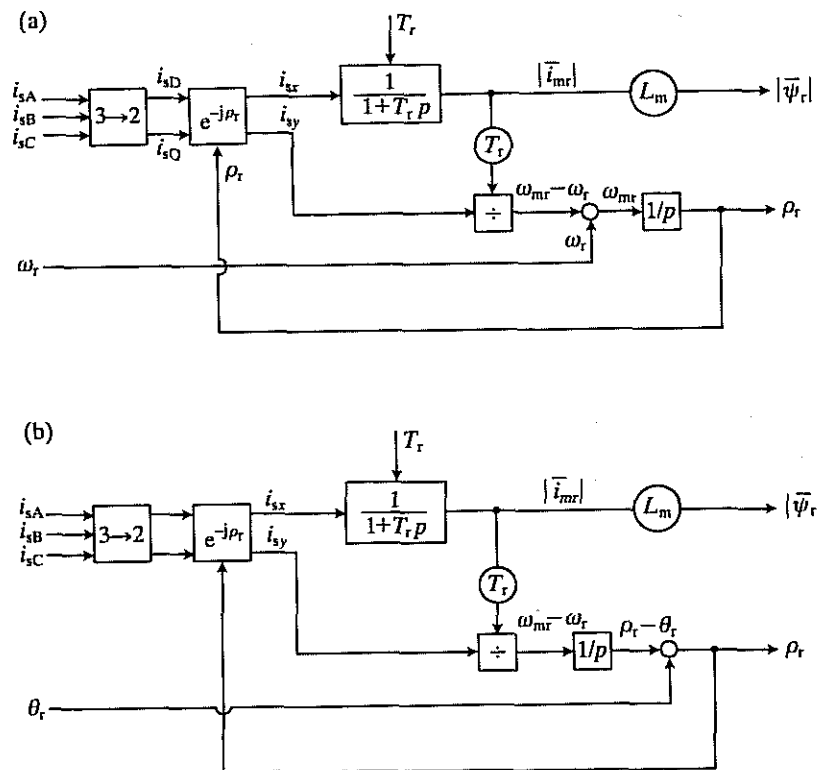


Fig. 4.6. Flux models in the rotor-flux-oriented reference frame. (a) Flux model with inputs  $i_{sA}$ ,  $i_{sB}$ ,  $i_{sC}$ ,  $\omega_r$ ; (b) flux model with inputs  $i_{sA}$ ,  $i_{sB}$ ,  $i_{sC}$ ,  $\theta_r$ .

It is an important feature of eqns (4.1-25) and (4.1-26) that there is a strong dependency on the rotor time constant. If there is an inaccurate value of  $T_r$  in the flux models described above, it could lead to an unwanted coupling between the  $x$  and  $y$  axes, and therefore to a deteriorated dynamic performance of the drive with unwanted instabilities. This problem can be avoided by, for example, the application of on-line parameter-adaption schemes which yield accurate values of the rotor time constant. However, without parameter adaption more acceptable performance can be obtained at lower power levels than at higher power levels. The technique of Model Reference Adaptive Control (MRAC) can also be used to obtain an identification algorithm for the rotor resistance of a squirrel-cage induction machine. In Section 8.2 other models are described to obtain the rotor parameters of induction machines. It should be noted that in contrast to the large sensitivity to the rotor parameters, the implemented drive is less sensitive to variations in the stator parameters (which are, however, needed in the decoupling circuit).

#### 4.1.1.4.2 Rotor voltage equations for flux models in the stationary reference frame

There are several ways to obtain the modulus and phase angle of the rotor-flux space phasor by utilizing certain machine parameters and various monitored quantities, such as the actual stator currents, the rotor speed and the stator voltages. Two different implementations will now be discussed. Since it is the intention to use actual stator voltages and/or currents, the equations will be formulated in the stationary reference frame fixed to the stator.

**Flux model utilizing the monitored rotor speed and stator currents:** It is possible to obtain the modulus and phase angle of the rotor-flux space phasor from a circuit, which in addition to the monitored rotor speed or rotor angle, also utilizes the monitored stator currents. However, in contrast to the implementation shown in Fig. 4.6, the stator currents do not have to be transformed into their values in the rotor-flux-oriented reference frame. For this purpose again the rotor voltage space-phasor equation is used, but in order to have an equation which directly contains the stator currents expressed in the reference frame fixed to the stator, the rotor voltage equation formulated in the stationary reference frame must be used. It should be noted that the effects of magnetic saturation are again neglected.

It follows from eqn (2.1-125) that in the stationary reference frame the rotor voltage equation takes the form,

$$0 = R_r \bar{i}'_r + \frac{d\bar{\psi}'_r}{dt} - j\omega_r \bar{\psi}'_r, \quad (4.1-27)$$

where  $\bar{i}'_r$  and  $\bar{\psi}'_r$  are the rotor-current and rotor-flux space phasors respectively, but expressed in the stationary reference frame. Similarly to the definition used in eqn (4.1-1), the rotor magnetizing-current space phasor expressed in the stationary reference frame is obtained by dividing the rotor flux-linkage space phasor expressed in the stationary reference frame by the magnetizing inductance,

$$\bar{i}_{mr} = \frac{\bar{\psi}'_r}{L_m} = \bar{i}_s + (1 + \sigma_r) \bar{i}'_r, \quad (4.1-28)$$

where  $\bar{i}_{mr}$  and  $\bar{i}_s$  are the rotor magnetizing current and stator phasor currents respectively in the stationary reference frame. By considering eqn (4.1-28), the rotor-current space phasor can be expressed in terms of the rotor magnetizing space phasor, and when this expression is substituted into eqn (4.1-27), the following equation is obtained:

$$T_r \frac{d\bar{i}_{mr}}{dt} = \bar{i}_s - \bar{i}_{mr} + j\omega_r T_r \bar{i}_{mr}. \quad (4.1-29)$$

In the stationary reference frame, the rotor magnetizing-current space phasor and the stator-current space phasor can be expressed in terms of their direct- and

quadrature-axis components as  $\bar{i}_{mr} = i_{mrD} + j i_{mrQ}$  and  $\bar{i}_s = i_{sD} + j i_{sQ}$ , and therefore resolution of eqn (4.1-29) into real and imaginary axis components gives the following two differential equations:

$$T_r \frac{di_{mrD}}{dt} = i_{sD} - i_{mrD} - \omega_r T_r i_{mrQ} \quad (4.1-30)$$

$$T_r \frac{di_{mrQ}}{dt} = i_{sQ} - i_{mrQ} + \omega_r T_r i_{mrD}. \quad (4.1-31)$$

An implementation of eqns (4.1-30) and (4.1-31) is shown in Fig. 4.7, where first the three-phase stator currents are transformed into their two-axis components by the application of the three-phase to two-phase transformation. According to eqns (4.1-30) and (4.1-31), first the signals  $i_{sD} - i_{mrD} - \omega_r T_r i_{mrQ}$  and  $i_{sQ} - i_{mrQ} + \omega_r T_r i_{mrD}$  are obtained. These are then divided by the rotor time constant ( $T_r$ ) and are integrated to yield the direct- and quadrature-axis rotor magnetizing current components ( $i_{mrD}, i_{mrQ}$ ). A rectangular-to-polar converter is used to obtain the modulus ( $|\bar{i}_{mr}|$ ) and the phase angle ( $\rho_r$ ) of the rotor magnetizing flux-linkage space phasor. If required,  $|\bar{i}_{mr}|$  can be multiplied by the magnetizing inductance ( $L_m$ ) to yield the modulus of the rotor flux-linkage space phasor. This scheme is also dependent on the rotor time constant of the machine

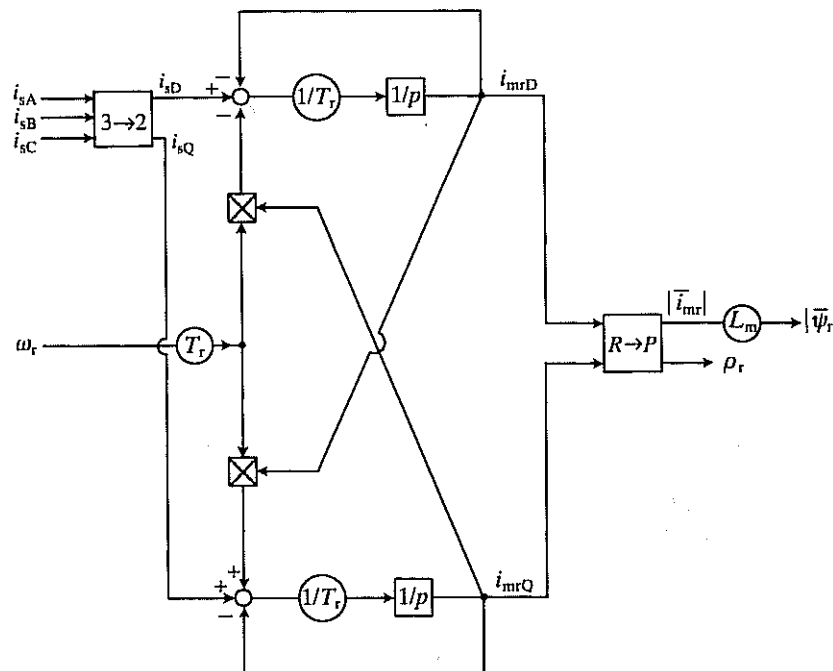


Fig. 4.7. Flux model in the stationary reference frame (the inputs are  $i_{sA}, i_{sB}, i_{sC}, \omega_r$ ).

and can be used over the entire speed range, including standstill. When this model is used, the angle  $\rho_r$  at the output of the model has to be differentiated to obtain  $\omega_{mr}$  which is required in the decoupling circuits described in Figs 4.1, 4.2, 4.3, and 4.4. When compared with the flux models shown in Fig. 4.6, the flux model described in Fig. 4.7 yields less accurate values of the modulus and position of the rotor flux-linkage space phasor.

From eqn (4.1-29), it can be shown that in the steady state, where  $p = d/dt = j\omega_1$ , the rotor magnetizing current can be expressed in terms of the stator current phasor as

$$\bar{I}_{mr} = \frac{\bar{I}_s}{1 + j(\omega_1 - \omega_r)T_r}, \quad (4.1-32)$$

from which it follows that at high speeds, where the difference  $(\omega_1 - \omega_r) = s\omega_1$  (where  $s$  is the slip) is small, a small error in the monitored value of the rotor speed will result in a large error in the rotor magnetizing current (in its modulus and space angle), and this is especially pronounced in its phase angle. The other source of errors is the rotor time constant, which is also temperature dependent, although it follows from eqn (4.1-32) that only at no load ( $s=0$ ) is the rotor magnetizing current (or the rotor flux) not influenced by the rotor time constant. This is of course a physically expected result, since at no load there are no currents in the rotor. However, it will be shown in the next section that it is possible to utilize a linear combination of the stator and rotor voltage equations, and these equations are not so sensitive to the rotor speed. Thus an implementation based on these equations requires less accurate rotor speed monitoring. Furthermore, it will also be shown that the system to be considered is affected by changes in the temperature only in the low speed region.

**Flux model utilizing monitored rotor speed and stator voltages and currents:** From eqns (2.1-148) and (2.1-149), which describe the stator voltage and flux-linkage equations respectively in the space-phasor form, it follows that in the stationary reference frame the stator voltage equations can be put into the following form, if again the effects of magnetic saturation are neglected:

$$\bar{u}_s = R_s \bar{i}_s + L_s \frac{d\bar{i}_s}{dt} + L_m \frac{d\bar{i}'_r}{dt}, \quad (4.1-33)$$

where  $R_s$  and  $L_s$  are the stator resistance and self-inductance  $L_m$  is the magnetizing inductance, and  $\bar{i}_s$  and  $\bar{i}'_r$  are the space phasors of the stator and rotor currents respectively in the stationary reference frame.

If in eqn (4.1-33) the rotor-current space phasor is expressed in terms of the rotor magnetizing current ( $\bar{i}_{mr}$ ) defined by eqn (4.1-28), the following space-phasor voltage equation is obtained for the stator:

$$\bar{u}_s = R_s \bar{i}_s + \sigma L_s \frac{d\bar{i}_s}{dt} + (1-\sigma) L_s \frac{d\bar{i}_{mr}}{dt}, \quad (4.1-34)$$

where  $\sigma$  is the resultant leakage constant  $\sigma = (1 - L_m^2/L_s L_r)$ . Thus it follows from eqn (4.1-34) that

$$(1 - \sigma)T_s \frac{d\bar{i}_{mr}}{dt} = \frac{\bar{u}_s}{R_s} - \bar{i}_s - T'_s \frac{di_s}{dt}, \quad (4.1-35)$$

where  $T_s = L_s/R_s$  are  $T'_s = L'_s/R_s$  are the stator time constant and stator transient time constant respectively. When this equation is added to eqn (4.1-29), the following differential equation is obtained:

$$\frac{d\bar{i}_{mr}}{dt} [T_r + T_s(1 - \sigma)] = \frac{\bar{u}_s}{R_s} + (j\omega_r T_r - 1)\bar{i}_{mr} - T'_s \frac{di_s}{dt}. \quad (4.1-36)$$

It follows that if certain machine parameters and the stator voltages and currents (in the stationary reference frame) are known, it is possible to use eqn (4.1-36) directly to obtain the rotor magnetizing-current space phasor. However, for this purpose, eqn (4.1-36) must be resolved into its real- and imaginary-axis components. Since in the stationary reference frame  $\bar{i}_{mr} = i_{mrD} + j i_{mrQ}$ ,  $\bar{i}_s = i_{sD} + j i_{sQ}$ , and  $\bar{u}_s = u_{sD} + j u_{sQ}$ , it follows from eqn (4.1-35) that its real- and imaginary-axis forms are

$$\frac{di_{mrD}}{dt} [T_r + T_s(1 - \sigma)] + i_{mrD} = \frac{u_{sD}}{R_s} - \omega_r T_r i_{mrQ} - T'_s \frac{di_{sD}}{dt} \quad (4.1-37)$$

$$\frac{di_{mrQ}}{dt} [T_r + T_s(1 - \sigma)] + i_{mrQ} = \frac{u_{sQ}}{R_s} + \omega_r T_r i_{mrD} - T'_s \frac{di_{sQ}}{dt}. \quad (4.1-38)$$

An implementation of eqns (4.1-37) and (4.1-38) is shown in Fig. 4.8, where the input quantities are the monitored value of the rotor speed  $\omega_r$ , and the monitored values of the three-phase stator voltages and currents. These are then transformed into the two-axis components of the stator currents ( $i_{sD}, i_{sQ}$ ) and stator voltages ( $u_{sD}, u_{sQ}$ ) by the application of the three-phase to two-phase transformation. There are two integrators, labelled in the block '1/p' ( $p = d/dt$ ). The two-axis components of the rotor magnetizing currents  $i_{mrD}, i_{mrQ}$  are then converted into the modulus  $|\bar{i}_{mr}|$  and phase angle  $\rho_r$  of the rotor magnetizing-current space phasor with a rectangular-to-polar converter. It follows that the machine parameters to be used in this circuit are the stator resistance, the total leakage constant, and the stator and rotor time constants. When off-line parameter identification is used, these can be obtained by the application of conventional tests. Other techniques are described in Section 8.2.

It can be shown by considering eqn (4.1-36) that in the steady state the following expression is obtained for the rotor magnetizing current phasor (by utilizing  $d/dt = j\omega_1$ ):

$$\bar{i}_{mr} = \frac{\bar{U}_s / R_s - j\omega_1 T'_s \bar{i}_s}{1 + j[(\omega_1 - \omega_r)T_r + \omega_1 T_s(1 - \sigma)]}, \quad (4.1-39)$$

from which it follows that at high speeds, where  $\omega_1 - \omega_r$  is small, a small error in the measured value of the rotor speed will not influence  $\bar{i}_{mr}$  as much as in

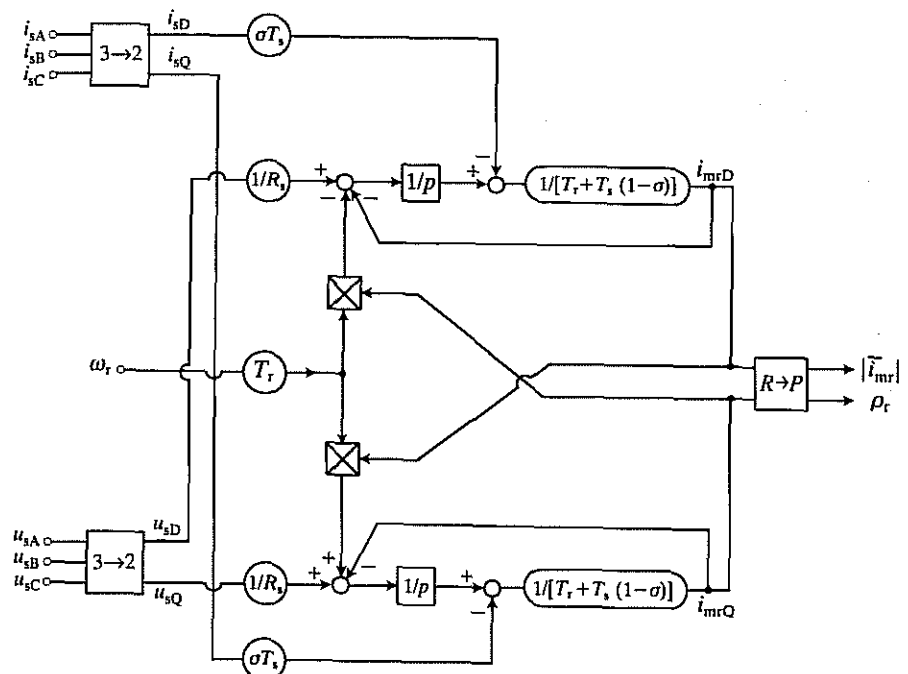


Fig. 4.8. Flux model in the stationary reference frame (the inputs are  $u_{sA}, u_{sB}, u_{sC}, i_{sA}, i_{sB}, i_{sC}, \omega_r$ ).

eqn (4.1-32), since at high values of the rotor speed in the imaginary part of the denominator of eqn (4.1-39), the term  $\omega_1 T_s(1 - \sigma)$  will dominate and this is independent of the speed.

To see the influence of the changes in temperature, eqn (4.1-39) is now rearranged into a form where the temperature-dependent parameters are only present in the denominator. For this purpose both the numerator and the denominator of eqn (4.1-39) are multiplied by  $R_s/L_s = 1/T_s$  and, with  $T'_s = \sigma T_s$ ,

$$\bar{i}_{mr} = \frac{\bar{U}_s / R_s - j\omega_1 \sigma \bar{i}_s}{1/T_s + j[(\omega_1 - \omega_r)T_r/T_s + \omega_1(1 - \sigma)]}. \quad (4.1-40)$$

When  $\omega_1 = \omega_r$ , the denominator becomes  $1/T_s + j\omega_1(1 - \sigma)$ , and the only parameter influenced by the change in the stator temperature is  $T_s$ , since it depends on  $R_s$ , but the effect is negligible. However, at low speeds or at standstill, large errors can arise in  $\bar{i}_{mr}$ , due to the change of  $R_s$  caused by the variation of the temperature. Higher precision can be obtained if instead of using the 'cold' value of the stator resistance a 'hot' value is used, if the temperature is sensed and a simple compensation circuit is implemented, or if a thermal model is used to correct the stator resistance.

It should be noted that instead of eqn (4.1-36), it is possible to use another equation, obtained in a similar way but by using different linear combinations of eqns (4.1-29) and (4.1-35). By increasing the effect of eqn (4.1-29), some improvement can be achieved in the sensitivity of  $\bar{I}_{mr}$  in the low-speed region, but this would be obtained at the expense of greater sensitivity to the errors (in the monitored rotor speed and due to temperature variation) at higher speeds.

#### 4.1.1.4.3 Flux model utilizing monitored stator voltages and currents; improved flux models

It is possible to establish a flux model which does not use the monitored rotor speed, but only the monitored values of the stator voltages and stator currents for the determination of the modulus and the space angle of the rotor magnetizing-current space phasor. For this purpose eqn (4.1-34) can be used. In the stationary reference frame  $\bar{u}_s = u_{sD} + j u_{sQ}$  and  $\bar{i}_s = i_{sD} + j i_{sQ}$ , and therefore resolution of eqn (4.1-34) into its real- and imaginary-axis components yields

$$(1-\sigma)T_s \frac{di_{mrD}}{dt} = \frac{u_{sD}}{R_s} - i_{sD} - T_s \frac{di_{sD}}{dt} \quad (4.1-41)$$

$$(1-\sigma)T_s \frac{di_{mrQ}}{dt} = \frac{u_{sQ}}{R_s} - i_{sQ} - T_s \frac{di_{sQ}}{dt}. \quad (4.1-42)$$

In Fig. 4.9(a) there is shown an implementation of eqns (4.1-41) and (4.1-42), where the input quantities are the monitored values of the three-phase stator voltages and currents respectively ( $u_{sA}, u_{sB}, u_{sC}, i_{sA}, i_{sB}, i_{sC}$ ) and the required parameters are the stator resistance, the total leakage constant, and the stator inductance. Similarly to Fig. 4.8, two integrators are used and the modulus ( $|\bar{I}_{mr}|$ ) and the phase angle ( $\rho_r$ ) of the rotor magnetizing-current space phasor are obtained from its two-axis components by the application of a rectangular-to-polar converter.

It follows from eqns (4.1-41) and (4.1-42) that when these equations are multiplied by the stator resistance, the direct- and quadrature-axis magnetizing-current components in the stator reference frame are essentially obtained by the integration of the direct- and the quadrature-axis magnetizing voltages respectively. These voltages are obtained by monitoring the two-axis components of the terminal voltages and by reducing them by the corresponding stator ohmic drops and by the corresponding voltage drops across the transient inductance of the stator ( $L'_s$ ). When the magnetizing inductance is assumed to be very large (infinite), a voltage drop across the transient stator inductance is equal to the voltage drop across a fictitious resultant leakage inductance, which is obtained by connecting the leakage inductances of the stator and rotor in series. It should be noted that such an assumption leads to only a few per cent error in the determination of the stator transient inductance. However, at low stator frequencies, the stator ohmic drops will dominate and accurate ohmic voltage drop compensation must be performed prior to the integration. However, due to the temperature

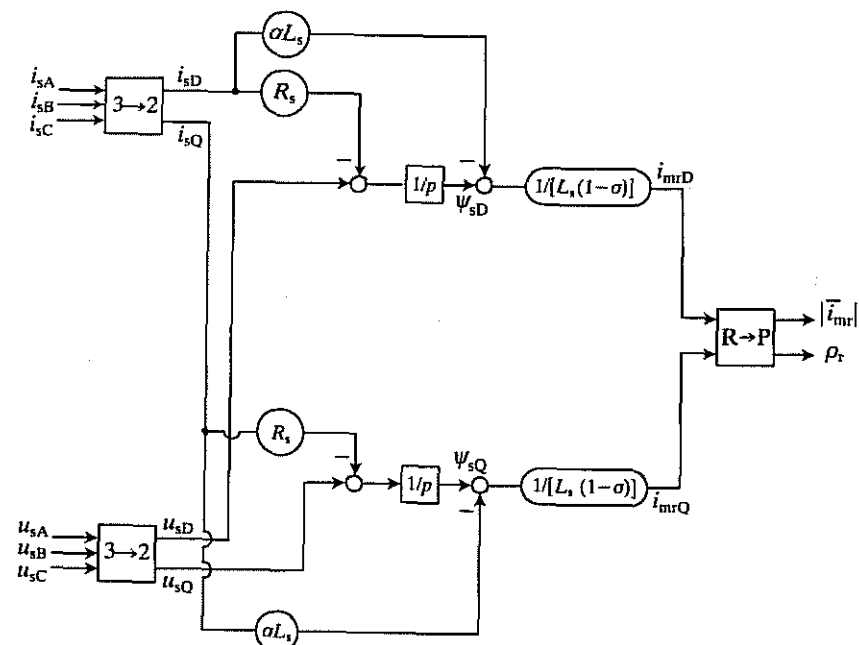


Fig. 4.9(a). Flux model in the stationary reference frame (the inputs are  $u_{sA}, u_{sB}, u_{sC}, i_{sA}, i_{sB}, i_{sC}$ ).

dependency of the stator resistance, this is difficult to perform and with such an implementation a lower frequency limit for useful operation is approximately 3 Hz with a 50 Hz supply. It should also be noted that at low frequencies it is not possible to perform drift-free analogue integration.

It should be noted that to obtain the direct- and quadrature-axis stator voltages, in practice only two stator line voltages are required (e.g.  $u_{AC}$  and  $u_{BA}$ ). This has been discussed in detail in Section 3.1.3.1 where it was shown that

$$u_{sD} = u_{sA} = \frac{1}{3}(u_{BA} - u_{AC})$$

$$u_{sQ} = \frac{1}{\sqrt{3}}(u_{sB} - u_{sC}) = \frac{1}{\sqrt{3}}u_{CB} = -\frac{1}{\sqrt{3}}(u_{AC} + u_{BA}).$$

It has also been discussed in Section 3.1.3.1, that  $i_{sD}$  and  $i_{sQ}$  can be obtained by using only two stator line currents (e.g.  $i_{sA}$  and  $i_{sB}$ ), since by assuming  $i_{sA} + i_{sB} + i_{sC} = 0$ , finally

$$i_{sD} = i_{sA}$$

$$i_{sQ} = \frac{1}{\sqrt{3}}(i_{sB} - i_{sC}) = \frac{1}{\sqrt{3}}(i_{sA} + 2i_{sB})$$

are obtained.

In Fig. 4.9(a), the quantities which are integrated are the direct- and quadrature-axis stator flux linkages in the stationary reference frame ( $\psi_{sD}$ ,  $\psi_{sQ}$ ). Various aspects of this type of stator flux estimator have been discussed in detail in Section 3.1.3.1 and the reader is advised to study that section. Section 3.1.3.1 also discussed the effects of integrator drift and a technique to obtain more accurate estimations of the stator flux-linkage components by subtracting the corresponding drift components of the drift vector. Furthermore, it should also be noted that in addition to the scheme shown in Fig. 4.9(a), it is possible to construct another rotor flux model, where the integration drifts are reduced at low frequency. For this purpose, instead of open-loop integrators, closed-loop integrators are introduced and a rotor flux model is now presented where the stator flux linkages are obtained by using closed-loop integrators. Since

$$\bar{\psi}_s = |\bar{\psi}_s| \exp(j\varphi_s) = \psi_{sD} + j\psi_{sQ},$$

in the rotor flux model shown in Fig. 4.9(b) the direct-axis stator flux can be obtained as  $\psi_{sD} = |\bar{\psi}_s| \cos \varphi_s$  and the quadrature-axis stator flux can be obtained as  $\psi_{sQ} = |\bar{\psi}_s| \sin \varphi_s$  (this is performed by the polar-to-rectangular (P→R) converter shown). However,  $|\bar{\psi}_s|$  and  $\varphi_s$  are obtained by considering the stator voltage equation in the stator-flux-oriented reference frame, eqn (3.1-56). This is now repeated here for convenience:

$$\bar{u}_{s\psi s} = R_s \bar{i}_{s\psi s} + \frac{d|\bar{\psi}_s|}{dt} + j\omega_{ms} |\bar{\psi}_s|.$$

In this voltage equation  $\omega_{ms} = d\varphi_s/dt$  is the speed of the reference frame, which is equal to the speed of the stator flux-linkage space vector. In agreement with eqns (3.1-57) and (3.1-58), resolution of this into its real and imaginary components gives the rate of change of the stator flux modulus as  $d|\bar{\psi}_s|/dt = u_{sx} - R_s i_{sx}$  and the speed of the stator flux space vector as  $\omega_{ms} = (u_{sy} - R_s i_{sy})/|\bar{\psi}_s|$ , where the subscripts  $x$  and  $y$  denote the direct- and quadrature-axis of the stator-flux-oriented reference frame respectively. These voltage equations are used in Fig. 4.9(b) to yield the first part of the circuit, which is the same as that shown

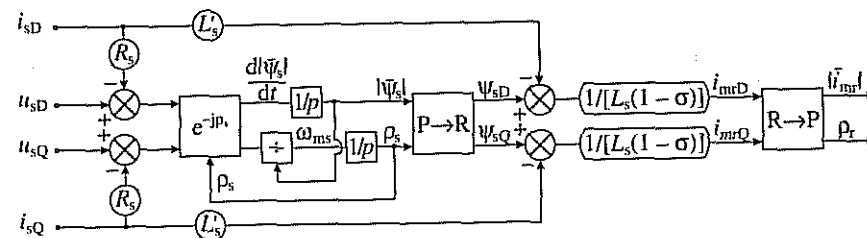


Fig. 4.9(b). Rotor flux model where stator flux linkages are obtained in the stator-flux-oriented reference frame.

in Fig. 3.20(b), and the extra parts of the circuit shown in Fig. 4.9(b) are the same as the corresponding parts shown in Fig. 4.9(a). It can be seen that these extra parts correspond physically to the fact that the rotor flux-linkage space vector (expressed in the stationary reference frame),  $\bar{\psi}'_r = L_m |i_{mr}| \exp(j\varphi_r)$ , is related to the stator flux-linkage space vector (expressed in the stationary reference frame) by

$$\bar{\psi}'_r = \frac{L_r}{L_m} (\psi_s - \sigma L_s i_s),$$

where  $\sigma L_s = L'_s$  is the transient stator inductance.

It should also be noted that, similarly to the discussion in Section 3.1.3.1, it is also possible to use flux estimators such that the stator voltages are not monitored but are reconstructed. If the machine is supplied by a voltage-source inverter, then it is possible to reconstruct the stator voltages from the d.c. link voltage ( $U_d$ ) by using the inverter switching states ( $S_A, S_B, S_C$ ). The details are shown in Section 3.1.3.1. However, it follows from eqn (3.1-39) that

$$\bar{u}_s = \frac{2}{3} U_d (S_A + aS_B + a^2 S_C) = u_{sD} + j u_{sQ};$$

thus the direct- and quadrature-axis voltages can be reconstructed as

$$u_{sD} = \frac{2}{3} U_d \left( S_A - \frac{S_B}{2} - \frac{S_C}{2} \right)$$

$$u_{sQ} = \frac{1}{\sqrt{3}} U_d (S_B - S_C).$$

It is possible to construct a stator flux or rotor flux estimator, in which the drift problems associated with ‘pure’ open-loop integrators at low frequency are avoided by a band-limited integration of the high-frequency components and by replacing the inaccurate flux estimation at frequencies below  $1/T$  by its reference value in a smooth transition. For this purpose a first-order delay element is used, as shown in Fig. 4.9(c).

The inputs to the stator flux estimator shown in Fig. 4.9(c) are the monitored values of the stator-voltage space vector ( $\bar{u}_s$ ) and stator-current space vector ( $\bar{i}_s$ ), expressed in the stationary reference frame. In addition, the third input is the modulus of the reference value of the stator flux-linkage space vector ( $|\bar{\psi}_{sref}|$ ), which is also expressed in the stationary reference frame. It should be noted that since the stationary reference frame is used, the reference flux-linkage space vector  $\bar{\psi}_{sref}$  contains two components,  $\psi_{sDref}$  and  $\psi_{sQref}$ . The space vector of the induced stator voltages is

$$\bar{u}_{si} = \bar{u}_s - R_s \bar{i}_s = \frac{d\bar{\psi}_s}{dt}$$

and in an open-loop stator flux estimator using a ‘pure’ integrator, its integrated value ( $\int \bar{u}_{si} dt$ ) would yield the stator flux-linkage space vector  $\bar{\psi}_s$ . However, in

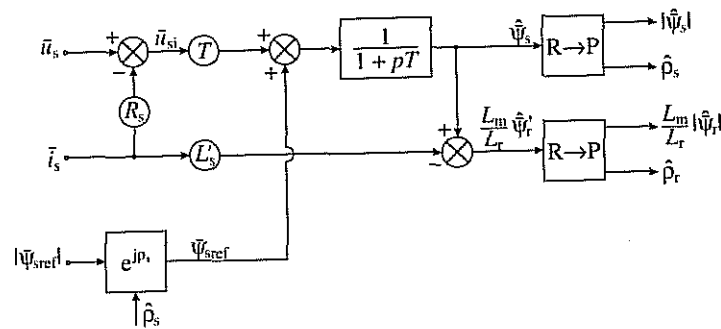


Fig. 4.9(c). Flux estimator using a time-delay element.

Fig. 4.9(c),  $\bar{u}_{si}$  is multiplied by  $T$ . The reference stator flux-linkage space vector is added to  $T\bar{u}_{si} + \bar{\psi}_{sref}$ . This is then the input to the first-order delay element,  $1/(1+pT)$ , on the output of which the estimated value of the stator flux-linkage space vector  $\hat{\psi}_s$  is obtained. It can be seen that if  $\bar{\psi}_{sref}$  is equal to  $\bar{\psi}_s$  then the output ( $\hat{\psi}_s$ ) is exactly  $\bar{\psi}_s$ . In Fig. 4.9(c) an R→P converter is used which yields the modulus  $|\hat{\psi}_s|$  and also angle  $\hat{\rho}_s$  of the stator flux-linkage space vector in the stationary reference frame. However, it is also possible to obtain an estimate of the rotor flux-linkage space vector expressed in the stationary reference frame,  $\bar{\psi}'_r$ , by considering that

$$\bar{\psi}_s = L'_s \bar{i}_s + \frac{L_m}{L_r} \bar{\psi}'_r,$$

where  $L'_s$  is the transient stator inductance, and this estimation is also shown in Fig. 4.9(c). Thus  $(L_m/L_r)\bar{\psi}'_r$  is obtained, and by using another R→P converter,  $(L_m/L_r)|\bar{\psi}'_r|$  and  $\hat{\rho}_r$  are obtained. This scheme can be used in both vector drives and also in direct-torque-controlled drives. In a vector drive with stator-flux-oriented control, the space vector  $\hat{\psi}'_{sref}$  can be obtained from the reference stator flux vector modulus  $|\bar{\psi}'_{sref}|$ , which is one of the inputs to a stator-flux-oriented control scheme, by considering that

$$\hat{\psi}'_{sref} = |\bar{\psi}'_{sref}| \exp(j\hat{\rho}_s),$$

where  $\hat{\rho}_s$  is the angle of the stator flux-linkage space vector with respect to the real-axis of the stationary reference frame. It should be noted that for low-frequency operation, in the scheme shown in Fig. 4.9(c), the time-delay element has approximately a transfer function of unity and thus its output becomes almost equal to  $\bar{\psi}'_{sref}$  since  $\bar{u}_{si}$  is small. This is in agreement to that emphasized above. Thus the integration is avoided at low stator frequencies. However, at high stator frequencies, the transfer function of the time-delay element is approximately equal to that of an integrator and it follows that the two actions are switched over smoothly around the stator frequency of  $1/T$ . The time constant must be selected so that it should minimize the estimation error when switching over takes place.

A suitable value for  $T$  is  $T=T_r$ , where  $T_r$  is the rotor time constant; this gives an estimator with minimum parameter sensitivity. The flux estimator scheme shown in Fig. 4.9(c) could be expanded to obtain the electromagnetic torque and also the rotor speed (see also Section 4.5.3.1 which discusses various techniques for the estimation of the rotor speed using flux-linkage estimates).

It is also possible to obtain a rotor flux-linkage estimator whose inputs are the stator voltage and current space vectors as above, but the third input is the reference value of the modulus of the rotor flux-linkage space vector,  $|\bar{\psi}'_{rref}|$ , which, for example, is a known quantity in a vector drive employing rotor-flux-oriented control. Such a scheme is shown in Fig. 4.9(d).

It can be seen that in Fig. 4.9(d) the estimated value of the rotor flux-linkage space vector in the stationary reference frame is  $\hat{\psi}'_r$ , and by using a R→P converter its modulus  $|\hat{\psi}'_r|$  and its angle  $\hat{\rho}_r$  are obtained. Furthermore, by using the measured stator currents and also the estimated rotor flux linkages (in the stationary reference frame), the torque-producing stator current component  $i_{sy}$  is also obtained as

$$i_{sy} = \frac{(\hat{\psi}'_r \times \bar{i}_s)}{|\hat{\psi}'_r|^2} = \frac{(\hat{\psi}'_{rd} i_{sQ} - \hat{\psi}'_{rq} i_{sD})}{(\hat{\psi}'_{rd}^2 + \hat{\psi}'_{rq}^2)^{1/2}}.$$

This can be proved by using eqn (2.1-192) and  $\cos \rho_r = \hat{\psi}'_{rd}/|\bar{\psi}'_{rq}|$ ,  $\sin \rho_r = \hat{\psi}'_{rq}/|\bar{\psi}'_{rq}|$ . The angular slip frequency,  $\omega_{sl}$ , can also be obtained, since by using the second term on the right-hand side of eqn (4.1-26),

$$\hat{\omega}_{sl} = \frac{(L_m/T_r)i_{sy}}{|\hat{\psi}'_r|}.$$

However, by using eqn (4.1-26), the angular rotor speed can also be obtained as  $\hat{\omega}_r = \hat{\omega}_{mr} - \hat{\omega}_{sl}$  where  $\hat{\omega}_{mr} = d\hat{\rho}_r/dt$ , where the estimation of  $\hat{\rho}_r$  has been discussed above; thus  $\hat{\rho}_r = \tan^{-1}(\hat{\psi}'_{rq}/\hat{\psi}'_{rd})$  or  $\hat{\rho}_r = \cos^{-1}(\hat{\psi}'_{rd}/|\hat{\psi}'_r|)$ , etc., where  $|\hat{\psi}'_r| = (\hat{\psi}'_{rd}^2 + \hat{\psi}'_{rq}^2)^{1/2}$ . It is an advantage of this scheme that it can give accurate estimates of the flux linkages and thus the electromagnetic torque as well

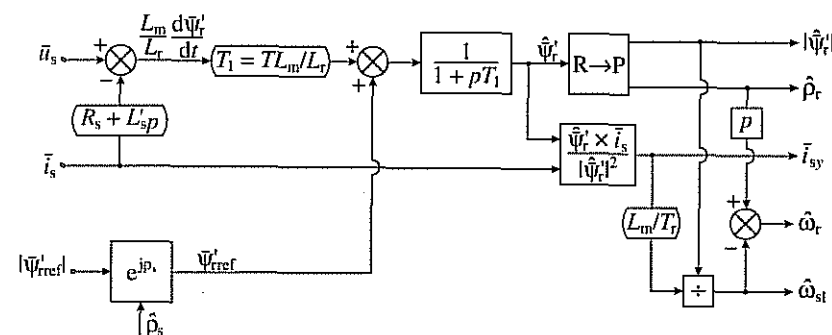


Fig. 4.9(d). Rotor flux estimator using a time-delay element.

$\dot{i}_e = (3/2)P(L_m/L_r)(\bar{\psi}_{rq}i_{sQ} - \bar{\psi}_{rQ}i_{sD})$  or the torque can be expressed directly in terms of the angular slip frequency], and also the rotor speed even at very low frequencies. Thus it can be used in speed-sensorless vector- and direct-torque-controlled induction motor drives (see also Section 4.5.3.1), but it is very important to select the appropriate  $T_1$  time constant used in Fig. 4.9(d) and very large and very small values of  $T_1$  should be avoided.

Another possibility to improve at low speed the stator flux-linkage and rotor flux-linkage estimates obtained by the application of the stator voltage model  $[\bar{\psi}_s = \int(\bar{u}_s - R_s\bar{i}_s)dt; \bar{\psi}_r = (L_r/L_m)(\bar{\psi}_s - L'_s\bar{i}_s) = |\bar{\psi}_r| \exp(j\rho_r)]$  is to use some form of stabilizing feedback in the voltage model. The correction term makes the modified voltage model insensitive to parameter deviation and measurement errors. The derivation of the modified voltage model is discussed briefly below.

As discussed earlier, due to feedforward integration, the voltage model is sensitive to parameter variations and measurement error and at low stator frequencies, these effects become more important. At zero stator frequency the induced voltage is zero and  $\bar{u}_s = R_s\bar{i}_s$ . It can be seen that at low frequency even a small deviation of the stator resistance will lead to an integration offset yielding incorrect estimates of  $\bar{\psi}_s$  and  $\bar{\psi}_r$ . However, it is possible to obtain the rotor flux-linkage space vector (and stator flux-linkage space vector) by using other models, thus  $\bar{\psi}'_r = |\bar{\psi}_r| \exp(j\rho_r^*)$  is obtained. It is then possible to obtain the difference vector  $\Delta\bar{\psi}_r = \bar{\psi}'_r - \bar{\psi}_r$ , and its components can be used to obtain correction voltage components, which are fed back to the voltage model. The obtained modified voltage model then contains modified stator voltage components, where a modified component voltage is the sum of the original voltage and the feedback voltage.

It can be assumed that at low frequency and also at standstill the modulus of the rotor flux-linkage space vector is constant, thus  $|\bar{\psi}_r| = \text{constant}$ , since this will not degrade the dynamic performance of the drive (at low speed). However, its position ( $\rho_r$ ) can also be estimated even at standstill, e.g. by using parameter-insensitive techniques, including the technique discussed in Section 3.2.2.2.3, where saturation effects are utilized. Thus  $\bar{\psi}'_r = |\bar{\psi}_r| \exp(j\rho_r^*)$  is known, and then by using

$$\Delta\bar{\psi}_r = \bar{\psi}'_r - \bar{\psi}_r = \Delta\psi_{rx} + j\Delta\psi_{ry},$$

the component rotor flux-linkage deviations are obtained as

$$\Delta\psi_{rx} = |\bar{\psi}_r^*| \sin \rho$$

$$\Delta\psi_{ry} = |\bar{\psi}_r^*| (\cos \rho - 1),$$

where  $\rho = \rho_r^* - \rho_r$  is the angle between the two rotor flux-linkage space vectors  $\bar{\psi}_r^*$  and  $\bar{\psi}_r$  and  $x$  and  $y$  are the real and imaginary axes of the reference frame fixed to the rotor flux-linkage space vector  $\bar{\psi}_r$ . These rotor flux-linkage deviation components are then used in the voltage feedback of the modified voltage model.

#### 4.1.1.5 Expression for the electromagnetic torque; utilization of the steady-state equivalent circuit

By considering the expression for the electromagnetic torque shown in eqn (2.1-197), which is repeated here for convenience,

$$t_e = \frac{3}{2}P \frac{L_m^2}{L_r} |\bar{i}_{mr}| i_{sy}, \quad (4.1-43)$$

it follows that if the parameters of the machine are considered to be constant and  $|\bar{i}_{mr}|$  is constant, then the electromagnetic torque is proportional to the quadrature-axis stator current expressed in the rotor-flux-oriented reference frame and thus the torque will respond instantaneously with  $i_{sy}$ . If there is a change in  $i_{sx}$ , it follows by considering eqns (4.1-25) and (4.1-26) that there will be a delayed response in the torque, and the delay is determined by the rotor time constant.

In the steady state, eqn (4.1-43) can also be derived by considering the steady-state equivalent circuit of the induction machine. This will now be discussed. The expression for the electromagnetic torque will be obtained by utilizing the relationship between the air-gap power and the torque, and the expression for the air-gap power will be obtained directly from the steady-state equivalent circuit.

In the steady state, if the induction machine is supplied by a sinusoidal symmetrical three-phase supply voltage system, the stator voltages are

$$u_{sA}(t) = \sqrt{2}U_s \cos(\omega_1 t) \quad u_{sB} = \sqrt{2}U_s \cos(\omega_1 t - 2\pi/3) \\ u_{sC} = \sqrt{2}U_s \cos(\omega_1 t - 4\pi/3),$$

where  $U_s$  is the r.m.s. value of the line-to-neutral voltages. Thus it follows from the definition of the stator-voltage space phasor in the stationary reference frame given by eqn (2.1-61) that  $\bar{u}_s = \sqrt{2}U_s e^{j\omega_1 t}$ . The space phasor of the stator currents can be similarly defined. Thus by considering that in the steady state, the instantaneous values of the stator currents are

$$i_{sA}(t) = \sqrt{2}I_s \cos(\omega_1 t - \phi_s) \quad i_{sB} = \sqrt{2}I_s \cos(\omega_1 t - \phi_s - 2\pi/3) \\ i_{sC} = \sqrt{2}I_s \cos(\omega_1 t - \phi_s - 4\pi/3),$$

it follows, by the application of eqn (2.1-4), that the space phasor of the stator currents in the stationary reference frame is

$$\bar{i}_s = \sqrt{2}I_s e^{j(\omega_1 t - \phi_s)} = \sqrt{2}I_s e^{j(\omega_1 t)}$$

Thus by considering eqns (4.1-27), (4.1-28), and (4.1-34) and the steady-state expressions for  $\bar{u}_s$  and  $\bar{i}_s$ , the resulting equations can be represented by the equivalent circuit shown in Fig. 4.10(a).

It is a main feature of the equivalent circuit shown in Fig. 4.10(a) that, in contrast to the well-known steady-state equivalent circuit of the induction

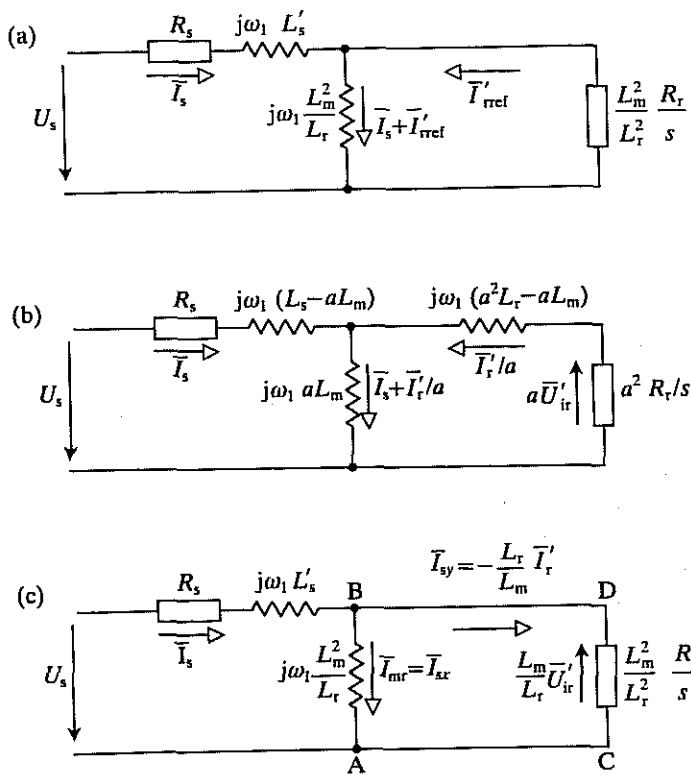


Fig. 4.10. Steady-state equivalent circuits of the induction machine. (a) Equivalent circuit where the rotor leakage inductance is not present in the rotor branch. (b) Equivalent circuit incorporating the effects of the general turns ratio. (c) Equivalent circuit which contains the torque- and flux-producing stator-current components.

machine, now the rotor leakage inductance is not present in the rotor branch. It should be noted that the rotor resistance ( $R_r$ ) is divided by the slip ( $s$ ) and  $R_r/s$  is multiplied by  $a^2$ , where  $a$  is a specially selected turns ratio  $a=L_m/L_r$ . In Fig. 4.10(a) the referred value of the rotor current phasor in the steady-state is present; this is  $\bar{I}'_{ref}=\bar{I}'_r/a$  and  $\bar{I}_{mr}=\bar{I}_s+\bar{I}'_{ref}$  is the rotor magnetizing-current phasor in the steady state in accordance with that stated in Section 2.1.3 and also in agreement with eqn (4.1-28). Furthermore, in the equivalent circuit shown, the referred value of the magnetizing inductance is present, which is equal to  $aL_m=L_m^2/L_r$  and owing to the special referring factor, instead of the stator leakage inductance, the stator transient inductance ( $L'_s=\sigma L_s$ ) is present.

The equivalent circuit shown in Fig. 4.10(a) could have also been obtained from the space-phasor stator and rotor voltage equations in the stationary reference frame, but by considering a general value of the turns ratio ( $a$ ). For this purpose, first eqns (2.1-35) and (2.1-51) are considered, which define the stator and rotor

flux-linkage space phasors respectively ( $\bar{\psi}_s, \bar{\psi}_r$ ) in the stationary reference frame. By considering the steady state and adding the term  $aL_m\bar{I}_s-aL_m\bar{I}'_s$  to the expression for  $\bar{\Psi}_s$ ,

$$\bar{\Psi}_s=(L_s-aL_m)\bar{I}_s+aL_m(\bar{I}_s+\bar{I}'_r/a)$$

is obtained. The referred value of the rotor flux-linkage space phasor is obtained by multiplying  $\bar{\Psi}'_r$  by the general turns ratio ( $a$ ), and by adding the term  $aL_m\bar{I}'_r/a-aL_m\bar{I}'_r/a$ . Thus

$$a\bar{\Psi}'_r=(a^2L_r-aL_m)\bar{I}'_r/a+aL_m(\bar{I}_s+\bar{I}'_r/a)$$

is obtained. When these expressions are combined with the stator and rotor voltage equations, the equivalent circuit shown in Fig. 4.10(b) is obtained. It follows from Fig. 4.10(b) that if the general turns ratio is selected as  $a=L_m/L_r$ , in the rotor branch the inductive part will vanish and the equivalent circuit shown in Fig. 4.10(a) is obtained.

It is possible to redraw the equivalent circuit shown in Fig. 4.10(a) as the equivalent circuit shown in Fig. 4.10(c), which contains the torque and rotor flux-producing stator-current components ( $\bar{I}_{sy}, \bar{I}_{sx}$ ). It follows from Fig. 4.10(c) that the stator current  $\bar{I}_s$  is divided into  $\bar{I}_{mr}=\bar{I}_{sx}$  and  $\bar{I}_{sy}$  components. The current  $\bar{I}_{mr}=\bar{I}_{sx}$  flows through the referred magnetizing reactance  $\omega_1 L_m^2/L_r$  and the current  $\bar{I}_{sy}$  flows through the referred rotor resistance  $(L_m^2/L_r^2)R_r/s$ . Furthermore,  $(L_m/L_r)\bar{U}'_{ir}$  is the referred value of the voltage drop across the referred rotor resistance and thus  $\bar{U}'_{ir}=-j\omega_1\bar{\Psi}'_r$ . In Fig. 4.10(c) the current  $\bar{I}_{sx}$  is the rotor flux-producing stator-current component and this can be proved by considering that the voltage across points A and B ( $\bar{U}_{AB}$ ) is equal to the voltage across points C and D ( $\bar{U}_{CD}$ ) and thus  $\bar{I}_{sx}\omega_1 L_m^2/L_r=j\omega_1(L_m/L_r)\bar{\Psi}'_r$  and it follows that  $\bar{\Psi}'_r=L_m\bar{I}_{sx}$ , so  $\bar{I}_{sx}$  is indeed the rotor flux-producing stator current.

That  $\bar{I}_{sy}$  is the torque-producing stator current can be proved by considering that in the steady state, the electromagnetic torque can be obtained as  $T_e=P_{ag}/\omega_1$ , where  $P_{ag}$  is the air-gap power, i.e. the power that crosses the air-gap. By considering the equivalent circuit shown in Fig. 4.10(c),  $P_{ag}$  can be expressed as  $P_{ag}=(3P/2)|\bar{U}_{AB}||\bar{I}_{sy}|$ , where  $|\bar{U}_{AB}|=\omega_1(L_m^2/L_r)|\bar{I}_{sx}|$ . Thus the electromagnetic torque can be expressed as

$$T_e=(3P/2)(L_m^2/L_r)|\bar{I}_{sx}||\bar{I}_{sy}|=(3P/2)(L_m/L_r)|\bar{\Psi}'_r||\bar{I}_{sy}|.$$

As expected, this is similar to eqn (4.1-43).

The equivalent circuit shown in Fig. 4.10(c) can also be used to obtain the expression for the angular slip frequency in the steady-state. If the modulus of the voltage across points A and B  $|\bar{I}_{sx}|\omega_1 L_m^2/L_r$  is equal to the modulus of the voltage across points C and D, which in terms of the referred rotor resistance can be expressed as  $|\bar{I}_{sy}|(L_m^2/L_r^2)R_r/s$ , it follows that  $s\omega_1=|\bar{I}_{sy}|/(T_r|\bar{I}_{sx}|)$ , where  $s\omega_1=\omega_{sl}$  is the angular slip frequency, and  $T_r$  is the rotor time constant ( $T_r=L_r/R_r$ ). The same result also follows from eqn (4.1-26) if the steady state is considered, and  $\omega_{mr}-\omega_r=s\omega_1$ .

Since in the steady state the torque-producing stator current varies linearly with the angular slip frequency, and thus there is no pull-out slip or pull-out torque (see also Section 4.3.4), static instability does not arise in the induction machine subjected to rotor-flux-oriented control. However, in contrast to this, when, say, stator-flux-oriented control of the induction machine is performed, as shown in Section 4.2, the torque-producing stator current does not vary linearly with the angular slip frequency and theoretically static instability can arise. The details of this will be discussed in Section 4.3.4, but it should be noted that from the general equivalent circuit shown in Fig. 4.10(b), if the general turns ratio is chosen to be  $a = L_s/L_m$ , the inductive term in the stator branch is eliminated. In this case the current  $\bar{I}_s + (L_m/L_s)\bar{I}'_r$  flows across the referred value of the magnetizing inductance and this current is equal to  $(L_m/L_s)$  times the so-called stator magnetizing current, which in the steady state takes the form  $\bar{I}_{ms} = (L_s/L_m)\bar{I}_s + \bar{I}'_r$ . A similar definition of this current will be used in Section 4.2. By choosing  $a = L_s/L_m$ , it is possible to use the equivalent circuit shown in Fig. 4.10(b) to obtain the expression for the electromagnetic torque in the steady state in terms of the stator flux-producing stator current component and the torque-producing stator current component, or to obtain the expression for the angular slip frequency in terms of the same two current components.

#### 4.1.1.6 Implementation of the PWM VSI-fed vector-controlled induction machine

##### 4.1.1.6.1 Implementation of the PWM VSI-fed induction machine drive utilizing a speed sensor and the actual values of $i_{sx}$ , $i_{sy}$

This implementation of the PWM voltage-source inverter-fed induction machine drive uses the concepts discussed in previous sections. Figure 4.11 shows the schematic of the rotor-flux-oriented control of a voltage-source inverter-fed induction machine.

In this and the following sections two different implementations are described for the PWM voltage-source inverter-fed induction machine drive which have found widespread applications. The first one utilizes one of the decoupling circuits described above, which uses the actual values of the direct- and quadrature-axis stator currents in the rotor-flux-oriented reference frame ( $i_{sx}$ ,  $i_{sy}$ ) and contains a closed-loop control of the rotor position, rotor speed, electromagnetic torque, and rotor flux. In the second, simpler implementation, decoupling is achieved by using the reference values of the same stator current components ( $i_{sxref}$ ,  $i_{syref}$ ); there is closed-loop control of the rotor speed, which is obtained by the application of a sensor. It should be noted that it is possible to have closed-loop control of the flux- and torque-producing currents and of the rotor speed in a scheme where a decoupling circuit is utilized which is similar to the one used in the first implementation, and uses the actual values of  $i_{sx}$  and  $i_{sy}$ . However, the rotor speed is not obtained by a sensor, but is estimated by utilizing Model Reference Adaptive Control.

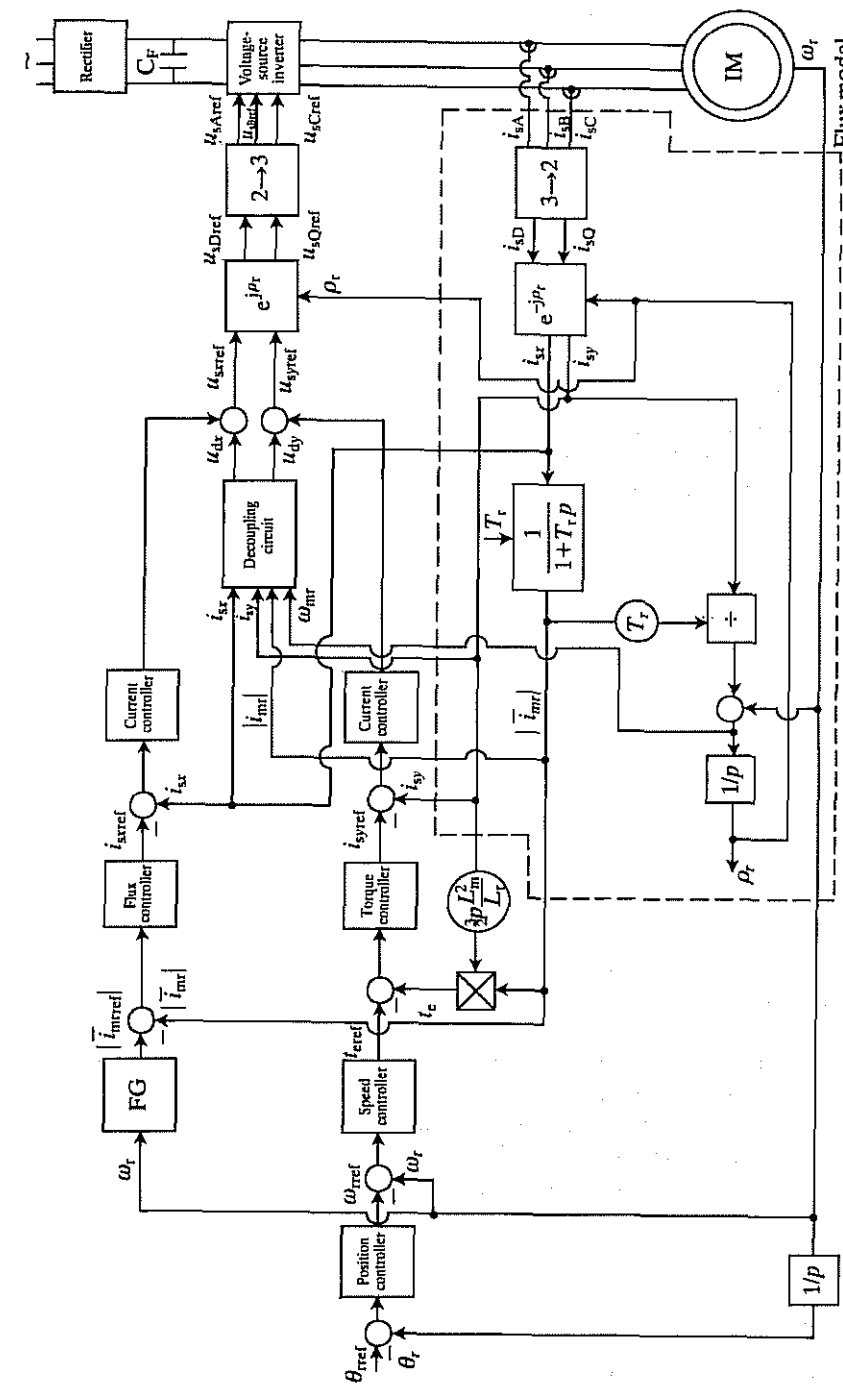


Fig. 4.11. Schematic of the rotor-flux-oriented control of a voltage-source inverter-fed induction machine.

In Fig. 4.11 the I.M. is supplied by a voltage-source PWM inverter, which is supplied by a diode bridge rectifier through a filter capacitor. The output voltages of the inverter are controlled by a pulse-width modulation technique. There are many types of modulation techniques which will not be discussed in detail here, but it should be noted that the so-called suboscillation technique has gained widespread application. When this technique is used, the output voltage of the inverter is generated by comparing a triangular carrier wave of frequency (switching frequency)  $f_s$  (in order to avoid beat effects, usually  $f_s = Nf_1$ , where  $f_1$  is the fundamental frequency and  $N$  is the pulse number, an integer) with a sinusoidal modulating wave with fundamental frequency; the natural points of intersection determine the switching instants. The pulse-width modulated output voltages contain time harmonics and these lead to unwanted losses in the machine. There are a number of so-called harmonic elimination techniques, but when such a technique is used, although certain time harmonics (e.g. the fifth and the seventh) are almost eliminated, other harmonics will have increased magnitudes (e.g. the ninth and the eleventh). However, since the harmonic losses in the machine are determined by the r.m.s. value of the harmonic currents, it is these currents which have to be minimized in order to reduce these losses. This concept has led to the development of the so-called minimum harmonic current technique. It is a common feature of these techniques that they are based on off-line computation of optimal pulse patterns for steady-state operation of the drive under consideration. Thus the optimum conditions can only be obtained in the steady state and not in the transient state. Furthermore, at low stator frequencies, off-line methods can be ineffective. To overcome this problem, on-line computation of the pulse patterns is required and by using on-line optimization algorithms it is possible to ensure, for example, minimum harmonic torque at minimum switching frequency or minimum torque pulsations. When the inverter switching frequency is reduced, the efficiency of the drive is increased as a result of the decrease in the switching losses, which can be especially important in thyristor inverters with forced commutation.

The flux model shown in Fig. 4.6 is used to obtain the angle  $\rho_r$ , which is used in the transformation blocks  $e^{j\rho_r}$  and  $e^{-j\rho_r}$ . Furthermore, this flux model is used to obtain the angular speed of the rotor flux  $\omega_{mr}$  and the modulus of the rotor magnetizing current  $|i_{mr}|$ , since these are also used in the decoupling circuit, which is now assumed to be the one shown in Fig. 4.1. The modulus of the rotor magnetizing-current space phasor is also used to obtain the electromagnetic torque, in accordance with eqn (4.1-43).

A position controller, which can be a proportional controller (since the rotor speed  $\omega_r$  is equal to the first time derivative of the rotor angle  $\theta_r$ ) provides as its output the reference value of the rotor speed ( $\omega_{rref}$ ). The speed controller, a PI controller, provides the reference torque ( $T_{rref}$ ), and the torque controller, also a PI controller, gives the reference value of the quadrature-axis stator current in the rotor-flux-oriented reference frame ( $i_{syref}$ ). Since in the steady state, the fundamental components of the stator voltages increase with stator frequency, but only a specific maximal output voltage of the inverter is available, it follows that with

constant rotor magnetizing current ( $|i_{mr}|$ ), at a specific frequency, these voltages would exceed the maximally available value. Thus above a certain frequency, an increase of speed is only possible if the rotor magnetizing current is reduced. In Fig. 4.11 field weakening is achieved by the application of the function generator FG, the output of which is the reference value of the modulus of the rotor magnetizing-current space phasor ( $|i_{mrref}|$ ), which is speed dependent. Below base speed a constant (maximal) value is obtained (this value is only limited by main flux saturation), and above base speed this is reduced, inversely proportional to the rotor speed. The reference signal  $|i_{mrref}|$  is compared with the actual value of the rotor magnetizing current and the error serves as input to the flux controller, also a PI controller. Its output is the direct-axis stator current reference expressed in the rotor-flux-oriented reference frame ( $i_{sxref}$ ). In Fig. 4.11 it is possible to leave out the quadrature-axis stator current controller, since the torque controller performs a similar role, and in this case there is no need to feed back the current  $i_{sy}$ ; there is only the torque feedback, which is, however, proportional to the quadrature-axis stator current if the magnetizing inductance is constant.

The error signals  $i_{sxref} - i_{sx}$  and  $i_{syref} - i_{sy}$  serve as inputs to the respective current controllers and the outputs from these are added to the corresponding outputs of the decoupling circuit, as described above for the ideal drive. Thus the direct- and quadrature-axis reference stator voltages  $u_{sxref}$  and  $u_{syref}$  are obtained; these are established in the rotor-flux-oriented reference frame, and therefore they have to be transformed by  $e^{j\rho_r}$  to obtain the two-axis stator voltages references in the stationary reference frame ( $u_{sDref}, u_{sQref}$ ). This is followed by the application of the two-phase to three-phase transformation indicated by the '2→3' block and finally the reference values of the three-phase stator voltages are obtained. These signals are used to control the pulse-width modulator which transforms these reference signals into appropriate on-off switching signals to command the inverter phases.

With the given scheme it is possible to produce full torque even at standstill, since the stator currents flow even at standstill and supply the magnetizing currents. The implementation shown in Fig. 4.11 gives a high dynamic performance drive. In addition to the high dynamic response resulting from the decoupling control, there is no pull-out effect and if there is too quick a change of the speed reference or if the induction machine is overloaded, the electromagnetic torque cannot exceed the specified maximal level, since the speed error signal will saturate.

It is possible to obtain a fully digital implementation of the total control system, where all the control tasks and pulse-width modulation (which can be an on-line technique) are performed by a single 16-bit microprocessor, the currents are sensed in an analog manner (e.g. by the application of Hall sensors), and the rotor position or rotor speed is obtained by using a single optical encoder. Since the pulse-width modulation and all the control tasks are performed by the same microprocessor, this allows the application of optimization criteria to the modulation, since all the machine quantities (e.g. voltages and currents) are known. The possibilities for using various optimization schemes have been discussed above.

It should be noted that there are other ways to obtain the reference value of the rotor magnetizing current. For example, it is also possible to have an implementation in which the function generator in Fig. 4.11 is not present but the two-axis voltages  $u_{sxref}$ ,  $u_{syref}$  are used to obtain the absolute value of the reference stator-voltage space phasor,  $|\bar{u}_{sref}| = (\bar{u}_{sxref}^2 + \bar{u}_{syref}^2)^{1/2}$ . Field weakening can be automatically performed by the application of an extra control loop which contains a limiting stator voltage controller (a PI controller) the input of which is the error  $u - |\bar{u}_{sref}|$ , where  $u$  is a constant voltage reference (the ceiling voltage of the inverter), and the output is  $|\bar{v}_{mref}|$ . The voltage controller attempts to remove the error  $(u - |\bar{u}_{sref}|)$  by adjusting the rotor magnetizing current  $|\bar{v}_{mr}|$ . When the motor operates below base speed,  $|\bar{u}_{sref}| < u$  and the voltage controller will be saturated and the maximal  $|\bar{v}_{mref}|$  is produced, so the rotor flux is kept at the saturation limit of the induction machine. However, when the speed increases above base speed, the inverter will approach its maximal output voltage and when the maximal output voltage of the inverter is reached ( $|\bar{u}_{sref}|$  is equal to  $u$ ), the voltage controller will give a smaller value of  $|\bar{v}_{mref}|$  in order to limit the modulus of the stator voltages. Thus it follows that field weakening is automatically performed with this implementation. In contrast to permanent-magnet synchronous machines, where there is only a limited field weakening range (because the large air-gap causes a small synchronous reactance), in the induction machine, field weakening can be achieved over a wide speed range with constant power. This feature is extremely useful in spindle-drive applications but it can be utilized in position-controlled feed drives as well.

#### 4.1.1.6.2 Implementation of the PWM VSI-fed induction machine utilizing a speed sensor and the reference values of $i_{sxref}$ , $i_{syref}$

*Decoupling circuit:* In this section an implementation of the rotor-flux-oriented control is presented for a voltage-source inverter-fed induction machine where the necessary decoupling circuit uses the reference values of the direct- and quadrature-axis components of the stator currents  $i_{sxref}$ ,  $i_{syref}$ . Operation with constant rotor flux is assumed and the effects of magnetic saturation are neglected.

When the rotor flux ( $\bar{\psi}_r$ ) is constant and since  $\bar{\psi}_r = L_m \bar{v}_{mr}$  and thus under linear magnetic conditions the rotor-magnetizing current  $|\bar{v}_{mr}|$  is also constant, it follows from eqn (4.1-25) that  $|\bar{v}_{mr}| = i_{sx}$ , where  $i_{sx}$  is the direct-axis component of the stator current in the rotor-flux-oriented reference frame. Under these conditions it follows from eqns (4.1-7) and (4.1-8) that if the term  $L'_s di_{sy}/dt$  is neglected, the stator voltage components in the rotor-flux-oriented reference frame are:

$$u_{sx} = R_s i_{sx} - \omega_{mr} L'_s i_{sy} \quad (4.1-44)$$

$$u_{sy} = R_s i_{sy} + \omega_{mr} L'_s i_{sx}. \quad (4.1-45)$$

It should be noted that in eqn (4.1-44), the stator transient inductance  $L'_s$  is present and in eqn (4.1-45) the stator inductance  $L_s$  is present in the direct- and quadrature-axis rotational voltage terms respectively. Furthermore, it follows

from eqns (4.1-44) and (4.1-45) that in the direct-axis voltage equation, the rotational voltage is affected by the quadrature-axis stator current ( $i_{sy}$ ) and in the quadrature-axis voltage equation, the rotational term is influenced by the direct-axis stator current ( $i_{sx}$ ). Thus the rotor flux (or  $i_{sx}$ ) is not solely determined by the direct-axis stator voltage expressed in the rotor-flux-oriented reference frame ( $u_{sx}$ ), but is also influenced by the quadrature-axis stator current and similarly, the torque-producing stator-current component is not solely determined by the quadrature-axis stator voltage expressed in the rotor-flux-oriented reference frame  $u_{sy}$ , but is also dependent on the direct-axis stator current. However, it is possible to have an independent control of the flux-producing stator-current component ( $i_{sx}$ ) and the torque-producing stator-current component ( $i_{sy}$ ), when the unwanted coupling terms are cancelled and thus the rotor flux is controlled by  $i_{sx}$  and the electromagnetic torque is controlled by  $i_{sy}$ , which are independent of each other. It follows from eqns (4.1-44) and (4.1-45) that in the decoupling circuit the actual values of  $i_{sx}$  and  $i_{sy}$  have to be used. However, by assuming that the lag time between  $i_{sy}$  and  $u_{sy}$  is small and thus can be neglected, it is possible to utilize the reference currents in the decoupling circuit and in this case  $\dot{i}_{sx} = R_s i_{sxref}$  and  $\dot{i}_{sy} = R_s i_{syref}$ . This concept is utilized in the implementation of the rotor-flux-oriented control of the voltage-source inverter-fed induction machine drive described in the following section.

*Drive implementation:* The schematic of the rotor-flux-oriented control of a voltage-source inverter-fed induction machine drive utilizing the concepts described above is shown in Fig. 4.12. This is simpler than the drive described in Fig. 4.11, but it can yield a satisfactory dynamic response.

In Fig. 4.12, the reference value of the rotor flux is  $|\bar{\psi}_{rref}|$  and when it is divided by the magnetizing inductance, the rotor magnetizing current is obtained, which is equal to the direct-axis stator current reference  $i_{sxref}$ . The reference value of the rotor speed ( $\omega_{rref}$ ) is compared with its actual value ( $\omega_r$ ) and the error serves as input to the speed controller (a PI controller). The output of the speed controller is the torque reference, which is, however, proportional to the quadrature-axis stator current reference ( $i_{syref}$ ).

The direct- and quadrature-axis stator current references are used in the decoupling circuit, which utilizes the principles described above. Thus  $i_{sxref}$  is multiplied by the stator resistance ( $R_s$ ) and the value obtained is reduced by  $-\omega_{mr} L'_s i_{syref}$ . Thus the direct-axis stator reference voltage component expressed in the rotor-flux-oriented reference frame ( $u_{sxref}$ ) is obtained. Similarly, the quadrature-axis stator current reference is multiplied by the stator resistance and the rotational voltage component  $\omega_{mr} L'_s i_{sxref}$  is added to this voltage, and thus the quadrature-axis stator voltage reference expressed in the rotor-flux-oriented reference frame ( $u_{syref}$ ) is obtained. The voltage references  $u_{sxref}$  and  $u_{syref}$  are transformed into the two-axis voltage components of the stationary reference frame ( $u_{sDref}$ ,  $u_{sQref}$ ), by utilizing the transformation  $e^{j\rho_r}$ , where  $\rho_r$  is the space angle of the rotor flux-linkage space phasor with respect to the real axis of the stationary reference frame. For completeness the transformed values are also

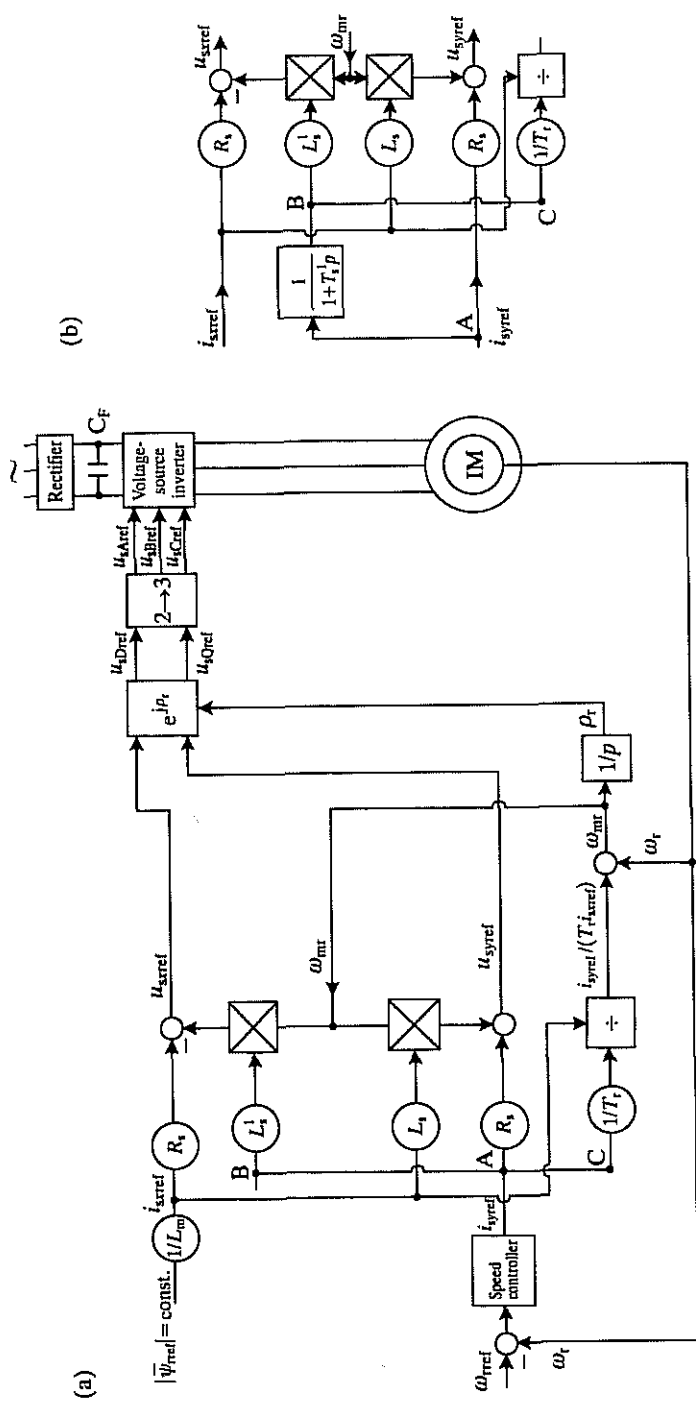


Fig. 4.12. Schematic of the rotor-flux-oriented control of a voltage-source induction machine drive. (a), (b) See text.

given in their expanded forms. Thus by considering eqn (4.1-4), but using reference values of the voltages,

$$u_{sD\text{ref}} + j u_{sQ\text{ref}} = (u_{sx\text{ref}} + j u_{sy\text{ref}}) e^{j\phi_r} \quad (4.1-46)$$

or, from the resolution of eqn (4.1-46) into its real and imaginary components,

$$u_{sD\text{ref}} = \cos \rho_r u_{sx\text{ref}} - \sin \rho_r u_{sy\text{ref}} \quad (4.1-47)$$

$$u_{sQ\text{ref}} = \sin \rho_r u_{sx\text{ref}} + \cos \rho_r u_{sy\text{ref}}. \quad (4.1-48)$$

These two-axis voltage references are then transformed into their three-phase reference values by the application of the two-phase to three-phase transformation indicated by the '2 → 3' block. It is possible to obtain the three-phase reference values by simply considering that in the absence of zero-sequence voltages, the projections of the voltage space phasor on the corresponding axes yield the instantaneous values of the phase voltages [see eqns (2.1-70), (2.1-71), and (2.1-72)]:

$$u_{sA\text{ref}} = \text{Re}(\bar{u}_{s\text{ref}}) = \text{Re}(u_{sD\text{ref}} + j u_{sQ\text{ref}}) = u_{sD\text{ref}}, \quad (4.1-49)$$

where  $\bar{u}_{s\text{ref}}$  is the reference value of the stator-voltage space phasor in the stationary reference frame,

$$u_{sB\text{ref}} = \text{Re}(a^2 \bar{u}_{s\text{ref}}) = \frac{-u_{sD\text{ref}}}{2} + \sqrt{3} \frac{u_{sQ\text{ref}}}{2} \quad (4.1-50)$$

and

$$u_{sC\text{ref}} = \text{Re}(a^2 \bar{u}_{s\text{ref}}) = \frac{-u_{sD\text{ref}}}{2} - \sqrt{3} \frac{u_{sQ\text{ref}}}{2}. \quad (4.1-51)$$

Of course it is also possible to use the Euler forms of the space-phasor equations. Thus the space phasor of the stator voltage references in the rotor-flux-oriented reference frame can be expressed as

$$\bar{u}'_{s\text{ref}} = u_{sx\text{ref}} + j u_{sy\text{ref}} = (u_{sx\text{ref}}^2 + u_{sy\text{ref}}^2)^{1/2} e^{j\phi_u} \quad (4.1-52)$$

where  $\phi_u = \tan^{-1}(u_{sy\text{ref}}/u_{sx\text{ref}})$ .

From eqn (4.1-46), in the stationary reference frame the space phasor of the stator reference voltages is

$$\bar{u}_{s\text{ref}} = \bar{u}'_{s\text{ref}} e^{j\rho_r} = (u_{sx\text{ref}}^2 + u_{sy\text{ref}}^2)^{1/2} e^{j(\rho_r + \phi_u)}, \quad (4.1-53)$$

where  $\bar{u}'_{s\text{ref}}$  has been substituted by the expression given in eqn (4.1-52). Thus by considering eqns (4.1-49), (4.1-50), and (4.1-51), the three-phase stator voltage reference values can be put into the following form:

$$u_{sA\text{ref}} = \text{Re}(\bar{u}_{s\text{ref}}) = (u_{sx\text{ref}}^2 + u_{sy\text{ref}}^2)^{1/2} e^{j(\rho_r + \phi_u)} \quad (4.1-54)$$

$$u_{sB\text{ref}} = \text{Re}(a^2 \bar{u}_{s\text{ref}}) = (u_{sx\text{ref}}^2 + u_{sy\text{ref}}^2)^{1/2} e^{j(\rho_r + \phi_u - 2\pi/3)} \quad (4.1-55)$$

$$u_{sC\text{ref}} = \text{Re}(a^2 \bar{u}_{s\text{ref}}) = (u_{sx\text{ref}}^2 + u_{sy\text{ref}}^2)^{1/2} e^{j(\rho_r + \phi_u + 2\pi/3)} \quad (4.1-56)$$

which could be utilized directly to obtain the three-phase reference voltages.

It is also possible to have an implementation where the decoupling and the transformation of the stator reference voltage components from the rotor-flux-oriented reference frame into the stationary reference frame is performed in one step. For this purpose eqns (4.1-44) and (4.1-45) are substituted into eqns (4.1-47) and (4.1-48) respectively, and the reference values of the stator current components ( $i_{sxref}, i_{syref}$ ) are used in the decoupling circuit instead of their actual values ( $i_{sx}, i_{sy}$ ). The following two new voltage equations are then obtained:

$$u_{sDref} = (R_s + L_s p) \cos \rho_r i_{sxref} - (R_s + L'_s p) \sin \rho_r i_{syref} \quad (4.1-57)$$

$$u_{sQref} = (R_s + L_s p) \sin \rho_r i_{sxref} - (R_s + L'_s p) \cos \rho_r i_{syref}, \quad (4.1-58)$$

an implementation of which is shown in Fig. 4.13. The inputs to the circuit shown in Fig. 4.13 are the reference values of the flux- and torque-producing currents ( $i_{sxref}, i_{syref}$ ) and the angle  $\rho_r$ . The angle  $\rho_r$  is obtained from  $i_{sxref}$ ,  $i_{syref}$  and the monitored rotor speed, as described below. The outputs of the circuit shown in Fig. 4.13 are the direct- and quadrature-axis stator voltage references in the stationary reference frame ( $u_{sDref}$  and  $u_{sQref}$ ).

The angular frequency of the stator voltages is  $\omega_{mr}$  and is obtained from  $i_{syref}$  by utilizing eqns (4.1-25) and (4.1-26). It follows from eqn (4.1-25) that if  $|\bar{i}_{mr}|$  is constant,  $|\bar{i}_{mr}| = i_{sx}$  and  $\omega_{mr} = \omega_r + i_{sy}/(T_r i_{sx})$ . Thus in accordance with the discussion presented above, by using the reference values of the stator currents instead of the actual values, finally

$$\omega_{mr} = \omega_r + \frac{i_{syref}}{T_r i_{sxref}} \quad (4.1-59)$$

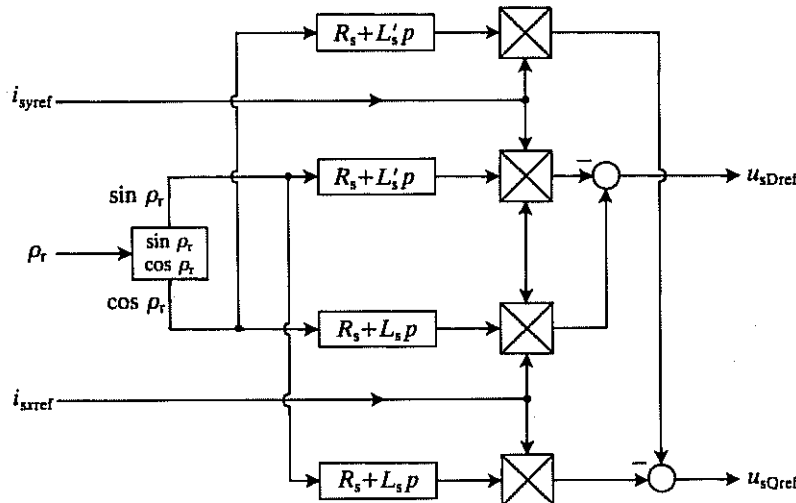


Fig. 4.13. Circuit to obtain reference voltages.

is obtained. In Fig. 4.12 eqn (4.1-59) is utilized to obtain  $\omega_{mr}$ , where  $\omega_r$  is the monitored value of the rotor speed. The integration of  $\omega_{mr}$  gives the angle  $\rho_r$ , which is required in the transformations described above. The integration is carried out by the block labelled '1/p'. It follows that accurate values for the rotor flux position are only obtained if the rotor time constant used is accurate. Under linear magnetic conditions this changes, mainly due to the variation of the rotor resistance. However, it is possible to implement relatively simple compensation of the rotor resistance variation because, according to experiments performed for the drive described in Fig. 4.12, the actual value of  $i_{sy}$  is approximately proportional to the inverse of the actual (correct) value of the rotor resistance.

The implementation shown in Fig. 4.12 uses eqns (4.1-44) and (4.1-45), and eqn (4.1-45) has been obtained by neglecting the term  $L'_s di_{sy}/dt$ , where  $L'_s$  is the transient stator inductance. This term can be neglected in a standard cage induction machine, where the transient inductance of the stator is much smaller than the magnetizing inductance, which is large. In this case the transient inductance of the stator is approximately equal to the sum of the stator and rotor leakage inductances. However, in induction machines for servo-applications, the magnetizing inductance is smaller than for normal applications, and in this case the effect of  $L'_s$  should be incorporated in the controller. If this is not done and there is a step change in the torque reference, there can be an unwanted overshoot in the electromagnetic torque. A solution to this problem can be obtained in several ways, and two of these are now briefly discussed.

The first solution can be obtained by adding the missing term  $L'_s di_{sy}/dt$  to eqn (4.1-45). In this way a quick response will be obtained, but it is necessary to differentiate the torque-producing stator current component. A second solution can be obtained by incorporating a small delay term which corresponds to the stator transient inductance in the decoupling compensator of Fig. 4.12. In this case the actual torque producing stator current ( $i_{sy}$ ) will be delayed by the stator transient time constant ( $T'_s = L'_s/R_s$ ) and thus, for accurate decoupling, the torque-producing stator current reference ( $i_{syref}$ ) should also be delayed by the same time constant. This can be achieved by inserting a new block in Fig. 4.12(a) between points A and B, which contains a first-order lag described by  $1/(1+T'_s p)$ , by connecting point C to point B and disconnecting points C and A as shown in Fig. 4.12(b). With this implementation, improved dynamic response is obtained and the unwanted overshoot in the electromagnetic torque is reduced. Compared to the first method, the second method results in a slightly slower response.

It is important to note that the implementation shown in Fig. 4.12 utilizes the fact that the rotor flux is constant, and thus is not suitable under field-weakening conditions. However, it can be extended to operate under field weakening. For this purpose eqns (4.1-7), (4.1-8), and (4.1-25) must be considered, but under the assumption that  $|\bar{i}_{mr}|$  is not constant. In this case when the expression for  $|\bar{i}_{mr}|$  obtained from eqn (4.1-25) is substituted into the direct-axis voltage equation defined by eqn (4.1-7), the resulting direct-axis voltage equation will contain three

terms. These are the direct-axis voltage across the stator impedance, which is equal to  $(R_s + L_s p) i_{sx}$ , the direct-axis rotational voltage component  $-\omega_{mr} L'_s i_{sy}$ , and finally an extra term  $-L_m^2 p^2 i_{sx}/(R_r + L_r p)$ , where  $p = d/dt$ . This third component contains the second time derivative of the direct-axis stator current component  $i_{sx}$ . Thus to get a direct relationship between  $u_{sx}$  and  $i_{sx}$ , the rotational component must be eliminated (this was achieved previously when  $|\bar{i}_{mr}|$  was assumed to be constant) and since the third component disturbs the simplified structure of the  $x$ -axis, it should also be cancelled. It should be noted that when  $|\bar{i}_{mr}| = \text{constant}$ , it follows by considering eqn (4.1-25) that this term is only present in the equations in the form of  $i_{sx} = |\bar{i}_{mr}|$ . The required cancellation of the unwanted third component can be performed by the application of such a direct-axis stator current ( $i_{sx}$ ) controller, which ensures that  $p i_{sx} = 0$ , i.e. the rate of change of the direct-axis stator current in the rotor-flux-oriented reference frame is zero. For this purpose it is also possible to use a model reference-frame proportional-output error-feedback controller and the actual control current at the output of this controller will replace the current  $i_{sxref}$  in Fig. 4.12, which is related to  $i_{sx}$  through the transfer function  $1/(1+T_s p)$ , where  $T_s$  is the stator time constant. It follows from eqn (4.1-25) that  $|\bar{i}_{mr}| = i_{sx}/(1+T_s p)$  where  $T_s$  is the rotor time constant and this current has to replace  $i_{sxref}$  in the terms  $L_s i_{sxref}$  and  $i_{syref}/(T_s i_{sxref})$  shown in Fig. 4.12.

Under field-weakening operation, it is possible to obtain  $i_{sxref}$  similarly to the method shown in Fig. 4.11, or it is possible to determine it from an optimal value of the rotor flux reference  $|\bar{\psi}_{rref}| = L_m |\bar{i}_{mrref}|$ , which has to be dependent on the rotor speed and which gives maximum efficiency of the induction machine subjected to rotor-flux-oriented control. The speed dependency of the rotor flux reference follows from the fact that two loss components, the hysteresis and eddy-current losses, are functions of the stator frequency, which, however, is the sum of the slip frequency and the rotor speed (see eqn (4.1-26)). However, when deciding which way to obtain  $i_{sxref}$ , it should be considered that in the transient state, the main goal is to obtain quick torque response, while efficiency optimization is more important in the steady state.

#### 4.1.2 CONTROL OF AN INDUCTION MACHINE WITH IMPRESSED CURRENTS

##### 4.1.2.1 General introduction

In contrast to inverters which function as voltage sources, inverters which function as current sources are becoming the main power sources for high-performance a.c. machine drives. In the lower-power region PWM inverters with fast current control are employed. In this case, because of the chopping mode of the inverter and the high gain of the current loops, the a.c. machine follows the current reference signals very quickly. At higher power levels the Current-Source Inverter (CSI) is used where a supply-side controlled rectifier is connected

through a large d.c. link reactor to the motor-side inverter. Its major advantages are:

- its simplicity;
- its inherent ability for regeneration (by reversing the d.c. link voltage) and reversal (by electronic reversal of the phase sequence of the machine currents, which is carried out by changing the sequence of operation of the inverter switches);
- it does not require silicon-controlled rectifiers with high switching speeds—it can use converter-grade thyristors. (As shown later, this follows because commutation causes voltage spikes superimposed on the nearly sinusoidal stator voltages and these can be reduced by the application of large commuting capacitors or by reducing the transient inductance of the stator. Thus commutation is relatively slow and therefore it is not necessary to use thyristors with high switching speed);
- the inverter will recover from a short-circuit across any two of its output terminals and is undamaged by the misfire of the output thyristors (because there is a large d.c. link reactor which prevents quick changes of the link current).

However, the current response of the conventional CSI with auto-sequential commutation is much slower than that of the current-controlled PWM voltage inverter. Furthermore, at low speed there can exist unwanted torque pulsations (this will be discussed later).

By the application of the conventional CSI, rapid control of both the phase and amplitude of an a.c. current cannot be achieved. In this case, the amplitude of the a.c. currents is determined by the magnitude of the d.c. link current, and as a result of the large filter inductance, the current response to an input command is greatly influenced by the d.c. link parameters (rectifier phase-control delay time, rated value of the rectifier output voltage, gain of the d.c. link current loop, inductance of the d.c. link). Although the response can be minimized by establishing high gain in the current-regulator loop of the controlled rectifier, the output of which is the d.c. link current, the large gain can result in control problems because of the saturation of the output voltage of the controlled rectifier and ripple current instabilities at light load. Thus the current response of the conventional CSI is slower than for the current-controlled PWM inverter. It should be noted that when a so-called notched auto-sequentially commutated inverter is employed, where the d.c. link current is kept constant and thus the influence of the d.c. link parameters on the dynamics of the system response can be neglected, rapid control of both the phase and amplitude of the a.c. current can be achieved.

In this section the rotor-flux-oriented control of induction machines will be discussed for four cases. The induction machine can be supplied by: (i) a voltage-source PWM inverter with fast current control; (ii) a conventional current-source inverter with auto-sequential commutation (CSI); (iii) a cycloconverter with fast current control; or (iv) impressed rotor currents. The main assumptions are those

used in Section 4.1.1, but unless stated otherwise, the time lag of the inverter is neglected although it could be considered by using the technique described in Section 3.1.1.

When a high-dynamic-performance induction machine drive with impressed currents is designed, ideally the following requirements should be satisfied:

- Smooth speed response without cogging or torque pulsations at low speed (it will be shown that sometimes it is difficult to satisfy this requirement);
- Smooth speed reversals under any torque condition;
- Capability of four-quadrant operation (this can be achieved by changing the phase sequence of the stator currents and the polarity of the d.c. link voltage);
- Operation of the drive with constant full torque below base speed and above base speed with reduced flux (field-weakening operation).

There are many control schemes known for induction machine drives with impressed currents, but rotor-flux-oriented control has emerged as one of the most frequently used techniques. The application of this technique yields fast dynamic response and most of the requirements mentioned above can also be satisfied. Similarly to that discussed in Section 4.1.1, in order to obtain high dynamic performance, the stator currents of the machine are transformed into flux- and torque-producing current components ( $i_{sx}$ ,  $i_{sy}$ ). These are defined in eqn (4.1-3), and Fig. 2.16 shows the relationship between various quantities in the reference frames fixed to the stator and rotor flux-linkage space phasors. Below base speed the modulus of the rotor magnetizing current ( $|\bar{i}_{mr}|$ ), defined by eqn (4.1-1), is maintained at its maximum possible value but is limited by magnetic saturation. Above base speed,  $|\bar{i}_{mr}|$  is reduced (field-weakening operation). The electromagnetic torque is controlled by the quadrature-axis stator current  $i_{sy}$ , (see, for example, eqn (2.1-197) and Section 2.1.8).

#### 4.1.2.2 Control of the induction machine supplied by a current-controlled PWM inverter

In this section the rotor-flux-oriented control of an induction machine supplied by a voltage-source inverter with fast current control will be described. The inverter can be a transistorized inverter with high switching frequency, such as the one shown in Fig. 3.5(b). Two types of implementation will be given, which use the direct method and the indirect method. As discussed at the beginning of this chapter, when the direct method is used (flux-feedback control), the space angle of the rotor flux-linkage space phasor is obtained by direct measurements (e.g. by using Hall sensors) or by using a so-called flux model. However, when the indirect method is used (feedforward control), the space angle of the rotor flux-linkage space phasor is obtained as the sum of the monitored rotor angle ( $\theta_r$ ) and the computed reference value of the slip angle ( $\theta_{sl}$ ), where the slip angle gives the position of the rotor flux-linkage space phasor relative to the rotor (or more precisely relative to the direct axis of the reference frame fixed to the rotor).

##### 4.1.2.2.1 Implementation using the direct method

Figure 4.14 shows the schematic of the direct implementation of the rotor-flux-oriented control of an induction machine supplied by a current-controlled PWM inverter. This is simpler than the implementation shown in Fig. 4.12 for a voltage-controlled PWM inverter, since now the stator currents are impressed by fast current control loops and thus the scheme does not utilize the stator voltage equations and there is no decoupling circuit in the implementation of Fig. 4.14.

In Fig. 4.14 the same cascade control structure is utilized as in Fig. 4.12. The monitored value of the rotor speed ( $\omega_r$ ) is integrated (the integration is denoted by  $1/p$ ) to give the actual value of the rotor angle ( $\theta_r$ ). This is compared with its reference value ( $\theta_{rref}$ ) and the resulting error serves as the input to the position controller, which is a PI controller. The output of this is the reference value of the rotor speed ( $\omega_{rref}$ ). When this is compared with the monitored value of the rotor speed, the error signal is supplied to the input of the speed controller, also a PI controller, and the output of which is the reference value of the electromagnetic torque ( $t_{eref}$ ). Comparison of  $t_{eref}$  and the actual value of the torque  $t_e$  gives an error which serves as input to the torque controller, again a PI controller, and its output is the reference value of the quadrature-axis stator current expressed in the rotor-flux-oriented reference frame ( $i_{syref}$ ).

The direct-axis stator current reference ( $i_{sxref}$ ), which is expressed in the rotor-flux-oriented reference frame, is obtained as the output of the flux controller (PI controller) the input of which is the difference between the reference value of the rotor magnetizing current  $|\bar{i}_{mrref}|$  and the actual value of the rotor magnetizing current  $|\bar{i}_{mr}|$ . The reference current  $|\bar{i}_{mrref}|$  is obtained as the output of the function generator FG, which allows field weakening to be implemented. Thus the input of FG is the monitored rotor speed and below base speed FG gives a constant value of  $|\bar{i}_{mrref}|$ , while above base speed  $|\bar{i}_{mrref}|$  is inversely proportional to the rotor speed.

In accordance with eqn (4.1-3), the stator current references  $i_{sxref}$  and  $i_{syref}$  are first transformed into the two-axis stator current references of the stationary reference frame ( $i_{sDref}$ ,  $i_{sQref}$ ) by the application of the transformation  $e^{j\theta_r}$  where  $\rho_r$  is the angle of the rotor magnetizing-current space phasor with respect to the direct-axis (SD) of the stationary reference frame. For convenience Fig. 4.15 shows the relationship of the space phasor of the stator currents in the stationary and in the special, rotor-flux-oriented reference frame. The space phasor of the rotor magnetizing current is also shown. Figure 4.15 is similar to Fig. 2.16.

Thus by resolving eqn (4.1-3) into its real and imaginary axes components, but using reference values, it follows that

$$i_{sDref} = \cos \rho_r i_{sxref} - \sin \rho_r i_{syref} \quad (4.1-60)$$

$$i_{sQref} = \sin \rho_r i_{sxref} + \cos \rho_r i_{syref}. \quad (4.1-61)$$

These two-axis current references are then transformed into their three-phase reference values ( $i_{sAref}$ ,  $i_{sBref}$ ,  $i_{sCref}$ ) by the application of the two-phase to

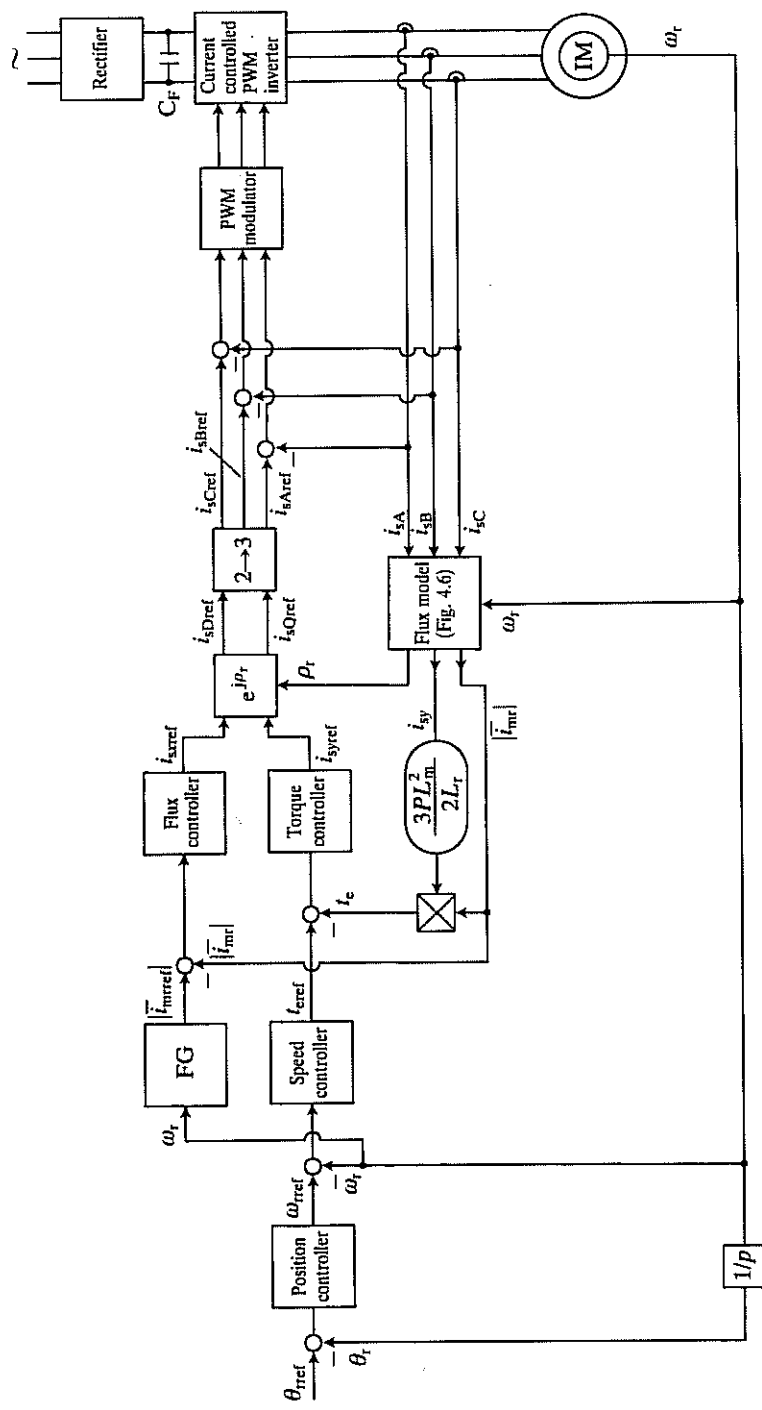


Fig. 4.14. Schematic of the direct implementation of the rotor-flux-oriented control of an induction machine supplied by a current-controlled PWM inverter.

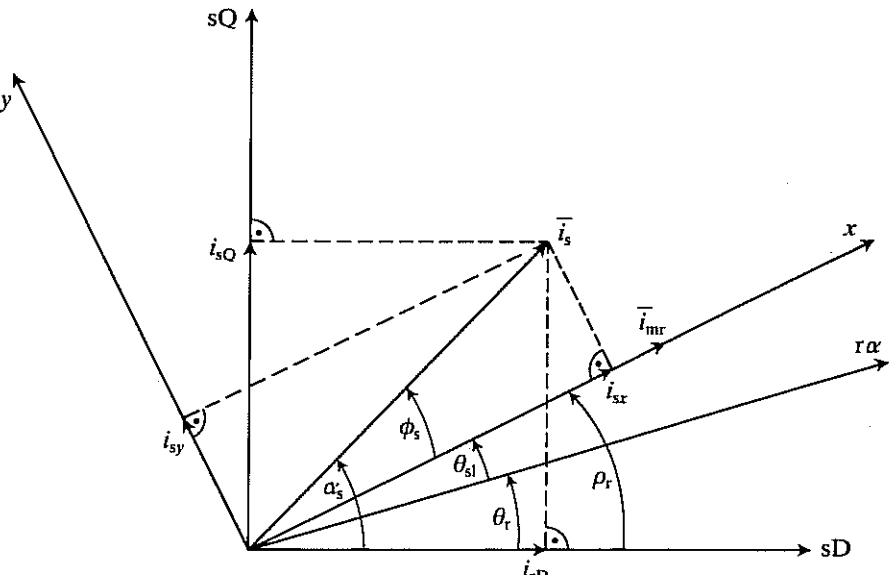


Fig. 4.15. Stator-current and rotor-current space phasors in the stationary and other reference frames.

three-phase transformation indicated by the block labelled '2→3'. These are used, together with the monitored three-phase currents ( $i_{sA}$ ,  $i_{sB}$ ,  $i_{sC}$ ), to obtain the gate signals necessary for the inverter which supplies the induction machine.

As in eqns (4.1-49), (4.1-50), and (4.1-51) in the case of voltages, it is possible to obtain the three-phase reference currents by simply considering that in the absence of zero-sequence currents, the projections of the current space phasor on the corresponding axes yield the instantaneous values of the phase currents; thus

$$i_{sAref} = \text{Re}(i_{sref}) = \text{Re}(i_{sDref} + j i_{sQref}) = i_{sDref}, \quad (4.1-62)$$

where  $i_{sref}$  is the reference value of the stator-current space phasor in the stationary reference frame,

$$i_{sBref} = \text{Re}(a^2 i_{sref}) = \frac{-i_{sDref}}{2} + \sqrt{3} \frac{i_{sQref}}{2} \quad (4.1-63)$$

and

$$i_{sCref} = \text{Re}(a i_{sref}) = \frac{-i_{sDref}}{2} - \sqrt{3} \frac{i_{sQref}}{2}. \quad (4.1-64)$$

Of course it is also possible to utilize the Euler forms of the space-phaser equations. Thus the space phasor of the stator current references in the rotor-flux-oriented reference frame can be expressed as

$$i'_{sref} = i_{sxref} + j i_{syref} = (i_{sxref}^2 + i_{syref}^2)^{1/2} e^{j\phi_s}, \quad (4.1-65)$$

where

$$\phi_s = \tan^{-1} \frac{i_{syref}}{i_{sxref}} \quad (4.1-66)$$

and  $\phi_s$  is the space angle of the stator-current space phasor with respect to the real axis of the rotor-flux-oriented reference frame, as shown in Fig. 4.15.

From eqn (4.1-3) or Fig. 4.15 in the stationary reference frame the space phasor of the stator reference currents is obtained as

$$\bar{i}_{sref} = \bar{i}'_{sref} e^{j\rho_r} = (i_{sxref}^2 + i_{syref}^2)^{1/2} e^{j(\rho_r + \phi_s)}, \quad (4.1-67)$$

where  $(\rho_r + \phi_s) = \alpha_s$  and  $\alpha_s$  is the space angle of the stator-current space phasor shown in Fig. 4.15. In eqn (4.1-67)  $\bar{i}'_{sref}$  has been substituted by the expression given in eqn (4.1-65). Thus from eqns (4.1-62), (4.1-63), (4.1-64), and (4.1-67), the three-phase current references can be put into the form,

$$i_{sAref} = \text{Re}(\bar{i}_{sref}) = (i_{sxref}^2 + i_{syref}^2)^{1/2} e^{j(\rho_r + \phi_s)} \quad (4.1-68)$$

$$i_{sBref} = \text{Re}(a^2 \bar{i}_{sref}) = (i_{sxref}^2 + i_{syref}^2)^{1/2} e^{j(\rho_r + \phi_s - 2\pi/3)} \quad (4.1-69)$$

$$i_{sCref} = \text{Re}(a \bar{i}_{sref}) = (i_{sxref}^2 + i_{syref}^2)^{1/2} e^{j(\rho_r + \phi_s + 2\pi/3)}. \quad (4.1-70)$$

Equations (4.1-68), (4.1-69) and (4.1-70) could be used directly to obtain the three-phase reference currents.

In Fig. 4.14 the monitored stator currents, together with the monitored rotor speed, are inputs to the flux model which has been described in Fig. 4.6. This contains the rotor time constant  $T_r$ . The outputs of the flux model are the rotor magnetizing current ( $|\bar{i}_{mr}|$ ), the torque-producing stator current ( $i_{sy}$ ), and the spatial position of the rotor flux-linkage space phasor ( $\rho_r$ ). In accordance with eqn (4.1-43), the electromagnetic torque ( $t_e$ ) is obtained by multiplying  $i_{sy}$  by the constant  $3PL_m^2/(2L_r)$ , where  $P$  is the number of pole pairs,  $L_m$  is the magnetizing inductance of the machine, and  $L_r$  is the self-inductance of the rotor.

The behaviour of the induction machine subjected to rotor-flux-oriented control shown in Fig. 4.14 is similar to that of the separately excited d.c. machine. The stator frequency is equal to the first time derivative of  $\rho_r$ . It should be noted that since the flux model uses the rotor time constant, the accuracy of the output signals of the flux model depends on the rotor time constant. Accurate values of  $T_r$  can be obtained, for example, by using Model Reference Adaptive Control to establish an on-line rotor time-constant estimator.

#### 4.1.2.2.1 Implementation using the indirect method

The implementation of indirect rotor-flux-oriented control of an induction machine supplied by a current-controlled PWM inverter is similar to that of the direct method, except that the space angle of the rotor magnetizing-current space phasor ( $\rho_r$ ) is obtained as the sum of the rotor angle ( $\theta_r$ ) and the reference value of the slip angle ( $\theta_{sl}$ ). These angles are shown in Fig. 4.15 and the required

equations follow from eqn (4.1-59), according to which the speed of the rotor magnetizing current space phasor is

$$\omega_{mr} = \omega_r + \omega_{sref} \quad (4.1-71)$$

where  $\omega_r$  is the rotor speed,

$$\omega_r = \frac{d\theta_r}{dt}, \quad (4.1-72)$$

and  $\omega_{sref}$  is the reference value of the slip frequency,

$$\omega_{sref} = \frac{i_{syref}}{T_r i_{sxref}} \quad (4.1-73)$$

where  $i_{sxref}$  and  $i_{syref}$  are the reference values of the direct- and quadrature-axis stator currents in the rotor-flux-oriented reference frame. Furthermore

$$\omega_{mr} = \frac{d\rho_r}{dt}. \quad (4.1-74)$$

Thus it follows from eqns (4.1-71)–(4.1-74) that

$$\rho_r = \int \omega_{mr} dt = \int (\omega_r + \omega_{sref}) dt = \theta_r + \theta_{sref}. \quad (4.1-75)$$

As shown in Fig. 4.15, the slip angle  $\theta_{sref}$  gives the position of the rotor magnetizing-current space phasor with respect to the direct axis ( $r\alpha$ -axis) of the reference frame fixed to the rotor. Thus by considering eqns (4.1-72) and (4.1-73)

$$\rho_r = \theta_r + \int \omega_{sref} dt = \theta_r + \int \frac{i_{syref}}{T_r i_{sxref}} dt, \quad (4.1-76)$$

which serves as the basis for obtaining the angle  $\rho_r$  when the indirect method is used in the implementation of the rotor-flux-oriented control of the induction machine. According to eqn (4.1-76) the division of the direct- and quadrature-axis stator currents ( $i_{sxref}, i_{syref}$ ) is controlled by the slip frequency  $\omega_{sl}$  and the two reference currents are used to determine the required slip frequency. When the rotor angle and the reference value of the slip frequency angle are added, the position of the rotor magnetizing-current space phasor is obtained. To obtain accurate values of  $\rho_r$ , the addition of the two angles must be performed very accurately; this can be done digitally, which also has the advantage of avoiding drift problems associated with analog implementation.

The schematic of the drive is shown in Fig. 4.16. In Fig. 4.16(a) the implementation uses Cartesian coordinates and in Fig. 4.16(b) polar coordinates are used. However, for simplicity, in Fig. 4.16(b) only that part of the scheme is shown which corresponds to the part shown in Fig. 4.16(a) within the dashed line.

In Fig. 4.16 an incremental rotor position sensor is used to obtain the rotor angle ( $\theta_r$ ) and the rotor speed ( $\omega_r$ ). The actual value of the rotor angle ( $\theta_r$ ) is compared with its reference value ( $\theta_{rref}$ ) and the resulting error serves as the input

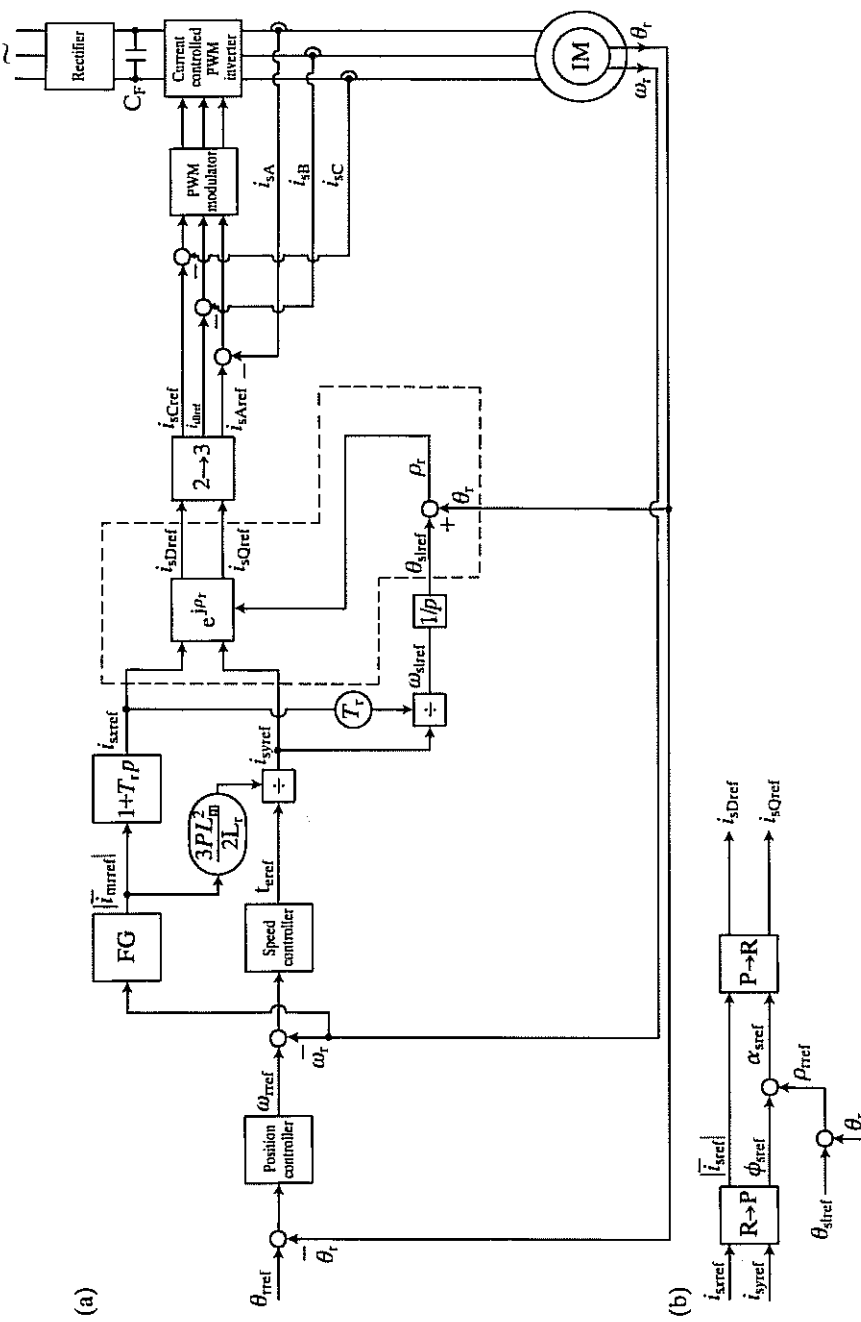


Fig. 4.16. Schematic of the indirect rotor-flux-oriented control of a current-controlled PWM inverter-fed induction machine. (a) In Cartesian coordinates; (b) in polar coordinates.

to the position controller, which is a PI controller. The output of the position controller is the reference value of the rotor speed ( $\omega_{ref}$ ). This is compared with the monitored value of the rotor speed and the error is supplied as the input to the speed controller, which is also a PI controller. Its output is the reference value of the electromagnetic torque ( $t_{ref}$ ) and in accordance with eqn (4.1-43) this is divided by the constant  $3PL_m^2/(2L_r)$  to yield the reference value of the stator current expressed in the rotor-flux-oriented reference frame ( $i_{sxref}$ ).

To enable field weakening to be performed, the monitored rotor speed serves as the input to the function generator FG shown in Fig. 4.16, the output of which is the reference value of the rotor magnetizing current ( $|i_{mref}|$ ). Below base speed FG gives a constant value of  $|i_{mref}|$ , while above base speed  $|i_{mref}|$  is inversely proportional to the rotor speed.

It follows from eqn (4.1-25) that, when the actual currents are replaced by their reference values,

$$i_{sxref} = (1 + T_r p) |i_{mref}| \quad (4.1-77)$$

and eqn (4.1-77) is used in the implementation shown in Fig. 4.16 to derive the reference value of the direct-axis stator current component expressed in the rotor-flux-oriented reference frame ( $i_{sxref}$ ).

As described in the previous section, the stator current references  $i_{sxref}, i_{syref}$  are first transformed into the two-axis stator current references of the stationary reference frame ( $i_{sDref}, i_{sQref}$ ) by the application of the transformation  $e^{ip_r}$ , where  $p_r$  is the angle of the rotor magnetizing-current space phasor with respect to the direct-axis (sD) of the stationary reference frame. These two-axis current references are then transformed into their three-phase reference values ( $i_{sAref}, i_{sBref}, i_{sCref}$ ) by the application of the two-phase to three-phase transformation indicated by the block labelled '2→3'. The corresponding equations have been given in the previous section. The reference stator currents together with the monitored three-phase stator currents ( $i_{sA}, i_{sB}, i_{sC}$ ) are used to obtain the gate signals necessary for the inverter which supplies the induction machine.

Finally eqn (4.1-76) is utilized to obtain the space angle  $\rho_r$  from  $i_{sxref}, i_{syref}$ , and the monitored value of the rotor angle. The block labelled '1/p' performs the required integration of the slip frequency.

In Fig. 4.16(b) the reference currents  $i_{sxref}$  and  $i_{syref}$  are converted by a rectangular-to-polar converter into the modulus of the stator-current space phasor ( $|i_{sref}|$ ) and also into the phase-angle of the stator-current space phasor with respect to the real axis of the rotor magnetizing-current reference frame ( $\phi_{sref}$ ), which according to Fig. 4.15 is equal to  $\alpha_{sref} - \rho_{ref}$ . Thus when  $\rho_{ref}$  is added to this angle,  $\alpha_{sref}$  is obtained, which according to Fig. 4.15 is the phase-angle of the stator-current space phasor with respect to the real axis of the stationary reference frame. Thus  $|i_{sref}|$  and  $\alpha_{sref}$  are inputs to a polar-to-rectangular converter, the outputs of which are  $i_{sDref}$  and  $i_{sQref}$ . In accordance with Fig. 4.15, the angle  $\rho_{ref}$  is obtained by adding the rotor angle to the slip frequency angle and the latter is obtained by the integration of the angular slip frequency. The slip angle is obtained in the same way as in Fig. 4.16(a).

The indirect implementation given in Fig. 4.16 is similar to the implementation used in a CSI-fed induction machine drive with the conventional slip frequency control. In that case the inverter frequency command is obtained as the sum of the slip frequency command and the rotational frequency of the motor, and the slip frequency command is obtained from the measured d.c. link current by utilizing a function generator. This function generator ensures that below base speed the magnetizing flux of the machine should be constant. In contrast to maintaining constant magnetizing flux, in rotor-flux-oriented control the rotor flux is kept constant. Furthermore, since the traditional slip-frequency control method of the CSI-fed induction machine is based on steady-state equations, during transient operation (i.e. when the machine is accelerated or decelerated) the angle between the stator-current space phasor and the rotor magnetizing-current space phasor is not controlled correctly. In contrast to this, when rotor-flux-oriented control is performed, the correct relationship is achieved between these two space phasors even under transient conditions.

#### 4.1.2.3 Control of the induction machine supplied by a conventional Current-Source Inverter (CSI)

##### 4.1.2.3.1 General introduction

In this section the rotor-flux-oriented control of an induction machine supplied by a conventional CSI with auto-sequential commutation is described. Again two implementations are discussed which correspond to the direct and indirect methods of obtaining the space angle of the rotor flux-linkage space phasor.

Figure 4.17 shows the schematic of a conventional six-step CSI with auto-sequential commutation. In Fig. 4.17, a.c. power is first converted to d.c., which is then inverted by a square-wave six-step inverter to produce variable-frequency a.c. currents. Thus the supply-side mains-commutated thyristor converter provides, through a high-inductance filter, the smooth d.c. link current ( $i_D$ ). This is supplied to the machine-side inverter. To maintain a constant direct link current specified by the reference value  $i_{Dref}$ , there is a current control loop, where  $i_{Dref}$  is compared with  $i_D$  and the difference serves as input to the current controller (which is a PI controller), whose output is used to control the firing angle of the supply-side converter. The phase-controlled rectifier can be replaced by an uncontrolled (diode) rectifier followed by a d.c. chopper to produce the required variable d.c. voltage source. Furthermore, it should also be noted that when the CSI supplies the stator windings of an induction machine, the d.c. link current is influenced by the back e.m.f. of the induction machine and under transient conditions the application of the PI current controller in the d.c. link current loop cannot give satisfactory current response. However, this problem can be overcome by the application of a function generator which compensates for the motor back e.m.f. This will be discussed in more detail below.

In Fig. 4.17, the machine-side converter contains six force-commutated thyristors. The function of the capacitors is to effect the successful commutation of

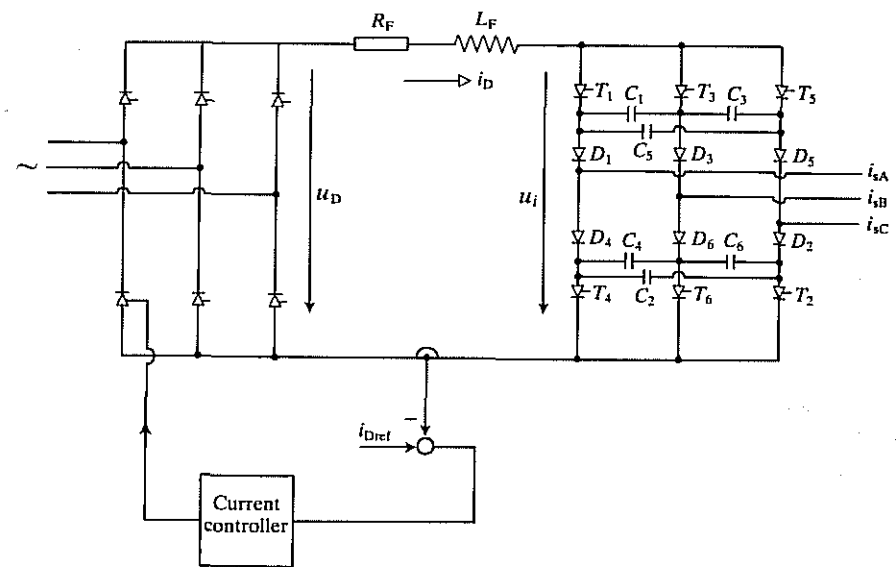


Fig. 4.17. Schematic of conventional six-step CSI with auto-sequential commutation.

current from each thyristor to the next thyristor in the same upper or lower row, i.e. thyristor  $T_1$  is extinguished when  $T_3$  is fired,  $T_2$  is turned-off when  $T_4$  is fired, etc. The six diodes decouple the commutating capacitors ( $C_1-C_6$ ) from the input and output terminals of the machine-side converter, except during commutation. Thus they allow the capacitors to remain charged to relatively high voltages. During commutation, the capacitors become charged to peak voltages, which are mainly determined by the magnitude of the motor current to be commutated. Thus the inverter can commutate satisfactorily over a wide range of output voltage and frequency.

As a result of the commutation, there are voltage spikes superimposed on the almost sinusoidal stator voltages. The amplitudes of these are proportional to the link current and to the square root of the stator transient inductance ( $L'_s$ ) and are inversely proportional to the square root of the commutating capacitance. They can be reduced by increasing the capacitance of the commutation capacitors. Since the capacitor voltages appear directly on the semiconductor components, this increases their required voltage rating even when the fundamental component of the voltage waveform is relatively small. These voltage spikes are one of the limiting factors of the horsepower rating of CSI-fed induction machine drives. Another limiting factor in extending the horsepower rating of the machine is the rather limited speed range, which is again due to commutation problems. Although generally it is desirable to increase the output frequency of the inverter to the highest possible value, since this can result in a reduction of the size and cost of the machine, and there exist solid-state devices with high switching

frequency, the commutation period for the CSI (which is affected by the commutating capacitor and the commutating inductance  $L'_s$ ) is significantly lower than for a voltage-source inverter of equal rating.

The d.c. link current is switched through the inverter thyristors to produce three-phase, six-stepped line currents. Each thyristor conducts for  $2\pi/3$  and at any instant one upper and one lower thyristor is conducting. If it is assumed that only two phases conduct at any instant, six distinct modes of operation result. A more detailed description of the operation of the machine-side converter will now be given. For this purpose it is assumed that the diodes and the thyristors are ideal switches, that the d.c. link current is constant and does not contain ripples, and that commutation of the currents is completed in less than one-sixth of a period ( $T$ ) of a stator current. The operation can be divided into three stages. If initially two thyristors  $T_1$  and  $T_2$  conduct, as shown in Fig. 4.18(a), the stator currents of the machine are  $i_{sA} = i_D$ ,  $i_{sB} = 0$ ,  $i_{sC} = -i_D$ , and thus from the definition of the space phasor of the stator currents  $\bar{i}_s$  (eqn (2.1-4)),

$$\bar{i}_s = \frac{2i_D(1-a^2)}{3} = \frac{2i_D e^{j\pi/6}}{\sqrt{3}}. \quad (4.1-78)$$

Thus the space phasor of the stator currents is in position 1 in Fig. 4.18(e). The first stage begins at the instant when thyristor  $T_3$  is triggered and simultaneously the gating signal is removed from  $T_1$ . Thus capacitor  $C_1$  (which was charged at a previous commutation) begins to discharge and turns off  $T_1$ . As soon as  $T_1$  turns off, the d.c. link currents flows through capacitor  $C_1$  and the series connected capacitors  $C_3$  and  $C_5$  (Fig. 4.18(b)). The first stage continues until diode  $D_3$  starts to conduct and at this instant the second stage begins (Fig. 4.18(c)). Thus there is three-phase conduction, where none of the stator currents are zero, so the space phasor of the stator currents must move from position 1 in the direction of position 2 shown in Fig. 4.18(e). During the second stage, the current gets diverted from the capacitor bank, diode  $D_1$  and stator phase sA to diode  $D_3$  and stator phase sB, and the second stage ends when the current in the capacitor bank is zero ( $D_1$  is blocked,  $T_3$ ,  $D_3$  and  $T_2$ ,  $D_2$  conduct—see Fig. 4.18(d)). Since  $i_{sA} = 0$ ,  $i_{sB} = i_D$  and  $i_{sC} = -i_D$ , it follows by considering eqn (2.1-4) that the space phasor of the stator currents is

$$\bar{i}_s = \frac{2a-a^2}{3} = \frac{2i_D j}{\sqrt{3}} \quad (4.1-79)$$

and this corresponds to position 2 of the stator-current space phasor in Fig. 4.18(e). The third stage lasts until thyristor  $T_4$  is triggered to turn off  $T_2$  and the d.c. link current flows across  $T_3$ ,  $D_3$ , the machine and  $T_2$ ,  $D_2$ .

It follows that the locus of the stator currents over one period of the stator currents is a hexagon. During one-sixth of a cycle, the space phasor remains in a fixed position and during three-phase conduction it rotates by  $2\pi/6$  along the hexagon. The locus is a closed curve (hexagon) and is symmetrical with respect to the origin of the stator reference frame as a result of the periodicity. It also

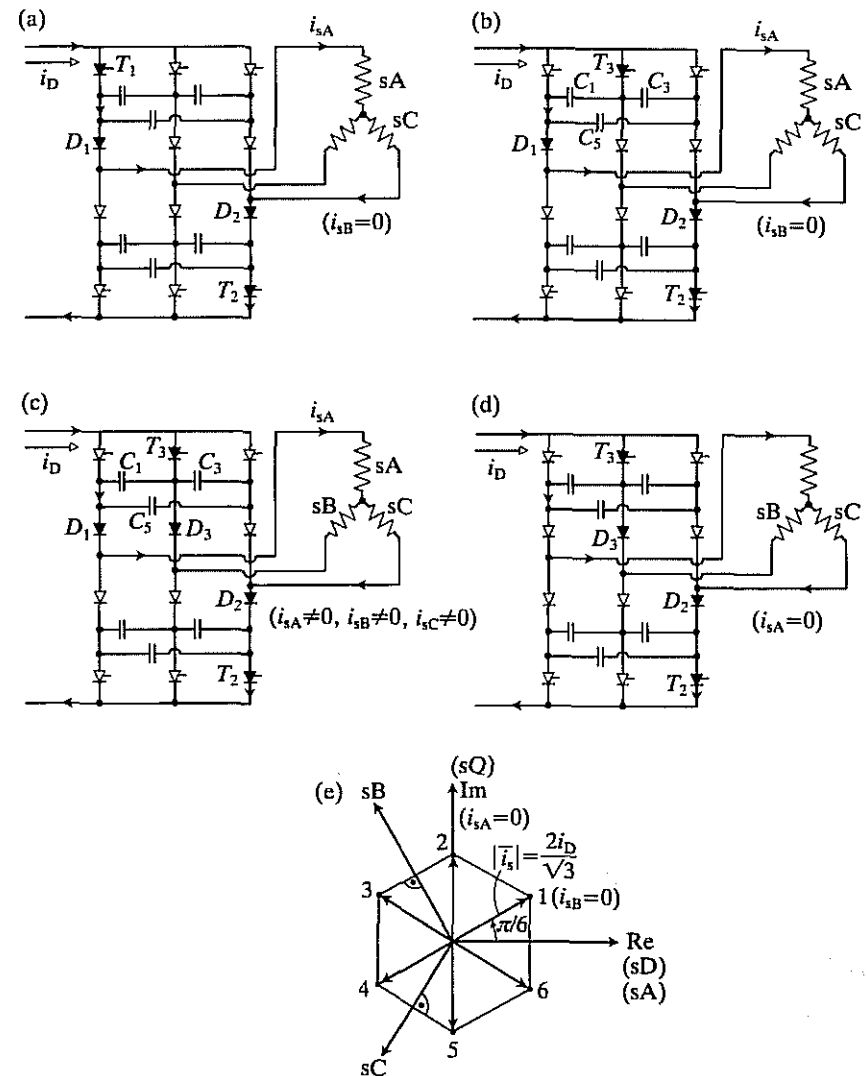


Fig. 4.18. Commutation process. (a) Initial stage of commutation; (b) first stage of commutation; (c) second stage of commutation; (d) third stage of commutation; (e) locus of stator-current space phasor.

follows that the magnitude of the three-phase currents is controlled by the regulation of the d.c. link current. The frequency of the three-phase currents is determined by the rate of switching of the inverter thyristors.

When the CSI shown in Fig. 4.17 supplies the stator windings of an induction machine, it should be noted that at low speed there can be undesirable torque pulsations, which are mainly due to the non-sinusoidal stator currents produced

by the inverter. The pulsations occur at six times the operating frequency and at very low frequency the frequency of the pulsations is reduced so much that the rotor moves in steps instead of rotating smoothly. This unsmooth rotation makes this drive unsuitable for servo-drive applications which require continuous position control.

In the case of the CSI-fed induction machine, one possibility for torque-ripple control is the pulse-width modulation of the stator currents by multiple commutations of the inverter in each half cycle. When this technique is used, the stator currents are notched at specific points to eliminate certain time harmonics. Each notch added to the current waveforms allows the elimination of a specific time harmonic, i.e. an appropriate double-notched waveform at each quarter cycle can result in the elimination of the fifth and seventh time harmonics in the stator currents and thus in the elimination of the sixth-harmonic torque. Pulse-width modulation can be achieved by the application of an angle loop, where the loop acts as a switching regulator which advances or reverses the sense of rotation of the space phasor of stator currents. A stator-current-angle control loop is utilized in the implementation of a rotor-flux-oriented control of a CSI-fed induction machine described in the next section.

#### 4.1.2.3.2 Implementation using the direct method

In the present section the rotor-flux-oriented control of a CSI-fed induction machine is described, where the angle of the rotor magnetizing-current space phasor is obtained by using the so-called direct method.

As discussed above, in the CSI-fed induction machine the d.c. link current is determined by the supply-side converter. Since the modulus of the stator-current space phasor ( $|i_s|$ ) must be proportional to the d.c. link current ( $i_D$ ), this is also determined by the supply-side converter. However, the space angle of the stator-current space phasor,  $\alpha_s$ , which is also shown in Fig. 4.15, is determined by the machine-side inverter. Both  $|i_s(t)|$  and  $\alpha_s(t)$  are continuous functions. By considering that one of the three stator currents is always zero outside the commutation intervals, the locus of the stator-current space phasor is a six-pointed star, whose radius is proportional to the d.c. link current, and according to eqns (4.1-78) and (4.1-79) is equal to  $|i_s| = (2i_D)/\sqrt{3}$ . It has been shown that when currents flow in all the three stator phases, the locus is characterized by a hexagon which connects the end points of the six-pointed star.

Outside the commutation interval the switching state of the inverter is characterized by  $e^{j\beta}$ , where the angle  $\beta$  changes discontinuously in increments of  $\pm \pi/3$ . The firing signals for the inverter can be derived by the application of a six-step bidirectional ring counter, which is stepped clockwise and anticlockwise. This method is utilized in Fig. 4.19.

The outer control loops of the drive shown in Fig. 4.19 are similar to those presented in Fig. 4.14. The instantaneous value of the angular rotor speed ( $\omega_r$ ) is obtained together with the instantaneous value of the rotor angle ( $\theta_r$ ). This is compared with the reference value of the rotor angle ( $\theta_{rref}$ ) and the resulting error

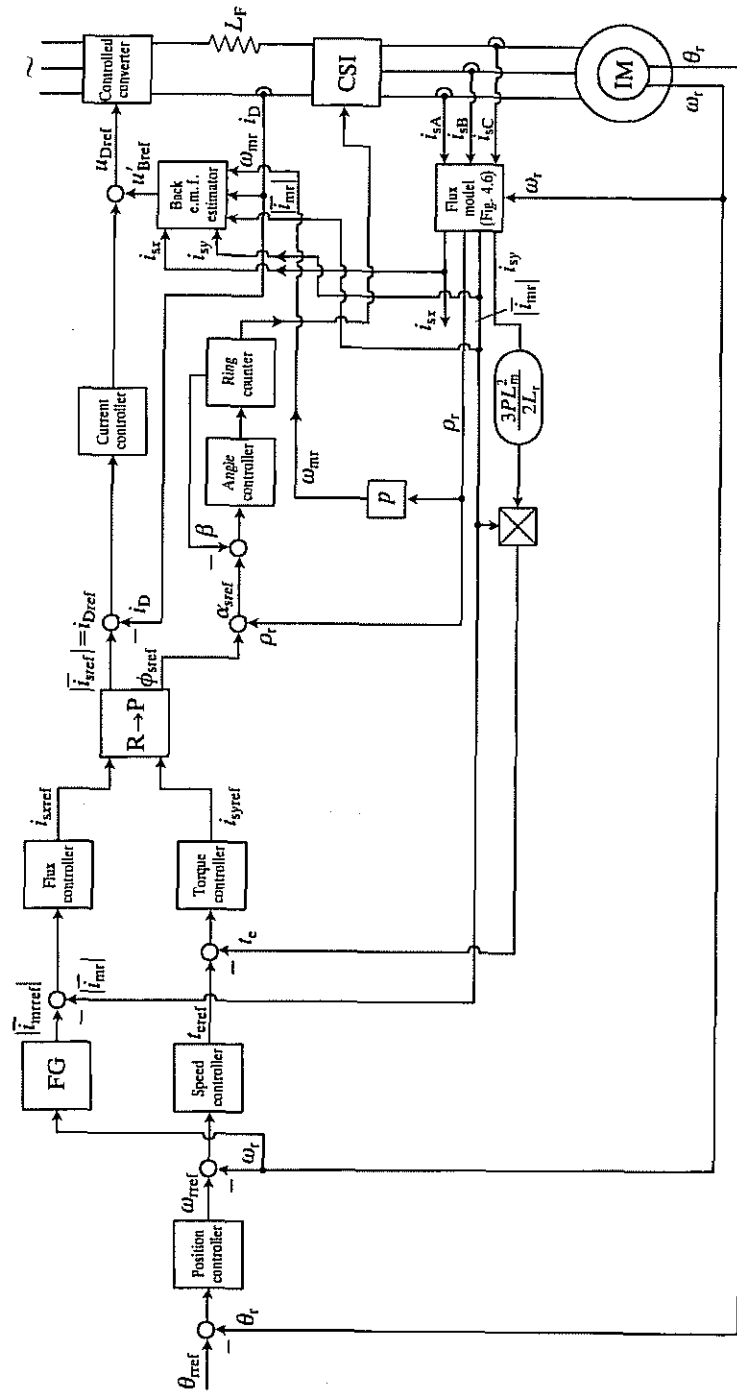


Fig. 4.19. Schematic of the direct rotor-flux-oriented control of a CSI-fed induction machine.

is the input to the position controller, which is a PI controller. The output of this is the reference value of the rotor speed ( $\omega_{r\text{ref}}$ ). When this is compared with the monitored value of the rotor speed ( $\omega_r$ ), the resulting error is supplied to the input of the speed controller, also a PI controller, the output of which is the reference value of the electromagnetic torque ( $t_{\text{ref}}$ ). Comparison of the torque reference with its actual value ( $t_e$ ) gives an error, which serves as input to the torque controller (PI controller) of which the output is the reference value of the quadrature-axis stator current expressed in the rotor-flux-oriented reference frame ( $i_{s\text{yref}}$ ).

The direct-axis stator current reference ( $i_{s\text{xref}}$ ), which is also expressed in the rotor-flux-oriented reference frame, is obtained as the output of the flux controller (PI controller), the input of which is the difference between the reference value of the rotor magnetizing current ( $|\bar{i}_{m\text{ref}}|$ ) and its actual value ( $|\bar{i}_{mr}|$ ). The reference current  $|\bar{i}_{m\text{ref}}|$  is obtained as the output of the function generator FG, which allows field weakening to be implemented. Therefore the input of FG is the monitored rotor speed and below base speed FG outputs a constant value of  $|\bar{i}_{m\text{ref}}|$ , while above base speed,  $|\bar{i}_{m\text{ref}}|$  is inversely proportional to the rotor speed. The two-axis stator current references are then inputs to the R-P block which performs the rectangular-to-polar conversion and its outputs are the modulus ( $|\bar{i}_{s\text{ref}}|$ ) and the space angle ( $\phi_{s\text{ref}}$ ) of the reference value of the stator-current space phasor in the rotor-flux-oriented reference frame. The angle ( $\phi_s$ ) has also been shown in Fig. 4.15.

In Fig. 4.19 the monitored stator currents, together with the monitored rotor speed, are inputs to the flux model. This has been described in Fig. 4.6. The outputs of the flux model are the rotor magnetizing current ( $|\bar{i}_{mr}|$ ), the torque-producing stator current ( $i_{sy}$ ), and the spatial position of the rotor flux-linkage space phasor ( $\rho_r$ ). In accordance with eqn (4.1-43), the electromagnetic torque is obtained by multiplying the torque-producing current by the constant  $3PL_m^2/(2L_r)$ , where  $P$  is the number of pole pairs,  $L_m$  is the magnetizing inductance of the machine, and  $L_r$  is the self-inductance of the rotor.

In Fig. 4.19 the angle  $\phi_{s\text{ref}}$  is first added to the angle  $\rho_r$  to yield the space angle of the reference value of the stator-current space phasor with respect to the real-axis of the stator reference frame ( $\alpha_{s\text{ref}}$ ). This angle has also been shown in Fig. 4.15. The angle  $\alpha_{s\text{ref}}$  is then compared with the angle  $\beta$  described above, which corresponds to the state of the inverter, and the resulting error serves as the input to the angle controller, which is a PI controller. With the aid of the angle-control loop, a six-step ring counter is switched forward and backward between two adjacent states. Another advantage of using the angle-control loop is that, at low speed, the torque pulsations, which have been discussed in the previous section and are caused by the interaction of the approximately sinusoidal rotor magnetizing currents and the non-sinusoidal stator currents, will be reduced because of the reduced distortions in the stator currents. However, as discussed in the previous section, the CSI-fed induction machine is not suitable for servo-drive applications, where at very low speed controlled torque is required. In contrast to this, in the voltage-source PWM inverter-fed induction machine there is no low-speed cogging effect.

As discussed above, the amplitude of the stator currents is controlled through the d.c. link current ( $i_D$ ) and conventionally a PI controller is used for this purpose. However, with this type of control the d.c. link current is influenced by the back e.m.f. of the motor. During transient conditions the conventional control cannot give satisfactory current response and, as a consequence, the performance of the drive deteriorates. The influence of the back e.m.f. can be reduced by increasing the gain of the PI current controller, which results in the narrowing of the bandwidth of the d.c. link current loop. However, this will not yield the desired current response since, as will be shown below, the back e.m.f. is a function of several variables whose dynamics are faster or as fast as that of the d.c. link current. Furthermore, the bandwidth of the d.c. link current loop is determined by a large time constant ( $T_B = L/R$  where  $R$  and  $L$  will be defined in eqns (4.1-87) and (4.1-88) respectively) and also by the stability requirements on the current response. A solution to this problem, and thus improved current response, can be obtained if, in addition to the PI current controller, a function generator is incorporated in the control to compensate for the back e.m.f.s of the induction machine. The details of the design of the required back-e.m.f. estimator will now be discussed. For this purpose the voltage equation of the d.c. link, which is valid under transient conditions, has to be obtained, and it has to contain the back e.m.f. of the machine but referred to the inverter input.

First the space phasor of the back e.m.f. of the machine is obtained. It is assumed that there are no time harmonics in the d.c. link current and voltage, and none on the output of the inverter, apart from the fundamental. The effects of magnetic saturation are also neglected. Equation (4.1-6), the space-phasor form of the stator voltage equation in the rotor-flux-oriented reference frame, is

$$\bar{u}_{s\psi r} = (R_s + L'_s p) \bar{i}_{s\psi r} + j\omega_{mr} L'_s \bar{i}_{s\psi r} + (L_s - L'_s)(p + j\omega_{mr}) \bar{i}_{mr}, \quad (4.1-80)$$

where  $p = d/dt$ ,  $R_s$  and  $L_s$  are the resistance and self-inductance of a stator winding respectively,  $L'_s$  is the transient inductance of the stator,  $\bar{u}_{s\psi r}$  and  $\bar{i}_{s\psi r}$  are the stator voltage and current space phasors in the rotor-flux-oriented reference frame, and  $\bar{i}_{mr}$  is the rotor magnetizing-current space phasor in the same reference frame ( $\bar{i}_{mr} = |\bar{i}_{mr}|$ ).  $\omega_{mr}$  is the speed of the reference frame and is equal to the sum of the rotor speed and the slip speed. The third term on the right-hand side of eqn (4.1-80) gives the space phasor of the back e.m.f.s of the induction machine,

$$\bar{u}_B = (L_s - L'_s)(p + j\omega_{mr}) \bar{i}_{mr}. \quad (4.1-81)$$

This will be utilized in the back-e.m.f. estimator, but it has to be referred to the inverter input.

The dynamic voltage equation of the d.c. link will now be obtained. It follows from Fig. 4.17 that the output voltage of the controlled rectifier ( $u_D$ ) and the input voltage of the inverter ( $u_i$ ) are related by

$$u_D = (R_F + L_F p) i_D + u_i, \quad (4.1-82)$$

where  $R_F$  and  $L_F$  are the resistance and inductance of the filter (smoothing reactor) and  $i_D$  is the d.c. link current. Furthermore, by assuming that there are

no losses in the inverter (and thus the power into the inverter is equal to the output power of the inverter), it follows from eqn (2.1-87) that

$$u_i i_D = \frac{2}{3} \operatorname{Re}(\bar{u}_{s\psi r} \bar{i}_{s\psi r}^*), \quad (4.1-83)$$

where the asterisk denotes the complex conjugate and  $\operatorname{Re}$  denotes the real part of a complex quantity.

If the expression for the voltage space phasor defined by eqn (4.1-80) is substituted into eqn (4.1-83), but its third term is replaced by  $u_B$ , the following equation is obtained after some rearrangement of the various terms:

$$\frac{\frac{2}{3} \operatorname{Re}(\bar{u}_B \bar{i}_{s\psi r}^*)}{i_D} = u_i - \frac{2}{3} (R_s + L'_s p) \frac{|\bar{i}_s|^2}{i_D} = u'_B. \quad (4.1-84)$$

The second term after the first equal sign of eqn (4.1-84) contains the ohmic and leakage voltage drops referred to the inverter input and the term on the left-hand-side is the motor back e.m.f. referred to the inverter input ( $u'_B$ ). When the expression for  $\bar{u}_B$  given by eqn (4.1-81) is substituted into the left-hand side of eqn (4.1-84), and substituting  $\bar{i}_{s\psi r} = i_{sx} + j i_{sy}$ ,

$$u'_B = \frac{\frac{2}{3} \operatorname{Re}(\bar{u}_B \bar{i}_{s\psi r}^*)}{i_D} = \frac{2}{3} L_s (1 - \sigma) (p |\bar{i}_{mr}| i_{sx} + \omega_{mr} |\bar{i}_{mr}| i_{sy}) / i_D, \quad (4.1-85)$$

where  $\sigma$  is the resultant leakage constant,  $\sigma = 1 - L_m^2 / (L_s L_r)$ . It can be seen that  $u'_B$  depends on the level of the rotor magnetizing current (rotor flux level), flux- and torque-producing stator currents, the d.c. link current and also on the rotor speed (this is contained in  $\omega_{mr}$ ). Thus by taking  $u_i$  from eqn (4.1-82) and substituting into eqn (4.1-84), the following equation is obtained, which describes the dynamics of the d.c. link in terms of  $u'_B$ :

$$u_D = (R + Lp) i_D + u'_B, \quad (4.1-86)$$

where  $u'_B$  is defined by eqn (4.1-85) and

$$R = R_F + \frac{2}{3} \left( R_s \frac{|\bar{i}_s|^2}{i_D^2} \right) \quad (4.1-87)$$

$$L = L_F + \frac{2}{3} \left( L'_s \frac{|\bar{i}_s|^2}{i_D^2} \right). \quad (4.1-88)$$

It follows from eqn (4.1-88) that  $u'_B$  acts as a feedback in the drive. The back e.m.f. can be compensated by the application of a back-e.m.f. estimator, which is also shown in Fig. 4.19, and which is based on eqn (4.1-85).

In general, it follows from eqn (4.1-85), that the inputs to the back-e.m.f. estimator shown in Fig. 4.19 are the d.c. link current ( $i_D$ ), the flux-producing stator current component ( $i_{sx}$ ), the torque-producing stator current component ( $i_{sy}$ ), and the speed of the rotor flux ( $\omega_{mr}$ ). When the back-e.m.f. estimator is used together with the PI current controller in the d.c. link loop, the d.c. link current is no longer disturbed by the back e.m.f. of the machine and its transient

behaviour is only determined by the PI current controller and a first-order lag, whose time constant is equal to  $L/R$ , where  $L$  and  $R$  are defined in eqns (4.1-87) and (4.1-88) respectively. When the rotor flux is constant,  $|\bar{i}_{mr}| = \text{constant}$ , eqn (4.1-85) takes a very simple form:

$$u'_B = \frac{2}{3} L_s (1 - \sigma) \frac{\omega_{mr} |\bar{i}_{mr}| i_{sy}}{i_D}. \quad (4.1-89)$$

This can be arranged into various forms for various implementations and, for example, by considering eqn (4.1-43) it follows that the product  $|\bar{i}_{mr}| i_{sy}$  is proportional to the electromagnetic torque ( $t_e$ ) and eqn (4.1-89) takes the form

$$u'_B = \frac{t_e \omega_{mr}}{P i_D}, \quad (4.1-90)$$

where  $P$  is the number of pole pairs. In eqn (4.1-90)  $\omega_{mr}$  can be replaced by using eqn (4.1-26) and thus

$$u'_B = \left[ t_e \left( \omega_r + \frac{i_{sy}}{T_r |\bar{i}_{mr}|} \right) \right] / P i_D, \quad (4.1-91)$$

where  $\omega_r$  is the rotor speed and  $T_r$  is the rotor time constant. It is also possible to use eqn (4.1-43) and to eliminate  $i_{sy}$  in eqn (4.1-91) to yield

$$u'_B = \left[ t_e \left( \omega_r + \frac{t_e R_r}{c |\bar{i}_{mr}|^2} \right) \right] / P i_D, \quad (4.1-92)$$

where  $c = \frac{3}{2} P L_m^2$  and  $R_r$  is the rotor resistance (referred to the stator winding). A very simple realization of the  $u'_B$  compensator is obtained if  $t_e$  is replaced by its reference value.

It should be noted that when the motor back-e.m.f. estimator is incorporated into the drive control, the improvement in the d.c. link current response also results in improved torque and flux responses. Furthermore, back e.m.f.s are also present in the output current control loops of the current-controlled PWM voltage-source inverter-fed induction machine. In this case these e.m.f.s can be obtained by the transformation of  $u'_B$  into the actual back e.m.f.s, and current control with e.m.f. compensation can be established, where the compensator can be designed on the basis of the space-phasor equation of the back e.m.f.s.

#### 4.1.2.3.3 Implementation using the indirect method

In this section the rotor-flux-oriented control of a CSI-fed induction machine is described, where the angle of the rotor magnetizing-current space phasor is obtained by using the so-called indirect method. Fig. 4.20 shows the schematic of the drive.

The implementation shown in Fig. 4.20 resembles the implementation shown in Fig. 4.16, which contains the control scheme of the indirect rotor-flux-oriented control of a current-controlled PWM inverter-fed induction machine. The outer control loops shown in Fig. 4.20 are the same as those shown in Fig. 4.16, and

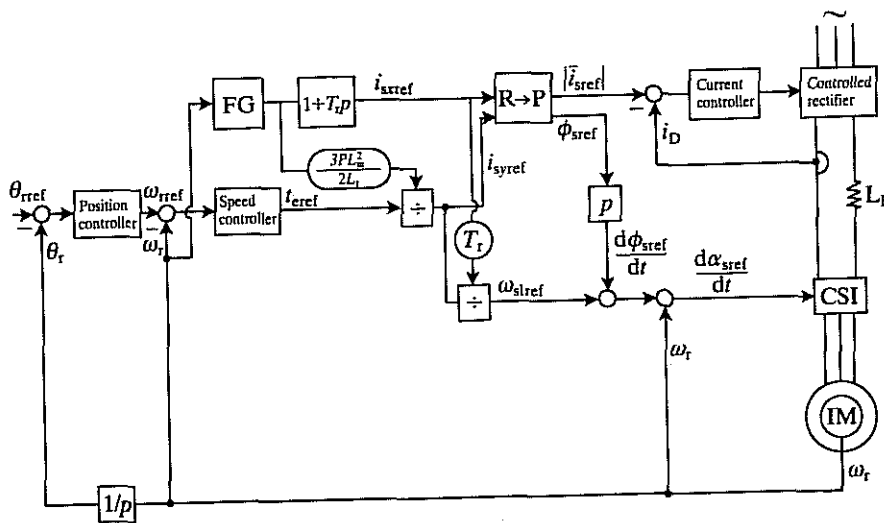


Fig. 4.20. Schematic of the indirect rotor-flux-oriented control of a CSI-fed induction machine.

therefore they are not described here. The reference values of the direct- and quadrature-axis stator currents expressed in the rotor-flux-oriented reference frame ( $i_{sxref}$ ,  $i_{syref}$ ) are obtained in the same way as shown in Fig. 4.16. Furthermore the reference value of the slip frequency ( $\omega_{sref}$ ) is obtained identically to that shown in Fig. 4.16, by utilizing  $i_{sxref}$  and  $i_{syref}$  and the known value of the rotor time constant ( $T_r$ ), which can also be obtained by on-line identification.

In Fig. 4.20, as in Fig. 4.19, the reference stator currents  $i_{sxref}$ ,  $i_{syref}$  are converted into polar coordinates by a rectangular-to-polar converter, and thus the outputs of the R→P converter are the modulus of the reference value of the stator-current space phasor ( $|i_{sref}|$ ) together with its space angle ( $\phi_{sref}$ ), which angle is shown in Fig. 4.15 and is the angle of the stator-current space phasor with respect to the real axis of the rotor-flux-oriented reference frame. It follows from Fig. 4.15 that

$$\alpha_{sref} = \theta_r + \theta_{sref} + \phi_{sref}, \quad (4.1-93)$$

where  $\alpha_s$  is the space angle of the stator-current space phasor with respect to the real axis of the stationary reference frame,  $\theta_r$  is the rotor angle, which gives the position of the real axis of the reference frame fixed to the rotor with respect to the real axis of the stationary reference frame,  $\theta_{sref}$  is the slip angle, which gives the position of the rotor flux-linkage space phasor with respect to the real axis of the reference frame fixed to the rotor, and  $\phi_s$  is the angle of the stator-current space phasor with respect to the real axis of the rotor-flux-oriented reference frame. The subscript 'ref' denotes the reference value. Thus differentiation of eqn (4.1-93) with respect to time yields

$$p\alpha_{sref} = p\theta_r + p\theta_{sref} + p\phi_{sref} = \omega_1 = \omega_r + \omega_{sref} + p\phi_{sref}, \quad (4.1-94)$$

where  $p = d/dt$ ,  $\omega_1$  is the required stator frequency,  $\omega_r$  is the rotor speed, and  $\omega_{sref}$  is the reference value of the slip frequency, which is defined in eqn (4.1-73), repeated here for convenience:

$$\omega_{sref} = \frac{i_{syref}}{T_r i_{sxref}}. \quad (4.1-95)$$

Thus in Fig. 4.20 the stator frequency  $\omega_1$  is obtained by considering eqns (4.1-94) and (4.1-95). The supply-side converter is controlled in the same way as in Fig. 4.17.

It should be noted that to obtain lower torque pulsations at low speeds, the technique described in Fig. 4.19 could be utilized. Furthermore, a more accurate value of the slip frequency can be obtained by utilizing the actual values of the flux- and torque-producing stator currents ( $i_{sx}$ ,  $i_{sy}$ ) instead of their reference values ( $i_{sxref}$ ,  $i_{syref}$ ), since the presence of the d.c. link inductor makes the stator current slow to respond to a change in the reference currents. During transient operation the slip frequency determined from  $i_{sxref}$  and  $i_{syref}$  differs from the slip frequency which is determined from the actual values of these currents and the difference is large at the beginning of the transient. As a consequence, an inappropriate value of the slip frequency results, and this affects adversely the torque response of the drive and leads to deteriorated performance. The actual values of the stator current components  $i_{sx}$  and  $i_{sy}$  can be obtained in several ways, including the utilization of the appropriate transformations of the monitored stator currents  $i_{sA}$ ,  $i_{sB}$ ,  $i_{sC}$ . In this case, by considering eqns (2.1-112) and (2.1-113), first the direct- and quadrature-axis stator currents in the stationary reference frame are obtained as follows, if it is assumed that there are no zero-sequence currents:

$$i_{sD} = i_{sA} \quad (4.1-96)$$

$$i_{sQ} = \frac{1}{\sqrt{3}}(i_{sB} - i_{sC}). \quad (4.1-97)$$

These are then transformed into the two-axis currents established in the rotor-flux-oriented reference frame by utilizing eqn (2.1-192):

$$i_{sx} = \cos \rho_r i_{sD} + \sin \rho_r i_{sQ} \quad (4.1-98)$$

$$i_{sy} = -\sin \rho_r i_{sD} + \cos \rho_r i_{sQ}. \quad (4.1-99)$$

However, this requires the angle  $\rho_r$ , which is the angle of the rotor magnetizing-current space phasor with respect to the real axis of the stationary reference frame. Furthermore, the two transformations required lead to large computation time in the case of a digital implementation or to complicated hardware in the case of analog implementation.

However, a much simpler implementation can be obtained if  $i_{sx}$  and  $i_{sy}$  are derived from the monitored d.c. link current ( $i_D$ ) and the angle of the stator-current space phasor with respect to the real axis of the rotor-flux-oriented reference frame ( $\phi_s$ ). This angle is also shown in Fig. 4.15. Since the commutation period is short in the CSI inverter, it can be neglected and according to Fig. 4.18(e)

the modulus of the stator-current space phasor  $|\bar{i}_s|$  is proportional to the d.c. link current ( $i_D$ ),

$$|\bar{i}_s| = \frac{2i_D}{\sqrt{3}}, \quad (4.1-100)$$

and the amplitude of the fundamental current is equal to  $(2\sqrt{3}/\pi)i_D$ . Thus, from Fig. 4.15, the space phasor of the stator currents in the rotor-flux-oriented reference frame can be expressed as

$$\bar{i}_{syf} = i_{sx} + ji_{sy} = |\bar{i}_s| e^{j\phi_s} \quad (4.1-101)$$

and the following expressions are obtained for the flux- and torque-producing stator current components:

$$i_{sx} = ci_D \cos \phi_s \quad (4.1-102)$$

$$i_{sy} = ci_D \sin \phi_s, \quad (4.1-103)$$

where  $c$  is a constant. Thus  $i_{sx}$  and  $i_{sy}$  can be obtained in a simple manner from  $i_D$  and  $\phi_s$  and the required transformation is not dependent on any machine parameter. A possible implementation is shown in Fig. 4.21, where  $\phi_s$  is replaced by  $\phi_{sref}$ , which is the space angle of the reference value of the stator-current space phasor.

In Fig. 4.21  $i_{sxref}$  and  $i_{syref}$  are converted by a rectangular-to-polar converter into  $|\bar{i}_{sref}|$  and  $\phi_{sref}$ . As shown in Fig. 4.20, the slip frequency  $\omega_{sl}$  is added to  $d\phi_{sref}/dt$  and to this is added the monitored rotor speed to yield  $\omega_1 = d\alpha_{sref}/dt$ . The monitored d.c. link current is first multiplied by the constant  $c$ , and  $ci_D$  and  $\phi_{sref}$  are inputs to a polar-to-rectangular converter, the outputs of which are  $i_{sy}$  and  $i_{sx}$ . By utilizing eqn (4.1-25),  $|\bar{i}_{mrl}|$  is obtained from  $i_{sx}$  in the block which contains  $1/(1+T_r p)$ , where  $p = d/dt$  and  $T_r$  is the rotor time constant. The slip frequency

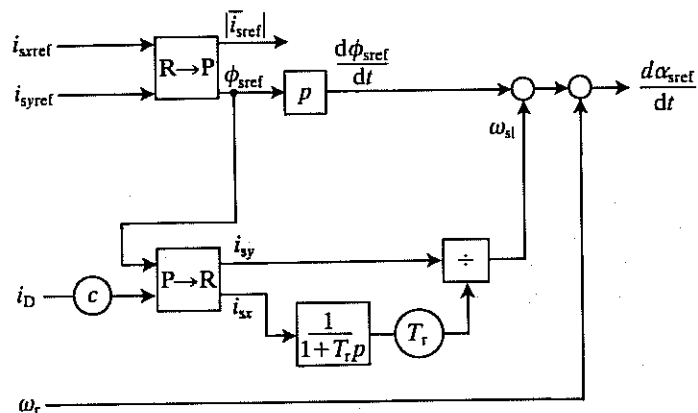


Fig. 4.21. Determination of  $i_{sx}$ ,  $i_{sy}$ , and  $\omega_{sl}$  by utilizing  $i_D$  and  $\phi_{sref}$ .

( $\omega_{sl}$ ) is obtained by utilizing eqn (4.1-26) and thus  $\omega_{sl} = i_{sy}/(T_r |\bar{i}_{mrl}|)$ . The full rotor-flux-oriented control scheme can be obtained by adding the parts of the circuit shown in Fig. 4.20 to Fig. 4.21.

#### 4.1.2.4 Control of the induction machine supplied by a current-controlled cycloconverter

A cycloconverter-fed induction machine drive is very suitable for high-power, low-speed applications. Some applications include rolling steel mills, temper mills, etc. and the characteristics of rolling mills have been described in Section 3.2.1. These characteristics can be satisfied by the vector-controlled cycloconverter-fed induction machine. Owing to the advantages of the induction machine over the d.c. machine (reliability, lower moment of inertia, ruggedness, absence of commutator and brushes, etc.) the cycloconverter-fed induction machine offers additional advantages over d.c. drives, and conventional d.c. drives can be replaced by high-performance vector-controlled cycloconverter-fed induction machines.

As a result of the application of line-commutated bridge converters, the output frequency of the cycloconverter varies between 0 and 25 Hz if the converter is supplied at a frequency of 50 Hz and between 0 and 20 Hz if the supply frequency is 60 Hz. This limits the speed range of the cycloconverter, but in low-speed drives this is of no importance. If necessary, the speed range can be increased by increasing the number of phases on the line-side of the cycloconverter, by employing a transformer with the required number of secondary windings between the line and the cycloconverter. However, it is a disadvantage of this technique that as a result of the increased number of phases, the number of thyristors has to be increased in the converter. The high input reactive power of the cycloconverter drive is also a disadvantage, but there are several well-known techniques to reduce this (asymmetrical voltage control, neutral potential bias control, etc.).

In this section the rotor-flux-oriented control of a current-controlled cycloconverter-fed induction machine is described. As described in Section 3.2.1 for the cycloconverter-fed salient-pole synchronous machine, each stator phase of the induction machine is supplied by two anti-parallel three-phase six-pulse bridge converters. These bridge converters have been shown in Fig. 3.20. The stator currents of the induction machine are separately controlled by fast current loops. Figure 4.22 shows an implementation of the drive.

The control structure is similar to that used for d.c. machines. The difference between the monitored rotor speed ( $\omega_r$ ) and the reference rotor speed ( $\omega_{rref}$ ) serves as the input to the speed controller, which is a PI controller, and this produces the required torque reference ( $t_{ref}$ ). The function generator FG has the same role as, for example, in Fig. 4.14; this allows field weakening to be achieved and its output is the reference value of the rotor magnetizing current ( $|\bar{i}_{mrref}|$ ). The output of the flux controller (which has the same role as in Fig. 4.14) is the reference value of the flux-producing stator current component ( $i_{sxref}$ ) and its input is  $|\bar{i}_{mrref}| - |\bar{i}_{mrl}|$ , where the actual value of the rotor magnetizing current ( $|\bar{i}_{mrl}|$ ) is obtained by utilizing the flux model shown in Fig. 4.6.

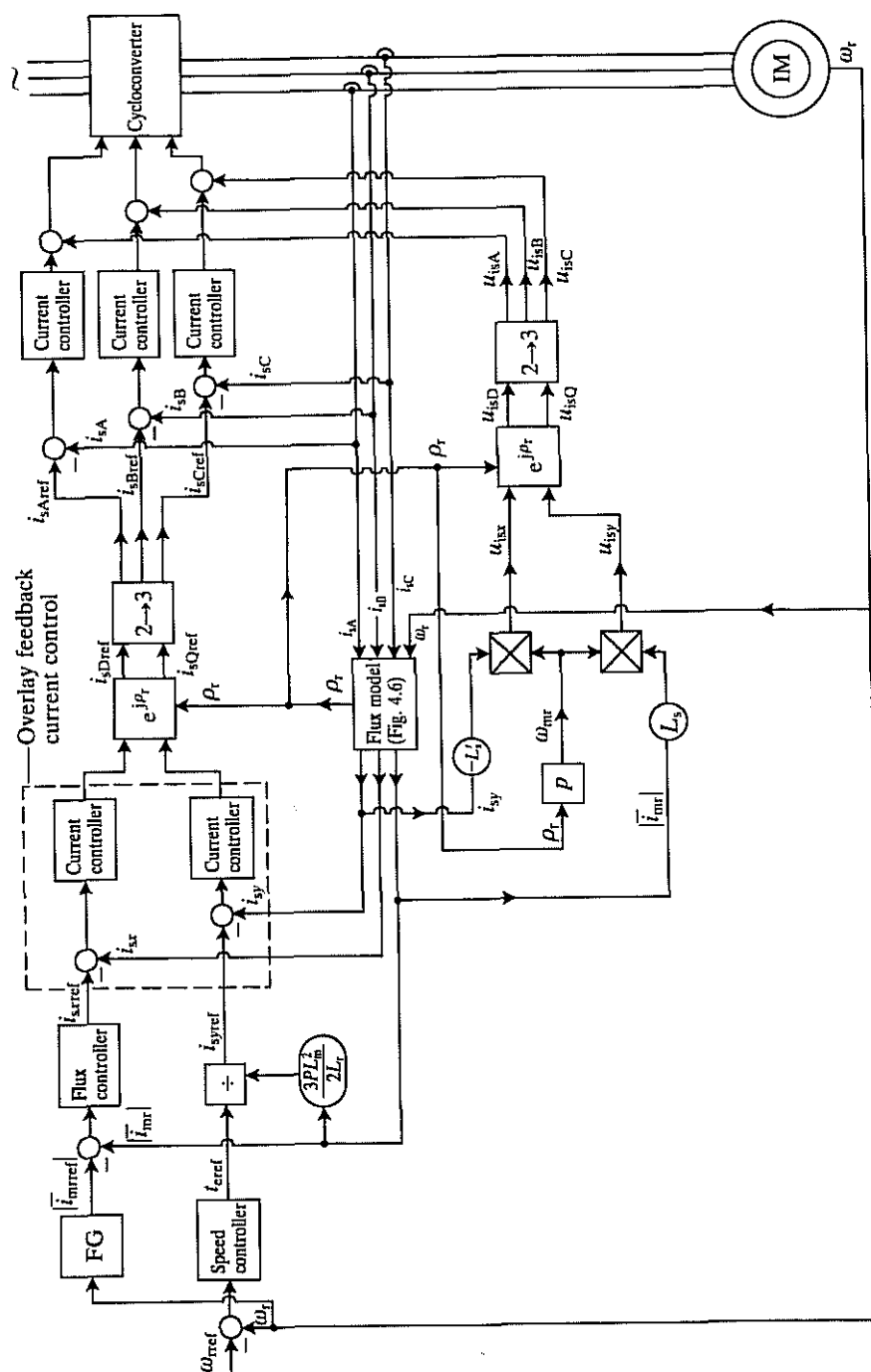


Fig. 4.22. Schematic of the rotor-flux-oriented control of a current-controlled cycloconverter.

The inputs to the flux model are the rotor speed ( $\omega_r$ ) and the stator currents (in the absence of zero-sequence currents only two line currents have to be monitored). The outputs of the flux model are the flux- and torque-producing stator currents ( $i_{sx}$ ,  $i_{sy}$ ), which are established in the rotor-flux-oriented reference frame,  $\rho_r$ , which is the angle of the rotor magnetizing-current space phasor with respect to the real axis of the stationary reference frame, and  $|i_{mr}|$ , which is the modulus of the rotor magnetizing-current space phasor. These quantities are also shown in Fig. 4.15. In accordance with eqn (2.1-197), the reference value of the torque-producing stator current ( $i_{syref}$ ) is obtained by dividing the torque reference by the factor  $3P|i_{mr}|L_m^2/(2L_r)$ , where  $P$  is the number of pole pairs and  $L_m$  and  $L_r$  are the magnetizing inductance and rotor self-inductance respectively.

To obtain high accuracy, overlay current control loops are used to control the flux- and torque-producing stator currents. The outputs of the controllers in these loops are inputs to the transformation block  $e^{j\rho_r}$ , which is required to obtain the reference values of the direct- and quadrature-axis stator currents ( $i_{sDref}$ ,  $i_{sQref}$ ) established in the stationary reference frame, as discussed in connection with Fig. 4.14. These currents are then transformed into their three-phase components by the application of the three-phase to two-phase transformation, and are then compared with their actual values. The resulting errors are inputs to the appropriate current controllers which control the cycloconverter.

It has been noted in Section 3.2.2 that at higher output frequencies of the cycloconverter, induced a.c. voltages will disturb the current control system and there will result phase and amplitude errors, which even in the steady-state cannot be eliminated by the current controllers which control the cycloconverter. However, one possible solution to this is to add feedforward voltages to the outputs of these current controllers. Thus in Fig. 4.22 e.m.f. compensation is realized by feedforward of the induced voltages ( $u_{isA}$ ,  $u_{isB}$ ,  $u_{isC}$ ). These are obtained from their two-axis values ( $u_{isD}$ ,  $u_{isQ}$ ) by the application of the two-phase to three-phase transformation. However, these are related to the induced voltages established in the rotor-flux-oriented reference frame ( $u_{isx}$ ,  $u_{isy}$ ) by the transformation  $e^{j\rho_r}$ . The required induced voltages  $u_{isx}$  and  $u_{isy}$  can be obtained from eqns (4.1-7) and (4.1-8) and by using the fact that in the steady state  $|i_{mr}|=constant$  and considering eqn (4.1-25), which yields  $|i_{mr}|=i_{sx}$ ; so finally

$$u_{isx} = -\omega_{mr} L'_s i_{sy} \quad (4.1-104)$$

$$u_{isy} = \omega_{mr} L_s |i_{mr}|. \quad (4.1-105)$$

$\omega_{mr}$  is the speed of the rotor-flux-oriented reference frame ( $\omega_{mr}=d\rho_r/dt$ ), and  $L_s$  and  $L'_s$  are the self-inductance and transient inductance of the stator respectively.

#### 4.1.2.5 Control of the slip-ring induction machine with impressed rotor currents

Rotor-flux-oriented control can also be used for the slip-ring induction machine with impressed rotor currents. For this purpose the converter in the rotor circuit can be a current-controlled cycloconverter (e.g. a six-pulse cycloconverter as

described in the previous section), a pulse-width modulated inverter with current control (again described earlier) or, for example, a static converter cascade. In the last case there is dual converter in the rotor and this is shown in Fig. 4.23.

In the implementation shown in Fig. 4.23 a forced commutated thyristor converter is connected to the slip rings of the induction machine and this is connected via a d.c. reactor to a naturally commutated controlled-thyristor bridge converter (special form of static Scherbius cascade). Thus slip power can flow in both directions (to the rotor from the supply and from the rotor to the supply) and the speed of the induction machine can be controlled in the supersynchronous and subsynchronous ranges. Below the synchronous speed in the motoring mode and above the synchronous speed in the regeneration mode the rotor-side converter operates as a rectifier and the line-side converter as an inverter, and slip power is returned to the stator, usually through a transformer. Below the synchronous speed in the regeneration mode and above the synchronous speed in the motoring mode, the rotor-side converter operates as an inverter and the line-side converter operates as a rectifier, and slip power is supplied to the rotor. At the synchronous speed, slip power is taken from the supply to excite the rotor windings, and in this case the machine behaves as a synchronous machine. It should be noted that if the rotor-side converter was a line-commutated bridge converter, near to the synchronous speed, when the a.c. voltage available to commutate the converter is small, the commutating ability of the converter would be lost. It is for this reason that a force-commutated rotor-side converter is used in the special form of the static Scherbius cascade shown in Fig. 4.23, and thus full torque capability can be produced near standstill.

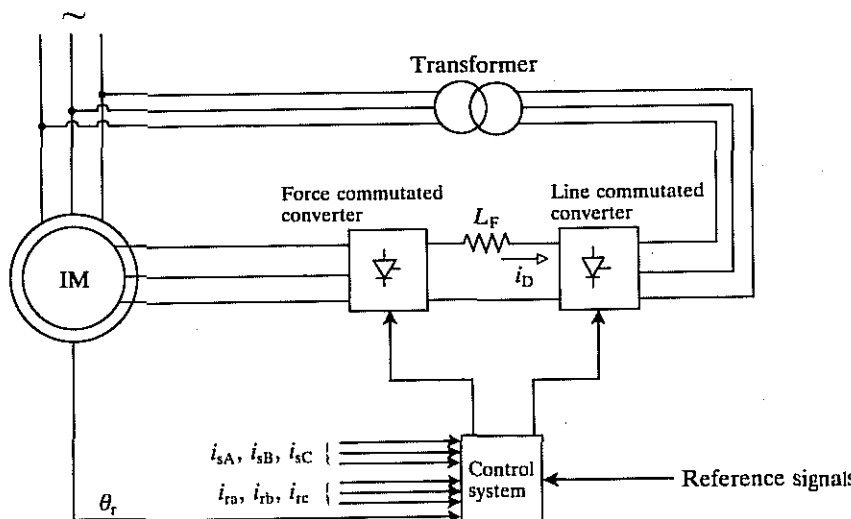


Fig. 4.23. Schematic of the control of a doubly-fed induction machine with converter cascade in the rotor.

Since impressed rotor currents are assumed, the rotor voltage equations can be disregarded from the point of view of the dynamics of the drive under consideration and this results in a simplified dynamic structure of the drive. Thus only the stator voltage equations have to be considered.

The space-phasor form of the stator voltage equation in the rotor-flux-oriented reference frame has been given as eqn (4.1-6) and its two-axis forms have been given as eqn (4.1-7) and eqn (4.1-8). These contain the rotor magnetizing current ( $|i_{mr}|$ ), which has been defined in eqn (4.1-1). These equations together with the equation of the electromagnetic torque, eqn (4.1-43), could be used to obtain the implementations of the rotor-flux-oriented control of a slip-ring induction machine with impressed rotor currents. However, in contrast to the implementations so far discussed for induction machines, where the rotor currents were not directly measurable quantities, in the slip-ring machine it is possible to monitor these and this results in simpler implementations than, say, in the case of a squirrel-cage machine. If the stator currents and the rotor currents are measured together with the rotor angle ( $\theta_r$ ) then  $|i_{mr}|$  and  $\rho_r$ , which is the space angle of the rotor magnetizing-current space phasor with respect to the direct-axis of the stationary reference frame (see Fig. 4.15), are known quantities. Mathematically this follows from eqn (4.1-1), which is now repeated here for convenience,

$$\bar{i}_{mr} = \bar{i}_{s\psi r} + (1 + \sigma_r) \bar{i}_{r\psi r}, \quad (4.1-106)$$

where  $\bar{i}_{s\psi r}$  and  $\bar{i}_{r\psi r}$  are the space phasors of the stator currents and rotor currents respectively in the rotor-flux-oriented reference frame. By considering eqn (4.1-3) and eqn (2.1-194) they can be expressed in terms of the space phasor of the stator currents and rotor currents expressed in the stationary reference frame ( $\bar{i}_s, \bar{i}_r'$ ) as

$$\bar{i}_{s\psi r} = \bar{i}_s e^{-j\rho_r} \quad (4.1-107)$$

$$\bar{i}_{r\psi r} = \bar{i}'_r e^{-j\rho_r}. \quad (4.1-108)$$

Substitution of eqns (4.1-107) and (4.1-108) into eqn (4.1-106) yields

$$\bar{i}_{mr} = \left[ \bar{i}_s + \frac{L_t}{L_m} \bar{i}'_r \right] e^{-j\rho_r}. \quad (4.1-109)$$

Thus it follows from eqn (2.1-133) and eqn (4.1-109) that

$$\bar{i}_{mr} = |i_{mr}| e^{j\rho_r} = \bar{i}_s + \frac{L_t}{L_m} \bar{i}'_r = \bar{i}_s + \frac{L_t}{L_m} \bar{i}_r e^{j\theta_r}, \quad (4.1-110)$$

where in terms of their two-axis components,

$$\bar{i}_s = i_{sD} + j i_{sQ} \quad (4.1-111)$$

$$\bar{i}_r = i_{rD} + j i_{rQ} \quad (4.1-112)$$

$$\bar{i}_r e^{j\theta_r} = i_{rd} + j i_{rq} \quad (4.1-113)$$

$$\bar{i}_{mr} = i_{mrD} + j i_{mrQ} \quad (4.1-114)$$

and  $\theta_r$  is the rotor angle. Equations (4.1-110)–(4.1-113) can be used to obtain  $|\bar{i}_{mr}|$  and  $\rho_r$  from the measured values of the stator and rotor currents and the rotor angle. Physically eqn (4.1-110) gives the rotor magnetizing-current space phasor in the stationary reference frame and, as expected, this contains two components; these are the stator-current space phasor and a component which would be equal to the rotor-current space phasor if there was no rotor leakage. In this case (when the rotor leakage inductance is zero)  $L_r = L_m$  and the rotor magnetizing-current space phasor is identical to the conventional magnetizing-current space phasor, which is equal to the sum of the stator- and rotor-current space phasors. Equation (4.1-110) can also be obtained directly by dividing the expression for the rotor flux-linkage space phasor expressed in the rotor reference frame (see eqn (2.1-134)) by the magnetizing inductance and this technique has been used for the derivation of eqn (4.1-28), which gives the same definition for the rotor magnetizing-current space phasor as eqn (4.1-110).

It should be noted that when  $|\bar{i}_{mr}|$  and  $\rho_r$  are determined from eqn (4.1-110), there is no dependency on the rotor resistance, in contrast to the derivation based on the flux models described in Figs 4.6 and 4.7. This is an advantage, since the rotor resistance varies as a result of changes in the temperature and the skin effect. By using eqn (4.1-110), Fig. 4.24 shows a possible implementation for obtaining  $|\bar{i}_{mr}|$  and  $\rho_r$ .

It follows from Fig. 4.24 that the monitored three-phase stator currents ( $i_{sA}$ ,  $i_{sB}$ ,  $i_{sC}$ ) are first transformed into the real- and imaginary-axis components of the stator-current space phasor expressed in the stationary reference frame ( $\bar{i}_s$ ) by

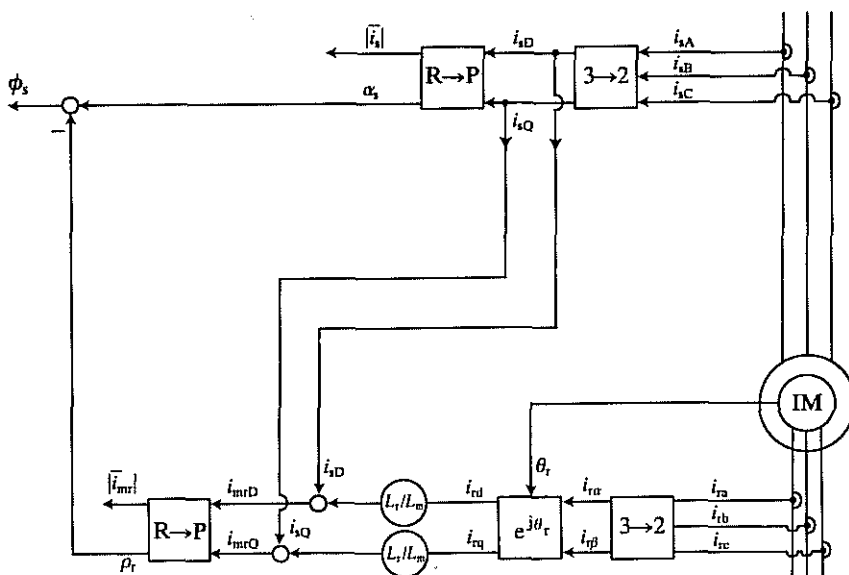


Fig. 4.24. Obtaining  $|\bar{i}_{mr}|$ ,  $|\bar{i}_s|$ ,  $\rho_r$ , and  $\phi_s$  by monitoring the stator and rotor currents and the rotor angle.

the application of the three-phase to two-phase transformation. The monitored rotor currents ( $i_{ra}$ ,  $i_{rb}$ ,  $i_{rc}$ ) are similarly transformed into the  $i_{rd}$ ,  $i_{rq}$  components (which are the direct- and quadrature-axis rotor currents in the rotor reference frame) by the application of the three-phase to two-phase transformation. These are then transformed into  $i_{rd}$  and  $i_{rq}$ , which are the two-axis rotor current components in the stator reference frame, by the application of the transformation  $e^{j\theta_r}$  (see eqn (4.1-113) and eqn (2.1-40)). Finally by considering eqn (4.1-110)  $i_{rd}$  and  $i_{rq}$  are multiplied by  $L_r/L_m$  and the newly obtained rotor currents are added to  $i_{sD}$  and  $i_{sQ}$  respectively to yield the two-axis components of the rotor magnetizing-current space phasor in the stationary reference frame ( $i_{mrD}$ ,  $i_{mrQ}$ ). These are inputs to a rectangular-to-polar converter the outputs of which are  $|\bar{i}_{mr}|$  and  $\rho_r$ .

By utilizing the implementation shown in Fig. 4.24, several other quantities can also be obtained which could be required in various implementations of the rotor-flux-oriented control of slip-ring induction machines with impressed rotor currents. Thus when  $\rho_r$  is differentiated,  $\omega_{mr}$ , the speed of the rotor flux-linkage space phasor, is obtained. From the monitored rotor angle ( $\theta_r$ ) and  $\rho_r$ , the slip angle  $\theta_{sl}$  is obtained (this angle is shown in the phasor diagram of Fig. 4.15). It follows from eqn (4.1-107) that the space phasor of the stator currents in the rotor-flux-oriented reference frame is

$$(i_{sx} + j i_{sy}) = (i_{sD} + j i_{sQ}) e^{-j \rho_r},$$

and resolution into real and imaginary terms gives eqns (4.1-98) and (4.1-99) which could be used to obtain  $i_{sx}$  and  $i_{sy}$  from  $i_{sD}$  and  $i_{sQ}$ . The modulus ( $|\bar{i}_s|$ ) and the space angle ( $\alpha_s$ ) of the stator-current space phasor expressed in the stationary reference frame are obtained in Fig. 4.24 by the application of a rectangular-to-polar converter by using  $i_{sD}$  and  $i_{sQ}$  as input quantities. The angle  $\alpha_s$  is also shown in Fig. 4.15. Finally, in accordance with Fig. 4.15, in Fig. 4.24 the torque angle ( $\phi_s$ ), which is the angle of the stator-current space phasor with respect to the real axis of the rotor-flux-oriented reference frame, is obtained as  $\phi_s = \alpha_s - \rho_r$ .

For the implementation of the rotor-flux-oriented slip-ring machine with impressed rotor currents, when the rotor speed is monitored and when this is compared with its reference value, the error signal can serve as input to a speed controller (PI controller) the output of which is the torque reference.

For the rotor-flux-oriented control of the doubly-fed induction machine with the static converter cascade shown in Fig. 4.23, the torque reference can be used to obtain the reference value of the d.c. link current ( $i_D$ ) which flows across the reactor connected between the two converters. Thus the line-side converter can be controlled by using the closed loop control of the d.c. link current, where the difference between the reference d.c. link current and the actual d.c. link current is fed into a PI controller. The rotor-side converter can be controlled by using the closed loop control of the torque angle. For this purpose a PI controller can be used, the input of which is the difference between the reference actual values of the torque angle (the latter can be obtained with the help of Fig. 4.24). A more detailed description will be given in Section 4.2.6, where stator-flux-oriented control of the same drive will be discussed.

The vector control of the slip-ring motor with impressed rotor currents using a cycloconverter will be discussed in detail in Section 4.2.6, where stator-flux-oriented control is discussed, since it will be shown that in the stator-flux-oriented system, the real- and imaginary-axis components of the rotor currents ( $i_{rx}, i_{ry}$ ) correspond directly to the two-axis stator currents expressed in the stator-flux-oriented reference frame. Thus control of the  $i_{rx}$  current can be used to maintain the reactive stator current at a fixed value (or at a value dependent on the voltage) and the current  $i_{ry}$  can be used for torque control. Beside the speed-independent control of active and reactive powers, it is also an advantage of the application of this control scheme that it leads to the avoidance of the instability problems associated with doubly fed machines.

## 4.2 Stator-flux-oriented control of induction machines

In this part of the chapter stator-flux-oriented control will be applied to induction machines. The main assumptions are the same as those used in connection with rotor-flux-oriented control of induction machines and, in particular, the effects of magnetic saturation are neglected. Since there is a large similarity between stator-flux-oriented control and rotor-flux-oriented control (see also Section 1.2.1.2), emphasis will only be laid on the differences between these two control techniques.

### 4.2.1 EXPRESSIONS FOR THE ELECTROMAGNETIC TORQUE

It follows from Sections 1.2.1.2 and 2.1.8 that in the stator-flux-oriented reference frame the electromagnetic torque of an induction machine is proportional to the product of the modulus of the stator magnetizing-current space phasor ( $|\bar{i}_{ms}|$ ) and the torque-producing stator current component ( $i_{sy}$ ); the torque can be controlled by independent control of these two currents. Thus from eqn (2.1-209),

$$t_e = c |\bar{i}_{ms}| i_{sy}, \quad (4.2-1)$$

where  $c = 3PL_m/2$  is a constant,  $P$  is the number of pole pairs, and  $L_m$  is the magnetizing inductance of the machine. In eqn (4.2-1) the stator magnetizing-current space phasor can be put in terms of the stator- and rotor-current space phasors expressed in the stator-flux-oriented reference frame ( $\bar{i}_{sy}, \bar{i}_{r\psi s}$ ) as, if eqn (2.1-208) is considered,

$$|\bar{i}_{ms}| = \bar{i}_{r\psi s} + \frac{\bar{i}_{sy}}{L_m} L_s = (i_{rx} + ji_{ry}) + (i_{sx} + ji_{sy}) \frac{L_s}{L_m}, \quad (4.2-2)$$

where  $L_s$  is the self-inductance of the stator and  $i_{rx}, i_{ry}, i_{sx}, i_{sy}$  are the two-axis components of the rotor- and stator-current space phasors respectively, expressed in the stator-flux-oriented reference frame. In eqn (2.1-201) the relation between the space phasors of the stator currents expressed in the stator (stationary) and stator-flux-oriented reference frames has been given, and it follows that

$$\bar{i}_{sy} = i_{sx} + ji_{sy} = (i_{sD} + ji_{sQ}) e^{-j\rho_s}, \quad (4.2-3)$$

where  $i_{sD}$  and  $i_{sQ}$  are the direct- and quadrature-axis components of the stator currents in the stationary reference frame and the angle  $\rho_s$  gives the position of the stator magnetizing current with respect to the real-axis (sD) of the stationary reference frame (this is shown in Fig. 2.17). The rotor-current space phasor in the reference frame fixed to the rotor can be expressed in terms of its two-axis components as  $\bar{i}_r = i_{rx} + ji_{ry} = |\bar{i}_r| e^{j\alpha_r}$ , and thus it follows from eqn (2.1-206) that the rotor-current space phasor in the stator-flux-oriented reference frame can be expressed as

$$\bar{i}_{r\psi s} = i_{rx} + ji_{ry} = (i_{rx} + ji_{r\beta}) e^{j\theta_r} e^{-j\rho_s} = |\bar{i}_r| e^{j(\alpha_r + \theta_r - \rho_s)}. \quad (4.2-4)$$

It is evident that the stator and rotor current components  $i_{sx}, i_{sy}, i_{rx}, i_{ry}$  defined above are not equal to the similar current components defined by eqns (2.1-192) and (2.1-194), which are established in the rotor-flux-oriented reference frame. Only for simplicity is the real axis of the stator-flux-oriented reference frame denoted as  $x$ , and its imaginary axis as  $y$ , but these should not be confused with the real and imaginary axes of the rotor-flux-oriented reference frame. For better understanding, the stator magnetizing-current space phasor and the rotor-current space phasor are shown in Fig. 4.25, where the new reference frame ( $x, y$ ) is also shown, together with the angles  $\alpha_r$ ,  $\theta_r$ , and  $\rho_s$ .

It follows from Fig. 4.25 that the angle  $\phi_r = (\alpha_r + \theta_r - \rho_s)$ , which is the torque angle, is the angle of the rotor-current space phasor with respect to the stator magnetizing-current space phasor.

It should be noted that in the steady state, the definition of  $\bar{i}_{ms}$  (expressed in the stationary reference frame) can also be obtained by considering Fig. 4.10(b) if the general turns ratio is selected as  $a = L_s/L_m$ .

A new expression will now be obtained for the electromagnetic torque which, instead of the quadrature-axis stator current ( $i_{sy}$ ), contains the modulus of the rotor-current space phasor and the torque angle. This will be useful for the implementation of stator-flux-oriented control of doubly fed induction machines. It follows from eqn (4.2-2) that the torque-producing stator current can be expressed as

$$i_{sy} = -i_{ry} \frac{L_m}{L_s} \quad (4.2-5)$$

and  $i_{ry}$  can be obtained from eqn (4.2-4) as  $i_{ry} = |\bar{i}_r| \sin(\alpha_r + \theta_r - \rho_s)$ . By substitution of this expression into eqn (4.2-5) and considering eqn (4.2-1), the following expression is obtained for the electromagnetic torque:

$$t_e = -3|\bar{i}_{ms}| |\bar{i}_r| \sin(\alpha_r + \theta_r - \rho_s) \frac{L_m^2}{2L_s}. \quad (4.2-6)$$

This expression will be used in Section 4.2.6, where stator-flux-oriented control of a doubly fed three-phase induction machine with impressed rotor currents will be discussed.

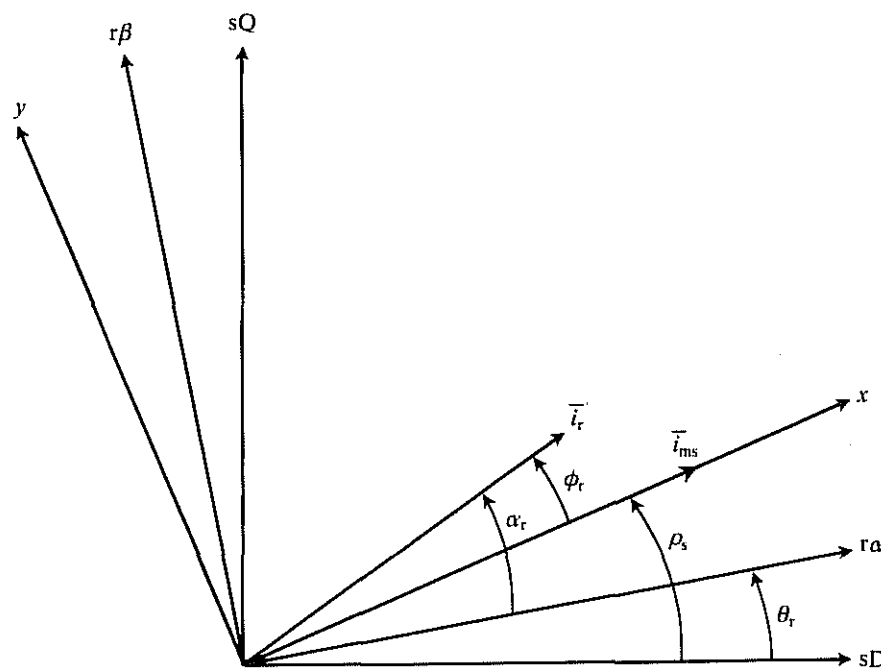


Fig. 4.25. Stator magnetizing-current space phasor and rotor-current space phasor.

#### 4.2.2 STATOR VOLTAGE EQUATIONS FOR THE SQUIRREL-CAGE MACHINE

In this section, the space-phasor form of the stator voltage equation is first obtained in the reference frame fixed to the stator magnetizing flux-linkage space phasor. This will then be resolved into its two-axis components. For this purpose the voltage equations formulated in the general reference frame are directly utilized. These have been given in Section 2.1.7. The stator-current space phasor will be expressed in terms of the stator magnetizing-current space phasor, which has been defined in the previous section. Thus the resulting stator voltage equation will contain the modulus and space angle (or speed) of the stator magnetizing-current space phasor. These quantities are required in the implementation of stator-flux-oriented control. Two alternatives will then be considered, which correspond to a squirrel-cage machine and to a slip-ring induction machine where there is direct access to the rotor currents.

By considering eqns (2.1-148) and (2.1-150), which define the stator voltage and flux-linkage space-phasor equations in the general reference frame respectively, and by neglecting the effects of magnetic saturation, the following stator voltage equation is obtained in the special reference frame fixed to the stator-linkage space phasor, which rotates at a speed  $\omega_{ms} = d\rho_s/dt$  (the angle  $\rho_s$  has been defined

in the previous section):

$$\bar{u}_{s\psi_s} = R_s \bar{i}_{s\psi_s} + L_s \frac{d\bar{i}_{s\psi_s}}{dt} + L_m \frac{d\bar{i}_{r\psi_s}}{dt} + j\omega_{ms} L_s \bar{i}_{s\psi_s} + j\omega_{ms} L_m \bar{i}_{r\psi_s}, \quad (4.2-7)$$

where as in eqn (4.2-3), which defines the stator-current space phasor in the stator-flux-oriented reference frame, the stator-voltage space phasor in the same reference frame can be expressed as

$$\bar{u}_{s\psi_s} = u_{sx} + j u_{sy} = (u_{sD} + j u_{sQ}) e^{-j\rho_s} = \bar{u}_s e^{-j\rho_s}. \quad (4.2-8)$$

In eqn (4.2-7)  $\bar{i}_{r\psi_s}$  is the space phasor of the rotor currents in the stator-flux-oriented reference frame and has been defined in eqn (4.2-4).

It is assumed that the squirrel-cage induction machine is supplied by a voltage-source inverter, as described in Section 4.1.1, and the stator currents cannot be impressed by fast current control loops. Thus to obtain the required reference voltages of the inverter, it is necessary to use the stator voltage equations.

It follows from eqn (4.2-7) that if a stator-flux-oriented control scheme for a squirrel-cage induction machine has to be obtained, the rotor currents have to be eliminated from the equations since these cannot be measured directly. However, it follows from eqn (4.2-2) that

$$\bar{i}_{r\psi_s} = |\bar{i}_{ms}| - \frac{L_s \bar{i}_{s\psi_s}}{L_m} \quad (4.2-9)$$

and substitution of eqn (4.2-9) into eqn (4.2-7) yields

$$\bar{u}_{s\psi_s} = R_s \bar{i}_{s\psi_s} + L_m \frac{d|\bar{i}_{ms}|}{dt} + j\omega_{ms} L_m |\bar{i}_{ms}|. \quad (4.2-10)$$

This is much simpler than the corresponding voltage equation expressed in the rotor-flux-oriented reference frame (eqn (4.1-6)). It should be noted that eqn (4.2-10) can also be obtained directly from eqn (2.1-148) by considering that  $\omega_{mg} = \omega_{ms}$  and  $\bar{\psi}_{ms} = L_m \bar{i}_{ms}$ . As a direct consequence of the selection of the stator-flux-oriented reference frame, there is no separate stator-leakage voltage component present in eqn (4.2-10). Furthermore, it does not contain the derivative of the stator-current space phasor, which is present when the rotor-flux-oriented reference frame is used. If the modulus of the stator magnetizing-current space phasor is constant, then eqn (4.2-10) takes an extremely simple form, which does not contain the derivative  $d|\bar{i}_{ms}|/dt$ . When eqn (4.2-10) is resolved into its two-axis components,

$$i_{sx} = \frac{u_{sx}}{R_s} - \frac{L_m}{R_s} \frac{d|\bar{i}_{ms}|}{dt} \quad (4.2-11)$$

$$i_{sy} = \frac{u_{sy}}{R_s} - \omega_{ms} L_m \frac{|\bar{i}_{ms}|}{R_s}. \quad (4.2-12)$$

These equations are much simpler than eqns (4.1-7) and (4.1-8). For stator-flux-oriented control,  $i_{sx}$  and  $i_{sy}$  have to be independently controlled. However,

it follows from eqn (4.2-12) that there is an unwanted coupling term and thus  $u_{sx}$  and  $u_{sy}$  cannot be considered as decoupled variables for the stator flux and electromagnetic torque. The stator current components  $i_{sx}$  and  $i_{sy}$  can only be independently controlled if eqns (4.2-11) and (4.2-12) are decoupled and the stator currents are indirectly controlled by controlling the terminal voltages of the induction machine. As in Section 4.1.1, it follows from eqns (4.2-11) and (4.2-12) that the required decoupling voltages are

$$\begin{aligned} u_{dx} &= 0 \\ u_{dy} &= \omega_{ms} L_m |\bar{i}_{ms}|. \end{aligned} \quad (4.2-13)$$

Thus a very simple decoupling circuit can be established, the inputs of which are  $\omega_{ms}$  and  $|\bar{i}_{ms}|$  and the output of which is  $u_{dy}$ . It follows from the simplicity of the stator voltage equations that when an induction machine is supplied by impressed stator voltages, the stator-flux-oriented control scheme will be simpler than the rotor-flux-oriented control scheme. When a squirrel-cage machine is supplied by a converter which functions as a current source, the stator equations can be omitted from the equations of the drive.

#### 4.2.3 ROTOR VOLTAGE EQUATIONS FOR THE SQUIRREL-CAGE INDUCTION MACHINE

The rotor voltage equations expressed in the stator-flux-oriented reference frame can be used to obtain the modulus and speed (or phase angle) of the stator flux-linkage space phasor (or stator magnetizing-current space phasor). The required flux model can be obtained by using the rotor voltage equations formulated in the stator-flux-oriented reference frame.

For this purpose, eqn (2.1-153) is used, which gives the space-phasor form of the rotor voltage equation in the general reference frame, but it is assumed that all the inductance parameters are constant. Thus in the stator-flux-oriented reference frame ( $\omega_g = \omega_{ms}$ ,  $\bar{u}_{rg} = \bar{u}_{r\psi s}$ ,  $\bar{i}_{sg} = \bar{i}_{s\psi s}$ ,  $\bar{i}_{rg} = \bar{i}_{r\psi s}$ ), this takes the form,

$$\bar{u}_{r\psi s} = R_r \bar{i}_{r\psi s} + L_r \frac{d\bar{i}_{r\psi s}}{dt} + L_m \frac{d\bar{i}_{s\psi s}}{dt} + j(\omega_{ms} - \omega_r)(L_r \bar{i}_{r\psi s} + L_m \bar{i}_{s\psi s}), \quad (4.2-14)$$

where  $\omega_r$  is the rotor speed and  $R_r$  and  $L_r$  are the rotor resistance and rotor self-inductance. Equation (4.2-14) contains the rotor-current space phasor, but since for a squirrel-cage machine this cannot be directly obtained, it is now eliminated. By the substitution of eqn (4.2-9) into eqn (4.2-14) and by considering that, since the rotor windings can be considered as short-circuited windings,  $\bar{u}_{r\psi s} = 0$ ,

$$0 = R_r \left[ |\bar{i}_{ms}| - \frac{L_s}{L_m} \bar{i}_{s\psi s} \right] + L_r \frac{d|\bar{i}_{ms}|}{dt} - \left( \frac{L'_s L_r}{L_m} \right) \frac{d\bar{i}_{s\psi s}}{dt} + j\omega_{sl} \left[ L_r |\bar{i}_{ms}| - \left( \frac{L'_s L_r}{L_m} \right) \bar{i}_{s\psi s} \right] \quad (4.2-15)$$

is obtained, where

$$\omega_{sl} = \omega_{ms} - \omega_r \quad (4.2-16)$$

is the angular slip frequency. This is equal to the first time derivative of the slip angle  $\theta_{sl}$ , which is equal to  $\rho_s - \theta_r$ , as shown in Fig. 4.25, and is the angle of the stator flux-linkage space phasor (or stator magnetizing-current space phasor) with respect to the real axis ( $r\alpha$ ) of the rotor reference frame. In eqn (4.2-15)  $L'_s$  is the transient stator inductance. It should be noted that eqn (4.2-15) is more complicated than the rotor voltage equation formulated in the rotor-flux-oriented reference frame (eqn (4.1-24)). This has the consequence that when the induction machine is supplied by impressed stator currents, the implementation of stator-flux-oriented control will be more complicated than the implementation of the rotor-flux-oriented control. Resolution of eqn (4.2-15) into its real- and imaginary-axis components yields

$$\frac{L_m}{L'_s} \frac{d|\bar{i}_{ms}|}{dt} + \frac{L_m}{L_s T'_r} |\bar{i}_{ms}| = \frac{di_{sx}}{dt} + \frac{i_{sx}}{T'_r} - \omega_{sl} i_{sy} \quad (4.2-17)$$

$$\omega_{sl} \left( \frac{L_m |\bar{i}_{ms}|}{L'_s} - i_{sx} \right) = \frac{di_{sy}}{dt} + \frac{i_{sy}}{T'_r}, \quad (4.2-18)$$

where  $T'_r$  is the transient rotor time constant.

For an induction machine with impressed stator currents eqns (4.2-17) and (4.2-18) have to be considered when stator-flux-oriented control is used. However, it follows from eqn (4.2-17) that there exists a coupling between the torque-producing stator current component  $i_{sy}$  and the stator magnetizing current. Therefore if there is a change in the torque-producing current, and if this is not followed by an appropriate change in  $i_{sx}$ , there will exist an unwanted transient in the stator magnetizing current. However, this undesirable coupling can be eliminated by the utilization of a decoupling circuit, as will now be described.

If the stator magnetizing current is regulated by a flux controller (as shown in Fig. 4.26), the input of which is the difference between the reference value ( $|\bar{i}_{msref}|$ ) and the actual value ( $|\bar{i}_{ms}|$ ) of the stator magnetizing current, and it is assumed that the output of this controller (which can be a PI controller) is the current  $\hat{i}_{sx}$ , then the required decoupling current  $i_{dx}$  has to be added to  $i_{sx}$  to yield the reference value of the stator current along the real axis of the stator-flux-oriented reference frame ( $i_{sxref}$ ). It follows that

$$i_{sx} = \hat{i}_{sx} + i_{dx} \quad (4.2-19)$$

and the substitution of eqn (4.2-19) into eqn (4.2-17) yields

$$\frac{L_m}{L'_s} \frac{d|\bar{i}_{ms}|}{dt} + \frac{L_m}{L_s T'_r} |\bar{i}_{ms}| = \frac{d\hat{i}_{sx}}{dt} + \frac{\hat{i}_{sx}}{T'_r} + \frac{di_{dx}}{dt} + \frac{i_{dx}}{T'_r} - \omega_{sl} i_{sy}. \quad (4.2-20)$$

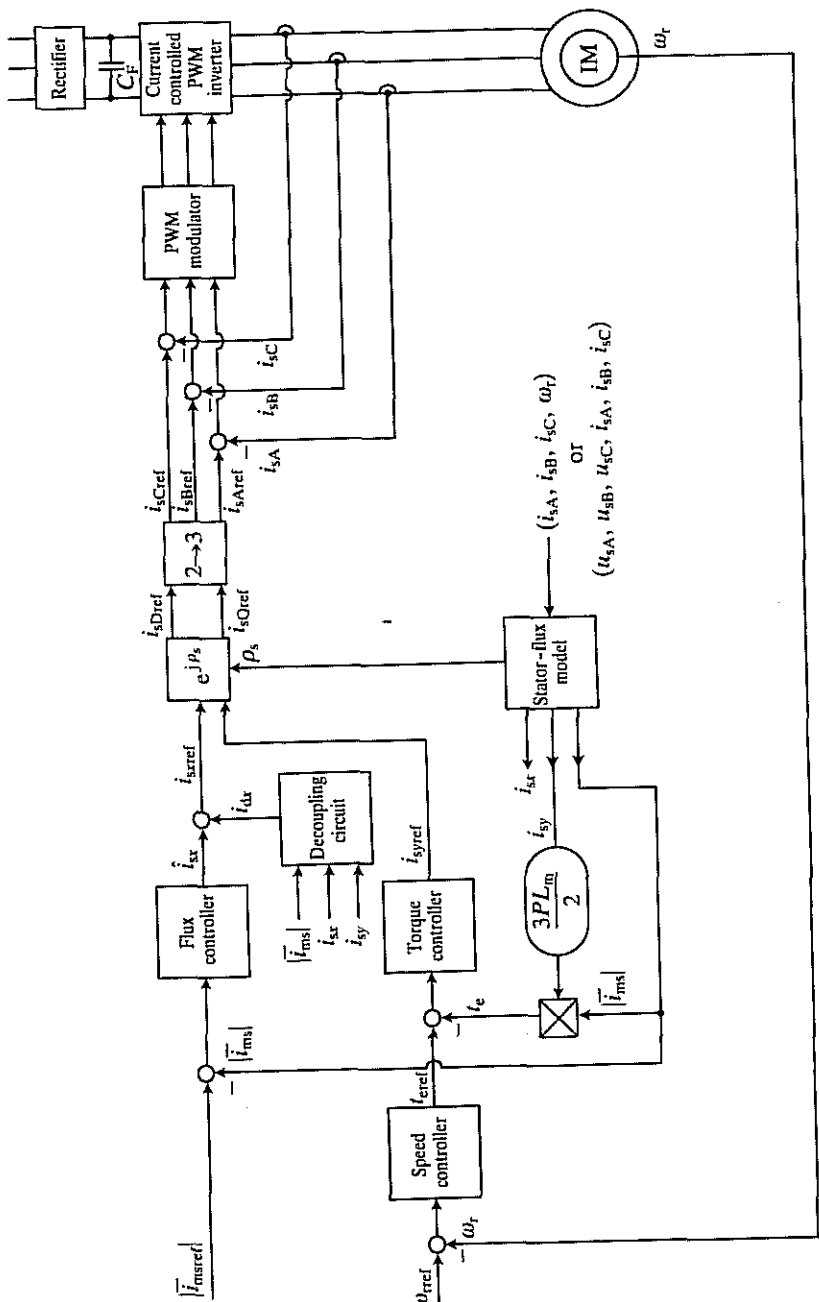


Fig. 4.26. Schematic of the stator-flux-oriented control of an induction machine with a current-controlled PWM inverter.

It follows from eqn (4.2-20) that  $|\bar{i}_{ms}|$  can be decoupled from  $i_{sy}$  if the three last terms on the right-hand side of eqn (4.2-20) are zero, i.e.

$$\left( p + \frac{1}{T'_r} \right) i_{dx} = \omega_{sl} i_{sy}, \quad (4.2-21)$$

where  $p = d/dt$ . Thus it follows from eqn (4.2-21) that the required current  $i_{dx}$  can be expressed as

$$i_{dx} = \omega_{sl} \frac{T'_r}{1 + T'_r p} i_{sy}. \quad (4.2-22)$$

In eqn (4.2-22) the angular slip frequency  $\omega_{sl}$  is present. This can be obtained by considering eqn (4.2-18). It follows from eqn (4.2-18) that

$$\omega_{sl} = \frac{(1 + T'_r p) L_s i_{sy}}{T_r (L_m |\bar{i}_{ms}| - L'_s i_{sx})}. \quad (4.2-23)$$

Equation (4.2-22), together with eqn (4.2-23), defines the required decoupling circuit. Thus when the correct machine parameters are used in these equations, the correct value of  $i_{sx}$  is obtained for a given value of  $i_{sy}$ , and thus  $|\bar{i}_{ms}|$  is not altered by any changes in the torque reference even during transient operation. By using the decoupling circuit defined by eqns (4.2-22) and (4.2-23), Fig. 4.26 shows as an example the schematic of the stator-flux-oriented control of an induction machine supplied by a current-regulated PWM inverter (which has also been used in the implementation shown in Fig. 4.14).

Since this scheme is similar to the one shown in Fig. 4.14 only the differences will be pointed out. The direct-axis stator reference current is obtained as the sum of  $i_{sx}$  (which is the output of the flux controller) and  $i_{dx}$ , which is the output of the decoupling circuit described above. A flux model is used to obtain the modulus ( $|\bar{i}_{ms}|$ ) and the space angle ( $\rho_s$ ) of the stator magnetizing-current space phasor. The torque-producing stator current component ( $i_{sy}$ ) is obtained from the two-axis stator currents of the stationary reference frame ( $i_{sD}, i_{sQ}$ ) by considering eqn (4.2-3). The flux model can use at its inputs the actual stator currents ( $i_{sA}, i_{sB}, i_{sC}$ ) and the monitored rotor speed ( $\omega_r$ ) and thus by considering eqns (4.2-16), (4.2-17), and (4.2-18) its outputs are  $i_{sy}$ ,  $|\bar{i}_{ms}|$ , and  $\omega_{ms}$ , and  $\rho_s$  is obtained by the integration of  $\omega_{ms}$ . There are several other alternatives and if, for example, the stator voltages and currents are monitored, it follows from eqn (2.1-24) that the space phasor of the stator flux linkages ( $\bar{\psi}_s$ ) can be obtained by the integration of  $\bar{u}_s - R_s \bar{i}_s$ , where  $\bar{u}_s$  and  $\bar{i}_s$  are the space phasors of the stator voltages and currents respectively in the stationary reference frame (in terms of their two-axis components  $\bar{u}_s = \bar{u}_{sD} + j\bar{u}_{sQ}$ , and  $\bar{i}_s = \bar{i}_{sD} + j\bar{i}_{sQ}$ ). When  $\bar{\psi}_s$  is divided by  $L_m$ , the space phasor of the stator magnetizing current in the stationary reference frame is obtained, and its modulus is equal to  $|\bar{i}_{ms}|$  and its phase angle is equal to  $\rho_s$ . However, when this technique is used, as pointed out previously, at lower stator frequencies the stator resistance will dominate and accurate ohmic voltage-drop compensation must be performed. Figure 4.27 shows this type of solution, but it

should be noted that as shown in Section 3.1.3.1, in practice only two stator line voltages are required (e.g.  $u_{AC}$  and  $u_{BA}$ ), and thus the direct- and quadrature-axis stator voltages can be obtained by using  $u_{sD} = (1/3)(u_{BA} - u_{AC})$  and  $u_{sQ} = -(1/\sqrt{3})(u_{AC} + u_{BA})$ .

It has also been shown in Section 3.1.3.1 that the direct- and quadrature-axis stator currents  $i_{sD}$  and  $i_{sQ}$  can be obtained by using only two stator line currents (e.g.  $i_{sA}$  and  $i_{sB}$ ) if  $i_{sA} + i_{sB} + i_{sC} = 0$  holds, and in this case  $i_{sD} = i_{sA}$  and  $i_{sQ} = (1/\sqrt{3})(i_{sA} + 2i_{sB})$  are obtained. Further details on other aspects of this scheme, including drift compensation, can be found in Sections 3.1.3.1 and 4.1.1.4, where improved schemes are also presented and where the reconstruction of the stator voltages from the monitored d.c. link voltage and inverter switching states is also discussed. For example, it should be noted that, as discussed in Section 4.1.1.4 in connection to Fig. 4.9(b), it is also possible to utilize directly the stator voltage equations in the stator-flux-oriented reference frame (eqns (4.2-11) and (4.2-12)). It follows from eqn (4.2-11) that the rate of change of the stator flux modulus is  $u_{sx} - R_s i_{sx}$  and from eqn (4.2-12) the speed of the stator flux-linkage space vector ( $\omega_{ms}$ ) is obtained as  $\omega_{ms} = (u_{sy} - R_s i_{sy})/|\bar{\psi}_s|$ . These equations are also used in Fig. 4.28.

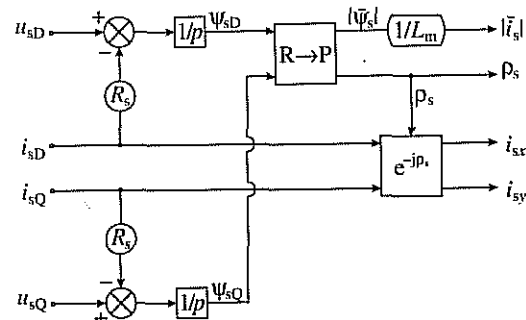


Fig. 4.27. Flux model (in stationary reference frame) and transformed stator currents.

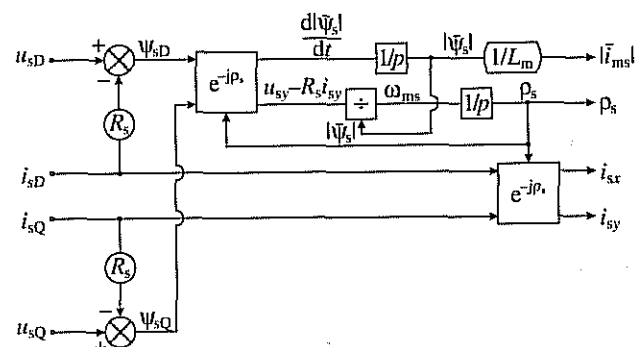


Fig. 4.28. Flux model (in stator-flux-oriented reference frame) and transformed stator currents.

In contrast to the scheme of Fig. 4.27, where open-loop integrations are present, in Fig. 4.28 closed-loop integrations are performed, and at low frequency this reduces the integrator drifts.

If the stator flux-linkage components are accurately estimated, then they can also be used for the estimation of the rotor speed in a speed-sensorless drive. For example, the scheme shown in Fig. 4.9(c) can also be used in a speed-sensorless vector-controlled drive even at low frequencies (see also Section 4.5.3.1).

#### 4.2.4 STATOR VOLTAGE EQUATIONS FOR THE DOUBLY FED INDUCTION MACHINE

For a doubly fed machine, it is useful to express  $\bar{i}_{s\psi s}$  in terms of  $|\bar{i}_{ms}|$  and  $\bar{i}_{r\psi s}$ . Thus it follows from eqn (4.2-2) that

$$\bar{i}_{s\psi s} = \frac{L_m}{L_s} (|\bar{i}_{ms}| - \bar{i}_{r\psi s}) \quad (4.2-24)$$

and when this is substituted into eqn (4.2-7),

$$\bar{u}_{s\psi s} = \frac{R_s L_m}{L_s} (|\bar{i}_{ms}| - \bar{i}_{r\psi s}) + \frac{L_m d|\bar{i}_{ms}|}{dt} + j\omega_{ms} L_m |\bar{i}_{ms}|. \quad (4.2-25)$$

This can be put into the form

$$T_s \frac{d|\bar{i}_{ms}|}{dt} + |\bar{i}_{ms}|(1 + j\omega_{ms} T_s) = \bar{u}_{s\psi s} \frac{L_s}{R_s L_m} + \bar{i}_{r\psi s}, \quad (4.2-26)$$

where  $T_s = L_s/R_s$  is the stator time constant. By considering the definitions of the stator-voltage, stator-current, and rotor-current space phasors in terms of their two-axis components established in the stator-flux-oriented reference frame (eqns (4.2-3), (4.2-4), and (4.2-8)), resolution of eqn (4.2-26) into its real- and imaginary-axis components yields

$$T_s \frac{d|\bar{i}_{ms}|}{dt} + |\bar{i}_{ms}| = \frac{L_s}{R_s L_m} u_{sx} + i_{rx} \quad (4.2-27)$$

$$\omega_{ms} T_s |\bar{i}_{ms}| = \frac{L_s}{R_s L_m} u_{sy} + i_{ry}. \quad (4.2-28)$$

For the doubly fed induction machine, the stator voltage components can be obtained as follows. By assuming a sinusoidal symmetrical three-phase supply voltage system, with frequency  $\omega_1$ , the stator-voltage space phasor in the stationary reference frame can be expressed as

$$\bar{u}_s = \sqrt{2} U_s e^{j\omega_1 t}, \quad (4.2-29)$$

where  $U_s$  is the r.m.s. value of the line-to-neutral voltages and  $t$  denotes time. Thus substitution of eqn (4.2-29) into eqn (4.2-8) gives

$$\bar{u}_{s\psi s} = \sqrt{2} U_s e^{j(\omega_1 t - \rho_s)} = u_{sx} + j u_{sy} \quad (4.2-30)$$

and thus

$$u_{sx} = \sqrt{2}U_s \cos(\omega_1 t - \rho_s) \quad (4.2-31)$$

$$u_{sy} = \sqrt{2}U_s \sin(\omega_1 t - \rho_s). \quad (4.2-32)$$

Compared with eqns (4.2-11) and (4.2-12), which contain the stator currents  $i_{sx}$ ,  $i_{sy}$ , eqns (4.2-27) and (4.2-28) contain the rotor currents  $i_{rx}$ ,  $i_{ry}$  because the rotor currents are subjected to stator-flux-oriented control. As mentioned earlier, two implementations will be discussed, where there is a current-controlled cycloconverter in the rotor of the slip-ring induction machine and where there is a static converter cascade in the rotor.

#### 4.2.5 ROTOR VOLTAGE EQUATIONS FOR THE DOUBLY FED INDUCTION MACHINE

By substitution of eqn (4.2-24) into eqn (4.2-14), the space-phasor form of the rotor voltage equation in the stator-flux-oriented reference frame is

$$\bar{u}_{r\psi s} = (R_r + L'_r p) \bar{i}_{r\psi s} + \frac{L_m^2}{L_s} p |\bar{i}_{ms}| + j \omega_{sl} \left[ \frac{L_m^2}{L_s} |\bar{i}_{ms}| + L'_r \bar{i}_{r\psi s} \right], \quad (4.2-33)$$

where it follows from eqn (4.2-16) that  $\omega_{sl} = \omega_{ms} - \omega_r$  is the angular slip frequency,  $\omega_{ms}$  is the speed of the reference frame, and  $\omega_r$  is the rotor speed. Equation (4.2-33) can be resolved into its direct- (x) and quadrature-axis (y) components and thus

$$T'_r \frac{di_{rx}}{dt} + i_{rx} = \frac{u_{rx}}{R_r} + \omega_{sl} T'_r i_{ry} - (T_r - T'_r) \frac{d|\bar{i}_{ms}|}{dt} \quad (4.2-34)$$

and

$$T'_r \frac{di_{ry}}{dt} + i_{ry} = \frac{u_{ry}}{R_r} - \omega_{sl} T'_r i_{rx} - \omega_{sl} (T_r - T'_r) |\bar{i}_{ms}|. \quad (4.2-35)$$

These equations are very similar to eqns (4.1-7) and (4.1-8) and they can be used to obtain the implementation of stator-flux-oriented control if the rotor currents are not impressed. When these two equations are compared with eqns (4.1-7) and (4.1-8), it can be seen that instead of the stator current components, the rotor current components are now present and the rotor magnetizing-current space phasor is replaced by the stator magnetizing-current space phasor. Furthermore, the stator voltage components are replaced by the rotor voltage components, the stator resistance is replaced by the rotor resistance, the speed of the rotor magnetizing-current space phasor is replaced by the speed of the stator magnetizing-flux-space phasor, and finally the stator time constant and stator transient time constant are replaced by the rotor time constant and rotor transient time constant respectively. It also follows from eqns (4.2-34) and (4.2-35) that there are unwanted coupling terms between the rotor circuits along the

x and y axes. These can be eliminated by utilizing the following decoupling voltage components, which are obtained by considering the rotational voltages in eqns (4.2-34) and (4.2-35) and assuming constant-stator-flux operation ( $|\bar{i}_{ms}| = \text{constant}$ ):

$$u_{dxr} = -\omega_{sl} L'_r i_{ry} \quad (4.2-36)$$

$$u_{dry} = \omega_{sl} L'_r i_{rx} + \omega_{sl} (L_r - L'_r) |\bar{i}_{ms}|. \quad (4.2-37)$$

These have to be added to the outputs of the current controllers which control the rotor currents  $i_{rx}$  and  $i_{ry}$ .

With impressed rotor currents it is not necessary to consider the rotor voltage equations but, to achieve improved dynamic performance, appropriate terms must be added to the outputs of the rotor current controllers, which in the case of  $|\bar{i}_{ms}| = \text{constant}$  compensate for the last term in eqn (4.2-35), which acts as a disturbance for rotor current controllers. Thus it follows from eqn (4.2-35) that in the stator-flux-oriented reference frame the necessary feedforward signal takes the form

$$\frac{u_{iy}}{R_r} = \omega_{sl} (T_r - T'_r) |\bar{i}_{ms}| \quad (4.2-38)$$

or, in space-phasor form,

$$\frac{\bar{u}_{i\psi s}}{R_r} = \frac{j u_{iy}}{R_r} = j \omega_{sl} (T_r - T'_r) |\bar{i}_{ms}|. \quad (4.2-39)$$

By considering Fig. 4.25, according to which the angle between the real axis of the stator-flux-oriented reference frame and the real axis of the reference frame fixed to the rotor is  $(\rho_s - \theta_r)$ , in the reference frame fixed to the rotor,  $\bar{u}_{i\psi s}/R_r$  can be expressed as

$$\frac{\bar{u}_i}{R_r} = \bar{u}_{i\psi s} \frac{e^{j(\rho_s - \theta_r)}}{R_r} = j \omega_{sl} (T_r - T'_r) |\bar{i}_{ms}| e^{j(\rho_s - \theta_r)} = i_x + j i_y, \quad (4.2-40)$$

where  $\bar{u}_i$  is the space phasor of the induced voltages in the rotor reference frame, and  $i_x$  and  $i_y$  are the required currents which have to be used as feedforward signals. Equation (4.2-40) also follows by considering the transformation of a space-phasor quantity from its natural reference frame into the general reference frame. Thus from eqn (2.1-143), the induced-voltage space phasor in the rotor reference frame ( $\bar{u}_i$ ) can be expressed in terms of the induced-voltage space phasor in the general reference frame as  $\bar{u}_i = \bar{u}_{ig} e^{j(\theta_g - \theta_r)}$ . Thus when, instead of the general reference frame, the stator-flux-oriented reference frame is used,  $\bar{u}_{ig} = \bar{u}_{i\psi s}$ ,  $\theta_g = \rho_s$ , and finally  $\bar{u}_i = \bar{u}_{i\psi s} e^{j(\rho_s - \theta_r)}$  is obtained, which agrees with the induced voltage space phasor used in eqn (4.2-40). Equation (4.2-40) will be utilized in the implementations discussed in the following two sections. When the currents  $i_x$  and  $i_y$  are added to the rotor currents  $i_{raref}$ ,  $i_{rpref}$ , which are the reference values of the rotor currents expressed in the rotor reference frame, then the effects of the

rotational voltages in the rotor windings due to the stator flux are cancelled (the stator flux has been assumed to be constant) and improved dynamic performance is obtained.

#### 4.2.6 CONTROL OF THE DOUBLY FED INDUCTION MACHINE WITH IMPRESSED ROTOR CURRENTS

First the stator-flux-oriented control of a doubly fed induction machine employing a cycloconverter in the rotor circuit is described. This is followed by a discussion on the stator-flux-oriented control of the doubly fed machine employing a converter cascade in the rotor.

##### 4.2.6.1 Control of the induction machine with a current-controlled cycloconverter in the rotor circuit

In many countries, pumps, fans, and blowers can be responsible for approximately half the electricity consumed by industry. Pump drives are used, for example, in sewage treatment, water supply applications, circulating water pumps, etc., and fans are used for mine ventilation, wind-tunnel applications, etc. These can represent very large loads—over 10 MW being common—and there is an increasing trend to use variable-speed drives in an attempt to improve the efficiency. In these applications the load torque is proportional to the square of the speed and there is a restricted range of speed control. For such applications the doubly fed slip-ring induction machine with its stator connected to a constant-frequency power supply and its rotor connected to a static converter represents an ideal solution. It is one of the most important features of a slip recovery system that, if the application requires only limited range of speed control (in pump and fan drives only a speed variation of 10–30% is usually required), then the control system has to be rated only for slip power, which is only a fraction of the stator power. The resulting reduction in the converter costs makes the slip recovery systems very attractive in all applications where only a limited speed-range is required and where energy saving is an important factor.

In this section a current-controlled cycloconverter is used in the rotor. The cycloconverter used is similar to that described in Section 3.2.1 (also used in Section 4.1.2), and it consists of three sets of anti-parallel six-pulse thyristor bridges without circulating currents. The rotor currents of the slip-ring machine are separately controlled by fast current loops.

If sinusoidal stator currents and the decoupling of the active and reactive stator power is required, it is useful to employ stator-flux-oriented control which ensures the required decoupling by appropriate control of the amplitude and phase angle of the rotor-current space phasor. The application of stator-flux-oriented control also has the advantage of stabilizing the drive. It should be noted that another area of application for a doubly fed induction machine with stator-flux-oriented control can be in large wind power stations, where wind gusts can cause power and torque fluctuations which can result in unwanted mechanical stresses on the

mechanical transmission system (shaft, gears) and can cause undesirable power fluctuations. When the doubly fed machine is used with a restricted speed range, the wind energy can be temporarily stored in the inertia of the rotor blades and the undesirable effects (power fluctuations, mechanical stresses) are reduced.

Figure 4.29 shows the schematic of the stator-flux-oriented control of an induction machine with a current-controlled cycloconverter in the rotor. The induction machine can operate as a motor or a generator in the supersynchronous and subsynchronous speed ranges with lagging or leading stator currents.

In Fig. 4.29 the input signals to the control system are the monitored stator and rotor currents, the monitored rotor angle ( $\theta_r$ ), and the active and reactive stator powers, respectively  $P_s$  and  $Q_s$ . The cycloconverter is connected to the grid via a three-phase transformer. The turns ratio of the transformer can be selected to minimize the voltage rating of the cycloconverter. The drive can be started in several ways. One possibility is to employ rotor resistances and to short-circuit them sequentially as the machine comes up to the operating speed when the cycloconverter is switched on. It is also possible to short-circuit the stator and to supply the rotor from the cycloconverter (which is connected to the grid) and which operates as a variable-frequency power supply. This arrangement corresponds to an inverted induction machine. The machine will accelerate and at approximately half speed the stator is connected to the grid. The rotor frequency will be approximately one half of the supply frequency and the motor can accelerate further.

It will now be shown that in the stator-flux-oriented system, the real- and imaginary-axis components of the rotor currents ( $i_{rx}, i_{ry}$ ) correspond directly to

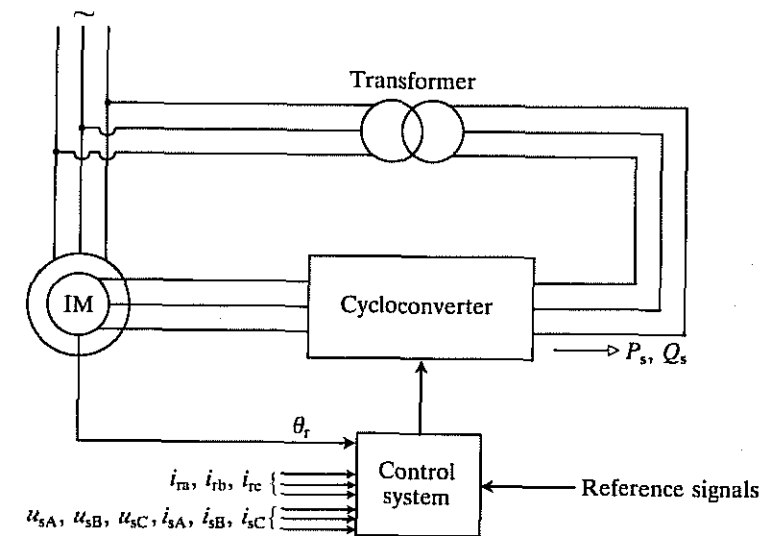


Fig. 4.29. Simplified schematic of the stator-flux-oriented control of an induction machine with a current-controlled cycloconverter in the rotor.

the two-axis stator currents ( $i_{sx}, i_{sy}$ ) expressed in the stator-flux-oriented reference frame. Thus control of the  $i_{rx}$  current can be used to maintain the reactive stator current ( $i_{sx}$ ) at a fixed value (or at a value dependent on the voltage) and the current  $i_{ry}$  can be used to control the electromagnetic torque.

By resolving eqn (4.2-24) into its two-axis components, it follows that the stator current components in the stator-flux-oriented reference frame ( $i_{sx}, i_{sy}$ ) can be expressed in terms of the rotor current components established in the same reference frame ( $i_{rx}, i_{ry}$ ) as follows:

$$i_{sy} = -i_{ry} \frac{L_m}{L_s}, \quad (4.2-41)$$

which is the same as eqn (4.2-5) but is repeated here for convenience, and

$$i_{sx} = (|\bar{i}_{ms}| - i_{ry}) \frac{L_m}{L_s}. \quad (4.2-42)$$

It follows from eqn (4.2-41) that the quadrature-axis rotor current ( $i_{ry}$ ) is proportional to the torque-producing (active) stator current component ( $i_{sy}$ ). However, in eqn (4.2-42) the stator magnetizing-current space phasor is also present, and this depends on the stator voltage. This dependency will now be obtained. For this purpose, it is assumed that the stator resistance ( $R_s$ ) of the induction machine can be neglected. This is usually justified in machines with a rating over 10 kW. Furthermore it is assumed that the frequency of the power supply on the stator is constant,  $\omega_1 = \text{constant}$ . In the steady state the modulus of the stator magnetizing current [which has been defined in eqn (4.2-2)] is constant ( $|\bar{i}_{ms}| = \text{constant}$ ) and the speed of the stator magnetizing-current space phasor ( $\omega_{ms} = d\rho_s/dt$ , where  $\rho_s$  is the angle of the stator magnetizing-current space phasor with respect to the real axis of the stationary reference frame and is shown in Fig. 4.25) is also constant.

Thus it follows from eqn (4.2-25) that

$$|\bar{u}_s| = \omega_1 L_m |\bar{i}_{ms}|, \quad (4.2-43)$$

where  $|\bar{u}_s|$  is the modulus of the stator-voltage space phasor and from eqn (4.2-30)  $|\bar{u}_s| = \sqrt{2} U_s$  is obtained. It follows from eqn (4.2-43) that the modulus of the stator magnetizing current is

$$|\bar{i}_{ms}| = \frac{|\bar{u}_s|}{\omega_1 L_m}, \quad (4.2-44)$$

which is an expected result since a steady state has been assumed together with negligible stator resistance. It should be noted that the same result follows from eqns (4.2-27)–(4.2-32), which under the same assumptions yield

$$u_{sx} = 0 \quad u_{sy} = |\bar{u}_s| \quad |\bar{i}_{ms}| = \frac{u_{sy}}{L_m \omega_1}. \quad (4.2-45)$$

Thus from eqns (4.2-42) and (4.2-44),

$$i_{sx} = (|\bar{u}_s|/\omega_1 - L_m i_{rx})/L_s, \quad (4.2-46)$$

from which it follows that, since the machine parameters ( $L_s, L_m$ ) and also  $|\bar{u}_s|$  and  $\omega_1$  are constant, the direct-axis (reactive) stator currents ( $i_{sx}$ ) can be controlled by the direct-axis rotor current ( $i_{rx}$ ). These results will be used in the implementation of the stator-flux-oriented control of the doubly fed machine shown in Fig. 4.30.

As in eqn (2.1-87), the stator active power can be defined as

$$P_s = \frac{3}{2} \operatorname{Re}(\bar{u}_{s\psi s} \bar{i}_{s\psi s}) = \frac{3}{2}(u_{sy} i_{sx} + u_{sx} i_{sy}), \quad (4.2-47)$$

and the stator reactive power as

$$Q_s = \frac{3}{2} \operatorname{Im}(\bar{u}_{s\psi s} \bar{i}_{s\psi s}) = \frac{3}{2}(u_{sy} i_{sx} - u_{sx} i_{sy}). \quad (4.2-48)$$

From eqn (4.2-45)  $u_{sx} = 0$  and  $u_{sy} = |\bar{u}_s|$ , and it follows from eqns (4.2-47) and (4.2-48) that

$$P_s = \frac{3}{2} |\bar{u}_s| i_{sy} \quad (4.2-49)$$

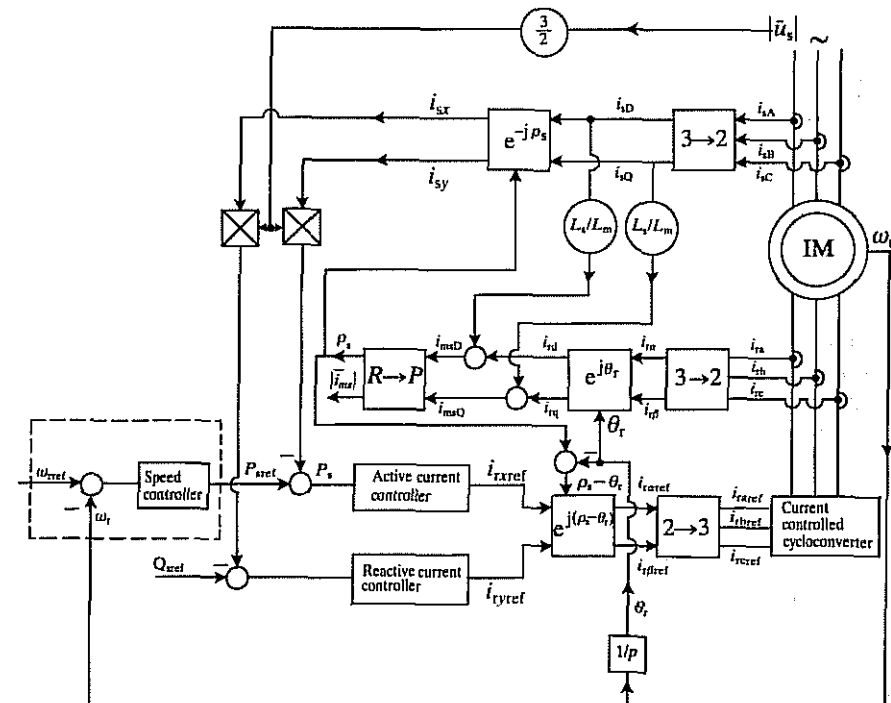


Fig. 4.30. Schematic of the stator-flux-oriented control of a doubly-fed induction machine with a current-controlled cycloconverter in the rotor.

and, since  $|\bar{u}_s|$  is a constant,  $P_s$  is equal to a constant times the torque-producing current, thus it also follows that

$$Q_s = \frac{3}{2} |\bar{u}_s| i_{sx} \quad (4.2-50)$$

and this is equal to a constant times the stator reactive current. Equations (4.2-49) and (4.2-50) are utilized in the implementation shown in Fig. 4.30. The modulus of the stator-voltage space phasor can be obtained from the monitored values of the stator voltages.

In Fig. 4.30 the space angle of the stator magnetizing-current space phasor ( $\rho_s$ ) is obtained from the direct-axis ( $i_{msD}$ ) and quadrature-axis ( $i_{msQ}$ ) components of the stator magnetizing-current space phasor expressed in the stationary reference frame, by utilizing a rectangular-to-polar converter. This can be obtained by considering eqns (4.2-2), (4.2-3), and (4.2-4) and thus

$$\begin{aligned} \bar{i}_{ms} &= i_{msD} + j i_{msQ} = \frac{L_s}{L_m} (i_{sD} + j i_{sQ}) + (i_{rd} + j i_{rq}) e^{j\theta_r} \\ &= \frac{L_s}{L_m} (i_{sD} + j i_{sQ}) + (i_{rd} + j i_{rq}) = |\bar{i}_{ms}| e^{j\rho_s}, \end{aligned} \quad (4.2-51)$$

where  $i_{sD}$ ,  $i_{sQ}$  are the stator current components in the stationary reference frame and are obtained from the monitored three-phase stator currents ( $i_{sA}$ ,  $i_{sB}$ ,  $i_{sC}$ ) by the application of the three-phase to two-phase transformation. The two-axis components of the rotor currents in the rotor reference frame ( $i_{rd}$ ,  $i_{rq}$ ) are obtained from the monitored rotor currents ( $i_{ra}$ ,  $i_{rb}$ ,  $i_{rc}$ ) by the application of the three-phase to two-phase transformation. The direct- and quadrature-axis rotor currents in the stator reference frame ( $i_{rd}$ ,  $i_{rq}$ ) are obtained from the rotor currents in the rotor reference frame ( $i_{ra}$ ,  $i_{rb}$ ) by the application of the transformation  $e^{j\theta_r}$  where  $\theta_r$  is the rotor angle. It should be noted that eqn (4.2-51) can be obtained directly from eqn (2.1-128), which defines the stator flux-linkage space phasor in the stationary reference frame, if it is divided by the magnetizing inductance. It is also possible to obtain  $i_{msD}$ ,  $i_{msQ}$  by using monitored stator voltages and currents. For this purpose  $i_{msD} + j i_{msQ} = (\psi_{sD} + j \psi_{sQ})/L_m$  could be utilized, where  $\psi_{sD} + j \psi_{sQ}$  can be obtained by the integration of  $(u_{sD} + j u_{sQ}) - R_s(i_{sD} + j i_{sQ})$ , where  $R_s$  is the stator resistance and  $u_{sD}$ ,  $u_{sQ}$  are the two-axis components of the stator voltages in the stator reference frame.

In Fig. 4.30 the stator currents  $i_{sx}$ ,  $i_{sy}$  are obtained from  $i_{sD}$ ,  $i_{sQ}$  by utilizing eqn (4.2-3). The difference between the reference and actual values of the stator active power is the input to the active current controller, which is a PI controller and the output of which is the direct-axis reference rotor current component established in the stator-flux-oriented reference frame ( $i_{rxref}$ ). Similarly, the reference value of the stator active power is compared with its actual value and their difference serves as the input to the reactive current controller, also a PI controller, and the output of which is  $i_{ryref}$ . The currents  $i_{rxref}$  and  $i_{ryref}$  are transformed into the two-axis rotor current references in the rotor reference frame  $i_{raref}$ ,  $i_{rbref}$  by using eqn (4.2-4). Finally by using the two-phase to three-phase

transformation, these are transformed into the three-phase rotor current references ( $i_{raref}$ ,  $i_{rbref}$ ,  $i_{rcref}$ ), which are required to control the cycloconverter.

It is also possible to implement a speed control loop, as shown in Fig. 4.30. In this case the output of the speed controller yields the reference value of the stator active power. To achieve improved dynamic performance, the currents  $i_x$  and  $i_y$ , defined in eqn (4.2-40), should be added to the currents  $i_{raref}$  and  $i_{rbref}$  respectively, since then the effects of the voltage induced in the  $y$ -axis rotor winding due to the stator flux are cancelled. However, the same effect can be achieved by adding the current defined in eqn (4.2-38) to the reference current  $i_{ryref}$ .

#### 4.2.6.2 Control of the induction machine with a static converter cascade in the rotor

It is possible to implement stator-flux-oriented control of a doubly fed induction machine with a static converter cascade in the rotor. This is similar to the control scheme described in Fig. 4.23, but there rotor-flux-oriented control was employed. Figure 4.31 shows the schematic of the drive system.

In the implementation shown in Fig. 4.31 a force-commutated thyristor converter is connected to the slip rings of the induction machine and this is connected via a d.c. link reactor to a naturally commutated controlled-thyristor bridge converter (a special form of static Scherbius cascade). Thus slip power can flow in both directions and the speed of the induction machine can be controlled in the supersynchronous and subsynchronous speed ranges. If the rotor-side converter was a line-commutated bridge converter, near to synchronous speed, when the a.c. voltage available to commutate this converter is small, the commutating ability of this converter would be lost. It is for this reason that a force-commutated rotor-side converter is used in the implementation shown in Fig. 4.31.

It follows from eqn (4.2-6) that in the stator-flux-oriented reference frame, if the stator magnetizing current  $|\bar{i}_{ms}|$  is constant, the electromagnetic torque of the doubly fed induction machine is proportional to the quadrature-axis rotor current component ( $i_{ry}$ ) and the torque can be controlled in the same way as for a separately excited d.c. machine where there is independent control of the excitation flux and the field current. For convenience eqn (4.2-6) is repeated here in a slightly different form,

$$t_e = c |\bar{i}_{ms}| i_{ry} = c |\bar{i}_{ms}| |\bar{i}_r| \sin(\alpha_r + \theta_r - \rho_s), \quad (4.2-52)$$

where  $c = -3L_m^2/(2L_s)$ ,  $|\bar{i}_r|$  is the modulus of the rotor-current space phasor and the various angles are shown in Fig. 4.25. Thus the angle  $\phi_r = (\alpha_r + \theta_r - \rho_s)$  is the angle of the rotor-current space phasor with respect to the real axis of the stator-flux-oriented reference frame (torque angle). In Fig. 4.31 the modulus of the rotor-current space phasor is controlled by the commutated converter and the angle  $\phi_r$  is controlled by the machine-side converter.

In Fig. 4.31 the line-side converter is controlled by utilizing the closed-loop control of the d.c. link current, where the difference between the reference d.c. link current and the actual d.c. link current is fed into a PI controller. The torque

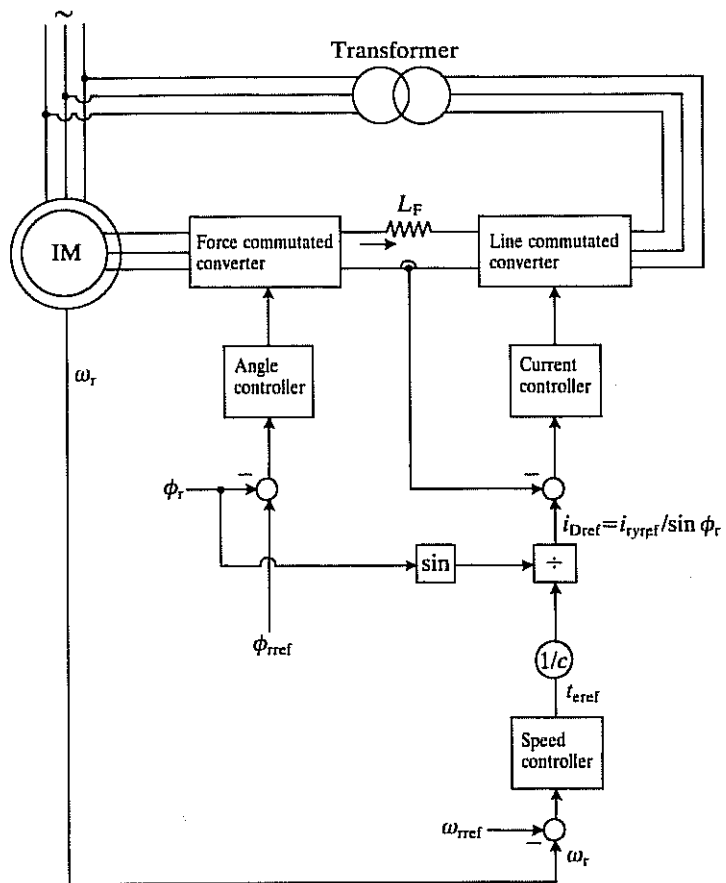


Fig. 4.31. Schematic of the stator-flux-oriented control of a doubly-fed induction machine with a static converter cascade in the rotor.

reference ( $t_{\text{ref}}$ ) is used to obtain the reference value of the d.c. link current ( $i_{\text{Dref}}$ ) and the torque reference appears as the output of the speed controller, also a PI controller, and the input of which is the difference between the reference rotor speed ( $\omega_{\text{ref}}$ ) and the monitored rotor speed ( $\omega_r$ ). The reference value  $i_{\text{Dref}}$  is obtained as  $i_{\text{Tyref}}/\sin \phi_r$ .

The rotor-side converter is controlled by utilizing the closed-loop control of the torque angle. For this purpose an angle controller is used, also a PI controller, the input of which is the difference between the reference ( $\phi_{\text{ref}}$ ) and the actual ( $\phi_r$ ) value of the torque angle.

It is possible to obtain the torque angle in several ways, and a method which does not utilize the stator voltages is now described. It has been shown that the torque angle is a function of three angles,  $\phi_r = \alpha_r + \theta_r - \rho_s$ . These can be obtained

as follows. If eqn (4.2-51) is utilized, then the angle  $\rho_s$  can be obtained by monitoring the stator and rotor currents and the rotor angle, as shown in Fig. 4.30, and during the process of the determination of the angle  $\rho_s$  the rotor current components established in the rotor reference frame ( $i_{rz}$  and  $i_{ry}$ ) are also obtained. Thus the angle  $\alpha_r$ , which according to Fig. 4.25 is the angle of the rotor-current space phasor with respect to the real axis of the rotor reference frame, can be obtained if these two currents are inputs to a rectangular-to-polar converter. Finally, the rotor angle ( $\theta_r$ ) can be obtained by direct measurement.

### 4.3 Magnetizing-flux-oriented control of induction machines

In this part of the chapter the magnetizing-flux-oriented control of induction machines will be discussed. The main assumptions are the same as those used in connection with rotor-flux-oriented control and stator-flux-oriented control of induction machines, and in particular the effects of magnetic saturation are neglected. Because of the similarity between magnetizing-flux-oriented control and stator- and rotor-flux-oriented control, (see Section 4.2.4.2), magnetizing-flux-oriented control will only be described briefly. However, it will be shown how this technique can be used in the case of a double-cage induction machine, whose space-phasor model will also be developed.

#### 4.3.1 EXPRESSION FOR THE ELECTROMAGNETIC TORQUE

From the results presented in Section 2.1.8, it follows that the electromagnetic torque produced by an induction machine is proportional to the product of the modulus of the magnetizing-current space phasor ( $|\bar{i}_{\text{mm}}|$ ) and the torque-producing stator current component ( $i_{\text{sy}}$ ), and the torque can be controlled by the independent control of these two current components. It follows from Section 2.1.8 and also from Fig. 4.32 that in the magnetizing-flux-oriented reference frame  $|\bar{i}_{\text{mm}}| = i_{\text{mx}}$ , where  $i_{\text{mx}}$  is the direct-axis component of the magnetizing flux-linkage space phasor in the magnetizing-flux-oriented reference frame.

Thus from eqns (2.1-186) and the relationship  $|\bar{i}_{\text{mm}}| = i_{\text{mx}}$ , it follows that the electromagnetic torque can be expressed as

$$t_e = \frac{3}{2} P L_m i_{\text{mx}} i_{\text{sy}} = \frac{3}{2} P L_m |\bar{i}_{\text{mm}}| i_{\text{sy}}, \quad (4.3-1)$$

where  $P$  is the number of pole pairs and  $L_m$  is the magnetizing inductance of the machine. In eqn (4.3-1) the magnetizing-current space phasor can be expressed in terms of the stator- and rotor-current space phasors in the magnetizing-flux-oriented reference frame  $\bar{i}_{\text{sy,m}}$ ,  $\bar{i}_{\text{ry,m}}$ , which for simplicity are denoted by  $\bar{i}_{\text{sm}}$  and  $\bar{i}_{\text{rm}}$ , as follows, if eqns (2.1-181), (2.1-184), and (2.1-185) are considered,

$$|\bar{i}_{\text{mm}}| = \bar{i}_{\text{sm}} + \bar{i}_{\text{rm}} = i_{\text{sx}} + j i_{\text{sy}} + i_{\text{rx}} + j i_{\text{ry}}, \quad (4.3-2)$$

where  $i_{\text{sx}}$  and  $i_{\text{sy}}$  are the direct- and quadrature-axis components of the stator currents in the magnetizing-flux-oriented reference frame and they are also shown

in Fig. 4.32.  $i_{rx}$  and  $i_{ry}$  are the direct- and quadrature-axis components of the rotor currents in the magnetizing-flux-oriented reference frame. It should be noted that the space phasor of the stator currents in the magnetizing-flux-oriented reference frame ( $\bar{i}_{sm}$ ) can be expressed as follows, if eqn (2.1-181) is considered,

$$\bar{i}_{sm} = \bar{i}_s e^{-j\mu_m} = (i_{sd} + j i_{sq}) e^{-j\mu_m} = i_{sx} + j i_{sy}, \quad (4.3-3)$$

where  $\bar{i}_s$  is the space phasor of the stator currents in the stationary reference frame,  $i_{sd}$  and  $i_{sq}$  are its two-axis components in the same reference frame, and  $\mu_m$  is the angle of the magnetizing-current (or magnetizing flux-linkage) space phasor with respect to the real axis of the stationary reference frame, as shown in Fig. 4.32. Similarly, the space phasor of the rotor currents in the magnetizing-flux-oriented reference frame can be expressed as follows, if eqn (2.1-185) is considered,

$$\bar{i}_{rm} = \bar{i}_r e^{-j(\mu_m - \theta_r)} = (i_{rx} + j i_{r\beta}) e^{-j(\mu_m - \theta_r)} = i_{rx} + j i_{ry}. \quad (4.3-4)$$

In eqn (4.3-4)  $\bar{i}_r$  is the space phasor of the rotor currents in the reference frame fixed to the rotor,  $i_{rx}$  and  $i_{r\beta}$  are its two-axis components in the rotor reference frame, and  $\theta_r$  is the rotor angle, also shown in Fig. 4.32.

If the induction machine is supplied by impressed stator voltages or currents, eqn (4.3-1) is utilized when the magnetizing-flux-oriented control scheme is developed, but for a doubly fed induction machine, as in Section 4.2.1, the expression for the torque is put into a form which contains the rotor currents. Thus it follows from eqn (4.3-2) that

$$i_{sy} = -i_{ry} \quad (4.3-5)$$

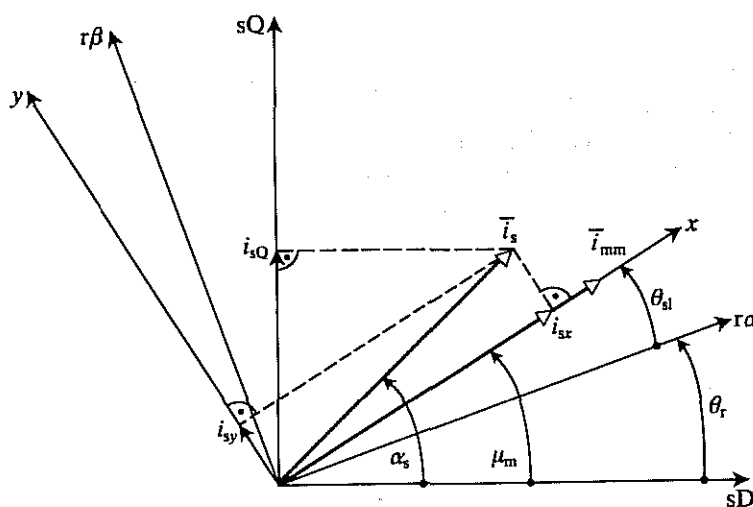


Fig. 4.32. Stator- and magnetizing-current space phasors.

and thus eqn (4.3-1) can be put into the form

$$t_e = -\frac{3}{2} PL_m |\bar{i}_{mm}| i_{ry} = -\frac{3}{2} PL_m |\bar{i}_{mm}| |\bar{i}_r| \sin(\alpha_r + \theta_r - \mu_m), \quad (4.3-6)$$

where  $i_{ry}$  has been obtained from eqn (4.3-4), and the Euler form of the space phasor of the rotor currents in the rotor reference frame,  $\bar{i}_r = |\bar{i}_r| e^{j\alpha_r}$  (the angle  $\alpha_r$  is the angle of  $\bar{i}_r$  with respect to the  $r\alpha$ -axis shown in Fig. 4.32) has been used. Equation (4.3-6) is similar to eqn (4.2-6), but as well as the differences in the constant parts, the modulus of the magnetizing-current space phasor is now present instead of the modulus of the stator magnetizing-current space phasor and the angle  $\rho_s$  is replaced by the angle  $\mu_m$ . Equation (4.3-6) can be utilized for magnetizing-flux-oriented control of the doubly fed induction machine with impressed rotor currents.

#### 4.3.2 STATOR VOLTAGE EQUATIONS

Here the space-phasor form of the stator voltage equation expressed in the magnetizing-flux-oriented reference frame will be obtained and this will be resolved into its two-axis components. For this purpose the voltage equations formulated in the general reference frame are utilized directly, these have been given in Section 2.1.7.

By considering eqns (2.1-148) and (2.1-150), which are the stator-voltage and flux-linkage space-phasor equations in the general reference frame, and by neglecting the effects of magnetic saturation, the space-phasor voltage equation of the stator will be as follows in the reference frame fixed to the magnetizing-flux-linkage space phasor, which rotates at the speed  $\omega_m = d\mu_m/dt$ , where the angle  $\mu_m$  has been defined above:

$$\bar{u}_{sm} = R_s \bar{i}_{sm} + L_s \frac{d\bar{i}_{sm}}{dt} + L_m \frac{d\bar{i}_{rm}}{dt} + j\omega_m (L_s \bar{i}_{sm} + L_m \bar{i}_{rm}). \quad (4.3-7)$$

$R_s$  and  $L_s$  are the stator resistance and self-inductance respectively and  $L_m$  is the magnetizing inductance and, as for the transformation of the stator currents given by eqn (4.1-27),  $\bar{u}_{sm}$  is related to the space phasor of the stator voltages in the stationary reference frame ( $\bar{u}_s$ ) by  $\bar{u}_{sm} = \bar{u}_s e^{-j\mu_m} = (u_{sd} + j u_{sq}) e^{-j\mu_m} = u_{sx} + j u_{sy}$ . By considering eqn (4.3-2), the rotor-current space phasor can be eliminated from eqn (4.3-7), since it follows that

$$\bar{i}_{rm} = |\bar{i}_{mm}| - \bar{i}_{sm} \quad (4.3-8)$$

and when eqn (4.3-8) is substituted into eqn (4.3-7),

$$\bar{u}_{sm} = R_s \bar{i}_{sm} + L_s \frac{d\bar{i}_{sm}}{dt} + L_m \frac{d|\bar{i}_{mm}|}{dt} + j\omega_m (L_{sl} \bar{i}_{sm} + L_m |\bar{i}_{mm}|), \quad (4.3-9)$$

where  $L_{sl}$  is the leakage inductance of a stator winding, and  $L_{sl} = L_s - L_m$  has been used. Physically it follows from eqn (4.3-9) that the stator-voltage space phasor is balanced by the stator ohmic drop ( $R_s \bar{i}_{sm}$ ), a voltage drop across the stator

leakage inductance ( $L_{sl} d\bar{i}_{sm}/dt$ ), the magnetizing voltage drop ( $L_m d|\bar{i}_{mm}|/dt$ ), and a rotational voltage component due to the rotation of the chosen reference frame: that last component is equal to  $j\omega_m(L_{sl}\bar{i}_{sm} + L_m|\bar{i}_{mm}|)$ , where  $L_{sl}\bar{i}_{sm}$  is the stator leakage flux-linkage space phasor and  $L_m|\bar{i}_{mm}|$  is the magnetizing flux-linkage space phasor, and of course both are expressed in the magnetizing-flux-oriented reference frame.

Equation (4.3-9) is more complicated than eqn (4.2-10), which was expressed in the stator-flux-oriented reference frame and does not contain the derivative of the stator currents. Furthermore, in contrast to eqn (4.2-10), which does not contain a separate stator leakage voltage drop, in eqn (4.3-9) the stator leakage voltage drop is also present. Thus if the induction machine is supplied by impressed stator voltages, it is simpler to use the stator-flux-oriented control scheme than the magnetizing-flux-oriented control scheme. When compared with the corresponding stator voltage equation expressed in the rotor-flux-oriented reference frame (eqn 4.1-6), whilst in eqn (4.3-9)  $L_{sl}$  is present in the two corresponding terms, in eqn (4.1-6) the stator transient inductance ( $L'_s$ ) is present. Furthermore, in eqn (4.3-9) in two respective terms the modulus ( $|\bar{\psi}_{mm}| = L_m|\bar{i}_{mm}|$ ) and the derivative of the magnetizing flux-linkage space phasor are present, whereas in the corresponding two terms of eqn (4.1-6)  $|\bar{i}_{mr}|(L_s - L'_s) = (L_m/L_r)|\bar{\psi}_{r\psi r}|$  and its derivative are present, where  $L_r$  is the self-inductance of the rotor and  $|\bar{\psi}_{r\psi r}|$  is the modulus of the rotor flux-linkage space phasor.

Resolution of eqn (4.3-9) into its real- and imaginary-axis components yields

$$i_{sx} = \frac{u_{sx}}{R_s} - T_{sl} \frac{di_{sx}}{dt} - \frac{L_m}{R_s} \frac{d|\bar{i}_{mm}|}{dt} + \omega_m T_{sl} i_{sy} \quad (4.3-10)$$

$$i_{sy} = \frac{u_{sy}}{R_s} - T_{sl} \frac{di_{sy}}{dt} - \frac{\omega_m (L_{sl}i_{sx} + L_m|\bar{i}_{mm}|)}{R_s}, \quad (4.3-11)$$

where  $T_{sl} = L_{sl}/R_s$  is the stator leakage time-constant. Equations (4.3-10) and (4.3-11) must be considered for the magnetizing-flux-oriented control scheme of an induction machine supplied by impressed stator voltages. However, for this purpose, a decoupling circuit must be utilized, as discussed in the next section.

### Decoupling circuit

It follows from eqns (4.3-10) and (4.3-11) that there are unwanted coupling terms, and independent control of the flux- and torque-producing stator currents  $i_{sx}$  and  $i_{sy}$  is only possible if eqns (4.3-10) and (4.3-11) are decoupled and  $i_{sx}$  and  $i_{sy}$  are indirectly controlled by controlling the terminal voltages of the induction machine. For this purpose, as described previously, the following decoupling voltages are introduced, if it is assumed that the magnetizing flux is constant,

$$u_{dx} = -\omega_m L_{sl} i_{sy} \quad (4.3-12)$$

$$u_{dy} = \omega_m (L_{sl} i_{sx} + L_m |\bar{i}_{mm}|). \quad (4.3-13)$$

These equations are similar to eqns (4.1-9) and (4.1-10), which define the decoupling voltages in the case of rotor-flux-oriented control and the required decoupling circuit shown in Fig. 4.33 is similar to the one shown in Fig. 4.1.

Thus the flux- and torque-producing stator current components can be independently controlled if  $u_{dx}$  and  $u_{dy}$  are added to the outputs of the current controllers ( $\hat{u}_{sx}$ ,  $\hat{u}_{sy}$ ) which control  $i_{sx}$  and  $i_{sy}$  respectively, since  $\hat{u}_{sx} + u_{dx}$  gives the direct-axis terminal voltage component in the magnetizing-flux-oriented reference frame and if the magnetizing flux is constant, it follows from eqn (4.3-10) that the voltage at the output of the direct-axis current controller is

$$\hat{u}_{sx} = R_s i_{sx} + L_{sl} \frac{di_{sx}}{dt}. \quad (4.3-14)$$

Thus  $\hat{u}_{sx}$  directly controls  $i_{sx}$  through a simple delay element with the stator leakage time constant ( $T_{sl} = L_{sl}/R_s$ ). Similarly,  $\hat{u}_{sy} + u_{dy}$  gives the quadrature-axis terminal voltage in the same reference frame and it follows from eqn (4.3-11) that the voltage on the output of the quadrature-axis current controller is

$$\hat{u}_{sy} = R_s i_{sy} + L_{sl} \frac{di_{sy}}{dt} \quad (4.3-15)$$

and  $\hat{u}_{sy}$  directly controls  $i_{sy}$  through a simple delay element with the time constant  $T_{sl}$ .

In the decoupling circuit shown in Fig. 4.33, the stator currents  $i_{sx}$  and  $i_{sy}$  can be obtained from the monitored three-phase stator currents by using eqn (4.3-3) and  $|\bar{i}_{mm}|$  and  $\omega_m$  (and  $\mu_m$ ) can be obtained either from a flux model which utilizes the rotor equations of the machine or by using direct measurements (e.g. Hall-sensors, special search coils, etc.). If the effect of inverter time delay is to be considered in the decoupling circuit, the method developed in Section 4.1.1 can be used and a decoupling circuit is obtained which is similar to that shown in Fig. 4.5.

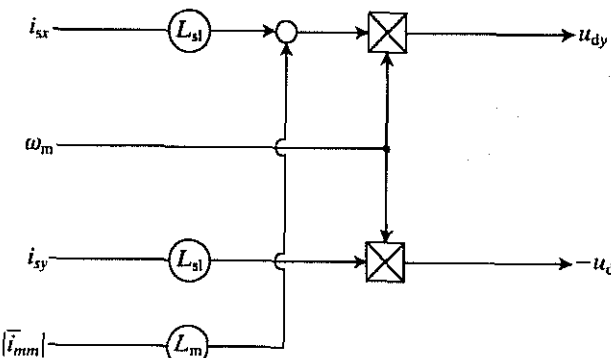


Fig. 4.33. Decoupling circuit to obtain the decoupling voltages  $u_{dx}$ ,  $u_{dy}$ .

When the machine is supplied by impressed stator currents, the stator voltage equations can be omitted from the equations of the drive.

#### 4.3.3 ROTOR VOLTAGE EQUATIONS

The rotor voltage equations expressed in the magnetizing-flux-oriented reference frame can be used to obtain the modulus of the magnetizing flux-linkage space phasor ( $|\bar{\psi}_{mm}| = L_m |\bar{i}_{mm}|$ ) and its speed ( $\omega_m$ ) or its phase angle ( $\mu_m$ ). For this purpose eqn (2.1-153) is used which gives the rotor voltage equation in a general reference frame. Thus by neglecting the effects of saturation, it follows from eqn (2.1-153) that in the magnetizing-flux-oriented reference frame ( $\omega_g = \omega_m$ ,  $\bar{i}_{rg} = \bar{i}_{rm}$ ,  $\bar{i}_{sg} = \bar{i}_{sm}$ ) the rotor voltage equation is as follows if short-circuited rotor windings are assumed:

$$0 = R_r \bar{i}_{rm} + L_r \frac{d\bar{i}_{rm}}{dt} + L_m \frac{d\bar{i}_{sm}}{dt} + j(\omega_m - \omega_r)(L_r \bar{i}_{rm} + L_m \bar{i}_{sm}), \quad (4.3-16)$$

where the stator- and rotor-current space phasors in the magnetizing-flux-oriented reference frame ( $\bar{i}_{sm}$  and  $\bar{i}_{rm}$ ) have been defined in eqns (4.3-3) and (4.3-4) respectively and  $\omega_r$  is the rotor speed. Since eqn (4.3-16) contains the rotor-current space phasor, and the rotor currents cannot be directly measured in the case of a squirrel-cage induction machine,  $\bar{i}_{rm}$  is eliminated by considering eqn (4.3-8) and

$$0 = R_r (|\bar{i}_{mm}| - \bar{i}_{sm}) + L_r \frac{d|\bar{i}_{mm}|}{dt} - L_{rl} \frac{d\bar{i}_{sm}}{dt} + j(\omega_m - \omega_r)(L_r |\bar{i}_{mm}| - L_{rl} \bar{i}_{sm}). \quad (4.3-17)$$

This equation is much more complicated than eqn (4.1-24), which defines the rotor voltage equation in the rotor-flux-oriented reference frame. Thus if the machine is supplied by impressed stator currents, magnetizing-flux-oriented control leads to more complicated implementation than the implementation based on rotor-flux-oriented control. When eqn (4.3-17) is compared with eqn (4.2-15), which gives the rotor voltage equation in the stator-flux-oriented reference frame, it can be seen that the two equations are similar.

Resolution of eqn (4.3-17) into its direct- and quadrature-axis components in the magnetizing-flux-oriented reference frame yields

$$\frac{|\bar{i}_{mm}| + T_r d|\bar{i}_{mm}|/dt}{T_{rl}} = \frac{di_{sx}}{dt} + \frac{i_{sx}}{T_{rl}} - \omega_{sl} i_{sy} \quad (4.3-18)$$

$$\omega_{sl} \left( |\bar{i}_{mm}| \frac{T_r}{T_{rl}} - i_{sx} \right) = \frac{di_{sy}}{dt} + \frac{i_{sy}}{T_{rl}}, \quad (4.3-19)$$

where  $\omega_{sl} = \omega_m - \omega_r$  is the angular slip frequency and  $T_r$  and  $T_{rl}$  are the rotor time constant and rotor leakage time constant respectively ( $T_r = L_r/R_r$ ,  $T_{rl} = L_{rl}/R_r$ ). For an induction machine with impressed stator currents eqns (4.3-18) and (4.3-19) have to be considered. However, there is unwanted coupling between these two equations and as a consequence  $|\bar{i}_{mm}|$  will be altered by a change in the

torque-producing stator current component. This coupling can be removed by the application of a decoupling circuit, as obtained in the following section, where the magnetizing-flux-oriented control scheme of an induction machine supplied by a current-controlled PWM inverter is also described.

#### Decoupling circuit; control scheme of a current-controlled PWM inverter-fed induction machine

If the magnetizing current is controlled by a flux controller (which can be a PI controller) and the output of this controller is  $i_{sx}$ , then the required decoupling current along the direct axis of the magnetizing-flux-oriented reference frame  $i_{dx}$  has to be added to  $i_{sx}$  to give the reference value  $i_{sxref}$ . Thus

$$i_{sx} = \hat{i}_{sx} + i_{dx} \quad (4.3-20)$$

and, when eqn (4.3-20) is substituted into eqn (4.3-18),

$$\frac{|\bar{i}_{mm}| + T_r d|\bar{i}_{mm}|/dt}{T_{rl}} = \frac{d\hat{i}_{sx}}{dt} + \frac{\hat{i}_{sx}}{T_{rl}} + \frac{di_{dx}}{dt} + \frac{i_{dx}}{T_{rl}} - \omega_{sl} i_{sy}. \quad (4.3-21)$$

Thus  $|\bar{i}_{mm}|$  can be decoupled from the torque-producing stator current if  $i_{dx}$  is selected in such a way that the term  $\omega_{sl} i_{sy}$  should disappear in eqn (4.3-21). Thus it follows from eqn (4.3-20) that this can be satisfied if

$$i_{dx} = \frac{\omega_{sl} i_{sy} T_{rl}}{1 + T_{rl} p} \quad (4.3-22)$$

where  $p = d/dt$ . The angular slip frequency in eqn (4.3-22) can be obtained from eqn (4.3-19) and it follows that it takes the form,

$$\omega_{sl} = \frac{(1 + T_{rl} p) i_{sy}}{T_r |\bar{i}_{mm}| - T_{rl} i_{sx}}. \quad (4.3-23)$$

Equations (4.3-22) and (4.3-23) can be used to construct the required decoupling circuit. When this is used, the magnetizing-flux-oriented control scheme of an induction machine supplied by a current-controlled PWM inverter will be similar to that shown in Fig. 4.26, which uses stator-flux-oriented control. Naturally for the magnetizing-flux-oriented control the transformation  $e^{j\theta_s}$  in Fig. 4.26 has to be replaced by the transformation  $e^{j\mu_m}$  and  $|\bar{i}_{ms}|$  and  $|\bar{i}_{msref}|$  have to be replaced by  $|\bar{i}_{mm}|$  and  $|\bar{i}_{mmref}|$  respectively.

The modulus and space angle of the magnetizing flux-linkage space phasor can also be obtained from the stator voltages and currents. For this purpose the stator voltage equation is formulated in the stationary reference frame. Thus by considering eqns (2.1-124) and (2.1-128), and also  $L_s = L_{sl} + L_m$  and by neglecting the effects of magnetic saturation,

$$\bar{u}_s = R_s \bar{i}_s + L_{sl} \frac{d\bar{i}_s}{dt} + \frac{d\bar{\psi}_m}{dt} = u_{sD} + j u_{sQ}, \quad (4.3-24)$$

where  $\bar{i}_s = i_{sD} + j i_{sQ}$  and  $\bar{\psi}_m$  is the magnetizing flux-linkage space phasor in the stationary reference frame which has also been used in eqn (2.1-178),

$$\bar{\psi}_m = L_m(\bar{i}_s + \bar{i}_r e^{j\theta_r}) = L_m \bar{i}_m = L_m(i_{mD} + j i_{mQ}) = L_m |\bar{i}_{mm}| e^{j\mu_m}. \quad (4.3-25)$$

In eqn (4.3-25)  $\bar{i}_m$  is the magnetizing flux-linkage space phasor in the stationary reference frame, which in polar form is  $|\bar{i}_{mm}| e^{j\mu_m}$  (for simplicity, instead of  $|\bar{i}_{mm}|$  the notation  $|\bar{i}_m|$  can be used, since the modulus of the magnetizing-current space phasor in the stationary reference,  $|\bar{i}_m|$ , is equal to the modulus of the same quantity in the magnetizing-flux-oriented reference frame  $|\bar{i}_{mm}|$ ). Thus it follows from eqns (4.3-24) and (4.3-25) that

$$\frac{di_{mD}}{dt} = u_{sD} - R_s i_{sD} - L_{sI} \frac{di_{sD}}{dt} \quad (4.3-26)$$

$$\frac{di_{mQ}}{dt} = u_{sQ} - R_s i_{sQ} - L_{sI} \frac{di_{sQ}}{dt} \quad (4.3-27)$$

and  $i_{mD}$  and  $i_{mQ}$  can be obtained by considering eqns (4.3-26) and (4.3-27) and by monitoring the terminal voltages and currents of the machine. Thus  $i_{mD} + j i_{mQ} = |\bar{i}_{mm}| e^{j\mu_m}$  can be used to obtain the modulus and the space angle of the magnetizing-current space phasor. In this case a flux model is obtained which is similar to that for an induction machine supplied by a voltage inverter. It is a disadvantage of the application of eqns (4.3-26) and (4.3-27) that they depend on the stator resistance and stator leakage inductance respectively and at low stator frequencies the stator ohmic drops will dominate. Thus prior to the integration of eqns (4.3-26) and (4.3-27), accurate stator voltage-drop compensation must be performed, which is a difficult task.

Equations (4.3-18) and (4.3-19) can be used to obtain the indirect magnetizing-flux-oriented control scheme of an induction machine with impressed stator currents. For this purpose the following expression for  $i_{sx}$  is obtained from eqn (4.3-18),

$$i_{sx} = \frac{(1+T_r p)|\bar{i}_{mm}| + i_{sy} T_r \omega_{sl}}{1+T_{rl} p}, \quad (4.3-28)$$

where  $\omega_{sl}$  has been defined in eqn (4.3-23).

Equations (4.3-28) and (4.3-23) are used in the indirect scheme shown in Fig. 4.34, where the induction machine is supplied by a current-controlled PWM inverter.

In Fig. 4.34(a) one of the inputs is the reference value of the modulus of the magnetizing current  $|\bar{i}_{mmref}|$ . The quadrature-axis stator current reference  $i_{sQref}$  is obtained from the torque reference ( $T_{tref}$ ) by utilizing eqn (4.3-1) and the torque reference is obtained as the output of the speed controller. In Fig. 4.34(a), within the dashed lines, the two-axis stator current references expressed in the stationary reference frame  $i_{sDref}$  and  $i_{sQref}$  are obtained by the application of the transformation  $e^{j\mu_m}$  in accordance with eqn (4.3-3). These are then transformed into the three-phase reference values by the application of the three-phase to two-phase

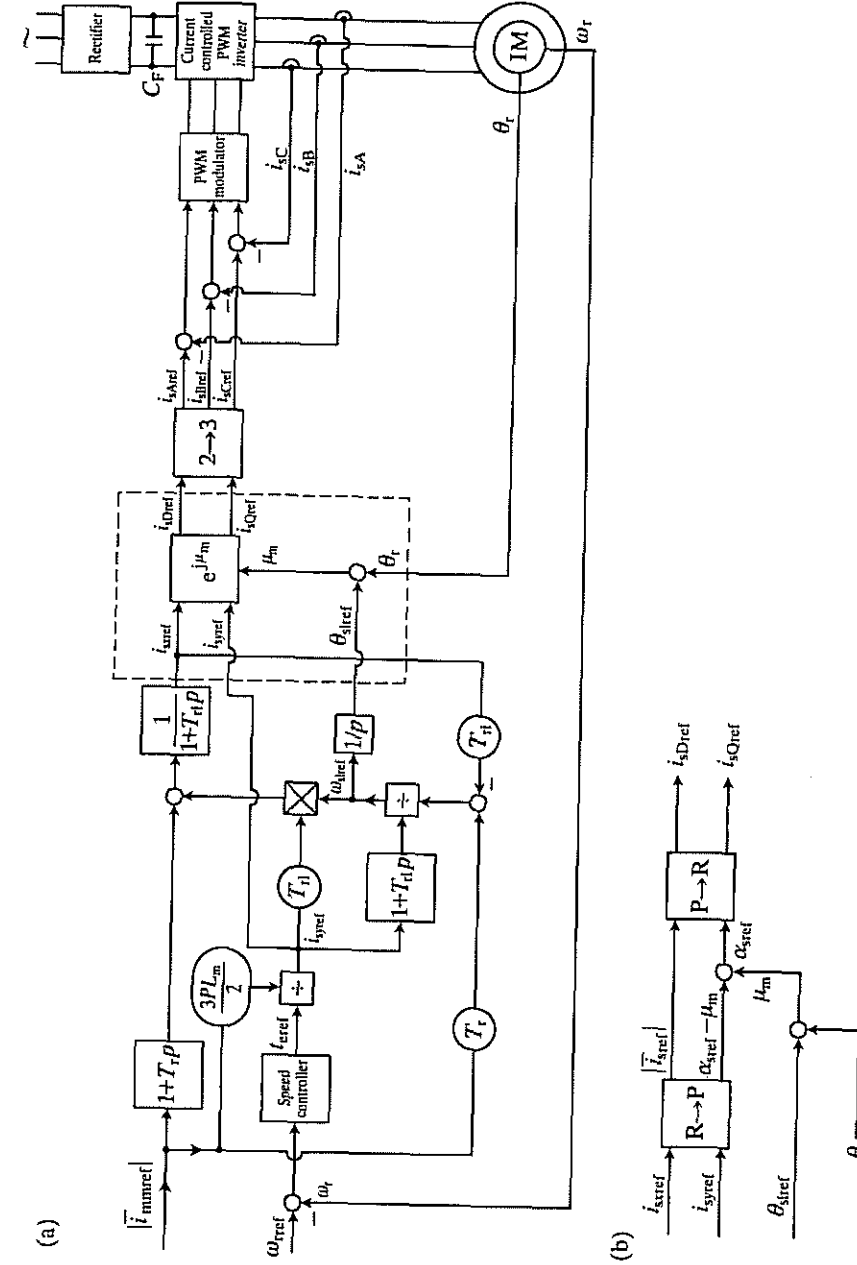


Fig. 4.34. Indirect magnetizing-flux-oriented control of a current-controlled PWM inverter-fed induction machine. (a) In Cartesian coordinates; (b) in polar coordinates.

transformation. The angle  $\mu_m$  is obtained in two steps; first the angular slip frequency is integrated and this gives the slip angle  $\theta_{sl}$ , which is also shown in Fig. 4.32 and is the angle of the magnetizing-current space phasor with respect to the real axis of the rotor reference frame. During the second step, the monitored value of the rotor angle ( $\theta_r$ ) is added to the slip angle, and thus the angle of the magnetizing-current space phasor with respect to the direct-axis of the stationary reference frame ( $\mu_m$ ) is obtained, as shown in Fig. 4.32.

In Fig. 4.34(a) the part shown within the dashed lines can be replaced by the part shown in Fig. 4.34(b). In this case,  $i_{sxref}$  and  $i_{syref}$  are inputs to a rectangular-to-polar converter, the inputs of which are the reference value of the modulus of the stator-current space phasor ( $|i_{sref}|$ ) and the space angle of the stator-current space phasor with respect to the direct axis of the magnetizing-flux-oriented reference frame ( $\alpha_{sref} - \mu_m$ ) (see Fig. 4.32). From Fig. 4.32 the sum of the slip angle and the rotor angle give  $\mu_m$ , and when this is added to  $(\alpha_{sref} - \mu_m)$ ,  $\alpha_{sref}$  is obtained, which is the angle of the stator-current space phasor with respect to the direct axis of the stationary reference frame. Finally, a polar-to-rectangular converter is used to obtain  $i_{sDref}$  and  $i_{sQref}$ .

When the implementation given in Fig. 4.34(a) is compared with the implementation shown in Fig. 4.16(a), which corresponds to indirect rotor-flux-oriented control of the induction machine supplied by a current-controlled PWM inverter, it can be seen that it is much simpler to implement the rotor-flux-oriented control.

Furthermore, in the steady state, with constant-magnetizing-flux control, the electromagnetic torque has a pull-out value ( $t_{emax}$ ) and this corresponds to the pull-out value of the angular slip frequency ( $\omega_{slmax}$ ). Beyond the pull-out value of the slip frequency, the induction machine can have a static stability limit. However, in contrast to this, in the steady state, with constant-rotor-flux control, there is no pull-out torque (if there is no limitation on the stator currents) and there is no static stability limit. With constant-stator-flux control, in the steady state there is also a pull-out torque and thus a static stability limit. These conclusions can be proved by considering the equations for the torque in the steady state. This will be discussed in the next section and the stability limits will be derived.

#### 4.3.4 STEADY-STATE STABILITY LIMIT

For magnetizing-flux-oriented control it follows from eqn (4.3-17) that in the steady state (when all the derivative terms are zero), the stator-current space phasor in the magnetizing-flux-oriented reference frame can be expressed as

$$\bar{i}_{sm} = |\bar{i}_{mm}| \frac{R_r + j\omega_{sl}L_r}{R_r + j\omega_{sl}L_{rl}} = i_{sx} + j i_{sy}. \quad (4.3-29)$$

The torque-producing stator current ( $i_{sy}$ ) is equal to the imaginary part of eqn (4.3-29) and thus

$$i_{sy} = \frac{\omega_{sl}R_rL_m|\bar{i}_{mm}|}{R_r^2 + \omega_{sl}^2L_{rl}^2} = \frac{\omega_{sl}R_r|\bar{\psi}_{mm}|}{R_r^2 + \omega_{sl}^2L_{rl}^2}, \quad (4.3-30)$$

where  $|\bar{\psi}_{mm}|$  is the modulus of the magnetizing flux-linkage space phasor. Thus by the substitution of eqn (4.3-30) into eqn (4.3-1), the following expression is obtained for the electromagnetic torque:

$$t_e = \frac{\frac{3}{2}PR_{rl}|\bar{\psi}_{mm}|^2\omega_{sl}}{R_r^2 + \omega_{sl}^2L_{rl}^2}. \quad (4.3-31)$$

This (and the torque-producing stator current) will have their maxima at the following value of the angular slip frequency,

$$\omega_{slmax} = \pm \frac{R_r}{L_{rl}} = \pm \frac{1}{T_{rl}}, \quad (4.3-32)$$

where  $T_{rl}$  is the leakage time constant of the rotor. Equation (4.3-32) can also be proved by differentiation of the electromagnetic torque (or the torque-producing stator current) with respect to the angular slip frequency, and setting this first derivative to zero. Substitution of eqn (4.3-32) into eqn (4.3-31) yields

$$t_{emax} = \pm \frac{\frac{3}{4}P|\bar{\psi}_{mm}|^2}{L_{rl}} = \pm \frac{\frac{3}{4}PL_m^2|\bar{i}_{mm}|^2}{L_{rl}} = \frac{3}{2}P|\bar{\psi}_{mm}|i_{symax}, \quad (4.3-33)$$

where  $i_{symax}$  is the maximal value of the torque-producing stator current. When the angular slip frequency is higher than  $\omega_{slmax}$ , static instability arises. It follows from eqns (4.3-32) and (4.3-33) that the pull-out angular slip frequency depends only on the rotor leakage time constant and does not depend on the magnetizing flux. However, the pull-out torque is proportional to the square of the modulus of the magnetizing flux-linkage space phasor and thus a small increase of the magnetizing flux will cause a significant increase in the electromagnetic torque.

It is also possible to obtain the limit of static stability in terms of the torque-producing stator current. From eqn (4.3-33)

$$i_{symax} = \frac{\pm L_m|\bar{i}_{mm}|}{2L_{rl}} \quad (4.3-34)$$

and it follows that unstable operation arises if the torque-producing stator current is larger than  $L_m|\bar{i}_{mm}|/(2L_{rl})$ . If  $L_{rl}/L_m = 1/30$  which is a typical value, instability only arises if  $i_{sy} > 15|\bar{i}_{mm}|$ , which is an unusually high value under steady-state conditions.

The static-stability limit in the case of stator-flux-oriented control with constant stator flux can be similarly determined by utilizing eqns (4.2-1) and (4.2-15). It follows from eqn (4.2-15) that the stator-current space phasor in the steady state is

$$\bar{i}_{sphs} = \frac{L_m}{L_s} \frac{|\bar{i}_{ms}|(R_r + j\omega_{sl}L_r)}{R_r + j\omega_{sl}L'_r} \quad (4.3-35)$$

and the torque-producing stator current ( $i_{sy}$ ) is equal to its imaginary-axis component. The maximum of this is at

$$\omega_{slmax} = \pm \frac{1}{T'_r}, \quad (4.3-36)$$

where  $T'_r$  is the rotor transient time constant and thus  $i_{sy\max}$  can also be obtained. By the substitution of  $i_{sy\max}$  into eqn (4.2-1), the pull-out torque is obtained as

$$\begin{aligned} t_{emax} &= \pm \frac{3}{4} P \left( \frac{L_m}{L_s} \right)^2 L_m^2 |\bar{l}_{ms}|^2 / L'_r = \pm \frac{3}{4} P \left( \frac{L_m}{L_s} \right)^2 |\bar{\psi}_s|^2 / L'_r \\ &= \frac{3}{2} P L_m |\bar{l}_{ms}| i_{sy\max}, \end{aligned} \quad (4.3-37)$$

where  $|\bar{\psi}_s|$  is the modulus of the stator flux-linkage space phasor. If the angular slip frequency is larger than  $\omega_{s1\max}$ , static instability arises. It follows from eqn (4.3-36) that this critical value of the angular slip frequency depends only on the rotor transient time constant and is not determined by the flux level. However, the pull-out torque depends on the square of the modulus of the stator linkage space phasor. It follows from eqn (4.3-37) that

$$i_{sy\max} = \pm \frac{L_m^3 |\bar{l}_{ms}|}{2 L_s^2 L'_r} \quad (4.3-38)$$

and static instability arises if  $i_{sy} > L_m^3 |\bar{l}_{ms}| / (2 L_s^2 L'_r)$ . By assuming equal stator and rotor leakages ( $L_{s1} = L_{r1}$ ), the following inequality is obtained

$$i_{sy} > \frac{(1-\sigma) |\bar{l}_{ms}|}{2\sigma(1+L_{r1}/L_m)},$$

where  $\sigma$  is the resultant leakage constant,  $\sigma = 1 - L_m^2 / (L_s L_r)$ . Thus when typical values of  $\sigma$  and  $L_{r1}/L_m$  are chosen, e.g.  $\sigma = 1/15$  and  $L_{r1}/L_m = 1/30$ , it follows that the instability only arises if the torque-producing stator current is greater than  $6.78 |\bar{l}_{ms}|$ . However, in the steady state it is unusual to have such a high torque-producing current and thus this instability does not cause a serious practical problem. It is also possible to obtain eqn (4.3-37) or eqn (4.3-38) by considering the general steady-state equivalent circuit of the induction machine shown in Fig. 4.10(b) and by utilizing the fact that the general turns ratio is equal to  $a = L_s / L_m$ .

Finally for the case of rotor-flux-oriented control it follows from eqn (4.1-26), that in the steady state the torque-producing stator current can be expressed as

$$i_{sy} = \omega_{s1} T_r |\bar{l}_{mr}|. \quad (4.3-39)$$

This varies linearly with  $\omega_{s1}$  (when  $|\bar{l}_{mr}| = \text{constant}$  and  $T_r = \text{constant}$ ), and thus the torque will also vary linearly with the angular slip frequency and there is no pull-out slip and no pull-out torque. This has also been discussed in Section 4.1.1.

#### 4.3.5 MAGNETIZING-FLUX-ORIENTED CONTROL OF DOUBLE-CAGE INDUCTION MACHINES

##### 4.3.5.1 General introduction

In all the previous sections, the squirrel-cage induction machine has been represented by its single-cage model and the effects of deep bars have not been

considered. However, during transient operation, in an induction machine with deep bars, the deep-bar effect can significantly influence the rotor time constants of the machine, which are important parameters during vector control. A similar situation exists in a squirrel-cage machine with double-cage rotor. If the rotor time constants are inaccurate, the angular slip frequency ( $\omega_{s1}$ ) will be inaccurate, and this will result in an inaccurate slip angle ( $\theta_{sl}$ ). Thus the angle of the magnetizing flux-linkage space phasor ( $\mu_m$ ), which is equal to the sum of the slip angle and the monitored rotor angle ( $\theta_r$ ) (see Fig. 4.32), will also be inaccurate. Therefore the desired decoupling of flux- and torque-producing stator current components ( $i_{sx}, i_{sy}$ ) cannot be achieved and this can lead to unwanted oscillations and a degradation of the performance of the induction machine. Compensation for the deep bar effects can improve the performance of the drive. For this purpose the angular slip frequency has to be calculated in such a way that it contains the effects of the deep bars (or double cage). In this section, the space-phasor model of the double-cage induction machine is developed and magnetizing-flux-oriented control of the double-cage machine with impressed stator currents is discussed in detail.

In practice, squirrel-cage rotors can have deep-bar rotors (with narrow and deep bars) or double-cage rotors with an outer and inner cage. In the case of the deep-bar rotor, it is possible to consider a bar with a large number of layers, and the leakage inductance of the bottom layer is greater than that of the top layer since the bottom layer links a greater amount of leakage flux. Thus the leakage inductance of the outer layer will be low and the leakage inductance of the inner layer will be high. Since all the layers can be considered to be electrically connected in parallel, when a.c. current flows in the cage (e.g. when the machine is started and the frequency of the rotor currents is high and equal to the stator frequency), the current in the upper layer (with low leakage reactance) will be larger than the current in a lower layer (with high leakage reactance). Thus the current will mainly flow in the top layers and the uneven rotor current distribution will result in an increase of effective rotor resistance and thus high starting torque is produced. When the machine accelerates, the rotor frequency decreases, so that at nominal speed the rotor frequency is very low and thus the effective rotor resistance is almost equal to the d.c. value. Thus in the induction machine with deep-bar rotor, high starting torque (resulting from high effective rotor resistance) and good running performance (resulting from low effective rotor resistance) are automatically ensured. As mentioned above, a rotor bar can be divided into several layers. In the dynamic state, to achieve high accuracy, several layers must be considered, but even the application of a model where a rotor bar is divided into two equal sections can give a substantial improvement in the computed characteristics, when compared with the application of a model where the rotor bar is not divided into layers. When a rotor bar is divided into two equal layers, the resistances of the two layers will be the same.

Similar conditions can be achieved by the application of a double-cage winding. In this case, the outer bars have smaller cross section, and thus they have a larger resistance than that of the inner bars. Furthermore, the leakage inductance of the

inner bars is larger than that of the outer bars, since the inner bars link more leakage flux. During starting, most of the rotor current will flow in the outer bars which have high resistance and small leakage reactance. Thus high starting torque is produced. At nominal speed, the rotor frequency is so low that the reactance of the inner cage is considerably lower than its resistance and the effective rotor resistance will be low and will be approximately equal to the d.c. resistance of the two cages in parallel.

In the following sections the dynamic model of the double-cage induction machine is established by the utilization of space-phasor theory. Although the goal is to obtain the dynamic model in the magnetizing-flux-oriented reference frame, which could be directly obtained by considering the voltage equations in the general reference frame, for better understanding of the various quantities (space phasors of various flux linkages, space phasors of rotor currents in the upper and lower cages, etc.) first the space-phasor voltage equations of the stator and rotor are established in the stationary reference frame. This will be followed by transformation of these into the magnetizing-flux-oriented reference frame.

#### 4.3.5.2 Stator- and rotor-voltage space-phasor equations in the stationary reference frame

The main assumptions are those used previously, in particular, the effects of magnetic saturation are neglected and the rotor is assumed to consist of two cages. Figure 4.35 shows the construction of the rotor. It is assumed that there is no mutual leakage between the stator and the upper cage (outer cage). Furthermore, in accordance with the discussion presented above, the leakage inductance of the upper cage is neglected. It is assumed that an upper bar and a lower bar occupy the same slot.

As in eqn (2.1-124), the space-phasor form of the stator voltage equation in the stationary reference frame is

$$\bar{u}_s = R_s \bar{i}_s + \frac{d\bar{\psi}_s}{dt}, \quad (4.3-40)$$

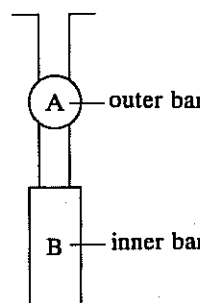


Fig. 4.35. Schematic of a double-cage.

where  $\bar{u}_s$  and  $\bar{i}_s$  are the space phasors of the stator voltages and currents respectively in the stationary reference frame,  $R_s$  is the stator resistance and  $\bar{\psi}_s$  is the space phasor of the stator flux linkages in the stationary reference frame. This contains three components. The first component is a flux linkage due to the stator currents,  $L_s \bar{i}_s$ , where  $L_s$  is the self-inductance of the stator, which is the sum of the stator leakage inductance  $L_{sl}$  and the magnetizing inductance  $L_m$  ( $L_s = L_{sl} + L_m$ ). The second component is a mutual flux linkage due to the rotor currents in the upper bars (denoted by A in Fig. 4.35),  $L_{mA} \bar{i}'_{rA}$ , where  $L_{mA}$  is the mutual inductance between the stator and the upper cage and  $\bar{i}'_{rA}$  is the space phasor of the rotor currents in the upper bars, but expressed in the stationary reference frame. Since the mutual leakage inductance between the stator and the upper cage has been neglected, it follows that  $L_{mA} = L_m$ . Finally the third component is a mutual flux-linkage component which is due to the rotor currents in the lower bars (denoted by B in Fig. 4.35),  $L_{mB} \bar{i}'_{rB}$ , where  $L_{mB}$  is the mutual inductance between the stator and the bottom cage and  $\bar{i}'_{rB}$  is the space phasor of the rotor currents in the bottom bars, but expressed in the stationary reference frame. From the assumptions made above  $L_{mA} = L_{mB} = L_m$ . Thus  $\bar{\psi}_s$  can be expressed as

$$\bar{\psi}_s = L_{sl} \bar{i}_s + L_m (\bar{i}_s + \bar{i}'_{rA} + \bar{i}'_{rB}) = L_{sl} \bar{i}_s + \bar{\psi}'_m, \quad (4.3-41)$$

where  $\bar{\psi}'_m$  is the magnetizing flux-linkage space phasor in the stationary reference frame,

$$\bar{\psi}'_m = L_m (\bar{i}_s + \bar{i}'_{rA} + \bar{i}'_{rB}) = L_m \bar{i}'_m = L_m |\bar{i}_{mm}| e^{j\mu_m} \quad (4.3-42)$$

and in eqn (4.3-42)  $\bar{i}'_m$  is the magnetizing current in the stationary reference frame,  $|\bar{i}_{mm}|$  is its modulus and  $\mu_m$  is its angle with respect to the real axis of the stationary reference frame, as shown in Fig. 4.32.

The space-phasor forms of the rotor voltage equations corresponding to the upper and lower cages, when expressed in the stationary reference frame, are similar to eqn (2.1-125),

$$0 = R_{rA} \bar{i}'_{rA} + \frac{d\bar{\psi}'_{rA}}{dt} - j\omega_r \bar{\psi}'_{rA} \quad (4.3-43)$$

and

$$0 = R_{rB} \bar{i}'_{rB} + \frac{d\bar{\psi}'_{rB}}{dt} - j\omega_r \bar{\psi}'_{rB}. \quad (4.3-44)$$

In eqn (4.3-43),  $\bar{\psi}'_{rA}$  is the space phasor of the rotor flux linkages which link the upper cage and it is expressed in the stationary reference frame.  $\bar{\psi}'_{rB}$  is the space phasor of the rotor flux linkages which link the bottom cage and it is also expressed in the stationary reference frame. From the assumptions made above,  $\bar{\psi}'_{rA}$  will contain three components, two of which are leakage components,  $L_{AB} \bar{i}'_{rA}$  and  $L_{AB} \bar{i}'_{rB}$ , where  $L_{AB}$  is the mutual leakage inductance between the upper and

lower cages. The third component is equal to the magnetizing flux-linkage space phasor  $\bar{\psi}'_m$  defined by eqn (4.3-42). Thus

$$\bar{\psi}'_{rA} = L_{AB}(\bar{i}'_{rA} + \bar{i}'_{rB}) + \bar{\psi}'_m. \quad (4.3-45)$$

In eqn (4.3-45) it has also been assumed that the leakage inductance of the upper cage is neglected. However, the leakage inductance of the lower cage ( $L_{rBI} = L_{rl}$ ) is not neglected and thus  $\bar{\psi}'_{rB}$  in eqn (4.3-44) can be expressed in a similar way to eqn (4.3-45), but it also has to include the leakage flux component  $L_{rl}\bar{i}'_{rB}$ . Thus

$$\bar{\psi}'_{rB} = L_{rl}\bar{i}'_{rB} + L_{AB}(\bar{i}'_{rA} + \bar{i}'_{rB}) + \bar{\psi}'_m. \quad (4.3-46)$$

Equations (4.3-40)–(4.3-46) define the voltage equations of the double-cage machine under dynamic conditions in the stationary reference frame. In the following section these equations will be expressed in the magnetizing-flux-oriented reference frame. It should be noted that, since there are two rotor flux-linkage space phasors (corresponding to the upper and lower cages respectively), in the case of the double-cage machine, it is not possible to establish a rotor-flux-oriented reference frame, where the stator currents can be decoupled into flux- and torque-producing components. This is in contrast to the single-cage induction machine, where it has been possible to use the rotor-flux-oriented reference frame and the stator currents have been decoupled into flux- and torque-producing components.

#### 4.3.5.3 Stator- and rotor-voltage space-phasor equations in the magnetizing-flux-oriented reference frame

The voltage equations of the double-cage machine, expressed in the magnetizing-flux-oriented reference frame, can be obtained directly from the corresponding voltage equations expressed in the stationary reference frame by utilizing the appropriate transformations between these two reference frames. These will be described in the present section. The stator voltage equations expressed in the magnetizing-flux-oriented reference frame are required for the magnetizing-flux-oriented control scheme of the double-cage machine supplied by impressed stator voltages, but are not required when the same machine is supplied by impressed stator currents. In the latter case only the rotor voltage equations are required.

##### 4.3.5.3.1 Stator voltage equations

By considering eqns (4.3-40) and (4.3-41), together with the required transformations of the stator voltage, current and flux-linkage space phasors [see eqns (4.3-48), (4.3-49), and (4.3-50)], it follows that in the special reference frame fixed to the magnetizing flux-linkage space phasor, which rotates at the speed of  $\omega_m$ , the stator-voltage space-phasor equation will be

$$\bar{u}_{sm} = R_s\bar{i}_{sm} + \frac{d\bar{\psi}_{sm}}{dt} + j\omega_m\bar{\psi}_{sm}. \quad (4.3-47)$$

This is similar to eqn (2.1-148), which gives the stator-voltage space-phasor equation in the general reference frame. The required transformations used for the derivation of eqn (4.3-47) are as follows. The space phasor of the stator currents in the magnetizing-flux-oriented reference frame ( $\bar{i}_{sm}$ ) has been defined in eqn (2.1-181), but for convenience it is repeated here,

$$\bar{i}_{sm} = \bar{i}_s e^{-j\mu_m} = (i_{sD} + j i_{sQ}) e^{-j\mu_m} = i_{sx} + j i_{sy}, \quad (4.3-48)$$

and the space phasor of the stator voltages in the same reference frame can similarly be defined as

$$\bar{u}_{sm} = \bar{u}_s e^{-j\mu_m} = (u_{sD} + j u_{sQ}) e^{-j\mu_m} = u_{sx} + j u_{sy}. \quad (4.3-49)$$

In these equations the components with the subscripts D and Q are direct- and quadrature-axis components in the stationary reference frame and the components with subscripts x and y are the direct- and quadrature-axis components in the magnetizing-flux-oriented reference frame (see Fig. 4.32). In eqn (4.3-47),  $\bar{\psi}_{sm}$  is the space phasor of the stator flux linkages in the magnetizing-flux-oriented reference frame and the following transformation has been utilized during the derivation of eqn (4.3-47):

$$\bar{\psi}_{sm} = \bar{\psi}_s e^{-j\mu_m} = (\psi_{sD} + j \psi_{sQ}) e^{-j\mu_m} = \psi_{sx} + j \psi_{sy}, \quad (4.3-50)$$

which is similar to the transformation defined by eqns (4.3-48) and (4.3-49). By substitution of eqn (4.3-41) into eqn (4.3-50) and by utilizing the definition of  $\bar{i}_{sm}$  given in eqn (4.3-48) and the definition of  $\bar{\psi}'_m$  given in eqn (4.3-42),

$$\begin{aligned} \bar{\psi}_{sm} &= \bar{\psi}_s e^{-j\mu_m} = (L_{sI}\bar{i}_s + \bar{\psi}'_m) e^{-j\mu_m} = L_{sI}\bar{i}_s e^{-j\mu_m} + \bar{\psi}'_m e^{-j\mu_m} \\ &= L_{sI}\bar{i}_{sm} + L_{mI}\bar{i}_{mm} = \psi_{sx} + j \psi_{sy}, \end{aligned} \quad (4.3-51)$$

where  $\psi_{sx}$  and  $\psi_{sy}$  are the direct- and quadrature-axis components of the stator flux-linkage space phasor in the magnetizing-flux-oriented reference frame, and it follows from eqn (4.3-51) that they can be expressed as

$$\psi_{sx} = L_{sI}i_{sx} + L_m|\bar{i}_{mm}| = L_{sI}i_{sx} + |\bar{\psi}_{mm}| \quad (4.3-52)$$

$$\psi_{sy} = L_{sI}i_{sy}, \quad (4.3-53)$$

where  $|\bar{\psi}_{mm}|$  is the modulus of the magnetizing flux-linkage space phasor and is equal to the space phasor of the magnetizing flux linkages in the magnetizing-flux-oriented reference frame. Thus the two-axis forms of the stator voltage equation in the magnetizing-flux-oriented reference frame are obtained by resolving eqn (4.3-47) into its real- and imaginary-axis components,

$$u_{sx} = R_s i_{sx} + \frac{d\psi_{sx}}{dt} - \omega_m \psi_{sy} \quad (4.3-54)$$

$$u_{sy} = R_s i_{sy} + \frac{d\psi_{sy}}{dt} + \omega_m \psi_{sx} \quad (4.3-55)$$

where  $\psi_{sx}$  and  $\psi_{sy}$  have been defined in eqns (4.3-52) and (4.3-53) respectively.

By multiplying eqn (4.3-42) by  $e^{-j\mu_m}$ , it follows that the space phasor of the magnetizing flux linkages in the magnetizing-flux-oriented reference frame is

$$\begin{aligned}\bar{\psi}'_m e^{-j\mu_m} &= L_m (\bar{i}_s e^{-j\mu_m} + \bar{i}'_{rA} e^{-j\mu_m} + \bar{i}'_{rB} e^{-j\mu_m}) \\ &= L_m |\bar{i}_{mm}| = |\bar{\psi}_{mm}| = \psi_{mx} + j\psi_{my},\end{aligned}\quad (4.3-56)$$

where according to eqn (4.3-48)  $\bar{i}_s e^{-j\mu_m} = \bar{i}_{sm}$  is the stator-current space phasor in the magnetizing-flux-oriented reference frame and the rotor-current phasors  $\bar{i}'_{rA} e^{-j\mu_m}$  and  $\bar{i}'_{rB} e^{-j\mu_m}$  are the space phasors of the rotor currents in the upper and lower cages respectively, but expressed in the magnetizing-flux-oriented reference frame,

$$\bar{i}_{rAm} = \bar{i}'_{rA} e^{-j\mu_m} = i_{rAx} + j i_{rAy} \quad (4.3-57)$$

$$\bar{i}_{rBm} = \bar{i}'_{rB} e^{-j\mu_m} = i_{rBx} + j i_{rBy}. \quad (4.3-58)$$

It should be noted that  $\bar{i}'_{rA}$  and  $\bar{i}'_{rB}$  are the space phasors of the rotor currents in the upper and lower cages respectively, but expressed in the stationary reference frame. Equations (4.3-57) and (4.3-58) are similar to eqn (4.3-4), which defines the space phasor of the rotor currents in the magnetizing-flux-oriented reference frame for a single-cage machine. In eqns (4.3-57) and (4.3-58)  $i_{rAx}$ ,  $i_{rAy}$ , and  $i_{rBx}$ ,  $i_{rBy}$  are the two-axis rotor currents of the upper and lower cages respectively in the magnetizing-flux-oriented reference frame. Thus by resolving eqn (4.3-56) into its real- and imaginary-axis components,

$$\psi_{mx} = |\bar{\psi}_{mm}| = L_m (i_{sx} + i_{rAx} + i_{rBx}) \quad (4.3-59)$$

$$\psi_{my} = 0 = L_m (i_{sy} + i_{rAy} + i_{rBy}). \quad (4.3-60)$$

These two equations will be used below, when the state-variable equations of the double-cage induction machine with impressed stator currents are obtained, to express  $i_{rAx} + i_{rBx}$  in terms of  $|\bar{\psi}_{mm}|$  and  $i_{sx}$ , and to express  $(i_{rAy} + i_{rBy})$  in terms of  $i_{sy}$ .

Equations (4.3-54), (4.3-55), (4.3-52), and (4.3-53) have to be considered if the double-cage induction machine is supplied by impressed stator voltages. They can be put into a form which is similar to eqns (4.3-10) and (4.3-11) for the single-cage machine. Thus the required decoupling circuit can be constructed in a similar way to that shown in Fig. 4.33 and it should be noted that  $|\bar{\psi}_{mm}| = L_m |\bar{i}_{mm}|$ . In such a decoupling circuit, the stator currents  $i_{sx}$  and  $i_{sy}$  can be obtained from the monitored three-phase stator currents by utilizing eqn (4.3-48), and  $|\bar{i}_{mm}|$  and  $\omega_m$  (and  $\mu_m$ ) can be obtained either from a flux-model which uses the rotor equations of the machine expressed in the magnetizing-flux-oriented reference frame or by using direct measurements (e.g. Hall-sensors, special search coils, etc.). The rotor voltage equations will be obtained in the following section. They will also be used to obtain the magnetizing-flux-oriented control scheme of the double-cage machine with impressed stator currents.

#### 4.3.5.3.2 Rotor voltage equations

By utilizing the required transformations [see eqns (4.3-57), (4.3-58), (4.3-63), and (4.3-64)], it follows from eqns (4.3-43) and (4.3-44) that the rotor-voltage

space-phasor equations in the magnetizing-flux-oriented reference frame will take the form,

$$0 = R_{rA} \bar{i}_{rAm} + \frac{d\bar{\psi}_{rAm}}{dt} + j(\omega_m - \omega_r) \bar{\psi}_{rAm} \quad (4.3-61)$$

$$0 = R_{rB} \bar{i}_{rBm} + \frac{d\bar{\psi}_{rBm}}{dt} + j(\omega_m - \omega_r) \bar{\psi}_{rBm}. \quad (4.3-62)$$

These are similar to the rotor voltage equations of a single-cage machine expressed in the same reference frame, which can be obtained from eqn (2.1-149). For the derivation of eqns (4.3-61) and (4.3-62), eqns (4.3-57) and (4.3-58) have also been utilized; they give the space-phasor forms of the rotor currents of the upper and lower cages respectively in the magnetizing-flux-oriented reference frame ( $\bar{i}_{rAm}$ ,  $\bar{i}_{rBm}$ ). A similar definition has been used for the space phasors  $\bar{\psi}_{rAm}$  and  $\bar{\psi}_{rBm}$ , which are the space phasors of the rotor flux linkages for the upper and lower cages, expressed in the magnetizing-flux-oriented reference frame,

$$\bar{\psi}_{rAm} = \bar{\psi}'_{rA} e^{-j\mu_m} = \psi_{rAx} + j\psi_{rAy} \quad (4.3-63)$$

$$\bar{\psi}_{rBm} = \bar{\psi}'_{rB} e^{-j\mu_m} = \psi_{rBx} + j\psi_{rBy}, \quad (4.3-64)$$

where  $\bar{\psi}'_{rA}$  and  $\bar{\psi}'_{rB}$  have been defined in eqns (4.3-45) and (4.3-46) respectively.

By substituting eqn (4.3-45) into eqn (4.3-63) and considering eqns (4.3-57), (4.3-58), and (4.3-56),

$$\bar{\psi}_{rAm} = [L_{AB}(\bar{i}'_{rA} + \bar{i}'_{rB}) + \bar{\psi}'_m] e^{-j\mu_m} = L_{AB}(\bar{i}_{rAm} + \bar{i}_{rBm}) + |\bar{\psi}_{mm}|. \quad (4.3-65)$$

Similarly, substituting eqn (4.3-46) into eqn (4.3-64) and considering eqns (4.3-57), (4.3-58), and (4.3-56) gives

$$\begin{aligned}\bar{\psi}_{rBm} &= [L_{rI} \bar{i}'_{rB} + L_{AB}(\bar{i}'_{rA} + \bar{i}'_{rB}) + \bar{\psi}'_m] e^{-j\mu_m} \\ &= L_{rI} \bar{i}_{rBm} + L_{AB}(\bar{i}_{rAm} + \bar{i}_{rBm}) + |\bar{\psi}_{mm}|.\end{aligned}\quad (4.3-66)$$

Resolution of eqns (4.3-61), (4.3-62), (4.3-65), and (4.3-66) into their real- and imaginary-axis components give

$$0 = R_{rA} i_{rAx} + \frac{d\psi_{rAx}}{dt} - (\omega_m - \omega_r) \psi_{rAy} \quad (4.3-67)$$

$$0 = R_{rA} i_{rAy} + \frac{d\psi_{rAy}}{dt} + (\omega_m - \omega_r) \psi_{rAx} \quad (4.3-68)$$

$$0 = R_{rB} i_{rBx} + \frac{d\psi_{rBx}}{dt} - (\omega_m - \omega_r) \psi_{rBy} \quad (4.3-69)$$

$$0 = R_{rB} i_{rBy} + \frac{d\psi_{rBy}}{dt} + (\omega_m - \omega_r) \psi_{rBx}, \quad (4.3-70)$$

where

$$\psi_{rAx} = L_{AB}(i_{rAx} + i_{rBx}) + |\bar{\psi}_{mm}| \quad (4.3-71)$$

$$\psi_{rAy} = L_{AB}(i_{rAy} + i_{rBy}) \quad (4.3-72)$$

$$\psi_{rBx} = L_{rl}i_{rBx} + L_{AB}(i_{rAx} + i_{rBx}) + |\bar{\psi}_{mm}| \quad (4.3-73)$$

$$\psi_{rBy} = L_{rl}i_{rBy} + L_{AB}(i_{rAy} + i_{rBy}), \quad (4.3-74)$$

where  $|\bar{\psi}_{mm}|$  has been defined in eqn (4.3-59). The stator voltage equations, eqns (4.3-54) and (4.3-55), which use the expressions for the stator flux linkages, eqns (4.3-52) and (4.3-53), together with the rotor voltage equations, eqns (4.3-67)–(4.3-70), which use the rotor flux-linkage equations, eqns (4.3-71)–(4.3-74), describe the dynamic behaviour of the double-cage induction machine if the equation of motion is also considered. The expression for the electromagnetic torque will be obtained in the next section.

#### 4.3.5.3.3 The electromagnetic torque

The electromagnetic torque can be obtained in a similar way to that shown in eqn (4.3-1) for the single-cage machine. Physically this must be the case since it has been shown earlier that the electromagnetic torque can be considered to be produced by the interaction of the stator flux linkages and the stator currents and from this point of view, it is irrelevant how many cages there are on the rotor. Mathematically, it is possible to prove in several ways that the expression for the electromagnetic torque in the double-cage machine is similar to that given by eqn (4.3-1), but, of course, the modulus of the magnetizing flux-linkage space phasor ( $|\bar{\psi}_{mm}|$ ) is different for the double-cage machine than for the single-cage machine, since as well as the stator currents, the rotor currents of both rotor cages contribute to the magnetization current. Furthermore the torque-producing stator current ( $i_{sy}$ ) is different in the double-cage machine from that of the single-cage machine. It is very convenient to utilize a form of the torque equation which contains the stator flux-linkage space phasor, rather than other forms where two rotor flux-linkage space phasors have to be used.

In eqn (2.1-167) the electromagnetic torque has been defined by utilizing the space phasors of the stator flux linkages and the stator current in the general reference frame. Thus when the magnetizing-flux-oriented reference frame is used, it follows from eqn (2.1-167) that

$$t_e = \frac{3}{2}P\bar{\psi}_{sm} \times \bar{i}_{sm}, \quad (4.3-75)$$

where  $\bar{\psi}_{sm}$  and  $\bar{i}_{sm}$  have been defined in eqns (4.3-48) and (4.3-51) respectively. By performing the vector product, the following expression is obtained for the electromagnetic torque, if the stator flux-linkage components are replaced by the expressions given in eqns (4.3-52) and (4.3-53)

$$\begin{aligned} t_e &= \frac{3}{2}P(\psi_{sx}i_{sy} - \psi_{sy}i_{sx}) \\ &= \frac{3}{2}P[(L_{sl}i_{sx} + |\bar{\psi}_{mm}|)i_{sy} - L_{sl}i_{sy}i_{sx}] = \frac{3}{2}P|\bar{\psi}_{mm}|i_{sy}, \end{aligned} \quad (4.3-76)$$

which as expected agrees with the form of eqn (4.3-1). In eqn (4.3-76) the modulus of the magnetizing flux-linkage space phasor, ( $|\bar{\psi}_{mm}|$ ), is defined in eqn (4.3-59) and the torque-producing stator current ( $i_{sy}$ ) is related to the direct-axis and quadrature-axis stator currents in the stationary reference frame by eqn (4.3-48).

#### 4.3.5.4 Magnetizing-flux-oriented control of the double-cage induction machine with impressed stator currents

In this chapter the indirect magnetizing-flux-oriented control scheme of the double-cage induction machine with impressed stator currents is developed. For this purpose the rotor equations derived in the stationary reference frame are utilized together with the expression for the electromagnetic torque given in eqn (4.3-76). However, the rotor voltage equations are reformulated in such a way that the stator currents  $i_{sx}$ ,  $i_{sy}$  are retained.  $|\bar{\psi}_{mm}|$  is an input command and  $\mu_m$  is controlled indirectly. Since there are four rotor voltage equations, two other state variables also have to be selected. These are chosen to be the real- and imaginary-axis components ( $\psi_{rBx}$ ,  $\psi_{rBy}$ ) of the space phasor of the rotor leakage flux linkages in the lower cage. This space phasor has been defined in eqn (4.3-66) as  $\bar{\psi}_{rBl} = L_{rl}\bar{i}_{rBm}$  and thus its two-axis components in the magnetizing-flux-oriented reference frame are

$$\psi_{rBx} = L_{rl}i_{rBx} \quad (4.3-77)$$

$$\psi_{rBy} = L_{rl}i_{rBy}. \quad (4.3-78)$$

These are selected as state variables since they are essential for the description of the double-cage (deep-bar) effect. The direct-axis stator current ( $i_{sx}$ ) and the angular slip frequency ( $\omega_{sl}$ ) are strongly dependent on these. It should be noted that  $L_{rl}$  is the leakage inductance of the bottom cage, and in the transient state, the non-uniform current distribution between the upper and lower cages depends on the energy stored in this inductance.

The four rotor voltage equations, eqns (4.3-67)–(4.3-70), are now rearranged to contain the required four state variables. For this purpose, first the rotor flux-linkage components given by eqns (4.3-71)–(4.3-74) are substituted into eqns (4.3-67)–(4.3-70). The resulting equations will thus contain the four rotor current components ( $i_{rAx}$ ,  $i_{rAy}$ ,  $i_{rBx}$ ,  $i_{rBy}$ ):

$$0 = R_{rA}i_{rAx} + \frac{d|\bar{\psi}_{mm}|}{dt} + L_{AB} \frac{d(i_{rAx} + i_{rBx})}{dt} - \omega_{sl}L_{AB}(i_{rAy} + i_{rBy}) \quad (4.3-79)$$

$$0 = R_{rA}i_{rAy} + L_{AB} \frac{d(i_{rAy} + i_{rBy})}{dt} + \omega_{sl}[|\bar{\psi}_{mm}| + L_{AB}(i_{rAx} + i_{rBx})] \quad (4.3-80)$$

$$\begin{aligned} 0 &= R_{rB}i_{rBx} + \frac{d|\bar{\psi}_{mm}|}{dt} + \frac{d(L_{rl}i_{rBx})}{dt} + L_{AB} \frac{d(i_{rAx} + i_{rBx})}{dt} \\ &\quad - \omega_{sl}[L_{rl}i_{rBy} + L_{AB}(i_{rAy} + i_{rBy})] \end{aligned} \quad (4.3-81)$$

$$0 = R_{rB}i_{rBy} + \frac{d(L_{rl}i_{rBy})}{dt} + L_{AB} \frac{d(i_{rAx} + i_{rBy})}{dt} + \omega_{sl}[L_{rl}i_{rBx} + L_{AB}(i_{rAx} + i_{rBx}) + |\bar{\psi}_{mm}|], \quad (4.3-82)$$

where  $\omega_{sl} = (\omega_m - \omega_r)$  is the angular slip frequency.

However, the rotor current components can be eliminated by expressing them in terms of the four state-variables, since it follows from eqns (4.3-77) and (4.3-78) that

$$i_{rBx} = \frac{\psi_{rBlx}}{L_{rl}} \quad (4.3-83)$$

$$i_{rBy} = \frac{\psi_{rBly}}{L_{rl}}, \quad (4.3-84)$$

and from eqns (4.3-59) and (4.3-60) that

$$i_{rAx} = \frac{|\bar{\psi}_{mm}|}{L_m} - i_{sx} - i_{rBx} = \frac{\bar{\psi}_{mm}}{L_m} - i_{sx} - \frac{\psi_{rBlx}}{L_{rl}} \quad (4.3-85)$$

$$i_{rAy} = -i_{sy} - i_{rBy} = -i_{sy} - \frac{\psi_{rBly}}{L_{rl}}, \quad (4.3-86)$$

where  $i_{rx}$  and  $i_{ry}$  have been substituted by the expressions given by eqns (4.3-83) and (4.3-84) respectively. Thus when eqns (4.3-83)–(4.3-86) are substituted into the rotor voltage equations, eqns (4.3-79)–(4.3-82), the following four equations are obtained. The direct-axis rotor voltage equation of the upper cage yields

$$\frac{d|\bar{\psi}_{mm}|}{dt} = -\frac{R_{rA}|\bar{\psi}_{mm}|}{L_m + L_{AB}} + \frac{L_m}{L_m + L_{AB}} \left( R_{rA}i_{sx} + L_{AB} \frac{di_{sx}}{dt} + \frac{R_{rA}\psi_{rBlx}}{L_{rl}} - L_{AB}\omega_{sl}i_{sy} \right). \quad (4.3-87)$$

The quadrature-axis rotor voltage equation of the upper cage yields

$$\omega_{sl} = \left[ R_{rA} \left( i_{sy} + \frac{\psi_{rBly}}{L_{rl}} \right) + L_{AB} \frac{di_{sy}}{dt} \right] / \psi_{rAx}, \quad (4.3-88)$$

where in the denominator,

$$\psi_{rAx} = |\bar{\psi}_{mm}| \frac{(L_m + L_{AB})}{L_m} - L_{AB}i_{sx} \quad (4.3-89)$$

is the direct-axis flux-linkage component of the upper cage. It follows from the direct-axis rotor voltage equation of the lower cage that

$$\frac{d\psi_{rBlx}}{dt} = -\frac{R_{rB}\psi_{rBlx}}{L_{rl}} - \frac{L_{AB} + L_m}{L_m} \frac{d|\bar{\psi}_{mm}|}{dt} + L_{AB} \frac{di_{sx}}{dt} - \omega_{sl}L_{AB}i_{sy} + \omega_{sl}\psi_{rBly}. \quad (4.3-90)$$

Finally, the following equation is obtained from the quadrature-axis rotor voltage equation of the lower cage:

$$\frac{d\psi_{rBly}}{dt} = -\frac{R_{rB}\psi_{rBly}}{L_{rl}} - \omega_{sl}\psi_{rBlx} + L_{AB} \frac{di_{sy}}{dt} - \omega_{sl}\psi_{rAx}, \quad (4.3-91)$$

where  $\psi_{rAx}$  has been defined in eqn (4.3-89). However, eqn (4.3-91) contains the first derivative  $di_{sy}/dt$  and this can be eliminated by using eqn (4.3-88). Thus from eqn (4.3-88)  $\psi_{rAx}$  is expressed in terms of  $\omega_{sl}$ ,  $i_{sy}$ , and  $\psi_{rBly}$  and, when this is substituted into eqn (4.3-91),

$$\frac{d\psi_{rBly}}{dt} = -\frac{R_{rA} + R_{rB}}{L_{rl}} \psi_{rBly} - R_{rA}i_{sy} - \omega_{sl}\psi_{rBlx}. \quad (4.3-92)$$

Thus eqns (4.3-87), (4.3-88), (4.3-89), (4.3-90), and (4.3-92), together with the expression of the electromagnetic torque, eqn (4.3-76), can be used to obtain the indirect magnetizing-flux-oriented control scheme of the double-cage induction machine supplied by impressed stator currents. For this purpose it should be considered that if the reference value of the modulus of the magnetizing flux-linkage space phasor ( $|\bar{\psi}_{mmref}|$ ) and the reference value of the torque-producing stator current ( $i_{syref}$ ) are known, in the indirect control scheme  $i_{sxref}$  and  $\omega_{slref}$  have to be determined. Thus these quantities have to be expressed in terms of ( $|\bar{\psi}_{mmref}|$ ) and ( $i_{syref}$ ), but in accordance with eqns (4.3-87)–(4.3-90) and eqn (4.3-92), they will depend on the leakage flux components  $\psi_{rBlx}$  and  $\psi_{rBly}$ . Therefore to obtain the control scheme, the equations given above have to be arranged for  $i_{sx}$  and  $\omega_{sl}$ , and the leakage fluxes of the bottom cages ( $\psi_{rBlx}$  and  $\psi_{rBly}$ ) have to be expressed in terms of  $|\bar{\psi}_{mm}|$ ,  $i_{sx}$ , and  $i_{sy}$ . Thus when eqn (4.3-87) is rearranged, the following equation is obtained for the direct-axis stator current:

$$(1 + T_{AB}p)i_{sx} = (1 + T_{mAB}p)|\bar{\psi}_{mm}| + T_{AB}\omega_{sl}i_{sy} - \frac{\psi_{rBlx}}{L_{rl}}, \quad (4.3-93)$$

where  $p = d/dt$  and the mutual time constants associated with the upper cage are

$$T_{AB} = \frac{L_{AB}}{R_{rA}}, \quad T_{mAB} = T_m + T_{AB}, \quad \text{and} \quad T_m = \frac{L_m}{R_{rA}}.$$

Equation (4.3-88) yields the following expression for the angular slip frequency:

$$\omega_{sl} = \frac{i_{sy}(1 + T_{AB}p) + \psi_{rBly}/L_{rl}}{T_{mAB}|\bar{\psi}_{mm}| - T_{AB}i_{sx}}. \quad (4.3-94)$$

In eqns (4.3-93) and (4.3-94) the rotor leakage-flux linkages are also present. These are obtained from eqns (4.3-89) and (4.3-90) as

$$(p + T_{Bl})\psi_{rBlx} = -pR_{rA}(T_{mAB}|\bar{\psi}_{mm}| - T_{AB}i_{sx}) - \omega_{sl}L_{AB}i_{sy} + \omega_{sl}\psi_{rBly}, \quad (4.3-95)$$

where  $T_{Bl} = R_{rB}/L_{rl}$  is the leakage time constant of the lower cage,

$$(p + T_{ABl})\psi_{rBly} = -R_{rA}i_{sy} - \omega_{sl}\psi_{rBlx} \quad (4.3-96)$$

and  $T_{ABl}$  is the total leakage time constant of the upper and lower cages,

$$T_{ABl} = T_{Bl} + T_{Al} \quad \text{where} \quad T_{Al} = \frac{R_{rA}}{L_{rl}}.$$

Equations (4.3-93)–(4.3-96) are used in Fig. 4.36, which shows the magnetizing-flux-oriented indirect control scheme of the double-cage induction machine with impressed stator currents. The converter which supplies the induction machine can be either a CSI or a current-controlled PWM inverter.

In Fig. 4.36 the required reference values of the stator currents are obtained in a way similar to that shown in Fig. 4.34 for the single-cage machine. Thus by using the reference values of the direct- and quadrature-axis stator current components expressed in the magnetizing-flux-oriented reference frame ( $i_{sxref}, i_{syref}$ ), it is possible to obtain the reference value of the space phasor of the stator currents in the magnetizing-flux-oriented reference frame,

$$(i_{sxref} + j i_{syref}) = |\bar{i}_{sref}| e^{j(\alpha_{sref} - \mu_m)} \quad (4.3-97)$$

(see Fig. 4.32). Equation (4.3-97) can be used to obtain the reference values of the direct- and quadrature-axis stator currents in the stationary reference frame ( $i_{sDref}, i_{sQref}$ ), by either of the methods shown in Fig. 4.34(a) or Fig. 4.34(b). If the method of Fig. 4.34(b) is used,  $|\bar{i}_{sref}|$  and  $(\alpha_{sref} - \mu_m)$  are obtained by polar-to-rectangular conversion from  $i_{sxref}$  and  $i_{syref}$ , since eqn (4.3-97) is utilized. When the angular slip frequency ( $\omega_{sl}$ ) obtained from eqn (4.3-94) is integrated, the slip angle ( $\theta_{sl}$ ) is obtained and when the monitored rotor angle ( $\theta_r$ ) is added to this, the angle of the magnetizing flux-linkage space phasor with respect to the direct-axis of the magnetizing-oriented reference frame ( $\mu_m$ ) is obtained (this also follows from Fig. 4.32) as

$$\mu_m = \theta_{sref} + \theta_r. \quad (4.3-98)$$

Thus when  $\mu_m$  is added to  $(\alpha_{sref} - \mu_m)$ ,  $\alpha_{sref}$  is obtained, which is the space angle of the stator-current space phasor with respect to the direct axis of the stationary reference frame (see Fig. 4.32).

In Fig. 4.36, the circuit which produces the required leakage-flux components of the bottom cage ( $\psi_{rBlx}, \psi_{rBly}$ ), contains a differentiator (indicated by the block containing the operator  $p$ ) and furthermore, it is asymmetrical. However, it is possible to construct a circuit which produces the required rotor leakage fluxes, where differentiation is not required and which is symmetrical. For this purpose, eqn (4.3-95) is rearranged to resemble the simple structure of eqn (4.3-96), but eqn (4.3-96) itself will not be changed.

Thus when the expression for the voltage component  $R_{rA}|\bar{\psi}_{mm}|/L_{rl}$  is taken from eqn (4.3-93) [or it may be easier to use eqn (4.3-87) directly] and the expression is added to the expression for the rotational voltage,  $\omega_{sl}\psi_{rBly}$ , which can be obtained from eqn (4.3-95) [or eqn (4.3-90)], the following voltage equation is obtained:

$$(p + T_{ABl})\psi_{rBlx} = R_{rA}(|\bar{i}_{mm}| - i_{sx}) + \omega_{sl}\psi_{rBly}. \quad (4.3-99)$$

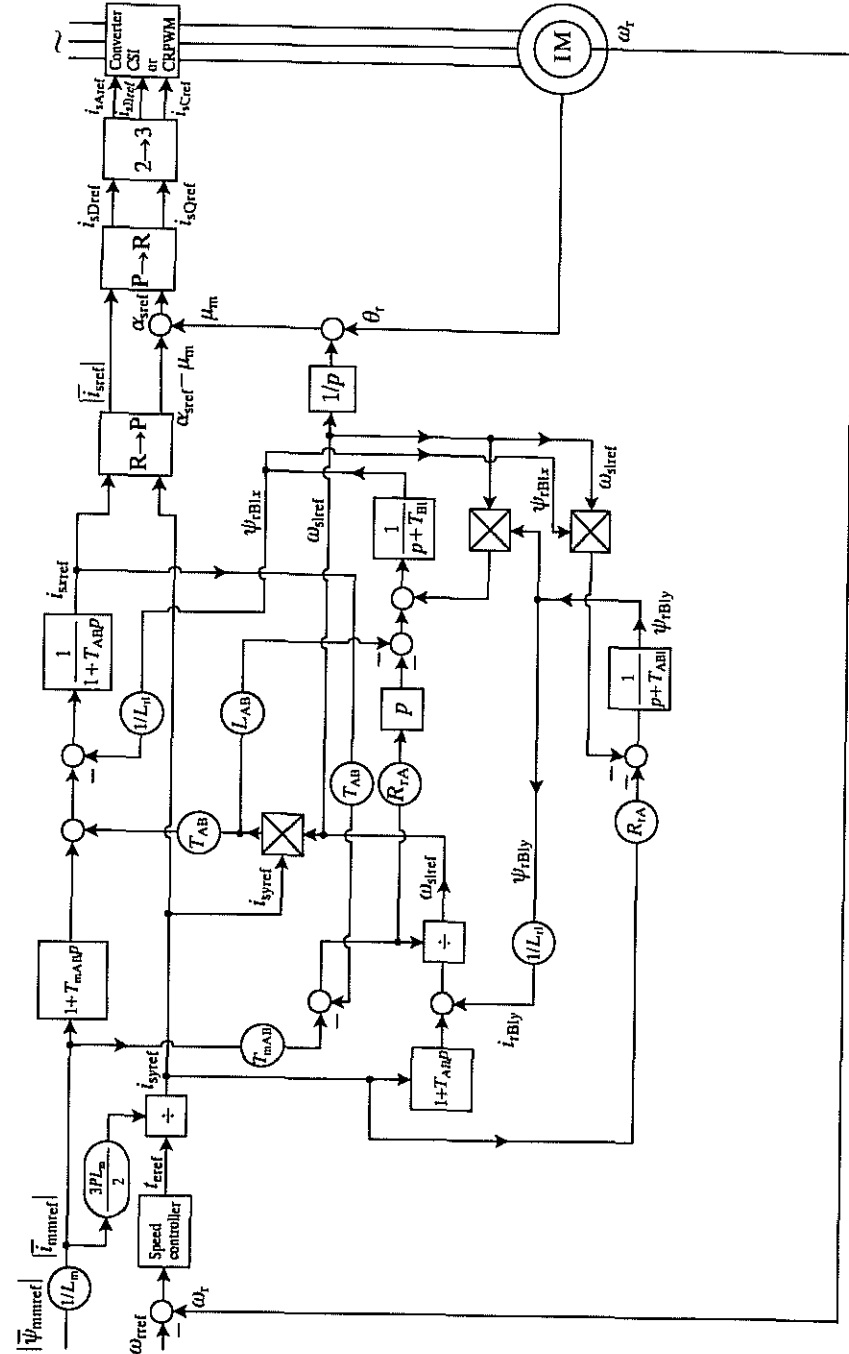


Fig. 4.36. Schematic of the indirect magnetizing-flux-oriented control of a double-cage induction machine with impressed stator currents utilizing an asymmetric rotor flux-linkage estimator.

The structure of eqn (4.3-99) resembles that of eqn (4.3-96) and thus eqns (4.3-96) and (4.3-99) describe a rotor flux-linkage estimator circuit which is symmetrical and does not contain a differentiator. Figure 4.37 shows the schematic of the indirect magnetizing-flux-oriented control of the double-cage induction machine with impressed stator currents where the rotor flux-linkage estimator circuit is symmetrical.

In the implementations shown in Fig. 4.36 and Fig. 4.37, the quadrature-axis stator current reference ( $i_{syref}$ ) is obtained from the torque reference ( $t_{erel}$ ), by using eqn (4.3-76). The torque reference is obtained as the output of the speed controller, which can be a PI controller. When the vector-control schemes shown in Fig. 4.36 and Fig. 4.37 are compared with the scheme shown in Fig. 4.34, which corresponds to the single-cage machine, there is a resemblance, although as a result of the double-cage, extra parts are present in Fig. 4.36 and Fig. 4.37. The main difference between the magnetizing-flux-oriented control schemes corresponding to the single-cage and double-cage machines is that in the scheme for the double-cage machine, an estimation circuit is present, which derives the direct- and quadrature-axis leakage flux-linkage components of the bottom cage. However, the required flux linkages can be obtained in real time at very high speed by using digital signal processors.

For indirect vector control of both the single-cage machine and the double-cage machine, it has been necessary to calculate the angular slip frequency by, for example, the circuits shown in Fig. 4.34(a) and Fig. 4.37 respectively. It follows from eqn (4.3-94) which defines  $\omega_{sl}$ , by considering eqns (4.3-93), (4.3-95), and (4.3-96), and by setting all the derivative terms to be zero, that the expression for  $\omega_{sl}$  is obtained in the steady state. This gives a fourth-order equation for  $\omega_{sl}$ . It follows from this equation that if  $i_{sx}/|\bar{I}_{mm}|$  and  $i_{sy}/i_{sx}$  are small and  $\omega_{sl}$  is also small, the angular slip frequency of the double-cage machine takes the same form as the angular slip frequency of the single-cage machine. However, while for the single-cage machine the angular slip frequency is proportional to the rotor resistance ( $R_r$ ) for the double-cage machine it is proportional to a resultant rotor resistance, which is obtained by connecting in parallel the resistors of the upper and lower cages, giving  $R_{rA}R_{rB}/(R_{rA} + R_{rB})$ . Usually the rotor resistance of the single-cage machine  $R_r$  and the resultant rotor resistance of the double-cage machine  $R_{rA}R_{rB}/(R_{rA} + R_{rB})$  are different and when a double-cage machine is subjected to vector control and  $\omega_{sl}$  is obtained by utilizing the equations of the double-cage machine, since the resistances of the upper and lower cages are independent of the rotor slip frequency, more accurate values of  $\omega_{sl}$  are obtained than by utilizing the single-cage equations. This also holds at low values of the torque-producing current. It can also be shown, by considering the steady-state expression for  $\omega_{sl}$ , that when  $\omega_{sl}$  is calculated as a function of  $i_{sx}/|\bar{I}_{mm}|$  or of  $i_{sy}/i_{sx}$ , it will have a maximum value. In the steady state this limits the stability region of the double-cage induction machine subjected to magnetizing-flux-oriented control.

When eqn (4.3-94) is used to obtain the expression for the angular slip frequency in the transient state, by also considering eqns (4.3-93), (4.3-95), and (4.3-96) it is

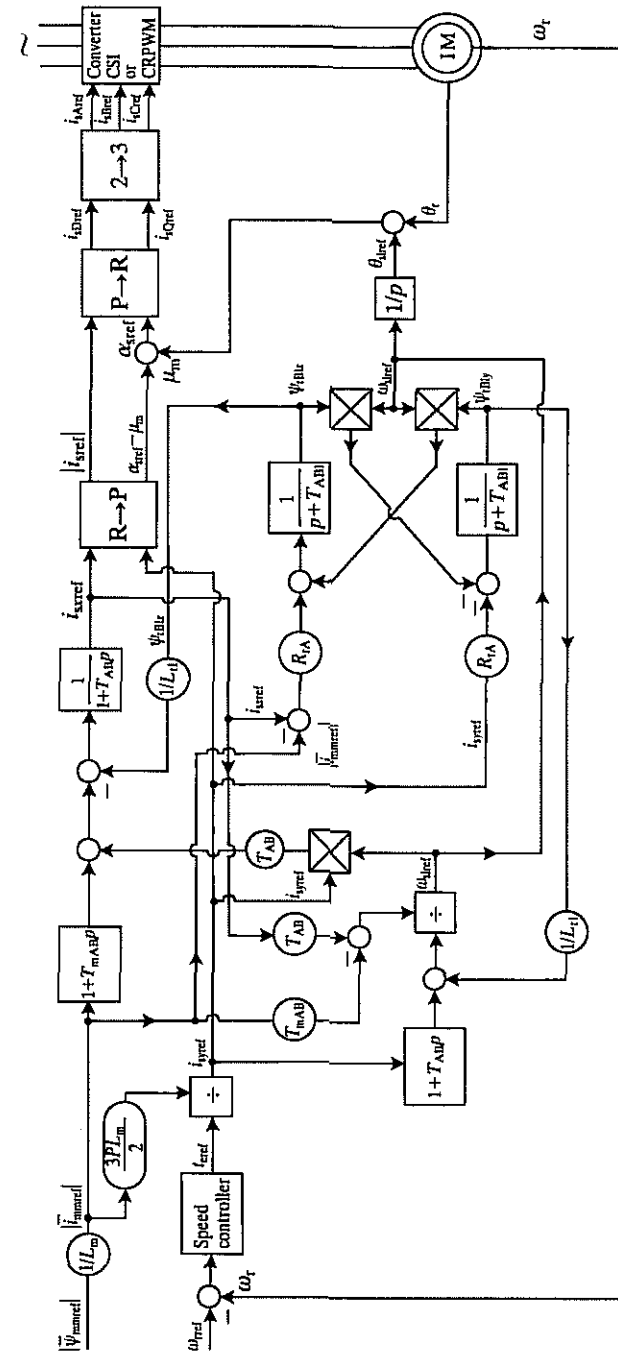


Fig. 4.37. Schematic of the indirect magnetizing-flux-oriented control of a double-cage induction machine with impressed stator currents utilizing a symmetrical rotor flux-linkage estimator.

possible to show that in the transient state,  $\omega_{sl}$  can be expressed in terms of  $i_{sy}$ ,  $i_{sx}$  and the various inductance and resistance parameters of the machine. If  $\omega_{sl}$  is small, the rotor time constant for slow and fast variations of  $i_{sx}$  decreases from  $T_{r1} = L_m/[R_{rA}R_{rB}/(R_{rA} + R_{rB})]$  to  $T_{r2} = L_{r1}/(R_{rA} + R_{rB})$ . If, say, a machine with deep rotor bars is considered and it is assumed that a rotor bar is divided into two equal sections, it follows that  $R_{rA} = R_{rB} = R_r$ . If  $L_m/L_{r1} = 30$ , the ratio of  $T_{r1}$  to  $T_{r2}$  is equal to 120, while if  $L_m/L_{r1} = 10$ , it is equal to 40. This shows that there can be a significant change in the rotor time constant. Thus to obtain fast torque response for high-performance a.c. servo applications, it is very important to incorporate the effects of the double-cage in the vector control scheme.

#### 4.4 Artificial-intelligence-based vector-controlled induction motor drives

In the present section vector-controlled drives using fuzzy-logic controllers and also fuzzy-neural controllers will be discussed. The main purpose of using artificial-intelligence-based controllers is to reduce the tuning efforts associated with the controllers and also to obtain improved responses. By using minimum configuration artificial-intelligence-based controllers, it is possible to have DSP implementations which do not have excessive memory and computation requirements.

##### 4.4.1 VECTOR DRIVES WITH FUZZY CONTROLLERS

###### 4.4.1.1 General introduction

In the literature there are many papers which discuss various vector drives with fuzzy-logic controllers. Most of these contain a single fuzzy-logic controller, which is a speed controller, and only a few papers discuss implementations and mainly concentrate on simulations. However, in the present section, a fully digital vector-controlled induction motor drive is discussed where all the controllers are fuzzy, i.e. the drive contains four fuzzy-logic controllers and the experimental results are also shown. The DSP used is the Texas Instruments TMS320C30. The drive considered is a vector drive using rotor-flux-oriented control and the machine is supplied by a voltage-source inverter and is similar to that discussed in Section 4.1.1.6.

Recent developments in the application of control theory are such that conventional techniques for the design of controllers are being replaced by alternatives that adopt radically different design strategies by making extensive use of artificial-intelligence-based (neural, fuzzy, fuzzy-neuro and genetic) concepts (see also Chapter 7). These methods are characterized by the different amount and type of the necessary *a priori* knowledge describing the system and the required performance. There is a strong industrial need for the development and exploitation of systems incorporating controllers based on these novel methods because of the numerous advantages offered (see Section 7.1). Recently,

fuzzy-logic control has emerged as an attractive area for research in the control application of fuzzy set theory. The main feature is the construction of fuzzy-logic controllers (FLCs) which utilize the linguistic knowledge of human experts.

###### 4.4.1.2 General structure of a fuzzy-logic controller

There are many types of fuzzy-logic controllers (FLCs), but now the Mamdani-type of fuzzy-logic controller [Mamdani 1974] is used. As shown in Fig. 4.38(a), in general this type of fuzzy-logic controller contains four main parts, two of which perform transformations; these are:

- fuzzifier (transformation 1);
- knowledge base;
- inference engine;
- defuzzifier (transformation 2).

The *fuzzifier* performs measurement of the input variables (input signals, real variables), scale mapping, and fuzzification (transformation 1). Thus all the monitored input signals are scaled and fuzzification means that the measured signals (crisp input quantities which have numerical values) are transformed into fuzzy quantities (which are also referred to as linguistic variables in the literature). This transformation is performed by using membership functions. For example, if an input signal is small, e.g. it is a speed error and has a crisp value of 0.001, then it belongs to the 'POSITIVE SMALL' fuzzy set, or -0.001 would belong to the 'NEGATIVE SMALL' fuzzy set; other speed errors may belong to other fuzzy

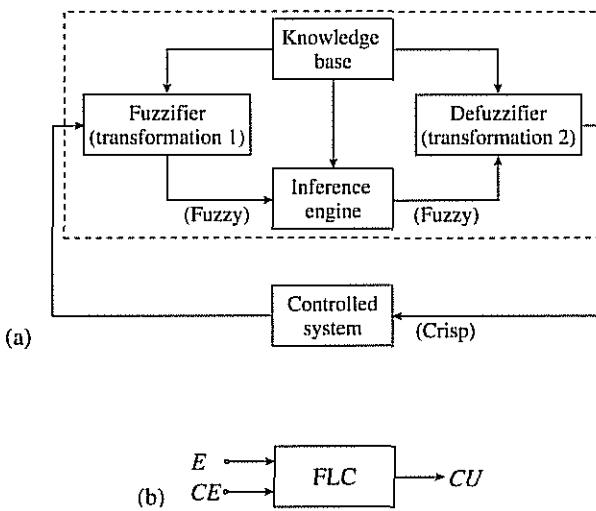


Fig. 4.38. Mamdani type of fuzzy-logic controller (FLC). (a) Schematic block diagram of a control system containing a Mamdani-type of FLC; (b) FLC with two inputs.

sets (e.g. POSITIVE LARGE, POSITIVE MEDIUM, etc.). In a ‘conventional’ fuzzy-logic controller (not a fuzzy-neural controller), the number of membership functions and the shapes of these are initially determined by the user. A membership function has a value between 0 and 1, and it indicates the degree of belongingness of a quantity to a fuzzy set. If it is absolutely certain that the quantity belongs to the fuzzy set, then its value is 1 (it is 100% certain that this quantity belongs to this set), but if it is absolutely certain that it does not belong to this set then its value is 0. Similarly if, for example, the quantity belongs to the fuzzy set to an extent of 50%, then the membership function is 0.5. The membership functions can take many forms including triangular, Gaussian, bell-shaped, trapezoidal, etc. For example, if the rotor speed error is 0.001, this is the input to the membership function of the positive small (PS) rotor speed errors,  $\mu_{\omega_r}^{PS}(E)$ , and e.g. on the output of this 0.99 is obtained,  $\mu_{\omega_r}^{PS}(E=0.001)=0.99$ , which means that it is 99% certain that the 0.001 rotor speed error is positive small. The initial forms of the membership functions can be obtained by using expert considerations or by clustering the input data. Final tuning of the membership functions can be performed on the DSP-controlled drive. Practical aspects of choosing the appropriate scaling factors and membership functions are also discussed below.

The *knowledge base* consists of the data base and the linguistic-control rule base. The data base provides the information which is used to define the linguistic control rules and the fuzzy data manipulation in the fuzzy-logic controller. The rule base (expert rules) specify the control goal actions by means of a set of linguistic control rules. In other words, the rule base contains rules which are those which would be provided by an expert. The FLC looks at the input signals and by using the expert rules determines the appropriate output signals (control actions). The rule base contains a set of if–then rules (see below). The main methods of developing the rule base are:

- using the experience and knowledge of an expert for the application and the control goals;
- modelling the control action of the operator;
- modelling the process;
- using a self-organized fuzzy controller;
- using artificial neural networks.

When the initial rules are obtained by using expert physical considerations, these can be formed by considering that the three main objectives to be achieved by the fuzzy-logic controller are:

- removal of any significant errors in the process output by suitable adjustment of the control output;
- ensuring a smooth control action near the reference value (small oscillations in the process output are not transmitted to the control input);
- preventing the process output exceeding user specified values.

The *inference engine* is the kernel of a fuzzy-logic controller and has the capability both of simulating human decision-making based on fuzzy concepts and of inferring fuzzy control actions by using fuzzy implication and fuzzy-logic rules of inference. In other words, once all the monitored input variables are transformed into their respective linguistic variables (by transformation 1 discussed above), the inference engine evaluates the set of if–then rules (given in the rule base) and thus a result is obtained which is again a linguistic value for the linguistic variable. This linguistic result has then to be transformed into a real output value of the FLC and this is why there is a second transformation in the FLC.

The second transformation is performed by the *defuzzifier* which performs scale mapping as well as defuzzification. The defuzzifier yields a non-fuzzy, real control action from the inferred fuzzy control action by using membership functions. There are many defuzzification techniques, but due to the simplicity of its implementation and simpler training algorithms, the centre of gravity method is adopted here. Physically this corresponds to taking a weighted average of the control action contributions from each of the various fuzzy rules. Since each of the rules (in the full rule base) can be considered to be rules provided by subexperts, this type of defuzzification simply means that the final decision is being made by taking the weighted average of all the recommendations of the subexperts.

When a classical controller (e.g. PI or PID) is used, then the input to the controller is the error signal. For example, for a PI speed controller, the input is the speed error, which is the difference between the reference speed and the actual speed,  $E(k)=\omega_{rref}(k)-\omega_r(k)$ . However, when a fuzzy-logic controller is used, there is more than one input to the controller. In the most frequently used fuzzy-logic controller, there are two inputs, these are the error ( $E$ ) and the change of the error ( $CE$ ) as shown in Fig. 4.38(b), and

$$E(k)=\omega_{rref}(k)-\omega_r(k) \quad CE(k)=E(k)-E(k-1).$$

This type of fuzzy-logic controller is used in the vector drive described in the present section, but it should be noted that there are other types of fuzzy-logic controllers as well, where the number of inputs is higher. It is a goal of the fuzzy-logic controller to obtain on its output a signal which is based on  $E$  and  $CE$ , e.g. this signal can be  $CU$ , which is the change of the output signal. If this is known, then it is possible to obtain the output signal from the change of the output by using  $u(k)=u(k-1)+CU(k)$ . It should also be noted that it is also possible to use another fuzzy-logic controller, where instead of obtaining the change of the output quantity, the output quantity is directly obtained.

As discussed above, in the heart of the fuzzy-logic controller there is a rule base and this contains the individual rules (subrules). In general, these linguistic rules are in the form of IF–THEN rules and take the form:

$$\text{IF } (E \text{ is } A \text{ AND } CE \text{ is } B) \text{ THEN } (CU \text{ is } C),$$

where  $A, B, C$  are fuzzy subsets for the universe of discourse of the error, change of the error and change of the output respectively. For example,  $A$  can denote the

subset NEGATIVE LARGE of the error, etc. To be more precise, for example, for a fuzzy speed controller, the following rules can be obtained by physical considerations:

Rule 1: IF ( $E$  is  $ZE$  AND  $CE$  is  $ZE$ ) THEN ( $CU$  is  $ZE$ )

Rule 2: IF ( $E$  is  $ZE$  AND  $CE$  is  $NS$ ) THEN ( $CU$  is  $NS$ )

Rule 3: IF ( $E$  is  $PS$  AND  $CE$  is  $NS$ ) THEN ( $CU$  is  $ZE$ )

and so on, where  $ZE$ ,  $NS$ ,  $PS$  denote the fuzzy sets ZERO, NEGATIVE SMALL, and POSITIVE SMALL respectively.

In general, for given numerical values of  $E$  and  $CE$  (which are the measured scaled inputs to the FLC), several rules can be activated simultaneously. This follows from the fact that a given numerical value can be a member of more than one fuzzy set (this is determined by the membership functions). Example 4.1 shows a numerical example of obtaining the output signal of a Mamdani-type of FLC, if two rules are assumed only for simplicity, and the two numerical (crisp) inputs to the FLC are  $x_1=4$  and  $y_1=8$ . It can be seen that  $x_1=4$  belongs to both the fuzzy set  $A1$  and fuzzy set  $A2$ ; the belongingness is described by the membership functions  $\mu^{A1}(x)$  and  $\mu^{A2}(x)$  respectively, and for the given  $x_1$  value they are  $\mu^{A1}(x_1)=2/3$  ( $x_1$  belongs to fuzzy set  $A1$  to a degree of 66.6%) and  $\mu^{A2}(x_1)=1/3$  ( $x_1$  also belongs to the fuzzy set  $A2$  to a degree of 33%). Although in general, several rules apply at the same time (several rules are 'fired' simultaneously), only a single control action must be performed, so the main task is to combine in an appropriate manner the contribution of each rule to obtain the control action. The inference engine determines the controller output on the basis of the contribution of each rule. In fuzzy-logic terms, the composition operation is used to perform this task. There are many types of composition operations, but the most commonly used is the sup-min (supremum–minimum) composition. In practice, the sup-min principle is applied to one rule at a time, which means that first, for each rule, an output membership function is computed, which gives the strength of the rule under consideration. This is obtained by using the 'min' operator (minimum operator) which corresponds to the fuzzy AND operation in the rules; thus the minimums of the appropriate membership functions are computed and then the combined fuzzy output is obtained by the supremum operator, or in other words, the outputs of each rule are combined into a single fuzzy set. When the supremum operator is applied, it means that after obtaining for each rule a truncated membership function (due to the min operator), then due to the supremum operator, a combined membership function is obtained, which is the outer envelope of the individual membership functions. For better understanding, this is illustrated in Example 4.1 which is related to a Mamdani-type of FLC, where for simplicity and there are only two rules. There are two inputs ( $x, y$ ) and an output ( $z$ ) and the input membership functions and output membership functions are given (they are triangular membership functions). It can be seen that for rule 1 the trapezoidal membership function  $\mu^{C1}(z)$  is obtained (its height is equal to the firing strength of the rule,  $w_1=2/3$ , and for rule 2 the membership function  $\mu^{C2}(z)$  is obtained (with height  $w_2=1/3$ ), and the combined

membership function,  $\mu(z)$ , is obtained from the outer envelopes of the two output membership functions. This combined output membership function is then used together with an appropriate defuzzification technique to obtain the crisp output value of the controller. In Example 4.1 the centre of gravity (COG) defuzzification method has been used, and the crisp output value of the controller is  $z^*=4.7$ .

#### Example 4.1 Mamdani-type of FLC with two rules

Inputs  $x_1=4$ ;  $y_1=8$

Determine (output):  $z^*$

Rule 1: IF  $x$  is  $A1$  AND  $y$  is  $B1$  THEN  $z$  is  $C1$

Rule 2: IF  $x$  is  $A2$  AND  $y$  is  $B2$  THEN  $z$  is  $C2$

Given membership functions:  $\mu^{A1}(x)$ ,  $\mu^{A2}(x)$ ,  $\mu^{B1}(y)$ ,  $\mu^{B2}(y)$ ,  $\mu^{C1}(z)$ ,  $\mu^{C2}(z)$

Input membership functions (for given inputs  $x_1, y_1$ )

In rule 1:  $\mu^{A1}(x_1)=2/3$ ;  $\mu^{B1}(y_1)=1$

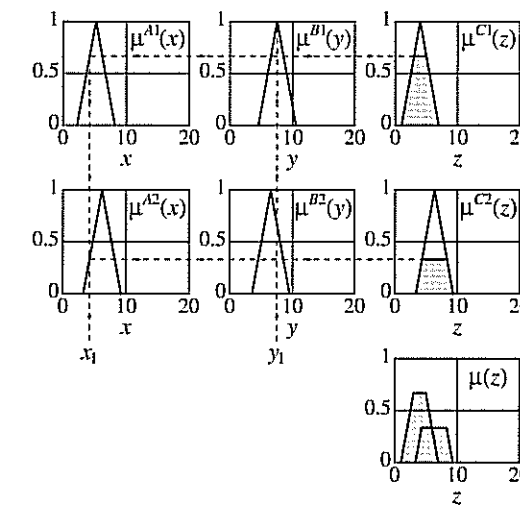
In rule 2:  $\mu^{A2}(x_1)=1/3$ ;  $\mu^{B2}(y_1)=2/3$

Firing strength of rule  $i(w_i)$ ; Fuzzy AND  $\Rightarrow$  min operator

Firing strength of rule 1:  $w_1=\min[\mu^{A1}(x_1), \mu^{B1}(y_1)]=\min(2/3, 1)=2/3$

Firing strength of rule 2:  $w_2=\min[\mu^{A2}(x_1), \mu^{B2}(y_1)]=\min(1/3, 2/3)=1/3$

Defuzzification Given: combined output membership function  $\mu(z)$ ; determine:  $z^*$



### Centre of gravity defuzzification (COG)

$$z^{*COG} = \sum z_k \mu(z_k) / \sum \mu(z_k) \quad (k=1, 2, \dots, 9)$$

$$z^{*COG} = \frac{2*(1/3) + 3*(2/3) + 4*(2/3) + 5*(2/3) + 6*(1/3) + 7*(1/3) + 8*(1/3) + 9*0}{1/3 + 2/3 + 2/3 + 2/3 + 1/3 + 1/3 + 1/3 + 0} \\ = 4.7$$

One possible initial rule base that can be used in drive systems consists of 64 linguistic rules as shown in Table 4.1. The 64 rules can be considered to be rules provided by 64 subexperts. It should be noted that a classical fixed-term controller (e.g. a PID controller) cannot achieve the three main control objectives listed above, unless extra logic is added. This extra heuristic logic is contained implicitly within the rules shown in Table 4.1.

In Table 4.1, the following fuzzy sets are used: *NM*=NEGATIVE MEDIUM, *NS*=NEGATIVE SMALL, *NZ*=NEGATIVE ZERO, *PZ*=POSITIVE ZERO, *PS*=POSITIVE SMALL, *PM*=POSITIVE MEDIUM, *PL*=POSITIVE LARGE. For example, it follows from Table 4.1 that the first ‘expert rule’ is: IF (*E* is *NL* AND *CE* is *NL*) THEN (*CU* is *NL*), where *CU* denotes the change of the output. It should be emphasized that although this initial rule base has given satisfactory responses in the DSP-controlled vector drive under consideration, it has been possible to significantly reduce the number of rules without degrading the drive performance. The reduced rule-base contains only 16 rules. The reduced rule-base has great influence on the overall complexity of the fuzzy system; this includes computational complexity and memory requirements. This is an important factor for industrial users, most of whom at present are reluctant to employ fuzzy techniques in variable-speed drives, since they associate fuzzy controllers with large computational and memory requirements. Fuzzy-controlled drives with minimal configuration fuzzy controllers is an important research topic [Vas 1996].

**Table 4.1** Fuzzy rule base with 64 rules

CE								
	<i>NL</i>	<i>NM</i>	<i>NS</i>	<i>NZ</i>	<i>PZ</i>	<i>PS</i>	<i>PM</i>	<i>PL</i>
<i>E</i>	<i>NL</i>	<i>NL</i>	<i>NL</i>	<i>NL</i>	<i>NL</i>	<i>NM</i>	<i>NS</i>	<i>NZ</i>
	<i>NM</i>	<i>NL</i>	<i>NL</i>	<i>NM</i>	<i>NM</i>	<i>NS</i>	<i>NZ</i>	<i>PS</i>
	<i>NS</i>	<i>NL</i>	<i>NL</i>	<i>NM</i>	<i>NS</i>	<i>NS</i>	<i>NZ</i>	<i>PM</i>
	<i>NZ</i>	<i>NL</i>	<i>NM</i>	<i>NS</i>	<i>NZ</i>	<i>PS</i>	<i>PM</i>	<i>PL</i>
	<i>PZ</i>	<i>NL</i>	<i>NM</i>	<i>NS</i>	<i>PZ</i>	<i>PZ</i>	<i>PS</i>	<i>PL</i>
	<i>PS</i>	<i>NM</i>	<i>NS</i>	<i>PZ</i>	<i>PS</i>	<i>PS</i>	<i>PM</i>	<i>PL</i>
	<i>PM</i>	<i>NS</i>	<i>PZ</i>	<i>PS</i>	<i>PM</i>	<i>PL</i>	<i>PL</i>	<i>PL</i>
	<i>PL</i>	<i>PZ</i>	<i>PS</i>	<i>PM</i>	<i>PL</i>	<i>PL</i>	<i>PL</i>	<i>PL</i>

### 4.4.1.3 Vector drive with four fuzzy controllers; design and tuning of fuzzy controllers

The overall structure of the system is shown in Fig. 4.39. The system contains a voltage-source inverter, a 3 kW squirrel-cage induction motor, analog circuits for the voltage and current transformations and a TMS320C30 DSP system board and interface board (DMB). The two boards are installed in a host computer. There are four A/D channels in the DMB which enable the input of four signals. The DSP software contains the algorithms for the fuzzy controllers, vector-control, PWM generation, machine soft-starting, and A/D calibration. During operation, up to fifteen drive quantities can be simultaneously shown on the host computer display in real-time. This greatly facilitates the tuning of the drive system. The PWM scheme uses an asynchronous symmetrical space-vector modulation technique. The digital signal conversion block is used for inverter fault detection, inverter protection, and the generation of the six firing (gating) signals.

As shown in Fig. 4.40, in the induction motor (IM) drive there are four fuzzy controllers; controller 1 is the speed controller, controller 2 is the torque-producing stator-current controller, controller 3 is the rotor-magnetizing-current (rotor-flux) controller, and controller 4 is the flux-producing stator-current controller. The four digital controllers implemented have been initially tuned by using a simulation of the drive system and fine tuning has been achieved on-line in the DSP implementation. The decoupling circuit has been described in Section 4.1.1.3 and is required in a VSI-fed drive (see also Fig. 4.11), to produce the required stator voltages  $u_{sxref}$ ,  $u_{syref}$ , which are also shown in Fig. 4.40. These are voltages in the rotor-flux-oriented reference frame, so they have to be transformed into

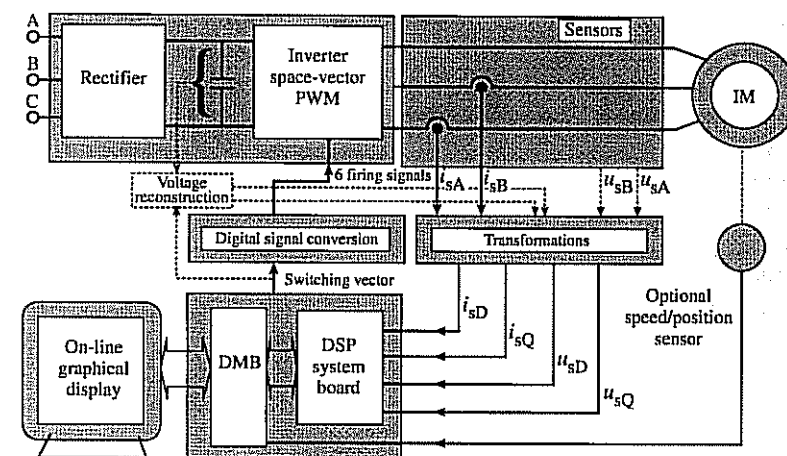


**Fig. 4.39.** Schematic diagram of vector-controlled PWM voltage-source inverter-fed induction motor drive.

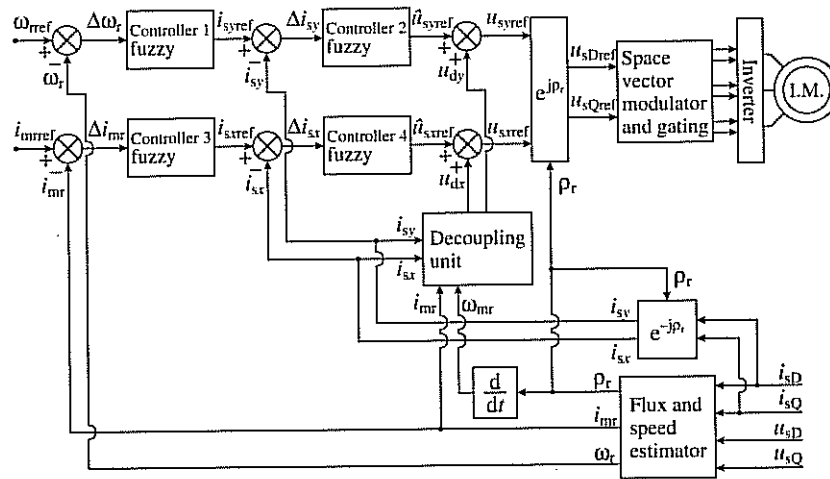


Fig. 4.40. Vector-controlled PWM voltage-source inverter-fed induction motor drive with four fuzzy controllers.

their stationary reference frame values ( $u_{sDref}$ ,  $u_{sQref}$ ) by using the complex transformation  $\exp(j\rho_r)$ , where  $\rho_r$  is the angle of the rotor flux-linkage space vector. The inverse transformation  $\exp(-j\rho_r)$  is used in Fig. 4.40 to transform the stator current components expressed in the stationary reference frame ( $i_{sD}$ ,  $i_{sQ}$ ) into the stator currents in the rotor-flux-oriented reference frame ( $i_{sx}$ ,  $i_{sy}$ ).

It should be noted that classical PI and PID controllers which are used in conventional converter-fed a.c. drive systems are mainly tuned using *ad hoc* methods. Several techniques exist which provide initial values of the controller parameters, the most commonly used being based on the Ziegler–Nichols methods. However, these techniques can be time-consuming and fixed controllers cannot necessarily provide acceptable dynamic performance over the complete operating range of the drive. Performance will degrade mainly because of machine non-linearities, parameter variation, etc. Adaptive controllers can be used to overcome these problems and also to eliminate the need to perform detailed *a priori* controller design. Alternatively, performance-index-based optimal control techniques can be adopted, but these may suffer from convergence-related problems. The fundamental aim of drive system optimization is to obtain the smallest overshoot with the shortest rise and settling times. It is not generally possible to fulfil all these criteria simultaneously, but a solution can be obtained by using some type of an integral criteria (performance index). When an integral criteria is used, the integrands are products of the control error and the time, each raised to some power. When the integral square error (ISE) criterion is used, the performance index is the integral of the square of the error. To obtain better damping of the controlled variable, the ITSE criterion is used. In this case the integral of the error squared multiplied by time is used. Further improvements of the settling

time can be obtained by using the ISTSE (integral of time squared multiplied by the error squared) criterion, but the computation time is increased. The ITAE criteria is commonly used in variable-speed drives, where the integrand is the absolute value of the error multiplied by time. However, the determination of the optimum controller parameters based on performance indexes may be very time consuming and, as mentioned above, may suffer from convergence-related problems.

For a practical DSP implementation of the four fuzzy controllers the following aspects should be considered:

- Discretization of membership functions** For ease of real-time implementation, and for the purposes of fuzzification and defuzzification, triangular membership functions have also been considered, and they can be conveniently described by using discrete values in a look-up table.
- Rule base look-up table** It should be noted that when a microprocessor or DSP-based fuzzy controller is designed, a look-up table for the rule base can also be used. This contains the discrete values of the change of the output of the fuzzy controller. However, care must be taken when a look up table is selected, otherwise errors could arise due to improper selection.

The absence of widespread industrial applications of fuzzy controllers in drives is also related to the fact that there are no straightforward procedures for the tuning of fuzzy controllers. However, it is possible to give guidelines for the developer of these controllers. The main tuning steps are:

- Tuning of input and output scaling factors** The output scaling factor in a fuzzy-logic controller has great influence on the stability of the system. The input scaling factor has great influence on the sensitivity of the fuzzy-logic controller with respect to the optimal choice of the operating ranges of the input signals. Both scaling factors are thus set during the initial tuning stage.
- Tuning of input and output membership functions** The number and shape of the input and output membership functions have a considerable influence on the controller behaviour. The second stage of the tuning process is concerned with the tuning of the membership functions. A variety of membership-function forms has been considered, including triangular and Gaussian membership functions. Finally, triangular membership functions have been selected.
- Tuning of the rules** It is possible to achieve optimal tuning by the appropriate adjustment of the base.

An extensive range of digital simulations has been performed to obtain the appropriate values of the scaling factors, membership functions, and rule base. This was followed by the real-time implementation of the fuzzy-logic controllers in various drive systems.

It should be noted that in addition to fuzzy controllers, fuzzified controllers (FPIC) [Vas 1995] may also be used. Sometimes industry prefers such a solution, since it only requires small changes to be made to an existing system. FPICs can

improve the performance of the system incorporating conventional PI controllers by using fuzzy logic. Small changes of the values of the controller coefficients may lead to considerable improvement in performance. In a FPIC, the rule base contains the following type of rules:

if  $E$  is  $A$  and  $CE$  is  $B$  then  $CP$  is  $C$   
if  $E$  is  $A$  and  $CE$  is  $B$  then  $CI$  is  $C$ ,

where  $E$  and  $CE$  describe the error and change in error respectively,  $CP$  and  $CI$  represent the changes of the proportional term and the integral term of the PI part in the FPIC separately. For example, there can be in total 72 rules. In these rules the linguistic variables  $A$ ,  $B$ , and  $C$  may take the values  $PM$ ,  $NS$ , etc. The parameters of the PI part of the fuzzified controller can be adjusted according to

$$P(k) = P(k-1) + K_p CP \quad (4.4-1)$$

for the proportional term and

$$I(k) = I(k-1) + K_i CI \quad (4.4-2)$$

for the integral term. In these equations  $K_p$  and  $K_i$  are proportional and integral coefficients on which the degree of dynamic parameter adjustment depends,  $P(k)$  and  $P(k-1)$  describe the proportional term of the PI part at the  $k$ th and  $(k-1)$ th sampling times respectively, and  $I(k)$  and  $I(k-1)$  correspond to the integral term of the PI part at these sampling instants. It should be emphasized that the performances of the FLC are far better than those of both the FPIC and optimal PI controller. In contrast to the computational times for the fuzzy-logic-based system, those for the optimized controller are excessive.

#### 4.4.1.4 Experimental results

Figure 4.41 shows some experimental characteristics obtained for the DSP-controlled induction motor drive system with four fuzzy controllers. It can be seen from Fig. 4.41(a) that the drive starts from rest. The reference rotor speed ( $\omega_{ref}$ ) is first set to zero then to  $220 \text{ rad s}^{-1}$  and then to  $-220 \text{ rad s}^{-1}$  and finally to zero again. As shown in Fig. 4.41(c), the torque-producing stator current ( $i_{sy}$ ) is maintained at its maximum value during both acceleration and deceleration. It follows well its reference value ( $i_{syref}$ ). It can be seen from Fig. 4.41(b) that the rotor magnetizing current ( $|i_{mr}|$ ) is effectively constant. As expected, the angular slip frequency ( $\omega_{sl}$ ) has a similar shape as  $i_{sy}$ , since if  $|i_{mr}| = \text{constant}$ , and the rotor time constant ( $T_r$ ) is also considered to be constant, then from eqn (4.1-26)  $\omega_{sl} = i_{sy}/(T_r |i_{mr}|) = ci_{sy}$ , where  $c$  is a constant.

It is very important to note that the tuning effort required with the fuzzy-controlled drive is significantly less than that required for the drive using four PI controllers. Similar conclusions for other fuzzy drives have also been obtained by Texas Instruments [Beierke 1995]. Furthermore, there is also some improvement in the responses, e.g. the stator flux-producing current ( $i_{sx}$ ) for the fuzzy-controlled

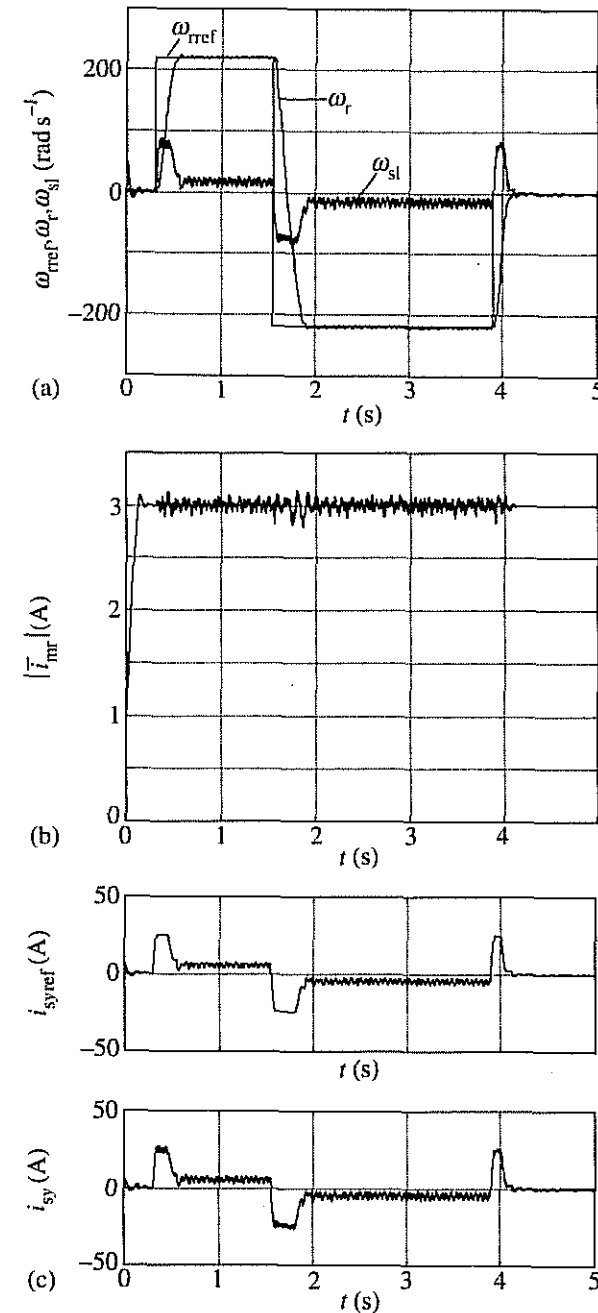


Fig. 4.41. Vector-controlled induction motor drive responses using four fuzzy controllers (experimental results). (a) Rotor speed reference, rotor speed, angular slip frequency ( $\omega_{ref}$ ,  $\omega_r$ ,  $\omega_{sl}$ ); (b) rotor magnetizing current ( $|i_{mr}|$ ); (c) torque-producing stator-current reference and its actual value ( $i_{syref}$ ,  $i_{sy}$ ).

drive shows an improved transient profile. An extensive simulation of the complete drive system has also been performed, which has also incorporated the effects of the space vector pulse-width modulator. For this purpose the simulation software described in [Vas 1993] has been extended to incorporate the four fuzzy-logic controllers.

Figures 4.42(a) and (b) show the highly non-linear 3-D controller profile of the implemented speed and flux fuzzy-logic controllers. For illustration purposes Figs 4.42(c) and 4.42(d) show the controller profiles of the discretized speed and flux PI controllers used above. Although the control profiles of the PI controllers are simpler, which also correspond to simpler digital implementations, it is still extremely useful to implement the more complicated fuzzy controllers resulting in more complex control surfaces. This is due to the fact that the fuzzy controllers are adaptive controllers. Therefore, by appropriate tuning it is possible to obtain better dynamic characteristics under all operating conditions. It should be noted that even the very first laboratory implementation of the discretized fuzzy controllers has been successful. This also proves the existence of the reduction in tuning effort associated with fuzzy controllers.

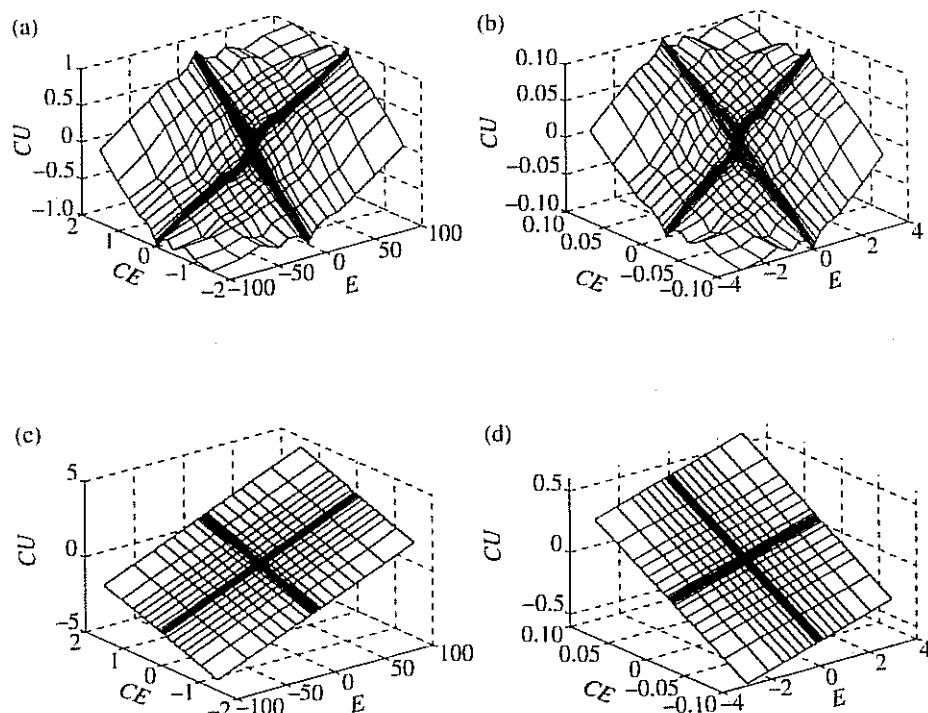


Fig. 4.42. PI and fuzzy-controller profiles. (a) Fuzzy speed-controller profile; (b) Fuzzy flux-controller profile; (c) PI speed-controller profile; (d) PI flux-controller profile.

#### 4.4.2 VECTOR DRIVE WITH FUZZY-NEURAL CONTROLLERS

##### 4.4.2.1 General introduction

In the previous section, a fuzzy-controlled vector drive has been described for a voltage-source inverter-fed induction motor. This contained four fuzzy-logic controllers and all the fuzzy-logic controllers required the use of their own rule base and membership functions (for fuzzification and defuzzification). However, it is possible to use such controllers where these rules and membership functions do not have to be known *a priori*. For this purpose fuzzy-neural controllers can be used (see also Chapter 7).

Fuzzy-neural control emerged as a powerful technique more than a decade ago. In fuzzy-neural control the ideas of a fuzzy-logic controller and an artificial neural network (ANN) structure are combined. The fuzzy-neural network is automatically constructed by a learning process. In a connectionist fuzzy-neural controller, the input and output nodes of the ANN represent the input and output signals, and in the hidden layer nodes take the roles of membership functions and rules. The learning algorithm for this network can be hybrid, combining unsupervised and supervised methods. The unsupervised learning produces the number of fuzzy sets for each input and output variable, the number of fuzzy rules, the rules themselves, and the centres and widths of the membership sets. This information is used to establish a fuzzy-neural controller which is then trained using a back-propagation algorithm to further tune the centres and widths of the membership functions. The structure of the controller is fixed. Hybrid learning outperforms purely supervised learning by reducing training times.

There are many architectures which can be used for fuzzy-neural controllers. The fuzzy-neural controller used here contains five layers: an input layer, a layer for the fuzzy membership sets, a fuzzy AND layer, a fuzzy OR layer, and an output layer (see Fig. 4.43 below). The input layer contains the input nodes, which represent linguistic variables. These distribute each input variable to its membership functions. There are three hidden layers: layer 2 generates the appropriate membership values, layer 3 defines the preconditions of the rule nodes, and the nodes in the fourth layer connect the output of the fuzzy AND nodes to the consequences in the rules. The last layer is the output layer and it performs defuzzification. Tuning can conveniently be performed using a back-propagation-type of algorithm.

The direct implementation of conventional fuzzy-logic controllers suffers from the disadvantage that there is no formal procedure for the direct incorporation of the expert knowledge during the development of the controller. The structure and detail of the fuzzy controller (number of rules, the rules themselves, number and shape of membership functions, etc.) is achieved through a time-consuming tuning process which is essentially *ad hoc*. The ability to automatically ‘learn’ characteristics and structure which may be obscure to the human observer is, however, an inherent feature of neural networks. However, in applying artificial neural

networks to control problems, there is no general systematic approach to choosing the network type or structure and it is also difficult to relate the final trained network (in terms of the activation functions, weights, etc.) to the original physical problem (see also Section 7.1). The combination of a fuzzy-logic controller with the structure of a neural network does, however, offer the control system designer the opportunity to make use of the advantages of both—the ability of the fuzzy logic to take account of expert human knowledge and the learning ability of the neural network—to overcome their respective disadvantages—the lack of a formal learning procedure for the fuzzy controller and the lack of a clear correlation with the physical problem when using artificial neural networks. This approach therefore provides a means of combining the use of imprecise, linguistic information but which has a clear physical significance with formalized mathematical structures and training algorithms. A fuzzy-neural controller offers a structure which enables ‘automated’ design, requiring a minimum of human intervention for the tuning.

#### 4.4.2.2 Fuzzy-neural controller design

This section provides a detailed description of both general and application-specific features of the development of a fuzzy-neural controller implementation. This is based on the Mamdani type of fuzzy logic system shown in Fig. 4.38(a), the basic elements of which are a fuzzy rule base, with associated fuzzy sets, and a fuzzy inference engine, with associated operators. The artificial neural network used is multi-layer feedforward ANN. The training algorithms used are of the competitive learning and the back-propagation types. A variety of activation functions associated with the nodes are used and are described in detail.

##### 4.4.2.2.1 Structure of fuzzy-neural controllers

The fuzzy-neural controller structure used is represented by a neural network consisting of five layers. Figure 4.43 shows an example of the network structure for a controller with two inputs and a single output.

In Fig. 4.43 the first layer is an input layer with one node for each controller input variable. The nodes in this layer act as single-input, multi-output, ‘fan-out’ nodes distributing each input variable to each of its associated membership function nodes in the second layer. The weights (strength of connection) between a  $j$ th node in the  $k$ th layer and an  $i$ th node in the previous layer are denoted by  $w_{ji}^k$ . The interconnection weights between the first and second layers are all unity and constant. The second layer is made up of nodes representing Gaussian membership functions. The total number of nodes in this layer is equal to the total number of fuzzy sets associated with the input variables. The input function,  $f$ , the activation function,  $g$ , and the output function,  $h$ , are such that the overall the node output,  $y$ , is given by

$$y = \exp[-(x^2 - m)^2/\sigma^2], \quad (4.4-3)$$

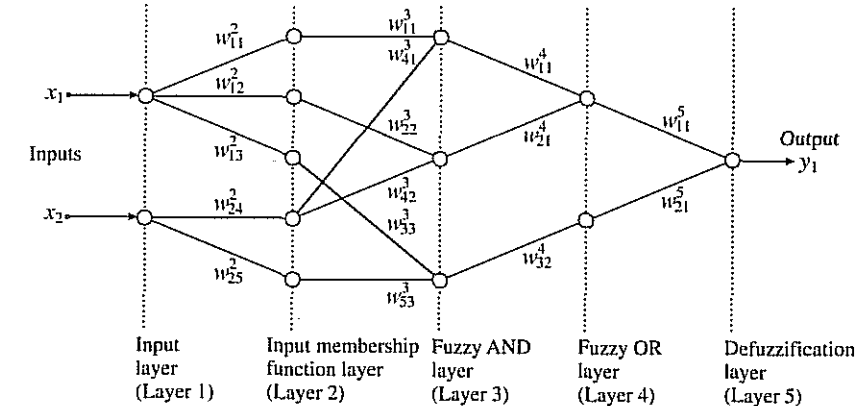


Fig. 4.43. Fuzzy-neural network.

where  $m$  and  $\sigma$  denote the centre and width of a fuzzy set respectively. The interconnection weights between the second and third layers are all unity and constant. The third layer is made up of nodes implementing the fuzzy intersection form of the fuzzy AND operator. Each node represents a fuzzy rule and the node output,  $y$ , is given by

$$y = \min(x_1, x_2, \dots, x_k). \quad (4.4-4)$$

The interconnection weights between the third and fourth layers are also all unity and constant. The fourth layer is made up of nodes implementing the bounded sum form of the fuzzy OR operator. The number of nodes is equal to the total number of fuzzy sets associated with the controller output variables. The node output,  $y$ , is given by

$$y = \min\left(1, \sum_{i=1}^k x_i\right). \quad (4.4-5)$$

The fifth and final layer comprises nodes implementing the centre-of-area defuzzification algorithm, with one node for each output variable. The weights of the interconnections between the nodes in the fourth and fifth layers are the products of the centre and width of the membership function associated with the fuzzy set for each layer-four node output variable. The node output,  $y$ , is given by

$$y = \frac{\sum_{i=1}^k m_i \sigma_i x_i}{\sum_{i=1}^k \sigma_i x_i}. \quad (4.4-6)$$

In order to establish the fuzzy-neural controller structure for a particular application the following must be determined:

- The number of membership sets associated with each input variable, i.e. the number of nodes in the second layer and the connections between layers 1 and 2.

- The number of membership sets associated with each output variable, i.e. the number of nodes in the fourth layer.
- What the fuzzy rules are, i.e. the connections between layers 2 and 3 and between layers 3 and 4.
- The initial estimates for the centre and width of each input variable fuzzy-set-membership function, i.e. the parameters of the activation functions of the layer-2 nodes.
- The initial estimates for the centre and width of each output variable fuzzy-set-membership function, i.e. the connection weights between layers 4 and 5 and the parameters of the activation function of the layer-5 nodes.

The determination of the required structure and the initial values of the membership function parameters is done in an initial tuning stage. Subsequent to this, a further tuning, using a back-propagation type of algorithm, adjusts the membership function parameters and the network connection weights to produce the final trained fuzzy-neural controller. The details of these two stages are given in the following sections.

#### *4.4.2.2.2 Determination of the fuzzy-neural network structure and parameters*

This section describes in detail the first stage of the fuzzy-neural controller development discussed above. This stage uses a separate, competitive-learning type of artificial neural network to determine the number of fuzzy rules, the fuzzy rules themselves, and the number and centre of the membership sets. The results from this give both the structure and the initial parameter and weight settings for the controller network.

The network used in this first stage consists of a layer of input nodes followed by a single layer of competitive nodes trained using a supervised instar learning algorithm. The number of nodes in the input layer is equal to the number of controller input and output variables—a total of three in the present application, two variables representing the controller inputs—error and change in error, the third representing the change in controller output. The number of nodes in the competitive layer is equal to the maximum number of fuzzy rules possible for the problem under consideration. For example, if eight membership sets are assumed for each of the three controller variables then the number of output nodes is 512.

The network is fully connected, i.e. all first layer nodes are connected to all nodes in the second layer. The initial setting of the weights associated with the network are assigned as uniformly distributed random values. The weights connecting each of the input nodes to an output node are regarded as a weight vector; all such vectors are normalized to a magnitude of unity. The input to the network consists of a sequence of training vectors. Each training vector comprises the values of the controller inputs and the corresponding controller output.

The network is then trained by establishing which weight vector is ‘closest’ to the input (training) vector. This is done by forming the inner product of the training vector with each of the weight vectors and finding the maximum of the

resulting products. This identifies the ‘winning’ output node which is assigned an output of unity; all other network outputs are set to zero. The weight vector associated with the ‘winning’ output node is adjusted to become closer to the training vector; all other remain unchanged. A count is kept of the number of times each output node ‘wins’. At the end of training, the training vectors have been ‘clustered’ by association with the ‘winning’ output nodes.

The clusters associated with output nodes which ‘win’ represent the fuzzy rules implied by the training data. A straightforward application of this procedure may, however, result in an unnecessarily high number of rules. The outcome of this stage of the training is therefore modified. This procedure eliminates ‘weak’ rules, of both a similar and conflicting nature, thereby enabling a minimal rule base to be established from the training data. Any available expert linguistic information can be included, as required, at this stage of the controller development.

Initial estimates of the centres of the membership functions are established from the mean of each variable associated with the remaining vector clusters. The widths of the membership functions are established using the ‘nearest neighbour’ and ‘overlap’ concepts [Stronach *et al.* 1996]. As an alternative, the standard deviation of the vector clusters can be used but experience has shown that problems arise in cases where standard deviation values are insufficiently large and overlap between adjacent membership sets is ‘inadequate’.

#### *4.4.2.2.3 Fuzzy-neural controller tuning*

This section describes the second-phase tuning of the fuzzy-neural controller development outlined above. The results of the first stage training, the number of fuzzy sets for each variable and the fuzzy rules, are used to establish the structure of the fuzzy-neural controller network, as described in Section 4.4.2.2.1 and typified by the network shown in Fig. 4.43. The network is initialized using the values for the membership function centres and widths obtained from the first-stage tuning. Once established, the network structure remains fixed during the second stage of tuning. Therefore the network interconnection weights between layers one and two, between layers two and three, and between layers three and four do not change in the second stage of tuning. Only the interconnection weights between layers four and five and the parameters (centres and widths) of the membership functions are altered. The second stage of tuning to improve these values uses a back-propagation-type algorithm with the same set of training data as was used for the first-stage competitive network. The final, trained form of this network gives the implementation form of the controller.

#### *4.4.2.2.4 Alternative fuzzy-neural controller designs*

In addition to the approach described in detail above, a number of alternative methods may be adopted for establishing a fuzzy-neural controller.

A back-propagation-based method which does not use clustering allows all fuzzy logic system parameters to be updated in a single optimization procedure. This approach can also incorporate linguistic information but the high

dependence on a non-linear optimization search results in a possible slow convergence to a local minimum. The numbers of fuzzy sets for each variable must be specified *a priori*. It has been found that the proposed clustering-based approach results in fewer such sets. An 'order of magnitude' reduction is typically achieved. Investigations using a much simpler 'nearest neighbour' type of clustering algorithm do not show such a reduction in the number of fuzzy sets.

An approach based on an orthogonal least-squares solution establishes fuzzy basis functions and uses these to set up a form of fuzzy-logic controller which is linear in the unknown parameters. This approach, however, is computationally expensive and again requires the *a priori* specification of the initial number of basis functions to be used from which a specified number of 'best' functions are selected.

Look-up-table methods have the advantage of simplicity and the resulting controller can be established in a one-pass operation. There is, however, no optimization and *a priori* specification of the numbers of fuzzy sets for each variable is again required. Equivalent and conflicting rules are eliminated by calculating a weight for each rule; rules with the highest weights are retained. Since there is no prior clustering of the training data, the elimination of such rules involves an exhaustive, and hence computationally expensive, evaluation of rule weights leading to an increased development time for the controller.

The method adopted and described above has been found to result in a considerably simplified controller structure when compared to those obtained by any of the alternative methods, and the proposed procedure also has the advantage that the number of fuzzy sets and fuzzy rules can be determined by an automatic procedure.

#### 4.4.2.3 Vector drive with a self-organizing fuzzy-neural controller; minimal configuration

The vector drive considered is similar to that shown in Fig. 4.40, where controller 1 is the speed controller, controller 2 is the torque-producing current controller, controller 3 is the magnetizing current controller, and controller 4 is the flux-producing current controller. Conventionally these are implemented as PI-type controllers, but any of these may be replaced by a fuzzy-neural controller, and now the speed controller (controller 1) is a fuzzy-neural controller.

There are various possibilities for obtaining the training data, e.g. it can be obtained from the PI-controlled drive. For this purpose, approximately 1500 data sets for the error, change of error, and controller output were recorded with the drive responding to a sequence of changes in reference speed going from standstill to 75% rated speed, followed by a speed reversal to -75% rated speed, followed by a reference speed change bringing the drive to rest. Data from this test was used to establish and train the fuzzy-neural speed controller by the two-stage, off-line procedure described in Sections 4.4.2.2.2 and 4.4.2.2.3. The first-stage training was carried out for approximately 60 epochs and the second-stage tuning was carried out for a further 30 epochs.

It is a feature of the proposed method that it results in a significant reduction (up to 50%) in the number of fuzzy sets required for each variable when compared to classical non-self-organizing fuzzy speed controllers used in drives. A corresponding reduction in the number of fuzzy rules is also obtained, in this case up to an order of magnitude. These reductions afford a significant advantage over conventional approaches to controller design, particularly regarding the DSP requirements of a practical implementation.

The results for the real-time performance obtained for the drive using the TMS320C30 DSP with the fuzzy-neural controller replacing the PI speed controller are shown in Figs 4.44(a) to 4.44(c). The sequence of speed reference changes is as indicated above. It follows from Fig. 4.44(a) that a satisfactory speed response is achieved. The torque-producing stator current component ( $i_{sy}$ ) shown in Fig. 4.44(b) has the expected form and follows the reference value ( $i_{syref}$ ) generated by the fuzzy-neural controller. As expected the rotor magnetizing current ( $|I_{mr}|$ ) shown in Fig. 4.44(c) is effectively constant.

It should be noted that similar experimental results have been obtained for the induction motor drive when various speed controllers have been used: for the case when a fuzzy speed controller was used, for the drive with a PI speed controller, and also for the drive with an artificial-neural speed controller. However, in the present scheme the fuzzy rules and the membership functions have been obtained by an automatic, systematic procedure. In addition, a reduced number of membership functions and fuzzy rules has been established.

Figure 4.45 shows the extremely non-linear 3-D controller characteristic of the fuzzy-neural speed controller. This results from a considerably reduced rule base established from the first phase of the network development followed by a second-stage tuning process with a duration of around 100 epochs.

In summary it can be concluded that the combination of artificial neural network and fuzzy-logic concepts allows the advantages of each approach to be utilized whilst at the same time overcoming their respective disadvantages. The design procedure adopted allows for two-stage tuning of the controller. The first stage involves a method for the determination of the detailed structure of the fuzzy-neural controller, the determination of a minimal rule-base together with initial estimates for the centres and widths of the membership functions. The first stage allows for the inclusion of expert linguistic information. The second stage involves further tuning of the membership functions of the fuzzy-neural controller using a back-propagation-type training algorithm. The fuzzy-neural-controller form of a vector-controlled induction motor drive has been compared to that using conventional PI-type and non-self-tuning fuzzy controllers. Although the responses obtained in these cases are similar, it is important to note that the two-stage approach results in a reduced overall development time compared to the conventional approaches. The proposed technique produces minimal fuzzy set and rule base configurations for the fuzzy-neural controller. This leads to simpler real-time implementation. It is believed that in the future fuzzy-neural controllers will find widespread applications in various variable-speed drives.

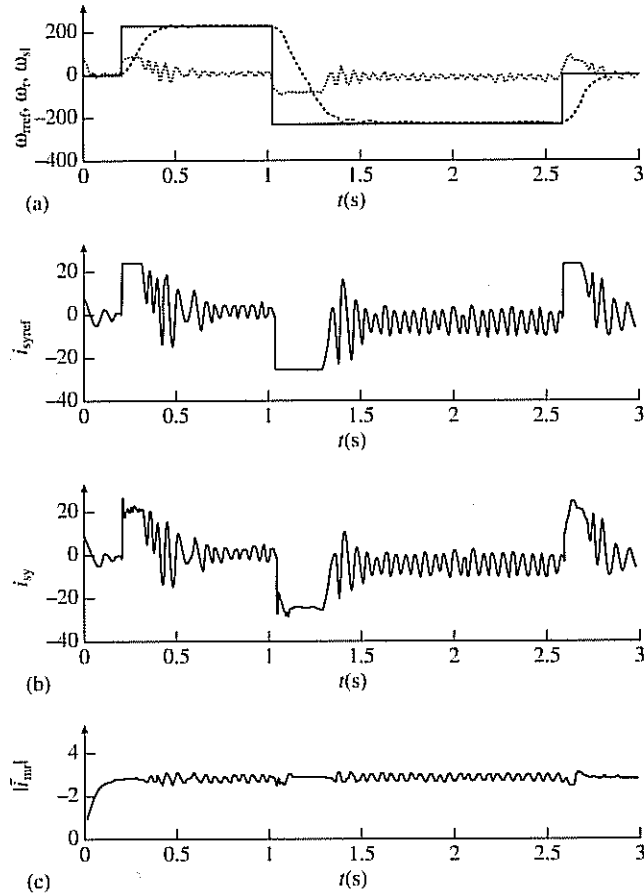


Fig. 4.44. Fuzzy-neural-controlled vector drive experimental responses. (a) Reference speed, rotor speed, slip frequency ( $\omega_{\text{ref}}, \omega_r, \omega_{\text{sl}}$ ); (b) torque-producing stator current reference, torque-producing stator current ( $i_{\text{sref}}, i_{sy}$ ); (c) rotor magnetizing current ( $i_{\text{mref}}$ ).

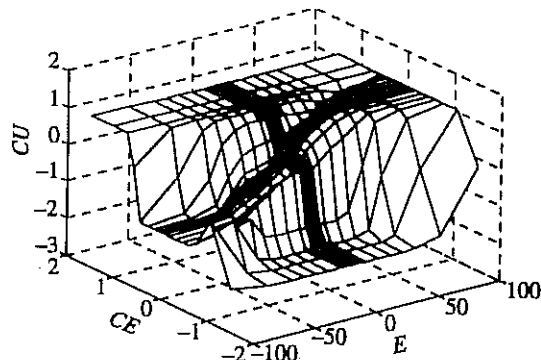


Fig. 4.45. Non-linear fuzzy-neural speed controller profile.

## 4.5 Main techniques of sensorless control of induction motors

### 4.5.1 GENERAL INTRODUCTION

Many attempts have been made in the past to extract the speed or position signal of an induction machine; Chapter 5 of a recent book [Vas 1993] describes in detail various solutions. However, the first attempts have been restricted to techniques which are only valid in the steady state, and as an example, such techniques will first be briefly described. These can be used in low-cost drive applications, not requiring high dynamic performance. However, other techniques will also be described which are applicable for high-performance applications in vector- and direct-torque-controlled drives.

It is a common feature of many of the ‘sensorless’ techniques that they depend on machine parameters: they may depend on the temperature, saturation levels, frequency, etc. To compensate for the parameter variations, various parameter-adaptation schemes have also been proposed in the literature. In an ideal sensorless drive, speed information and control is provided with an accuracy of 0.5% or better, from zero speed to the highest speed, for all operating conditions and independent of saturation levels and parameter variations. In the only industrial sensorless implementation of a direct-torque-controlled drive, an improved mathematical model is used to estimate the speed, and it is claimed that the drive can work even at zero speed. However, it is believed that in the not-distant future, artificial-intelligence-based techniques (fuzzy, neural, fuzzy-neural, etc.) will have a more dominant role in sensorless drives and in particular, complicated mathematical models will not be required for speed or position estimation.

Conventional techniques are not suitable to achieve stable, very low speed operation in a speed or position sensorless high-performance induction motor drive. In this case the estimation of the speed is problematic, due to parameter mismatch and noise. If the induction motor is represented by its fundamental model, then it becomes unobservable at zero frequency. However, as will be discussed in Section 4.5.3, it is possible to utilize various effects (rotor slot harmonics, saliency, etc.) for the speed estimation, but e.g. the rotor slot harmonic signal is insufficient in bandwidth as a speed feedback signal in a high-performance drive, and specially introduced saliencies require non-standard rotors. On the other hand, it is possible to estimate the rotor position at very low rotor speed and even at zero frequency with high bandwidth in a standard squirrel cage induction motor by utilizing the rotor angle variation of the machine inductances  $u_{sA}/(di_{sA}/dt)$ ,  $u_{sB}/(di_{sB}/dt)$ , and  $u_{sC}/(di_{sC}/dt)$ .

In Chapter 7 artificial-intelligence-based speed-sensorless drives are also discussed.

#### 4.5.2 SLIP AND SPEED ESTIMATORS FOR LOW-PERFORMANCE APPLICATIONS

It is possible to construct a low-cost slip-sensing device, which uses the stator voltages and currents of the induction motor. This can be obtained by simply considering the steady-state equivalent circuit of the induction motor, and then it can be seen that for small values of the slip, the slip ( $s$ ) can be expressed as

$$s = \frac{(R'_r/3)\omega_1 T_e}{|\bar{U}_m|^2}, \quad (4.5-1)$$

where  $R'_r$  is the referred rotor resistance,  $\omega_1$  is the stator angular frequency,  $T_e$  is the steady-state electromagnetic torque, and  $|\bar{U}_m|$  is the absolute value of the magnetizing (air-gap) voltage. Thus the slip monitor uses the monitored electromagnetic torque and also the magnetizing voltage, which can be simply obtained by subtracting the ohmic and stator leakage voltage drops from the terminal voltage. The electromagnetic torque can be obtained from monitored stator voltages and currents (by using the fact that the torque can be expressed as the cross-vectorial product of the stator flux-linkage and current space vectors, and the stator flux-linkage vector can be obtained by integrating the stator-voltage space vector reduced by the stator-voltage space vector of the ohmic drops).

As an alternative, the electromagnetic torque can be obtained from the air-gap power,

$$T_e = \frac{P_{gap}}{\omega_1}, \quad (4.5-2)$$

which can be determined as the difference of the d.c. link power and the power losses for the inverter, stator, and choke:

$$P_{gap} = P_{dc} - P_{loss} = U_{dc} I_{dc} - (P_s + P_{inv} + P_{choke}). \quad (4.5-3)$$

In this scheme the d.c. link voltage and d.c. link current are monitored. The inaccuracy in the determination of the various losses has a significant effect on the accuracy of the estimated slip at low values of the slip, since at low slip values, these losses constitute a large percentage of the input power. The steady-state angular rotor speed can then be obtained as

$$\omega_r = \omega_1(1-s). \quad (4.5-4)$$

It is important to note that the monitoring schemes described above cannot be used under dynamic conditions and the first scheme can only be used for the estimation of the slip near to its rated value, i.e. for small values of the slip. Thus the speed range is limited. Furthermore, in the first scheme, when obtaining the magnetizing voltage, the stator leakage voltage contains the derivative of the stator currents, and this can cause significant problems due to the noise content in the stator currents. The techniques described can only be used in low-performance applications and not in high-performance drives.

It is also possible to utilize the Kloss formula for the determination of the steady-state slip, if the pull-out slip ( $s_{max}$ ) and pull-out torque ( $T_{e_{max}}$ ) values are known:

$$\frac{T_e}{T_{e_{max}}} \approx \frac{2}{(s/s_{max} + s_{max}/s)}, \quad (4.5-5)$$

where the electromagnetic torque can be estimated by using one of the techniques described above. Furthermore, it follows from eqn (4.5-5) that for low values of the slip, the slip estimation can be based on

$$\frac{T_e}{T_{e_{max}}} \approx \frac{2s}{(s_{max})} \quad (4.5-6)$$

and at large values of the slip it can be obtained from

$$\frac{T_e}{T_{e_{max}}} \approx \frac{2s_{max}}{s}. \quad (4.5-7)$$

In a conventional speed-controlled voltage-source inverter-fed induction motor drive with open-loop flux control using the steady-state machine model (V/f control), the speed is monitored and the reference value of the slip frequency is obtained on the output of a speed controller as shown in Fig. 4.46.

In this scheme the reference angular stator frequency is obtained by using

$$\omega_{1ref} = \omega_{sref} + \omega_r \quad (4.5-8)$$

and  $\omega_{1ref}$  is an input to the function generator  $f(\omega_1)$ , which outputs the modulus of the reference stator voltages,  $|\bar{u}_{sref}|$ . If the effects of the stator resistance are neglected, then to ensure constant stator flux,  $|\bar{u}_{sref}|$  is varied linearly with the stator frequency (thus the function  $f$  is a linear function of  $\omega_1$ ). However, at low stator frequencies, it is important to consider the effects of the stator resistance, and then the stator voltage has to be boosted (thus the function  $f$  is not linear). Such an induction motor drive has good steady-state performance but low dynamic performance, since it is based on the steady-state equivalent circuit. Similarly to all types of open-loop drives, such an open-loop drive is sensitive to various secondary effects (parameter variations, e.g. due to temperature variation).

In a low-cost implementation of the V/f drive, no slip compensation is used, thus there is no need to monitor the speed. Such a low-cost, low-dynamic-performance

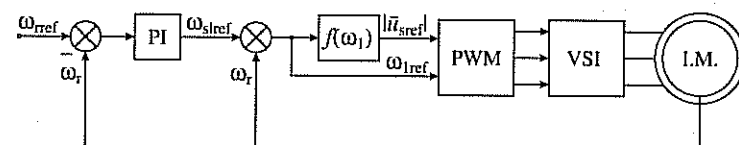


Fig. 4.46. V/f control scheme using speed sensor.

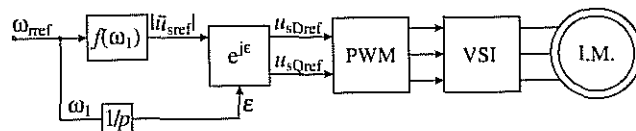


Fig. 4.47. Low-cost V/f control scheme without speed sensor.

VSI-fed induction motor drive scheme is shown in Fig. 4.47. In this scheme, the slip frequency is not considered, thus  $\omega_1 = \omega_{\text{ref}}$  is assumed.

When the stator frequency is integrated, it gives the position ( $\epsilon$ ) of the stator-voltage space vector (with respect to the direct-axis of the stationary reference frame). Thus

$$\epsilon(t) = \int \omega_1(t) dt. \quad (4.5-9)$$

On the other hand, the output of the  $f(\omega_1)$  function generator gives the stator-voltage reference modulus ( $|\bar{u}_{\text{sref}}|$ ). This function generator implements the V/f characteristic as discussed above. In the stator-voltage-oriented reference frame, the reference stator-voltage space vector has only a direct-axis component,  $u_{sDref} = |\bar{u}_{\text{sref}}|$ , and its quadrature-axis components ( $u_{sQref}$ ) is zero. It follows that the two-axis components of the reference stator-voltage space vector in the stationary reference frame ( $u_{sDref}, u_{sQref}$ ) can be obtained by using the transformation

$$u_{sDref} + j u_{sQref} = \exp(j\epsilon)(u_{sxref} + j u_{syref}). \quad (4.5-10)$$

Thus  $u_{sDref} = |\bar{u}_{\text{sref}}| \cos \epsilon$  and  $u_{sQref} = |\bar{u}_{\text{sref}}| \sin \epsilon$ , which are the inputs to the modulator, as shown in Fig. 4.47. If the three-phase reference stator voltages are required, these can also be obtained as

$$u_{sAref} = |\bar{u}_{\text{sref}}| \cos \epsilon \quad u_{sBref} = |\bar{u}_{\text{sref}}| \cos(\epsilon - 2\pi/3) \quad u_{sCref} = |\bar{u}_{\text{sref}}| \cos(\epsilon - 4\pi/3). \quad (4.5-11)$$

However, the scheme shown in Fig. 4.47 will result in speed errors caused by a load (for large loads the error is large), since it has been assumed above that the stator frequency is equal to the reference speed, which is only correct if the slip is zero (there is no load). It follows that to ensure good steady-state speed regulation, slip compensation must be employed.

In various implementations of the V/f control scheme with slip compensation, it is possible to obtain the slip frequency using the concepts discussed above for slip estimation. However, a simple scheme shown in Fig. 4.48 can also be obtained, which contains the slip frequency compensation, but where the slip frequency is obtained in another easier way. For this purpose it is utilized that the slip frequency is proportional to the torque, which is however proportional to the quadrature-axis stator current ( $i_{sy}$ ) in the stator-voltage-oriented reference frame (this reference frame was introduced in connection with the scheme

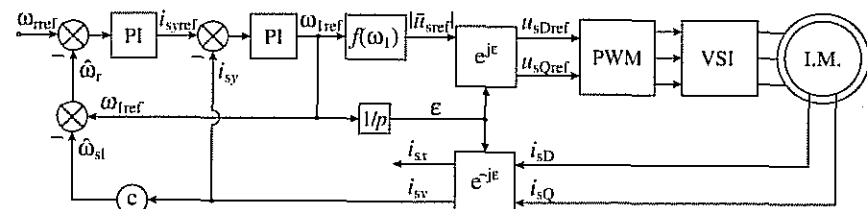


Fig. 4.48. Speed-sensorless V/f scheme with slip frequency compensation and using the position of the stator-voltage space vector.

described in Fig. 4.47). However, for this purpose the active stator current ( $i_{sy}$ ) component must be monitored. This can be obtained from the monitored stator currents, since the stator-current space vector in the stator-voltage-oriented reference frame can be expressed as

$$i_{sx} + j i_{sy} = \exp(-j\epsilon)(i_{sD} + j i_{sQ}), \quad (4.5-12)$$

where  $i_{sD} + j i_{sQ}$  is the stator-current space vector in the stator (stationary) reference frame. Thus  $i_{sy} = -i_{sD} \sin \epsilon + i_{sQ} \cos \epsilon$ . This is the reason why the  $\exp(-j\epsilon)$  transformation is also present in the control scheme shown in Fig. 4.48. The voltage transformation is the same as in the scheme of Fig. 4.47. The slip frequency can be estimated by considering that it is proportional to the active stator current, thus  $\hat{\omega}_{sl} = ci_{sy}$ , where  $c$  is a constant. The speed controller in Fig. 4.47 outputs the reference value of the active stator current ( $i_{syref}$ ) and when this is compared with the actual value of the active current, the error is an input to the active stator-current controller. This outputs the reference value of the angular stator frequency ( $\omega_{1ref}$ ), and when integrated gives the angle  $\epsilon$  as discussed above. Furthermore, the difference of  $\omega_{1ref}$  and the estimated slip frequency ( $\hat{\omega}_{sl}$ ) gives the estimated speed ( $\hat{\omega}_r$ ). By considering that  $i_{sA} + i_{sB} + i_{sC} = 0$ , the two-axis stator currents  $i_{sD}, i_{sQ}$  can be obtained by only measuring two stator currents (e.g.  $i_{sA}, i_{sB}$ ), where  $i_{sD}$  is proportional to  $i_{sA}$  and  $i_{sQ}$  is proportional to  $i_{sB} - i_{sC} = i_{sB} + 2i_{sC}$ .

It follows that this scheme contains closed-loop control of both the speed and the active stator current. It can be used for the accurate steady-state speed control of the induction machine for any value of the load. However, the dynamic performance of the drive is low, since the scheme is based on the steady-state equivalent circuit of the machine. Speed estimation schemes which allow high dynamic performance are discussed in the next section.

#### 4.5.3 SLIP, SPEED, ROTOR ANGLE, AND FLUX-LINKAGE ESTIMATORS FOR HIGH-PERFORMANCE APPLICATIONS

In the present section, various techniques are described which can be used in high-performance drives for the estimation of the slip, rotor speed, rotor

angle, and various machine flux linkages. Thus the following techniques are described:

1. Open-loop estimators using monitored stator voltages/currents and improved schemes;
2. Estimators using the spatial-saturation stator phase third-harmonic voltage;
3. Estimators using saliency (geometrical, saturation) effects;
4. Model reference adaptive systems (MRAS);
5. Observers (Kalman, Luenberger);
6. Estimators using artificial intelligence (neural network, fuzzy-logic-based systems, fuzzy-neural networks, etc.).

#### 4.5.3.1 Open-loop speed estimators using monitored stator voltages and currents; improved schemes

##### 4.5.3.1.1 General introduction

In the present section various rotor speed and slip frequency estimators are obtained by considering the voltage equations of the induction machine. The schemes described below use the monitored stator voltages and currents or the monitored stator currents and reconstructed stator voltages. Some of these estimation schemes are used in recently introduced commercially available speed-sensorless induction motor drives. However, it is important to note that in general, the accuracy of open-loop estimators depends greatly on the accuracy of the machine parameters used. At low rotor speed, the accuracy of the open-loop estimators is reduced, and in particular, parameter deviations from their actual values have great influence on the steady-state and transient performance of the drive system which uses an open-loop estimator. Furthermore, higher accuracy is achieved if the stator flux is obtained by a scheme which avoids the use of pure integrators (see also Sections 3.1.3.2, 3.2.2.2, and 4.1.1.4).

In general, open-loop speed estimators depend on various parameters of the induction machine. The stator resistance ( $R_s$ ) has important effects on the stator flux linkages, especially at low speeds, and if the rotor flux linkage is obtained from the stator flux linkage, then the rotor flux-linkage accuracy is also influenced by the stator resistance. However, it is possible to have a rather accurate estimate of the appropriate 'hot' stator resistance by using a thermal model of the induction machine.

In some schemes, the rotor flux-linkage estimation requires the rotor time constant, which can also vary, since it is the ratio of the rotor self-inductance and the rotor resistance, and the rotor resistance can vary due to temperature effects and skin effect (current-displacement effect), and the rotor self-inductance can vary due to skin effect and saturation effects. The changes of the rotor resistance due to temperature changes are usually slow changes. Due to main flux saturation, the magnetizing inductance ( $L_m$ ) can change and thus the stator self-inductance

( $L_s = L_{sl} + L_m$ ) and rotor self-inductance ( $L_r = L_{rl} + L_m$ ) can also change even if the leakage inductances ( $L_{sl}, L_{rl}$ ) are constant. The changes of the rotor self-inductance due to saturation can be fast. Due to leakage flux saturation,  $L_{sl}$ ,  $L_{rl}$  and the stator transient inductance ( $L'_s$ ) can also change. In a vector-controlled drive, where the rotor flux amplitude is constant, the variations of  $L_m$  are small. In a machine with closed rotor slots, the stator transient inductance varies due to leakage flux saturation, and is a function of the stator currents, due to the saturable closing bridge around the rotor slots. In a torque-controlled drive, the effects of incorrect parameters result in incorrect torque, flux, degradation of system performance, etc.

In Section 8.1 and also in a recent book [Vas 1993] on-line parameter identification techniques are discussed, where the most important four induction motor parameters (stator resistance, rotor time constant, stator transient inductance, stator self-inductance) are also identified during a self-commissioning stage of a torque-controlled induction motor drive system (vector drive or direct-torque-controlled drive). Various commercial drives use parameter estimation techniques which are identical or similar to that described in Section 8.1. It should be noted that in this self-commissioning stage, the machine is at standstill during all measurements. The stator resistance is identified by injecting a d.c. current in the stator winding and measuring the corresponding d.c. voltage in the steady state. The rotor time constant is identified from the exponential voltage waveform when a step change in the stator current is applied. Finally the stator transient time constant is identified from the slope of the stator currents when a step voltage is applied.

Five rotor-speed estimator schemes are described below, but where possible, small modifications of a scheme are also discussed within the scheme. In every subsection, first the expression for the rotor speed used by the scheme is given and this is then followed by a mathematical proof and the description of various aspects of implementation details.

##### 4.5.3.1.2 Rotor speed estimation scheme 1

$$\omega_r = \left[ -\frac{d\psi_{rd}}{dt} - \frac{\psi_{rd}}{T_r} + \frac{L_m i_{sd}}{T_r} \right] / \psi_{rq}$$

It is possible to obtain an expression for the rotor speed directly by using the rotor-voltage space-vector equation expressed in the stationary reference frame ( $\omega_g = 0$ ). It follows from eqn (2.1-149) that for the induction motor, the direct-axis rotor-voltage equation becomes

$$0 = R_r i_{rd} + \frac{d\psi_{rd}}{dt} + \omega_r \psi_{rq}, \quad (4.5-13)$$

where

$$\psi_{rd} = L_r i_{rd} + L_m i_{sd}. \quad (4.5-14)$$

Equation (4.5-13) can be rearranged for the rotor speed, but it contains the direct-axis rotor current which cannot be measured directly. However, by considering eqn (4.5-14) it can be expressed in terms of the direct-axis stator current and direct-axis rotor flux and when this is substituted into eqn (4.5-13),

$$\omega_r = \left[ -\frac{d\psi_{rd}}{dt} - \frac{\psi_{rd}}{T_r} + \frac{L_m}{T_r} i_{sD} \right] / \psi_{rq} \quad (4.5-15)$$

is obtained. This equation can be used for the estimation of the rotor speed. However, for this purpose, the direct- and quadrature-axis rotor flux linkages have to be estimated. Various techniques have been discussed in Section 4.1.1 for the estimation of the stator flux and rotor magnetization current from terminal quantities. For example, the rotor flux-linkage space vector can be obtained from the monitored terminal voltages and currents by using the circuit of Fig. 4.9(a), and by utilizing  $\psi_{rd} = L_m i_{mrD}$ ,  $\psi_{rq} = L_m i_{mrQ}$ , or  $\bar{\psi}_r = L_m |I_{mr}| \exp(j\phi_r)$ . However, other circuits have been shown in Figs 4.9(b), 4.9(c), and 4.9(d) which result in smaller integrator drift at low frequency (two of the circuits use closed-loop integrators). However, as discussed in Section 3.1.3.1 and also in Section 4.1.1, it is also possible to reconstruct the stator voltages by using the monitored d.c. link voltage together with the inverter switching functions. For clarity, some of the equations will now be summarized.

In eqn (4.5-15)  $T_r$  is the rotor time constant ( $T_r = L_r/R_r$ ) and it can be seen that this equation contains the derivative of the direct-axis rotor flux-linkage component. By using eqns (2.1-150) and (2.1-151), the rotor flux-linkage space vector can be expressed in terms of the stator flux-linkage space vector, and in the stationary reference frame  $\bar{\psi}_r = (L_r/L_m)(\bar{\psi}_s - L'_s i_s)$  is obtained, where  $L'_s$  is the stator transient inductance. Resolution of this into its real and imaginary parts gives

$$\psi_{rd} = \frac{L_r}{L_m} (\psi_{sD} - L'_s i_{sD}) \quad (4.5-16)$$

$$\psi_{rq} = \frac{L_r}{L_m} (\psi_{sQ} - L'_s i_{sQ}). \quad (4.5-17)$$

The derivative of  $\psi_{rq}$  is used in eqn (4.5-15), and if magnetic saturation is neglected, it follows from eqn (4.5-16) that

$$\frac{d\psi_{rd}}{dt} = \frac{L_r}{L_m} \left( \frac{d\psi_{sD}}{dt} - L'_s \frac{di_{sD}}{dt} \right). \quad (4.5-18)$$

Eqns (4.5-16)–(4.5-18) contain the stator flux-linkage components which can be obtained from eqn (2.1-148) in the stationary reference frame by using

$$\frac{d\psi_{sD}}{dt} = u_{sD} - R_s i_{sD} \quad (4.5-19)$$

$$\frac{d\psi_{sQ}}{dt} = u_{sQ} - R_s i_{sQ}. \quad (4.5-20)$$

However, greater accuracy can be obtained by using the flux estimation techniques discussed in Section 4.1.1.4.3. The rotor speed can finally be obtained from eqn (4.5-15), by considering eqns (4.5-16)–(4.5-20). To summarize:

$$\omega_r = \left[ -\frac{d\psi_{rd}}{dt} - \frac{\psi_{rd}}{T_r} + \frac{L_m}{T_r} i_{sD} \right] / \psi_{rq}, \quad (4.5-21)$$

where

$$\frac{d\psi_{rd}}{dt} = \frac{L_r}{L_m} \left( u_{sD} - R_s i_{sD} - L'_s \frac{di_{sD}}{dt} \right) \quad (4.5-22)$$

and  $\psi_{rd}$  is obtained from this by integration. Similarly,  $\psi_{rq}$  is obtained from

$$\frac{d\psi_{rq}}{dt} = \frac{L_r}{L_m} \left( u_{sQ} - R_s i_{sQ} - L'_s \frac{di_{sQ}}{dt} \right) \quad (4.5-23)$$

by integration. A possible implementation is shown in Fig. 4.49. It can be seen that this requires several machine parameters, some of which vary with temperature, skin effect, and saturation. Thus the speed can only be obtained accurately if these parameters are accurately known. It is possible to have a rather accurate estimate of the stator resistance by utilizing the ‘cold’ value of the stator resistance together with a thermal model of the induction machine. At low speeds the accuracy of this scheme is limited, but improvements can be obtained by using the flux estimation techniques discussed in Section 4.1.1.4.3. It should be noted that a similar scheme could be obtained if the speed is estimated by using the quadrature-axis rotor equation in the stationary reference frame. The stator voltages can be monitored or reconstructed from the d.c. link voltage and the inverter switching states, as discussed in Section 3.1.3.1 and Section 4.1.1.

As mentioned above, it is possible to improve the speed estimation by employing improved flux estimators (e.g. those shown in Figs 4.9(b), 4.9(c), or 4.9(d)). For illustration purposes one of the improved schemes which is obtained by utilizing the technique described in connection with Fig. 4.9(b) is shown in Fig. 4.50.

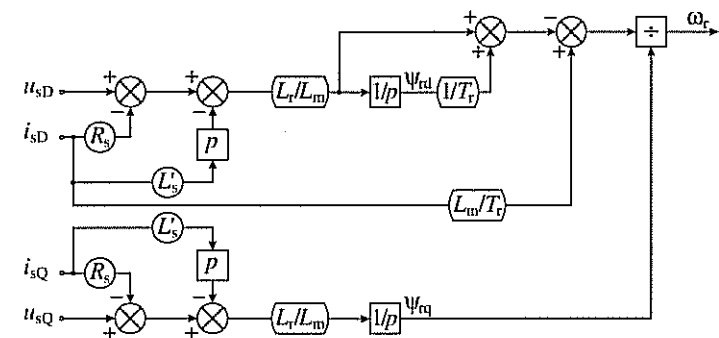


Fig. 4.49. Rotor speed estimator using two integrators, two differentiators, and 5 machine parameters.

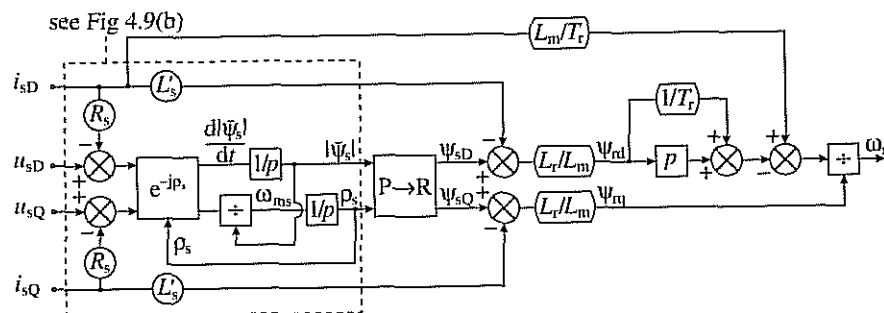


Fig. 4.50. Rotor speed estimator using 2 integrators, 1 differentiator, and 4 machine parameters.

In this case, first, the modulus ( $|\bar{\psi}_s|$ ) and angle ( $\rho_s$ ) of the stator flux-linkage space vector are obtained (by the circuit shown in Fig. 4.9(b)) and then the rotor flux linkages are obtained by using eqns (4.5-16) and (4.5-17). These are then used in eqn (4.5-21).

The estimator shown in Fig. 4.50 contains a differentiator to obtain  $d\psi_{rd}/dt$ . When a suitable numerical algorithm is used, this can be performed accurately. However, it is also possible to use another combined scheme, where  $d\psi_{rd}/dt$  is obtained by using eqn (4.5-22) and  $\psi_{rq}$  is obtained by using the technique described in Fig. 4.50.

#### 4.5.3.1.3 Rotor speed estimation scheme 2

$$\omega_r = - \left[ u_{sD} - \left( R_s + \frac{L_s}{T_r} \right) i_{sD} - L'_s \frac{di_{sD}}{dt} + \frac{\psi_{sD}}{T_r} \right] / (\psi_{sQ} - L'_s i_{sQ})$$

or

$$\omega_r = \left[ u_{sQ} - \left( R_s + \frac{L_s}{T_r} \right) i_{sQ} - L'_s \frac{di_{sQ}}{dt} + \frac{\psi_{sQ}}{T_r} \right] / (\psi_{sD} - L'_s i_{sD})$$

It is possible to obtain another rotor speed estimation scheme, which can be obtained from eqn (4.5-15) by the substitution of eqns (4.5-16), (4.5-17), and (4.5-22). Thus

$$\omega_r = - \left[ u_{sD} - \left( R_s + \frac{L_s}{T_r} \right) i_{sD} - L'_s \frac{di_{sD}}{dt} + \frac{\psi_{sD}}{T_r} \right] / (\psi_{sQ} - L'_s i_{sQ}). \quad (4.5-24)$$

It should be noted that this expression can also be directly obtained by considering the quadrature-axis rotor voltage equation, eqn (4.5-13), and by substitution into this eqns (4.5-17), (4.5-22), and  $i_{rd} = (\psi_{sD} - L_s i_{sD})/L_m$  (which follows from the

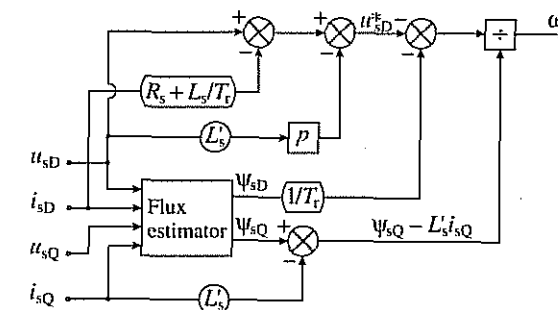


Fig. 4.51. Rotor speed estimator using 2 integrators, 1 differentiator, and 4 machine parameters.

definition of the direct-axis stator flux linkage,  $\psi_{sD} = L_s i_{sD} + L_m i_{rd}$ ). A scheme using eqn (4.5-24) is shown in Fig. 4.51. The flux estimator block can be implemented by using any of the improved techniques discussed earlier.

The speed estimator shown in Fig. 4.51 requires four machine parameters and accuracy of the speed estimator greatly depends on these. However, it is possible to obtain satisfactory results down to 1–2 Hz.

Equation (4.5-24) has been derived by using the quadrature-axis rotor equation, but if the direct-axis rotor voltage equation is used, then a similar expression can be obtained:

$$\omega_r = \left[ u_{sQ} - \left( R_s + \frac{L_s}{T_r} \right) i_{sQ} - L'_s \frac{di_{sQ}}{dt} + \frac{\psi_{sQ}}{T_r} \right] / (\psi_{sD} - L'_s i_{sD}). \quad (4.5-25)$$

An implementation based on eqn (4.5-25) requires the same complexity as that shown in eqn Fig. 4.51. However, it can be seen from (4.5-25) that if another speed estimator is used where the quadrature-axis stator flux is forced to be zero, then the scheme is simplified and the numerator will not contain the quadrature-axis stator flux-linkage space vector. This is indeed the case if the rotor voltage equation is expressed in a reference frame rotating with the speed of the stator flux. This is now discussed below.

#### 4.5.3.1.4 Rotor speed estimation scheme 3

$$\omega_r = u_{sQ}^*/(|\bar{\psi}_s| - L'_s i_{sx})$$

There are many possibilities for obtaining the expression for the rotor speed for this scheme, but it is very straightforward to use first the rotor voltage equation in the stationary reference frame, and the resulting equation is then transformed into the stator-flux-oriented reference frame. By following this approach, of course eqns (4.5-24) and (4.5-25) will also result. For this purpose the rotor-voltage space vector equation is considered in the stationary reference frame. This can be

obtained from eqn (2.1-149) by assuming  $\omega_g = 0$  and thus  $0 = R_s \bar{i}_r' + d\bar{\psi}_r'/dt - j\omega_r \bar{\psi}_r'$  is obtained. However, the rotor-current space vector can be eliminated by considering  $\bar{i}_r' = (\bar{\psi}_s - L_s \bar{i}_s)/L_m$  and the rotor flux-linkage space vector can be substituted by  $\bar{\psi}_r' = (L_r/L_m)(\bar{\psi}_s - L'_s \bar{i}_s)$ . Hence

$$\frac{d\bar{\psi}_r'}{dt} = \frac{L_r}{L_m} \left( \bar{u}_s - R_s \bar{i}_s - L'_s \frac{d\bar{i}_s}{dt} \right)$$

and substitution of the expressions for  $\bar{i}_r'$ ,  $\bar{\psi}_r'$ , and  $d\bar{\psi}_r'/dt$  into the rotor voltage equation gives

$$\bar{u}_s - \left( R_s + \frac{L_s}{T_r} \right) \bar{i}_s - L'_s \frac{d\bar{i}_s}{dt} = -\frac{\bar{\psi}_s}{T_r} + j\omega_r(\bar{\psi}_s - L'_s \bar{i}_s). \quad (4.3-26)$$

It should be noted that, as expected, the real and imaginary parts of eqn (4.3-26) yield eqns (4.5-24) and (4.5-25) respectively. Equation (4.3-26) is a specific form of the rotor voltage equation in the stationary reference frame. When this is transformed into the reference frame rotating with the stator flux-linkage space vector, whose speed is  $\omega_{ms} = d\rho_s/dt$  (stator-flux-oriented reference frame, where  $\rho_s$  is the angle of the stator flux-linkage space vector with respect to the real-axis of the stator reference frame as shown in Fig. 4.25), then

$$\begin{aligned} & \left[ \bar{u}_s - \left( R_s + \frac{L_s}{T_r} \right) \bar{i}_s - L'_s \frac{d\bar{i}_s}{dt} \right] \exp(-j\rho_s) \\ &= -\bar{\psi}_s \exp(-j\rho_s)/T_r + j\omega_r[\bar{\psi}_s \exp(-j\rho_s) - L'_s \bar{i}_s \exp(-j\rho_s)] \end{aligned} \quad (4.5-27)$$

is obtained. However, on the right-hand side of eqn (4.5-27),

$$\bar{\psi}_s \exp(-j\rho_s) = \bar{\psi}'_s = \psi_{sx} + j\psi_{sy} = |\bar{\psi}_s|$$

and

$$\bar{i}_s \exp(-j\rho_s) = \bar{i}'_s = i_{sx} + j i_{sy}$$

are the stator-flux and stator current space vectors respectively in the stator-flux-oriented reference frame (whose real and imaginary axes are denoted by  $x$  and  $y$  respectively). Thus it follows that

$$\left[ \bar{u}_s - \left( R_s + \frac{L_s}{T_r} \right) \bar{i}_s - L'_s \frac{d\bar{i}_s}{dt} \right] \exp(-j\rho_s) = -\frac{|\bar{\psi}_s|}{T_r} + j\omega_r(|\bar{\psi}_s| - L'_s \bar{i}'_s). \quad (4.5-28)$$

The real and imaginary parts of eqn (4.5-28) give

$$u_{sx}^* = -\frac{|\bar{\psi}_s|}{T_r} + \omega_r L'_s i_{sy} \quad (4.5-29)$$

$$u_{sy}^* = \omega_r (|\bar{\psi}_s| - L'_s i_{sx}), \quad (4.5-30)$$

where

$$u_{sx}^* + j u_{sy}^* = \left[ \bar{u}_s - \left( R_s + \frac{L_s}{T_r} \right) \bar{i}_s - L'_s \frac{d\bar{i}_s}{dt} \right] \exp(-j\rho_s) \quad (4.5-31)$$

and  $\bar{u}_s = u_{sD} + j u_{sQ}$ ,  $\bar{i}_s = i_{sD} + j i_{sQ}$ . It follows from eqn (4.5-30) that

$$\omega_r = u_{sy}^*/(|\bar{\psi}_s| - L'_s i_{sx}). \quad (4.5-32)$$

As expected, the numerator of eqn (4.5-32) contains only  $u_{sy}^*$  and not the quadrature-axis stator flux. This is physically due to the fact that in the stator-flux-oriented reference frame the quadrature-axis stator flux is zero. This should be contrasted with eqn (4.5-25), whose numerator contains the quadrature-axis stator flux (expressed in the stationary reference frame). Equation (4.5-32) has been implemented in Fig. 4.52. This scheme again depends on four machine parameters and can give satisfactory results even at very low speeds. The voltages can either be monitored or they can be reconstructed from the measured d.c. link voltage and inverter switching states. A speed estimator based on eqn (4.5-32) can be effectively used in a stator-flux-oriented vector control scheme even at relatively low stator frequency. The flux estimator can use any of the improved techniques discussed earlier, including the estimator shown in Fig. 4.9(b) or (c).

It should be noted that if the rotor speed is determined by eqn (4.5-32), then by using this in eqn (4.5-29), it is possible to obtain an expression for the rotor time constant, and this can be used to monitor the changes of  $T_r$ .

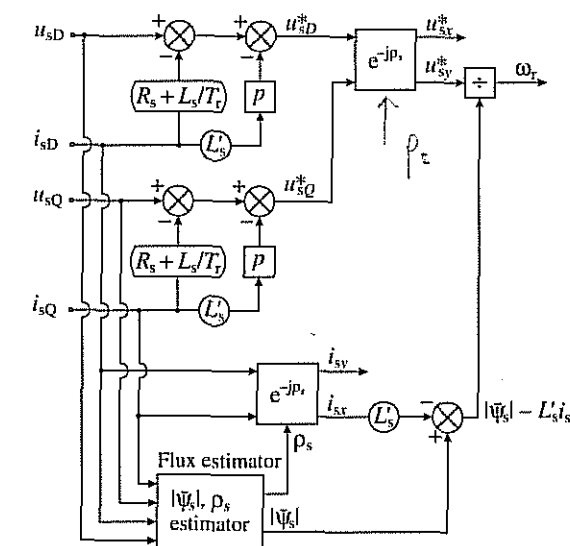


Fig. 4.52. Rotor speed estimator using scheme 3.

### 4.5.3.1.5 Rotor speed estimation scheme 4

$$\omega_r = \omega_{mr} - \omega_{sl} = \left( \psi_{rd} \frac{d\psi_{rq}}{dt} - \psi_{rq} \frac{d\psi_{rd}}{dt} \right) / |\bar{\psi}_r|^2 - \frac{L_m}{T_r |\bar{\psi}_r|^2} (-\psi_{rq} i_{sD} + \psi_{rd} i_{sQ})$$

or

$$\omega_r = \omega_{mr} - \omega_{sl} = \left( \psi_{rd} \frac{d\psi_{rq}}{dt} - \psi_{rq} \frac{d\psi_{rd}}{dt} \right) / |\bar{\psi}_r|^2 - \frac{2t_e R_r}{3P |\bar{\psi}_r|^2}$$

or

$$\omega_r = \left( \psi_{sD} \frac{d\psi_{sQ}}{dt} - \psi_{sQ} \frac{d\psi_{sD}}{dt} \right) / (\psi_{sD}^2 + \psi_{sQ}^2) - \frac{d}{dt} [\sin^{-1}(t_e / (c |\bar{\psi}_s| |\bar{\psi}_r|))] - \frac{2t_e R_r}{3P |\bar{\psi}_r|^2}$$

Various rotor speed estimators are now described, which use the speed of the rotor flux-linkage space vector or the speed of the stator flux-linkage space vector. These require the estimate of the appropriate slip frequency. This type of scheme is one of those schemes which are used in recently introduced speed-sensorless, commercially available high-performance induction motor drives. In these commercial implementations the stator voltages are not monitored but are reconstructed from the d.c. link voltage and switching states of the inverter (see Sections 3.1.1 and 4.1.1). It should be noted that a similar scheme has been described in Section 3.1.3 for a permanent-magnet synchronous machine [e.g. see eqn (3.1-48)], but in the PM synchronous machine the speed estimation is simpler, since the rotor speed is equal to the speed of the stator flux (slip speed is zero).

It is possible to implement an angular rotor-slip-frequency estimator ( $\omega_{sl}$ ) by considering the rotor voltage equation of the induction motor. It has been shown in Section 4.1.1 that if the rotor voltage equation is expressed in the rotor-flux-oriented reference frame, then eqn (4.1-26) is obtained, which contains the angular slip frequency,  $\omega_{sl} = i_{sy} / (T_r |\bar{l}_{mr}|)$ . If the expression of  $i_{sy}$  given by (2.1-192) is substituted into this, then

$$\omega_{sl} = \frac{i_{sy}}{T_r |\bar{l}_{mr}|} = \frac{-i_{sD} \sin \rho_r + i_{sQ} \cos \rho_r}{T_r |\bar{l}_{mr}|} \quad (4.5-33)$$

is obtained, where  $\rho_r$  is the angle of the rotor flux with respect to the real-axis of the stationary reference frame. By considering that the rotor flux modulus can be expressed as  $|\bar{\psi}_r| = L_m |\bar{l}_{mr}|$ , where  $|\bar{l}_{mr}|$  is the modulus of the rotor magnetizing-current space vector, and also using  $\sin \rho_r = \psi_{rq} / |\bar{\psi}_r|$  and  $\cos \rho_r = \psi_{rd} / |\bar{\psi}_r|$ , which expressions follow from  $\bar{\psi}'_r = |\bar{\psi}_r| \exp(j\rho_r)$ , eqn (4.5-33) can be rewritten as

$$\omega_{sl} = \frac{L_m}{T_r |\bar{\psi}_r|^2} (-\psi_{rq} i_{sD} + \psi_{rd} i_{sQ}). \quad (4.5-34)$$

Equation (4.5-34) can be used to monitor the angular slip frequency by monitoring the stator currents, and also by using the rotor flux linkages. The rotor flux

linkages can be estimated in various ways, e.g. by using eqns (4.5-16) and (4.5-17). These expressions include the stator flux linkages, which can be estimated from the stator voltages and currents as described above (see also Section 4.1.1.4). It should be noted that it is possible to reformulate eqn (4.5-34) by considering the expression for the electromagnetic torque given by eqn (2.1-191), where  $\psi_{rx} = |\bar{\psi}_r|$  is the modulus of the rotor flux. Thus

$$\omega_{sl} = \frac{2t_e R_r}{3P |\bar{\psi}_r|^2} \quad (4.5-35)$$

is obtained, where  $t_e$  is the electromagnetic torque,  $P$  is the number of pole pairs, and  $R_r$  is the rotor resistance. This expression contains the modulus of the rotor flux and also the electromagnetic torque. The electromagnetic torque can also be substituted by  $t_e = (3P/2)(\psi_{sD} i_{sQ} - \psi_{sQ} i_{sD})$ , where  $\psi_{sD}$  and  $\psi_{sQ}$  are the stator flux linkages in the stationary reference frame, and their monitoring has also been discussed above.

It is also possible to obtain an expression for the rotor speed by considering that from eqn (4.1-26) it follows that

$$\omega_r = \omega_{mr} - \omega_{sl}, \quad (4.5-36)$$

where  $\omega_{mr}$  is the speed of the rotor flux (relative to the stator)  $\omega_{mr} = d\rho_r/dt$ , and  $\omega_{sl}$  the angular slip frequency [e.g. given by eqns (4.5-34) and (4.5-35)]. In other words,  $\omega_{mr}$  is the speed of the rotor flux-linkage space vector with respect to the rotor. It is possible to obtain an expression for  $\omega_{mr}$  in terms of the rotor flux-linkage components by expanding the expression for the derivative  $d\rho_r/dt$ . Since the rotor flux-linkage space vector expressed in the stationary reference frame is

$$\bar{\psi}'_r = \psi_{rd} + j\psi_{rq} = |\bar{\psi}_r| \exp(j\rho_r),$$

thus  $\rho_r = \tan^{-1}(\psi_{rq}/\psi_{rd})$  and it follows that

$$\omega_{mr} = \frac{d\rho_r}{dt} = \frac{d}{dt} [\tan^{-1}(\psi_{rq}/\psi_{rd})] = \frac{\psi_{rd} d\psi_{rq}/dt - \psi_{rq} d\psi_{rd}/dt}{\psi_{rd}^2 + \psi_{rq}^2}. \quad (4.5-37)$$

The numerator contains  $|\bar{\psi}_r|^2$ . By substituting eqn (4.5-37) into eqn (4.5-36) and by also considering (4.5-34) or (4.5-35), finally we obtain

$$\omega_r = \omega_{mr} - \omega_{sl} = \frac{\psi_{rd} d\psi_{rq}/dt - \psi_{rq} d\psi_{rd}/dt}{|\bar{\psi}_r|^2} - \frac{L_m}{T_r |\bar{\psi}_r|^2} (-\psi_{rq} i_{sD} + \psi_{rd} i_{sQ}) \quad (4.5-38)$$

and

$$\omega_r = \omega_{mr} - \omega_{sl} = \frac{\psi_{rd} d\psi_{rq}/dt - \psi_{rq} d\psi_{rd}/dt}{|\bar{\psi}_r|^2} - \frac{2t_e R_r}{3P |\bar{\psi}_r|^2}. \quad (4.5-39)$$

A rotor speed estimator can then be constructed which uses the monitored stator currents and the rotor flux components, which, however, can be obtained from the stator flux linkages as discussed above. The stator flux linkages can be obtained by using monitored stator currents and monitored or reconstructed

stator voltages as discussed above. The accuracy of a speed estimator using eqn (4.5-38) or (4.5-39) depends greatly on the machine parameters used, and also on the model used for the estimation of the rotor flux-linkage components. A possible implementation is shown in Fig. 4.53. This contains the following three machine parameters:  $R_s$ ,  $L'_s$ , and  $k = L_m/L_r$ . However, an improved scheme is obtained if improved flux-linkage estimation is used. For this purpose it is also possible to use any of the techniques discussed earlier (see Section 4.1.1.4) and then, for example, the speed estimator shown in Fig. 4.9(d) is obtained.

For digital implementation it is possible to use various forms, including the following discrete form:

$$\begin{aligned}\omega_r(k) = & [\psi_{rd}(k-1)\psi_{rq}(k) - \psi_{rq}(k-1)\psi_{rd}(k)]/|\bar{\psi}_r(k)|^2 \\ & - [L_m/(T_r|\bar{\psi}_r(k)|^2)][-\psi_{rq}(k)i_{sD}(k) + \psi_{rd}(k)i_{sQ}(k)],\end{aligned}\quad (4.5-40)$$

where  $|\bar{\psi}_r(k)|^2 = [\psi_{rd}(k-1)]^2 + [\psi_{rq}(k-1)]^2$ . Since this equation contains a modelling error, which results in an error of the estimated rotor speed, in practice a low-pass filter can be used to remove this error.

It should be noted that in a vector-controlled drive, rather accurate estimation of the rotor speed may be obtained if the slip frequency term in eqn (4.5-39) is replaced by its reference value. For example, in a vector-controlled drive with rotor-flux-oriented control where  $i_{syref}$  and  $|\bar{i}_{mref}|$  are used,  $\omega_{sref} = i_{syref}/(T_r|\bar{i}_{mref}|)$  or  $\omega_{sref} = (2i_{eref}R_r)/(3P|\bar{\psi}_{ref}|^2)$ .

It is also possible to estimate the rotor speed in another way, which is similar to that described by eqn (4.5-39), but which instead of using the speed of the rotor flux ( $\omega_{mr}$ ), uses the speed of the stator flux,  $\omega_{ms}$ . If the direct and quadrature-axis

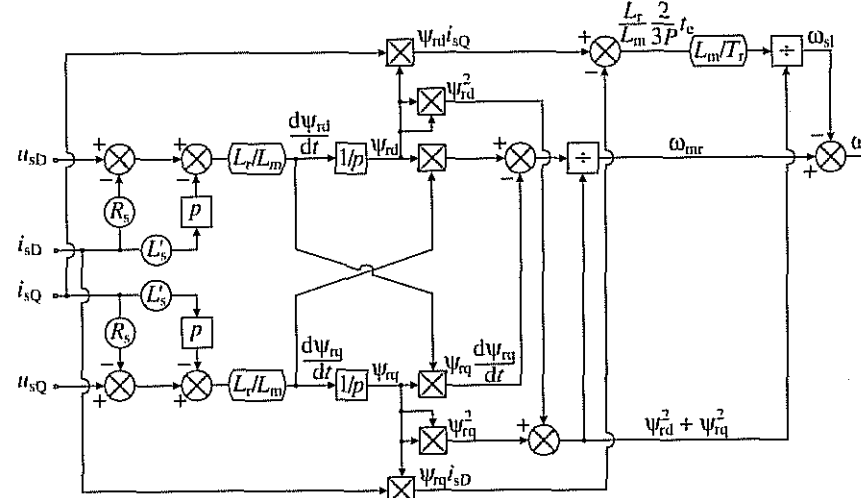


Fig. 4.53. Rotor speed estimator using 2 integrators, 2 differentiators, and 3 parameters.

stator flux linkages ( $\psi_{sD}$ ,  $\psi_{sQ}$ ) in the stationary reference frame are known (they are estimated by one of the techniques described above, which uses the monitored stator voltages and currents or the reconstructed stator voltages and currents), then since  $\psi_s = \psi_{sD} + j\psi_{sQ} = |\bar{\psi}_s| \exp(j\rho_s)$ , where  $\rho_s$  is the angle of the stator flux-linkage space vector with respect to the real-axis of the stationary reference frame, it follows that

$$\omega_{ms} = \frac{d\rho_s}{dt} = \frac{d}{dt}[\tan^{-1}(\psi_{sQ}/\psi_{sD})]. \quad (4.5-41)$$

In eqn (4.5-41)  $\omega_{ms}$  is the speed of the stator flux-linkage space vector with respect to the stator. By performing the differentiation, this can be put into the following form:

$$\omega_{ms} = \frac{\psi_{sD} d\psi_{sQ}/dt - \psi_{sQ} d\psi_{sD}/dt}{\psi_{sD}^2 + \psi_{sQ}^2}, \quad (4.5-42)$$

where the numerator contains  $|\bar{\psi}_s|^2$ . This is similar to eqn (4.5-37). By using eqns (4.5-19) and (4.5-20), it is possible to express  $\omega_{ms}$  in terms of the stator voltages and stator currents. The upper part of the circuit shown in Fig. 4.54 shows a possible implementation of eqn (4.5-42).

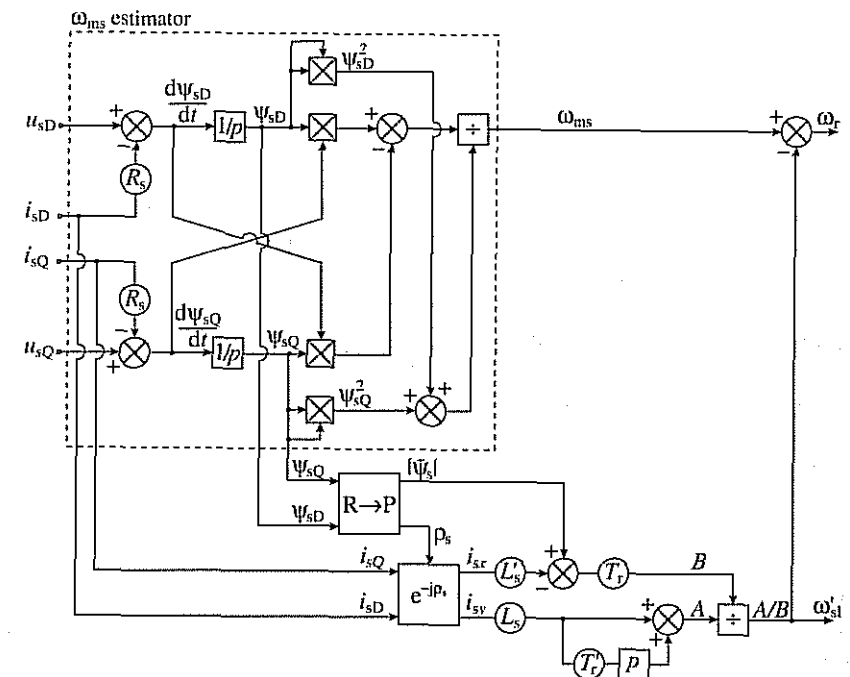


Fig. 4.54. Estimation of the rotor speed by using the speed of the stator flux-linkage space vector.

This requires the use of two integrators and only one machine parameter: the stator resistance. It should be noted that by using the concepts discussed in Sections 3.1.3.1 and 4.1.1, it is possible to obtain other schemes where the problems associated with pure integrator initial values and drift are reduced. For example, the pure integrator can be replaced by a low-pass filter.

To obtain a rotor speed estimator, which uses  $\omega_{ms}$  [defined by eqn (4.5-42)], it is possible to proceed in various ways. A specific solution can be obtained by considering eqns (4.2-16) and (4.2-23), from which  $\omega_r = \omega_{ms} - \omega'_{sl}$ , where now  $\omega'_{sl}$  is the speed of the stator flux-linkage space vector relative to the rotor (not the speed of the rotor flux relative to the rotor, which is denoted by  $\omega_{sl}$ ):

$$\omega'_{sl} = \frac{L_s(i_{sy} + T'_r di_{sy}/dt)}{T_r(|\bar{\psi}_s| - L'_s i_{sx})}. \quad (4.5-43)$$

It should be noted that eqn (4.5-43) has been directly obtained from the rotor voltage equation of the induction machine, but expressed in the stator-flux-oriented reference frame (which rotates at the speed of  $\omega_{ms}$ ). Thus the stator currents  $i_{sx}$  and  $i_{sy}$  are the stator currents in the stator-flux-oriented reference frame, and they can be obtained from the stator currents  $i_{sD}$ ,  $i_{sQ}$  (expressed in the stationary reference frame) by considering  $i_{sx} + j i_{sy} = (i_{sD} + j i_{sQ}) \exp(-j \rho_s)$ . Hence by using eqn (4.5-43), the scheme shown in Fig. 4.54 can be extended to obtain  $\omega'_{sl}$ . For this purpose  $\cos \rho_s$  and  $\sin \rho_s$  can be obtained from the stator flux-linkage components shown in Fig. 4.54, by using  $\cos \rho_s = \psi_{sD}/|\bar{\psi}_s|$  and  $\sin \rho_s = \psi_{sQ}/|\bar{\psi}_s|$  to obtain  $i_{sx}$  and  $i_{sy}$ , or  $\rho_s$  can be obtained by using a rectangular-to-polar converter (where the inputs are  $\psi_{sD}$  and  $\psi_{sQ}$  and the outputs are  $|\bar{\psi}_s|$  and  $\rho_s$ ). By using the obtained  $i_{sx}$ ,  $i_{sy}$ , and  $|\bar{\psi}_s|$ , the slip frequency  $\omega'_{sl}$  can be obtained by the application of eqn (4.5-43), and finally when this is subtracted from  $\omega_{ms}$ , the rotor speed,  $\omega_r$  is obtained. This is also shown in Fig. 4.54. However, it can be seen that this speed estimator is more complicated than the one shown in Fig. 4.53.

It should be noted that it is possible to obtain other solutions as well, which use the speed of the stator and rotor flux-linkage space vectors. For example, such a scheme can be derived by considering that the rotor speed is equal to the sum of the speed of the stator flux-linkage space vector,  $\omega_{ms} = d\rho_s/dt$ , minus the speed difference between the stator and rotor flux-linkage space vectors,  $\omega_d = d\rho/dt$ , minus the speed of the rotor flux-linkage space vector (relative to the rotor),  $\omega_{sl} = d\theta_{sl}/dt$ . This last term is now defined as in eqn (4.5-35), and can be expressed as in eqns (4.5-34) or (4.5-35). Thus

$$\omega_r = \omega_{ms} - \omega_d - \omega_{sl}. \quad (4.5-44)$$

Equation (4.5-44) can be simply proved by considering Fig. 4.55 which shows the stator and rotor flux-linkage space vectors and their angles with respect to different reference frames. As discussed above,  $\rho_s$  is the angle of the stator flux-linkage space vector with respect to the real axis of the stator reference frame,  $\rho_r$  is the angle of the rotor flux-linkage space vector with respect to the real axis

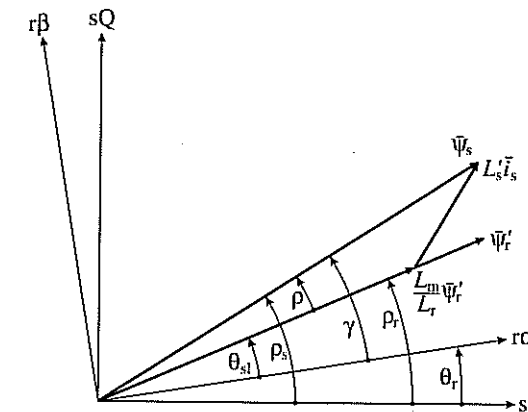


Fig. 4.55. Stator flux and rotor flux-linkage space vectors, and their positions in various reference frames.

of the stator reference frame, and  $\rho$  is the angle between the stator and rotor flux-linkage space vectors,  $\rho = \rho_s - \rho_r$ . It follows that

$$\omega_d = \frac{d\rho}{dt} = \frac{d\rho_s}{dt} - \frac{d\rho_r}{dt} = \omega_{ms} - \omega_{mr}$$

is indeed the difference between the speed of the stator flux-linkage space vector and the speed of the rotor flux-linkage space vector. Furthermore, as shown in Fig. 4.55,  $\theta_r$  is the rotor angle, and  $\theta_r = \rho_s - \rho - \theta_{sl}$ . Thus

$$\omega_r = \frac{d\theta_r}{dt} = \frac{d\rho_s}{dt} - \frac{d\rho}{dt} - \frac{d\theta_{sl}}{dt} = \omega_{ms} - \omega_d - \omega_{sl},$$

in agreement with eqn (4.5-44). In eqn (4.5-44),  $\omega_{ms}$  can be obtained as given by eqn (4.5-42), and  $\omega_{sl}$  can be obtained as shown by eqn (4.5-35). However,  $\omega_d$  can be obtained by considering that

$$t_e = \frac{3}{2} PL_m / (L'_s/L_r) |\bar{\psi}_s| |\bar{\psi}_r| \sin \rho = c |\bar{\psi}_s| |\bar{\psi}_r| \sin \rho,$$

where  $c = (3/2)PL_m / (L'_s/L_r)$ , from which

$$\omega_d = \frac{d\rho}{dt} = \frac{d}{dt} [\sin^{-1}(t_e / (c |\bar{\psi}_s| |\bar{\psi}_r|))].$$

It should be noted that  $t_e = c |\bar{\psi}_s| |\bar{\psi}_r| \sin \rho$  follows from  $t_e = (3/2)P \bar{\psi}_s \times \bar{\psi}_r$ , by considering that  $\bar{\psi}_s = [\bar{\psi}_s - (L_m/L_r) \bar{\psi}_r]/L'_s$  [this last equation follows from eqns (2.1-150) and (2.1-151)]. Finally eqn (4.5-44) can be put into the form

$$\omega_r = \frac{\psi_{sD} d\psi_{sQ}/dt - \psi_{sQ} d\psi_{sD}/dt}{\psi_{sD}^2 + \psi_{sQ}^2} - \frac{d}{dt} [\sin^{-1}(t_e / (c |\bar{\psi}_s| |\bar{\psi}_r|))] - \frac{2t_e R_r}{3P |\bar{\psi}_r|^2}, \quad (4.5-45)$$

where it is possible to use different expressions for the electromagnetic torque [e.g.  $t_e = (3/2)P(\psi_{sD}i_{sQ} - \psi_{sQ}i_{sD})$  or  $t_e = (3/2)P(L_m/L_r)(\psi_{rd}i_{sQ} - \psi_{rq}i_{sD})$ ]. Equation (4.5-45) can also be used for the estimation of the rotor speed of an induction machine, but this is not simpler than that described by eqn (4.5-38) or (4.5-39).

In Fig. 4.55, the angle  $\rho_s - \rho$  is equal to the angle  $\rho_r$  and thus

$$\omega_r = \frac{d\theta_r}{dt} = \frac{d}{dt}(\rho_s - \rho) - \frac{d\theta_{sl}}{dt} = \omega_{mr} - \omega_{sl},$$

which, as expected, agrees with eqn (4.5-36). It follows that when the rotor speed is determined by using the speed ( $\omega_{mr}$ ) of the rotor flux-linkage space vector and the speed of the rotor flux with respect to the rotor ( $\omega_{sl}$ ), then  $\omega_r = \omega_{mr} - \omega_{sl}$  holds. However, when the rotor speed is determined by using the speed of the stator flux-linkage space vector ( $\omega_{ms}$ ) and also the speed of the rotor flux-linkage space vector with respect to the rotor ( $\omega_{sl}$ ), then an extra speed term,  $\omega_d$ , has also to be considered, and  $\omega_r = \omega_{ms} - \omega_d - \omega_{sl}$ . On the other hand, it also follows that the rotor speed can be determined by considering that  $\theta_r = \rho_s - (\rho + \theta_{sl}) = \rho_s - \gamma$ , where as shown in Fig. 4.55,  $\gamma = \rho + \theta_{sl}$  is the angle of the stator flux-linkage space vector with respect to the real axis of the rotor, since it follows that

$$\omega_r = \frac{d\theta_r}{dt} = \frac{d\rho_s}{dt} - \frac{d\gamma}{dt} = \omega_{ms} - \omega'_{sl}.$$

This means that the rotor speed is equal to the speed of the stator flux-linkage space vector (with respect to the stator) minus the speed of the stator flux-linkage space vector with respect to the rotor,  $\omega'_{sl}$  (which has been given by eqn (4.5-43)). This last approach has been used in the scheme of Fig. 4.54.

Various other simplified rotor-speed estimation schemes can be obtained directly by considering eqns (4.5-44) and (4.5-45), if it is assumed that the speeds of the stator and rotor flux-linkage space vectors are equal. In this case  $\omega_d = 0$ , and

$$\omega_r \approx \frac{\psi_{sD}d\psi_{sQ}/dt - \psi_{sQ}d\psi_{sD}/dt}{\psi_{sD}^2 + \psi_{sQ}^2} - \frac{2t_e R_r}{3P|\bar{\psi}_r|^2}. \quad (4.5-46)$$

This is similar in form to eqn (4.5-39), but eqn (4.5-39) is more accurate, since eqn (4.5-46) assumes that  $\omega_d = 0$ .

In summary it should be noted that among the various speed estimators discussed above in connection with the Scheme shown in Fig. 4.53, those using eqns (4.5-38) or (4.5-39) are the simplest and most accurate. These rely heavily on the accuracy of the estimated flux-linkage components. If the stator voltages and currents are used to obtain the flux-linkage estimates, then by considering the thermal variations of the stator resistance (e.g. by using a thermal model), and also by using appropriate saturated inductances, the estimation accuracy can be greatly improved. However, a speed-sensorless high-performance torque-controlled drive (vector- or direct-torque-controlled drive) using this type of speed estimator will only work successfully at extremely low speeds (including zero speed) if the flux-linkage estimator is a closed-loop observer.

#### 4.5.3.1.6 Rotor speed estimation scheme 5

$$\omega_r = \left[ \frac{d\psi_{rq}}{dt} \psi'_{sD} - \frac{d\psi_{rd}}{dt} \psi'_{sQ} \right] / [\psi_{rd}\psi'_{sD} + \psi_{rq}\psi'_{sQ}]$$

$$\psi'_{sD} = \psi_{sD} - L_s i_{sD} \quad \psi'_{sQ} = \psi_{sQ} - L_s i_{sQ}$$

It is also possible to obtain directly an expression for the rotor speed from the rotor space-vector voltage equation of the induction machine in the stationary reference frame, by eliminating from this the unmeasurable rotor-current space vector. However, due to its limitations, this estimation technique has been deliberately considered as the last scheme, since it will be shown that this direct approach cannot be used in two cases: under sinusoidal steady-state conditions and also when the rotor flux is constant. The rotor voltage equation can also be used for the estimation of the rotor resistance, but again, the estimation cannot be used in the sinusoidal steady-state and when the rotor flux is constant. The details will be considered below, and these are mainly useful for educational purposes.

It follows from eqn (2.1-149) that

$$0 = R_r \tilde{i}'_r + \frac{d\bar{\psi}'_r}{dt} - j\omega_r \bar{\psi}'_r, \quad (4.5-47)$$

where the primed rotor quantities denote quantities in the stationary reference frame. However, by considering that the stator flux-linkage space vector can be expressed as  $\bar{\psi}_s = L_s \tilde{i}_s + L_m \tilde{i}_r'$ , it follows that the rotor-current space vector expressed in the stationary reference frame is

$$\tilde{i}'_r = \frac{\bar{\psi}_s - L_s \tilde{i}_s}{L_m}. \quad (4.5-48)$$

Substitution of eqn (4.5-48) into (4.5-47) gives the rotor voltage equation in terms of the stator flux-linkage, rotor flux-linkage, and stator-current space vector respectively, and when this voltage equation is resolved into its real and imaginary parts,

$$R_r \frac{(\psi_{sD} - L_s i_{sD})}{L_m} + \omega_r \psi_{rq} = - \frac{d\psi_{rd}}{dt} \quad (4.5-49)$$

$$R_r \frac{(\psi_{sQ} - L_s i_{sQ})}{L_m} - \omega_r \psi_{rd} = - \frac{d\psi_{rq}}{dt} \quad (4.5-50)$$

are obtained. Equations (4.5-49) and (4.5-50) can be put into the form

$$a_1 x_1 + b_1 x_1 = c_1 \quad (4.5-51)$$

$$a_2 x_2 + b_2 x_2 = c_2, \quad (4.5-52)$$

where

$$\begin{aligned} a_1 &= \frac{\psi_{sD} - L_s i_{sD}}{L_m} & b_1 &= \psi_{rq} & a_2 &= \frac{\psi_{sQ} - L_s i_{sQ}}{L_m} & b_2 &= -\psi_{rd} \\ c_1 &= -\frac{d\psi_{rd}}{dt} & c_2 &= -\frac{d\psi_{rq}}{dt} & x_1 &= R_r & x_2 &= \omega_r. \end{aligned} \quad (4.5-53)$$

Equations (4.5-51) and (4.5-52) can be solved for the 'unknowns'  $x_1$  and  $x_2$  when the resulting determinant  $D = a_1 b_2 - a_2 b_1$  is not zero, and finally

$$x_1 = R_r = -\frac{L_m [\psi_{rd}(d\psi_{rd}/dt) + \psi_{rq}(d\psi_{rq}/dt)]}{\psi_{rd}(\psi_{sD} - L_s i_{sD}) + \psi_{rq}(\psi_{sQ} - L_s i_{sQ})} \quad (4.5-54)$$

$$x_2 = \omega_r = \frac{(d\psi_{rq}/dt)(\psi_{sD} - L_s i_{sD}) - (d\psi_{rd}/dt)(\psi_{sQ} - L_s i_{sQ})}{\psi_{rd}(\psi_{sD} - L_s i_{sD}) + \psi_{rq}(\psi_{sQ} - L_s i_{sQ})} \quad (4.5-55)$$

are obtained. These equations depend on the stator flux linkages, rotor flux linkages and stator currents, where the various flux-linkage components can be obtained from the stator voltages and currents by considering eqns (4.5-16), (4.5-17), (4.5-19), and (4.5-20) as follows, or by using the improved flux estimators described earlier:

$$\psi_{sD} = \int (u_{sD} - R_s i_{sD}) dt \quad (4.5-56)$$

$$\psi_{sQ} = \int (u_{sQ} - R_s i_{sQ}) dt \quad (4.5-57)$$

$$\psi_{rd} = \frac{L_r}{L_m} (\psi_{sD} - L_s' i_{sD}) \quad (4.5-58)$$

$$\psi_{rq} = \frac{L_r}{L_m} (\psi_{sQ} - L_s' i_{sQ}). \quad (4.5-59)$$

In general the rotor speed can be determined from eqn (4.5-55), which can also be put into the following form by considering eqns (4.5-48), (4.5-58), and (4.5-59):

$$\begin{aligned} \omega_r &= \frac{\bar{t}'_r \times (d\bar{\psi}'_r/dt)}{\bar{t}'_r \cdot \bar{\psi}'_r} = \frac{|\bar{t}'_r| d\bar{\psi}'_r/dt | \sin \alpha}{|\bar{t}'_r| |\bar{\psi}'_r| \cos \beta} \\ &= \frac{|d\bar{\psi}'_r/dt| \sin \alpha}{|\bar{\psi}'_r| \cos \beta} \end{aligned} \quad (4.5-60)$$

where  $\times$  denotes the vectorial product and  $\bullet$  denotes the scalar (dot) product,  $\alpha$  is the phase angle between the rotor-current space vector and the space vector  $d\bar{\psi}'_r/dt$ , and  $\beta$  is the angle between the rotor-current space vector and the rotor flux-linkage space vector expressed in the stationary reference frame ( $\bar{\psi}'_r$ ). However, in the sinusoidal steady-state of an induction machine, where the stator voltages and currents are sinusoidal, eqn (4.5-55) cannot be used, since its

numerator and denominator become zero at every instant of time. This can be simply proved by considering that it follows from eqn (4.5-47) [by replacing the derivative by  $j\omega_1$ ] that in the sinusoidal steady-state (where the supply frequency is  $\omega_1$ ) the rotor-current space vector ( $\bar{t}'_r$ ) is in phase with  $d\bar{\psi}'_r/dt$  (thus  $\alpha=0$ ) and  $\bar{t}'_r$  is in quadrature to the rotor flux vector  $\bar{\psi}'_r$  (thus  $\beta=90^\circ$ ). It follows that  $|d\bar{\psi}'_r/dt| \sin \alpha = 0$ , and  $|\bar{\psi}'_r| \cos \beta = 0$ , and it can be seen that both the numerator and denominator of eqn (4.5-60) are zero in the sinusoidal steady-state. Furthermore, if steady-state is not assumed, but  $|\bar{\psi}'_r| = \text{constant}$  is assumed, then  $d\bar{\psi}'_r/dt = j\omega_{mr} \bar{\psi}'_r$ , where  $\omega_{mr} = d\rho_r/dt$  is the speed of the rotor flux-linkage space vector, since

$$\frac{d\bar{\psi}'_r}{dt} = \frac{d}{dt} [|\bar{\psi}'_r| \exp(j\rho_r)] = \exp(j\rho_r) \frac{d}{dt} (|\bar{\psi}'_r|) + j \frac{d\rho_r}{dt} |\bar{\psi}'_r| \exp(j\rho_r) = j\omega_{mr} \bar{\psi}'_r,$$

and it can be seen that the phase shift between  $d\bar{\psi}'_r/dt$  and  $\bar{\psi}'_r$  is  $90^\circ$  (similarly to that in the steady-state). Thus it follows from eqn (4.5-60) that if the angle of  $\bar{t}'_r$  is  $\delta_i$  (with respect to the real-axis of the stationary reference frame) and  $\rho_r$  is the angle of  $\bar{\psi}'_r$  (with respect to the real-axis of the stationary reference frame), then

$$\omega_r = \frac{|d\bar{\psi}'_r/dt| \sin \alpha}{|\bar{\psi}'_r| \cos \beta} = \frac{\omega_{mr} |\bar{\psi}'_r| \sin(\rho_r + \pi/2 - \delta_i)}{|\bar{\psi}'_r| \cos(\rho_r - \delta_i)} = \omega_{mr},$$

and hence the rotor speed is equal to the speed of the rotor flux-linkage space vector. However, in general, this is not correct; it is only correct when the slip frequency is zero ( $\omega_{sl}=0$ ) [e.g. it follows from eqn (4.5-39) that when  $\omega_{sl}=0$ ,  $\omega_r = \omega_{mr} - \omega_{sl} = \omega_{mr}$ ]. The slip frequency is only zero now because the rotor resistance, which can be obtained from eqn (4.5-54), is zero when the rotor flux-linkage space vector is assumed to be constant. This follows since under the special condition of  $|\bar{\psi}'_r| = \text{constant}$ , the flux-linkage space vector and its derivative are displaced by  $90^\circ$  and therefore their dot product ( $\bar{\psi}'_r \cdot d\bar{\psi}'_r/dt$ ) is zero, which leads to  $R_r=0$  in eqn (4.5-54), which can also be expressed in general as

$$R_r = -\frac{\bar{\psi}'_r \cdot (d\bar{\psi}'_r/dt)}{\bar{t}'_r \cdot \bar{\psi}'_r}.$$

Although eqn (4.5-55) cannot be used in the sinusoidal steady-state of an induction machine, it can be used for an induction machine supplied by non-sinusoidal voltages and currents, e.g. the case of a PWM-fed induction machine. This follows from the fact that in this case the special phase relationships described above ( $\alpha=0, \beta=90^\circ$ ) do not hold in every instant of time. However, due to the flux ripples, resulting from the non-sinusoidal stator voltages, both the denominator and numerator of the speed expression will have periodic waveforms, which contain many zero-crossings, and at the time instants where the denominator zero-crossings occur, it is not possible to perform the required division. It is also important to note that, since the amplitudes of the harmonic components (ripples) present in the waveforms of the numerator and denominator are small, high accuracy of the estimated rotor speed can only be obtained if high accuracy voltage and current sensors are used together with high accuracy A/D converters.

In the steady-state of a PWM-fed machine, the numerator and denominator have similar waveforms, but the amplitudes of these two are different, and thus the ratio of the numerator and denominator gives a constant value.

It has been stated above that when the denominator of eqn (4.5-60) becomes zero (at the zero-crossing instants), it is impossible to use eqn (4.5-60). However, this problem can be avoided by considering that the numerator and denominator waveforms have different amplitudes, and the same zero-crossings. Therefore the correct speed estimate will result if the absolute value of the numerator is divided by the absolute value of the denominator, but since the estimated speed can be positive or negative, this ratio has to be multiplied by the sign of the expression given by eqn (4.5-60).

Thus

$$\omega_r = \text{sign} \left\{ \frac{\bar{i}'_r \times (\text{d}\bar{\psi}'_r / \text{d}t)}{\bar{i}'_r \cdot \bar{\psi}'_r} \right\} \frac{|[\bar{i}'_r \times (\text{d}\bar{\psi}'_r / \text{d}t)]|}{|(\bar{i}'_r \cdot \bar{\psi}'_r)|}. \quad (4.5-61)$$

Furthermore, when the absolute values in eqn (4.5-61) are small, the estimated rotor speed may become inaccurate. This problem can be avoided by low-pass filtering the absolute values of the numerator and denominator waveforms respectively. To obtain high accuracy, the two low-pass filters must be identical. The speed estimator described above depends on various machine parameters,  $R_s$ ,  $L'_s$ ,  $L_s$ ,  $L_r/L_m$ , but does not depend on the rotor resistance. The stator resistance has important effects on the stator flux linkages, especially at low speeds. Due to main flux saturation  $L_m$  can change and  $L_s = L_{s1} + L_m$ ,  $L_r = L_{r1} + L_m$  can also change even if the leakage inductances are constant. However, due to leakage flux saturation,  $L_{s1}$ ,  $L_{r1}$ , and  $L'_s$  can also change. In a vector-controlled drive, where the rotor flux amplitude is constant, the variations of  $L_m$  are small. It follows that in this drive, accurate speed estimation based on eqn (4.5-61) depends mostly on  $R_s$  and  $L'_s$ . In an induction machine with closed rotor slots,  $L'_s$  varies due to leakage flux saturation, and  $L'_s$  is a function of the stator currents, due to the saturable closing bridge around the rotor slots. Furthermore, higher accuracy is obtained if the stator flux is obtained by a scheme which avoids the use of pure integrators (some solutions for this are discussed elsewhere in the book, e.g. see Sections 3.1.3, 4.1.1).

It should be noted that, in general, eqn (4.5-55) can be used for the identification of the rotor resistance. As mentioned above, this can be put into the following form:

$$R_r = -\frac{\bar{\psi}'_r \cdot (\text{d}\bar{\psi}'_r / \text{d}t)}{\bar{i}'_r \cdot \bar{\psi}'_r}. \quad (4.5-62)$$

In the sinusoidal steady-state, incorrect rotor resistance is obtained, since in the steady state the rotor flux-linkage space vector and the derivative of the rotor flux-linkage space vector are displaced by  $90^\circ$  (see above), and thus the numerator in eqn (4.5-62) is zero. However, in the sinusoidal steady-state, the denominator of eqn (4.5-62) is also zero, since the rotor-current space vector and the rotor

flux-linkage space vector are also displaced by  $90^\circ$  (see above). Furthermore, it has been shown above that when  $|\bar{\psi}'_r| = \text{constant}$ , this expression gives the incorrect  $R_r = 0$ , since in this case the rotor flux-linkage space vector and its derivative are displaced by  $90^\circ$ .

It should be noted that since  $|\bar{\psi}'_r| = \text{constant}$  results in  $\text{d}\bar{\psi}'_r / \text{d}t = j\omega_{mr}\bar{\psi}'_r$  (see above), and thus  $\text{d}\psi_{rd} / \text{d}t = -\omega_{mr}\psi_{rq}$  and  $\text{d}\psi_{rq} / \text{d}t = \omega_{mr}\psi_{rd}$ , it follows from (4.5-49) and (4.5-50) that  $\omega_r = \omega_{mr}$ , which is in agreement with that shown above, using a different derivation.

It should also be noted that, as shown above, the simultaneous estimation of the rotor resistance and rotor speed is impossible if the rotor flux-linkage space vector does not change (e.g. this occurs in the sinusoidal steady-state, or in a drive where the voltages and currents are not sinusoidal but constant rotor flux linkage is imposed). This impossibility can also be simply proved in a slightly different way by directly considering eqn (4.5-47). It follows that when  $|\bar{\psi}'_r| = \text{constant}$ , and thus  $\text{d}\bar{\psi}'_r / \text{d}t = j\omega_{mr}\bar{\psi}'_r$ , then

$$0 = R_r \bar{i}'_r + j(\omega_{mr} - \omega_r) \bar{\psi}'_r = R_r \bar{i}'_r + j\omega_{sl} \bar{\psi}'_r$$

( $\omega_{sl}$  is the slip frequency) and hence  $0 = (R_r/\omega_{sl}) \bar{i}'_r + j\bar{\psi}'_r$ . However, since for given  $\bar{i}_s$  and  $\bar{i}_s$  (and machine parameters) the rotor flux-linkage space vector and rotor-current space vector ( $\bar{\psi}'_r$  and  $\bar{i}'_r$ ) are uniquely determined, e.g.  $\bar{\psi}'_s = \int (\bar{i}_s - R_s \bar{i}_s) \text{d}t$ ,  $\bar{\psi}'_r = (L_r/L_m)(\bar{\psi}'_s - L'_s \bar{i}_s)$ , and  $\bar{i}'_r = (\bar{\psi}'_s - L'_s \bar{i}_s)/L_m$ , it follows that it is only possible to estimate the combined parameter  $R_r/\omega_{sl}$  and it is not possible to have a separate, simultaneous estimation of  $R_r$  and  $\omega_{sl}$  (or  $R_r$  and  $\omega_r$ ). In the sinusoidal steady-state, the same result can also be obtained directly by considering the equivalent circuit of the induction machine (Fig. 4.10), which shows that when the rotor flux is constant ( $L_m |\bar{i}_{mr}| = \text{const.}$ ), only the ratio of the rotor resistance and slip can be estimated.

However, when the special conditions (sinusoidal steady-state or rotor flux constant) do not apply, and when the induction machine is supplied by a voltage-source PWM inverter, thus there are time harmonics in the stator voltages and currents (and therefore in the flux linkages as well), these special phase relationships do not apply at every instant of time and  $R_r$  can be estimated by using eqn (4.5-62). To avoid the problems associated with the zero-crossing of the numerator and denominator waveforms of this expression, a similar technique is used as before. However, since the rotor resistance is always positive, there is no need to take the sign of the ratio given by eqn (4.5-62) and the rotor resistance is estimated from

$$R_r = \frac{|-\bar{\psi}'_r \cdot (\text{d}\bar{\psi}'_r / \text{d}t)|}{|(\bar{i}'_r \cdot \bar{\psi}'_r)|}. \quad (4.5-63)$$

In practice, the rotor resistance can be estimated by dividing the low-pass filtered absolute value of  $|-\bar{\psi}'_r \cdot (\text{d}\bar{\psi}'_r / \text{d}t)|$  by the low-pass filtered absolute value  $|(\bar{i}'_r \cdot \bar{\psi}'_r)|$ . As before, the two low-pass filters used in the rotor resistance estimator must have identical characteristics in order to obtain high accuracy. This scheme

can be used in a torque-controlled drive. When this rotor resistance estimator is used in a speed-sensorless torque-controlled drive which requires the rotor resistance, and e.g. the rotor speed estimator is described by eqn (4.5-61), further improvements in the speed response are expected.

Finally it should be noted that the accuracy of open-loop estimators depends greatly on the accuracy of the machine parameters used. In general, at low rotor speed the accuracy of the open-loop estimators is reduced, and in particular, parameter deviations from their actual values have great influence on the steady-state and transient performance of the drive system. The robustness against parameter mismatch and noise (in the measured signals) can be greatly reduced by using closed-loop observers for the estimation of the state-variables (e.g. flux linkages, speed, etc.). Various closed-loop observers are discussed in Section 4.5.3.5.

#### 4.5.3.2 Estimators using spatial saturation third-harmonic voltage

##### 4.5.3.2.1 General introduction

In the present section saturation phenomena are utilized to obtain the rotor speed and also the magnitude and position of the magnetizing flux-linkage space vector. This information can then also be used to obtain the rotor flux-linkage space vector and the stator flux-linkage space vector, and their applications in vector-controlled drives is discussed. The same saturation phenomena can also be used to obtain a signal proportional to the electromagnetic torque.

For better understanding, first the main features of this technique will now be summarized. In a symmetrical three-phase induction motor with stator windings without a neutral point, the sum of the stator voltages is monitored. This is a spatial saturation third-harmonic voltage component and is due to stator and rotor teeth saturation, which saturation condition is normal in a standard motor. The third-harmonic voltage is then integrated to give the third-harmonic flux, and the fundamental component of the magnetizing flux ( $\psi_{ml}$ ) is then determined by using a saturation function that can be obtained experimentally by performing the conventional no-load test (a look-up table stored in the memory of a microprocessor or DSP can be used which gives the relationship of the fundamental magnetizing flux and third-harmonic flux). The obtained magnetizing-flux modulus is large and is practically free of noise.

It is also possible to obtain the angle of the magnetizing-flux space vector by utilizing the monitored third-harmonic voltage. For this purpose the current in stator phase sA is also monitored and the displacement angle ( $\gamma$ ) between this stator current maximum and the fundamental magnetizing-flux maximum is determined. It should be noted that the fundamental magnetizing-flux component does not have to be monitored, since only the location of its maximum point is required and this can be obtained from the third-harmonic stator voltage (the suitable zero-crossing point of this voltage). By knowing the angle of the fundamental magnetizing-current space vector with respect to the stator-current space vector ( $\gamma$ ), and also by measuring the angle of the stator-current space vector with

respect to the direct-axis of the stationary reference frame ( $\alpha_s$ ), it is possible to obtain the angle of the magnetizing-flux space vector with respect to the direct-axis of the stationary reference frame ( $\mu_m$ ). The details will be described below.

By using the modulus of the fundamental magnetizing vector and also its phase angle with respect to the stationary reference frame, the magnetizing flux-linkage space vector  $\bar{\psi}_m = |\bar{\psi}_m| \exp(j\mu_m)$  is known, and this can be used to construct the rotor flux-linkage space vector or the stator flux-linkage space vector. The magnetizing flux-linkage, rotor flux-linkage, and stator flux-linkage space vectors can be used in vector control schemes using magnetizing-flux-oriented, rotor-flux-oriented, or stator-flux-oriented control. The rotor speed can be obtained, for example, by also considering the first derivative of the angle of the stator-flux space vector with respect to the direct-axis of the stationary reference frame (see also Section 4.5.3.1).

##### 4.5.3.2.2 Physical picture due to saturation; teeth and core saturation

For better utilization, a modern induction machine is designed to operate in the saturated region of the magnetizing characteristic. If the stator windings of a symmetrical three-phase induction machine are assumed to be sinusoidally distributed, the stator currents will create a sinusoidally distributed m.m.f in an unsaturated machine and this establishes a sinusoidal air-gap flux density distribution. However, if the machine is saturated, the sinusoidal distribution becomes distorted. Two cases must be considered, saturation of the stator/rotor teeth and saturation of the stator/rotor core.

Saturation in the teeth is more common in a practical machine, since the volume of the iron is generally greater in the core where a much higher flux density exists. Therefore the techniques described below will only utilize teeth saturation phenomena, although some physical aspects of core saturation will also be briefly discussed for clarity. Considering the saturation of the teeth, the teeth with the highest flux density will saturate first, thus the sinusoidal flux density distribution will become flattened. The flattened flux density distribution,  $B_{sat}^{teeth}(\theta)$  is shown in Fig. 4.56 together with the fundamental flux density distribution,  $B_{gap1}(\theta)$ . It can be seen that its peak value is smaller than the peak of the fundamental distribution. The flattening of the curve is mainly caused by the presence of a third-harmonic air-gap flux density component  $B_{gap3}^{teeth}(\theta)$ , which is also shown in Fig. 4.56. By using Fourier analysis, it can be shown that the flattened curve contains other odd harmonics as well, but the dominant component is the third harmonic for all saturation levels. The speed of the third-harmonic component is identical to that of the fundamental component and both rotate in the same direction. It also follows that if a model of the induction machine with saturated teeth is required, it can be simply obtained by superposition of the third harmonic on the fundamental air-gap flux component. It can also be seen that teeth saturation decreases the permeability of the iron parts and this increases the reluctances of the teeth for the region around the resultant air-gap flux density.

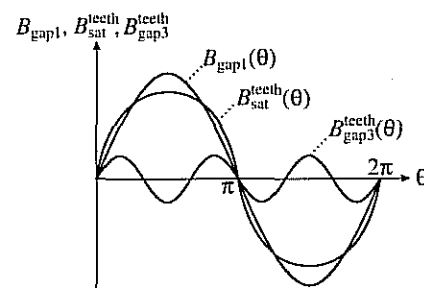


Fig. 4.56. Fundamental, flattened, and third-harmonic flux density distributions for teeth saturation.

By keeping the necessary assumption of constant and infinite iron permeability, the reluctance variation of the teeth can also be viewed as a variation of the air-gap reluctance. However, the air-gap has a constant permeability, thus the air-gap length has to be made variable (to ensure variation of the air-gap reluctance). It is therefore also possible to model an induction motor with saturated teeth by incorporating a variable air-gap length into its linear model, where the air-gap length is a function of the saturation level and spatial position. This also explains the resemblance between a saturated smooth-air-gap two-axis model and a non-saturated two-axis salient-pole model, which has been discussed in detail in [Vas 1992], where in the latter case, there exists real (physical) air-gap length variation.

When saturation occurs in the stator or rotor core, it also distorts the air-gap flux density distribution. However, in this case, since the core with the highest flux density will saturate first, the core flux density distribution will have a flattened sinusoidal form, and the air-gap flux density distribution will be peaked. This can also be explained by the fact that the air-gap flux-density distribution is proportional to the spatial derivative of the core flux-density distribution. This can be understood by considering the fluxes in the two-pole induction machine shown in Fig. 4.57. It can be seen that in the magnetic axis of the coil (which corresponds to the position  $\theta = \pi/2$ ), the core flux is zero, but the air-gap flux is maximal, but  $90^\circ$  away (which corresponds to  $\theta = 0$ ), the core flux is maximal and the air-gap flux is zero. It clearly follows that the core flux-density distribution is the spatial integral of the teeth flux-density distribution.

As in the case of teeth saturation, again the third harmonic is the dominant component  $B_3^{core}(\theta)$ , but this third harmonic is in phase opposition to that produced by teeth saturation (see Fig. 4.56) thus enforcing the fundamental component, and leading to the peaked resultant core density distribution,  $B_{sat}^{core}(\theta)$ . This is shown in Fig. 4.58.

It is important to note that the presence of a third-harmonic component in the air-gap flux density distribution is only a sufficient but not necessary condition for the occurrence of saturation. It has been shown that the mechanisms of teeth and core saturation cause opposite effects; the two types of third-harmonic

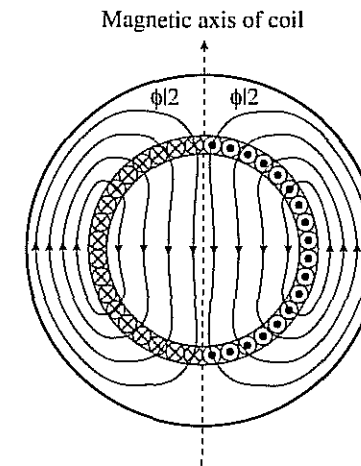


Fig. 4.57. Fluxes in the air-gap and core of a two-pole induction machine.

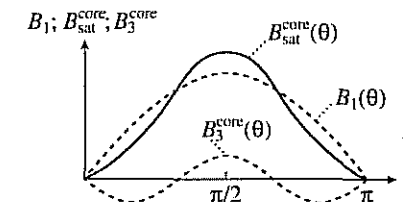


Fig. 4.58. Fundamental, third-harmonic, and peaked flux-density distributions for core saturation,

waves are in direct phase opposition. Thus a highly saturated machine does not necessarily have a high third-harmonic air-gap flux component.

#### 4.5.3.2.3 General aspects of magnetizing flux-linkage monitoring using saturation phenomena

For an induction machine with wye-connected stator windings without a neutral point, it is possible to have a simple direct-vector-control scheme utilizing saturation effects in the stator/rotor teeth. For this purpose, first the fundamental component of the magnetizing-flux space vector (e.g. its modulus  $|\bar{\psi}_{m1}|$  and its phase angle  $\gamma$ , with respect to the stator current vector) can be obtained by processing of the monitored (spatial saturation) zero-sequence third-harmonic voltage ( $u_{s3}$ ) together with the monitored stator line current (e.g.  $i_{sA}$ ), and also by utilizing a saturation function ( $f$ ) obtained by a conventional no-load test. The saturation function  $f$  gives the relationship between the rms value of the third-harmonic magnetizing voltage and the rms value of the fundamental

magnetizing voltage under no-load condition. The zero-sequence third-harmonic voltage component ( $u_{s3}$ ) is due to the stator and rotor teeth saturation, and this saturation condition is normal in a modern induction motor.

The zero-sequence voltage can be obtained by adding the three stator phase voltages (e.g. by using potential transformers, or by using operational amplifiers as discussed below) and by eliminating the high frequency slot harmonic voltage component,  $u_{sh}$ , (by using an analog or digital filter). Of course for this purpose access is required to the neutral point of the stator windings. Figure 4.59 shows the fundamental stator voltage,  $u_{s1}$ , and the third-harmonic zero-sequence stator voltage  $u_{s0}$ , which is modulated by the high frequency slot harmonics,  $u_{s0} = u_{s3} + u_{sh}$ .

For rotor-flux-oriented control, the rotor flux-linkage space vector (its modulus and phase angle) can be obtained from  $|\psi_{m1}|$  and  $\gamma$ , as discussed below. Figures 4.60 and 4.61 show two implementations respectively of obtaining the zero-sequence stator voltage,  $u_{s0}$ . In Fig. 4.60 three potential transformers are used and the secondary windings of the transformers are connected in series.

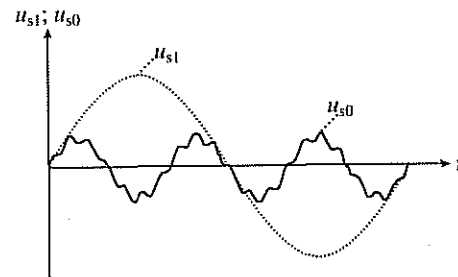


Fig. 4.59. Fundamental stator voltage and zero-sequence stator voltage with slot ripples.

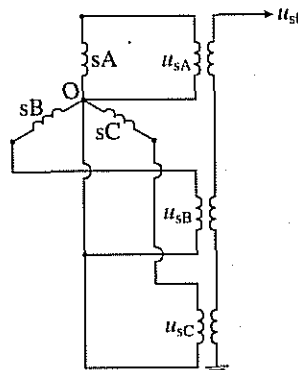


Fig. 4.60. Monitoring of the zero-sequence stator voltage using three potential transformers.

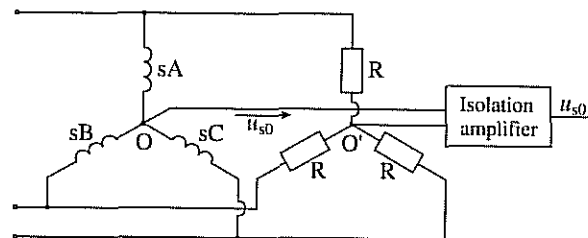


Fig. 4.61. Monitoring of the zero-sequence stator voltage using three identical external resistors.

However, in Fig. 4.61, three identical resistors are connected in star, and this arrangement is connected in parallel with the stator windings of the induction motor.

In Fig. 4.61 the zero-sequence stator voltage is obtained across the neutral point of the stator winding (point 0) and the pseudo-neutral point of the three external resistors (0'). This must then be isolated. If the induction motor is directly supplied from a PWM inverter, high transient intercoil voltages are also created at the line end of the windings. The magnitude of these transient voltages varies due to reflections at the end points and therefore the switching transients, which are present at both the pseudo-star (0') and motor-star (0) point, may not exactly cancel when the motor signal is formed. Thus additional filtering of this feedback signal is necessary.

It has been discussed above that due to teeth saturation a flattened magnetizing flux-density distribution will arise, which contains a dominant third-harmonic flux component. This links the stator windings and induces a third-harmonic voltage component in each stator phase ( $u_{sA3}$ ,  $u_{sB3}$ ,  $u_{sC3}$ ), which are all in phase, forming a zero-sequence set of stator voltages. However, if the stator windings of the saturated induction machine are connected in star with no neutral connection, no third-harmonic currents (zero-sequence current components) will circulate in the stator and therefore there will be no third-harmonic ohmic and leakage voltage drops across the stator impedance. Hence the third harmonic stator voltage ( $u_{s0}$ ), whose monitoring has been discussed above, can be used to obtain directly the third-harmonic magnetizing voltage ( $u_{m3} = u_{s0}$ ). The third-harmonic magnetizing flux ( $\psi_{m3}$ ) can be obtained from this by integration:

$$\int u_{s0} dt = \int (u_{s3} + u_{sh}) dt = \int u_{s3} dt = \psi_{m3}$$

( $u_{sh}$  is filtered out, e.g. by a low-pass filter with high cut-off frequency).

It should be noted that if the stator winding distribution contains a third-harmonic spatial component, then the zero-sequence currents can flow in the stator. Furthermore, induction of a third-harmonic voltage in the stator windings due to stator and rotor currents is also possible. However, for a star-connected machine, without neutral return, these components can only exist if positive-sequence or

negative-sequence third-harmonic current components flow in the stator windings. The summation of these voltages will cancel out these harmonics. If the machine is delta-connected, zero-sequence third-harmonic currents can flow around the delta path, provided that the stator winding distribution contains the third-harmonic spatial components. In this case, with practical windings, the current is only very small (a few per cent of the rated current).

The third-harmonic stator voltage (which has been shown to be equal to the third-harmonic magnetizing voltage) is always in phase with the fundamental magnetizing voltage. Thus the fundamental magnetizing flux ( $\psi_{m1}$ ) is in phase with the third-harmonic magnetizing flux ( $\psi_{m3}$ ) for all load conditions. This is shown in Fig. 4.62, where the temporal variations of  $\psi_{m1}$  and  $\psi_{m3}$  are shown for no-load and rated conditions respectively. However, since  $\psi_{m3}$  is small, for clarity,  $40\psi_{m3}$  is shown in both diagrams.

The fact that the fundamental magnetizing flux is in phase with the third-harmonic magnetizing flux for all load conditions is a direct consequence of the physical phenomenon that when saturation of the teeth occurs, the magnetizing-flux density distribution keeps its flattened sinusoidal form, independent of the load. This can also be seen by considering that the third-harmonic rotor currents

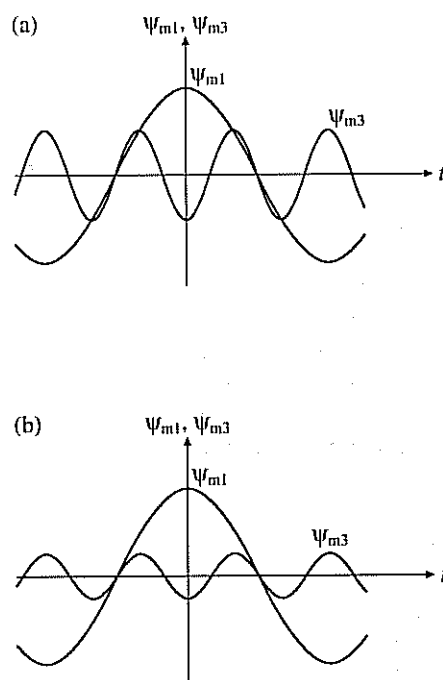


Fig. 4.62. Variation of  $\psi_{m1}$  and  $\psi_{m3}$  at no-load and rated load. (a) No-load condition; (b) rated load condition.

are not large enough to produce a rotor m.m.f. that would change the position of the third-harmonic magnetizing flux with respect to the fundamental magnetizing flux. It follows that the third-harmonic magnetizing flux always maintains a constant position with respect to the fundamental magnetizing flux. This is why the position of the third-harmonic magnetizing flux coincides with the position of the fundamental magnetizing flux, and thus the third-harmonic magnetizing voltage can be used to obtain the position (angle) of the fundamental magnetizing flux. This principle is utilized below in the next section.

To conclude: when the three stator voltages are added, the resultant zero-sequence voltage ( $u_{s0}$ ) contains a third-harmonic component ( $u_{s3}$ ) and the high frequency slot harmonic component ( $u_{sh}$ ),  $u_{s0} = u_{s3} + u_{sh}$ . However, the third-harmonic component is dominant, since the fundamental and other, non-triple, so-called characteristic harmonics (e.g. 5th, 7th, 11th, etc.) which could be present in the currents and thus in the air-gap m.m.f. and magnetizing flux, will cancel. The slot harmonic component can be filtered out, as discussed above.

#### 4.5.3.2.4 Estimation of the modulus of the magnetizing flux-linkage space-vector and the angle between the stator current vector and the magnetizing flux-linkage space-vectors

As shown above, by assuming a star-connected induction machine, where saturation of the teeth is present, the third-harmonic stator voltage  $u_{s3}$  will be a component of the stator zero-sequence voltage  $u_{s0}$  (which is obtained by the addition of the individual stator phase voltages,  $u_{s0} = u_{sA} + u_{sB} + u_{sC}$ ), and  $u_{s0} = u_{s3} + u_{sh}$ , where  $u_{sh}$  is the high-frequency slot harmonic voltage component. The voltage component,  $u_{s3}$ , can be obtained from  $u_{s0}$ , by filtering out the high frequency slot harmonic voltage component (by using a bandpass filter). The monitored third-harmonic stator voltage,  $u_{s3}$ , and a stator line current ( $i_{sA}$ ) are used for the determination of the phase angle ( $\gamma$ ) of the fundamental component of the magnetizing flux.

As shown in Fig. 4.63,  $\gamma$  is equal to the displacement angle between the maximum of the stator current  $i_{sA}$  and maximum of the fundamental magnetizing

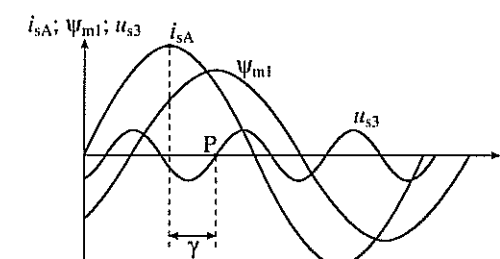


Fig. 4.63. Time variation of stator current  $i_{sA}$ , third-harmonic stator voltage  $u_{s3}$ , and fundamental magnetizing flux  $\psi_{m1}$ .

flux  $\psi_{m1}$ . This would imply that first  $\psi_{m1}$  has to be determined. However, the fundamental magnetizing flux does not have to be monitored, since for the determination of  $\gamma$ , only the location of the maximum point of  $\psi_{m1}$  is required, and this can be obtained from the suitable zero-crossing point of the third-harmonic voltage  $u_{s3}$  (since the zero-crossing of the voltage  $u_{s3}$  corresponds to a maximum value of the flux  $\psi_{m1}$ ). The zero-crossing point is P in Fig. 4.63.

The displacement angle,  $\gamma$ , is very small for no-load condition, since a small mechanical output power is developed only to overcome windage and friction losses. However, when the induction machine is loaded, this angle will increase in response to the torque required by the load. It should be noted that this angle is positive for motoring and negative for generating.

The determination of the modulus of  $\psi_{m1}$  will next be discussed. However, it should be noted that for this purpose it does not have to be monitored; it can be obtained from the modulus of the third-harmonic magnetizing flux,  $\psi_{m3}$ , which is obtained from the monitored voltage  $u_{s3}$ .

The integration of the third-harmonic stator voltage  $u_{s3}$  gives the third-harmonic magnetizing flux linkage  $\psi_{m3}$ ,

$$\psi_{m3} = \int u_{s3}(t) dt, \quad (4.5-64)$$

and from this the amplitude of the third-harmonic magnetizing flux,  $|\psi_{m3}|$ , can be directly obtained. However, the integration of the offsets and noise present in the third-harmonic voltage can lead to inaccurate third-harmonic magnetizing-flux-linkage estimates. It should be noted that at low speeds a highly distorted third-harmonic voltage signal is obtained since the signal/noise ratio for the third-harmonic voltage increases considerably, which makes difficult a correct flux estimation. However, if proper filtering and averaging is used, useful information can be obtained. This information can be derived from the zero-crossings of  $u_{s3}$  to estimate the position ( $\theta_{s3}$ ) of the third-harmonic voltage (the estimated value

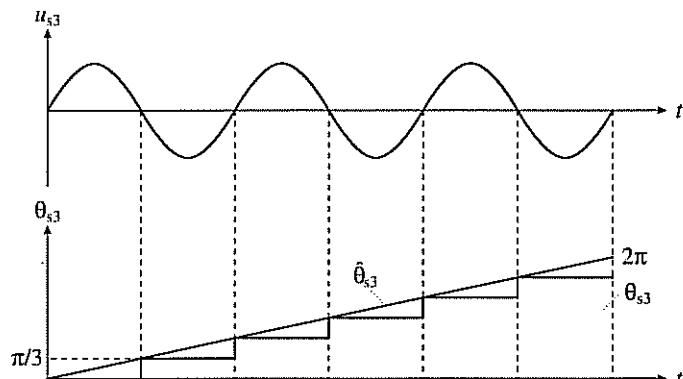


Fig. 4.64. Absolute position detection using  $u_{s3}$  and the phase voltages.

is  $\hat{\theta}_{s3}$ ), and the position of the magnetizing flux linkage with an accuracy of 60 electrical degrees. As shown in Fig. 4.64 at every zero crossing of  $u_{s3}$ , a 60 electrical degree increment in the third-harmonic voltage position (and with the corresponding shift of the third-harmonic magnetizing flux) is obtained. It follows that an exact magnetizing flux-linkage position is available in a convenient manner.

However, for absolute position sensing further measurements must be made and  $\theta_{s3}$  must also be estimated during positions between the zero crossings of  $u_{s3}$ . This problem (absolute position sensing) can be solved by using the relative positions of the stator phase voltages to detect the absolute positions of  $u_{s3}$ . If the voltage drops across the stator impedances are neglected, then at each zero crossing of  $u_{s3}$ , one of the phase voltages is zero (others have opposite signs), and this can be used to determine which of the six zero crossings has taken place, in order to obtain the absolute position. However, in a realistic approach the voltage drops must be compensated for each stator phase. It is possible to obtain an estimate for the stator impedance using the measured value of the phase voltage (at a zero crossing of  $u_{s3}$ ) and also of the corresponding stator current. Thus the absolute position of the fundamental magnetizing flux can be determined at each zero crossing of  $u_{s3}$ . Problems arise at extremely low speeds, where high values of harmonics in the stator voltages may lead to incorrect flux estimation. The problem of absolute position sensing could also be solved by using a relative incremental scheme. In this case the induction machine is initially positioned in a known position and any further zero-crossings of  $u_{s3}$  are used to increment or decrement the absolute position information depending on the sign of the speed. This method is easier to implement than the first one, since it does not require the measurement of the phase voltages and currents or the stator impedance voltage-drop corrections. However, in this case, any false zero-crossings of  $u_{s3}$  will lead to an unacceptable position error.

As mentioned above, the second problem to be solved is the accurate estimation of the position between the zero-crossings of  $u_{s3}$ , since only at the zero-crossings of  $u_{s3}$  is the exact position available (only six steps have been used above with 60 degree accuracy). Between the six instants, a special estimation technique is required. A solution is obtained by using the position information of the stator-voltage space vector expressed in the stator reference frame (which requires the monitoring of the stator voltages) between the zero crossings of  $u_{s3}$ . However, mainly at low speeds, several factors influence the monitored voltages. These are: measurement noise, impedance voltage drop, harmonics, etc. Therefore it is better to use the variation of the position of the stator-voltage space vector for the determination of the position between the zero-crossings. In an alternative scheme, the position between the zero-crossings can be determined by utilizing the average speed of the magnetizing flux,  $\omega_{av}$ , then the position is incremented by  $\pi/3$  radians between two switchings which occur at consecutive zero-crossing instants  $t_1$  and  $t_2$ , thus  $\omega_{av} = (\pi/3)(t_2 - t_1)$ . Such an estimator will work well in the steady state, but in the transient state correction terms are required to take account of the motor and load models.

A similar signal/noise problem to that discussed above occurs when the motor operates at a flux level which is lower than the rated level, since the amplitude of

$u_{s3}$  reduces due to the lower saturation level. Thus an accurate estimation of the flux under these conditions requires special considerations.

The amplitude of the third-harmonic stator voltage is a function of the saturation level in the induction machine, which is dictated by the amplitude of the fundamental magnetizing flux. Thus there exists a function  $f$  between the third-harmonic stator voltage (amplitude) and the fundamental magnetizing voltage (amplitude). This function is the so-called saturation function. It can be obtained from a conventional no-load test (where the rms value of the fundamental stator voltage,  $u_{s1}$ , is measured together with the rms value of the third harmonic voltage,  $u_{s3}$ ), yielding the required relationship for the amplitudes:  $|u_{s1}| = f(|u_{s3}|)$ . Since  $|u_{s3}| = |u_{m3}|$  for a star-connected machine, where  $u_{m3}$  is the third-harmonic magnetizing voltage, thus  $|\psi_{m1}| = f(|\psi_{m3}|)$  also holds. Therefore the amplitude of the fundamental magnetizing flux-linkage space vector can be obtained as  $|\psi_{m1}| = f(|\psi_{m3}|)$ . It follows that for the microprocessor or DSP implementation of the saturation function, a look-up table stored in the memory of the microprocessor or DSP can be used, which gives the relationship between the fundamental magnetizing flux and the third-harmonic flux (relationship of rms value of fundamental stator line voltage and rms value of third-harmonic stator voltage under no-load condition). In general, the thus obtained magnetizing-flux modulus is large, it is practically free of noise, and problems arise only at low frequency.

#### 4.5.3.2.5 Estimation of the magnetizing-, stator-, and rotor flux-linkage space vectors; utilization in torque control schemes; estimation of the electromagnetic torque

By using the technique described above, the modulus of the magnetizing-flux space vector  $|\bar{\psi}_m| = |\psi_{m1}|$  (the subscript 1 is usually omitted in the literature) is obtained together with the angle  $\gamma$ , which is the angle between the magnetizing flux-linkage space vector and the stator-current space vector. These quantities, together with the angle of the stator-current space vector,  $\alpha_s$ , can be used to obtain the magnetizing flux-linkage space vector and also the stator and rotor flux-linkage space vectors, which are required in various vector control implementations. For clarity Fig. 4.65 shows the magnetizing-flux space vector, stator-current space vector, and the relationship of various angles.

In Fig. 4.65  $\mu_m$  is the angle of the magnetizing flux-linkage space vector with respect to the real axis of the stationary reference frame. By using the angle  $\alpha_s$  (stator-current vector angle with respect to the real-axis stationary reference frame), which can be obtained as

$$\alpha_s = \tan^{-1}(i_{sQ}/i_{sD}), \quad (4.5-65)$$

the angle  $\mu_m$  can be obtained by using

$$\mu_m = \alpha_s - \gamma. \quad (4.5-66)$$

Thus the magnetizing flux-linkage space vector in the stationary reference frame is

$$\bar{\psi}_m = \psi_{mD} + j\psi_{mQ} = |\bar{\psi}_m| \exp(j\mu_m) = |\bar{\psi}_m| \exp[j(\alpha_s - \gamma)], \quad (4.5-67)$$

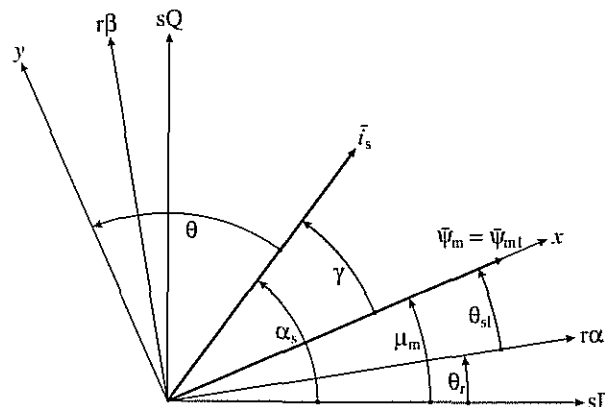


Fig. 4.65. Magnetizing flux-linkage and stator-current space vectors and the various angles.

or alternatively its components in the stationary reference frame are

$$\psi_{mD} = |\bar{\psi}_m| \cos(\alpha_s - \gamma) \quad (4.5-68)$$

$$\psi_{mQ} = |\bar{\psi}_m| \sin(\alpha_s - \gamma). \quad (4.5-69)$$

Of course in the magnetizing-flux-oriented reference frame (whose real axis is  $x$ , as shown in Fig. 4.65),  $\bar{\psi}'_m = \bar{\psi}_m \exp(-j\mu_m) = \psi_{mx} + j\psi_{my}$ , thus

$$\psi_{mx} = |\bar{\psi}_m| \quad (4.5-70)$$

$$\psi_{my} = 0. \quad (4.5-71)$$

The magnetizing flux-linkage space vector can then be used to obtain the stator or rotor flux space vectors. Thus the space vector of the stator flux linkages in the stationary reference frame can be obtained by considering

$$\bar{\psi}_s = L_s \bar{i}_s + L_m \bar{i}'_r = L_{s1} \bar{i}_s + L_m (\bar{i}_s + \bar{i}'_r) = L_{s1} \bar{i}_s + L_m \bar{i}_m,$$

but since  $\bar{\psi}_m = L_m \bar{i}_m$ , thus

$$\bar{\psi}_s = L_{s1} \bar{i}_s + \bar{\psi}_m = L_{s1} \bar{i}_s + |\bar{\psi}_m| \exp[j(\alpha_s - \gamma)] = \psi_{sD} + j\psi_{sQ}, \quad (4.5-72)$$

where  $L_{s1}$  is the stator leakage inductance. The rotor flux-linkage space vector can be obtained as follows in terms of the magnetizing-flux space vector by considering that

$$\begin{aligned} \bar{\psi}'_r &= L_r \bar{i}'_r + L_m \bar{i}_s = L_r \bar{i}'_r + (L_r - L_{rl})(\bar{i}_s + \bar{i}'_r) = -L_{rl} \bar{i}_s + L_r \bar{i}_m \\ \bar{\psi}_m &= L_m \bar{i}_m, \end{aligned}$$

thus

$$\bar{\psi}'_r = -L_{rl} \bar{i}_s + \frac{L_r}{L_m} \bar{\psi}_m = -L_{rl} \bar{i}_s + \frac{L_r}{L_m} |\bar{\psi}_m| \exp[j(\alpha_s - \gamma)] = \psi_{rd} + j\psi_{rq}, \quad (4.5-73)$$

or in terms of the stator flux-linkage space vector, similarly to that shown in eqns (4.5-16) and (4.5-17), as

$$\bar{\psi}'_r = \frac{L_r}{L_m} (\bar{\psi}_s - L'_s \bar{i}_s) = \psi_{rd} + j\psi_{rq}, \quad (4.5-74)$$

where  $L_r$  and  $L'_s$  are the rotor leakage and rotor self-inductance respectively and  $L_m$  and  $L'_s$  are the magnetizing inductance and stator transient inductance respectively. In general these inductances are saturation dependent, and for correct flux-linkage estimation this has to be considered. It follows from eqn (4.5-73) that if it is used in a rotor-flux-oriented control scheme, then even if the magnetizing flux linkage can be obtained with high accuracy, the estimated rotor flux linkage will be sensitive to the rotor leakage inductance.

The flux space vectors obtained above can be used in various torque-controlled drives. In sensorless schemes, it is possible to obtain from these the rotor speed (or rotor position), similarly to that described in Section 4.5.3.1, where the rotor speed is obtained by utilizing the speed of the flux vector under consideration.

For better understanding, Fig. 4.66 shows the schematic of the flux estimators using the spatial saturation third-harmonic stator voltage. In Fig. 4.66(a), first the zero-sequence voltage  $u_{s0}$  is obtained by the technique shown in Figs 4.60 or 4.61, e.g. by a circuit which sums the three line-to-neutral stator voltages of the induction machine. This is followed by an isolation circuit on the output of which the isolated zero-sequence voltage is present. This could be an isolation amplifier. By using a filter (low-pass filter), which removes the high-frequency slot harmonics, the third-harmonic stator voltage,  $u_{s3}$ , is obtained. The third harmonic magnetizing-flux modulus,  $|\bar{\psi}_{m3}|$ , is then obtained by integration and taking the absolute value of the integrated signal. For this purpose a low-pass digital filter with a low cut-off frequency (e.g. 0.1 Hz) can be used to minimize the integration error at low frequencies. This signal is then applied to a function generator, where the function  $f$  is the saturation function described above and which can be obtained by using the no-load magnetizing curve. In a digital implementation this is a look-up table. On the output of this, the modulus of the fundamental magnetizing flux-linkage space vector amplitude,  $|\bar{\psi}_m|$ , is obtained. The angle of the magnetizing flux-linkage space vector,  $\mu_m$ , is obtained as follows. The monitored direct- and quadrature-axis stator currents ( $i_{sD}, i_{sQ}$ ) are inputs to a rectangular-to-polar ( $R \rightarrow P$ ) converter, on the outputs of which the angle  $\alpha_s$  and the modulus  $|\bar{i}_s|$  of the stator-current space vector is present. This angle is then added to the angle  $\gamma$ , which is the angle between the magnetizing-flux space vector and the stator-current space vector (as shown in Fig. 4.65). The angle  $\gamma$  is obtained on the output of the  $\gamma$ -estimator block, which obtains  $\gamma$  by using  $u_{s3}$  and  $i_{sA}$  as described above. To be more specific, this angle is obtained by considering that it is the angle between the maximum value of the line current in stator phase sA and the zero-crossing of  $u_{s3}$  (since the zero-crossing occurs at the maximum value of the fundamental magnetizing flux). As discussed above, the angle  $\gamma$  for no-load conditions is very small, since the mechanical output power is developed only to overcome the windage and friction losses. However, when the machine is

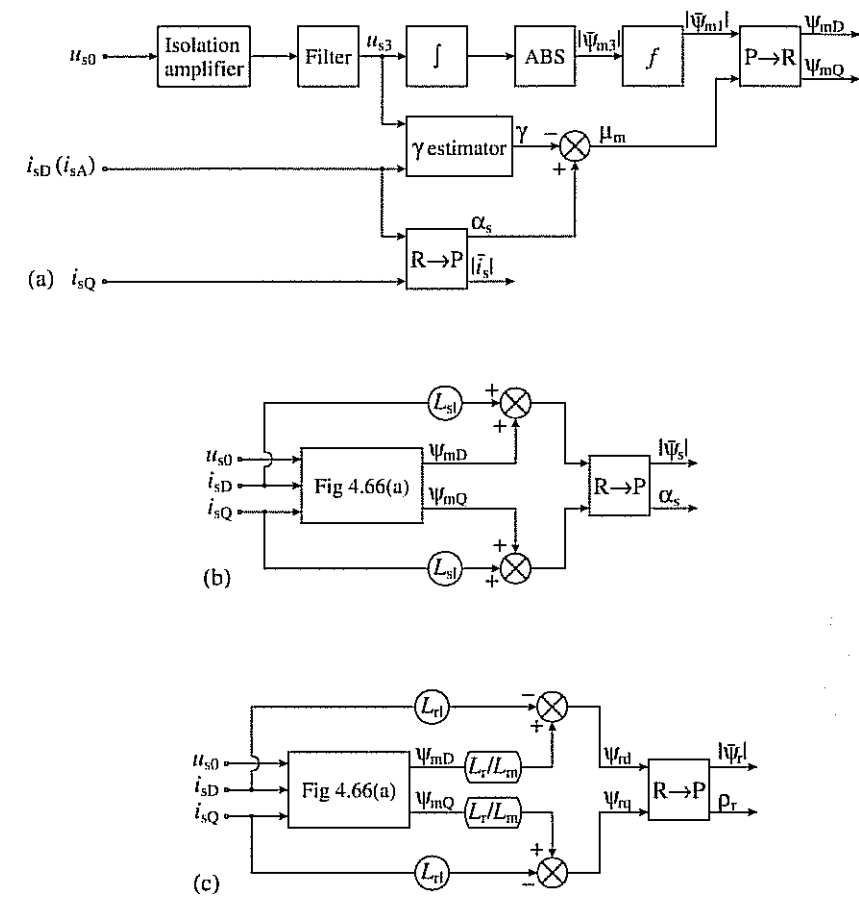


Fig. 4.66. Schematic of flux-linkage estimators using the saturation third-harmonic stator voltage. (a) Estimation of magnetizing flux linkages; (b) estimation of stator flux linkages; (c) estimation of rotor flux linkages.

loaded, this angle increases to respond to the torque required by the load. Finally, in the last part of the circuit shown in Fig. 4.66(a), a polar-to-rectangular ( $P \rightarrow R$ ) converter is used, on the output of which the direct-and quadrature-axis components of the magnetizing-flux space vector are obtained in the stationary reference frame,  $\psi_{md}$ ,  $\psi_{mq}$ .

For completeness, in Fig. 4.66(b) the schematic of a circuit is shown, which is based on eqn (4.5-72) and can be used to obtain the direct- and quadrature-axis components of the stator flux-linkage components in the stationary reference frame,  $\psi_{sd}$ ,  $\psi_{sq}$ . A rectangular-to-polar converter is then used to obtain the modulus and phase angle of the stator flux-linkage space vector. On the output of the circle with

$L_{sl}$  inside, the appropriate leakage flux component is present and when this is added to the corresponding magnetizing-flux component, the corresponding total stator flux-linkage component is obtained. It should be noted that in this circuit the only extra machine parameter to be used is the stator leakage inductance.

Similarly, in Fig. 4.66(c) a circuit is shown which is based on eqn (4.5-73), on the outputs of which the modulus and phase angle of the rotor-flux space vector in the stationary reference frame are obtained. It should be noted that  $L_r/L_m = 1 + L_{rl}/L_m$ , so this circuit only requires two machine parameters, the rotor leakage inductance and the magnetizing inductance ( $L_{rl}, L_m$ ). For normal operating conditions the constancy of the rotor leakage inductance is a very good approximation. If the effects of leakage flux saturation cannot be neglected, the entire scheme may become problematic, since due to leakage flux saturation, the zero-sequence stator voltage  $u_{so}$  will contain an extra voltage component (in addition to the high-frequency component described above). If the magnetizing inductance changes (with the flux or load), a correction can be applied to  $L_m$  via a non-linear function, which relates the estimated value of the magnetizing inductance to the magnitude of the third-harmonic magnetizing flux component,  $|\psi_{m3}|$ . This function can be obtained from the saturation function described above and can be realized by a look-up table in a digital implementation.

Finally it should be noted that the instantaneous value of the electromagnetic torque can also be determined by using the fundamental component of the magnetizing flux-linkage space vector (which has been determined from the third-harmonic stator voltage component and also the phase angle of the fundamental magnetizing flux, with respect to the stator current in phase sA). For this purpose it is utilized that the electromagnetic torque is produced by the interaction of the stator flux-linkage space vector and stator-current space vector, and the stator flux-linkage space vector can be expressed in terms of the magnetizing flux-linkage space vector as  $\bar{\psi}_s = L_{sl}\bar{i}_s + \bar{\psi}_m$ , where  $L_{sl}$  is the stator leakage inductance. Thus

$$t_e = \frac{3}{2} P \bar{\psi}_s \times \bar{i}_s = \frac{3}{2} P \bar{\psi}_{m1} \times \bar{i}_s = \frac{3}{2} P \bar{\psi}_m |\bar{i}_s| \sin \gamma = \frac{3}{2} P |i_s| f(|\psi_{m3}|) \sin \gamma, \quad (4.5-75)$$

where  $P$  is the number of pole-pairs,  $f$  is the saturation function described above, and  $\gamma$  is the angle of the magnetizing flux with respect to the stator current  $i_{sA}$ . All the other expressions derived earlier for the electromagnetic torque can also be used, e.g. if they contain the magnetizing flux-linkage components, then these can be substituted by their values shown in eqns (4.5-68) and (4.5-69). However, if they contain the stator or rotor flux-linkage components, then these components can be substituted by their values shown in eqns (4.5-72), (4.5-73), and (4.5-74).

It should be noted that there are many vector-controlled induction motor implementations in the literature (e.g. Kreindler *et al.* 1994) which utilize the saturation third-harmonic stator voltage for the estimation of the modulus of the fundamental magnetizing flux linkages and which contain a speed or position sensor. The main advantage compared to other schemes is that this type of solution is less dependent on machine parameters. The sensorless torque-controlled drive implementations of an induction machine using the saturation third-harmonic

voltage will not be discussed in further detail, since they can be readily derived by using the information provided on sensorless drives presented in the present and other sections.

#### 4.5.3.3 Estimators using saliency (geometrical, saturation) effects

##### 4.5.3.3.1 General introduction and various schemes

In high-performance induction motor drives it is possible to estimate the rotor speed, rotor position, and various flux linkages of a squirrel-cage induction motor by utilizing different types of geometrical effects (normal slotting, inherent air-gap asymmetry, intentional rotor magnetic saliency created by spatial modulation of rotor-slot leakage inductance) and saliency effects created by saturation. Thus the rotor speed can also be estimated by utilizing slot harmonics or eccentricity harmonics. Furthermore it is also possible to estimate flux-linkage space vector position (and using this information, the rotor position) by using flux-linkage detection based upon saturation-induced inductance variations (see also Sections 3.1.3.6 and 3.2.2.2.3), where test voltages are applied to the stator terminals of the machine and the flux-linkage space-vector position is detected from measured current responses. However, in the presence of injected high frequency stator voltages, for the estimation of flux-linkage space-vector position and the rotor position, it is also possible to use saliency effects, which are due to magnetic saturation (main flux or leakage flux saturation) or saliency effects intentionally created by using special rotor construction, where spatial modulation of the rotor leakage inductance is created (e.g. by periodically varying the rotor slot-opening widths or by varying the depths of the rotor slot openings, etc.).

In the following sections the various techniques listed above will be discussed in some detail. The first technique to be discussed uses slot-harmonic effects and for this purpose two alternatives will be examined: the first one uses monitored stator voltages and the second uses monitored stator currents.

##### 4.5.3.3.2 Estimators using rotor slot harmonics

The slip frequency and rotor speed of a three-phase induction machine can also be estimated by utilizing the rotor slot harmonics. However, in a speed-sensorless high-performance drive, up to now, due to the measurement bandwidth limitation, such an estimator has not been directly used for rotor speed estimation, but it has only been used indirectly to help the tuning of MRAS speed estimators (see also Section 4.5.3.4). It is a great advantage of this technique that variations in the motor parameters do not influence the accuracy of the estimation and the technique can also be used for all loads. The rotor slot harmonics can be detected by using various techniques:

- Utilizing monitored stator voltages;
- utilizing monitored stator currents.

The details of these two techniques are presented below, but in a speed-sensorless high-dynamic performance drive, the second technique is preferred since the monitoring of the stator currents is always required, but the voltage monitoring can be avoided.

*Slip frequency and speed estimation using monitored stator voltages* If a symmetrical three-phase induction motor is supplied by a system of symmetrical three-phase voltages, the air-gap flux will contain space harmonics. Neglecting the effects of magnetic saturation, some of these space harmonics are due to the non-sinusoidal distribution of the stator windings; these are usually referred to as m.m.f. space harmonics. However, due to slotting, there are also slot harmonics produced by the variation of the reluctance due to stator and rotor slots; these are the so-called stator and rotor slot harmonics respectively. The rotor slot harmonics can be utilized for the detection of the angular slip frequency and the angular rotor speed of an induction machine. When the air-gap m.m.f. contains slot harmonics, slot-harmonic voltages are induced in the stator windings when the rotor rotates. Both the amplitude and frequency of these depend on the rotor speed. However, it is difficult to extract information on the rotor speed from the magnitude, because it depends not only on the rotor speed but also on the magnitude of the flux level and the loading conditions. The rotor speed and the slip frequency are obtained from the frequency of these slot-harmonic voltages. It should be noted that if the induction machine does not have skewed rotor slots, stronger slot harmonics will be produced, but usually skewed rotor slots are employed, in order to reduce the audible noise and to eliminate asynchronous crawling (created by these harmonics) during line starts.

In a stator phase of an induction machine the magnitude of the induced slot-harmonic voltages is small and thus to separate these from the dominating fundamental voltage, the stator phase voltages are added. In general, if the monitored stator voltages of the induction machine are added, the resulting voltage ( $u_s = u_{sA} + u_{sB} + u_{sC}$ ) will contain a slot-harmonic component  $u_{sh}$ , due to the fundamental m.m.f. wave, but due to main flux saturation it will also contain a third-harmonic component  $u_{s3}$ . Furthermore, when an inverter supplies the induction machine, the stator voltage ( $u_s$ ), will also contain extra time harmonic voltages,  $u_{shk}$ , where  $k$  is the time-harmonic order. Thus in general

$$u_s = u_{sh} + u_{s3} + u_{shk}. \quad (4.5-76)$$

The frequency of the slot harmonic voltage components ( $u_{sh}$ ,  $u_{shk}$ ) is given below and it will be shown how it is related to the stator frequency and rotor speed (and the number of rotor slots, which is assumed to be known). It can be proved (e.g. see [Vas 1993]) that if the stator voltages of the induction machine ( $u_{sA}$ ,  $u_{sB}$ ,  $u_{sC}$ ) are added, and if the m.m.f. distribution is assumed to be sinusoidal, then the resulting stator voltage  $u_s = u_{sA} + u_{sB} + u_{sC}$  will contain the rotor slot harmonic voltages ( $u_{sh}$ ) and the frequency of their dominant component (fundamental slot-harmonic frequency) is

$$f_{sh} = N_r f_r \pm f_1 = 3Nf_1 - N_r f_{sl} \quad N_r = 3N \mp 1. \quad (4.5-77)$$

In eqn (4.5-77)  $f_r$  is the rotational frequency of the rotor,  $f_r = \omega_r / 2\pi$ , where  $\omega_r$  is the angular rotor speed. Furthermore,  $f_1$  is the stator frequency ( $f_1 = \omega_1 / 2\pi$ , where  $\omega_1$  is the angular stator frequency) and  $f_{sl}$  is the slip frequency,  $f_{sl} = f_1 - f_r = (\omega_1 - \omega_r) / 2\pi = \omega_{sl} / 2\pi$ , where  $\omega_{sl}$  is the angular slip frequency. Finally  $N_r$  is the number of rotor slots per pole-pair ( $N_r = Z_r / P$ ), where  $Z_r$  is the number of rotor slots and  $P$  is the number of pole-pairs. It follows that the rotor slot-harmonic frequency only depends on  $f_1$ ,  $f_r$ , and  $N_r$ . By considering that  $\omega_r = \omega_1(1-s)$ , where  $s$  is the slip, it is also possible to express  $f_{sh}$  as

$$f_{sh} = \left[ \frac{Z_r(1-s)}{P} \pm 1 \right] f_1. \quad (4.5-78)$$

When the induction machine is supplied by a three-phase inverter, in general, the output currents and voltages of the inverter contain time harmonics ( $u_{shk}$ ,  $i_{shk}$ ). Since in the output voltage of the three-phase inverter, there are no harmonic voltages with harmonic orders  $3k$ , where  $k=1, 2, \dots$  the voltage ( $u_s$ ) which is obtained by adding the three stator phase voltages ( $u_{sA}$ ,  $u_{sB}$ ,  $u_{sC}$ ) does not contain time harmonics if the induction motor is symmetrical. However, slot-harmonic voltages are present in the stator winding due to the time-harmonic fluxes produced by the time-harmonic currents. The slot-harmonic frequency due to the  $k$ th time harmonic can be expressed as

$$f_{shk} = \begin{cases} N_r f_r \pm kf_1 = 3Nf_1 \pm 6mf_1 - N_r f_{sl} & k=6m-1 \\ N_r f_r \mp kf_1 = 3Nf_1 \mp 6mf_1 - N_r f_{sl} & k=6m+1 \end{cases} \quad (4.5-79)$$

where  $N_r = 3N \pm 1$ ,  $m=1, 2, \dots$

If saturation of the main flux paths occurs, a third-harmonic voltage ( $u_3$ ) is produced in each stator phase voltage. These third-harmonic voltages are in phase with each other and therefore are present in the sum of the phase voltages. It should be noted that in general the magnitude of the third-harmonic voltage in a stator phase is smaller than the magnitude of the fundamental voltage in the corresponding stator phase, but the slot-harmonic voltage is also small and thus  $u_3$  cannot be ignored even if the motor operates at rated voltage. The third-harmonic voltage is approximately one fifth of the slot-harmonic component.

If an induction motor with star-connected stator windings is assumed with the neutral point accessible, then the summation of the stator voltages can be performed by using three potential transformers, whose secondary windings are connected in series (e.g. see Fig. 4.60). It is also possible to use operational amplifiers to add the three stator voltages, but in a DSP-controlled drive the addition can be simply done numerically. Thus  $u_s$  is obtained. It follows from eqn (4.5-76) that  $u_{sh}$  can be obtained by removing the voltage components  $u_{s3}$  and  $u_{shk}$ . This can be achieved by using various circuits (e.g. see [Vas 1993]) and then the frequency of the rotor slot harmonic ( $f_{sh}$ ) can be obtained from  $u_{sh}$ . By subtracting the stator frequency,  $f_{sh} - f_1 = N_r f_r$  is obtained and multiplication of this by  $2\pi/N_r$  gives the angular rotor speed  $\omega_r = 2\pi(f_{sh} - f_1)/N_r$ . The slip

frequency can be obtained by using  $f_{sl} = f_1 - f_r$ , where  $f_r = \omega_r / 2\pi$ . However, special considerations are required in the low speed range, because at low speeds the amplitude of the slot-harmonic voltages decrease.

*Slip frequency and speed estimation using monitored stator currents* The rotor speed can also be obtained by using the monitored stator line currents and performing harmonic spectral estimation. This is the preferred technique, since in a speed-sensorless high-dynamic-performance torque-controlled induction motor drive there is always the need for current monitoring, and it is useful to reduce the number of sensors required (by eliminating the voltage sensors). The stator-current slot harmonics can be similarly obtained as given above by eqn (4.5-79), thus if a stator line current of a PWM inverter-fed induction motor is monitored, then  $f_{shk} = N_r f_r \pm k f_1$  holds, where  $f_r = f_1(1-s)$ . For example, Fig. 4.67 shows the measured frequency spectrum of a loaded inverter-fed induction motor (the slip is 0.01133) which has  $Z_2 = 28$  rotor slots,  $2p = 4$ ,  $f_1 = 50$  Hz.

As expected, it follows from Fig. 4.67 that due to the inverter, in the window shown, the time harmonics  $k \times 50$  Hz are present, these are  $3 \times 50 = 150$  Hz;  $5 \times 50 = 250$  Hz;  $7 \times 50 = 350$  Hz;  $9 \times 50 = 450$  Hz. Furthermore, in agreement with

$$f_{shk} = N_r f_r (1-s) \pm k f_1 = 14 \times 50 \times (1-s) \pm k \times 50,$$

the slot-harmonic frequencies  $14 \times 50 \times 0.988 - 5 \times 50 = 442$  Hz;  $14 \times 50 \times 0.988 - 7 \times 50 = 342$  Hz, and  $14 \times 50 \times 0.988 - 9 \times 50 = 242$  Hz are also present.

For the purpose of speed estimation, in a PWM inverter-fed induction motor drive, a line current is monitored, scaled, and low-pass filtered (to eliminate high frequency PWM harmonics) and e.g. digital FFT can be used to detect the

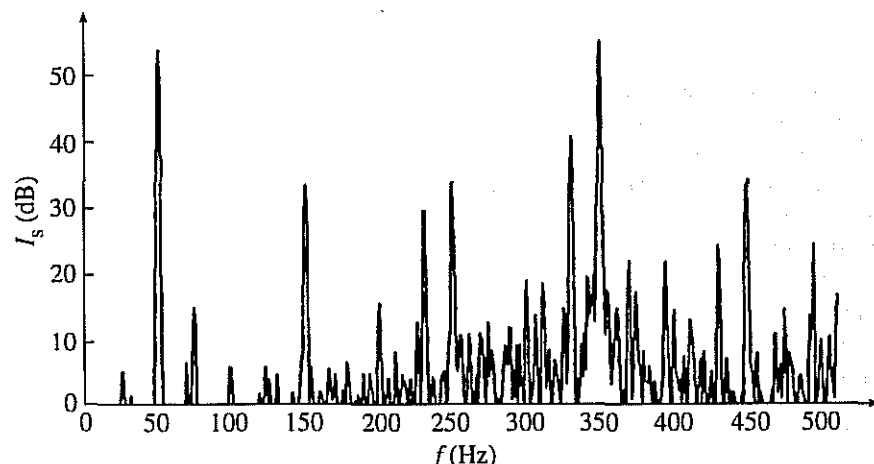


Fig. 4.67. Measured stator-current frequency spectrum of an induction motor ( $Z_2 = 28$  rotor slots,  $2p = 4$ ,  $f_1 = 50$  Hz).

speed-dependent rotor slot harmonic ( $f_{sh}$ ). When  $f_{sh}$  is known, by using eqn (4.5-77) the rotor speed can be obtained as

$$\omega_r = 2\pi f_r = 2\pi \frac{(f_{sh} \mp f_1)}{N_r}, \quad (4.5-80)$$

where  $f_1$  is the fundamental stator frequency and  $N_r$  is the number of rotor slots per pole-pair,  $N_r = Z_r / P$ , where  $Z_r$  is the number of slots and  $P$  is the number of pole-pairs. It follows from eqn (4.5-80) that the accuracy of the estimated rotor speed depends on the accuracy of the measurement of  $f_{sh}$  and  $f_1$ . In a speed-sensorless vector-controlled drive, with rotor-flux-oriented control, the derivative of the angle of the rotor flux-linkage space vector can be used to obtain  $f_1$ . The accuracy of obtaining  $f_{sh}$  by using the Fast Fourier Transform (FFT) is also discussed below. It is important to note that the rotor-speed detection scheme based on eqn (4.5-80) requires the knowledge of the number of rotor slots per pole-pair.

The five main steps of the  $f_{sh}$  estimation are as follows:

1. Identification of  $f_1$  (see also discussion above).
2. Determination of the no-load slot harmonic ( $f_{sh0}$ ) around a specific stator harmonic. For example by considering  $k = \pm 1$ , the no-load slot harmonic frequency is  $f_{sh0} = N_r f_1 \pm k f_1 = N_r f_1 + f_1$  (in general it follows from eqn (4.5-77) that  $f_{sh} = f_{sh0} - N_r s f_1$ , where  $s$  is the slip).
3. Defining the width of the slot-harmonic tracking window;  $\Delta f_{sh} = N_r f_{slmax}$ , where  $f_{slmax}$  is the maximum value of the slip frequency (e.g. rated slip frequency). For motoring operation, the window is placed at  $[f_{sh0} - \Delta f_{sh}, f_{sh0}]$ , while for motoring and generating operations it is placed at  $[f_{sh0} - \Delta f_{sh}, f_{sh0} + \Delta f_{sh}]$ .
4. Searching for the highest-amplitude harmonic (highest spectrum line) in the window which is a non-triple harmonic of  $f_1$ .
5. Increasing the accuracy of the  $f_{sh}$  estimation (e.g. by interpolation, see below).

It is possible to isolate the rotor-slot harmonic from its neighbouring harmonics at any load over a wide speed-range if an adequate frequency resolution is used. The separation of the slot harmonics from their no-load values increases with load (this follows from  $f_{sh} = f_{sh0} - N_r s f_1$ ). A digital FFT can give satisfactory results above a few Hz, but below this, noise and other factors prevent a correct estimation. For digital implementation, a real-value FFT based on the split-radix algorithm (Soresen *et al.* 1987) is ideal, since it requires a minimal number of multiplications and additions. For the purposes of the algorithm,  $2^N$  samples are used over an acquisition time  $T_a$  with sampling frequency  $f_s$ . This gives a spectrum of base resolution  $1/T_a$  over the frequency range 0 to  $f_s/2$ . In a practical application, the determination of the spectral lines is terminated at the maximum frequency of interest (which also depends on  $N_r$  and the maximum  $f_1$ ). It is important to note that the resulting spectrum also includes the PWM harmonics of the excitation frequency, which will interfere with the detection of the slot harmonics. Thus when using the FFT approach, in a PWM-fed induction motor drive, care should be taken since the slot harmonics can cross over a succession

of PWM harmonics as the rotor speed decreases. The inverter harmonics interfere with the detection of the slot harmonics and this interference at low speed contributes to a low speed limit of a few Hertz for speed estimation. It should also be considered that the FFT will provide inaccurate frequency estimates when the frequencies to be detected are not integer multiples of  $1/T_a$ . This has two immediate effects. The first one is that for an estimated frequency, a spectrum quantization error ( $\Delta f$ ) is present (with respect to the real frequency), which results in a speed error. The second effect is the spectral leakage effect (spreading of the energy distribution of each harmonic; also see below) and this effect is important when small-amplitude harmonics are close to large-amplitude harmonics. At low speeds, the slot harmonics are close to the PWM harmonics, and this effect must be considered. Machines with a large number of rotor slots have rotor-slot harmonics at higher frequencies, and the frequency at which the rotor-slot harmonics become close to large PWM harmonics is lower, and thus the rotor speed estimation can be performed at lower frequencies.

The accuracy of the speed estimation can be increased by using appropriate windowing (e.g. Hanning data window, Hamming window, rectangular window, etc.) and interpolation techniques. Windowing means that the FFT analyser sees the signal to be analysed through a window (it only sees a short length of the signal). However, in general, major discontinuities exist at the window edges. When these are transformed into the frequency domain, false results are obtained. The effect of windowing causes sidelobes to appear either side of the peaks. Some of the energy in the signal is leaking away into these sidelobes (hence the terminology: spectral leakage). This effect can be prevented by avoiding the discontinuities by arranging for the window length to be an exact multiple of the signal period. However, the problem is that most signals contain more than one fundamental frequency and also on most analysers the window length is not adjustable. This means that these discontinuities have to be accommodated some way. In practice, the effect is suppressed by using 'weighting'. Weighting is a function applied to the samples of the signal prior to processing by the FFT algorithm. For the case of rectangular weighting, all the samples have a weighting of one (from this point of view all the samples are considered to be of equal importance). However, there exist other weightings, which reduce the importance of the samples at the edges of the window, and correspondingly increase the importance, or weight, of the samples towards the middle. For example, the Hamming weighting is such a technique. The main effects of these weightings are to

- reduce the discontinuity to zero;
- modulate the signal by the 'shape' of the window;
- reduce the sidelobe height in the frequency domain;
- increase the effective bandwidth.

The increased bandwidth is an important factor for practical applications in torque-controlled speed-sensorless drives. The bandwidth considered is that of each

point in the frequency domain. In a perfect system, each point would represent a perfect band-pass filter of very small width and virtually 'brick-wall' characteristics either side. However, in practice, the filter has a finite width and finite cut-off slope, which determines the selectivity of the system. The time and frequency domains have an inverse relationship. If the window shapes are considered in the time domain, it is clear that the maximum effective window width is obtained with a rectangular window. All other windows can intuitively be seen to have a reduced effective width (e.g. consider the 3 dB points). Reduced width in the time domain is equivalent to increased width in the frequency domain, thus the effect of windows other than rectangular is to increase the bandwidth of each frequency point. Therefore this effectively reduces the ability of the FFT analyser to resolve the close components. It also reduces the so-called 'picket fence' effect.

The accuracy of the FFT can be improved by using the method of interpolation. It has been emphasized above that spectral leakage causes the spreading of the energy distribution of each harmonic. This results in a number of spectral lines for each harmonic. If the largest peak exists at the  $i$ th spectral line with amplitude  $A_i$ , then the speed estimation accuracy can be increased by using interpolation, which means that the frequency resolution is enhanced by using an appropriate frequency correction factor,  $\delta$ . For a rectangular window using interpolation,  $\delta = 1/(1+x)$ , where  $x$  is obtained from  $x = A_i/\max(A_{i+1}, A_{i-1})$ , where  $A_{i+1}$ ,  $A_{i-1}$  are known magnitudes of the surrounding desired frequency. For the Hanning window, when interpolation is used, the expression of the correction factor is simple,

$$\delta = \frac{2-x}{1+x},$$

and for the Hamming window it is more complicated,

$$\delta = \frac{(x-2)(0.16x^2 - 0.18)}{(x+1)(0.16x^2 - 0.32x - 0.92)}.$$

However, in practice, the application of the Hanning window can give accurate results in many cases. The interpolation technique is analogous to the use of a phase-locked-loop frequency multiplier acting on an encoder pulse train [Vas 1993].

As an example of the speed estimation of a  $2p=4$ , 50 Hz, 1.8 kW three-phase induction machine with 28 rotor slots Table 4.2 shows the speeds which have been estimated with interpolation (I) and without interpolation (NI) and using

Table 4.2 Estimation of the rotor speed

$\Delta f$ (Hz)	$\omega_r$ (rpm)(I, Rectangular)	$\omega_r$ (rpm)(I, Hanning)	$\omega_r$ (rpm)(NI, Rectangular)
0.5	1430.74	1430.83	1429.96
1	1430.15	1430.71	1428.03
2	1429.38	1430.14	1426.65

rectangular and Hamming windows, for various spectrum quantisation ( $\Delta f$ ) errors. It should be noted that the correct speed is 1431 rpm.

As expected, larger errors are present when no interpolation is used, and the errors are larger when the rectangular window is used compared to the errors for the case of using the Hanning window. This is due to the fact that the rectangular window exhibits larger spectral leakage. The Hanning window can give relatively accurate results even for large values of the spectrum quantization error. For the example discussed, with the Hamming window, the speed errors for the three quantization errors are 0.17 rpm, 0.29 rpm, and 0.86 rpm respectively. The example given only illustrates some possible improvements, but it is possible to obtain larger accuracies.

It has been shown above that the described speed-detection scheme requires the knowledge of the number of rotor slots per pole-pair. However, if information is not available from the manufacturer, then it is possible to obtain information on this parameter by conducting additional experiments see discussion following eqn (4.5-82) below).

In practice, the air-gap m.m.f. also contains space harmonics due to various types of asymmetries, e.g. eccentricity ([Vas 1993], [Hurst *et al.* 1994]). By neglecting the effects of magnetic saturation, and assuming sinusoidally distributed stator windings, the stator current contain harmonics with the frequencies

$$f = [(cZ_2 \pm n_d)(1-s)/P \pm k]f_1, \quad (4.5-81)$$

where  $f_1$  is the fundamental stator frequency,  $c$  is any integer,  $Z_2$  is the number of rotor slots, and  $n_d$  is the eccentricity order number, which for static eccentricity is zero and for dynamic eccentricity is 1. Furthermore, in eqn (4.5-81)  $s$  is the slip,  $P$  is the number of pole-pairs, and  $k$  is the order of the time harmonics ( $k=1, 3, 5, 7$ , etc.). It should be noted that if  $c=1$  and  $k=1$  and  $n_d=0$ , eqn (4.5-81) reduces to eqn (4.5-77). It follows from eqn (4.5-81) that for 'pure' dynamic eccentricity ( $c=0, n_d=1, k=1$ ), the current harmonics due to eccentricity are

$$f = [1 \pm (1-s)/P]f_1. \quad (4.5-82)$$

This expression is independent of the  $Z_2$  and only requires knowledge of the pole-pair number, which can however be obtained by simple measurement. The most commonly used pole-pair number is four. It follows from eqn (4.5-82) that if the pole-pair number is known, and in an initial test the harmonics associated with 'pure' dynamic eccentricity are first detected by FFT from the measured stator current, then it is possible to estimate the slip (and also the speed). It should be noted that although the harmonics caused by pure eccentricity enable  $Z_2$ -independent speed and slip estimation, they provide much lower slip resolution than the slot harmonics for a given sampling time. Thus the slot harmonics can be used to provide the accurate speed estimation and the eccentricity harmonics are only used to give extra information for initialization of the slot-harmonic estimator. By using the estimated slip and also eqn (4.5-81), it is then possible to use a search algorithm to obtain  $Z_2$ ,  $n_d$ , and  $k$ , from a table containing possible

values of these parameters. When these are known, these parameters can be used in a speed-sensorless induction motor drive using current-harmonic spectral estimation. The number of rotor slots influences crawling, cogging, acoustic noise, stray losses, etc. In a squirrel-cage induction motor with die-casted rotor, the number of rotor slots is generally lower than the number of stator slots. For induction machines in the 4 kW–100 kW range, the most common number of poles is four, and the stator slot numbers usually employed are 36, 48, 60, 72. The rotors of the 4-pole induction machine usually have eight slots less than the stator. This information can be used to obtain an initial estimate of the number of rotor slots.

#### 4.5.3.3.3 Estimation utilizing saturation-induced saliency

In Sections 3.1.3.6.1 and 3.2.2.2.3 a simple technique has been discussed for the rotor position estimation of PM synchronous machines and also synchronous reluctance machines. This technique [Schroedl 1988] can also be used for induction machines even at standstill. This is based on the fact that in the induction motor, due to saturation of the stator and rotor teeth, the stator inductances depend not only on the level of saturation but also on the position of the main flux. It follows from the stator voltage equation of the saturated induction machine that at standstill the rate of change of the stator currents can be expressed as  $d\bar{I}_s/dt = \bar{u}_s/L$ . In this equation  $L$  is the complex stator transient inductance of the induction machine, whose magnitude and angle depend on the magnetic operating point and the direction of the magnetizing flux-linkage space vector. By applying appropriate stator-voltage test vectors ( $\bar{u}_s$ ), the rate of change of the stator-current space vector ( $d\bar{I}_s/dt$ ) can be measured. The angle of the magnetizing flux-linkage space vector can then be obtained, since the locus of the modulus of the complex transient inductance is an ellipse and the minimum of this ellipse is in the direction of the magnetizing flux-linkage space vector.

It is also possible to estimate flux-linkage space-vector position in an induction machine by the tracking of high-frequency magnetic saliency created by magnetic saturation (main flux or leakage flux saturation) at zero or low rotor speeds [Jansen and Lorenz 1995b]. For this purpose high-frequency voltages are injected in the stator. The injected voltages can also be produced by the PWM VSI used in the drive scheme. It will be shown below that this technique is only possible in a saturated smooth-air-gap machine, because of the physically existing cross-saturation effect (this effect is due to the saliency caused by saturation).

It is well known (see e.g. [Vas 1992] and also Section 6.1 of the present book) that as a consequence of magnetic saturation, saliency is created and the stator direct- and quadrature-axis inductances become asymmetrical ( $L_{SD} \neq L_{SQ}$ ), and also coupling will exist between the two axes (cross-saturation effect,  $L_{DQ} \neq 0$ ). It has been shown [Vas 1992] that due to saturation, all the inductances are functions of the saliency position ( $\mu$ ), and

$$L_{SD} = L_1 + \Delta L \cos(2\mu) \quad L_{SQ} = L_1 - \Delta L \cos(2\mu) \quad L_{DQ} = L_{QD} = \Delta L \sin(2\mu).$$

It then follows that due to saturation, the stator transient inductances in the direct- and quadrature-axis (of the stationary reference frame) are also asymmetrical. It can be concluded that due to saturation, the stator transient inductances are spatially modulated, i.e. in the stationary reference frame the stator transient inductances also depend on the position of the saturation-induced saliency. Thus the direct- and quadrature-axis stator transient inductances ( $L'_{sd}$ ,  $L'_{sq}$ ) and also the cross-coupling transient inductances ( $L'_{DQ} = L'_{QD}$ ) are functions of the angle  $\mu$ , and similarly to that shown above,

$$L'_{sd} = L'_1 + \Delta L' \cos(2\mu) \quad L'_{sq} = L'_1 - \Delta L' \cos(2\mu) \quad L'_{DQ} = L'_{QD} = \Delta L' \sin(2\mu),$$

where  $L'_1 = (L'_{sd} + L'_{sq})/2$  and  $\Delta L' = (L'_{sd} - L'_{sq})/2$ . In these expressions  $L'_{sd}$  and  $L'_{sq}$  are the direct- and quadrature-axis transient stator inductances in the direct- and quadrature-axes of the existing saliency respectively. As expected the cross-saturation coupling and inductance asymmetry disappears when  $L'_{sd} = L'_{sq}$ .

The stator current responses will now be obtained, when high-frequency stator voltages are injected into the stator windings. These currents can then be used to obtain information on the position of the saliency. For high stator frequencies, the stator equations of the saturated induction machine in the stationary reference frame can be well approximated by the voltages across the appropriate stator transient inductances. Thus when a symmetrical three-phase high-frequency stator voltage system with amplitude  $U_{si}$  and angular frequency  $\omega_i$  ( $\omega_i$  is high) is injected into the stator, in the steady state the stator currents will be displaced from the stator voltages by  $90^\circ$  (since the stator transient inductances are dominant), and it follows from the stator voltage equations (in the stationary reference frame) that the space vector of the stator currents in the stationary reference frame can be expressed as

$$\bar{i}_{si} = I_{si0} \exp(j\omega_i t) + I_{si1} \exp[j(2\mu - \omega_i t)].$$

This current response can be measured.

It can be seen that the first term in the current response is independent of the angle  $\mu$ , thus in practice the second term can be used to estimate  $\mu$ . For completeness it should be noted that the amplitudes of the two current components are

$$I_{si0} = (U_{si}/\omega_i) L'_1 / (L'^2_1 - \Delta L'^2)$$

$$I_{si1} = (U_{si}/\omega_i) \Delta L' / (L'^2_1 - \Delta L'^2).$$

It follows that in the absence of cross-saturation (no saliency)  $\Delta L' = 0$  and it is not possible to estimate the second term in the expression of the currents (since  $I_{si1} = 0$ ). Furthermore, the first term is a direct measure of the saliency present; it characterizes the average stator transient inductance.

By resolving the stator-current space vector ( $\bar{i}_{si}$ ) into its real- and imaginary-axis components,  $i_{sd}$  and  $i_{sq}$  are obtained. The angle  $\mu$ , which is present in the stator-current components, can then be extracted in a number of ways. One possibility is to use a demodulation scheme involving heterodyning [Jansen and Lorenz 1995a], where the direct-axis stator current ( $i_{sd}$ ) is multiplied by

$\sin(2\hat{\mu} - \omega_i t)$ , and the quadrature-axis stator current ( $i_{sq}$ ) is multiplied by  $\cos(2\hat{\mu} - \omega_i t)$ , where  $\hat{\mu}$  is the estimated saliency angle (in electrical radians), and then the difference of these two signals is obtained:

$$\varepsilon = i_{sq} \sin(2\hat{\mu} - \omega_i t) - i_{sd} \cos(2\hat{\mu} - \omega_i t).$$

When the expressions for the direct- and quadrature-axis stator currents are substituted into this expression, then the newly obtained expression is  $\varepsilon = I_{si0} \sin[2(\omega_i t - \hat{\mu})] + I_{si1} \sin[2(\mu - \hat{\mu})]$ . The second term of this contains the spatial position information, and approaches zero as  $\hat{\mu} \rightarrow \mu$  (where  $\hat{\mu}$  is the estimated and  $\mu$  is the actual saliency position). The first term can be removed by a low-pass filter. The remaining second part (heterodyned and filtered signal,  $\varepsilon_f$ ) is in the form of a linear position error (as  $\hat{\mu} \rightarrow \mu$ ),

$$\varepsilon_f = I_{si1} \sin[2(\mu - \hat{\mu})] \approx 2I_{si1} (\mu - \hat{\mu}).$$

This signal can then be used to drive a controller, described by  $K_1 + K_2/p$ , where  $K_1$  and  $K_2$  are gains of the controller. It follows that the saliency position is obtained as  $\hat{\mu} = \int \dot{\hat{\mu}} dt$ , where  $\dot{\hat{\mu}} = (K_1 + K_2/p)\varepsilon_f$ . By using the saliency position, it is also possible to obtain estimates of the rotor flux linkages. For this purpose a flux model can be used; thus the measured stator-current components of the induction machine are first transformed into the reference frame rotating with the saliency [by using the transformation  $\exp(-j\hat{\mu})$ ], and the obtained transformed stator currents are then used as inputs into the flux model of the machine [e.g. eqns (4.1-25) and (4.1-26)]. The obtained flux-linkage components can then be transformed into their stationary axis components ( $\hat{\psi}_{rd}$ ,  $\hat{\psi}_{rq}$ ), by using the transformation  $\exp(j\hat{\mu})$ .

The best machine configurations for saturation-induced saliency tracking appear to be those with open or semi-closed rotor slots and are designed so that main flux saturation has a much greater impact on the stator transient inductance than localized leakage saturation. It is important to note that robust tracking of saturation-induced saliency may require operation at flux levels which are considerably higher than normal or rated. The maximum operational speed is then limited by core loss and/or stator voltage. Field-weakening greatly beyond base speed may then be not possible. The generation of the high-frequency injected stator voltages by the inverter requires the inverter to remain in a PWM or pulse-density modulation mode. It follows that to obtain a wide range operation, including field weakening, the scheme discussed above must be combined with another scheme which is suitable for high-frequency operation.

Another technique has been described recently [Blaschke *et al.* 1996], which allows sensorless vector control at zero flux frequency. With this scheme it is possible to hold a load stationary for a long time even at zero frequency. For this purpose, saturation effects are again utilized to obtain the position of the rotor flux-linkage space vector (namely that the dynamic inductance is not equal to the static magnetizing inductance, i.e. there is magnetic saliency in the induction machine due to saturation). The quantities to be measured are the stator voltages and currents. As shown in Fig. 4.68(c), a special test-current space vector ( $\Delta \bar{i}_s$ ) is

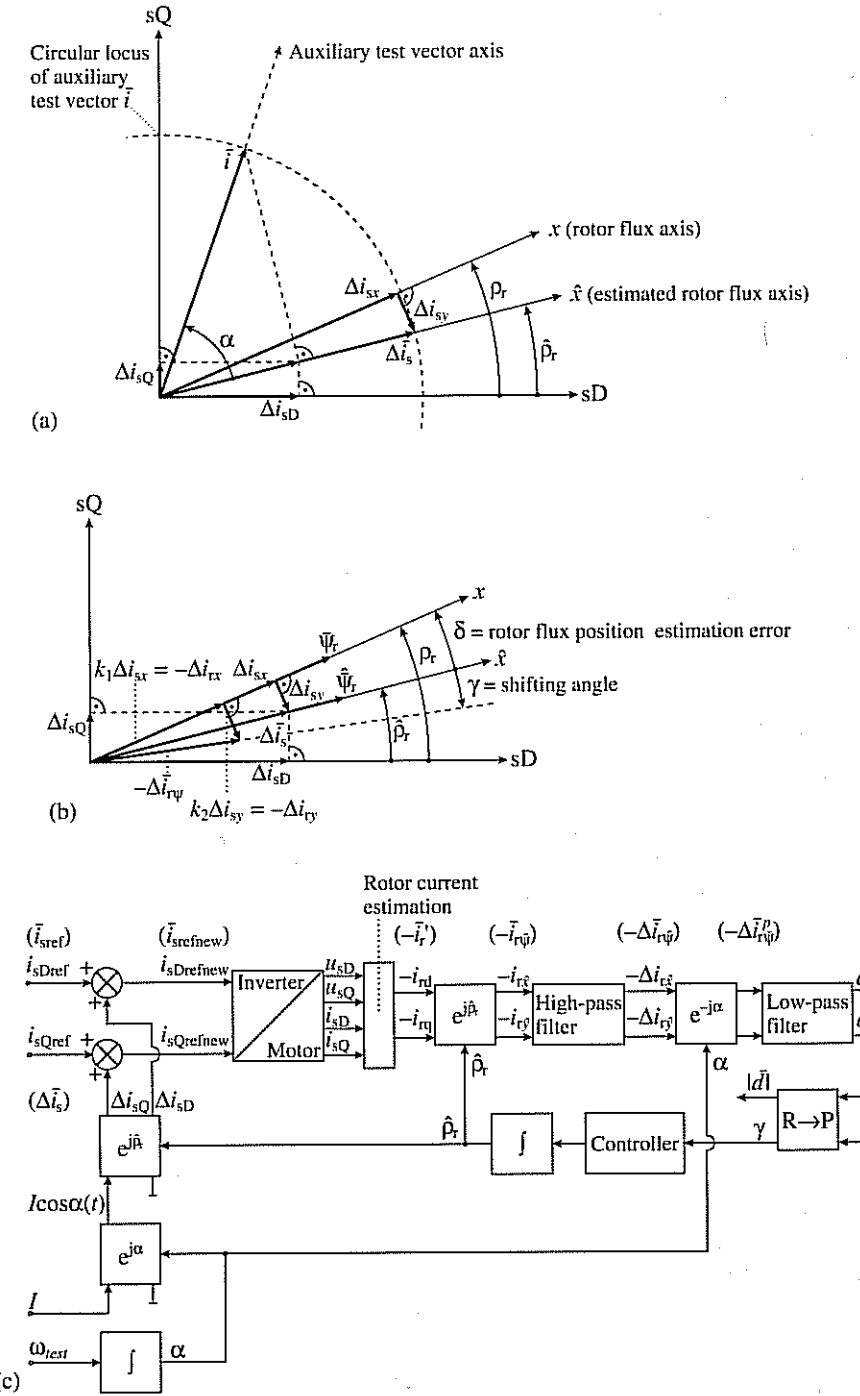


Fig. 4.68. Estimation of rotor flux angle at zero and low frequencies. (a) Vector diagram, production of test vector; (b) vector diagram, effect of saturation on rotor currents; (c) basic estimation scheme.

added to the reference stator-current space vector ( $\bar{i}_{sref}$ ), where the test-current space vector is pulsating in parallel with the direction of the estimated rotor-flux vector. It also follows that the angle between the test-current space vector and the direct-axis of the stationary reference frame is equal to the position of the estimated rotor flux-linkage space vector ( $\hat{\psi}_r$ ). Due to the special selection of the test-current space vector, it has no influence on the produced electromagnetic torque. As shown in Fig. 4.68(c), due to the test currents, modified stator reference currents are obtained; these can be described by  $\bar{i}_{srefnew} = \bar{i}_{sref} + \Delta\bar{i}_s$ , where  $\Delta\bar{i}_s = [I \cos \alpha(t)] \exp(j\hat{\psi}_r)$ , and  $\hat{\psi}_r$  is the estimated position of the rotor flux-linkage space vector (with respect to the real axis of the stationary reference frame). The transformation  $\exp(j\hat{\psi}_r)$  is required to ensure that the test-current space vector in the stationary reference frame is coaxial with the real axis of the estimated rotor flux-linkage space vector (see also Fig. 4.68(b)). In the expression above,  $I$  is the amplitude of the test current (it is also shown in Fig. 4.68(c), since it is one of the inputs) and the angle  $\alpha(t)$  is obtained by integration of a constant test frequency,  $\omega_{test}$ , since  $\omega_{test} = d\alpha/dt$  holds (see also Fig. 4.68(c)). The stator-current test signal,  $I \cos \alpha(t)$ , can be considered as a projection of an auxiliary test-current vector  $\bar{i}$  (which rotates at the speed of  $\omega_{test}$ ) on the real axis of the estimated rotor flux-linkage space vector, and this projection moves along a straight curve when the auxiliary vector rotates. This is shown in Fig. 4.68(a). In this way, the test vector  $\Delta\bar{i}_s$  is indeed pulsating in the direction ( $\hat{x}$ ) of the estimated rotor flux-linkage space vector ( $\hat{\psi}_r$ ).

It is a very important feature of the scheme that due to magnetic saturation, the rotor-current space vector produced by the test stator-current space vector ( $-\Delta\bar{i}_{r\psi}$ ) is displaced by an angle ( $\gamma$ ) with respect to the test-current space vector (see also Fig. 4.68(b)); this is now discussed. This follows from the fact that by assuming fast and small variations of the stator currents, it can be shown by using eqns (4.1-5) and (6.1-18) that

$$\Delta\bar{i}_{r\psi} = \Delta i_{rx} + j\Delta i_{ry},$$

where

$$\Delta i_{rx} = -[1/(1+L_r/L)]\Delta i_{sx} = k_1 \Delta i_{sx}$$

$$\Delta i_{ry} = -[1/(1+L_r/L)]\Delta i_{sy} = k_2 \Delta i_{sy},$$

where  $k_1$  and  $k_2$  are saturation-dependent gains,  $L_r$  is the rotor leakage inductance, and  $L$  and  $L_m$  are the dynamic and static inductances respectively ( $L$  is the tangent slope and  $L_m$  is the static (chord) slope of the magnetizing curve as discussed in Chapter 6). Under saturated conditions  $L < L_m$ , and thus  $k_2 > k_1$  and therefore the test motion of the stator-current space vector ( $\Delta\bar{i}_s$ ) is transferred into the motion of the rotor-current space vector without any delay, and the current transfer in the  $x$ -axis (axis coaxial with the rotor flux-linkage space vector) takes place with smaller gain than current transfer in the  $y$ -axis (axis in space-quadrature to the rotor flux-linkage space vector). In other words, under saturated conditions the space vector  $-\Delta\bar{i}_{r\psi}$  is displaced from the space vector  $\Delta\bar{i}_s$

by the shifting angle  $\gamma$  as shown in Fig. 4.68(b). In a saturated machine, it is this effect which causes the shifting angle  $\gamma$  to be different from zero when the estimated rotor flux position ( $\hat{\rho}_r$ ) is different from the actual rotor flux position ( $\rho_r$ ), i.e. when the error angle is  $\delta = \hat{\rho}_r - \rho_r \neq 0$ . It is the angle  $\gamma$  which is used to obtain the position of the rotor flux-linkage space vector. It is important to note that if  $\rho_r = \hat{\rho}_r$  ( $\delta = 0$ ) then  $\gamma = 0$  and when the shifting angle is not zero, in general, it has an opposite direction to the error angle. It follows from the above that, to obtain the shifting angle, the negative rotor-current components  $-\Delta i_{r\ddot{x}}$ ,  $-\Delta i_{r\ddot{y}}$  due to the test stator-current space vector have to be known in the estimated-rotor-flux-oriented reference frame. The estimation of the required rotor currents is now discussed briefly.

The current components  $-\Delta i_{r\ddot{x}}$  and  $-\Delta i_{r\ddot{y}}$ , which are also shown in Fig. 4.68(c), can be obtained in a few steps. As shown in Fig. 4.68(c), first the negative rotor-current space vector expressed in the stationary reference frame,  $-\bar{i}'_r = -(i_{rd} + j i_{rq})$ , is monitored and this is then transformed into the negative rotor-current space vector in the estimated-rotor-flux-oriented reference frame  $-\bar{i}_{r\ddot{\psi}} = -(i_{r\ddot{x}} + j i_{r\ddot{y}}) = -\bar{i}'_r \exp(-j\hat{\rho}_r)$ . This transformation is then followed by high-pass filtering, which yields the pulsating negative rotor-current space vector (in the estimated-rotor-flux-oriented reference frame) due to the test stator-current space vector  $-\Delta \bar{i}_{r\ddot{\psi}} = -(\Delta i_{r\ddot{x}} + j \Delta i_{r\ddot{y}})$ . This pulsating current vector can be described by two counter-rotating vectors, which have the same amplitude. The component which rotates at the constant speed of  $\omega_{test}$  is the positive-sequence system and the other, which rotates at the  $-\omega_{test}$  speed, corresponds to a negative-sequence system. As shown in Fig. 4.68(c), the positive-sequence current vector  $-\Delta \bar{i}_{r\ddot{\psi}}^p$  is obtained by performing the transformation  $-\Delta \bar{i}_{r\ddot{\psi}} \exp(-j\alpha)$  and then by low-pass filtering of this signal. The resulting vector is a stationary vector,  $\bar{d} = d_1 + j d_2$ , which is displaced from the axis of the auxiliary test-current vector ( $\bar{i}$ ) by angle  $\gamma$ , and thus  $\gamma$  can be obtained, e.g. by considering  $\gamma = \tan^{-1}(d_2/d_1)$ . This shifting angle is then input into a controller on the output of which the derivative of the estimated rotor flux-linkage position is obtained, this is then integrated to yield  $\hat{\rho}_r$ . The estimated  $\hat{\rho}_r$  is changed until  $\gamma = 0$  is obtained (and in this case  $\hat{\rho}_r = \rho_r$ ).

It has been discussed above that the scheme requires the monitored values of the rotor currents in the stationary reference frame. However, these can be obtained from the measured stator voltages and currents by considering the stator voltage equation in the stationary reference frame. The stator voltage equation is simplified by considering a high test frequency and also that the speed of the rotor flux-linkage space vector,  $\omega_{mr} = d\rho_r/dt$ , is low. The details of the rotor-current estimation circuit shown in Fig. 4.77(c) can be found in the literature, where the technique has been verified in a vector-controlled induction machine, fed by a current-controlled PWM inverter [Blaschke *et al.* 1996]. The test results reported prove that the scheme can work at exactly zero flux frequency, i.e. a loaded machine was running in a stable manner at exactly zero frequency for a long period.

Finally it should be noted that instead of utilizing saturation effects, it is also possible to estimate the rotor position of the induction machine by tracking of

high-frequency saliency created by spatial modulation of the rotor leakage inductance. This is briefly discussed in the next section.

#### 4.5.3.3.4 Estimation utilizing saliency introduced by special rotor construction

For the estimation of the rotor position and rotor speed even at zero and low speeds, it is also possible to use saliency effects, which are intentionally created by using special rotor construction, where spatial modulation of the rotor leakage inductance is created. This can be achieved, for example, by periodically varying the rotor-slot opening widths or by varying the depths of the rotor-slot openings, etc. [Jansen and Lorenz 1995b]. The technique resembles the one described in the previous section, but the main difference is that in the present case there exists a deliberately introduced saliency due to physical asymmetry, whilst in the previous case magnetic saliency existed due to saturation. It should, however, be noted that the introduced rotor saliency is symmetric about each pole, i.e. it is 90 mechanical degrees for a four-pole machine. In order to be able to track the saliency, similarly to that discussed in the previous section, symmetrical three-phase high-frequency voltages are injected into the stator (the amplitude and angular frequency of these are  $U_{si}$  and  $\omega_i$  respectively). First, it is shown below that when special (asymmetrical) rotor constructions are used, the stator transient inductances due to asymmetry are position dependent. It is this position dependency of the inductances which causes position-dependent current responses, when the stator is supplied by high-frequency voltages. By measuring these stator currents, it is then possible to extract the information on the rotor position.

Due to the special rotor construction, the rotor leakage inductances ( $L_{rid}$ ,  $L_{rlq}$ ) in the direct and quadrature axes of the rotor reference frame are different. However, when these are transformed into the stator reference frame, rotor-position ( $\theta_r$ )-dependent inductances,

$$L_{rid} = L_1 + \Delta L \cos(2\theta_r) \quad L_{rlq} = L_1 - \Delta L \cos(2\theta_r) \quad L_{ridQ} = L_{rlqD} = \Delta L \sin(2\theta_r)$$

are obtained, where  $L_1 = (L_{rid} + L_{rlq})/2$  and  $\Delta L = (L_{rid} - L_{rlq})/2$ . A simple proof of this can be obtained e.g. by performing the transformation of the rotor leakage-flux space vector expressed in the rotor reference frame,  $\bar{\psi}_{ri} = L_{rid} i_{rd} + j L_{rlq} i_{rq}$ , into the rotor flux-linkage space vector expressed in the stationary reference frame,  $\bar{\psi}'_{ri} = \bar{\psi}_{ri} \exp(j\theta_r)$ , and then by resolving the obtained flux linkages into their real- and imaginary-axis components. For this purpose the expressions of the rotor-current space vector in the rotor reference frame,  $\bar{i}_r = i_{rd} + j i_{rq}$ , and also in the stationary reference frame,  $\bar{i}'_r = \bar{i}_r \exp(j\theta_r)$ , are introduced. Thus

$$\begin{aligned} \bar{\psi}'_{ri} &= \bar{\psi}_{ri} \exp(j\theta_r) = (L_{rid} i_{rd} + j L_{rlq} i_{rq}) \exp(j\theta_r) \\ &= [(L_{rid} + L_{rlq})/2] i_r \exp(j\theta_r) + [(L_{rid} - L_{rlq})/2] \bar{i}'_r \exp(j\theta_r) \\ &= L_1 \bar{i}'_r + \Delta L \bar{i}'_r \exp(2j\theta_r) \end{aligned}$$

is obtained, and resolution into its components yields the inductances defined above. As expected, the cross-coupling inductances ( $L_{ridQ} = L_{rlqD}$ ) are zero,

if  $L_{rd} = L_{rq}$ . As a consequence of this rotor leakage asymmetry, four stator transient inductances can be defined: the direct-axis transient inductance,  $L'_{sd} = L_{sl} + L_{rd} = L'_1 + \Delta L' \cos(2\theta_r)$ , the quadrature-axis transient inductance  $L'_{sq} = L_{sl} + L_{rq} = L'_1 - \Delta L' \cos(2\theta_r)$ , and also the cross-coupling transient inductances  $L'_{dq} = L'_{qd} = \Delta L' \sin(2\mu)$ . In these expressions  $L'_1 = L_1$  and  $\Delta L = \Delta L'$ , where as shown above  $L_1 = (L_{rd} + L_{rq})/2$  and  $\Delta L = (L_{rd} - L_{rq})/2$ .

When high-frequency stator voltages ( $\bar{u}_{si}$ ) are injected into the stator of the induction machine, it follows from the stator voltage equation of the induction machine in the stationary reference frame that  $\bar{u}_{si} \approx d\bar{\psi}_s/dt$ , where the stator flux-linkage component is mainly a leakage flux component. This contains the appropriate stator transient inductances (sum of stator and rotor leakage inductances). It follows that the stator currents due to the injected stator voltages can be formally expressed in the same way as in the previous section. Thus the current response to the injected stator voltages is obtained as

$$\bar{i}_{si} = I_{si0} \exp(j\omega_i t) + I_{si1} \exp[j(2\theta_r - \omega_i t)],$$

where

$$I_{si0} = (U_{si}/\omega_i)(L_{sl} + L'_1)/[(L_{sl} + L'_1)^2 - \Delta L'^2],$$

$$I_{si1} = (U_{si}/\omega_i)\Delta L'/[(L_{sl} + L'_1)^2 - \Delta L'^2].$$

The second component of the stator current contains the rotor angle, and this can be used to estimate the rotor position, by using the same technique as discussed in the previous section.

It follows that the signal

$$e = (i_{sQi}) \cos(2\hat{\theta}_r - \omega_i t) - (i_{sDi}) \sin(2\hat{\theta}_r - \omega_i t)$$

is first obtained, which can be expressed as

$$e = I_{si0} \sin[2(\omega_i t - \hat{\theta}_r)] + I_{si1} \sin[2(\theta_r - \hat{\theta}_r)].$$

The second term contains the rotor position information, and approaches zero as  $\hat{\theta}_r \rightarrow \theta_r$  (where  $\hat{\theta}_r$  is the estimated and  $\theta_r$  is the actual rotor position). The first term can be removed by a low-pass filter. The remaining second part (heterodyned and filtered signal) is in the form of a linear position error (as  $\hat{\theta}_r \rightarrow \theta_r$ ), thus  $e_f = I_{si1} \sin[2(\theta_r - \hat{\theta}_r)] \approx 2I_{si1}(\theta_r - \hat{\theta}_r)$ . This can then be used to drive a controller,  $K_1 + K_2/p$ , where  $K_1$  and  $K_2$  are gains of the controller, thus the rotor position is obtained as  $\hat{\theta}_r = \int \hat{\omega}_r dt$ , where  $\hat{\omega}_r = (K_1 + K_2/p)e_f$  is the estimated rotor speed.

As discussed in the previous section, saturation causes magnetic saliences and as a consequence, an extra term will be added to  $I_{si1} \sin[2(\theta_r - \hat{\theta}_r)]$ . However, this extra term can be avoided by appropriate machine design. For example, the effects of leakage saturation can be avoided in the rotor by selecting minimal slot-opening widths.

Finally it should be noted that variation of the rotor slot-opening width may also influence adversely the magnetizing inductance and may result in torque pulsations. If the depths of the rotor slot openings are varied in order to create a spatial modulation of the rotor leakage inductance, then the magnetizing inductance is

almost unchanged, but the rotor lamination asymmetry can be undesirable for a manufacturer. The rotor leakage inductance modulation can also be achieved by a variation in rotor slot opening fill, but this can also have some adverse effects.

#### 4.5.3.4 Model reference adaptive systems (MRAS)

##### 4.5.3.4.1 General introduction

In Section 4.5.3.1 various open-loop speed and flux-linkage estimators have been discussed. These have utilized the stator and rotor voltage equations of the induction machine. However, the accuracy of these open-loop observers depends strongly on the machine parameters. In closed-loop estimators the accuracy can be increased. Five rotor speed observers using the Model Reference Adaptive System (MRAS) are described below. In a MRAS system, some state variables,  $x_d$ ,  $x_q$  (e.g. rotor flux-linkage components,  $\psi_{rd}$ ,  $\psi_{rq}$ , or back e.m.f. components,  $e_d$ ,  $e_q$ , etc.) of the induction machine (which are obtained by using measured quantities, e.g. stator voltages and currents) are estimated in a reference model and are then compared with state variables  $\hat{x}_d$ ,  $\hat{x}_q$  estimated by using an adaptive model. The difference between these state variables is then used in an adaptation mechanism, which outputs the estimated value of the rotor speed ( $\hat{\omega}_r$ ) and adjusts the adaptive model until satisfactory performance is obtained. Such a scheme is shown in Fig. 4.69(a), where the compact space-vector notation is used. However, Fig. 4.69(b) corresponds to an actual implementation, and here the components of the space vectors are shown.

The appropriate adaptation mechanism can be derived by using Popov's criterion of hyperstability. This results in a stable and quick response system, where the differences between the state-variables of the reference model and adaptive model (state errors) are manipulated into a speed tuning signal ( $\epsilon$ ), which is then an input into a PI-type of controller (shown in Fig. 4.69(c)), which outputs the estimated rotor speed. Four schemes will be discussed in the following sections; these use the speed tuning signals  $\epsilon_w = \text{Im}(\bar{\psi}'_r \bar{\psi}'^*_r)$ ,  $\epsilon_e = \text{Im}(\bar{e}\bar{e}^*)$ ,  $\epsilon_{Ac} = \text{Im}(\Delta\bar{e}\bar{i}_s^*)$  and  $\epsilon_{Ae} = \text{Im}(\Delta\bar{e}\bar{p}i_s^*)$  respectively, and are indicated in Fig. 4.69(c). In these expressions  $\bar{\psi}'_r$  and  $\bar{i}_s$  denote the rotor flux-linkage and stator-current space vectors respectively in the stationary reference frame,  $\bar{e}$  denotes the back-e.m.f. space vector also in the stationary reference frame  $\bar{e} = (L_m/L_r) d\bar{\psi}_r/dt$ , and finally the error back-e.m.f. space vector is defined as  $\Delta\bar{e} = \bar{e} - \hat{\bar{e}}$ . The symbol  $\hat{\cdot}$  denotes the quantities estimated by the adaptive model. In addition to these four schemes, artificial-intelligence-assisted MRAS speed estimators are also discussed below in Section 4.5.3.4.6 and also in Section 4.5.3.6, estimators which do not contain any mathematical adaptive model, and the adaptation mechanism is incorporated into the tuning of the appropriate artificial-intelligence-based network (which can be a neural network, a fuzzy-neural network, etc.).

To improve the performance of the observers described, various practical techniques are also discussed which avoid the use of pure integrators. One of the schemes described is robust to stator resistance and rotor resistance variations,

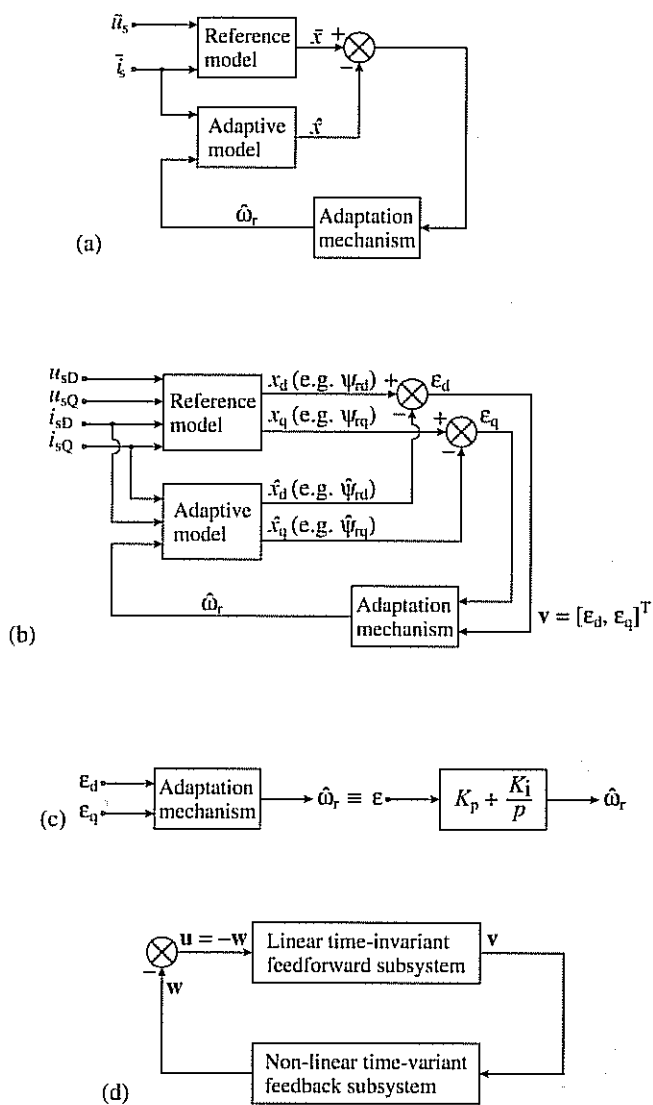


Fig. 4.69. MRAS-based speed estimator scheme. (a) Basic scheme (using space-vector notation); (b) basic scheme (using space-vector components); (c) adaptation mechanism; speed tuning signal

$$\varepsilon = \begin{cases} e_\omega = \text{Im}(\bar{\psi}'_r \hat{\psi}'_r^*) & \text{where } \bar{\psi}'_r = \psi_{rd} + j\psi_{rq} \\ e_e = \text{Im}(\bar{e} \hat{e}^*) & \text{where } \bar{e} = e_d + j e_q = \frac{L_m}{L_r} \psi_{rd} + j \frac{L_m}{L_r} \psi_{rq} \\ e_{\Delta e} = \text{Im}(\Delta \bar{e} \bar{t}_s^*) & \text{where } \Delta \bar{e} = \bar{e} - \hat{e} = (e_d - \hat{e}_d) + j(e_q - \hat{e}_q); \\ e_{\Delta \omega} = \text{Im}(\Delta \bar{e} \rho \bar{t}_s^*) & \end{cases}$$

(d) equivalent non-linear feedback system.

and can even be used at very low speeds, e.g. 0.3 Hz (but not zero speed). All the observers described below use monitored stator currents and stator voltages, but in a voltage-source inverter-fed drive, it is not necessary to monitor the stator voltages, since it is possible to reconstruct them by using the inverter switching states and also the monitored value of the d.c. link voltage (see also Section 3.1.3.2.1). An artificial-intelligence-based MRAS speed estimator seems to offer the most satisfactory performance even at very low speeds.

#### 4.5.3.4.2 Application of Popov's hyperstability theorem and integral inequality

This section is only given here for completeness and contains a short description of the selection of the appropriate adaptation mechanism, proves why there is a PI controller in the schemes described below, and also shows the form of the speed tuning signal to be used. However, this section can be skipped by those who do not require a proof of the fact that the application of Popov's theorem yields the various MRAS systems described, e.g. that shown in Fig. 4.69, which contains a PI controller and the appropriate speed tuning signal.

In general, a model reference adaptive speed estimator system can be represented by an equivalent non-linear feedback system which comprises a feed-forward time-invariant linear subsystem and a feedback non-linear time-varying subsystem. This is shown in Fig. 4.69(d).

In Fig. 4.69(d) the input to the linear time-variant system is  $u$  (which contains the stator voltages and currents), its output is  $v$ , which is the speed tuning signal (generalized error),  $v = [e_d, e_q]^T$ . The output of the non-linear time-variant system is  $w$ , and  $u = -w$ . The rotor speed estimation algorithm (adaptation mechanism) is chosen according to Popov's hyperstability theory, whereby the transfer function matrix of the linear time-invariant subsystem must be strictly positive real and the non-linear time-varying feedback subsystem satisfies Popov's integral inequality, according to which  $\int v^T w dt \geq 0$  in the time interval  $[0, t_1]$  for all  $t_1 \geq 0$ . Thus to obtain the adaptation mechanism, first the transfer function  $F(s)$  of the linear time-invariant feedforward subsystem has to be obtained. It can be shown by lengthy calculations that in all the schemes described below this is strictly positive real.

A possible proof uses the state-variable form of the error equation,  $dv/dt = Av - w$ , which is obtained by subtracting the state-variable equations of the adjustable model from the state-variable equations of the reference model. The equations of the adjustable model (rotor model) are the rotor voltage equations in the stationary reference frame, which can be obtained from eqn (4.1-27) by eliminating the rotor-current space vector. Thus

$$\hat{\psi}'_r = \int \left\{ \left[ -\frac{1}{T_r} + j\omega_r \right] \hat{\psi}'_r + \frac{L_m}{T_r} \bar{t}_s \right\} dt$$

is obtained, which is then resolved into its two-axis components. The reference model (stator model) equations are the two-axis stator voltage equations in the

stationary reference frame, which have been defined by eqns (4.5-22) and (4.5-23), and the space-vector form of this is

$$\bar{\psi}'_r = \frac{L_r}{L_m} \left[ \int (\bar{u}_s - R_s \bar{i}_s) dt - L'_s i_{sQ} \right].$$

In the resulting state-variable form of the error equations, the state matrix is  $\mathbf{A}$ , where

$$\mathbf{A} = \begin{bmatrix} -1/T_r & -\omega_r \\ \omega_r & -1/T_r \end{bmatrix}.$$

The feedforward path transfer matrix of the linear time-invariant subsystem shown in Fig. 4.69(d) is  $\mathbf{F}(s) = [sI - \mathbf{A}]^{-1}$ , where  $I$  is an identity matrix. It follows from the derivation of the error state equation that  $\mathbf{w} = [\hat{\omega}_r - \omega_r] [-\hat{x}_q x_d]^T$  (where  $\hat{x}_d$  and  $\hat{x}_q$  are the states estimated by the adaptive model), thus when  $\mathbf{w}$  is substituted into Popov's integral inequality,  $\int \mathbf{v}^T \mathbf{w} dt \geq 0$ , it can be shown that this inequality can be satisfied by letting  $\hat{\omega}_r = (K_p + K_i/p)\epsilon$ . In this equation  $1/p$  represents an integrator and  $\epsilon$  is the appropriate speed tuning signal. In general, the state variables in the reference and adaptive models are  $x_d$ ,  $x_q$  and  $\hat{x}_d$ ,  $\hat{x}_q$  respectively and when these are the rotor flux linkages  $\psi_{rd}$ ,  $\psi_{rq}$ ,  $\hat{\psi}_{rd}$ ,  $\hat{\psi}_{rq}$ , then the speed tuning signal is  $\text{Im}(\bar{\psi}_r \hat{\bar{\psi}}_r^*)$ , where the asterisk denotes the complex conjugate. This signal is used in the first scheme discussed below, thus  $\epsilon_\omega = \text{Im}(\bar{\psi}_r \hat{\bar{\psi}}_r^*)$ . In the second scheme to be discussed it has a similar form,  $\epsilon_e = \text{Im}(\bar{e} \hat{\bar{e}}^*)$ , etc. It can be seen that when a specific state variable is used (on the outputs of the reference and adaptive models), then a corresponding speed tuning signal of a specific form is obtained by using Popov's integral inequality. It has been discussed above that when the rotor speed to be estimated is changed in the adaptive model in such a way that the difference between the output of the reference model and the adaptive model is zero, then the estimated rotor speed is equal to the actual rotor speed. The error signal actuates the rotor-speed identification algorithm, which makes this error converge asymptotically to zero. The physical reason for the integrator (in the PI controller) is that this ensures that the error converges asymptotically to zero.

#### 4.5.3.4.3 Scheme 1: speed tuning signal is $\epsilon_\omega = \text{Im}(\bar{\psi}_r \hat{\bar{\psi}}_r^*)$

As shown in the previous section, it is possible to estimate the rotor speed by using two estimators (a reference-model-based estimator and an adaptive-model-based one), which independently estimate the rotor flux-linkage components in the stator reference frame ( $\psi_{rd}$ ,  $\psi_{rq}$ ), and by using the difference between these flux-linkage estimates to drive the speed of the adaptive model to that of the actual speed. The expressions for the rotor flux linkages in the stationary reference frame can be obtained by using the stator voltage equations of the induction machine (in the stationary reference frame). These give eqns (4.5-22) and (4.5-23), which are now rearranged for the rotor flux linkages:

$$\psi_{rd} = \frac{L_r}{L_m} \left[ \int (u_{sd} - R_s i_{sd}) dt - L'_s i_{sD} \right] \quad (4.5-83)$$

$$\psi_{rq} = \frac{L_r}{L_m} \left[ \int (u_{sq} - R_s i_{sq}) dt - L'_s i_{sQ} \right], \quad (4.5-84)$$

where  $L'_s$  is the stator transient inductance. These two equations represent a so-called stator *voltage* model, which does not contain the rotor speed and is therefore a reference model. However, when the rotor voltage equations of the induction machine are expressed in the stationary reference frame, they contain the rotor fluxes and the speed as well. They can be obtained from eqn (4.1-27) and, by eliminating the rotor-current space vector by using  $\bar{i}_r = (\bar{\psi}_r - L_m \bar{i}_s)/L_r$  or from eqns (4.1-30) and (4.1-31) by considering that  $\psi_{rd} = L_m i_{md}$ ,  $\psi_{rq} = L_m i_{mq}$ , thus

$$\hat{\psi}_{rd} = \frac{1}{T_r} \int (L_m i_{sD} - \hat{\psi}_{rd} - \omega_r T_r \hat{\psi}_{rq}) dt \quad (4.5-85)$$

$$\hat{\psi}_{rq} = \frac{1}{T_r} \int (L_m i_{sQ} - \hat{\psi}_{rq} + \omega_r T_r \hat{\psi}_{rd}) dt, \quad (4.5-86)$$

where  $T_r$  is the rotor time constant. These two equations correspond to a *current* model, which contains the rotor speed, and therefore represent the adjustable (adaptive) model. The reference and adaptive models are used to estimate the rotor flux linkages and the angular difference of the outputs of the two estimators  $\epsilon_\omega = \text{Im}(\bar{\psi}_r \hat{\bar{\psi}}_r^*) = \psi_{rq} \hat{\psi}_{rd} - \psi_{rd} \hat{\psi}_{rq}$  is used as the speed tuning signal. This tuning signal is the input to a linear controller (PI controller) which outputs the estimated rotor speed as shown in Fig. 4.70.

As discussed in the previous section, the reason for using a PI controller and  $\epsilon_\omega = \text{Im}(\bar{\psi}_r \hat{\bar{\psi}}_r^*) = \psi_{rq} \hat{\psi}_{rd} - \psi_{rd} \hat{\psi}_{rq}$  is that this will give a stable non-linear feedback system, and a rigorous proof uses Popov's hyperstability criterion. The PI controller tunes the rotor speed value when the error between the two rotor flux-linkage space vectors is not zero ( $\bar{\psi}_r \neq \hat{\bar{\psi}}_r$ ). In other words, when the rotor speed to be estimated ( $\hat{\omega}_r$ ) is changed in the adjustable model in such a way that the difference between the output of the reference model and the output of the

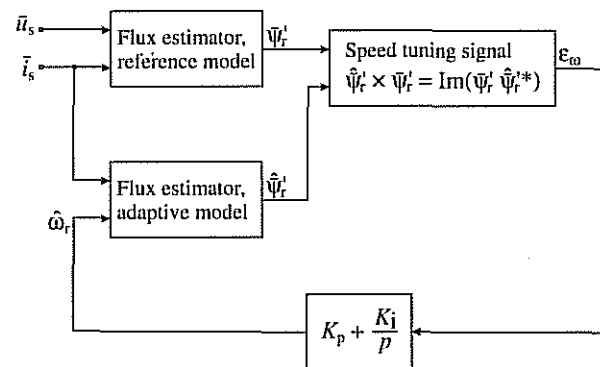


Fig. 4.70. MRAS-based rotor speed observer using rotor flux linkages for the speed tuning signal and employing pure integrators.

adjustable model becomes zero, then the estimated rotor speed is equal to the actual rotor speed ( $\omega_r$ ). The error signal actuates the rotor-speed identification algorithm, which makes this error converge to zero. The algorithm is chosen to give quick and stable response. It should be noted that it is also possible to construct similar MRAS schemes which, however, use the back-e.m.f. components instead of the rotor flux-linkage components, or they can use the components of the power vector ( $\bar{u}_s \bar{i}_s^*$ ), etc. Some aspects of these schemes will be discussed at the end of the present section and it will be shown that they have some advantages (e.g. absence of pure integrator, reduced noise sensitivity, etc.) over the scheme using the rotor flux estimates in the speed tuning signal.

It follows from Fig. 4.70 that the estimated speed can be expressed as

$$\hat{\omega}_r = K_p \varepsilon_\omega + K_i \int \varepsilon_\omega dt, \quad (4.5-87)$$

and it can be shown by using the linearized state-variable equations that arbitrary  $K_p$  and  $K_i$  cannot be used to obtain satisfactory performance. The complete

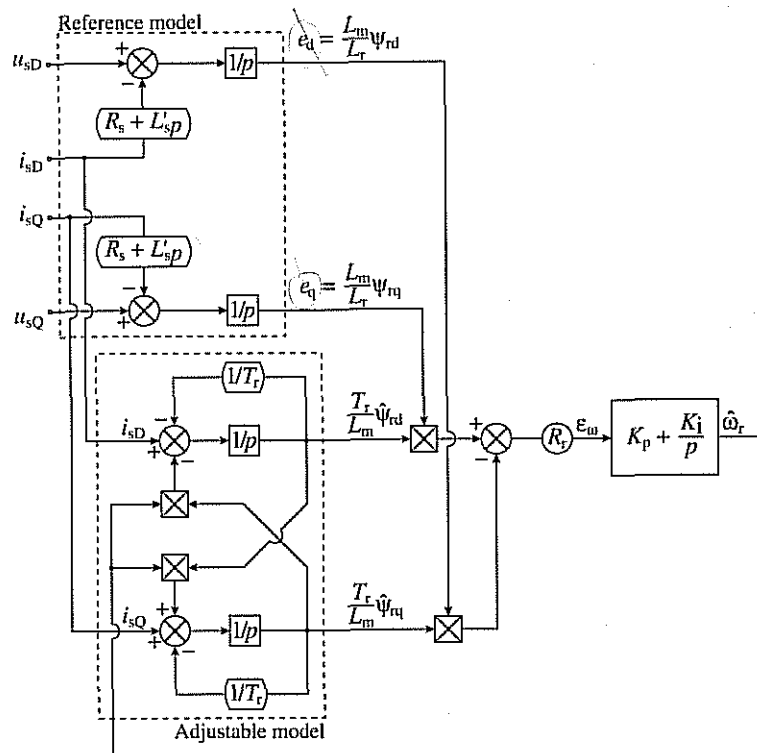


Fig. 4.71. Complete scheme of MRAS-based speed observer using rotor flux linkages for the speed tuning signal.

scheme of the MRAS-based rotor speed observer is shown in Fig. 4.71. It should be noted that in Fig. 4.71 the speed tuning signal  $\varepsilon_\omega$  is multiplied by  $1/R_r$ , and thus to obtain  $\varepsilon_\omega$ , it is multiplied by  $R_r$ . However, this separate multiplication is not required, since  $R_r$  could be incorporated in the proportional and integral gain constants of the PI controller. The stator voltages can be obtained from the monitored terminal voltages or they can be obtained in an inverter-fed drive by reconstructing the stator voltages from the inverter switching states and by using the monitored value of the d.c. link voltage (see Sections 3.1.1 and 4.1.1 for further detail).

In practice, the reference model is difficult to implement due to the pure integrators required by eqns (4.5-83) and (4.5-84), which have initial value and drift problems. However, to avoid these problems, in a practical implementation a low-pass filter, with the transfer function  $1/(p+1/T)$ , can be used instead of a pure integrator. However, since  $1/(p+1/T) = (1/p)[p/(p+1/T)]$ , thus in the practical system, the reference model (which contains  $1/p$ ) is followed by a high-pass filter [ $p/(p+1/T)$ ], as shown in Fig. 4.72.

In this case the modified rotor flux linkages of the reference model ( $\psi'_{rd}$ ,  $\psi'_{rq}$ ) can be obtained from eqns (4.5-83) and (4.5-84) and thus

$$\left( p + \frac{1}{T} \right) \psi'_{rd} = \frac{L_r}{L_m} (u_{sd} - R_s i_{sd} - L'_s p i_{sd}) \quad (4.5-88)$$

$$\left( p + \frac{1}{T} \right) \psi'_{rq} = \frac{L_r}{L_m} (u_{sq} - R_s i_{sq} - L'_s p i_{sq}). \quad (4.5-89)$$

Since the output of the modified reference model gives the modified rotor flux linkages  $\psi'_{rd}$  and  $\psi'_{rq}$ , the adaptive model must also be adjusted to give the corresponding modified values, and therefore the high-pass filter block [ $p/(p+1/T)$ ] is placed in front of the original adaptive model in Fig. 4.72. In practice the cut-off frequency of the high-pass filter is a few Hertz (e.g.  $T=0.05$  s gives  $f=1/(2\pi T)=3.2$  Hz). Below the cut-off frequency, the rotor speed estimation

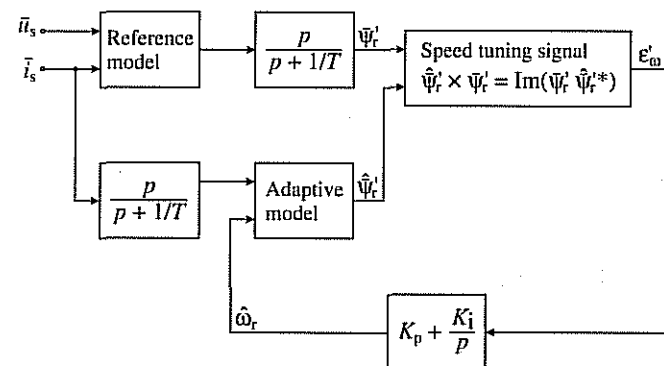


Fig. 4.72. Practical MRAS-based rotor speed observer using rotor flux linkages for the speed tuning signal and avoiding pure integrators.

becomes inaccurate. Furthermore, at low speeds, the stator voltages are small and therefore an accurate value of the stator resistance is required to have a satisfactory response. However, when the MRAS scheme described above is used in a vector-controlled induction motor drive, speed reversal through zero during a fast transient process is possible, but if the drive is operated at zero frequency for more than a few seconds, then speed control is lost due to the incorrect flux-linkage estimation. It should be noted that the problems associated with pure integrators in the reference model can be also avoided by using another flux estimator in the reference model (e.g. see Sections 3.1.3.2 and 4.1.1.4, where such stator flux estimators are also described, which avoid the use of pure integrators, use the monitored stator voltages and currents, and contain a feedback of the flux angle). However, it is also possible to avoid the use of pure integrators by using another speed tuning signal in the MRAS system, which does not require pure integration. Since in the above scheme the integrator was present only because the rotor flux linkage is estimated from the stator flux linkage,  $\bar{\psi}_r = (L_r/L_m)(\bar{\psi}_s - L'_s \bar{i}_s)$ , and the stator flux-linkage estimation from the stator voltages and currents requires an integration, it follows that if a signal (e.g. back e.m.f.) proportional to  $d\bar{\psi}_r/dt$  is used (the space vector of the back e.m.f. is  $\bar{e} = (L_m/L_r) d\bar{\psi}_r/dt$ ), then no integration is required. Such a scheme is discussed in the next section.

#### 4.5.3.4.4 Scheme 2: speed tuning signal is $e_e = \text{Im}(\bar{e}\hat{e}^*)$

It has been mentioned above that it is also possible to construct other MRAS schemes which, instead of using the rotor flux-linkage estimates in the speed tuning signal, use the back e.m.f.s or some other quantities, e.g. the components of the power vector ( $\bar{u}_s \bar{i}_s^*$ ), etc. When the back e.m.f.s are used, then the problems associated with the pure integrators in the reference model disappear, since in this case the reference model does not contain any integrator. The equations for the direct- and quadrature-axis back e.m.f.s follow from eqns (4.5-83) and (4.5-84):

$$e_d = \frac{L_m}{L_r} \frac{d\bar{\psi}_{rd}}{dt} = u_{sD} - R_s i_{sD} - L'_s \frac{di_{sD}}{dt} \quad (4.5-90)$$

$$e_q = \frac{L_m}{L_r} \frac{d\bar{\psi}_{rq}}{dt} = u_{sQ} - R_s i_{sQ} - L'_s \frac{di_{sQ}}{dt}, \quad (4.5-91)$$

and these are used in a new reference model, shown in Fig. 4.73.

As expected, the component back e.m.f.s  $e_d$  and  $e_q$  can be obtained without integration. Similarly to scheme described in the previous section (Scheme 1), the direct- and quadrature-axis stator voltages can be obtained from monitored terminal voltages, or in an inverter-fed drive, they can be reconstructed by using the inverter switching states and the monitored d.c. link voltage.

The corresponding back e.m.f. equations for the adaptive model are obtained from eqns (4.5-85) and (4.5-86):

$$\hat{e}_d = \frac{L_m}{L_r} \frac{d\bar{\psi}_{rd}}{dt} = \frac{L_m}{L_r} \frac{(L_m i_{sD} - \psi_{rd} - \omega_r T_r \psi_{rq})}{T_r} \quad (4.5-92)$$

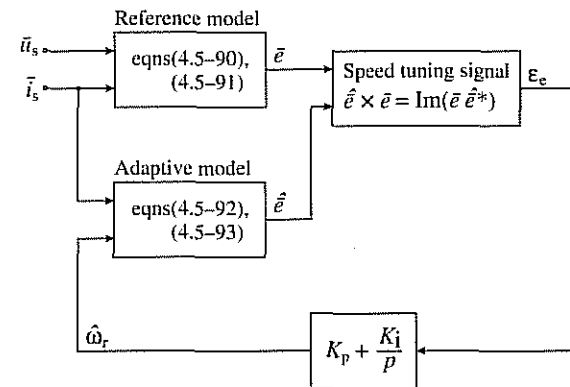


Fig. 4.73. MRAS-based speed observer using back e.m.f.s for the speed tuning signal.

$$\dot{e}_q = \frac{L_m}{L_r} \frac{d\bar{\psi}_{rq}}{dt} = \frac{L_m}{L_r} \frac{(L_m i_{sQ} - \psi_{rq} + \omega_r T_r \psi_{rd})}{T_r}. \quad (4.5-93)$$

Equations (4.5-92) and (4.5-93) are used in the adaptive model shown in Fig. 4.73. In Fig. 4.73 the speed tuning signal is  $e_e = \text{Im}(\bar{e}\hat{e}^*) = \hat{e} \times \bar{e} = e_d \hat{e}_d - e_q \hat{e}_q$ , which is proportional to the angular difference between the back e.m.f. vectors of the reference and adjustable models respectively,  $\bar{e}$ ,  $\hat{e}$  ( $\times$  denotes the cross-vectorial product). The full scheme is shown in Fig. 4.74.

It should be noted that in Fig. 4.74 the speed tuning signal  $e_e$  is multiplied by  $L'_m/T_r$ , which has been assumed to be constant, where  $L'_m = L_m^2/L_r$  is the referred value of the magnetizing inductance (this inductance was used in Fig. 4.10(a)). Thus multiplication by the constant  $L'_m/T_r$  is used to obtain  $e_e$ , which is then the input to the PI controller. However, this multiplication can be omitted since  $L'_m/T_r$  can be incorporated in the proportional and integral gain constants of the PI controller (which become  $K'_p = K_p L'_m/T_r$  and  $K'_i = K_i L'_m/T_r$ ).

When the scheme shown in Fig. 4.74 is employed in a speed-sensorless vector-controlled drive, satisfactory performance can be obtained even at low speeds if an accurate value of the stator resistance is used, since the reference model does not contain pure integration. However, the stator resistance varies with temperature, and this effects the stability and performance of the speed observer, especially at very low speeds. A MRAS scheme which is insensitive to stator resistance variation can be obtained by using such a speed tuning signal, which is obtained from a quantity which does not contain the stator resistance. This is discussed in the next section.

#### 4.5.3.4.5 Scheme 3: speed tuning signal is $e_{\Delta e} = \text{Im}(\Delta \bar{e} \bar{i}_s^*)$

In Schemes 2 and 3 described above, the speed tuning signal is obtained from  $\text{Im}(\bar{\psi}'_r \bar{\psi}'^*)$  and from  $\text{Im}(\bar{e}\hat{e}^*)$  respectively. In the new scheme (Scheme 3), the speed

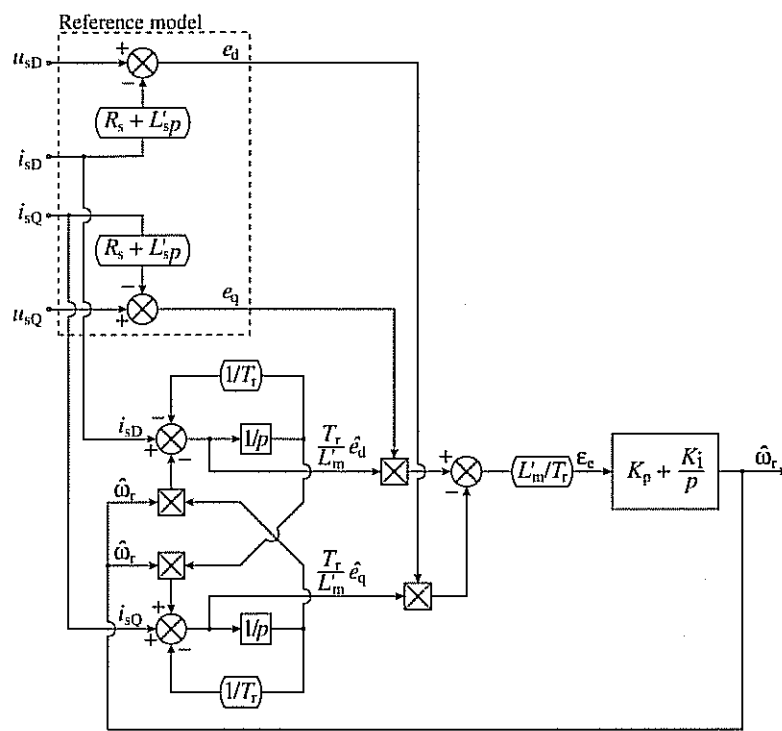


Fig. 4.74. Complete scheme of MRAS-based speed observer using back e.m.f.s for the speed tuning signal.

tuning signal is deliberately chosen to be  $\text{Im}(\Delta\bar{e}\bar{i}_s^*)$ , where  $\Delta\bar{e}=\bar{e}-\hat{e}$  and  $\bar{e}, \hat{e}$  are the space vectors of the back e.m.f.s in the reference model and adaptive model respectively. It follows that  $\text{Im}(\Delta\bar{e}\bar{i}_s^*)=\bar{i}_s \times \Delta\bar{e}=\bar{i}_s \times \bar{e}-\bar{i}_s \times \hat{e}$ , and by considering eqns (4.5-90), (4.5-91), and  $\bar{e}=e_d+je_q$ ,  $\bar{u}_s=u_{sd}+ju_{sq}$ ,  $\bar{i}_s=i_{sd}+ji_{sq}$ ,

$$y=\bar{i}_s \times \bar{e}=\bar{i}_s \times \left(\bar{u}_s-L'_s \frac{d\bar{i}_s}{dt}\right) \quad (4.5-94)$$

is obtained, which is the output of the reference model. It can be seen that this does not contain the stator resistance, and this is why  $y$  has been chosen to be a component of the speed tuning signal. In other words, since the stator-voltage space vector ( $\bar{u}_s$ ) is equal to the sum of the stator ohmic voltage drop ( $R_s\bar{i}_s$ ) plus  $L'_s d\bar{i}_s/dt$ , plus the back e.m.f.  $\bar{e}=(L_m/L_r)d\bar{\psi}_r/dt$ , therefore the vectorial product  $\bar{i}_s \times \bar{u}_s$  does not contain the stator resistance and takes the form  $\bar{i}_s \times \bar{u}_s=\bar{i}_s \times L'_s d\bar{i}_s/dt+\bar{i}_s \times \bar{e}$ , and this gives eqn (4.5-94) as expected. The first term on the right-hand side of eqn (4.5-94) is  $(\bar{i}_s \times \bar{u}_s)$ , the reactive input power. Similarly to the other two schemes discussed in the previous two sections, the

stator voltage components  $u_{sd}, u_{sq}$  can be obtained from the monitored line voltages, or in an inverter-fed induction motor drive, they can be reconstructed from the inverter switching states and the monitored value of the d.c. link voltage.

The output of the adaptive model is obtained by considering eqns (4.5-92), (4.5-93) and  $\hat{e}=e_d+je_q$ , as follows:

$$\hat{y}=\bar{i}_s \times \hat{e}=\bar{i}_s \times \frac{L_m}{L_r} \left[ \frac{L_m}{T_r} \bar{i}_s + \frac{\bar{\psi}_r(j\omega_r-1)}{T_r} \right] = \frac{L_m}{L_r} \left[ \frac{1}{T_r} \bar{\psi}_r \times \bar{i}_s + \omega_r(\bar{i}_s \times j\bar{\psi}_r) \right]. \quad (4.5-95)$$

Figure 4.75 shows the schematic of the rotor speed observer using the speed tuning signal  $e_{\Delta e}=\text{Im}(\Delta\bar{e}\bar{i}_s^*)$ . The reference model is represented by eqn (4.5-94) and the adaptive model by eqn (4.5-95).

The component forms of eqns (4.5-94) and (4.5-95) yield

$$y=\bar{i}_s \times \bar{e}=u_{sq}i_{sd}-u_{sd}i_{sq}-L'_s \left( i_{sd} \frac{di_{sq}}{dt} - i_{sq} \frac{di_{sd}}{dt} \right) \quad (4.5-96)$$

and

$$\hat{y}=\bar{i}_s \times \hat{e}=i_{sd}\hat{e}_q-i_{sq}\hat{e}_d \\ = \frac{L_m}{L_r} \left[ \frac{1}{T_r} (\psi_{rd}i_{sq}-\psi_{rq}i_{sd}) + \omega_r(\psi_{rd}i_{sd}+\psi_{rq}i_{sq}) \right] \quad (4.5-97)$$

respectively. Equations (4.5-96) and (4.5-97) can then be used in a final implementation of the rotor speed observer. When this observer is used in a vector-controlled drive, it is possible to obtain satisfactory performance even at very low speeds. The observer can track the actual rotor speed with a bandwidth that is only limited by noise, so the PI controller gains should be as large as possible. The scheme is insensitive to stator resistance variations and it can be shown that if in a rotor-flux-oriented vector drive, the same  $T_r$  is used as in the MRAS-based speed observer, then the drive will be robust to the variation of  $T_r$  as well [Peng *et al.* 1994]. Thus rotor-flux alignment is maintained, despite the fact that

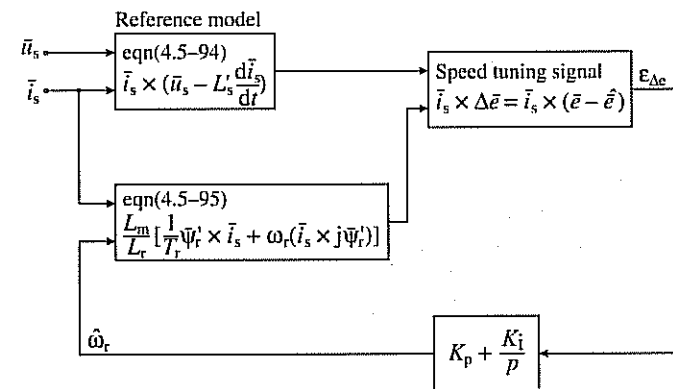


Fig. 4.75. Rotor speed observer using the tuning signal  $\text{Im}(\Delta\bar{e}\bar{i}_s^*)$ .

an incorrect value of the rotor time constant is used. This is due to the accumulative effects of the errors. This also holds for the other MRAS-based speed observers described above. However, the accuracy of the speed estimation system discussed above depends on the transient stator inductance ( $L'_s$ ) and also on the referred magnetizing inductance ( $L_m^2/L_r$ ). The latter quantity is not too problematic, since it does not change with the temperature. Furthermore, deviation of  $T_r$  from its correct value produces a steady-state error in the estimated speed and this error can become significant at low speed. In general, the scheme can be used at very low speeds as well, e.g. at 0.3 Hz, but not at zero stator frequency. Special care must be taken for the design of this scheme for applications where there are negative step changes in the torque-producing stator current, otherwise it is difficult to keep the speed stable.

Finally it should be noted that by using a simple space-vector model of the induction machine, which takes into account the effects of iron losses, it is possible to estimate the effects of iron losses on the estimated rotor speed. It can then be shown that in the field-weakening range the iron losses may have an important effect on the accuracy of the speed estimation. In a simple space-vector model of the induction machine, the iron losses can be considered in a similar way to that used in the conventional steady-state equivalent circuit of the induction machine. Thus in the model expressed in the stationary reference frame, the resistor taking account of iron losses is connected in parallel with the magnetizing inductance. In a model expressed in the general reference frame rotating at the general speed  $\omega_g$ , this resistance is connected in parallel with a circuit which contains the sum of the transformer voltage  $L_m p \bar{i}_{mg}$  ( $p = d/dt$  and  $\bar{i}_{mg}$  is the magnetizing-current space vector in the general reference frame) and the rotational voltage  $j\omega_g \bar{\psi}_{mg}$  ( $\bar{\psi}_{mg}$  is the magnetizing flux-linkage space vector in the general reference frame). For simplicity the magnetizing inductance has been assumed to be constant, but it is possible to use a similar dynamic model of the induction machine which takes account of both the iron losses and saturation effects. This could be used for the analysis and compensation of the speed estimation error caused by iron losses and main flux saturation in a MRAC-based speed-sensorless induction motor drive.

#### 4.5.3.4.6 Scheme 4: speed tuning signal is $e_{\Delta e'} = \text{Im}(\Delta \bar{e} \bar{i}_s^*)$

As discussed in the MRAS scheme of the previous section, the presence of the stator transient inductance ( $L'_s$ ) is undesirable, since this affects the accuracy of the estimated rotor speed in the entire speed range. For the purposes of the present scheme it is a goal to eliminate the need for using the stator transient inductance. Furthermore, it is another goal that the MRAS scheme should not require pure integration (similarly to the schemes described previously). It will be shown that it is possible to fulfil these conditions by using a suitable speed-tuning signal, but accurate speed estimation can only be achieved if the stator resistance and rotor time constant are accurately known (e.g. they are adapted on-line).

By examining the stator and rotor voltage space-vector equations of the induction machine, it can be physically deduced that both of these requirements

can be fulfilled if the speed tuning signal contains the derivative of the stator currents and is chosen as  $e_{\Delta e'} = \text{Im}(\Delta \bar{e} \bar{i}_s^*)$ . Similarly to the notation used in the earlier schemes, in this expression  $\bar{e}$  is the space vector of the back e.m.f.s,  $\bar{e} = (L_m/L_r) d\bar{\psi}_r / dt$ ,  $p$  is the differential operator ( $p = d/dt$ ) and  $\Delta \bar{e} = \bar{e} - \hat{\bar{e}}$  is the error back-e.m.f. space vector (difference between the back-e.m.f. space vector of the reference model and that of the adaptive model of the MRAS speed estimator scheme). Alternatively, this tuning signal can also be expressed as  $e_{\Delta e'} = p \bar{i}_s \times \Delta \bar{e}$ . It should be noted that by using the expressions for  $\bar{e}$  and  $\hat{\bar{e}}$  which can be obtained from the stator and rotor voltage equations respectively (both expressed in the stationary reference frame), it is possible to obtain the tuning signal in terms of the direct- and quadrature-axis components of the stator currents, stator voltages, and rotor flux linkages (all expressed in the stationary reference frame). Thus the following expression is obtained

$$\begin{aligned} e_{\Delta e'} = & [u_{sQ} p i_{sD} - u_{sD} p i_{sQ} - R_s (i_{sQ} p i_{sD} - i_{sD} p i_{sQ})] - \frac{L_m}{L_r} [\hat{\omega}_r (\psi_{rd} p i_{sD} \\ & + \psi_{rq} p i_{sQ}) + (\psi_{rd} p i_{sQ} - \psi_{rq} p i_{sD} + i_{sQ} p i_{sD} - i_{sD} p i_{sQ})/T_r], \end{aligned}$$

where  $\hat{\omega}_r$  is the estimated speed, which is used in the adjustable model of the MRAS speed-estimation scheme. As expected, this expression does not contain the direct- and quadrature-axis voltage drops across the stator transient inductance. The term within the first square brackets is implemented by the use of the reference model, which uses at its inputs the actual stator voltage and stator current components ( $u_{sD}$ ,  $u_{sQ}$ ,  $i_{sD}$ ,  $i_{sQ}$ ), but it can be seen that, in contrast to the scheme described in the previous section, it also uses  $R_s$ . Thus the success of an accurate speed estimation at low speeds depends on accurate knowledge of the stator resistance. It can also be seen that in space-vector terms this term is equal to  $[(p \bar{i}_s) \times \bar{e}]$  or alternatively  $[(p \bar{i}_s) \times (p \bar{\psi}_s)] = [(p \bar{i}_s) \times (\bar{u}_s - R_s \bar{i}_s)]$  and obviously  $(p \bar{i}_s) \times \bar{i}_s \neq 0$ . Therefore it is an advantage that the derivative of the stator flux-linkage space vector is present here and not the stator flux-linkage space vector itself, and thus there is no pure integration involved. Furthermore, it can also be seen that the term within the second square brackets contains the rotor flux-linkage components, which are obtained in the adjustable model, which uses the rotor voltage equations of the induction machine [eqns (4.5-85) and (4.5-86)] together with the monitored stator currents ( $i_{sD}$ ,  $i_{sQ}$ ) and the estimated rotor speed ( $\hat{\omega}_r$ ). However, this term also depends on the rotor time constant. In space-vector terms, when this term is multiplied by  $(L_m/L_r)$ , then it can be expressed as  $[(p \bar{i}_s) \times \hat{\bar{e}}]$ .

Similarly to all the other MRAS estimation schemes described in the previous sections, by using a rigorous mathematical proof, which e.g. involves Popov's hyperstability theory (discussed in Section 4.5.3.4.2), or Lyapunov's stability theory (discussed in Section 4.5.3.5.1), it can be shown that the adaptation mechanism is again  $K_p + K_i/p$ , where  $K_p$  and  $K_i$  are gain constants. Thus the estimated speed used by the adjustable model of the MRAS system is obtained from  $\hat{\omega}_r = (K_p + K_i/p) e_{\Delta e'}$ .

#### 4.5.3.4.7 Scheme 5: MRAS-based system with AI-based adaptive model and various possibilities for speed tuning signal

All the MRAS-based schemes described in Sections 4.5.3.4.3–4.5.3.4.6 contain a reference model and an adaptive model. An input to the adaptive model has been the estimated rotor speed, which was the output of a suitable adaptation mechanism, which utilized at its inputs the difference of the estimated state variables of the reference and adaptive models. Furthermore, in all the four schemes discussed above, the adaptation mechanism is based on using Popov's hyperstability criterion. This has eventually resulted in an adaptation mechanism in which the estimated state variables of the reference and adaptive model were manipulated into a speed tuning signal, which was then input into a PI controller, containing the proportional and integrator gains of the adaptation mechanism ( $K_p$  and  $K_i$ ). This approach has also required the use of a mathematical model for the adaptive model. A digital implementation of such a scheme is relatively simple and, in terms of processor requirements, Scheme 2 described in Section 4.5.3.4.4 is the simplest. However, greater accuracy and robustness can be achieved if this mathematical model is not used at all and instead, an artificial-intelligence-based non-linear adaptive model is employed. It is then also possible to eliminate the need for the separate PI controller, since this can be integrated into the tuning mechanism of the artificial-intelligence-based model.

The artificial-intelligence-based model can take various forms: it can be an artificial neural network (ANN), or a fuzzy-neural network, etc. (see also Chapter 7 and Section 4.4), and there is also the possibility of using different types of speed tuning signals. Furthermore, the adaptation-mechanism input signals can take various forms, as in the non-artificial-intelligence-based, conventional type of schemes discussed above. Thus there are various possibilities for the speed tuning signal. It follows that if only one ANN configuration is considered (e.g. a back-propagation feedforward multi-layer ANN), and only one specific fuzzy-neural network is used (see also Chapter 7 and Section 4.4), then it is possible to have eight different implementations by considering the four different types of speed tuning signals discussed in the previous sections. However, the possibilities are even greater, since there are many types of ANNs and fuzzy-neural networks. It is believed that some of these solutions can give high accuracy and are robust to parameter variations even at extremely low stator frequency. For illustration purposes of this technique, one specific solution will be described in Section 4.5.3.6, where the ANN contains adjustable and constant weights, and the adjustable weights are proportional to the rotor speed.

#### 4.5.3.5 Observers

##### 4.5.3.5.1 General, Luenberger, and Kalman observers

In general an estimator is defined as a dynamic system whose state variables are estimates of some other system (e.g. electrical machine). There are basically two

forms of the implementation of an estimator: open-loop and closed-loop, the distinction between the two being whether or not a correction term, involving the estimation error, is used to adjust the response of the estimator. A closed-loop estimator is referred to as an observer (see also Section 3.1.3.5).

In Section 4.5.3.1 different types of open-loop speed estimators have been discussed. In open-loop estimators, especially at low speeds, parameter deviations have a significant influence on the performance of the drive both in the steady-state and transient state. However, it is possible to improve the robustness against parameter mismatch and also signal noise by using closed-loop observers.

An observer can be classified according to the type of representation used for the plant to be observed. If the plant is considered to be deterministic, then the observer is a deterministic observer; otherwise it is a stochastic observer. The most commonly used observers are Luenberger and Kalman types (Du *et al.* 1994). The Luenberger observer (LO) is of the deterministic type and the Kalman filter (KF) is of the stochastic type. The basic Kalman filter is only applicable to linear stochastic systems, and for non-linear systems the extended Kalman filter (EKF) can be used, which can provide estimates of the states of a system or of both the states and parameters (joint state and parameter estimation). The EKF is a recursive filter (based on the knowledge of the statistics of both the state and noise created by measurement and system modelling), which can be applied to a non-linear time-varying stochastic system. The basic Luenberger observer is applicable to a linear, time-invariant deterministic system. The extended Luenberger observer (ELO) is applicable to a non-linear time-varying deterministic system. In summary it can be seen that both the EKF and ELO are non-linear estimators and the EKF is applicable to stochastic systems and the ELO to deterministic systems. The deterministic extended Luenberger observer (ELO) is an alternative solution for real-time implementations in industrial drive systems. The simple algorithm and the ease of tuning of the ELO may give some advantages over the conventional extended Kalman filter.

Various types of speed observers are discussed in the present section, which can be used in high-performance induction machine drives. These include a full-order (fourth-order) adaptive state observer (Luenberger observer) which is constructed by using the equations of the induction machine in the stationary reference frame by adding an error compensator. Furthermore, the extended Kalman filter (EKF) and the extended Luenberger observer (ELO) are also discussed. In the full-order adaptive state observer the rotor speed is considered as a parameter, but in the EKF and ELO the rotor speed is considered as a state variable. Furthermore, as discussed above, whilst the ELO is a deterministic observer, the EKF is a stochastic observer which also uses the noise properties of measurement and system noise. It is shown that when the appropriate observers are used in high-performance speed-sensorless torque-controlled induction motor drives (vector-controlled drives, direct-torque-controlled drives), stable operation can be obtained over a wide speed-range, including very low speeds. Various industrial a.c. drives already incorporate observers and it is expected that, in the future,

observers will have an increased role in industrial high-performance vector- and direct-torque-controlled drives.

#### 4.5.3.5.2 Application of a full-order adaptive state observer

In the present subsection, an adaptive speed and stator-resistance observer is discussed for the induction machine. However, first, a state estimator is described which can be used to estimate the rotor flux linkages of an induction machine. This estimator is then modified so it can also yield the speed estimate, and thus an adaptive speed estimator is derived (to be precise, a speed-adaptive flux observer is obtained). To obtain a stable system, the adaptation mechanism is derived by using the state-error dynamic equations together with Lyapunov's stability theorem. The design of the observer is also discussed. In an inverter-fed drive system, the observer uses the monitored stator currents together with the monitored (or reconstructed) stator voltages, or reference stator voltages. However, when the reconstructed stator voltages or reference voltages are used, some error compensation schemes must also be used and some aspects of this are also discussed below.

A state observer is a model-based state estimator which can be used for the state (and/or parameter) estimation of a non-linear dynamic system in real time. In the calculations, the states are predicted by using a mathematical model (the estimated states are denoted by  $\hat{x}$ ), but the predicted states are continuously corrected by using a feedback correction scheme. This scheme makes use of actual measured states ( $x$ ) by adding a correction term to the predicted states. This correction term contains the weighted difference of some of the measured and estimated output signals (the difference is multiplied by the observer feedback gain,  $G$ ). Based on the deviation from the estimated value, the state observer provides an optimum estimated output value ( $\hat{x}$ ) at the next input instant. In an induction motor drive a state observer can also be used for the real-time estimation of the rotor speed and some of the machine parameters, e.g. stator resistance. This is possible since a mathematical dynamic model of the induction machine is sufficiently well known. For this purpose the stator voltages and currents are monitored on-line and for example, the speed and stator resistance of the induction machine can be obtained by the observer quickly and precisely. The accuracy of the state observer also depends on the model parameters used. By using a DSP, it is possible to implement the adaptive state observer conveniently in real time. The state observer is simpler than the Kalman observer (e.g. see Section 3.1.3.5), since no attempt is made to minimize a stochastic cost criterion.

To obtain the full-order non-linear speed observer, first the model of the induction machine is considered in the stationary reference frame and then an error compensator term is added to this. The simplest derivation uses the stator and rotor space-vector equations of the induction machine given by eqns (2.1-148)–(2.1-151). These yield the following state variable equations in the stationary reference frame ( $\omega_g = 0$ ) if the space vectors of the stator currents ( $\bar{i}_s$ )

and rotor flux linkages ( $\bar{\psi}'_r$ ) are selected as state variables:

$$\frac{d}{dt} \begin{bmatrix} \bar{i}_s \\ \bar{\psi}'_r \end{bmatrix} = \begin{bmatrix} -[1/T'_s + (1-\sigma)/T'_r] & [L_m/(L'_s L_r)](-1/T_r + j\omega_r) \\ L_m/T_r & -1/T_r + j\omega_r \end{bmatrix} \begin{bmatrix} \bar{i}_s \\ \bar{\psi}'_r \end{bmatrix} + \begin{bmatrix} \bar{u}_s/L'_s \\ 0 \end{bmatrix}, \quad (4.5-98)$$

where  $\bar{u}_s$  is the space vector of stator voltages,  $L_m$  and  $L_r$  are the magnetizing inductance and rotor self-inductance respectively,  $L'_s$  is the stator transient inductance,  $T'_s = L'_s/R_s$  and  $T'_r = L'_r/R_r$  are the stator and rotor transient time constants respectively, and  $\sigma = 1 - L_m^2/(L_s L_r)$  is the leakage factor. Since  $\bar{i}_s = i_{sD} + j i_{sQ}$ ,  $\bar{\psi}'_r = \psi_{rd} + j \psi_{rq}$ , eqn (4.5-98) can also be put into the following component form:

$$\begin{aligned} \frac{d\bar{x}}{dt} &= \mathbf{Ax} + \mathbf{Bu} & (4.5-99) \\ \mathbf{A} &= \begin{bmatrix} -[1/T'_s + (1-\sigma)/T'_r]\mathbf{I}_2 & [L_m/(L'_s L_r)][\mathbf{I}_2/T_r - \omega_r \mathbf{J}] \\ L_m \mathbf{I}_2/T_r & -\mathbf{I}_2/T_r + \omega_r \mathbf{J} \end{bmatrix} \\ \mathbf{B} &= [\mathbf{I}_2/L'_s, \mathbf{O}_2]^T \\ \mathbf{J} &= \begin{bmatrix} 0 & -1 \\ 1 & 0 \end{bmatrix} \end{aligned}$$

The output equation is defined as

$$\mathbf{i}_s = \mathbf{Cx}. \quad (4.5-100)$$

In eqn (4.5-99),  $\mathbf{x} = [\mathbf{i}_s, \bar{\psi}'_r]$  is the state vector, which contains the stator-current column vector,  $\mathbf{i}_s = [i_{sD}, i_{sQ}]^T$  and also the rotor flux-linkage column vector,  $\bar{\psi}'_r = [\psi_{rd}, \psi_{rq}]^T$ .

Furthermore,  $\mathbf{u}$  is the input column vector, which contains the direct- and quadrature-axis stator voltages  $\mathbf{u} = \mathbf{u}_s = [u_{sD}, u_{sQ}]^T$ ,  $\mathbf{A}$  is the state matrix, which is a four-by-four matrix and is dependent on the speed ( $\omega_r$ ). Furthermore,  $\mathbf{B}$  is the input matrix,  $\mathbf{I}_2$  is a second-order identity matrix,  $\mathbf{I}_2 = \text{diag}(1, 1)$ , and  $\mathbf{O}_2$  is a two-by-two zero matrix. In eqn (4.5-100)  $\mathbf{C}$  is the output matrix  $\mathbf{C} = [\mathbf{I}_2, \mathbf{O}_2]^T$ . It can be seen that the space-vector form of the state equations, eqn (4.5-98), and its component form, eqn (4.5-99), are very similar. However, in the component equation matrix  $\mathbf{J}$  is used in contrast to  $\mathbf{j}$ , which is used in the space-vector equations, and also the identity matrix  $\mathbf{I}_2$  is present in the component equations instead of the 1 in the space vector equations. Both of these equations can be used to design the observer.

By using the derived mathematical model of the induction machine, e.g. if the component form of the equations, eqn (4.5-99), is used, since this is required in an actual implementation, and adding the correction term described above, which contains the difference of actual and estimated states, a full-order state-observer,

which estimates the stator currents and rotor flux linkages, can be described as follows:

$$\frac{d\hat{x}}{dt} = \hat{\mathbf{A}}\hat{x} + \mathbf{B}u + \mathbf{G}(i_s - \hat{i}_s) \quad (4.5-101)$$

$$\hat{\mathbf{A}} = \begin{bmatrix} -[1/T'_s + (1-\sigma)/T'_r]I_2 & [L_m/(L'_s L'_r)][I_2/T_r - \hat{\omega}_r \mathbf{J}] \\ L_m I_2/T_r & -I_2/T_r + \hat{\omega}_r \mathbf{J} \end{bmatrix}$$

and the output vector is

$$\hat{i}_s = \mathbf{C}\hat{x}, \quad (4.5-102)$$

where  $\hat{\cdot}$  denotes estimated values. It can be seen that the state matrix of the observer ( $\hat{\mathbf{A}}$ ) is a function of the rotor speed, and in a speed-sensorless drive, the rotor speed must also be estimated. The estimated rotor speed is denoted by  $\hat{\omega}_r$ , and in general  $\hat{\mathbf{A}}$  is a function of  $\hat{\omega}_r$ . It is important to note that the estimated speed is considered as a parameter in  $\hat{\mathbf{A}}$ ; however, in some other types of observers (e.g. extended Kalman filter), the estimated speed is not considered as a parameter, but it is a state variable. In eqns (4.5-101) and (4.5-102) the estimated state variables are  $\hat{x} = [\hat{i}_s, \hat{\psi}_r]^T$  and  $\mathbf{G}$  is the observer gain matrix, which is selected so that the system will be stable. In eqn (4.5-101) the gain matrix is multiplied by the error vector  $e = (i_s - \hat{i}_s)$ , where  $i_s$  and  $\hat{i}_s$  are the actual and estimated stator-current column vectors respectively,  $i_s = [i_{sD}, i_{sQ}]^T$ ,  $\hat{i}_s = [\hat{i}_{sD}, \hat{i}_{sQ}]^T$ . By using eqns (4.5-101) and (4.5-102) it is possible to implement a speed estimator which estimates the rotor speed of an induction machine by using the adaptive state observer shown in Fig. 4.76.

In Fig. 4.76 the estimated rotor flux-linkage components and the stator-current error components are used to obtain the error speed tuning signal, which can be

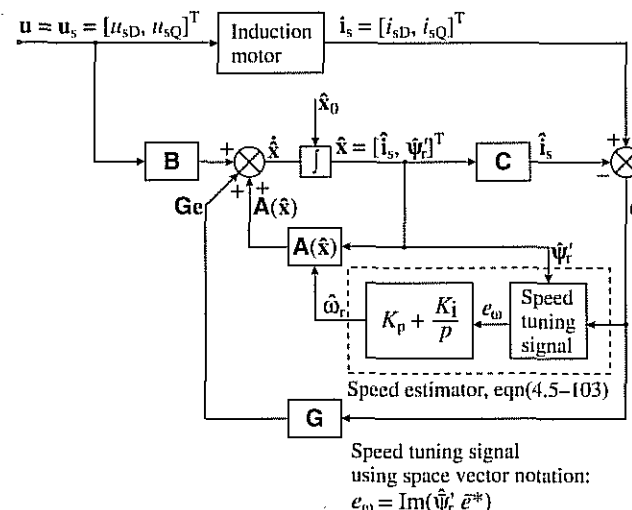


Fig. 4.76. Adaptive speed observer (speed-adaptive flux observer).

put into a very compact, simple form when the space-vector notation is used:  $e_\omega = \text{Im}(\hat{\psi}_r \bar{e}^*)$ , where  $\hat{\psi}_r = \psi_{rd} + j\psi_{rq}$  and  $\bar{e} = e_{sD} + j e_{sQ}$ . The estimated speed is obtained from the speed tuning signal by using a PI controller thus,

$$\hat{\omega}_r = K_p(\hat{\psi}_{rq} e_{sD} - \hat{\psi}_{rd} e_{sQ}) + K_i \int (\hat{\psi}_{rq} e_{sD} - \hat{\psi}_{rd} e_{sQ}) dt, \quad (4.5-103)$$

where  $K_p$  and  $K_i$  are proportional and integral gain constants respectively,  $e_{sD} = i_{sD} - \hat{i}_{sD}$  and  $e_{sQ} = i_{sQ} - \hat{i}_{sQ}$  are the direct- and quadrature-axis stator current errors respectively. The adaptation mechanism is similar to that discussed in the MRAS-based speed estimators in Section 4.5.3.4 where the speed adaptation has been obtained by using the state-error equations of the system considered. Since the goal is to obtain a stable observer, a rigorous proof of eqn (4.5-103) also uses the state-error equation of the system, together with Lyapunov's stability theorem. It should be noted that, instead of determining the stability of the observer itself, it is advantageous to determine the stability of its error dynamics. By using the error dynamics, the objective of a stability analysis is very clear: the states in the error dynamics should decay to the origin. To obtain the error dynamics, eqn (4.5-101) is subtracted from eqn (4.5-99), yielding the following observer-error equation:

$$\frac{de}{dt} = \frac{d}{dt}(x - \hat{x}) = (\mathbf{A} - \mathbf{GC})(x - \hat{x}) + (\mathbf{A} - \hat{\mathbf{A}})\hat{x} = (\mathbf{A} - \mathbf{GC})e - \Delta\mathbf{A}\hat{x}. \quad (4.5-104)$$

In eqn (4.5-104)  $e = x - \hat{x}$  is the estimation-error column vector (of the stator currents and rotor flux linkages) and the error state matrix is

$$\Delta\mathbf{A} = \hat{\mathbf{A}} - \mathbf{A} = \begin{bmatrix} \mathbf{O}_2 & -(\hat{\omega}_r - \omega_r) \mathbf{J} (L_m/L_r) L'_s \\ \mathbf{O}_2 & (\hat{\omega}_r - \omega_r) \mathbf{J} \end{bmatrix}, \quad (4.5-105)$$

where matrix  $\mathbf{J}$  has been defined in eqn (4.5-99). It can be seen that the error dynamics are described by the eigenvalues of  $\mathbf{A} - \mathbf{GC}$  and these could also be used to design a stable observer (gain matrix). However, to determine the stability of the error dynamics of the observer, it is also possible to use Popov's hyperstability theorem (which has been used in Section 4.5.3.4 for MRAS-based systems) or Lyapunov's stability theorem, which gives a sufficient condition for the uniform asymptotic stability of a non-linear system by using a Lyapunov function  $V$ . This function has to satisfy various conditions, e.g. it must be continuous, differentiable, positive definite, etc. Such a function exists and the following Lyapunov function is introduced:

$$V = e^T e + (\hat{\omega}_r - \omega_r)/c, \quad (4.5-106)$$

where  $c$  is a positive constant. This function is zero when the error ( $e$ ) is zero and when the estimated speed ( $\hat{\omega}_r$ ) is equal to the actual speed ( $\omega_r$ ). Since a sufficient condition for uniform asymptotic stability is that the derivative Lyapunov function,  $dV/dt$ , is negative definite, the derivative of  $V$  is now obtained. By using

the chain differentiation rule, it follows from eqn (4.5-106) that the time derivative of  $V$  becomes as follows:

$$\frac{dV}{dt} = \mathbf{e}^T \left[ \frac{d(\mathbf{e}^T)}{dt} \right] + \mathbf{e}^T \left[ \frac{d\mathbf{e}}{dt} \right] + 2 \frac{d\hat{\omega}_r}{dt} \frac{(\hat{\omega}_r - \omega_r)}{c} \quad (4.5-107)$$

By substitution of  $d\mathbf{e}/dt$  by its expression given by eqn (4.5-104), eqn (4.5-107) becomes

$$\frac{dV}{dt} = \mathbf{e}^T [(\mathbf{A} - \mathbf{GC})^T + (\mathbf{A} - \mathbf{GC})] \mathbf{e} - (\hat{\mathbf{x}}^T \Delta \mathbf{A}^T \mathbf{e} + \mathbf{e}^T \Delta \mathbf{A} \hat{\mathbf{x}}) + 2 \frac{d\hat{\omega}_r}{dt} \frac{(\hat{\omega}_r - \omega_r)}{c}. \quad (4.5-108)$$

When  $\mathbf{e} = \mathbf{x} - \hat{\mathbf{x}}$ ,  $\mathbf{x} = [i_s, \psi_r]^T$  and  $\hat{\mathbf{x}} = [\hat{i}_s, \hat{\psi}_r]^T$  are substituted into eqn (4.5-108), where  $i_s = [i_{sD}, i_{sQ}]^T$  and  $\psi_r = [\psi_{rd}, \psi_{rq}]^T$ , finally the derivative of the Lyapunov function can be expressed as follows:

$$\frac{dV}{dt} = \mathbf{e}^T [(\mathbf{A} - \mathbf{GC})^T + (\mathbf{A} - \mathbf{GC})] \mathbf{e} - 2 \frac{L_m}{L_r} (\hat{\omega}_r - \omega_r) \frac{(e_{sD} \hat{\psi}_{rq} - e_{sQ} \hat{\psi}_{rd})}{L_s} + \frac{2}{c} (\hat{\omega}_r - \omega_r) \frac{d\hat{\omega}_r}{dt}, \quad (4.5-109)$$

where  $e_{sD} = i_{sD} - \hat{i}_{sD}$  and  $e_{sQ} = i_{sQ} - \hat{i}_{sQ}$ . Since a sufficient condition for uniform asymptotic stability is that the derivative Lyapunov function,  $dV/dt$ , is negative definite, e.g.  $V$  has to decrease when the error is not zero, this can be satisfied by ensuring that the sum of the last two terms in eqn (4.5-109) is zero (the other terms on the right-hand side of eqn (4.5-109) are always negative). Thus it follows that the adaptive scheme (adjustment law) for the speed estimation is obtained as

$$\frac{d\hat{\omega}_r}{dt} = K_i (e_{sD} \hat{\psi}_{rq} - e_{sQ} \hat{\psi}_{rd}), \quad (4.5-110)$$

where  $K_i = c L_m / (L_s' L_r)$  ( $c$  is a positive constant introduced above). From eqn (4.5-110) the speed is estimated as follows:

$$\hat{\omega}_r = K_i \int (e_{sD} \hat{\psi}_{rq} - e_{sQ} \hat{\psi}_{rd}) dt. \quad (4.5-111)$$

However, to improve the response of the speed observer, this is modified to

$$\hat{\omega}_r = K_p (e_{sD} \hat{\psi}_{rq} - e_{sQ} \hat{\psi}_{rd}) + K_i \int (e_{sD} \hat{\psi}_{rq} - e_{sQ} \hat{\psi}_{rd}) dt \quad (4.5-112)$$

and eqn (4.5-112) is used for speed estimation, which agrees with eqn (4.5-103). In summary it can be seen that an adaptive observer can be used to obtain the rotor flux estimates ( $\hat{\psi}_{rq}$ ,  $\hat{\psi}_{rd}$ ) and the rotor speed is estimated by using the estimated rotor flux linkages and using the stator current errors ( $e_{sD}$ ,  $e_{sQ}$ ). This is why the precise name of this speed observer is ‘speed-adaptive flux observer’. The same result can also be obtained by applying Popov’s hyperstability theorem.

If the chosen PI constants  $K_p$  and  $K_i$  are large, then the convergence of the rotor speed estimation will be fast. However, in a PWM inverter-fed induction

machine, the estimated speed will be rich in higher harmonics, due to the PWM inverter. Thus the PI gains must be limited when the stator voltages and currents are obtained asynchronously with the PWM pattern. It should be noted that eqn (4.5-108) can also be used to obtain the gain matrix. If the observer gain matrix  $\mathbf{G}$  is chosen so the first term of eqn (4.5-108) is negative semi-definite, then the speed observer will be stable. To ensure stability (at all speeds), the conventional procedure is to select observer poles which are proportional to the motor poles [Kubota *et al.* 1990] (the proportionality constant is  $k$ , and  $k \geq 1$ ). This makes the observer dynamically faster than the induction machine. However, to make the sensitivity to noise small, the proportionality constant is usually small. Thus by using this conventional pole-placement technique, the gain matrix is obtained as

$$\mathbf{G} = - \begin{bmatrix} g_1 \mathbf{I}_2 + g_2 \mathbf{J} \\ g_3 \mathbf{I}_2 + g_4 \mathbf{J} \end{bmatrix} \quad (4.5-113)$$

which yields a two-by-four matrix. The four gains in  $\mathbf{G}$  can be obtained from the eigenvalues of the induction motor as follows:

$$\begin{aligned} g_1 &= -(k-1) \left( \frac{1}{T'_s} + \frac{1}{T'_r} \right) \\ g_2 &= (k-1) \hat{\omega}_r \\ g_3 &= (k^2 - 1) \left\{ - \left[ \frac{1}{T'_s} + \frac{(1-\sigma)}{T'_r} \right] \frac{L'_s L_m}{L_r} + \frac{L_m}{T'_r} \right\} + L'_s \frac{L_m}{L_r} (k-1) \left( \frac{1}{T'_s} + \frac{1}{T'_r} \right) \\ g_4 &= -(k-1) \hat{\omega}_r \frac{L'_s L_m}{L_r} \end{aligned} \quad (4.5-114)$$

It follows that the four gains depend on the estimated speed,  $\hat{\omega}_r$ . With this selection, the estimated states converge to the actual states in all the speed range. The observer can be implemented by using a DSP (e.g. Texas Instruments TMS320C30). However, in a discrete implementation of the speed observer, for small sampling time and low speed, accurate computation is required, otherwise (due to computational errors) stability problems can occur (roots are close to stability limit). For this purpose, another pole-placement procedure could be used, which ensures that the low-speed roots are moved away from the stability limit. Some of the issues related to DSP implementation are now discussed.

For DSP implementation the discretized form of the observer, eqn (4.5-101), and the adaptation mechanism, eqn (4.5-112), has to be used. Thus the discretized observer is described by

$$\hat{\mathbf{x}}(k+1) = \mathbf{A}_d \hat{\mathbf{x}}(k) + \mathbf{B}_d \mathbf{u}(k) + \mathbf{G}_d [\mathbf{i}_s(k) - \hat{\mathbf{i}}_s(k)],$$

where  $\mathbf{G}_d$  is the discretized observer gain matrix,

$$\mathbf{A}_d = \exp(\mathbf{AT}) \approx \mathbf{I}_4 + \mathbf{AT} + \frac{(\mathbf{AT})^2}{2}$$

is the discretized system matrix, where  $T$  is the sampling time, and

$$\mathbf{B}_d = \int_0^T [\exp(\mathbf{A}T)] \mathbf{B} d\tau \approx \mathbf{B}T + \frac{\mathbf{AB}T^2}{2}.$$

Since matrices  $\mathbf{A}$  and  $\mathbf{A}_d$  depend on the rotor speed, the gain matrix has to be computed at each time step and, as discussed above, the observer poles are chosen to be proportional to the poles of the induction machine. To make the scheme insensitive to measurement noise, the proportionality constant ( $k$ ) is selected to be low. In a real-time implementation, due to the complexity of the induction motor model, first the gain matrix  $\mathbf{G}$  is updated directly and then the discretized gain matrix  $\mathbf{G}_d$  is computed. However, this pole-placement technique may have some disadvantages and may not ensure good observer dynamics. It is a disadvantage that it requires extensive computation time, due to the updating of matrix  $\mathbf{G}$  and the discretization procedure. The observer dynamics can be adversely affected by the fact that, for small sampling time and low rotor speed, the discrete-root locus is very close to the stability limit and if there are computational errors, then instability may arise. However, it is possible to overcome some of these difficulties by using a simpler pole-placement technique. For this purpose, the symmetrical structure of  $\mathbf{G}$  is preserved, but the elements of  $\mathbf{G}$  are determined so that at low speed the poles are further displaced from the stability limit. Since these gain matrix elements can lead to a higher sensitivity on noise, beyond a specific rotor-speed value they are decreased. In this way two different, constant gain matrices ( $\mathbf{G}, \mathbf{G}'$ ) are predetermined and used according to the rotor speed (one for speed values less than a specified value and the other for speed values higher than this specific value). In the first 2-by-4 discretized gain matrix,  $\mathbf{G}_d$ , the elements are  $g_{11d} = g_{12d} = -g_{21d} = g_{22d} = g_{31d} = g_{32d} = -g_{41d} = g_{42d} = c$ , where  $c$  is a constant. The second discretized observer gain matrix  $\mathbf{G}'_d$  can also be approximated by a 2-by-4 matrix, which has four zero elements,  $g_{12d} = g_{21d} = g_{31d} = g_{34d} = 0$  but four constant elements,  $g_{11d} = g_{22d} = c_1$  and  $g_{32d} = -g_{42d} = c_2$ , where  $c_1$  and  $c_2$  are constants. This approach leads to a reduced computation time.

The speed estimator discussed above will only give correct speed estimates if correct machine parameters are used in the system matrix and in the input matrix. However, these also contain the stator and rotor transient time constants ( $T'_s$  and  $T'_r$ ), which also vary with the temperature (since they depend on the temperature-dependent stator and rotor resistances respectively). The variation of the stator resistance has significant influence on the estimated speed, especially at low speeds. On the other hand, in a high-dynamic-performance induction motor drive, where the rotor flux is constant, the influence of the rotor resistance variation is constant, independent of the speed, since the speed estimation error and the rotor resistance error cannot be separated from the stator variables (see also the discussion in Section 4.5.3.1, Scheme 5). The influence of the stator resistance variation on the speed estimation can be removed by using an adaptive stator-resistance estimation scheme. A rigorous mathematical derivation of the stator resistance

estimator is similar to that shown above for the speed estimator, and in this case again the state error equations of the observer have first to be obtained. These are obtained by subtracting from the original machine equations the new observer equation, which now contains a new state matrix, but this contains the stator resistance to be estimated  $\hat{R}_s$  (where  $\hat{R}_s = R_s + \Delta R_s$ , and  $\Delta R_s$  is the stator resistance error). It then follows that the following matrix form of the state error equation contains the error state matrix due to the stator resistance mismatch:

$$\Delta \mathbf{A}_{Rs} = \begin{bmatrix} -I_2/L'_s & 0_2 \\ 0_2 & 0_2 \end{bmatrix}, \quad (4.5-115)$$

where  $I_2$  and  $0_2$  are second-order identity and zero matrices respectively. By using the state error equations and applying Popov's hyperstability theorem, or Lyapunov's stability theorem, the estimate of the stator resistance can be obtained. Both of these approaches yield the following stator resistance estimate:

$$\hat{R}_s = -K'_i \int (e_{sD}\hat{i}_{sD} + e_{sQ}\hat{i}_{sQ}) dt - K'_p(e_{sD}\hat{i}_{sD} + e_{sQ}\hat{i}_{sQ}), \quad (4.5-116)$$

and e.g. this can be rigorously checked by using a similar procedure to that described above in conjunction with Lyapunov's stability theorem. When this stator resistance estimation is used on-line in a speed-sensorless high-performance induction motor drive employing torque control (vector control or direct torque control) which also uses the on-line estimation of the rotor speed based on eqn (4.5-112), the drive can be operated in a stable manner in a very wide speed-range, including extremely low speeds. However, it should be noted that the speed observer discussed above uses the monitored stator voltages. In a PWM inverter-fed induction machine the stator voltages contain harmonics due to the inverter and also the degree of voltage measurement deteriorates at low speeds. These problems can be overcome in various ways, e.g. by reconstructing the stator voltages from the inverter switching states by using the monitored d.c. link voltage (see also Sections 3.1.3.1, 4.1.1). Alternatively, in a drive system, it is also possible to use the reference voltages, e.g. these are the inputs to a space-vector PWM modulator (see also Section 3.1.3.5.1), where the reference voltages have been used in a PMSM drive. If this technique is used for the induction machine, to obtain high accuracy, it is necessary to compensate the error between the reference and actual stator voltages by the estimation of the voltage error. For this purpose the adaptive observer shown in Fig. 4.76 must be complemented by a voltage-error estimator block. This voltage error contains both a d.c. and an a.c. component, corresponding to a constant bias error between the real and reference voltage and also to an amplitude error. These errors are present due to the dead time which is required to prevent the short circuits of the inverter arms, errors caused by A/D quantization, voltage drops of the switching devices, etc. The modified observer with stator-voltage error compensator is simple to implement and significantly improves the system behaviour. The extra parts of this observer scheme contain

a stator-voltage error estimator. It can be shown by simple considerations that this voltage error estimator outputs the integral of  $\mathbf{G}(\mathbf{i}_s - \hat{\mathbf{i}}_s)$ , and this signal is manipulated into other signals which are then added to the reference voltages to obtain the correct stator voltages.

#### 4.5.3.5.3 Application of the extended Kalman filter (EKF)

In the present section the extended Kalman filter (EKF) is used for the estimation of the rotor speed of an induction machine. The details of the EKF have been discussed in Section 3.1.3.5, where it has been used in PMSM drives. Two induction-motor models will be derived which can be used by the EKF; one of them contains 5 induction machine parameters and the other one uses only 4 parameters. The details and practical aspects of the EKF algorithm are also discussed. The EKF is suitable for use in high-performance induction motor drives, and it can provide accurate speed estimates in a wide speed-range, including very low speeds. It can also be used for joint state and parameter estimation. However, it is computationally more intensive than the full-order state observer described in the previous section.

The EKF is a recursive optimum stochastic state estimator which can be used for the joint state and parameter estimation of a non-linear dynamic system in real-time by using noisy monitored signals that are disturbed by random noise. This assumes that the measurement noise and disturbance noise are uncorrelated. The noise sources take account of measurement and modelling inaccuracies. The EKF is a variant of the Kalman filter, but the extended version can deal with a non-linear system. It should be noted that in the full-order state-observer (speed-adaptive flux observer) discussed in Section 4.5.3.5.2, the noise has not been considered (it is a deterministic observer, in contrast to the EKF which is a stochastic observer). Furthermore, in the speed-adaptive flux observer, the speed was considered as a parameter, but in the EKF it is considered as a state. Similarly to the speed-adaptive flux observer, where the state variables are adapted by the gain matrix ( $\mathbf{G}$ ), in the EKF the state variables are adapted by the Kalman gain matrix ( $\mathbf{K}$ ).

In a first stage of the calculations of the EKF, the states are predicted by using a mathematical model of the induction machine (which contains previous estimates) and in the second stage, the predicted states are continuously corrected by using a feedback correction scheme. This scheme makes use of actual measured states by adding a term to the predicted states (which are obtained in the first stage). The additional term contains the weighted difference of the measured and estimated output signals. Based on the deviation from the estimated value, the EKF provides an optimum output value at the next input instant. In an induction motor drive the EKF can be used for the real-time estimation of the rotor speed, but it can also be used for joint state and parameter estimation. For this purpose the stator voltages and currents are measured (or the stator voltages are reconstructed from the d.c. link voltage and the inverter switching signals) and, for example, the speed of the machine can be obtained by the EKF quickly and precisely.

The main design steps for a speed-sensorless induction motor drive implementation using the discretized EKF algorithm are as follows (see also Section 3.1.3.5):

1. Selection of the time-domain induction machine model;
2. Discretization of the induction machine model;
3. Determination of the noise and state covariance matrices  $\mathbf{Q}$ ,  $\mathbf{R}$ ,  $\mathbf{P}$ ;
4. Implementation of the discretized EKF algorithm; tuning.

These steps are now discussed.

*1. Time-domain, augmented induction-machine model* For the purpose of using an EKF for the estimation of the rotor speed of an induction machine, it is possible to use various machine models. For example, it is possible to use the equations expressed in the rotor-flux-oriented reference frame ( $\omega_g = \omega_{mr}$ ), or in the stator-flux-oriented reference frame ( $\omega_g = 0$ ). When the model expressed in the rotor-flux-oriented reference frame is used, the stator current components in the rotor-flux-oriented reference frame ( $i_{sx}, i_{sy}$ ) are also state variables and the input and output matrices contain the sine and cosine of  $\rho_r$ , which is the angle of the rotor flux-linkage space vector (with respect to the direct-axis of the stationary reference frame). This is due to the fact that in the state-variable equations the actual stator voltages must be transformed into the rotor-flux-oriented reference frame (to give the required transformed input voltages,  $u_{sx}, u_{sy}$ ) and also since the output matrix must contain the actual stator currents ( $i_{sD}, i_{sQ}$ ) which are obtained from  $i_{sx}, i_{sy}$ . These transformations introduce extra non-linearities, but these transformations are not present in the model established in the stationary reference frame. The main advantages of using the model in the stationary reference frame are:

- reduced computation time (e.g. due to reduced non-linearities);
- smaller sampling times;
- higher accuracy;
- more stable behaviour.

It follows from eqn (4.5-98) or (4.5-99) that the two-axis state-space equations of the induction machine in the stationary reference are as follows, when the stator currents and rotor flux linkages are the state variables and these are augmented with the estimated quantity, which in this application is the rotor speed ( $\omega_r$ ):

$$\frac{d}{dt} \begin{bmatrix} i_{sD} \\ i_{sQ} \\ \psi_{rd} \\ \psi_{rq} \\ \omega_r \end{bmatrix} = \begin{bmatrix} -1/T_s^* & 0 & L_m/(L'_s L_r T_r) & \omega_r L_m/(L'_s L_r) & 0 \\ 0 & -1/T_s^* & -\omega_r L_m/(L'_s L_r) & L_m/(L'_s L_r T_r) & 0 \\ L_m/T_r & 0 & 0 & -1/T_r & -\omega_r \\ 0 & L_m/T_r & \omega_r & 0 & -1/T_r \\ 0 & 0 & 0 & 0 & 0 \end{bmatrix} \begin{bmatrix} i_{sD} \\ i_{sQ} \\ \psi_{rd} \\ \psi_{rq} \\ \omega_r \end{bmatrix} + \begin{bmatrix} 1/L'_s & 0 \\ 0 & 1/L'_s \\ 0 & 0 \\ 0 & 0 \\ 0 & 0 \end{bmatrix} \begin{bmatrix} u_{sD} \\ u_{sQ} \end{bmatrix} \quad (4.5-117)$$

and

$$\begin{bmatrix} i_{sD} \\ i_{sQ} \end{bmatrix} = \begin{bmatrix} 1 & 0 & 0 & 0 & 0 \\ 0 & 1 & 0 & 0 & 0 \end{bmatrix} [i_{sD} i_{sQ} \psi_{rd} \psi_{rq} \omega_r]^T = \mathbf{C} [i_{sD} i_{sQ} \psi_{rd} \psi_{rq} \omega_r]^T, \quad (4.5-118)$$

where  $T_s'^*$  is defined as

$$\frac{1}{T_s'^*} = \frac{1}{T_s'} + \frac{(1-\sigma)}{T_r'} = \frac{R_s + R_r(L_m/L_r)^2}{L'_s} = \frac{R_s + R_{ref}}{L'_s}. \quad (4.5-119)$$

It should be noted that in eqn (4.5-117) it has been assumed that the rotor speed derivative is negligible,  $d\omega_r/dt=0$ . Although this last equation corresponds to infinite inertia, however, in reality this is not true, but the required correction is performed by the Kalman filter (by the system noise, which also takes account of the computational inaccuracies). Furthermore, it should be noted that the effects of saturation of the magnetic paths of the machine have been neglected. This assumption is justified, since it can be shown that the EKF is not sensitive to changes in the inductances, since any changes in the stator parameters are compensated by the current loop inherent in the EKF. The application of eqn (4.5-117) in the EKF will give not only the rotor speed but also the rotor flux-linkage components (and as a consequence the angle and modulus of the rotor flux-linkage space vector will also be known). This is useful for high-performance drive implementations. It is important to emphasize that the rotor speed has been considered as a state variable and the system matrix  $\mathbf{A}$  is non-linear—it contains the speed,  $\mathbf{A}=\mathbf{A}(x)$ .

The compact forms of eqns (4.5-117) and (4.5-118) are

$$\frac{dx}{dt} = \mathbf{Ax} + \mathbf{Bu} \quad (4.5-120)$$

$$y = \mathbf{Cx}, \quad (4.5-121)$$

where

$$\mathbf{A} = \begin{bmatrix} -1/T_s'^* & 0 & L_m/(L'_s L_r T_r) & \omega_r L_m/(L'_s L_r) & 0 \\ 0 & -1/T_s'^* & -\omega_r L_m/(L'_s L_r) & L_m/(L'_s L_r T_r) & 0 \\ L_m/T_r & 0 & -1/T_r & -\omega_r & 0 \\ 0 & L_m/T_r & \omega_r & -1/T_r & 0 \\ 0 & 0 & 0 & 0 & 0 \end{bmatrix}, \quad \mathbf{B} = \begin{bmatrix} 1/L'_s & 0 \\ 0 & 1/L'_s \\ 0 & 0 \\ 0 & 0 \\ 0 & 0 \end{bmatrix}, \quad \mathbf{C} = \begin{bmatrix} 1 & 0 & 0 & 0 & 0 \\ 0 & 1 & 0 & 0 & 0 \end{bmatrix}, \quad (4.5-122)$$

and  $x = [i_{sD} i_{sQ} \psi_{rd} \psi_{rq} \omega_r]^T$  is the state vector,  $u$  is the input vector,  $u = [u_{sD} u_{sQ}]^T$ ,  $\mathbf{A}$  is the system matrix, and  $\mathbf{C}$  is the output matrix.

Equation (4.5-117) contains five machine parameters, these are  $R_s + R_{ref}$ ,  $L'_s$ ,  $L_m$ ,  $L_r$ ,  $T_r$ , where  $R_s + R_{ref}$  is a combined machine parameter: it is the sum of the

stator resistance and the referred value of the rotor resistance,  $R_r^{ref} = R_r(L_m/L_r)^2$ . This referred rotor resistance ( $R_{ref}$ ) is also present in the equivalent circuit shown in Fig. 4.10(a) and 4.10(c). However, it is possible to obtain another state-space model of the induction machine which contains only four machine parameters; these are:  $(R_s R_{ref}, L'_s, T_r)$  or  $(R_s, L'_s, L_M, T_r)$ , where  $L_M$  is the referred value of the magnetizing inductance,  $L_M = L_m^2/L_r$  (and  $R_{ref} = L_M/T_r$  also holds). These four parameters are the ones which are present in the equivalent circuit of Fig. 4.10(a) (or Fig. 4.10(c)), and this is a consequence of the fact that the special referring factor  $a = L_m/L_r$  was used. To obtain the state-variable equations with these four machine parameters, instead of using the rotor flux linkages as state variables, the referred values of the rotor flux linkages are used as state variables. This also follows directly from eqn (4.5-117), since in the stator equations all the parameters which are multiplied by the rotor flux linkages contain  $L_m/L_r$ . For convenience, the equivalent circuit of the induction machine using these four parameters is shown in Fig. 4.77. These four parameters can be conveniently determined in the self-commissioning stage of an induction motor drive by standstill tests, as discussed in Chapter 8. Such a self-commissioning stage is used in a wide range of commercial drives.

The space vector of the referred rotor flux linkages in the stationary reference frame ( $\bar{\psi}'_{ref}$ ) is obtained from the non-referred rotor flux-linkage space vector ( $\bar{\psi}'_r$ ) as follows:

$$\bar{\psi}'_{ref} = \psi_{rdref} + j\psi_{rqref} = \frac{L_m}{L_r} \bar{\psi}'_r = \frac{L_m}{L_r} (\psi_{rd} + j\psi_{rq}). \quad (4.5-123)$$

Thus when the state variables are  $i_{sD}$ ,  $i_{sQ}$ ,  $\psi_{rdref}$ ,  $\psi_{rqref}$  and the augmented state-variable is  $\omega_r$ , then the following state-variable equation is obtained from eqn (4.5-117):

$$\frac{d}{dt} \begin{bmatrix} i_{sD} \\ i_{sQ} \\ \psi_{rdref} \\ \psi_{rqref} \\ \omega_r \end{bmatrix} = \begin{bmatrix} -1/T_s'^* & 0 & 1/(L'_s T_r) & \omega_r/L'_s & 0 & i_{sD} \\ 0 & -1/T_s'^* & -\omega_r/L'_s & 1/(L'_s T_r) & 0 & i_{sQ} \\ L_m/T_r & 0 & -1/T_r & -\omega_r & 0 & \psi_{rdref} \\ 0 & L_m/T_r & \omega_r & -1/T_r & 0 & \psi_{rqref} \\ 0 & 0 & 0 & 0 & 0 & \omega_r \end{bmatrix} \begin{bmatrix} 1/L'_s & 0 \\ 0 & 1/L'_s \\ 0 & 0 \\ 0 & 0 \\ 0 & 0 \end{bmatrix} \begin{bmatrix} u_{sD} \\ u_{sQ} \end{bmatrix}, \quad (4.5-124)$$

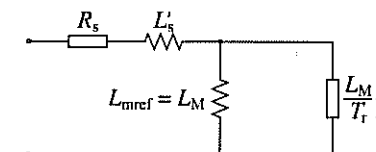


Fig. 4.77. Equivalent circuit of an induction machine using special referred parameters ( $a = L_m/L_r$ ).

and

$$\begin{bmatrix} i_{sD} \\ i_{sQ} \end{bmatrix} = \begin{bmatrix} 1 & 0 & 0 & 0 & 0 \\ 0 & 1 & 0 & 0 & 0 \end{bmatrix} [i_{sD} i_{sQ} \psi_{rdref} \psi_{rqref} \omega_r]^T. \quad (4.5-125)$$

It can be seen that the output equation [eqn (4.5-124)] contains the same output matrix  $\mathbf{C}$  as before.

Of course when eqns (4.5-124) and (4.5-125) are used in the EKF, then in addition to the rotor speed, the referred rotor flux-linkage components are obtained, and not the un-referred values. However, this is not a disadvantage, since the angle of  $\bar{\psi}'_{ref}$  is the same ( $\rho_r$ ) as for  $\bar{\psi}'_r$  and the rotor magnetizing-current modulus can be obtained as  $|\bar{i}_{mrl}| = |\bar{\psi}'_{ref}| / L_M$  (where  $L_M$  is the referred magnetizing inductance), in contrast to the usual  $|\bar{i}_{mrl}| = |\bar{\psi}'_r| / L_m$ . As discussed in Section 4.1.1, in vector drives with rotor-flux-oriented control these quantities ( $|\bar{i}_{mrl}|$  and  $\rho_r$ ) are the usual outputs of the rotor flux model. Furthermore, by considering eqn (4.1-43), the electromagnetic torque can also be expressed in terms of the referred rotor flux-linkage space vector as

$$t_e = \frac{3}{2} P \frac{L_m}{L_r} |\bar{\psi}_r| i_{sy} = \frac{3}{2} P |\bar{\psi}'_{ref}| i_{sy} \quad (4.5-126)$$

or as

$$\begin{aligned} t_e &= \frac{3}{2} P \frac{L_m}{L_r} \bar{\psi}'_r \times \bar{i}_s = \frac{3}{2} P \frac{L_m}{L_r} (\psi_{rd} i_{sQ} - \psi_{rq} i_{sD}) = \frac{3}{2} P \bar{\psi}'_{ref} \times \bar{i}_s \\ &= \frac{3}{2} P (\psi_{rdref} i_{sQ} - \psi_{rqref} i_{sD}). \end{aligned} \quad (4.5-127)$$

Thus in a torque-controlled high-performance drive, if the referred rotor flux linkages are determined by the EKF, then it is possible to obtain the electromagnetic torque in terms of the referred rotor flux linkages and stator currents, and  $L_m/L_r$  is not present in the expression for the electromagnetic torque.

**2. Discretized augmented induction-machine model** For digital implementation of the EKF, the discretized machine equations are required. These can be obtained from eqns (4.5-120), (4.5-121) or (4.5-124), (4.5-125) as follows:

$$\mathbf{x}(k+1) = \mathbf{A}_d \mathbf{x}(k) + \mathbf{B}_d(k) \mathbf{u}(k) \quad (4.5-128)$$

$$\mathbf{y}(k) = \mathbf{C} \mathbf{x}(k). \quad (4.5-129)$$

It should be noted that for the sampled value of  $\mathbf{x}$  in the  $t_k$  instant, the notation  $\mathbf{x}(t_k)$  could be used, or the corresponding more simple  $\mathbf{x}(k)$ , which strictly means  $\mathbf{x}(kT)$ , which corresponds to sampling at the  $k$ th instant, and the sampling time is  $T$  ( $T = t_{k+1} - t_k$ ). In eqns (4.5-128) and (4.5-129)  $\mathbf{A}_d$  and  $\mathbf{B}_d$  are the discretized system and input matrices respectively,

$$\mathbf{A}_d = \exp[\mathbf{A}T] \approx \mathbf{I} + \mathbf{A}T + \frac{(\mathbf{A}T)^2}{2} \quad (4.5-130)$$

$$\mathbf{B}_d \approx \mathbf{B}T + \frac{\mathbf{AB}T^2}{2}, \quad (4.5-131)$$

and it should be noted that the discrete output matrix is  $\mathbf{C}_d = \mathbf{C}$ , where  $\mathbf{C}$  has been defined in eqns (4.5-121) and (4.5-125). It should be noted that when the last terms are ignored in eqns (4.5-130) and (4.5-131), then they require very short sampling times to give a stable and accurate discretized model. However, a better approximation is obtained with the second-order series expansion, when these last terms are also considered. In general, to achieve adequate accuracy, the sampling time should be appreciably smaller than the characteristic time-constants of the machine. The final choice for this should be based on obtaining adequate execution time of the full EKF algorithm and also satisfactory accuracy and stability. The second-order technique obviously increases the computational time.

As an example of the discretized equations, the discrete form of eqn (4.5-120) is now first given, if the second-order terms are neglected in eqns (4.5-130) and (4.5-131):

$$\mathbf{x}(k+1) = \mathbf{A}_d \mathbf{x}(k) + \mathbf{B}_d \mathbf{u}(k) \quad (4.5-132)$$

$$\mathbf{y}(k) = \mathbf{C} \mathbf{x}(k). \quad (4.5-133)$$

$$\mathbf{A}_d = \begin{bmatrix} 1 - T/T_s^{**} & 0 & TL_m/(L'_s L_r T_r) & \omega_r TL_m/(L'_s L_r) & 0 \\ 0 & 1 - T/T_s^{**} & -\omega_r TL_m/(L'_s L_r) & TL_m/(L'_s L_r T_r) & 0 \\ TL_m/T_r & 0 & 1 - T/T_r & -T\omega_r & 0 \\ 0 & TL_m/T_r & T\omega_r & 1 - T/T_r & 0 \\ 0 & 0 & 0 & 0 & 1 \end{bmatrix}$$

$$\mathbf{B}_d = \begin{bmatrix} T/L'_s & 0 \\ 0 & T/L'_s \\ 0 & 0 \\ 0 & 0 \\ 0 & 0 \end{bmatrix}, \quad \mathbf{C}_d = \begin{bmatrix} 1 & 0 & 0 & 0 & 0 \\ 0 & 1 & 0 & 0 & 0 \end{bmatrix}, \quad (4.5-134)$$

where

$$\begin{aligned} \mathbf{x}(k) &= [i_{sD}(k) i_{sQ}(k) \psi_{rd}(k) \psi_{rq}(k) \omega_r(k)]^T \\ \mathbf{u}(k) &= [u_{sD}(k) u_{sQ}(k)]^T. \end{aligned}$$

By considering the system noise  $\mathbf{v}(k)$  ( $\mathbf{v}$  is the noise vector of the states), which is assumed to be zero-mean, white Gaussian, which is independent of  $\mathbf{x}(k)$ , and which has covariance matrix  $\mathbf{Q}$ , the system model becomes

$$\mathbf{x}(k+1) = \mathbf{A}_d \mathbf{x}(k) + \mathbf{B}_d \mathbf{u}(k) + \mathbf{v}(k). \quad (4.5-135)$$

By considering a zero-mean, white Gaussian measurement noise,  $w(k)$  (noise in the measured stator currents), which is independent of  $y(k)$  and  $v(k)$  and whose covariance matrix is  $R$ , the output equation becomes

$$y(k) = Cx(k) + w(k). \quad (4.5-136)$$

**3. Determination of the noise and state covariance matrices  $Q$ ,  $R$ ,  $P$**  The goal of the Kalman filter is to obtain unmeasurable states (e.g. rotor speed) by using measured states, and also statistics of the noise and measurements [i.e. covariance matrices  $Q$ ,  $R$ ,  $P$  of the system noise vector, measurement noise vector, and system state vector ( $x$ ) respectively]. In general, by means of the noise inputs, it is possible to take account of computational inaccuracies, modelling errors, and errors in the measurements. The filter estimation ( $\hat{x}$ ) is obtained from the predicted values of the states ( $x$ ) and this is corrected recursively by using a correction term, which is the product of the Kalman gain ( $K$ ) and the deviation of the estimated measurement output vector and the actual output vector ( $y - \hat{y}$ ). The Kalman gain is chosen to result in the best possible estimated states. Thus the filter algorithm contains basically two main stages, a prediction stage and a filtering stage. During the prediction stage, the next predicted values of the states  $x(k+1)$  are obtained by using a mathematical model (state-variable equations) and also the previous values of the estimated states. Furthermore, the predicted state covariance matrix ( $P$ ) is also obtained before the new measurements are made, and for this purpose the mathematical model and also the covariance matrix of the system ( $Q$ ) are used. In the second stage, which is the filtering stage, the next estimated states,  $\hat{x}(k+1)$  are obtained from the predicted estimates  $x(k+1)$  by adding a correction term  $K(y - \hat{y})$  to the predicted value. This correction term is a weighted difference between the actual output vector ( $y$ ) and the predicted output vector ( $\hat{y}$ ), where  $K$  is the Kalman gain. Thus the predicted state estimate (and also its covariance matrix) is corrected through a feedback correction scheme that makes use of the actual measured quantities. The Kalman gain is chosen to minimize the estimation-error variances of the states to be estimated. The computations are realized by using recursive relations. The algorithm is computationally intensive, and the accuracy also depends on the model parameters used. A critical part of the design is to use correct initial values for the various covariance matrixes. These can be obtained by considering the stochastic properties of the corresponding noises. Since these are usually not known, in most cases they are used as weight matrices, but it should be noted that sometimes simple qualitative rules can be set up for obtaining the covariances in the noise vectors (see also Section 3.1.3.5.1 and the last part of the present section, Section 4.5.3.5.2). With advances in DSP technology, it is possible to conveniently implement an EKF in real time.

The system noise matrix  $Q$  is a five-by-five matrix, the measurement noise matrix  $R$  is a two-by-two matrix, so in general this would require the knowledge of 29 elements. However, by assuming that the noise signals are not correlated, both  $Q$  and  $R$  are diagonal, and only 5 elements must be known in  $Q$  and 2 elements in  $R$ . However, the parameters in the direct and quadrature axes are the

same, which means that the two first elements in the diagonal of  $Q$  are equal ( $q_{11}=q_{22}$ ), the third and fourth elements in the diagonal of  $Q$  are equal ( $q_{33}=q_{44}$ ), so  $Q=\text{diag}(q_{11}, q_{11}, q_{33}, q_{33}, q_{55})$  contains only 3 elements which have to be known. Similarly, the two diagonal elements in  $R$  are equal ( $r_{11}=r_{22}=r$ ), thus  $R=\text{diag}(r, r)$ . It follows that in total only 4 noise covariance elements must be known.

**4. Implementation of the discretized EKF algorithm; tuning** As discussed above, the EKF is an optimal, recursive state estimator, and the EKF algorithm contains basically two main stages, a prediction stage and a filtering stage. During the prediction stage, the next predicted values of the states  $x(k+1)$  [which will be denoted by  $x^*(k+1)$ ] and the predicted state covariance matrix ( $P$ ) [which will be denoted by  $P^*$ ] are also obtained. For this purpose the state-variable equations of the machine are used, and also the system covariance matrix ( $Q$ ). During the filtering stage, the filtered states ( $\hat{x}$ ) are obtained from the predicted estimates by adding a correction term to the predicted value ( $x^*$ ); this correction term is  $K_e=K(y - \hat{y})$ , where  $e=(y - \hat{y})$  is an error term, and it uses measured stator currents,  $y=i_s$ ,  $\hat{y}=\hat{i}_s$ . This error is minimized in the EKF. The EKF equation is

$$\frac{d\hat{x}}{dt} = A(\hat{x})\hat{x} + Bu + K(i_s - \hat{i}_s). \quad (4.5-137)$$

The structure of the EKF is shown in Fig. 4.78. The state estimates are obtained by the EKF algorithm in the following seven steps:

**Step 1: Initialization of the state vector and covariance matrices**

Starting values of the state vector  $x_0=x(t_0)$  and the starting values of the noise covariance matrixes  $Q_0$  (diagonal  $5 \times 5$  matrix) and  $R_0$  (diagonal  $2 \times 2$  matrix) are set, together with the starting value of the state covariance matrix  $P_0$  (which is a  $5 \times 5$  matrix), where  $P$  is the covariance matrix of the state vector (the terminology

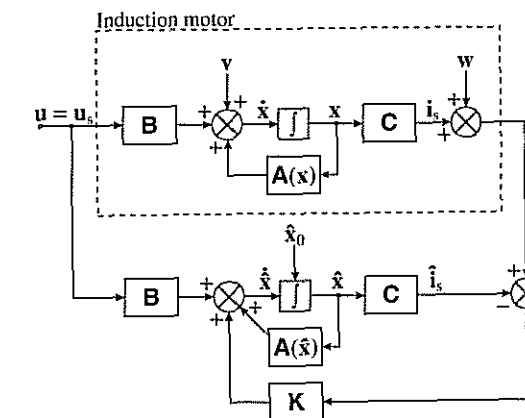


Fig. 4.78. Structure of the EKF.

'covariance matrix of prediction', 'error covariance matrix' are also used in the literature). The starting-state covariance matrix can be considered as a diagonal matrix, where all the elements are equal. The initial values of the covariance matrices reflect on the degree of knowledge of the initial states: the higher their values, the less accurate is any available information on the initial states. Thus the new measurement data will be more heavily weighted and the convergence speed of the estimation process will increase. However, divergence problems or large oscillations of state estimates around a true value may occur when too high initial covariance values are chosen. A suitable selection allows us to obtain satisfactory speed convergence, and avoids divergence problems or unwanted large oscillations.

The accuracy of the state estimation is affected by the amount of information that the stochastic filter can extract from its mathematical model and the measurement data processing. Some of the estimated variables, especially unmeasured ones, may indirectly and weakly be linked to the measurement data, so only poor information is available to the EKF. Finally it should be noted that another important factor which influences the estimation accuracy is due to the different sizes of the state variables, since the minimization of the trace of the estimation covariance ( $\hat{\mathbf{P}}$ ) may lead to high-percentage estimation errors for the variables with small size. This problem can be overcome by choosing normalized state-variables.

#### Step 2: Prediction of the state vector

Prediction of the state vector at sampling time ( $k+1$ ) from the input  $\mathbf{u}(k)$ , state vector at previous sampling time,  $\hat{\mathbf{x}}(k)$ , by using  $\mathbf{A}_d$  and  $\mathbf{B}_d$  is obtained by performing

$$\mathbf{x}^*(k+1|k) = \mathbf{x}^*(k+1) = \mathbf{A}_d \hat{\mathbf{x}}(k) + \mathbf{B}_d \mathbf{u}(k). \quad (4.5-138)$$

The notation  $\mathbf{x}^*(k+1|k)$  means that it is a predicted value at the  $(k+1)$ -th instant, and it is based on measurements up to the  $k$ th instant. However, to simplify the notation, this has been replaced by  $\mathbf{x}^*(k+1)$ . Similarly,  $\hat{\mathbf{x}}(k|k)$  has been replaced by  $\hat{\mathbf{x}}(k)$ .

Thus from eqn (4.5-135)

$$\mathbf{x}^*(k+1) = [a \ b \ c \ d \ e]^T,$$

where

$$\begin{aligned} a &= (1 - T/T_s') \hat{i}_{sD}(k) + [TL_m/(L'_s L_r T_r)] \hat{\psi}_{rd}(k) \\ &\quad + [\dot{\omega}_r(k) TL_m/(L'_s L_r)] \hat{\psi}_{rq}(k) + (T/L'_s) u_{sD}(k) \\ b &= (1 - T/T_s'') \hat{i}_{sQ}(k) - [\dot{\omega}_r(k) TL_m/(L'_s L_r)] \hat{\psi}_{rd}(k) \\ &\quad + [TL_m/(L'_s L_r T_r)] \hat{\psi}_{rq}(k) + (T/L'_s) u_{sQ}(k) \\ c &= (TL_m/T_r) \hat{i}_{sD}(k) + (1 - T/T_r) \hat{\psi}_{rd}(k) - T \dot{\omega}_r(k) \hat{\psi}_{rq}(k) \\ d &= (TL_m/T_r) \hat{i}_{sQ}(k) + (1 - T/T_r) \hat{\psi}_{rq}(k) + T \dot{\omega}_r(k) \hat{\psi}_{rd}(k) \\ e &= \dot{\omega}_r(k) \end{aligned} \quad (4.5-139)$$

#### Step 3: Covariance estimation of prediction

The covariance matrix of prediction is estimated as

$$\mathbf{P}^*(k+1) = \mathbf{f}(k+1) \hat{\mathbf{P}}(k) \mathbf{f}^T(k+1) + \mathbf{Q}, \quad (4.5-140)$$

where, to have simpler notation,  $\mathbf{P}^*(k+1|k)$  has been replaced by  $\mathbf{P}^*(k+1)$ ,  $\hat{\mathbf{P}}(k|k)$  has been replaced by  $\hat{\mathbf{P}}(k)$  [where  $k|k$  denotes prediction at time  $k$  based on data up to time  $k$ ] and  $\mathbf{f}(k+1|k)$  has been replaced by  $\mathbf{f}(k+1)$ , where  $\mathbf{f}$  is the following gradient matrix:

$$\mathbf{f}(k+1) = \frac{\partial}{\partial \mathbf{x}} \left( \mathbf{A}_d \mathbf{x} + \mathbf{B}_d \mathbf{u} \right) \Big|_{\mathbf{x}=\hat{\mathbf{x}}(k+1)}. \quad (4.5-141)$$

By using eqn (4.5-134),

$$\mathbf{f}(k+1) = \begin{bmatrix} 1 - T/T_s'^* & 0 & TL_m/(L'_s L_r T_r) & \omega_r TL_m/(L'_s L_r) & [TL_m/(L'_s L_r)] \psi_{rq} \\ 0 & 1 - T/T_s'^* & -\omega_r TL_m/(L'_s L_r) & TL_m/(L'_s L_r T_r) & -[TL_m/(L'_s L_r)] \psi_{rd} \\ TL_m/T_r & 0 & 1 - T/T_r & -T \omega_r & T \psi_{rq} \\ 0 & TL_m/T_r & T \omega_r & 1 - T/T_r & T \psi_{rd} \\ 0 & 0 & 0 & 0 & 1 \end{bmatrix} \quad (4.5-142)$$

where  $\omega_r = \dot{\omega}_r(k+1)$ ,  $\psi_{rd} = \hat{\psi}_{rd}(k+1)$ ,  $\psi_{rq} = \hat{\psi}_{rq}(k+1)$ . There are 17 elements in  $\mathbf{f}$  which are constant and 8 elements ( $f_{14}, f_{15}, f_{23}, f_{25}, f_{34}, f_{35}, f_{43}, f_{45}$ ) which are variable. In a practical DSP application it is useful to compute first the gradient matrix elements, since this contains the constants required in  $\mathbf{x}^*(k+1)$ . This leads to reduced memory requirements and reduced computational time, since space is only reserved once for the constant elements and the products involving the speed and the flux linkages have to be computed only once in one recursive step.

#### Step 4: Kalman filter gain computation

The Kalman filter gain (correction matrix) is computed as

$$\mathbf{K}(k+1) = \mathbf{P}^*(k+1) \mathbf{h}^T(k+1) [\mathbf{h}(k+1) \mathbf{P}^*(k+1) \mathbf{h}^T(k+1) + \mathbf{R}]^{-1}. \quad (4.5-143)$$

For the induction machine application, the Kalman gain matrix contains two columns and five rows. For simplicity of the notation,  $\mathbf{P}^*(k+1)$  has been replaced by  $\mathbf{P}^*(k+1)$ , and  $\mathbf{h}(k+1)$  is a gradient matrix, defined as

$$\mathbf{h}(k+1) = \frac{\partial}{\partial \mathbf{x}} \left[ \mathbf{C}_d \mathbf{x} \right] \Big|_{\mathbf{x}=\mathbf{x}^*(k+1)} \quad (4.5-144)$$

$$\mathbf{h}(k+1) = \begin{bmatrix} 1 & 0 & 0 & 0 & 0 \\ 0 & 1 & 0 & 0 & 0 \end{bmatrix}.$$



**Step 5: State-vector estimation**

The state-vector estimation (corrected state-vector estimation, filtering) at time  $(k+1)$  is performed as:

$$\hat{x}(k+1) = \hat{x}^*(k+1) + K(k+1)[y(k+1) - \hat{y}(k+1)], \quad (4.5-146)$$

where for simplicity of the notation,  $\hat{x}(k+1|k+1)$  has been replaced by  $\hat{x}(k+1)$ ,  $x^*(k+1|k)$  has been replaced by  $x^*(k+1)$ , and

$$\hat{y}(k+1) = C_d x^*(k+1), \quad (4.5-147)$$

where

$$\hat{y}(k+1) = [i_{sD}^*(k+1), i_{sQ}^*(k+1)]^T. \quad (4.5-148)$$

**Step 6: Covariance matrix of estimation error**

The error covariance matrix can be obtained from

$$\hat{P}(k+1) = P^*(k+1) - K(k+1)h(k+1)P^*(k+1), \quad (4.5-149)$$

where for simplicity of notation  $\hat{P}(k+1|k+1)$  has been replaced by  $\hat{P}(k+1)$ , and  $P^*(k+1|k)$  has been replaced by  $P^*(k+1)$ .

**Step 7: Put  $k=k+1$ ,  $x(k)=x(k-1)$ ,  $P(k)=P(k-1)$  and goto Step 1.**

For the realization of the EKF algorithm it is very convenient to use a signal processor (e.g. Texas Instruments TMS320C30, TMS320C40, TMS320C50, etc.), due to the large number of multiplications required and also due to the fact that all of the computations have to be performed fast: within one sampling interval. The calculation time of the EKF is  $130\mu s$  on the TMS320C40. However, the calculation times can be reduced by using optimized machine models.

The EKF described above can be used under both steady-state and transient conditions of the induction machine for the estimation of the rotor speed. By using the EKF in the drive system, it is possible to implement a PWM inverter-fed induction motor drive without the need of an extra speed sensor. It should be noted that accurate speed sensing is obtained in a very wide speed-range, down to very low values of speed (but not zero speed). However, care must be taken in the selection of the machine parameters and covariance values used. The speed estimation scheme requires the monitored stator voltages and stator currents. Instead of using the monitored stator line voltages, the stator voltages can also be reconstructed by using the d.c. link voltage and inverter switching states, but especially at low speeds it is necessary to have an appropriate dead-time compensation, and also the voltage drops across the inverter switches (e.g. IGBTs) must be considered (see also Section 3.4.3.2.1). Furthermore in a VSI inverter-fed vector-controlled induction motor drive, where a space-vector modulator is used, it is also possible to use the reference voltages (which are the inputs to the modulator) instead of the actual voltages, but this requires an appropriate error compensation (see also Section 4.5.3.5.1 on the full-order state observer).

The tuning of the EKF involves an iterative modification of the machine parameters and covariances in order to yield the best estimates of the states. Changing the covariance matrices  $Q$  and  $R$  affects both the transient duration and steady-state operation of the filter. Increasing  $Q$  corresponds to stronger system noises, or larger uncertainty in the machine model used. The filter gain matrix elements will also increase and thus the measurements will be more heavily weighted and the filter transient performance will be faster. If the covariance  $R$  is increased, this corresponds to the fact that the measurements of the currents are subjected to a stronger noise, and should be weighted less by the filter. Thus the filter gain matrix elements will decrease and this results in slower transient performance. Finally it should be noted that in general, the following qualitative tuning rules can be obtained: Rule 1: If  $R$  is large then  $K$  is small (and the transient performance is faster). Rule 2: If  $Q$  is large then  $K$  is large (and the transient performance is slower). However, if  $Q$  is too large or if  $R$  is too small, instability can arise. It is possible to derive similar rules to these rules, and to implement a fuzzy-logic-assisted system for the selection of the appropriate covariance elements.

In summary it can be stated that the EKF algorithm is computationally more intensive than the algorithm for the full-order state observer described in the previous section. The EKF can also be used for joint state and parameter estimation. It should be noted that to reduce the computational effort and any steady state error, it is possible to use various EKFs, which utilize reduced-order machine models and different reference frames (e.g. a reference frame fixed to the stator current vector).

**4.5.3.5.4 Application of the extended Luenberger observer (ELO)**

To develop a speed-sensorless high-dynamic-performance a.c. drive system, both the rotor speed and flux-linkage signals have to be estimated. Conventionally these have been obtained by using open-loop estimators. A voltage model or a current model of the induction machine, or a combination of these (hybrid estimators), are often used to estimate the speed and some other machine quantities. The problem with this kind of approach is that the estimation error introduced in the speed estimation cannot be overcome and can lead to an increasing deviation of the result from the actual value. If the error is significant, the detuning of the drive system may result. Therefore, for a speed-sensorless control system, it may be advisable that the estimation of the speed and the estimation of the flux should not be treated separately because there always exist mutual interactions between the two estimation systems. Otherwise, any error introduced by the flux-linkage estimator may be amplified by the action of the speed estimator, and vice versa. Thus it is a main objective to describe below an implementation of a real-time joint-flux-and-speed ELO estimation scheme.

It has been discussed in Section 4.5.3.5.1 that the basic Luenberger observer is applicable to a linear, time-invariant deterministic system. The extended Luenberger observer (ELO) is applicable to a non-linear time-varying deterministic system. However, in the past, extended Kalman filters (EKF) have been used almost uniquely for the joint state and parameter estimation problem in a.c. drive

systems (see also Section 4.5.3.5.3). However, this stochastic approach appears to have some inherent disadvantages. Difficulties may arise in situations where the noise content of the system and associated measurements are too low. The tuning of the EKF is *ad hoc*. In contrast to the standard linear Kalman filter, the EKF is not optimal (this important point is not well recognized) [Du *et al.* 1995]. There may be a bias problem when the assumed characteristics of stochastic noises do not match those of the real ones [Ljung 1979, Du *et al.* 1995]. Perhaps the most adverse drawback is that there is no means in the EKF design and implementation which can be utilized to tune its dynamic performance without affecting its steady-state accuracy. Therefore this traditional approach may sometimes not be efficient due to its computation burden, and sometimes even be unacceptable due to its bias.

*Basic Luenberger observer* A basic Luenberger observer (LO) can only be applied to the estimation of states of a linear-time-invariant system described by

$$\dot{\mathbf{x}}(t) = \mathbf{A}\mathbf{x}(t) + \mathbf{B}\mathbf{u}(t) \quad (4.5-150)$$

$$\mathbf{y}(t) = \mathbf{C}\mathbf{x}(t), \quad (4.5-151)$$

and the LO is described by

$$\hat{\mathbf{x}}(t) = \mathbf{A}\hat{\mathbf{x}}(t) + \mathbf{B}\mathbf{u}(t) + \mathbf{G}[\mathbf{y}(t) - \mathbf{C}\hat{\mathbf{x}}(t)], \quad (4.5-152)$$

where  $\hat{\mathbf{x}}(t)$  is the state vector of the estimates and  $\mathbf{G}$  is the observer gain matrix.

*Extended Luenberger observer* In contrast to the LO, the ELO can be applied to the estimation of the states of a non-linear time-invariant system, described by

$$\dot{\mathbf{x}}(t) = \mathbf{f}[\mathbf{x}(t)] + \mathbf{B}\mathbf{u}(t) \quad (4.5-153)$$

$$\mathbf{y}(t) = \mathbf{C}\mathbf{x}(t). \quad (4.5-154)$$

Equations (4.5-153) and (4.5-154) represent an extended induction-motor model. The model of a symmetrical three-phase single-cage induction machine can be described by five first-order differential equations, where four equations correspond to the stator and rotor voltage equations. The simplest derivation uses the stator and rotor space-vector equations of the induction machine given by eqns (2.1-148)–(2.1-151). These yield the following state-variable equations in the reference frame rotating with the rotor flux-linkage space vector ( $\omega_g = \omega_{mr}$ ) if the space vectors of the stator currents ( $\bar{i}_s'$ ) and rotor flux linkages ( $\bar{\psi}'_r$ ) are selected as state variables:

$$\frac{d}{dt} \begin{bmatrix} \bar{i}_s' \\ \bar{\psi}'_r \end{bmatrix} = \begin{bmatrix} -1/T_s'^* + j\omega_{mr} & -[L_m/(L'_s L_r)](-1/T_r + j\omega_r) \\ L_m/T_r & -1/T_r + j(\omega_r - \omega_{mr}) \end{bmatrix} \begin{bmatrix} \bar{i}_s' \\ \bar{\psi}'_r \end{bmatrix} + \begin{bmatrix} \bar{u}_s'/L'_s \\ 0 \end{bmatrix} \quad (4.5-155)$$

where  $\bar{u}_s'$  is the space vector of stator voltages (in the rotor-flux-oriented reference frame),  $L_m$  and  $L_r$  are the magnetizing inductance and rotor self-inductance respectively, and  $L'_s$  is the stator transient inductance. Furthermore, in eqn (4.5-155)  $T_s'^*$  has been defined by eqn (4.5-119), which is now repeated here for convenience:

$$\frac{1}{T_s'^*} = \frac{1}{T_s'} + \frac{(1-\sigma)}{T_r'} = \frac{R_s + R_r(L_m/L_r)^2}{L'_s} = \frac{R_s + R_{ref}}{L'_s}, \quad (4.5-156)$$

where  $T_s' = L'_s/R_s$  and  $T_r' = L'_r/R_r$  are the stator and rotor transient time-constants respectively and  $\sigma = 1 - L_m^2/(L_s L_r)$  is the leakage factor. Resolving eqn (4.5-155) into its real- and imaginary-axis components gives the following state-variable form of the voltage equations:

$$\dot{\mathbf{x}}_n(t) = \mathbf{f}_n[\mathbf{x}_n(t), \omega_r] + \mathbf{B}_n \mathbf{u}(t), \quad (4.5-157)$$

where  $\mathbf{x}_n = [i_{sx}, i_{sy}, \psi_{rx}, \psi_{ry}]^T$  is the state vector of the states,  $\mathbf{u} = [u_{sx}, u_{sy}]^T$  contains the stator-voltage components in the rotor-flux-oriented reference frame, and the input matrix is

$$\mathbf{B}_n = \begin{bmatrix} 1/L'_s & 0 & 0 & 0 \\ 0 & 1/L'_s & 0 & 0 \end{bmatrix}. \quad (4.5-158)$$

Furthermore,  $\mathbf{f}_n(\mathbf{x}_n, \omega_r) = \mathbf{A}_n(\omega_r)\mathbf{x}_n$ , where the state matrix of the induction motor is defined as  $\mathbf{A}_n(\omega_r)$ , where

$$\mathbf{A}_n(\omega_r) = \begin{bmatrix} -1/T_s'^* & \omega_{mr} & L_m/(L_r L_s T_r') & \omega_r L_m/(L_r L_s) \\ -\omega_{mr} & -1/T_s'^* & -\omega_r L_m/(L_r L_s) & L_m/(L_r L_s T_r') \\ L_m/T_r & 0 & -1/T_r & \omega_{mr} - \omega_r \\ 0 & L_m/T_r & \omega_r - \omega_{mr} & -1/T_r \end{bmatrix} \quad (4.5-159)$$

It should be noted that it is possible to obtain a somewhat simpler state matrix if, instead of the rotor flux-linkage components, the referred values of these are used as state variables [see also derivation of eqn (4.5-124)]. In agreement with the definition of the referred rotor flux-linkage space vector [eqn (4.5-123)], in this case the  $L_m/L_r$  coefficients are not present in the stator voltage equation, and as a direct consequence, in the rotor voltage equation,  $L_m$  is replaced by the referred magnetizing inductance  $L_M = L_m^2/L_r$ .

The fifth equation of the induction machine corresponds to the equation of motion,

$$\dot{\omega}_r = c_1 (i_{sy} \psi_{rx} - i_{sx} \psi_{ry}) - c_2 t_L. \quad (4.5-160)$$

In eqn (4.1-160) the first term is the electromagnetic torque given by eqn (2.1-177), and e.g. for a two-pole machine  $c_1$  and  $c_2$  are defined as  $c_1 = 3L_m/(2JL_r)$ ,  $c_2 = 1/J$ , where  $J$  is the inertia. It should be noted that when the referred flux linkages are used as state variables, then  $c_1$  does not contain  $L_m/L_r$ . The damping torque caused by windage and friction has been ignored in the equation of motion. However, the equation of motion contains the load torque, which in general is unknown. This makes the direct estimation of the rotor speed difficult. However, there are three possible approaches to this problem. The first approach is to ignore the load torque and the second approach is to assume that the rate of change of the rotor speed is zero,

$$\dot{\omega}_r = 0. \quad (4.5-161)$$

In this case satisfactory rotor-speed estimates can be obtained if the mechanical time constant is much larger than the electromagnetic time constants. The third method uses the equation of motion but assumes a constant load torque, so that both the speed and the load torque can be estimated. In the present book the second approach is discussed, since it is believed that in general this gives the most accurate estimates.

The first step for the joint rotor speed and rotor flux-linkage estimation is to construct the extended motor model. For this purpose an extended state vector is defined as  $\mathbf{x} = [\mathbf{x}_n, \mathbf{x}_p]^T$ , where in general  $\mathbf{x}_p$  denotes the parameter vector to be estimated, and for the present application  $\mathbf{x}_p = \omega_r$ . Thus it follows from eqns (4.5-157) and (4.5-161), and also considering that the equation defining the measurement variables  $\mathbf{y} = [i_{sx}, i_{sy}]^T$  is

$$\mathbf{y}(t) = \mathbf{C}_n \mathbf{x}_n(t) \quad (4.5-162)$$

where

$$\mathbf{C}_n = \begin{bmatrix} 1 & 0 & 0 & 0 \\ 0 & 1 & 0 & 0 \end{bmatrix}, \quad (4.5-163)$$

and the extended induction motor model can be described by

$$\dot{\mathbf{x}}(t) = \mathbf{f}[\mathbf{x}(t)] + \mathbf{B}\mathbf{u}(t) = [\mathbf{f}_n(\mathbf{x}_n, \mathbf{x}_p), \mathbf{f}_p(\mathbf{x}_n, \mathbf{x}_p)]^T + [\mathbf{B}_n, 0]^T \mathbf{u}(t) \quad (4.5-164)$$

$$\mathbf{y}(t) = \mathbf{C}\mathbf{x}(t) = [\mathbf{C}_n, 0][\mathbf{x}_n, \mathbf{x}_p]^T. \quad (4.5-165)$$

In eqn (4.5-165)  $\mathbf{y}$  is the extended measurement vector.

In contrast to the design of an LO, which results in a time-invariant observer, the ELO is fundamentally time-varying and requires continuous updating of the observer coefficients. Therefore the design of the ELO is based on the linearized form of eqn (4.5-164). Thus the linearized extended induction motor model (around the estimate of the augmented state  $\mathbf{x}$  in the last step, denoted by  $\tilde{\mathbf{x}}$ ) is obtained as

$$\dot{\tilde{\mathbf{x}}}(t) = \mathbf{f}'_{\tilde{\mathbf{x}}}[\tilde{\mathbf{x}}(t)] + \mathbf{B}\mathbf{u}(t) + \mathbf{g}[\tilde{\mathbf{x}}(t)] = \mathbf{A}(\tilde{\mathbf{x}})\mathbf{x} + \mathbf{B}\mathbf{u}(t) + \mathbf{g}(\tilde{\mathbf{x}}), \quad (4.5-166)$$

where  $\tilde{\mathbf{x}}(t)$  is the reference trajectory, which is usually chosen as the estimate in the last step,  $\hat{\mathbf{x}}(t-\tau)$ . In eqn (4.5-166)  $\mathbf{f}'_{\tilde{\mathbf{x}}} = d\mathbf{f}/d\tilde{\mathbf{x}}$  is the system Jacobian matrix (gradient matrix), which is a 5-by-5 matrix,

$$\mathbf{A} = \frac{d\mathbf{f}}{d\tilde{\mathbf{x}}} = \begin{bmatrix} \mathbf{A}_n(\tilde{\mathbf{x}}_p) & \mathbf{A}_2(\tilde{\mathbf{x}}_n) \\ 0 & 0 \end{bmatrix}, \quad (4.5-167)$$

where

$$\mathbf{A}_2(\tilde{\mathbf{x}}_n) = \frac{\partial(\mathbf{A}_n \mathbf{x}_n)}{\partial \tilde{\omega}_r} = [c\tilde{\psi}_{ry}, -c\tilde{\psi}_{rx}, -c\psi_{ry}, c\tilde{\psi}_{rx}]^T \quad (4.5-168)$$

( $c = L_m/L_s' L_r$ ).

The term  $\mathbf{g}[\tilde{\mathbf{x}}(t)]$  is defined as  $\mathbf{g}[\tilde{\mathbf{x}}(t)] = \mathbf{f}(\tilde{\mathbf{x}}) - \mathbf{f}'_{\tilde{\mathbf{x}}}(\tilde{\mathbf{x}})\tilde{\mathbf{x}}$  and thus

$$\mathbf{g}(\tilde{\mathbf{x}}) = [\mathbf{A}(\tilde{\mathbf{x}}) - \mathbf{A}(\tilde{\mathbf{x}})]\tilde{\mathbf{x}}. \quad (4.5-169)$$

The resulting full-order extended Luenberger observer can be written as

$$\dot{\hat{\mathbf{x}}}(t) = \mathbf{A}[\hat{\mathbf{x}}(t-\tau)]\hat{\mathbf{x}}(t) + \mathbf{B}\mathbf{u}(t) + \mathbf{G}[\hat{\mathbf{x}}(t-\tau)][\mathbf{y}(t) - \mathbf{C}\hat{\mathbf{x}}(t-\tau)] + \mathbf{g}[\hat{\mathbf{x}}(t-\tau)], \quad (4.5-170)$$

where

$$\mathbf{g}[\hat{\mathbf{x}}(t-\tau)] = \mathbf{f}[\hat{\mathbf{x}}(t-\tau)] - \mathbf{f}'_{\hat{\mathbf{x}}(t-\tau)}[\hat{\mathbf{x}}(t-\tau)]\hat{\mathbf{x}}(t-\tau) \quad (4.5-171)$$

and

$$\mathbf{f}'_{\hat{\mathbf{x}}(t-\tau)}[\hat{\mathbf{x}}(t-\tau)] = \mathbf{A}[\hat{\mathbf{x}}(t-\tau)]. \quad (4.5-172)$$

It should be noted that in eqn (4.5-170), the gain matrix  $\mathbf{G}$  is not constant, but depends on the past estimates of the system state vector.

In applications where all of the states are not required, a reduced ELO may be used (Du *et al.* 1995). This is described by

$$\dot{\hat{\mathbf{x}}}(t) = \mathbf{F}[\hat{\mathbf{x}}(t-\tau)]\mathbf{z}(t) + \mathbf{G}[\hat{\mathbf{x}}(t-\tau)]\mathbf{y}(t) + \mathbf{H}[\hat{\mathbf{x}}(t-\tau)]\mathbf{u} + \mathbf{D}[\hat{\mathbf{x}}(t-\tau)], \quad (4.5-173)$$

where the coefficient matrices are chosen to satisfy the constraints

$$\begin{aligned} \mathbf{T} f'_{\tilde{\mathbf{x}}}(\mathbf{x}(t))[\tilde{\mathbf{x}}(t-\tau)] - \mathbf{F}[\hat{\mathbf{x}}(t-\tau)]\mathbf{T} &= \mathbf{GC} \\ \mathbf{TB} &= \mathbf{H} \\ \mathbf{D} &= \mathbf{Tg}[\hat{\mathbf{x}}(t-\tau)], \end{aligned} \quad (4.5-174)$$

where  $\mathbf{T}$  is a transformation matrix. If  $\mathbf{T}$  is chosen as a unity matrix, with dimension equal to the number of components in  $\mathbf{x}(t)$ , then a full-order ELO results. Equation (4.5-174) is used to determine the gain matrix  $\mathbf{G}$ .

For convenience, the ELO algorithm is now summarized for a continuous-time ELO:

- Step 1** Specify the system function  $f$  and derive the system Jacobian  $f'_{\tilde{\mathbf{x}}}$ .
- Step 2** Input data: input the input coefficient matrix  $\mathbf{B}$  and output coefficient matrix  $\mathbf{C}$ .
- Step 3** Initialize all observer states.
- Step 4** Specify required observer poles. Construct suitable observer matrix  $\mathbf{F}$  with specified poles.
- Step 5** Evaluate  $\mathbf{g}$  using eqn (4.5-171).
- Step 6** Compute gain matrix  $\mathbf{G}$ :
  - (a) for a full-order ELO: use  $\mathbf{F} = \mathbf{A} - \mathbf{GC}$ , with  $\mathbf{A} = f'_{\tilde{\mathbf{x}}}$  evaluated at the present time instant;
  - (b) for a reduced-order ELO, use eqn (4.5-174) to obtain the gain matrix  $\mathbf{G}$ , the transformation matrix  $\mathbf{T}$ , the observer input coefficient matrix  $\mathbf{H}$ , and the matrix  $\mathbf{D}$ .

- Step 7** Using a suitable numerical integration routine, compute the state vector:
- for the full-order ELO compute the state vector  $\hat{x}$  at the next time instant by solving eqn (4.5-170);
  - for the reduced-order ELO compute the state vector  $z$  at the next time instant by solving eqn (4.5-173) and calculate  $\hat{x}$  using the relationship  $z = T\hat{x}$ . In practice, direct evaluation of this equation is avoided [Orlowska-Kowalska 1989; Du *et al.* 1995].

**Step 8** Go to Step 4

Finally, to indicate clearly the types of problems to which the ELO is applicable, to emphasize the main design features, and also to allow comparisons with the EKF, the important features of the ELO are now summarized:

- it is applicable to a majority of industrial systems since they can be regarded as deterministic;
- its performance can be altered by adjusting the gain matrix so that rapid convergence of the estimates and a robust design may be obtained;
- its computational requirements may be no more demanding than that for other estimation algorithms such as the EKF, as matrix inversion is required in the implementation of the EKF;
- its design incorporates a considerable amount of flexibility owing to the fact that redundancy exists in the constraints imposed by eqn (4.5-174) when specifying the gain matrix  $G$ . This flexibility can be used to meet any prescribed criteria such as speed of response, speed of convergence, robustness against parameter drift, etc.

For real-time implementation a discrete form of the ELO is required, where the estimate at the previous sampling instant is often taken as the reference trajectory, thus

$$\hat{x}(t-\tau) = \hat{x}(t-T_s), \quad (4.5-175)$$

where  $T_s$  is the sampling time. It should be noted that at time  $t$ ,  $\hat{x}(t-T_s)$  is constant, so that for a full-order ELO, eqn (4.5-170) at the  $k$ th sampling time becomes

$$\dot{\hat{x}}(t) = F[\hat{x}(t-T_s)]\hat{x}(t) + Bu(t) + G[\hat{x}(t-T_s)]y(t) + g[\hat{x}(t-T_s)] \quad (4.5-176)$$

$$F[\hat{x}(t-T_s)] = A[\hat{x}(t-T_s)] - GC \quad (4.5-176)$$

$(kT_s < t \leq (k+1)T_s)$ .

It is important to note that this represents a linear time-invariant system over the current sampling interval. Thus by using

$$\Phi_k = \exp(F_k T_s) \quad (4.5-177)$$

$$\Gamma_k = \int_0^{T_s} \exp(F_k t) dt \quad (4.5-178)$$

then the estimation is obtained as

$$\hat{x}_{k+1|k} = \Phi_k \hat{x}_{k|k-1} + \Gamma_k (G_k y_k + Bu_k + g_k). \quad (4.5-179)$$

If  $F_k$  is chosen as a constant matrix,  $\Phi_k$  and  $\Gamma_k$  will also be constant and their values can be computed in advance. Thus the computation time of eqn (4.5-179) is significantly reduced.

To allow comparison with the EKF, the main features of the EKF are summarized here:

- it is based on an extension of a readily implementable algorithm, the Kalman filter;
- it is effective for applications in industrial systems which can be regarded as stochastic in nature;
- its performance can be tuned by adjusting the covariance matrices;
- its design incorporates no flexibility owing to the fact that a constraint implying optimality must be satisfied. Thus no additional prescribed performance criteria such as speed of response, speed convergence, robustness against parameter variation, etc. can be accommodated directly into the design procedure;
- in contrast to the basic Kalman filter, *ad hoc* covariance matrix tuning adjustments, and the non-linear nature of the plant, may result in a non-optimal estimator;
- *ad hoc* covariance matrix adjustments may also result in a bias problem [Ljung 1979].

It appears from a comprehensive study of the ELO in high-performance torque-controlled induction motor drives that the ELO is always capable of producing unbiased estimates. It is important to note that the transient behaviour of the ELO can be conveniently tuned by the common control-system design procedure of adjusting the pole positions. This tuning does not degrade the steady-state performance. When the ELO is used for joint rotor speed and rotor flux-linkage estimation in a torque-controlled induction motor drive, then accurate speed estimates can be obtained even for fast speed transients. However, when the speed is very low, its non-linear observability becomes weak for joint flux-linkage and speed estimation. However, this weak observability does not constitute a severe problem if the drive does not operate constantly around zero speed.

#### 4.5.3.6 Estimators using artificial intelligence

In Section 3.1.3.7 and Chapter 7 the possibilities of using different types of artificial-intelligence-based speed and position estimators are discussed. The two main solutions considered use artificial neural networks (ANN) and fuzzy-neural networks, and the advantages of the fuzzy-neural implementations are also highlighted in Section 3.1.3.7 and Chapter 7. It is believed that this type of approach will find increasing application in the future. This is mainly due to the

fact that the development time of such an estimator is short and the estimator can be made robust to parameter variations and noise. Furthermore, in contrast to all conventional schemes, it can avoid the direct use of a speed-dependent mathematical model of the machine. Two types of ANN-based speed estimators are discussed below for an induction machine. The first one uses a simple two-layer ANN, where the rotor speed is proportional to the appropriate weights, and this ANN is part of a Model Reference Adaptive System (MRAS). In this system, the ANN takes the role of the adaptive model. However, in the more general, second implementation, which is not related to a MRAS, a multi-layer feedforward ANN with hidden layers is used, and the rotor speed is directly present on the output of the ANN.

#### 4.5.3.6.1 MRAS containing two-layer ANN: speed proportional to weights

In Section 4.5.3.4 various MRAS-based speed estimation schemes have been described. All of them have contained a reference model and also an adaptive model. The inputs to the adaptive model were the estimated rotor speed and the stator currents. The estimated rotor speed was the output of a suitable adaptation mechanism, which utilized at its inputs the difference of the estimated state variables of the reference and adaptive models. The main differences between the various MRAS-based speed estimator schemes lie basically in the type of speed tuning signal used, but the adaptation mechanisms in all cases have used Popov's hyperstability criterion. This has eventually resulted in an adaptation mechanism in which the estimated state-variables of the reference and adaptive models were manipulated into a speed tuning signal, which was then input into a PI controller containing the proportional and integrator gains ( $K_p$  and  $K_i$ ) of the adaptation mechanism (e.g. see Fig. 4.68). This approach has also required the use of a mathematical model for the adaptive model. However, greater accuracy and robustness can be achieved if this mathematical model is not used at all and instead, an artificial-intelligence-based no-linear adaptive model is employed. It is then also possible to eliminate the need for the separate PI controller, since this can be integrated into the tuning mechanism of the appropriate artificial-intelligence-based model.

An AI-based model can take various forms: it can be an artificial neural network (ANN) or a fuzzy-neural network, etc. Furthermore, different types of adaptation mechanism input signals (speed tuning signal) can be used, similarly to that used in the conventional schemes discussed in Section 4.5.3.4. Thus there are various possibilities for the speed tuning signal. It follows that if only one ANN configuration is considered (e.g. a back-propagation multi-layer feedforward ANN), and only one specific fuzzy-neural network is used (e.g. ANFIS [Jang 1993]), then it is possible to have eight different implementations by considering four different types of speed tuning signals. However, in practice the possibilities are even greater, since there are many types of ANNs and fuzzy-neural networks. It is believed that some of these solutions can give high accuracy and are robust to parameter variations even at extremely low stator frequency.

For illustration purposes, one specific implementation of this technique will now be discussed where the ANN contains adjustable and constant weights, and the adjustable weights are proportional to the rotor speed. The adjustable weights are changed by using the error between the outputs of the reference model and the adjustable model, since any mismatch between the actual speed and the estimated speed results in an error between the outputs of the reference and adaptive estimators.

Figure 4.79 shows the MRAS-based speed estimation scheme, which contains an ANN. It follows from Fig. 4.79 that the inputs to the reference model are the monitored stator voltages and currents of the induction machine. The outputs of the reference model are the rotor flux-linkage components in the stationary reference frame ( $\psi_{rd}$ ,  $\psi_{rq}$ ). These are obtained by considering eqns (4.5-83) and (4.5-84) in Section 4.5.3.4, which are now repeated here for convenience:

$$\psi_{rd} = \frac{L_r}{L_m} \left[ \int (u_{sd} - R_s i_{sd}) dt - L'_s i_{sd} \right] \quad (4.5-180)$$

$$\psi_{rq} = \frac{L_r}{L_m} \left[ \int (u_{sq} - R_s i_{sq}) dt - L'_s i_{sq} \right]. \quad (4.5-181)$$

These two equations do not contain the rotor speed and describe the reference model. However, when the rotor voltage equations of the induction machine are expressed in the stationary reference frame, they contain the rotor flux linkages and the rotor speed as well. These are the equations of the adaptive model and have been given by eqns (4.5-85) and (4.5-86) respectively, which are also given here for convenience:

$$\hat{\psi}_{rd} = \frac{1}{T_r} \int (L_m i_{sd} - \hat{\psi}_{rd} - \omega_r T_r \hat{\psi}_{rq}) dt \quad (4.5-182)$$

$$\hat{\psi}_{rq} = \frac{1}{T_r} \int (L_m i_{sq} - \hat{\psi}_{rq} + \omega_r T_r \hat{\psi}_{rd}) dt. \quad (4.5-183)$$

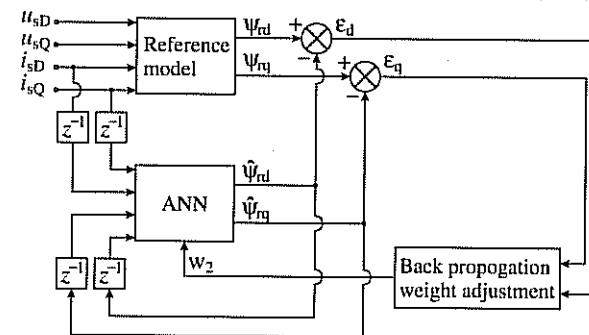


Fig. 4.79. MRAS-based rotor-speed estimator containing an ANN.

In these equations  $\hat{\psi}_{rd}$  and  $\hat{\psi}_{rq}$  are the rotor flux linkages estimated by the adaptive model, and they are also shown in Fig. 4.79. Equations (4.5-182) and (4.5-183) contain the rotor speed, which in general is changing, and it is our purpose to estimate this speed by using an ANN. For this purpose, eqns (4.5-182) and (4.5-183) can be implemented by a two-layer ANN which contains variable weights, and the variable weights are proportional to the rotor speed (a proof of this will also be given below).

For given stator voltages and currents and induction machine parameters, the actual rotor speed ( $\omega_r$ ) must be the same as the speed estimated by the ANN ( $\hat{\omega}_r$ ), when the outputs of the reference model and the adaptive model are equal. In this case the errors  $\varepsilon_d = \psi_{rd} - \hat{\psi}_{rd}$  and  $\varepsilon_q = \psi_{rq} - \hat{\psi}_{rq}$  are zero (these errors are also shown in Fig. 4.79).

When there is any mismatch between the rotor speed estimated by the ANN and the actual rotor speed, then these errors are not zero, and they are used to adjust the weights of the ANN (or in other words the estimated speed). The weight adjustment is performed in such a way that the error should converge fast to zero.

To obtain the required weight adjustments in the ANN, the sampled data forms of eqns (4.5-182) and (4.5-183) are considered. By using the backward difference method, e.g. by considering that the rate of change of an estimated rotor flux linkage can be expressed as

$$\frac{d\hat{\psi}_{rd}(t)}{dt} = \frac{\hat{\psi}_{rd}(k) - \hat{\psi}_{rd}(k-1)}{T}, \quad (4.5-184)$$

where  $T$  is the sampling time, the sampled data forms of the equations for the rotor flux linkages can be written as

$$\frac{\hat{\psi}_{rd}(k) - \hat{\psi}_{rd}(k-1)}{T} = -\frac{\hat{\psi}_{rd}(k-1)}{T_r} - \frac{\omega_r \hat{\psi}_{rq}(k-1)}{T} + \frac{L_m}{T_r} i_{sd}(k-1) \quad (4.5-185)$$

$$\frac{\hat{\psi}_{rq}(k) - \hat{\psi}_{rq}(k-1)}{T} = -\frac{\hat{\psi}_{rq}(k-1)}{T_r} + \frac{\omega_r \hat{\psi}_{rd}(k-1)}{T} + \frac{L_m}{T_r} i_{sq}(k-1). \quad (4.5-186)$$

Thus the rotor flux linkages at the  $k$ th sampling instant can be obtained from the previous  $(k-1)$ -th values as

$$\hat{\psi}_{rd}(k) = \hat{\psi}_{rd}(k-1) \left( 1 - \frac{T}{T_r} \right) - \omega_r T \hat{\psi}_{rq}(k-1) + \frac{L_m T}{T_r} i_{sd}(k-1) \quad (4.5-187)$$

$$\hat{\psi}_{rq}(k) = \hat{\psi}_{rq}(k-1) \left( 1 - \frac{T}{T_r} \right) + \omega_r T \hat{\psi}_{rd}(k-1) + \frac{L_m T}{T_r} i_{sq}(k-1). \quad (4.5-188)$$

By introducing  $c = T/T_r$  and assuming that the rotor time constant ( $T_r$ ) is constant, the following weights are introduced:

$$\begin{aligned} w_1 &= 1 - c \\ w_2 &= \omega_r c T_r = \omega_r T \\ w_3 &= c L_m. \end{aligned} \quad (4.5-189)$$

It can be seen that  $w_1$  and  $w_3$  are constant weights, but  $w_2$  is a variable weight, and is proportional to the speed. Thus equations (4.5-187) and (4.5-188) take the following forms:

$$\hat{\psi}_{rd}(k) = w_1 \hat{\psi}_{rd}(k-1) - w_2 \hat{\psi}_{rq}(k-1) + w_3 i_{sd}(k-1) \quad (4.5-190)$$

$$\hat{\psi}_{rq}(k) = w_1 \hat{\psi}_{rq}(k-1) + w_2 \hat{\psi}_{rd}(k-1) + w_3 i_{sq}(k-1). \quad (4.5-191)$$

These equations can be visualized by the very simple two-layer ANN shown in Fig. 4.80. This contains four input nodes. The input signals to these input nodes are the past values of the estimated rotor flux-linkage components expressed in the stationary reference frame  $[\hat{\psi}_{rd}(k-1), \hat{\psi}_{rq}(k-1)]$ , and also the past values of the stator current components expressed in the stationary reference frame  $[i_{sd}(k-1), i_{sq}(k-1)]$ . There are two output nodes which output the present values of the estimated rotor flux-linkage components  $[\hat{\psi}_{rd}(k), \hat{\psi}_{rq}(k)]$ . Thus all the nodes are well defined. The connections between the nodes are represented by weights (synapses), and a weight shows the strength of the connection considered. In general a weight can be positive or negative, corresponding to excitatory and inhibitory weights.

In the ANN shown in Fig. 4.80, the adaptive  $w_2$  weights are shown with thick solid lines and, as noted above, these are proportional to the speed ( $w_2 = \omega_r c T_r = \omega_r T$ ), where the proportionality factor is the sampling time. The adaptive weights are adjusted so that  $E = (1/2)\varepsilon^2(k)$  should be a minimum, where  $\varepsilon(k) = \psi_r(k) - \hat{\psi}_r(k)$ ,  $\psi_r(k) = [\psi_{rd}(k), \psi_{rq}(k)]^T$ ,  $\hat{\psi}_r(k) = [\hat{\psi}_{rd}(k), \hat{\psi}_{rq}(k)]^T$ . Thus the weight adjustments to give minimum squared error have to be proportional to the negative of the gradient of the error with respect to the weight,  $-\partial E / \partial w_2$ , since in this way it is possible to move progressively towards the optimum solution, where the squared error is minimal. The proportionality factor is the so-called learning rate,  $\eta$ , which is a positive constant, and larger learning rates yield larger changes in the weights. In practice as large a value is chosen for the learning rate as possible, since this gives the fastest learning, but a large learning rate can yield

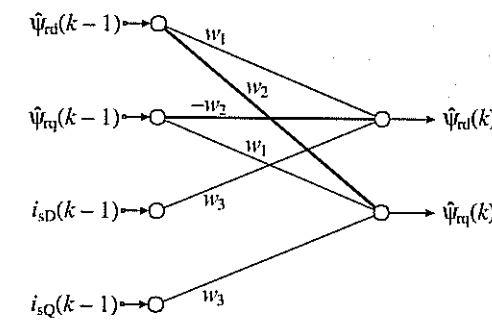


Fig. 4.80. ANN representation of estimated rotor flux linkages.

oscillations in the output of the ANN. It follows from the above that the mathematical expression for the weight adjustment has to be

$$\Delta w_2(k) = -\eta \frac{\partial E}{\partial w_2} \quad (4.5-192)$$

(see also Chapter 7). However, eqn (4.5-192) can be rewritten as follows

$$\Delta w_2(k) = -\eta \frac{\partial E}{\partial w_2} = -\eta \frac{\partial E}{\partial \hat{\Psi}_r(k)} \frac{\partial \hat{\Psi}_r(k)}{\partial w_2}. \quad (4.5-193)$$

Equation (4.5-193) is now expanded. By using the definition of  $E$ , the term  $\partial E / \partial \hat{\Psi}_r(k)$ , which is present on the right-hand side of eqn (4.5-193), can be expressed as

$$\frac{\partial E}{\partial \hat{\Psi}_r(k)} = \frac{1}{2} \frac{\partial [e^2(k)]}{\partial \hat{\Psi}_r(k)} = \frac{1}{2} \frac{\partial \{[\psi_r(k) - \hat{\psi}_r(k)]^2\}}{\partial \hat{\Psi}_r(k)} = -e^T(k). \quad (4.5-194)$$

Furthermore, the other term  $\partial \hat{\Psi}_r(k) / \partial w_2$  which is present in eqn (4.5-193) can be expanded as follows:

$$\frac{\partial \hat{\Psi}_r(k)}{\partial w_2} = [-\hat{\psi}_{rq}(k-1), \hat{\psi}_{rd}(k-1)]^T. \quad (4.5-195)$$

This follows directly from Fig. 4.80 or by considering eqns (4.5-190) and (4.5-191). Thus the substitution of eqns (4.5-194) and (4.5-195) into eqn (4.5-193) gives the following expression, if  $e(k) = [e_d(k), e_q(k)]^T$  is also considered:

$$\begin{aligned} \Delta w_2(k) &= -\eta \frac{\partial E}{\partial w_2} = \eta e^T(k) [-\hat{\psi}_{rq}(k-1), \hat{\psi}_{rd}(k-1)]^T \\ &= \eta [-e_d(k)\hat{\psi}_{rq}(k-1) + e_q(k)\hat{\psi}_{rd}(k-1)], \end{aligned} \quad (4.5-196)$$

where  $e_d(k) = \psi_{rd}(k) - \hat{\psi}_{rd}(k)$  and  $e_q(k) = \psi_{rq}(k) - \hat{\psi}_{rq}(k)$ . Equation (4.5-196) is a well-known type of expression in neural networks using the method of steepest gradient for weight adjustment (see also Chapter 7), and it can be seen that the appropriate errors are multiplied by the appropriate inputs of the neural network shown in Fig. 4.80. When the expressions for the errors ( $e_d, e_q$ ) are substituted into eqn (4.5-196), it follows that

$$\Delta w_2(k) = \eta \{ -[\psi_{rd}(k) - \hat{\psi}_{rd}(k)]\hat{\psi}_{rq}(k-1) + [\psi_{rq}(k) - \hat{\psi}_{rq}(k)]\hat{\psi}_{rd}(k-1) \} \quad (4.5-197)$$

is obtained. Thus in Fig. 4.80 the weight adjustments can be obtained from

$$\begin{aligned} w_2(k) &= w_2(k-1) + \Delta w_2(k) \\ &= w_2(k-1) + \eta \{ -[\psi_{rd}(k) - \hat{\psi}_{rd}(k)]\hat{\psi}_{rq}(k-1) \\ &\quad + [\psi_{rq}(k) - \hat{\psi}_{rq}(k)]\hat{\psi}_{rd}(k-1) \}. \end{aligned} \quad (4.5-198)$$

It has been discussed above that for rapid learning, the learning rate ( $\eta$ ) has to be selected to be large, but this can lead to oscillations in the outputs of the ANN. However, to overcome this difficulty, a so-called momentum term is added to eqn (4.5-198), which takes into account the past [( $k-1$ )-th] weight changes on the present [ $k$ th] weight. This ensures accelerated convergence of the algorithm (see also Chapter 7). Thus the current weight adjustment  $\Delta w_2(k)$  described by eqn (4.5-198) is supplemented by a fraction of the most recent weight adjustment,  $\Delta w_2(k-1)$ :

$$\begin{aligned} w_2(k) &= w_2(k-1) + \Delta w_2(k) + \alpha \Delta w_2(k-1) \\ &= w_2(k-1) + \eta \{ -[\psi_{rd}(k) - \hat{\psi}_{rd}(k)]\hat{\psi}_{rq}(k-1) \\ &\quad + [\psi_{rq}(k) - \hat{\psi}_{rq}(k)]\hat{\psi}_{rd}(k-1) \} + \alpha \Delta w_2(k-1), \end{aligned} \quad (4.5-199)$$

where  $\alpha$  is a positive constant called the momentum constant. The term  $\alpha \Delta w_2(k-1)$  is called the momentum term, and is a scaled value of the most recent weight adjustment. Usually  $\alpha$  is in the range between 0.1 and 0.8. The inclusion of the momentum term into the weight adjustment mechanism can significantly increase the convergence, which is extremely useful when the ANN shown in Fig. 4.80 is used to estimate in real-time the speed of the induction machine. Since it follows from eqn (4.5-189) that the weight  $w_2$  is proportional to the speed,  $w_2 = \omega_r T$ , finally the estimated rotor speed can be obtained from

$$\begin{aligned} \hat{\omega}_r(k) &= \hat{\omega}_r(k-1) + \frac{\Delta w_2(k)}{T} + \frac{\alpha}{T} \Delta w_2(k-1) \\ &= \hat{\omega}_r(k-1) + \frac{\eta}{T} \{ -[\psi_{rd}(k) - \hat{\psi}_{rd}(k)]\hat{\psi}_{rq}(k-1) \\ &\quad + [\psi_{rq}(k) - \hat{\psi}_{rq}(k)]\hat{\psi}_{rd}(k-1) \} + \frac{\alpha}{T} \Delta w_2(k-1). \end{aligned} \quad (4.5-200)$$

The simple structure of the ANN shown in Fig. 4.80 has various advantages. In a multi-layer feedforward neural network, which contains one or several hidden layers, and which uses the back-propagation algorithm (see Section 4.5.3.6.2), a supervised (off-line) training stage is required before the ANN can be used. This is usually a slow process. In contrast to this, the simple two-layer ANN shown above does not require a separate learning stage, since the learning takes place during the on-line speed estimation process. However, the multi-layer feedforward ANN with hidden layers can give more accurate speed estimates, especially at low speeds. It should be noted that it has been assumed above that  $T_r = \text{constant}$ , but in practice this is not a valid assumption and as a result incorrect speed can be estimated. Furthermore, the reference model has used open-loop integration, but this can be avoided by using other techniques developed earlier (see Sections 3.1.3.2, 4.1.1.4, 4.5.3.4).

It is also possible to implement other algorithms, where the error is not obtained from the respective rotor flux linkages, but it is an error between other

quantities which can also be obtained from the terminal voltages and currents of the induction machine, and e.g. which do not depend on the stator resistance (see various schemes in Section 4.5.3.4). The application of such algorithms can lead to improved speed estimation in the low-speed region, but in general, more accurate estimation can be achieved by using the technique discussed in the following section.

#### 4.5.3.6.2 Multi-layer feedforward ANN: speed is an output quantity

In addition to the speed estimation scheme shown in Fig. 4.79, which resembles a classical MRAS estimator (but the adaptive model is an ANN), it is also possible to use other ANN-based speed estimators for an induction machine, which are not related to a MRAS estimator. Such a system can use various types of learning techniques, some of which can be fuzzy-assisted. However, it is also possible to use fuzzy-neural networks for this purpose and an appropriate design can be made to be robust to noise and parameter variations, even at extremely low speeds. It is expected that such solutions will also appear in commercial drive applications in the future.

For example, as shown in Section 7.3.2.2, it is possible to use a multi-layer feedforward ANN speed estimator for an induction machine, which has four layers: an input layer, two hidden layers, and an output layer. The inputs to the ANN are the stator voltages and stator currents:  $u_{sD}(k)$ ,  $u_{sD}(k-1)$ ,  $u_{sQ}(k)$ ,  $u_{sQ}(k-1)$ ,  $i_{sD}(k)$ ,  $i_{sD}(k-1)$ ,  $i_{sQ}(k)$ ,  $i_{sQ}(k-1)$  and the output is the rotor speed,  $\omega_r(k)$ . The activation functions used in the hidden layers can be, for example, tansigmoid functions. In Section 7.3.2.2.1 two ANNs are considered for the speed estimation of a specific induction machine; they have 8-9-7-1 structure (there are eight input nodes, nine hidden nodes in the first hidden layer, seven hidden nodes in the second hidden layer, and a single output node) and 8-8-6-1 structure. It should be noted that other induction machines may require other ANN structures. In Section 7.3.2.2.2 a much more complex ANN with the structure 8-12-10-4 is applied, since it was the goal to obtain on its outputs four quantities: the rotor speed, the electromagnetic torque, and the direct- and quadrature-axis stator flux linkages in the stationary reference frame ( $\psi_{sD}$ ,  $\psi_{sQ}$ ). In Section 7.3.2.2.3 the details of an ANN speed estimator used in a voltage-source inverter-fed induction motor drive employing rotor-flux-oriented control are given, and for this purpose various ANN structures (8-15-13-1), (9-9-8-1) and (5-12-11-1) are considered. It is shown that the rotor speed estimation can be obtained when, instead of using an ANN with 8 inputs, there are 9 inputs, where a past rotor speed value,  $\omega_r(k-1)$ , is also present at the inputs.

It is believed that the ANNs discussed in the present section can be used in various torque-controlled induction motor drives. Different artificial-intelligence-based approaches for fully digital DSP-controlled speed-sensorless drives are under investigation by the research group (Intelligent Motion Control Group) of the author at Aberdeen University (see also Chapter 7).

## 4.6 Direct torque control (DTC) of induction machines

### 4.6.1 GENERAL INTRODUCTION

High-dynamic-performance instantaneous electromagnetic-torque-controlled induction motor (and other a.c. motor) drives have been used for more than 20 years. Based on the pioneering works of Blaschke, Hasse, and Leonhard, vector-controlled drives have become increasingly popular, and have become the standard in the drives industry. The most significant industrial contributions in this field have been made by Siemens. Direct-torque-controlled induction motor drives were developed more than 10 years ago by Depenbrock [Depenbrock 1985] and Takahashi [Takahashi and Noguchi 1985]. However, at present, ABB is the only industrial company who have introduced (in 1995) a commercially available direct-torque-controlled induction motor drive. This is a significant industrial contribution, and in numerous papers by ABB it has been claimed that ‘direct torque control’ is the latest a.c. motor control method developed by ABB (e.g. see [Tiitinen 1996]).

In the present section, the general and fundamental aspects of the direct torque control of induction machines is examined in great detail by using both mathematical and physical analyses of the processes involved. Torque and flux estimation, optimum switching-vector selection, reduction of torque and flux ripples, field weakening, speed-sensorless implementations, and predictive schemes are also discussed in great detail. Some aspects of direct torque control have also been discussed in Sections 1.2.2 and 3.3.

### 4.6.2 DTC OF A VSI-FED INDUCTION MOTOR

#### 4.6.2.1 General, mathematical, and physical fundamentals of producing fast torque response

In a direct-torque-controlled (DTC) induction motor drive, supplied by a voltage source inverter, it is possible to control directly the stator flux linkage (or rotor flux linkage, or magnetizing flux linkage) and the electromagnetic torque by the selection of optimum inverter switching modes. The selection is made to restrict the flux and torque errors within respective flux and torque hysteresis bands, to obtain fast torque response, low inverter switching frequency, and low harmonic losses. In the present section such a DTC drive will be described in which, in addition to controlling the electromagnetic torque, the controlled flux linkage is the stator flux linkage. However, it should be noted that it is possible to have other implementations in which the rotor flux linkage or the magnetizing flux linkage is controlled. DTC allows very fast torque responses and flexible control of an induction machine. Due to the importance of DTC drives, and also due to the great interest in these types of drives, and also since it is expected that various DTC drives will emerge in the future, for better understanding a very detailed description will be given below.

In general, in a symmetrical three-phase induction machine, the instantaneous electromagnetic torque is proportional to the cross-vectorial product of the stator flux-linkage space vector and the stator-current space vector,

$$t_e = \frac{3}{2} P \bar{\psi}_s \times \bar{i}_s, \quad (4.6-1)$$

where  $\bar{\psi}_s$  is the stator flux-linkage space vector and  $\bar{i}_s$  is the stator-current space vector. In eqn (4.6-1), both space vectors are expressed in the stationary reference frames. By considering that  $\bar{\psi}_s = |\bar{\psi}_s| \exp(j\rho_s)$ , where  $\rho_s$  is the angle of the stator flux-linkage space vector with respect to the direct-axis of the stator reference frame (see Fig. 4.81), and  $\bar{i}_s = |\bar{i}_s| \exp(j\alpha_s)$  (see Fig. 4.81), it is possible to put eqn (4.6-1) into the following form:

$$t_e = \frac{3}{2} P |\bar{\psi}_s| |\bar{i}_s| \sin(\alpha_s - \rho_s) = \frac{3}{2} P |\bar{\psi}_s| |\bar{i}_s| \sin \alpha, \quad (4.6-2)$$

where  $\alpha = \alpha_s - \rho_s$  is the angle between the stator flux-linkage and stator-current space vector.

It can be shown by using the voltage equations of the induction machine that, for a given value of the rotor speed, if the modulus of the stator flux-linkage space vector is kept constant and the angle  $\rho_s$  is changed quickly, then the electromagnetic torque can be rapidly changed. The mathematical proof is now briefly discussed, but it should be noted that a much simpler proof will also be presented below, which gives a very clear physical description of the processes involved.

For the purposes of the mathematical proof, the electromagnetic torque response of the machine for a step change in  $\rho_s$  at  $t=0$  is now derived. Therefore the time variation of the electromagnetic torque must be determined. For this purpose, first the rotor-current space vector (formulated in the stationary reference frame) is expressed in terms of the stator flux-linkage space vector,  $\bar{i}'_r = (\bar{\psi}_s - L_s \bar{i}_s)/L_m$ , and also the rotor flux-linkage space vector is expressed in terms of the stator flux-linkage space vector by using  $\bar{\psi}'_r = L_r \bar{i}'_r + L_m \bar{i}_s$ , where  $\bar{i}'_r = (\bar{\psi}_s - L_s \bar{i}_s)/L_m$ , thus  $\bar{\psi}'_r = (L_r/L_m)(\bar{\psi}_s - L_s \bar{i}_s)$ . The thus-obtained expressions for

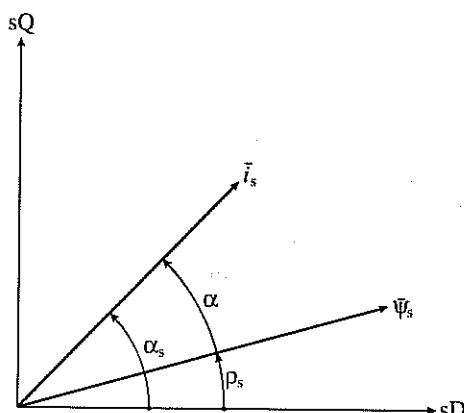


Fig. 4.81. Stator flux-linkage and stator current space vectors.

$\bar{i}'_r$  and  $\bar{\psi}'_r$  are substituted into the rotor voltage equation expressed in the stationary reference frame (which is obtained from eqn (2.1-125) as  $0 = R_r \bar{i}'_r + d\bar{\psi}'_r/dt - j\omega_r \bar{\psi}'_r$ ). The derived rotor voltage equation contains  $\bar{i}_s$  and  $\bar{\psi}_s$ , and this can be used to express the stator-current space vector in terms of the stator flux-linkage space vector. This expression for the stator-current space vector is then substituted into eqn (4.6-1). However, by also utilizing in this expression the fact that the stator flux-linkage space vector modulus is constant ( $|\bar{\psi}_s| = c_1$ ), thus  $\bar{\psi}_s = |\bar{\psi}_s| \exp(j\rho_s) = c_1 \exp(j\rho_s)$  and therefore  $d\bar{\psi}_s/dt = j|\bar{\psi}_s| d\rho_s/dt$ , finally it is possible to obtain an equation for the electromagnetic torque whose inverse Laplace transform gives the required temporal variation of the electromagnetic torque. An examination of this expression shows that for constant  $|\bar{\psi}_s|$ , the rate of change of the increasing electromagnetic torque is almost proportional to the rate of change of  $\rho_s$ . Thus by forcing the largest  $d\rho_s/dt$  under the condition of constant stator flux-linkage modulus, the fastest (minimum) electromagnetic torque response time is obtained.

In other words, if such stator voltages are imposed on the motor, which keep the stator flux constant (at the demanded value), but which quickly rotate the stator flux-linkage space vector into the position required (by the torque demand), then fast torque control is performed. It follows that if in the DTC induction motor drive, the developed actual electromagnetic torque of the machine is smaller than its reference value, the electromagnetic torque should be increased as fast as possible by using the fastest  $d\rho_s/dt$ . However, when the electromagnetic torque is equal to its reference value, the rotation is stopped. If the stator flux-linkage space vector is accelerated in the forward direction, then positive electromagnetic torque is produced, and when it is decelerated backwards, negative electromagnetic torque is produced. However, the stator flux-linkage vector can be adjusted by using the appropriate stator-voltage space vector, which is generated by the VSI inverter which supplies the induction machine (see details of voltage generation below). To summarize: the electromagnetic torque can be quickly changed by controlling the stator flux-linkage space vector, which, however, can be changed by using the appropriate stator voltages (generated by the inverter which supplies the induction motor). It can be seen that there is direct stator-flux and electromagnetic torque control achieved by using the appropriate stator voltages. This is why this type of control is usually referred to as direct torque control.

It is very useful to consider another form of the expression for the instantaneous electromagnetic torque, which gives an extremely clear physical picture of the processes involved but leads to the same results as shown above. By considering that  $\bar{\psi}_s = L_s \bar{i}_s + L_m \bar{i}'_r$  and  $\bar{\psi}'_r = L_r \bar{i}'_r + L_m \bar{i}_s$ , where again the primed rotor quantities are expressed in the stationary reference frame, it follows that  $\bar{i}_s = \bar{\psi}_s / L'_s - [L_m / (L_r L'_s)] \bar{\psi}'_r$ ; thus eqn (4.6-1) takes the following form:

$$\begin{aligned} t_e &= \frac{3}{2} P \frac{L_m}{L'_s L_r} \bar{\psi}'_r \times \bar{\psi}_s = \frac{3}{2} P \frac{L_m}{L'_s L_r} |\bar{\psi}'_r| |\bar{\psi}_s| \sin(\rho_s - \rho_r) \\ &= \frac{3}{2} P \frac{L_m}{L'_s L_r} |\bar{\psi}'_r| |\bar{\psi}_s| \sin \gamma. \end{aligned} \quad (4.6-3)$$

In eqn (4.6-3)  $\gamma$  is the angle between the stator and rotor flux-linkage space vectors,  $\gamma = \rho_s - \rho_r$ , where  $\rho_r$  is the angle of the rotor flux-linkage space vector with respect to the real-axis of the stationary reference frame, as shown in Fig. 4.82.

The rotor time constant of a standard squirrel-cage induction machine is large (e.g. a typical value is greater than 0.1 s, but it should be noted that for larger machines this is much larger); thus the rotor flux linkage changes only slowly compared to the stator flux linkage. It can be assumed to be constant. This also follows from the rotor voltage equation of the induction machine if the stator flux linkage is assumed to be constant. However, if the stator and rotor flux linkages are assumed to be constant, it follows from eqn (4.6-3) that the electromagnetic torque can be rapidly changed by changing  $\gamma$  in the required direction (which is determined by the torque command). This is the essence of direct torque control. However, as discussed below, the angle  $\gamma$  can be easily changed by switching on the appropriate stator-voltage space vector (produced by the appropriate inverter voltage). If the modulus of the stator flux-linkage space vector is not constant (e.g. in the field-weakening range), then it still possible to control both the angle  $\gamma$  and  $|\bar{\psi}_s|$  by switching on the appropriate inverter voltage.

In contrast to a vector-controlled induction motor drive, where the stator currents are used as control quantities, in the direct-torque-controlled drive, the stator flux linkages are controlled. It should be noted that if  $|\bar{\psi}_r| = \text{constant}$ , then it follows from eqn (2.1-191) that

$$t_e = \frac{3}{2} P \frac{L_r}{L_m} |\bar{\psi}_r| i_{sy},$$

where  $i_{sy}$  is the torque-producing stator current (quadrature-axis stator current in the rotor-flux-oriented reference frame whose axes are denoted by  $x$  and  $y$  respectively in Fig. 4.82), and the electromagnetic torque can be quickly changed

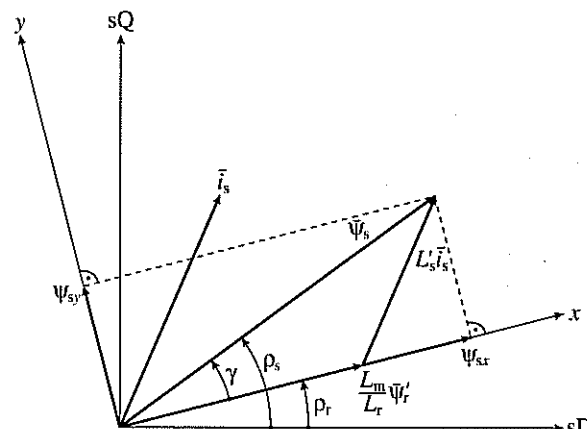


Fig. 4.82. Stator flux-linkage, rotor flux-linkage, and stator-current space vectors.

by quickly changing  $i_{sy}$ . In a vector-controlled drive, the stator currents are the controlled quantities ( $i_{sy}$  controls the torque and  $i_{sx}$  controls the rotor flux). This is one of the reasons why, in a vector-controlled drive employing rotor-flux-oriented control, the stator currents expressed in the stationary reference frame must be transformed into the stator currents in the rotor-flux-oriented reference frame. However, it follows from Fig. 4.82 [or eqn (4.6-3)] that  $|\bar{\psi}_s| \sin \gamma = \psi_{sy}$  is the torque-producing stator flux-linkage component and  $\psi_{sx}$  is collinear with the rotor flux. Thus the flux is controlled by the direct-axis stator flux and the torque is controlled by the quadrature-axis stator flux and again it can be seen that, in contrast to vector control, now the flux-linkage components are the control quantities. Equation (4.6-3) is similar to that of a synchronous machine, where the electromagnetic torque is controlled by the load angle between the stator and rotor flux linkages. During a short transient, the rotor flux is almost unchanged, thus rapid changes of the electromagnetic torque can be produced by rotating the stator flux in the forward direction (phase advancing) or by rotating it in the negative direction (retarding), or by stopping it, according to the demanded torque. In summary: in the direct-torque-controlled drive rapid instantaneous torque control can be achieved by quickly changing the position of the stator flux-linkage space vector (relative to the rotor flux-linkage space vector), or in other words, by quickly changing its speed (speed of the stator flux-linkage space vector). However, the stator flux-linkage space vector (both its modulus and its angle) can be changed by the stator voltages.

If for simplicity it is assumed that the stator ohmic drops can be neglected, then  $d\bar{\psi}_s/dt = \bar{u}_s$ , and it can be seen that the inverter voltage ( $\bar{u}_s = \bar{u}_i$ ) directly impresses the stator flux, and thus the required stator-flux locus will be obtained by using the appropriate inverter voltages (obtained by using the appropriate inverter switching states). For better understanding this is now discussed in detail. It follows from  $d\bar{\psi}_s/dt = \bar{u}_s$  that in a short  $\Delta t$  time, when the voltage vector is applied,  $\Delta \bar{\psi}_s = \bar{u}_s \Delta t$ . Thus the stator flux-linkage space vector moves by  $\Delta \bar{\psi}_s$  in the direction of the stator-voltage space vector at a speed which is proportional to the magnitude of the stator-voltage space vector (which is proportional to the d.c. link voltage). By selecting step-by-step the appropriate stator voltage vector, it is then possible to change the stator flux in the required way. Decoupled control of the torque and stator flux is achieved by acting on the radial and tangential components of the stator flux-linkage space vector in the locus. These two components are directly proportional (stator ohmic drop was neglected) to the components of the stator-voltage space vector in the same directions, and thus they can be controlled by the appropriate inverter switchings. It should be emphasized that for torque production, the angle  $\gamma$  plays a vital role, or in other words, the relative position of the stator and rotor flux-linkage space vectors determines the electromagnetic torque. By assuming a slow motion of the rotor flux-linkage space vector, if a stator-voltage space vector is applied, which causes a quick movement of the stator flux-linkage space vector away from the rotor flux linkage, then the electromagnetic torque will increase since the angle  $\gamma$  is increased. However, if a voltage space vector is applied (a zero-voltage space

vector, see below) which almost stops the rotation of the stator flux-linkage space vector, then the electromagnetic torque will decrease, since the rotor flux-linkage space vector is still moving and the angle  $\gamma$  decreases. If the duration of the zero-voltage space vector is sufficiently long, then since the stator flux-linkage space vector will almost not move (in practice it will move slightly due to the stator ohmic voltage drop), then the rotor flux-linkage space vector will overtake the stator flux-linkage space vector, the angle  $\gamma$  will change its sign, the electromagnetic torque will change its direction.

By considering the six-pulse VSI shown in Fig. 4.83(a), there are six non-zero active voltage-switching space vectors ( $\bar{u}_1, \bar{u}_2, \dots, \bar{u}_6$ ) and two zero space vectors ( $\bar{u}_7, \bar{u}_8$ ). These are shown in Fig. 4.83(c), and Fig. 4.83(b) shows the corresponding eight switching states. The six active inverter-switching vectors can be expressed as

$$\bar{u}_s = \bar{u}_k = \frac{2}{3} U_d \exp[j(k-1)\pi/3] \quad k=1, 2, \dots, 6, \quad (4.6-4)$$

where  $U_d$  is the d.c. link voltage (see also the book on space-vector theory [Vas 1992]). However, for  $k=7, 8$ ,  $\bar{u}_k=0$  holds for the two zero switching states where the stator windings are short-circuited,  $\bar{u}_s=\bar{u}_k=0$ . It follows from the definition of the switching vectors given above that since  $\bar{u}_s=u_{sD}+ju_{sQ}$ ,  $\bar{u}_1$  is aligned with the real axis ( $sD$ ) of the stationary reference frame, and this definition is used in Europe. It should be noted that in the USA, usually the quadrature-axis of the stator reference frame is aligned with  $\bar{u}_1$ , which means that all switching vectors would be displaced by  $90^\circ$  in the positive direction with respect to the switching vectors defined above.

Since  $\Delta\bar{\psi}_s = \bar{u}_s \Delta t$ , it can be seen that the stator flux-linkage space vector will move fast if non-zero (active) switching vectors are applied, for a zero switching vector it will almost stop (it will move very slowly due to the small ohmic voltage drop). For a six-pulse VSI, the stator flux linkage moves along a hexagonal path with constant linear speed, due to the six switching vectors. For a sinusoidal PWM (where the inverter switching states are chosen to give stator flux-linkage variations which are almost sinusoidal), a suitable sequence of the zero and active (non-zero) switching vectors is applied to obtain the required flux-linkage locus. In the DTC drive, at every sampling period, the switching vectors are selected on the basis of keeping the stator flux-linkage errors in a required tolerance band (hysteresis band), and keeping the torque error in the hysteresis band. It is assumed that the widths of these hysteresis bands are  $2\Delta\bar{\psi}_s$  and  $2\Delta t_e$  respectively. (The factor 2 appears in this definition since it is assumed that e.g. for the stator flux linkage, the upper limit value is above the reference value by  $\Delta\bar{\psi}_s$ , and the lower limit value is below the reference value by  $\Delta\bar{\psi}_s$ , thus the width of the hysteresis band is indeed  $2\Delta\bar{\psi}_s$ ). If the stator flux-linkage space vector lies in the  $k$ th sector, where  $k=1, 2, \dots, 6$ , its magnitude can be increased by using the switching vectors  $\bar{u}_k, \bar{u}_{k+1}, \bar{u}_{k-1}$ ; however, its magnitude can be decreased by selecting  $\bar{u}_{k+2}, \bar{u}_{k-2}$  and  $\bar{u}_{k+3}$ . Obviously the selected voltage switching vectors affect the electromagnetic torque as well. The speed of the stator flux-linkage

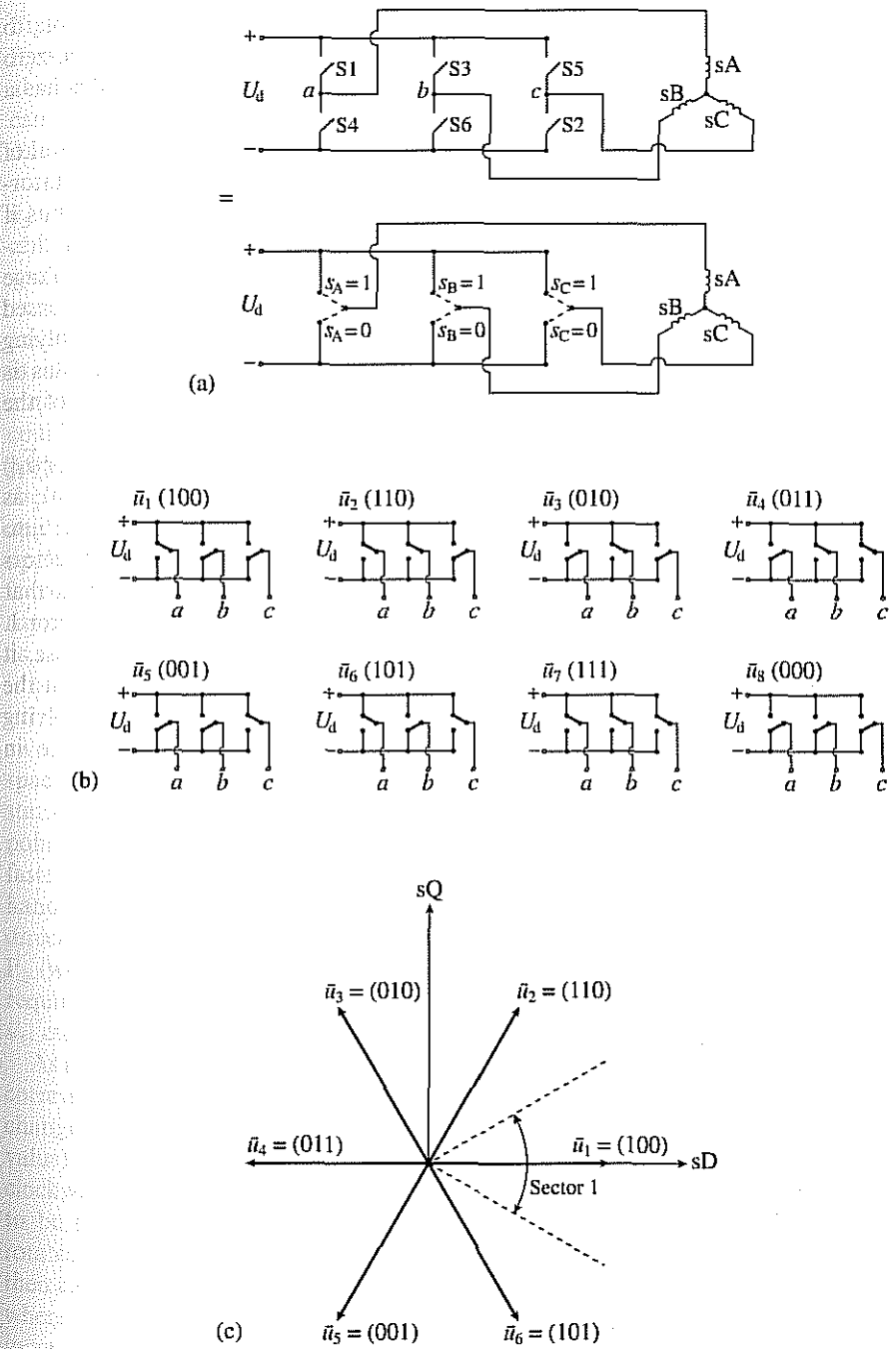


Fig. 4.83. Schematic of PWM VSI inverter, the eight switching states and the corresponding switching space vectors. (a) PWM VSI; (b) switching stages; (c) switching-voltage space vectors.

space vector is zero if a zero switching vector is selected, and it is possible to change this speed by changing the output ratio between the zero and non-zero voltage vectors. It is important to note that the duration of the zero states has a direct effect on the electromagnetic torque oscillations.

As shown above, the stator flux-linkage space vector is basically the integral of the stator-voltage space vector and it will move in the direction of the stator-voltage space vector for as long as the voltage space vector is applied. Thus if a reduced stator flux-linkage space-vector modulus is required, the stator flux-linkage space-vector modulus can be controlled by applying switching voltage vectors which are directed towards the centre of the rotor, and if an increased stator flux-linkage space-vector modulus is required, it is controlled by applying voltage vectors which are directed out from the centre of the rotor. This is illustrated in the example of Fig. 4.84, where  $|\bar{\psi}_{sref}|$  is the reference value of the stator flux-linkage space vector.

It is our goal to keep the modulus of the stator flux-linkage space vector ( $|\bar{\psi}_s|$ ) within the hysteresis band (denoted by the two circles), whose width is  $2\Delta\psi_s$  as shown in Fig. 4.84. The locus of the flux-linkage space vector is divided into several sectors, and due to the six-step inverter, the minimum number of sectors required is six. The six sectors are also shown in Fig. 4.84. It is assumed that initially the stator flux-linkage space vector is at position  $P_0$ , thus is in sector 1. Assuming that the stator flux-linkage space vector is rotating anticlockwise, it follows that since at position  $P_0$  the stator flux-linkage space-vector flux is at the upper limit ( $|\bar{\psi}_{sref}| + \Delta\psi_s$ ), it must be reduced. This can be achieved by applying the suitable switching vector, which is the switching vector  $\bar{u}_3$ , as shown in

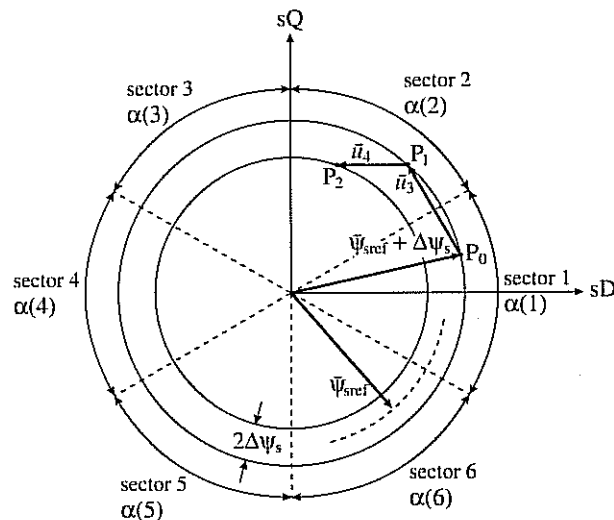


Fig. 4.84. Control of the stator flux-linkage space vector: stator flux-linkage space-vector locus [stator flux variations ( $\Delta\psi_s$ )], and inverter switching vectors.

Fig. 4.84. Thus the stator flux-linkage space vector will move rapidly from point  $P_0$  to point  $P_1$ , and it can be seen that point  $P_1$  is in sector 2. As mentioned above, altogether there are six  $60^\circ$ -wide sectors (due to the six-step inverter). It can also be seen that at point  $P_1$  the stator flux-linkage space vector is again at its upper limit. On the other hand, it should be noted that if the stator flux space vector moves in the clockwise direction from point  $P_0$ , then the switching vector  $\bar{u}_5$  would have to be selected, since this would ensure the required rotation and also the required flux decrease. Since at point  $P_1$ , the stator flux-linkage space vector again reaches the upper limit, it has again to be reduced when it is rotated anticlockwise, hence for this purpose the switching vector  $\bar{u}_4$  has to be selected, and then  $\bar{\psi}_s$  moves from point  $P_1$  to point  $P_2$  as shown in Fig. 4.84, which is also in sector 2. It should be noted that if, for example, at point  $P_1$  a quick anticlockwise rotation is required, then it can be seen that the quickest rotation could be achieved by applying the switching vector  $\bar{u}_6$ . On the other hand, if at point  $P_1$  the rotation of the stator flux-linkage space vector has to be stopped, then a zero switching vector would have to be applied, so either  $\bar{u}_7$  or  $\bar{u}_8$  can be applied. However, since prior to this the last switching was performed by the application of the switching vector  $\bar{u}_3 = \bar{u}_3(010)$ , which means that the first switch is connected to the (lower) negative d.c. rail, the second switch is connected to the (upper) positive d.c. rail, and the third switch is connected to the negative d.c. rail as shown in Fig. 4.83(b), to minimize the number of switchings, the state  $\bar{u}_8(000)$  is selected, since this requires only switching of the second switch (from 1 to 0), in contrast to selecting  $\bar{u}_7(111)$ , which would require two switchings (of the first switch from 0 to 1 and of the third switch from 0 to 1). If the stator flux-linkage space vector is at point  $P_2$ , then the lower limit ( $|\bar{\psi}_{sref}| - \Delta\psi_s$ ) is reached and the stator flux-linkage space vector can be rotated in the anticlockwise direction to point  $P_3$  by increasing it, and for this purpose the switching vector  $\bar{u}_3$  gives the fastest rotation. It can be seen that point  $P_3$  is still in sector 2. If on the other hand, the flux-linkage space vector has to be rotated from  $P_2$  in the opposite direction (clockwise), then by selecting the switching vector which rotates  $\bar{\psi}_s$  from  $P_2$  (where the flux-linkage space vector is at the lower limit, thus flux increase is required) in the fastest way in the clockwise direction gives the switching vector  $\bar{u}_1$ , etc.

As discussed above, stopping the rotation of the stator flux-linkage space vector corresponds to the case when the electromagnetic torque does not have to be changed (reference value of the electromagnetic torque is equal to its actual value). However, when the electromagnetic torque has to be changed (in the clockwise or anticlockwise direction) than the stator flux-linkage space vector has to be rotated in the appropriate direction. For example, when the stator flux rotates anticlockwise, and if an increase in the electromagnetic torque is required, then e.g. if the stator flux-linkage space vector is in the second sector at point  $P_1$  where the flux linkage has to be decreased, then the electromagnetic torque increase can be achieved by applying switching vector  $\bar{u}_4$ . On the other hand, if the stator flux-linkage space vector is in the second sector, but a torque decrease is required, but the flux-linkage has to be increased, then this can be achieved by

applying the switching vector  $\bar{u}_1$ , since this moves the stator flux-linkage space vector in the clockwise direction (which is the direction for the negative torque), and also increases the stator flux linkage. If the stator flux-linkage space vector is in the second sector and a torque decrease is required, but the stator flux linkage has to be decreased, then switching vector  $\bar{u}_1$  has to be applied, etc. Figure 4.85 shows the position of the various stator flux-linkage vectors if the stator flux-linkage space vector is in one of the six sectors. It is also shown which switching vector has to be selected to obtain the required increase or decrease of the stator flux linkage and the required increase or decrease of the electromagnetic torque (by creating positive or negative torques).

It can be seen that, in general, if an increase of the torque is required, then the torque is controlled by applying voltage vectors that advance the flux-linkage space vector in the direction of rotation and if a decrease is required, voltage vectors are applied which oppose the direction of the torque. If zero torque is required then that zero switching vector is applied ( $\bar{u}_7$  or  $\bar{u}_8$ ), which minimizes

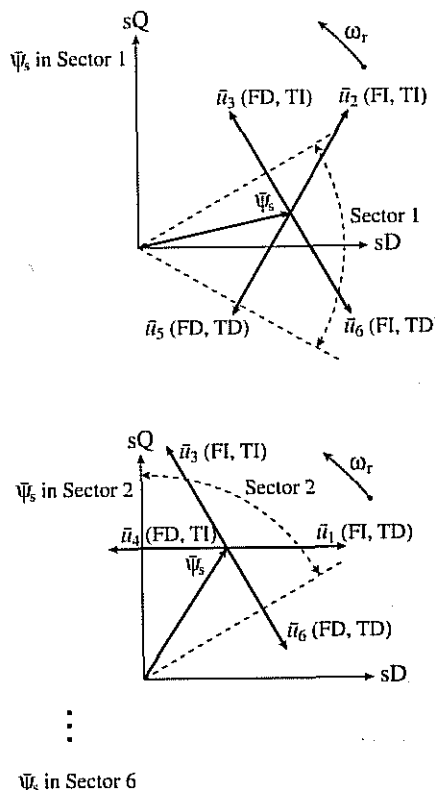


Fig. 4.85. Position of various stator flux-linkage space vectors, and selection of the optimum switching voltage vectors. FI: flux increase; FD: flux decrease; TI: torque increase; TD: torque decrease.

the inverter switching. It follows that the angle of the stator-voltage space vector is indirectly controlled through the flux vector modulus and torque, and increasing torque causes an increased angle. The torque demand is reduced to a choice of increase (positive torque), decrease (negative torque), or zero. Similarly, the stator flux-linkage vector modulus is limited to a choice of increase (flux increase) or decrease.

#### 4.6.2.2 Optimum switching vector selection (drive with non-predictive switching vector selection)

The results obtained in the previous section can be tabulated in the so-called optimum switching vector selection table shown in Table 4.3. This gives the optimum selection of the switching vectors for all the possible stator flux-linkage space-vector positions [six positions, corresponding to the six sectors shown in Fig. 4.84, where sector 1 is in the range of  $\alpha(1)$ , sector 2 is in the range of  $\alpha(2), \dots$ , sector 6 is in the range of  $\alpha(6)$ ] and the desired control inputs (which are the reference values of the stator flux-linkage modulus and the electromagnetic torque respectively). If a stator flux increase is required then  $d\psi = 1$ ; if a stator flux-linkage decrease is required  $d\psi = 0$ . The notation corresponds to the fact that the digital output signals of a two-level flux hysteresis comparator are  $d\psi$ , where

$$d\psi = 1 \text{ if } |\bar{\psi}_s| \leq |\bar{\psi}_{sref}| - |\Delta\psi_s|$$

$$d\psi = 0 \text{ if } |\bar{\psi}_s| \geq |\bar{\psi}_{sref}| + |\Delta\psi_s|.$$

If a torque increase is required then  $dt_e = 1$ , if a torque decrease is required then  $dt_e = -1$ , and if no change in the torque is required then  $dt_e = 0$ . The notation corresponds to the fact that the digital output signals of a three-level hysteresis comparator are  $dt_e$ , where for anticlockwise rotation (forward rotation)

$$dt_e = 1 \text{ if } |t_e| \leq |t_{eref}| - |\Delta t_e|$$

$$dt_e = 0 \text{ if } t_e \geq t_{eref},$$

Table 4.3 Optimum voltage switching vector look-up table

$d\psi$	$dt_e$	$\alpha(1)$ sector 1	$\alpha(2)$ sector 2	$\alpha(3)$ sector 3	$\alpha(4)$ sector 4	$\alpha(5)$ sector 5	$\alpha(6)$ sector 6
1	1	$\bar{u}_2$	$\bar{u}_3$	$\bar{u}_4$	$\bar{u}_5$	$\bar{u}_6$	$\bar{u}_1$
	0	$\bar{u}_7$	$\bar{u}_8$	$\bar{u}_7$	$\bar{u}_8$	$\bar{u}_7$	$\bar{u}_8$
	-1	$\bar{u}_6$	$\bar{u}_1$	$\bar{u}_2$	$\bar{u}_3$	$\bar{u}_4$	$\bar{u}_5$
0	1	$\bar{u}_3$	$\bar{u}_4$	$\bar{u}_5$	$\bar{u}_6$	$\bar{u}_1$	$\bar{u}_2$
	0	$\bar{u}_8$	$\bar{u}_7$	$\bar{u}_8$	$\bar{u}_7$	$\bar{u}_8$	$\bar{u}_7$
	-1	$\bar{u}_5$	$\bar{u}_6$	$\bar{u}_1$	$\bar{u}_2$	$\bar{u}_3$	$\bar{u}_4$

Active switching vectors:  $\bar{u}_1(100)$ ;  $\bar{u}_2(110)$ ;  $\bar{u}_3(010)$ ;  $\bar{u}_4(011)$ ;  $\bar{u}_5(001)$ ;  $\bar{u}_6(101)$

Zero switching vectors:  $\bar{u}_7(111)$ ;  $\bar{u}_8(000)$ .

and for clockwise rotation (backward rotation)

$$\begin{aligned} dt_e &= -1 \quad \text{if } |t_e| \geq |t_{e\text{ref}}| + |\Delta t_e| \\ dt_e &= 0 \quad \text{if } t_e \leq t_{e\text{ref}}. \end{aligned}$$

The selection of the width of the hysteresis bands has important effects, a too-small value may have the effect of losing the control, e.g. the stator flux linkage may exceed the values required by the tolerance band (the width of which is  $2|\Delta\psi_s|$ ). The duration of the zero states directly influences the torque oscillations.

The optimum switching look-up table requires knowledge of the position of the stator flux-linkage space vector, since it must be known in which sector is the stator flux-linkage space vector. For this purpose the angles  $\alpha(1), \alpha(2), \dots, \alpha(6)$  shown in Fig. 4.84 are required. Since  $\bar{\psi}_s = |\bar{\psi}_s| \exp(j\rho_s) = \psi_{sD} + j\psi_{sQ}$ , the stator flux angle ( $\rho_s$ ) can be determined by using the estimated values of the direct- and quadrature-axis stator flux linkages in the stationary reference frame ( $\psi_{sD}, \psi_{sQ}$ ); thus

$$\rho_s = \tan^{-1}(\psi_{sQ}/\psi_{sD}). \quad (4.6-5)$$

Alternatively

$$\rho_s = \cos^{-1}(\psi_{sD}/|\bar{\psi}_s|) \quad (4.6-6)$$

can also be used, where  $|\bar{\psi}_s| = (\psi_{sD}^2 + \psi_{sQ}^2)^{1/2}$  or the expression

$$\rho_s = \sin^{-1}(\psi_{sQ}/|\bar{\psi}_s|) \quad (4.6-7)$$

can be used. The angle  $\rho_s$  can then be used to obtain the angles  $\alpha(1), \alpha(2)$ , etc. However, it is possible to eliminate the need for using trigonometric functions (e.g. the inverse tangent, or inverse sine or inverse cosine), since it is not the accurate position of the stator flux-linkage space vector which has to be known, but only the sector (number) in which the stator flux-linkage space vector is positioned. This information can be simply obtained by considering only the signs of the various stator flux-linkage components, and this allows a simple implementation which requires only the use of comparators. For this purpose it should be considered that e.g. in sector 1,  $\psi_{sD} > 0$ , but since in sector 1,  $\psi_{sQ}$  can be both positive and negative, the sign of  $\psi_{sQ}$  will not give any useful information on the position of the stator flux-linkage space vector in sector 1. However, instead of  $\psi_{sQ}$  it is possible to use the stator flux linkage in stator phase sB ( $\psi_{sB}$ ), and it follows from Fig. 4.86 that  $\psi_{sB} < 0$  if  $\bar{\psi}_s$  is in the first sector (at point P<sub>1</sub> in Fig. 4.86, where it has the value  $\bar{\psi}_{s1}$ ). Similarly if  $\bar{\psi}_s$  is in sector 2, then  $\psi_{sD} > 0$ ,  $\psi_{sQ} > 0$ , and  $\psi_{sB} > 0$ , etc. These results are summarized in Table 4.4.

It can be seen that the sign of  $\psi_{sQ}$  does not give useful information in sectors 1 and 4, since in both of these sectors this sign can be both positive (+) and negative (-). In accordance with the very simple physical picture, Table 4.4 shows correctly that for  $\psi_{sD}$  three plus signs (in sectors 6, 1, 2) are followed by three minus signs (in sectors 3, 4, 5) and similarly for  $\psi_{sB}$  three plus signs (in sectors 2, 3, 4) are followed by three minus signs (in sectors 5, 6, 1).

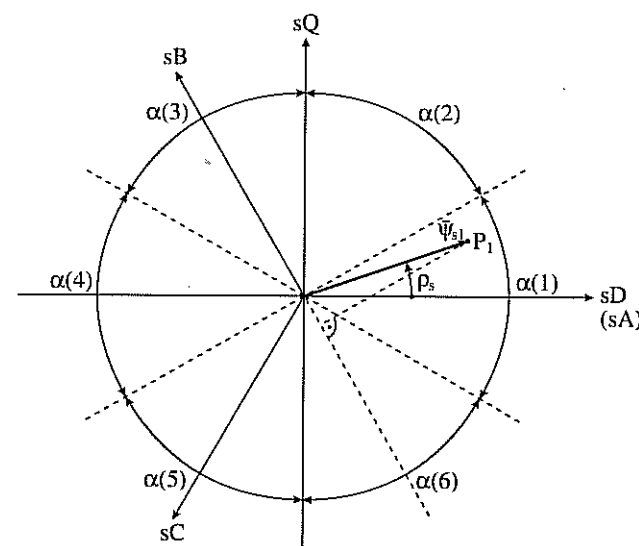


Fig. 4.86. Relationship of the space vector  $\bar{\psi}_s$  to the stator flux-linkage components  $\psi_{sD}$ ,  $\psi_{sQ}$ , and  $\psi_{sB}$ .

Table 4.4 Selection of the stator flux-linkage space-vector sector

Sectors Signs of flux linkages	$\alpha(1)$ sector 1	$\alpha(2)$ sector 2	$\alpha(3)$ sector 3	$\alpha(4)$ sector 4	$\alpha(5)$ sector 5	$\alpha(6)$ sector 6
Sign of $\psi_{sD}$	+	+	-	-	-	+
Sign of $\psi_{sQ}$	(nu; -+)	+	+	(nu; +-)	-	-
Sign of $\psi_{sB}$ = sign of $[\sqrt{3}\psi_{sD} - \psi_{sQ}]$	-	+	+	+	-	-

nu = not useful

It should also be noted for the determination of the appropriate sector that the computation of  $\rho_s$  by using eqn (4.6-5), eqn (4.6-6), or eqn (4.6-7) can also be avoided by using another technique, where first the signs of  $\psi_{sD}$  and  $\psi_{sQ}$  are determined. These give information on the quadrant where the space vector of the stator flux linkages is located (there are four quadrants, and every quadrant spans 90°: the first quadrant starts at the sD-axis and spans until the sQ-axis, the second quadrant starts at the sQ-axis and spans until the negative sD-axis, etc.). Since every quadrant contains only one full sector and half of another sector, thus there are two possible sectors (in a quadrant), but the specific sector where  $\bar{\psi}_s$  is located can be obtained by also using the ratio of  $\psi_{sQ}/\psi_{sD}$ . However, it is also possible to use other techniques as well, which minimize the computation burden.

It should also be noted that the application of the switching vectors shown in Table 4.3 yields excellent results when the speed of the machine is not too low. However, at very low speeds flux control can be lost. For example, when the

machine is started, problems can occur. In this case although at  $t=0$  the constant reference stator flux-linkage is applied and at  $t>t_1$ , a step electromagnetic torque reference is applied, the modulus of the actual stator flux-linkage space vector will be zero until  $t=t_1$ , and even after  $t_1$  it will not reach its reference value and will vary. Thus instead of having the circular path corresponding to the constant reference flux, the space-vector locus of the stator flux-linkage space vector will not be circular, but will be a six-sided symmetrical locus, (not a symmetrical hexagon), where during 1/6 of the cycle the modulus of the stator flux-linkage space vector changes (at a 'corner' point it is maximum, then it decreases, and then it reaches the maximum value again at the next 'corner' point). The problems are related to the inappropriate use of the switching voltage vectors in the low speed region.

Improved DTC schemes, including improved switching vector selection schemes and predictive switching vector selection schemes, will be discussed in Sections 4.6.2.4 and 4.6.2.9.

#### 4.6.2.3 Fundamentals of stator flux-linkage estimation; estimation problems

In the DTC induction motor drive the stator flux-linkage components have to be estimated due to two reasons. First, these components are required in the optimum switching vector selection table discussed in the previous section. Secondly, they are also required for the estimation of the electromagnetic torque. It should be noted that, in general, it follows directly from the stator voltage equation in the stator reference frame that

$$\psi_{sD} = \int (u_{sD} - R_s i_{sD}) dt \quad (4.6-8)$$

$$\psi_{sQ} = \int (u_{sQ} - R_s i_{sQ}) dt, \quad (4.6-9)$$

and as shown below

$$\psi_{sB} = \frac{\sqrt{3}\psi_{sD} - \psi_{sQ}}{2}. \quad (4.6-10)$$

If the non-power-invariant forms of the space vectors are used, then

$$\bar{\psi}_s = \frac{2}{3}(\psi_{sA} + a\psi_{sB} + a\psi_{sC}) = \psi_{sD} + j\psi_{sQ}$$

$$\psi_{sD} = \psi_{sA} = \int (u_{sD} - R_s i_{sD}) dt,$$

where  $u_{sD} = u_{sA}$  and  $i_{sD} = i_{sA}$ . Furthermore

$$\psi_{sQ} = \frac{\psi_{sB} - \psi_{sC}}{\sqrt{3}} = \int (u_{sQ} - R_s i_{sQ}) dt,$$

where  $u_{sQ} = (u_{sB} - u_{sC})/\sqrt{3}$  and  $i_{sQ} = (i_{sB} - i_{sC})/\sqrt{3}$ . However, since  $\psi_{sC} = -(\psi_{sA} + \psi_{sB})$ , thus  $\psi_{sB} = [\sqrt{3}\psi_{sQ} - \psi_{sD}]/2$  is obtained in agreement with eqn (4.6-10).

As discussed in Section 3.1.3, it is not necessary to use three stator-voltage sensors and three stator-current sensors since it is possible to show, by considering  $u_{sA} + u_{sB} + u_{sC} = 0$  and  $i_{sA} + i_{sB} + i_{sC} = 0$ , that  $u_{sD}$  and  $u_{sQ}$  can be obtained by monitoring only two stator line voltages (e.g.  $u_{BA}, u_{AC}$ ), and  $i_{sD}, i_{sQ}$  can be obtained by monitoring only two stator currents (e.g.  $i_{sA}, i_{sB}$ ). Thus

$$u_{sD} = \frac{1}{3}(u_{BA} - u_{AC}) \quad u_{sQ} = -\frac{(u_{AC} + u_{BA})}{\sqrt{3}} \quad i_{sD} = i_{sA} \quad i_{sQ} = \frac{i_{sA} + 2i_{sB}}{\sqrt{3}}.$$

It follows from eqn (4.6-10) that the sign of  $\psi_{sB}$  can be obtained by examining the sign of the flux linkage  $[\sqrt{3}\psi_{sD} - \psi_{sQ}]$  (physically this corresponds to twice the stator flux linking stator phase sB).

It is very important to note that the performance of the DTC drive using eqns (4.6-8) and (4.6-9) will depend greatly on the accuracy of the estimated stator flux-linkage components, and these depend on the accuracy of the monitored voltages and currents, and also on an accurate integration technique. However, errors may occur in the monitored stator voltages and stator currents due to the following factors: phase shift in the measured values (due to the sensors used), magnitude errors due to conversion factors and gain, offsets in the measurement system, quantization errors in the digital system, etc. Furthermore, an accurate value has to be used for the stator resistance. For accurate flux estimation, the stator resistance must be adapted to temperature changes. The integration can become problematic at low frequencies, where the stator voltages become very small and are dominated by the ohmic voltage drop. At low frequencies the voltage drop of the inverter must also be considered. This is a typical problem associated with open-loop flux estimators used in other a.c. drives as well, which use measured terminal voltages and currents.

Drift compensation is also an important factor in a practical implementation of the integration, since drift can cause large errors of the flux position. In an analog implementation the source of drift is the thermal drift of analog integrators. However, a transient offset also arises from the d.c. components which result after a transient change. If an open-loop speed estimator is used in the DTC induction motor drive (see Section 4.6.2.10), which utilizes the estimated stator flux-linkage components, the speed is determined by also using the flux-linkage space-vector position, thus a drift in the flux-linkage space vector will cause incorrect and oscillatory speed values. An open-loop flux linkage estimator can work well down to 1–2 Hz, but not below this unless special techniques are used (see also Sections 3.1.3.2, 4.1.1.4, 4.5.3.1).

#### 4.6.2.4 Stator-flux-based DTC induction motor drives

##### 4.6.2.4.1 Basic DTC schemes

Figure 4.87 shows the schematic of one simple form of the DTC induction motor drive, employing a VSI inverter. In this scheme the stator flux is the

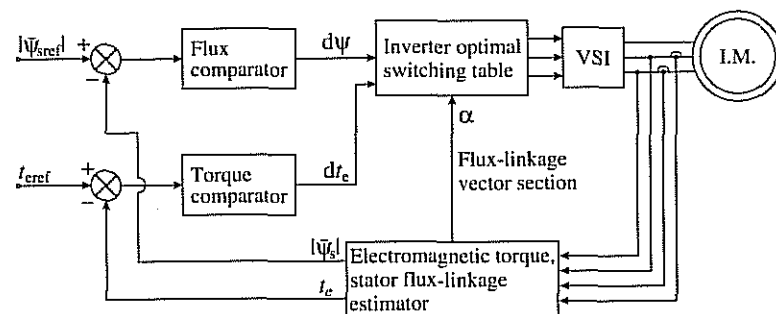


Fig. 4.87. Schematic of stator-flux-based DTC induction motor drive with VSI.

controlled flux, thus it will be referred to as a stator-flux-based DTC induction motor drive.

In Fig. 4.87 a voltage-source (VSI) six-pulse inverter-fed stator-flux-based DTC induction motor drive is shown. As discussed above, direct torque control involves the separate control of the stator flux and torque through the selection of optimum inverter switching modes. The optimum switching table has been shown in Section 4.6.2.2, Table 4.3. In Fig. 4.87 the reference value of the stator flux-linkage space vector modulus,  $|\psi_{sref}|$ , is compared with the actual modulus of the stator flux-linkage space vector,  $|\psi_s|$ , and the resulting error is fed into the two-level stator flux hysteresis comparator. Similarly, the reference value of the electromagnetic torque ( $t_{ref}$ ) is compared with its actual value ( $t_e$ ) and the electromagnetic torque error signal is fed into the three-level torque hysteresis comparator. The outputs of the flux and torque comparators ( $d\psi, dt_e$ ) are used in the inverter optimal switching table (look-up table), which also uses the information on the position of the stator flux-linkage space vector.

In Fig. 4.87, the flux-linkage and electromagnetic torque errors are restricted within their respective hysteresis bands, which are  $2\Delta\psi_s$  and  $2\Delta t_e$  wide respectively. The flux hysteresis band mainly affects the stator-current distortion in terms of low-order harmonics, and the torque hysteresis band affects the switching frequency and thus the switching losses. The DTC scheme requires flux-linkage and electromagnetic torque estimators. As discussed in Section 4.6.2.3, the stator flux-linkage components can be obtained by integrating appropriate monitored terminal voltages reduced by the ohmic losses, as shown by eqns (4.6-8) and (4.6-9), but at low frequencies large errors can occur due to the variation of the stator resistance, integrator drift, and noise. However, it is not necessary to monitor the stator voltages since they can be reconstructed by using the inverter switching modes and the monitored d.c. link voltage (see also Section 3.1.3.2.1). Improved stator flux estimators are also discussed in Section 4.5.3.1. For completeness, some simple schemes are briefly discussed below in Section 4.6.2.6. The electromagnetic torque can be estimated by using eqn (4.6-1); thus

$$t_e = \frac{3}{2} P(\psi_{sD} i_{sQ} - \psi_{sQ} i_{sD}). \quad (4.6-11)$$

Closed-loop speed control can be obtained by using a speed controller (e.g. a PI controller or a fuzzy-logic controller, etc.), whose output gives the torque reference, and the input to the speed controller is the difference between the reference speed and the actual speed.

#### 4.6.2.4.2 Reduction of stator flux and torque ripples

In the DTC induction motor drive there are torque and flux ripples, since none of the inverter switching vectors is able to generate the exact stator voltage required to produce the desired changes in the electromagnetic torque and stator flux linkage in most of the switching instances. However, the ripples in the electromagnetic torque and stator flux linkages can be reduced by using various techniques, some of which involve the use of high switching frequencies or changed inverter topology, but it is also possible to use schemes which do not involve high switching frequency and change of inverter topology (e.g. duty ratio control).

In a DTC induction motor drive, increased switching frequency is desirable since it reduces the harmonic content of the stator currents, and also leads to reduced torque harmonics. However, if high switching frequency is used, this will result in significantly increased switching losses (leading to reduced efficiency) and increased stress on the semiconductor devices of the inverter. This is the reason why inverters of higher power-rating (e.g. in diesel-electric traction) are operated at low switching frequency (to reduce the switching losses), e.g. they are a few hundred Hertz. Furthermore, in the case of high switching frequency, a fast processor is required since the control processing time becomes small. This increases the costs. However, it should be noted that in the ABB DTC drive a high-speed, 40 MHz digital signal processor is used [together with application-specific integrated circuit (ASIC) hardware] to determine the switching frequency of the inverter. The inverter switches in the ABB drive are supplied with the optimum switching pattern every 25 microseconds.

When changed inverter topology is used, it is possible to use an increased number of switches, but this will also increase the costs. For a delta-connected induction machine the switching state number can be increased by the use of two GTO inverters connected in parallel [Takahashi and Ohmori 1989]. Although in this system the number of non-zero switching states is increased to 18, zero-sequence stator currents are produced which have to be reduced by using special techniques, which also require the monitored zero-sequence stator current. However, it is also possible to use schemes, e.g. duty ratio control, which do not involve using inverters with a higher number of switches.

In the conventional DTC induction motor drive (discussed in detail above) a voltage vector is applied for the entire switching period, and this causes the stator current and electromagnetic torque to increase over the whole switching period. Thus for small errors, the electromagnetic torque exceeds its reference value early during the cycle, and continues to increase, causing a high torque ripple. This is then followed by switching cycles in which the zero switching vectors are applied in order to reduce the electromagnetic torque to its reference value. A solution

can be obtained where the ripples in the torque and flux can be reduced by employing a selected inverter switching vector not for the entire switching period, as in the conventional DTC induction motor drive, but only for a part of the switching period (which is defined as the duty ratio,  $\delta$ ) and by using the zero switching vector for the rest of the period. The time for which a non-zero voltage vector has to be applied is chosen so as to increase the electromagnetic torque to its reference value. When the electromagnetic torque reaches its reference value, a zero switching vector is applied. During the application of the zero switching vector, zero voltage is forced on the machine, and thus the electromagnetic torque is almost constant; it only decreases slightly (as also discussed earlier). The average input voltage to the induction motor during the application of each switching vector is  $\delta U_d$  ( $U_d$  is the inverter d.c. link voltage). By varying the duty ratio between 0 and 1, it is possible to apply any voltage between 0 and  $U_d$  during each switching period. This increases the choice of the voltage vector, which is limited by the number of switching vectors in the conventional DTC induction motor drive. As stated above, the duty ratio is selected to give a voltage vector whose average over the switching cycle gives the desired torque change, thus resulting in reduced torque ripples.

The duty ratio of each switching state is a non-linear function of the electromagnetic torque error and stator flux-linkage error, and it is also a function of the position of the stator flux-linkage space vector. Thus it is difficult to model this non-linear function. However, by using a fuzzy-logic-based DTC system, it is possible to perform fuzzy-logic-based duty-ratio control, where the duty ratio is determined during every switching cycle. In such a fuzzy-logic system, there are two inputs, the electromagnetic torque error  $e_{te} = t_{e\text{ref}} - t_e$ , and the stator flux-linkage position  $\rho_s$ . The output of the fuzzy-logic controller (FLC) is the duty ratio ( $\delta$ ). The fuzzy-logic duty-ratio estimator is shown in Fig. 4.88(a).

The general aspects of fuzzy-logic controllers (FLC) have been discussed in Section 4.4.1. A Mamdani-type of FLC contains a rule base, a fuzzifier, and also a defuzzifier. The fuzzy logic controller shown in Fig. 4.88(a) is a Mamdani-type of controller and contains a rule base, but this comprises two groups of rules, each of which contains nine rules (these are expert statements). The first group is used when the stator flux linkage is smaller than its reference value and the second group of rules is used when it is greater than its reference value. The rules can also be generated by simulating a non-fuzzy DTC induction motor drive using different switching states. As shown in Table 4.5, altogether there are 18 simple rules and there are only a minimal number (three) fuzzy sets used for the two input variables and also for the three output variables; these are: small, medium, and large.

It can be seen that there are five rules in group 2 which are the same as in group 1; the four different rules are shown in bold.

The nine membership functions are selected as follows. The membership function 'small' for the smallest stator-flux position  $\rho_s=0$  is  $\mu_{\rho_s}^{\text{small}}(\rho_s=0^\circ)=1$ , since it is absolutely certain that  $\rho_s=0$  belongs to the fuzzy set of small position angles (the absolute certainty gives the membership value 1, e.g. 50% certainty

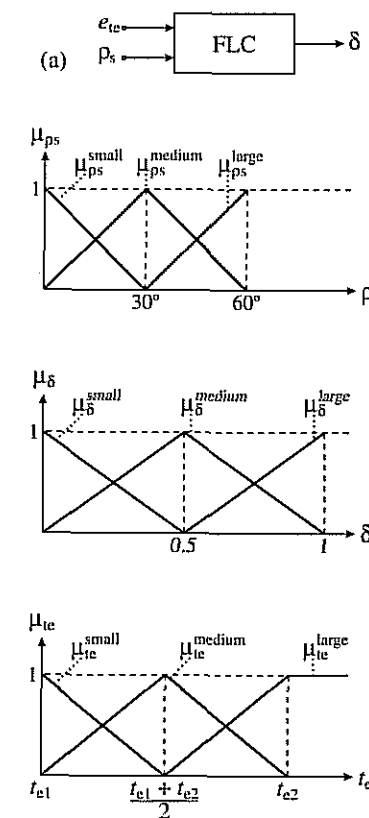


Fig. 4.88. Fuzzy-logic duty-ratio estimator, and membership functions. (a) FLC duty-ratio estimator; (b) membership functions.

would give a membership value of 0.5). Similarly, the membership function 'large' for the largest stator-flux position  $\rho_s=60^\circ$  is  $\mu_{\rho_s}^{\text{large}}(\rho_s=60^\circ)=1$ , since it is absolutely certain that  $\rho_s=60^\circ$  belongs to the large position angle. The membership function 'medium' for the medium stator-flux position  $\rho_s=30^\circ$  is  $\mu_{\rho_s}^{\text{medium}}(\rho_s=30^\circ)=1$ , since it is absolutely certain that  $\rho_s=30^\circ$  belongs to the medium position angle. Thus these three points are the extreme points of the  $\mu_{\rho_s}(\rho_s)$  membership functions shown in Fig. 4.88(b). The three membership functions are obtained by connecting the extreme points with straight lines, and are shown in the top part of Fig. 4.88(b). The three membership functions for the duty ratio can be similarly obtained and are also shown in the middle part of Fig. 4.88(b); these are  $\mu_\delta^{\text{small}}(\delta)$ ,  $\mu_\delta^{\text{medium}}(\delta)$ ,  $\mu_\delta^{\text{large}}(\delta)$ . The three membership functions for the electromagnetic torque error [ $\mu_{te}^{\text{small}}(t_e)$ ,  $\mu_{te}^{\text{medium}}(t_e)$ ,  $\mu_{te}^{\text{large}}(t_e)$ ] can also be constructed in a similar way, but of course these vary with the electromagnetic torque, and the constant values shown for the torque ( $t_{e1}, t_{e2}$ ) depend on the specific machine used. These three membership functions are shown in the bottom part of Fig. 4.88(b).

**Table 4.5** Fuzzy rule-base

Group 1 rules					
If $e_{te}$ is small	and	$\rho_s$ is	small	then	$\delta$ is medium
If $e_{te}$ is small	and	$\rho_s$ is	medium	then	$\delta$ is small
If $e_{te}$ is small	and	$\rho_s$ is	large	then	$\delta$ is small
If $e_{te}$ is medium	and	$\rho_s$ is	small	then	$\delta$ is medium
If $e_{te}$ is medium	and	$\rho_s$ is	medium	then	$\delta$ is medium
If $e_{te}$ is medium	and	$\rho_s$ is	large	then	$\delta$ is medium
If $e_{te}$ is large	and	$\rho_s$ is	small	then	$\delta$ is large
If $e_{te}$ is large	and	$\rho_s$ is	medium	then	$\delta$ is large
If $e_{te}$ is large	and	$\rho_s$ is	large	then	$\delta$ is large
Group 2 rules					
If $e_{te}$ is small	and	$\rho_s$ is	small	then	$\delta$ is small
If $e_{te}$ is small	and	$\rho_s$ is	medium	then	$\delta$ is small
If $e_{te}$ is small	and	$\rho_s$ is	large	then	$\delta$ is medium
If $e_{te}$ is medium	and	$\rho_s$ is	small	then	$\delta$ is medium
If $e_{te}$ is medium	and	$\rho_s$ is	medium	then	$\delta$ is medium
If $e_{te}$ is medium	and	$\rho_s$ is	large	then	$\delta$ is large
If $e_{te}$ is large	and	$\rho_s$ is	small	then	$\delta$ is medium
If $e_{te}$ is large	and	$\rho_s$ is	medium	then	$\delta$ is large
If $e_{te}$ is large	and	$\rho_s$ is	large	then	$\delta$ is large

The ripples in electromagnetic torque, stator flux, stator currents, and speed are reduced by the duty-ratio-controlled DTC. However, to obtain minimal torque ripples, the decrease in the electromagnetic torque during the application of the zero switching vector has to be minimized. Since this decrease of the electromagnetic torque also depends on the modulus of the reference stator flux-linkage space vector, an optimized stator flux-linkage reference value has to be used. For this purpose such a reference stator flux linkage is selected which is just large enough to generate the reference electromagnetic torque. This implies that the maximum electromagnetic torque reference has to be found and the optimum stator flux reference corresponds to this. The maximum torque reference can be obtained by using eqn (4.3-37), and equating the torque reference to this gives

$$t_{ref} = \frac{3}{4} P \left( \frac{L_m}{L_s} \right)^2 \frac{|\bar{\psi}_s|^2}{L'_r}, \quad (4.6-12)$$

where  $L'_r$  is the rotor transient inductance. Thus it follows by using  $|\bar{\psi}_{sref}| = |\bar{\psi}_s|$  that the optimized reference flux linkage for the given electromagnetic torque reference is

$$|\bar{\psi}_{sref}| = \left[ \frac{4L_s^2 L'_r}{3PL_m^2} \right]^{1/2}. \quad (4.6-13)$$

When the optimized reference stator flux linkage given by eqn (4.6-13) is used in the DTC induction motor drive with duty-ratio control, then the torque ripples are reduced.

When the conventional DTC induction motor drive is operated in the zero-speed region, problems occur as discussed at the end of Section 4.6.2.2. This is due to the fact that, during magnetization, the stator flux comparator selects only non-zero switching vectors (see optimum switching table, Table 4.3 shown in Section 4.6.2.2), and at this time the output of the torque comparator takes one state and the inverter cannot apply zero switching vectors to the motor. However, one possible solution to this problem can be obtained by the application of an additional carrier signal to the input of the electromagnetic torque comparator [Kazmierkowski and Sulkowski 1991]. The injected carrier signal is e.g. a 500 Hz square wave and is only applied in the zero speed region. This forces the zero switching vectors and improves both stator flux-linkage and stator-current waveforms. Furthermore, it ensures robust start and operation in the zero-speed region. However, many other types of solutions can also be obtained which solve the problems in the low speed region, and it is possible to get a satisfactory solution even without using the zero switching vectors (at low speed). However, it is useful to implement another technique where the zero vectors are applied, since in this case the switching frequency is reduced. Such a technique can also be developed by using simple physical considerations and when this is employed, high-dynamic performance is obtained in addition to the reduced switching frequency in the steady state.

A new switching vector selection scheme is proposed in [Damiano *et al.* 1997], which can be used at low speed as well.

#### 4.6.2.5 Main features, advantages, and disadvantages of DTC

The main features of the DTC are:

- direct control of flux and torque (by the selection of optimum inverter switching vectors);
- indirect control of stator currents and voltages;
- approximately sinusoidal stator fluxes and stator currents;
- possibility for reduced torque oscillations; torque oscillations depend on duration of zero-switching vectors;
- high dynamic performance;
- inverter switching frequency depends on widths of flux and torque hysteresis bands.

The main advantages of the DTC are:

- absence of coordinate transformations (which are required in most of the vector-controlled drive implementations);
- absence of separate voltage modulation block (required in vector drives);
- absence of voltage decoupling circuits (required in voltage-source vector drives);
- absence of several controllers (e.g. in a VSI PWM-fed induction motor drive employing rotor-flux-oriented control, there are minimally four controllers);

- only the sector where the flux-linkage space vector is located, and not the actual flux-linkage space-vector position, has to be determined (and the minimum accuracy required is 60 electrical degrees, in contrast to approx. minimum 1.4 degrees in vector drives);
- minimal torque response time.

However, the main disadvantages of a conventional DTC are:

- possible problems during starting and low speed operation and during changes in torque command;
- requirement for flux and torque estimators (same problem exists for vector drives);
- changing switching frequency;
- high ripple torque.

However, it is possible to overcome some of these difficulties, e.g. the difficulties during starting, low speed operation, high ripple torque, etc. (see later sections). In the only known industrially available DTC drive (ABB, 1996), torque response times typically better than 2 ms have been claimed [Tiitinen 1996] together with high torque-control linearity even down to low frequencies including zero speed. It has also been claimed by ABB that the new a.c. drive technology rests chiefly on a new motor model which enables the computation of the motor states without using a speed or position sensor. The motor model used by ABB is a mathematical model (using various machine parameters i.e. the stator resistance, mutual inductance, etc.) and not an artificial-intelligence-based model (e.g. it does not use a neural network or a fuzzy-neural network, etc.). Further details of the ABB DTC induction motor drive are discussed in Section 4.6.2.11.

#### 4.6.2.6 Improved stator flux-linkage estimation

##### 4.6.2.6.1 Application of low-pass filters

As also shown in the first book totally devoted to vector controlled drives [Vas 1990], due to the initial value and drift problems associated with pure integrators, it is useful to replace the pure integrators by a low-pass filter; thus the stator flux linkages can be obtained from

$$\bar{u}_s = R_s \bar{i}_s + \frac{(1+pT)}{T} \bar{\psi}_s. \quad (4.6-14)$$

In eqn (4.6-14)  $p = d/dt$ , and  $T$  is a suitably chosen time constant which gives a low cut-off frequency and thus allows eqn (4.6-14) to approximate a pure integration in the widest speed range [e.g.  $T = 0.2$  gives a cut-off frequency of  $f = 1/(2\pi T) = 0.795$  Hz]. It follows from eqn (4.6-14) that

$$\psi_{sD} = \frac{u_{sD} - R_s i_{sD}}{p + 1/T} \quad (4.6-15)$$

$$\psi_{sQ} = \frac{u_{sQ} - R_s i_{sQ}}{p + 1/T}. \quad (4.6-16)$$

##### 4.6.2.6.2 Application of first-order delay elements

It is also possible to use a stator flux estimator in which the drift problems associated with 'pure' open-loop integrators at low frequency are avoided by a band-limited integration of the high-frequency components, and by replacing the inaccurate flux estimation at frequencies below  $1/T$  by its reference value in a smooth transition. For this purpose a first-order delay element  $1/(1+pT)$  is used, thus the stator flux-linkage space vector is obtained from

$$\bar{\psi}_s = \frac{T(\bar{u}_s - R_s \bar{i}_s) + \bar{\psi}_{sref}}{1 + pT}, \quad (4.6-17)$$

where  $\bar{\psi}_{sref}$  is the stator flux-linkage space vector in the stationary reference frame,  $\bar{\psi}_{sref} = |\bar{\psi}_{sref}| \exp(j\phi_s)$ . As discussed in Section 4.1.1.4, the inputs to this stator flux estimator are the measured values of the stator-voltage space vector ( $\bar{u}_s$ ) and stator-current space vector ( $\bar{i}_s$ ), expressed in the stationary reference frame. However, there is also a third input, which is the modulus of the reference value of the stator flux-linkage space vector ( $|\bar{\psi}_{sref}|$ ). It should be noted that since the stationary reference frame is used,  $\bar{\psi}_{sref}$  contains two components,  $\psi_{sDref}$  and  $\psi_{sQref}$ . In eqn (4.6-17) the space vector of the induced stator voltages is  $\bar{u}_{si} = \bar{u}_s - R_s \bar{i}_s$  and in an open-loop stator flux-linkage estimator using a 'pure' integrator, its integrated value ( $\int \bar{u}_{si} dt$ ) would yield the stator flux-linkage space vector  $\bar{\psi}_s$ . However, in eqn (4.6-17)  $\bar{u}_{si}$  is multiplied by  $T$  and the reference stator flux-linkage space vector is added to  $T\bar{u}_{si}$ , yielding  $T\bar{u}_{si} + \bar{\psi}_{sref}$ . This is then the input to the first-order delay element,  $1/(1+pT)$ , on the output of which the estimated value of the stator flux-linkage space vector is obtained.

##### 4.6.2.6.3 Application of hybrid flux estimators

It is also possible to use hybrid stator flux estimators, where the rotor voltage equation is also utilized (see also Section 3.3.4). Thus the hybrid flux estimator uses two models; a stator-voltage-equation-based model and also a rotor-voltage-equation-based model. Such an estimator utilizes the fact that at high speeds, accurate stator flux estimation can be obtained by using the stator voltage equation, but at low speeds accurate stator flux estimation can be obtained by using the rotor voltage equation. Several simple solutions can be obtained, but it is important to have smooth transition from the stator-voltage-equation-based estimation to the rotor-voltage-based flux estimation. If a speed sensor can be used, then it is relatively simple to construct the hybrid model by the direct use of the stator and rotor voltage equations, and the inputs are then the measured stator voltages and currents and also the rotor speed.

It is also possible to improve the estimation of the stator flux linkages by using the stabilizing feedback in the voltage model discussed in Section 4.1.1.4.

#### 4.6.2.6.4 Application of observers

To obtain greater accuracy it is possible to use observers (Luenberger, Kalman). In particular, greater robustness to parameter variations can be obtained by using a full-order Luenberger observer (see also Section 4.5.3.3.1), yielding estimations of the stator flux-linkage components which are less sensitive to parameter variations. For this purpose, the observer contains a correction term, which contains the product of the observer gain matrix and the difference between the measured and estimated stator-current components. If the rotor speed is monitored, then it is very simple to use a full-order Luenberger observer which in general is described by

$$\frac{d\hat{\mathbf{x}}}{dt} = \mathbf{A}\hat{\mathbf{x}} + \mathbf{B}\mathbf{u} + \mathbf{K}(\mathbf{y}_s - \hat{\mathbf{y}}_s), \quad (4.6-18)$$

where  $\hat{\mathbf{x}}$  denotes the estimated states, which are the stator currents and flux-linkage components in the stationary reference frame,  $\hat{\mathbf{x}} = [\hat{i}_{sD}, \hat{i}_{sQ}, \hat{\psi}_{sD}, \hat{\psi}_{sQ}]^T$ , and  $\mathbf{u}$  is the input vector,  $\mathbf{u} = [u_{sD}, u_{sQ}]^T$ . Furthermore, matrices  $\mathbf{A}$  and  $\mathbf{B}$  can be obtained from the stator and rotor voltage equations of the induction machine in the stationary reference frame (the state-variable form of these equations is  $dx/dt = \mathbf{Ax} + \mathbf{Bu}$ ). For example, since  $\bar{i}_s$  and  $\bar{\psi}_s$  are state variables and the stator voltage equation is  $\bar{u}_s = R_s \bar{i}_s + d\bar{\psi}_s/dt$ , it immediately follows that the state-variable form of the component stator voltage equations are

$$\frac{d\psi_{sD}}{dt} = -R_s i_{sD} + u_{sD}$$

$$\frac{d\psi_{sQ}}{dt} = -R_s i_{sQ} + u_{sQ}.$$

Thus the system matrix  $\mathbf{A}$ , which is a 4-by-4 matrix, will contain the following elements:  $a_{31} = -R_s$ ,  $a_{32} = a_{33} = a_{34} = 0$ , and  $a_{42} = -R_s$ ,  $a_{41} = a_{43} = a_{44} = 0$ . The other 8 elements of  $\mathbf{A}$  can be obtained by considering the rotor voltage equation ( $0 = R_r \bar{i}'_r + d\bar{\psi}'_r/dt - j\omega_r \bar{\psi}'_r$ ) and by eliminating  $\bar{i}'_r$  and  $\bar{\psi}'_r$  (for this purpose  $\bar{i}'_r = (\bar{\psi}'_r - L_m \bar{i}_s)/L_r$  and  $\bar{\psi}'_r = (L_r/L_m)(\bar{\psi}_s - L'_s \bar{i}_s)$  are used). Thus the elements  $a_{12}$ ,  $a_{14}$  and  $a_{21}$  and  $a_{23}$  will contain the rotor speed, and there are four other non-zero elements as well. Thus the system matrix  $\mathbf{A}$  contains the rotor speed ( $\omega_r$ ), which is obtained by using a speed sensor.

In eqn (4.6-18)  $\mathbf{K}$  is the observer gain matrix,  $\mathbf{y}$  is the actual output vector,  $\mathbf{y} = \mathbf{Cx}$ ,  $\hat{\mathbf{y}}$  is the estimated output vector,  $\hat{\mathbf{y}} = \mathbf{C}\hat{\mathbf{x}}$ . The output matrix  $\mathbf{C}$  is a two-by-four matrix:  $\mathbf{C} = [\mathbf{I}_2, \mathbf{0}_2]$ , where  $\mathbf{I}_2$  is a second-order identity matrix and  $\mathbf{0}_2$  is a second-order null matrix. The estimation error of the stator currents and stator flux linkages (error dynamics) can be obtained by defining the error as  $\mathbf{e} = \mathbf{x} - \hat{\mathbf{x}}$ . Thus if eqn (4.6-18) is subtracted from  $dx/dt = \mathbf{Ax} + \mathbf{Bu}$ , then

$$\frac{de}{dt} = (\mathbf{A} - \mathbf{KC})e \quad (4.6-19)$$

is obtained. This is simpler than the observer error equation given by eqn (4.5-104), since eqn (4.5-104) also contains a term with  $\Delta\hat{\mathbf{A}} = \hat{\mathbf{A}} - \mathbf{A}$ , but now this term is not present since now  $\mathbf{A} = \hat{\mathbf{A}}$ . It follows from eqn (4.6-19) that the speed of error convergence is determined by the poles of the matrix  $\mathbf{A} - \mathbf{KC}$ . The gain matrix  $\mathbf{K}$  contains four rows and two columns, so it contains 8 elements:

$$\mathbf{K}^T = \begin{bmatrix} k_{11} & k_{12} & k_{13} & k_{14} \\ k_{21} & k_{22} & k_{23} & k_{24} \end{bmatrix}$$

For fast convergence, the elements of the gain matrix  $\mathbf{K}$  are selected in such a way that the observer poles should be more negative (faster) than the motor poles. However, care should be taken, since if the observer poles are made too negative, the observer gain may become too large, leading to stability problems resulting from amplified measurement noise. In addition, the motor poles change with the rotor speed, and thus the gain matrix can become large at low speeds if the observer poles are positioned in a fixed location. However, this problem can be overcome by selecting observer poles which are proportional to those of the induction motor (see also Section 4.5.3.5.1). In this way fast convergence and improved robustness to measurement noise is achieved. The poles of the induction motor are described by two sets of complex conjugate pairs,  $\Lambda_1 = a_1 \pm jb_1$ ,  $\Lambda_2 = a_2 \pm jb_2$  (see for example the book on space vector theory [Vas 1992]); these can be computed for the entire speed range. It is then possible to obtain values of  $\mathbf{K}$  such that the observer gains are proportional to the motor gains (it can be shown that in  $\mathbf{K}$ , the gains  $k_{12}$  and  $k_{21}$  are proportional to the rotor speed). When such an estimator is used, improved robustness to parameter variations is obtained (compared to the open-loop flux-linkage estimator using pure integrators), and in particular more accurate stator flux-linkage estimates can be obtained even if the stator resistance is not known accurately. However, when inaccurate stator resistance is used, this will also result in inaccurate stator flux-linkage estimates. A substantial improvement can be obtained for stator flux-linkage estimation if a thermal model of the machine is used and this is utilized for accurate stator resistance calculation. However, the thermal model can also be implemented by an observer.

It is also possible to use a Kalman filter for stator flux estimation. (The details of the Kalman filter are described in Section 4.5.3.5.2). When an extended Kalman filter is used, it is possible to estimate the rotor speed in addition to the stator flux linkages and some machine parameters (joint state and parameter estimation).

The stator flux-linkage components can also be estimated by using a model reference adaptive control (MRAS) system. The details of the MRAS systems are described in Section 4.5.3.4, so such a system will not be discussed here.

Finally it is very important to note that it is possible to obtain accurate stator flux-linkage estimates by using an artificial neural network, or a fuzzy-neural estimator. It is also possible to combine fuzzy-logic techniques with conventional observer-based techniques (see also Chapter 7).

#### 4.6.2.7 Field weakening

In the speed range above rated speed, field weakening has to be performed. In a vector-controlled induction motor drive with stator-flux-oriented control, the conventional technique is to decrease the stator flux-linkage reference in inverse proportion to the rotor speed. Thus the electromagnetic torque will decrease inversely with speed. It has been discussed above that in a direct-torque-controlled induction motor, fast torque control is achieved by fast changes of the angle (torque angle) between the stator and rotor flux linkages, and this can be achieved by phase advancing (increase of the torque) or by retarding (decrease of torque) the stator flux-linkage space vector.

It is assumed that the induction machine is supplied by the voltage-source inverter and the inverter is working in the six-step square-wave operation mode. This allows us to exploit the full voltage of the inverter. For the six-step square-wave operation, in the steady state the rotor flux-linkage space vector rotates on an almost circular locus, with a synchronous speed. However, the locus of the stator flux-linkage space vector is a hexagon and the angle between the stator flux and rotor flux-linkage space vectors is constant. This angle (torque angle) at rated torque is around 0.2 rad for a usual induction machine at rated flux. However, in the field-weakening range the rotor speed is in the order of few hundred,  $\text{rad s}^{-1}$ , and it follows that fast torque control can be achieved by very fast retardation of the stator flux linkage which, however, can be performed by stopping it only for a moment, by applying a short zero stator voltage vector (pulse), as shown in Fig. 4.89(a).

In Fig. 4.89(a), point  $P_1$  is the momentary stop point. This short zero stator-vector pulse is also called a stop pulse. For example, at 50 Hz, a load angle reduction of 0.2 rad can be achieved in 0.6 ms. It should be noted that if the inverter has a restricted minimum time between commutations, the stop pulse cannot be applied

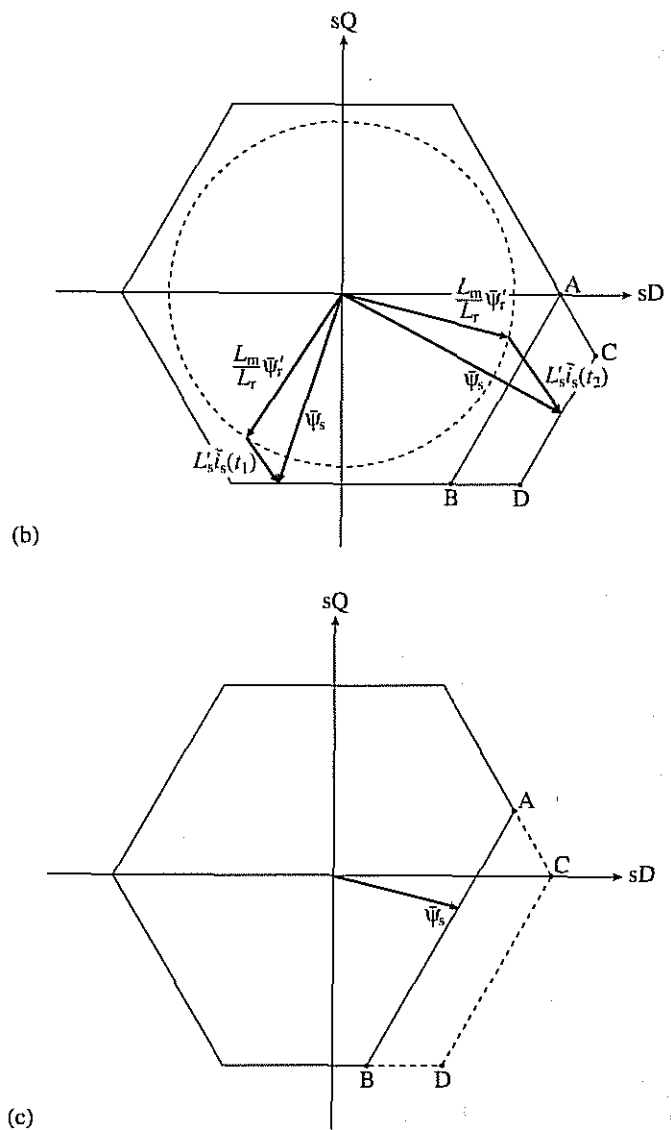
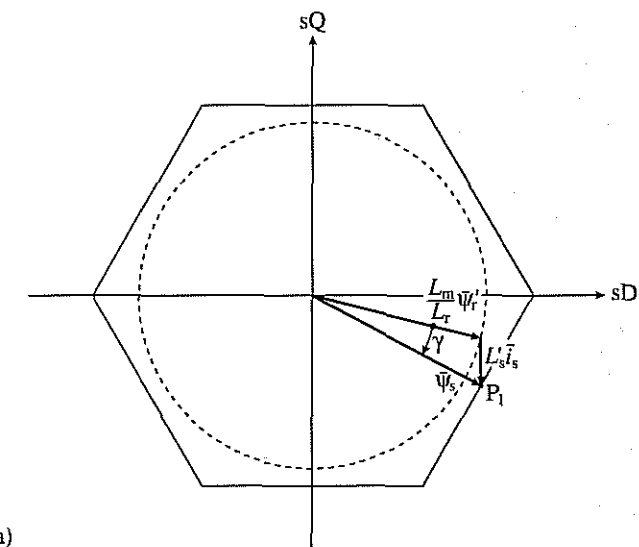


Fig. 4.89. Field-weakening operation: phase retard and phase advance of stator flux-linkage space vector. (a) Phase retard (torque reduction) by applying stop pulse; (b) phase retard (torque reduction) by increasing peripheral length of hexagon around a corner; (c) phase advance (torque increase) by decreasing peripheral length of a hexagon side.

and in this case small retardation of the stator flux linkage is possible by using another technique, which is the deformation technique, shown in Fig. 4.89(b). In this case, the peripheral length of the stator flux linkage hexagon is increased from AB to AC+CD+BD. This causes stator flux-linkage retardation (torque reduction) in the field-weakening range, since the peripheral length along the corner of the stator flux-linkage locus is increased from the original AB length to the length  $l=AC+CD+BD$ . Thus if the stator flux-linkage space vector is rotating from point B to point A, it will reach point B later than in the original locus and therefore the stator flux-linkage vector is phase retarded. It can also be seen from Fig. 4.89(b) that there is a momentary stator flux increase accompanied by a momentary increase of the stator current (since  $\bar{i}_s = [\bar{\psi}_s - (L_m/L_r)\bar{\psi}_r]/L'_s$ , and the rotor flux is constant). Thus torque reduction (phase retardation of the stator flux-linkage space vector) in the field-weakening range can be performed in two ways; by employing a stop pulse or by performing the hexagon deformation shown in Fig. 4.89(b) [Angquist 1986]. However, if the inverter commutation time does not impose any restrictions (see above), then the stop-pulse technique should be used, since this does not result in momentary high values of the stator currents and it also gives faster torque reduction.

If on the other hand a torque increase must be performed, then the stator flux-linkage space vector must be phase advanced. However, since the stator flux-linkage space vector is already running at its maximum speed, phase advance can only be achieved by shortening the peripheral length of the stator flux-linkage locus (hexagon) along one of its sides. This produces a momentary flux weakening as shown in Fig. 4.89(c). It follows from Fig. 4.89(c) that in the original flux hexagon, the peripheral length along the hexagon side is  $l=AC+CD+BD$ . However, in the new flux locus, this length has been shortened to AB ( $AB < l$ ), and therefore when the stator flux-linkage space vector moves along the locus in the direction from point A to point B, it will reach point B sooner. Since the time of movement through this new locus side is very short (typically between 1 to 5 ms), the rotor flux-linkage space vector will mainly follow the mechanical motion of the rotor and thus the stator flux-linkage space vector is phase advanced.

#### 4.6.2.8 Optimal control of efficiency

In a torque-controlled induction motor drive, in addition to ensuring high dynamic performance, it is also possible to obtain optimal efficiency. This can be very important, for example in a battery-driven electrical vehicle application of the DTC induction motor drive. There are many possibilities to maximize the efficiency, and for this purpose the motor, the inverter, and the controller must be considered.

In general, some of the possible methods of optimal efficiency control are:

##### *Conventional techniques*

**Constant flux control** In this case constant flux is used until the voltage limit of the inverter is reached, and for higher supply frequencies (when the machine speed is larger than the base speed), the flux is reduced in inverse proportion to

the supply frequency (conventional method of field weakening). However, when this technique is used, the drive may not achieve maximum torque capability over the full speed region, since the curve which gives the optimal flux level as a function of the rotor speed may differ from the inverse of the rotor speed.

**Stator current-ratio control** In this case the ratio of the direct- and quadrature-axis stator currents is controlled. This can involve constant, modified, or optimized current-ratio control. For example, for constant stator-current-ratio control, when the induction motor is operating with rotor-flux-oriented quantities, the ratio of the direct- and quadrature-axis stator currents is constant. This ratio can be unity to give maximum torque-to-stator-current ratio. When the modified stator current ratio is used, saturation effects are also considered. For optimal stator-current-ratio control, the stator current ratio depends on the stator frequency as well [Nilsen and Kasteenpohja 1995].

**Optimal flux control** In this case the control strategy can be found by measuring the efficiency in many points of the speed torque plane, and e.g. by using a look-up table for the flux reference as a function of the torque reference. These measurements also contain information on the saturation effects, but temperature variations are uncompensated.

##### *Artificial-intelligence-based control*

Due to the non-linearities involved, it is possible to use very effectively a simple fuzzy-logic-based efficiency controller, which can optimize the efficiency on-line by minimizing the d.c. link power. For this purpose the d.c. link voltage and d.c. link current are also measured and optimum stator-current ratio is obtained, which gives maximum efficiency.

When a conventional, non-artificial-intelligence-based efficiency control technique is used, the control strategy should be a combination of constant current-ratio control and optimal current-ratio control.

#### 4.6.2.9 Improved switching-vector selection schemes; predictive schemes

##### *4.6.2.9.1 General introduction; various predictive schemes*

In a DTC induction motor drive using the switching table shown in Section 4.6.2.2, sluggish response can be obtained during start-up and during a change in the reference stator flux linkage and reference electromagnetic torque. Although the switching voltage vectors are determined by the stator flux-linkage position and the errors in the electromagnetic torque and modulus of the stator flux-linkage space vector, large and small errors are not distinguished. Thus the switching vectors chosen for large errors (e.g. during start-up or during a step change in the torque) are the same as the switching vectors chosen for normal operation, when these errors are small. However, it is possible to choose switching vectors which are in accordance with the range of the errors (and stator flux-linkage space-vector

position). In this case the responses at start-up and change in reference stator flux and reference electromagnetic torque can be increased. There are several possible solutions, e.g. it is possible to use a fuzzy-logic-based system. In this system those switching states are used during start-up which give faster increase of the stator flux (during this time the change in torque is small). However, when the stator flux-linkage error becomes small, those switching states are chosen which give faster increase of the electromagnetic torque.

It should also be noted that in addition to using a fuzzy-logic-based optimal switching-vector selection strategy, it is also possible to have improvements by using a non-artificial-intelligence-based scheme, where the stator flux-linkage and electromagnetic torque errors are not quantized to two and three levels, and where more than six stator flux-linkage sectors are used. Although it is possible to have an implementation of this system which also uses a look-up table, the computational requirements will be increased.

It is also possible to implement DTC drive schemes in which the required switching voltage vectors are obtained by using predictive algorithms. For this purpose a suitable mathematical model of the induction machine is used and the electromagnetic torque is estimated for each sampling period for all possible inverter modes. The predictive algorithm then selects the inverter switching states to give minimum deviation between the predicted electromagnetic torque and the reference torque. This approach is discussed in some detail below; however, since there are many possibilities for the mathematical model to be used, only the main concepts will be discussed.

For the purposes of the predictive switching-vector estimation scheme, a suitable mathematical model of the induction machine can be obtained by considering the stator and rotor voltage equations (4.1-6), (4.1-24), and the expression of the electromagnetic torque, eqn (4.1-43). Thus the voltage equations in the rotor-flux-oriented reference frame (rotating at the speed of  $\omega_{mr}$ ) are as follows, if for simplicity the effects of magnetic saturation are neglected:

$$\bar{u}'_s = R_s \bar{i}'_s + \frac{L'_s d\bar{i}'_s}{dt} + j\omega_{mr} L'_s \bar{i}'_s + \frac{L_m}{L_r} \left( j\omega_{mr} |\bar{\psi}_r| + \frac{d|\bar{\psi}_r|}{dt} \right) \quad (4.6-20)$$

$$0 = \frac{|\bar{\psi}_r|}{T'_r} + \frac{d|\bar{\psi}_r|}{dt} - \frac{L_m \bar{i}'_s}{T'_r} + j(\omega_{mr} - \omega_r) |\bar{\psi}_r| \quad (4.6-21)$$

$$t_e = \frac{3}{2} P \frac{L_m}{L_r} |\bar{\psi}_r| i_{sy}. \quad (4.6-22)$$

In these equations, the primed quantities are expressed in the rotor-flux-oriented reference frame,  $L'_s$  is the stator transient inductance,  $T'_r$  is the rotor transient time constant. It is possible to combine these three equations into a single (vector) equation for the stator-voltage space vector expressed in the stationary reference frame, which contains the electromagnetic torque, modulus of the rotor flux-linkage space vector, the rotor speed, and the machine parameters. By assuming that within a sampling time interval, the rotor speed is constant, and also by

assuming that the reference electromagnetic torque is a step function, a simple and compact (vector) expression for  $\bar{u}_s$  is obtained in terms of the reference values of the electromagnetic torque and reference value of the rotor flux-linkage modulus. This voltage space vector is the reference voltage space vector in the stationary reference frame ( $\bar{u}_{sref}$ ). Thus the appropriate switching state of the inverter can then be determined by using space-vector modulation.

It is also possible to estimate the required stator voltage switching vectors by using a predictive scheme in which there is deadbeat control of the electromagnetic torque and stator flux linkage over a constant switching cycle. For this purpose the stator-voltage space vector is calculated, which is required to control the electromagnetic torque and stator flux-linkage space vector on a cycle-by-cycle basis, by using the electromagnetic torque error and stator flux-linkage errors of the previous cycle, and also the estimated back e.m.f. of the induction machine. It is one of the advantages of this algorithm that it gives constant switching frequency. However, it is important to note that under overmodulation (when  $a > 1$ , see eqn (4.6-43) below) and general transient conditions (when there is a transient in both the flux and torque references), deadbeat control is not possible. However, when there is only a torque transient (which is the most important practical case), it is possible to have deadbeat control of the flux, as discussed in Section 4.6.2.9.2, and in this case two switching voltage vectors are selected in a sampling interval. Similarly, if there is a transient in the stator flux linkage, then it is possible to have deadbeat control of the torque; this will also be discussed in Section 4.6.2.9.2 and again, two switching voltage vectors are applied in a sampling interval. If there is a simultaneous transient in the torque and flux then a single switching vector has to be selected for the entire sampling period. However, if there is no transient in the flux and torque (steady-state) then it is possible to implement deadbeat control of the flux and torque by using the technique described in the next section.

#### 4.6.2.9.2 A predictive control algorithm in the steady state

The eight steps of a predictive algorithm (in an arbitrary  $n$ th sampling period  $T_s$ ) in the steady state are now described.

##### Step 1 Estimation of stator flux linkages from monitored voltages and currents

If  $t_n$  is the time at the beginning of an arbitrary  $T_s$  sampling period, then by using the monitored values of stator currents and voltages ( $u_{sD}, u_{sQ}, i_{sD}, i_{sQ}$ ) the stator flux linkages,  $\psi_{sD}, \psi_{sQ}$ , (at the beginning of period  $T_s$ ) can be obtained by using a suitable technique, e.g.

$$\psi_{sD}(t_n) = \int (u_{sD} - R_s i_{sD}) dt$$

$$\psi_{sQ}(t_n) = \int (u_{sQ} - R_s i_{sQ}) dt.$$

However, it should be noted that the stator voltages do not have to be monitored, since it is possible to reconstruct the stator voltages from the monitored d.c. link voltage and inverter switching states (e.g. see Section 3.1.3.2.1). Furthermore, it is also possible to utilize any of the simple improved flux-estimation schemes described earlier (e.g. see Sections 4.1.1.4, 4.6.2.6).

#### Step 2 Estimation of back-e.m.f. components from flux linkages and currents

The back-e.m.f. components ( $e_{sD}$ ,  $e_{sQ}$ ) are estimated by using eqn (4.6-24) given below, thus

$$\bar{e} = e_{sD} + j e_{sQ} = \frac{d\bar{\psi}_s}{dt} - L'_s \frac{d\bar{i}_s}{dt} \quad (\bar{\psi}_s = \psi_{sD} + j\psi_{sQ}; \quad \bar{i}_s = i_{sD} + j i_{sQ}).$$

#### Step 3 Estimation of the electromagnetic torque from flux linkages and currents

The 'present' value of the electromagnetic torque is estimated, e.g. by using

$$t_e(t_n) = \frac{3}{2} P(\psi_{sD} i_{sQ} - \psi_{sQ} i_{sD}).$$

#### Step 4 Estimation of change of electromagnetic torque

$$\Delta t_e = t_e(t_n) - t_{eref}$$

#### Step 5 Estimation of required direct-axis stator reference voltage $v_{sDref}$ (by assuming $R_s=0$ )

Estimate  $v_{sDref}$  by solving eqn (4.6-34) given below, thus solve

$$\left[ T_s^2 + \left( \frac{\psi_{sQ} T_s}{\psi_{sD}} \right)^2 \right] v_{sDref}^2 + \left[ 2a\psi_{sQ} \left( \frac{T_s}{\psi_{sD}} \right)^2 + 2T_s \psi_{sD} + \frac{2\psi_{sQ}^2 T_s}{\psi_{sD}} \right] v_{sDref} \\ + 2aT_s \frac{\psi_{sQ}}{\psi_{sD}} + \left( \frac{aT_s}{\psi_{sD}} \right)^2 + \psi_{sD}^2 + \psi_{sQ}^2 - \psi_{sref}^2 = 0,$$

where

$$a = \frac{2\Delta t_e L'_s}{3PT_s} + (\psi_{sD} e_{sQ} - \psi_{sQ} e_{sD})$$

(see eqn (4.6-30) below).

#### Step 6 Estimation of required direct-axis stator reference voltage $v_{sQref}$ (by assuming $R_s=0$ )

Estimate  $v_{sQref}$  by using eqn (4.6-29) given below, thus

$$v_{sQref} = \frac{\psi_{sD} v_{sDref} + a}{\psi_{sD}}.$$

#### Step 7 Estimation of the required reference voltage space vector $\bar{u}_{sref}$ (adding correction term due to $R_s \neq 0$ )

Estimate the reference voltage space vector by using eqn (4.6-35) given below, thus

$$\bar{u}_{sref} = u_{sDref} + j u_{sQref} = \bar{v}_{sref} + R_s \bar{i}_s(t_n) = v_{sDref} + j v_{sQref} + R_s [i_{sD}(t_n) + j i_{sQ}(t_n)].$$

#### Step 8 Estimation of time duration of adjacent and zero switching-voltage vectors ( $t_a$ , $t_b$ , and $t_0$ )

Estimate the time duration of the switching voltage vectors which are adjacent to the reference stator voltage vector ( $t_a$ ,  $t_b$ ) by using eqns (4.6-39) and (4.6-40) or eqns (4.6-41)–(4.6-43). Estimate the time duration of the zero switching vector ( $t_0$ ) by using eqn (4.6-44). Thus e.g.

$$t_a = \frac{3T_s}{2U_d} \left[ u_{sDref} - \frac{u_{sQref}}{\sqrt{3}} \right]$$

$$t_b = \frac{\sqrt{3}}{U_d} T_s u_{sQref}$$

$$t_0 = T_s - t_a - t_b.$$

If a solution exists, then output switching states and switching intervals to base drives of the inverter. If solution does not exist (since it is not possible to have deadbeat control of stator flux linkage and electromagnetic torque), then proceed according to the method described below. However, first a mathematical and physical proof of the equations used will be presented.

#### Mathematical and physical proof of predictive steady-state algorithm

##### 1. Estimation of change of torque over a sampling period

In this computation step, the change of the electromagnetic torque is obtained over a period which is half of the switching period, in terms of the stator flux-linkage components, the reference values of the stator voltage components, and the back-e.m.f. components. For this purpose the stator voltage equation of the induction machine is used together with the expression for the electromagnetic torque. In contrast to the general predictive scheme described above, the rotor voltage equation is not used for the determination of the required switching voltage vectors, since the stator voltage equation is formulated in terms of the back e.m.f. (which implicitly contains the rotor flux) and the change of the electromagnetic torque is obtained in terms of the back e.m.f.

It follows from eqn (4.1-34) that the stator voltage equation of the induction machine in the stationary reference frame can be expressed as

$$\bar{u}_s = R_s \bar{i}_s + \frac{d\bar{\psi}_s}{dt} = R_s \bar{i}_s + L'_s \frac{d\bar{i}_s}{dt} + \bar{e} = R_s \bar{i}_s + \bar{v}, \quad (4.6-23)$$

where  $\bar{e}$  is the space vector of the back e.m.f. and  $\bar{v} = L'_s d\bar{i}_s / dt + \bar{e}$  is the voltage behind the stator transient inductance ( $L'_s$ ). Thus if the stator ohmic voltage drop is neglected, it is possible to estimate the direct- and quadrature-axis back e.m.f. components as

$$\bar{e} = e_{sD} + j e_{sQ} = \frac{d\bar{\psi}_s}{dt} - L'_s \frac{d\bar{i}_s}{dt}. \quad (4.6-24)$$

However, it should be noted that if it is assumed that  $\bar{\psi}_s$  and  $\bar{e}$  are sinusoidal, then  $\bar{e} = j\omega_1(\bar{\psi}_s - L'_s \bar{i}_s)$ , where  $\omega_1$  is the excitation frequency, and it can be simply

estimated by using  $\omega_1 = [\bar{\psi}_s \times (\bar{u}_s - R_s \bar{i}_s)] / |\bar{\psi}_s|^2$ . This can be proved by considering eqn (2.1-124), and by substitution of  $d/dt$  by  $j\omega_1$ .

It also follows from eqn (4.6-23) that if the stator ohmic voltage drop is neglected, then the rate of change of the stator-current space vector is simply

$$\frac{d\bar{i}_s}{dt} = (\bar{v} - \bar{e}) / L'_s. \quad (4.6-25)$$

If  $T_s$  is the time, which is equal to half the switching period, and it is assumed that this is sufficiently short, then  $d\bar{i}_s/dt \approx \Delta\bar{i}_s/T_s$  and the change of the stator current can be obtained from eqn (4.6-25) as

$$\Delta\bar{i}_s = \frac{T_s(\bar{v} - \bar{e})}{L'_s}. \quad (4.6-26)$$

By assuming that the stator electrical time constant is much longer than  $T_s$  (the change of the stator current over the  $T_s$  period is linear), the change of the electromagnetic torque over the time  $T_s$  can be obtained as  $(3/2)P\bar{\psi}_s \times \Delta\bar{i}_s$ , and thus by considering eqn (4.6-26),

$$\begin{aligned} \Delta t_e &= t_{ref} - t_e \approx \frac{3}{2} P(\bar{\psi}_s \times \Delta\bar{i}_s) \approx \frac{3}{2} PT_s \bar{\psi}_s \times \frac{(\bar{v}_{sref} - \bar{e})}{L'_s} \\ &= \frac{3}{2} PT_s \frac{(\bar{\psi}_s \times \bar{v}_{sref} - \bar{\psi}_s \times \bar{e})}{L'_s} \end{aligned} \quad (4.6-27)$$

is obtained. It can be seen that the change of the electromagnetic torque over a period  $T_s$  can be obtained from the stator voltage reference (which is now  $\bar{v}_{sref} = \bar{u}_{sref}$  since the stator ohmic drop has been neglected) and also the voltage vector ( $\bar{e}$ ) behind the stator transient inductance. By using the two-axis form of eqn (4.6-27), and considering that  $\bar{e} = e_{sD} + j e_{sQ}$ ,  $\bar{\psi}_s = \psi_{sD} + j \psi_{sQ}$ ,  $\bar{u}_{sref} = u_{sDref} + j u_{sQref}$ , we obtain

$$\Delta t_e = \frac{3PT_s}{2L'_s} [(\psi_{sD}v_{sQref} - \psi_{sQ}v_{sDref}) + (\psi_{sQ}e_{sD} - \psi_{sD}e_{sQ})]. \quad (4.6-28)$$

It follows from eqn (4.6-28) that the reference value of the quadrature-axis stator voltage is

$$v_{sQref} = \frac{\psi_{sD}v_{sDref} + a}{\psi_{sD}}, \quad (4.6-29)$$

where

$$a = \frac{2\Delta t_e L'_s}{3PT_s} + (\psi_{sD}e_{sQ} - \psi_{sQ}e_{sD}). \quad (4.6-30)$$

## 2. Stator voltages required for deadbeat control

The change of the stator flux can be obtained from eqn (4.6-23) and, by neglecting the ohmic drop (which is a valid assumption if the stator frequency is above a few Hz) and considering  $d\bar{\psi}_s/dt \approx \Delta\bar{\psi}_s/T_s$ ,

$$\Delta\bar{\psi}_s = T_s \bar{v} \quad (4.6-31)$$

is obtained. However, since  $|\bar{\psi}_{sref}| - |\bar{\psi}_s| = \Delta|\bar{\psi}_s| = \Delta\bar{\psi}_s$ , it follows by considering eqn (4.6-31) that

$$\bar{v}_{sref} = |\bar{\psi}_{sref}| = |\bar{\psi}_s| + \Delta|\bar{\psi}_s| = |\bar{\psi}_s(t_n)| + T_s \bar{v}_{ref}, \quad (4.6-32)$$

where  $t_n$  is the beginning of an  $n$ th  $T_s$  period and  $\bar{\psi}_s(t_n) = \psi_{sD} + j \psi_{sQ}$  is the space vector of the stator flux linkages at the beginning of the sampling period (the flux-linkage components are known, since they are determined by integrating the appropriate stator voltage). Equation (4.6-32) can be used to obtain the stator voltage required for deadbeat control of the stator flux linkages. By using the two-axis form of eqn (4.6-32),

$$\bar{v}_{sref}^2 = (\psi_{sD} + v_{sDref}T_s)^2 + (\psi_{sQ} + v_{sQref}T_s)^2, \quad (4.6-33)$$

where  $\psi_{sD}$  and  $\psi_{sQ}$  are the direct- and quadrature-axis stator flux linkages at the beginning of the  $n$ th sampling period. Thus the reference stator-voltage components  $v_{sDref}$ ,  $v_{sQref}$  can be obtained from eqns (4.6-29) and (4.6-33). Substitution of eqn (4.6-29) into (4.6-33) gives a quadratic equation, where the unknown is  $v_{sDref}$ ,

$$\begin{aligned} &\left[ T_s^2 + \left( \frac{\psi_{sQ}T_s}{\psi_{sD}} \right)^2 \right] v_{sDref}^2 + \left[ 2a\psi_{sQ} \left( \frac{T_s}{\psi_{sD}} \right)^2 + 2T_s\psi_{sD} + \frac{2\psi_{sQ}^2 T_s}{\psi_{sD}} \right] v_{sDref} \\ &+ 2aT_s \frac{\psi_{sQ}}{\psi_{sD}} + \left( \frac{aT_s}{\psi_{sD}} \right)^2 + \psi_{sD}^2 + \psi_{sQ}^2 - \bar{v}_{sref}^2 = 0. \end{aligned}$$

However, eqn (4.6-34) gives two solutions for  $v_{sDref}$ , but the solution with the smallest absolute value is chosen, since this corresponds to the smallest direct-axis stator voltage which is required to drive the stator flux linkage and electromagnetic torque to their reference values. When the obtained  $v_{sDref}$  is substituted into eqn (4.6-29), finally  $v_{sQref}$  is obtained. Thus  $\bar{v}_{sref} = v_{sDref} + j v_{sQref}$  is obtained (which corresponds to the reference-voltage space vector if the stator ohmic voltage drop is neglected). Therefore the corrected reference stator-voltage space vector (which incorporates the effects of the stator ohmic voltage drop) is obtained as

$$\bar{u}_{sref} = \bar{v}_{sref} + R_s \bar{i}_s(t_n). \quad (4.6-35)$$

In eqn (4.6-35) the stator ohmic drop from the previous cycle  $R_s \bar{i}_s(t_n)$  is added to  $\bar{v}_{sref}$ . However, this is justified, since as discussed above the change of the stator current is assumed to be linear over the period  $T_s$  (since the ohmic drop is small compared to the voltage drop across the stator transient inductance).

## 3. Inverter switching-state determination in the steady state (space-vector PWM)

The appropriate switching state of the inverter is determined by using space-vector pulse-width modulation (PWM). Therefore  $\bar{u}_{sref}$  [defined by eqn (4.6-35)] is used to select the optimal switching voltage vectors in such a way that the two switching vectors  $(\bar{u}_k, \bar{u}_{k+1})$  closest to  $\bar{u}_{sref}$  are selected, and the amount of time during which these vectors are applied ( $t_a, t_b$ ) is determined from

$$\bar{u}_{sref} T_s = \bar{u}_k t_a + \bar{u}_{k+1} t_b + \bar{u}_0 t_0. \quad (4.6-36)$$

In eqn (4.6-36)

$$T_s = t_a + t_b, \quad (4.6-37)$$

where  $T_s$  is the sampling time. Equation (4.6-36) follows from the fact that the time average of the three switching states (two active states and one zero state) during the sampling interval is equal to the reference voltage space vector, and also the switching voltage vectors and the reference voltage vector are constant over one switching cycle. In eqn (4.6-36),  $\bar{u}_k$  are the switching vectors in the 8 switching states of the voltage source inverter [see also eqn (4.6-4)]:

$$\bar{u}_k = \begin{cases} \frac{\sqrt{3}}{2} U_d \exp[j(k-1)\pi/3] & k=1, 2, \dots, 6 \\ 0 & k=7, 8 \end{cases} \quad (4.6-38)$$

where  $U_d$  is the d.c. link voltage,  $k=1, 2, \dots, 6$  corresponds to the active (non-zero) switching voltage vectors, and  $k=7, 8$  correspond to the two zero switching voltage vectors. The different switching states have been shown in Fig. 4.83(b). If eqn (4.6-38) is substituted into eqn (4.6-36) and the resulting equation is resolved into its real and imaginary parts, then  $t_a$  and  $t_b$  can be determined. Thus by using  $\bar{u}_{\text{ref}} = u_{sD\text{ref}} + j u_{sQ\text{ref}}$ ,

$$t_a = \frac{3T_s}{2U_d} \left[ \frac{u_{sD\text{ref}} - u_{sQ\text{ref}}}{\sqrt{3}} \right] \quad (4.6-39)$$

$$t_b = \frac{\sqrt{3}}{U_d} T_s u_{sQ\text{ref}}, \quad (4.6-40)$$

or by using polar coordinates,  $\bar{u}_{\text{ref}} = |\bar{u}_{\text{ref}}| \exp(j\alpha_{\text{ref}})$ :

$$t_a = a \left[ T_s \frac{(\cos \alpha_{\text{ref}} - \sin \alpha_{\text{ref}})}{\sqrt{3}} \right] \quad (4.6-41)$$

$$t_b = 2a T_s \frac{\sin \alpha_{\text{ref}}}{\sqrt{3}}, \quad (4.6-42)$$

where 'a' is the modulation index,

$$a = \frac{3|\bar{u}_{\text{ref}}|}{2U_d}. \quad (4.6-43)$$

The time during which the appropriate zero switching vector is selected is

$$t_0 = T_s - t_a - t_b. \quad (4.6-44)$$

Switching from the zero state to two adjacent states involves commutation of each inverter leg exactly once, thus  $T_s$  is a half-period of the switching frequency. Hence the stator flux linkage and the electromagnetic torque are controlled twice per switching frequency. Furthermore, when this control algorithm is used, then the oscillations in the stator currents are reduced.

Under transient conditions, it is not possible to have the deadbeat control. This is due to the fact that, in this case, there is no sufficient d.c. link voltage to cause

an adequate change in the electromagnetic torque and/or in the stator flux linkage to achieve deadbeat control. It follows from eqns (4.6-37), (4.6-39), and (4.6-40) that when there is an electromagnetic torque transient and/or stator flux-linkage transient (e.g. step changes), then the electromagnetic torque and stator flux-linkage errors are large in one switching period and thus  $t_a + t_b > T_s$  is obtained. This means that  $\bar{u}_{\text{ref}}$  is too large to be synthesized in a single switching period and thus an alternative control technique must be used. To summarize: the deadbeat control scheme presented above is suitable for the determination of the switching vectors in the steady state of the drive, and it is one advantage of the technique that the switching frequency is constant.

#### 4.6.2.9.3 Predictive control in the transient state

In the following the predictive control strategy (switching vector selection) to be used under transient conditions is discussed. If there is a transient in the electromagnetic torque reference (e.g. step change), then the controller must drive the electromagnetic torque in the required direction (to reduce the torque error over the period  $T_s$ ) while still maintaining deadbeat stator flux-linkage control. If there is a transient in the reference stator flux linkage, then the stator flux linkage has to be driven in the direction of its reference, while maintaining deadbeat control of the electromagnetic torque. In this way the selection of the appropriate switching vectors can be performed by first considering the position of the stator flux-linkage space vector (with respect to the sD-axis of the stationary reference frame),  $\rho_s$ , and then the sign of the electromagnetic torque or stator flux-linkage error is also considered. This is now discussed in some detail.

First a transient in the torque reference is assumed, where the electromagnetic torque cannot be driven to its reference value in a single  $T_s$  period (i.e. it is not possible to have deadbeat torque control). This is the most important case which arises most frequently, and in general a step change in the stator flux linkages is not required. In most of the cases the flux linkage is changed only during field weakening. However, in this operating mode, when the flux starts to be weakened, there is an almost linear change and then it varies continuously. Thus to obtain a simplified predictive switching-vector selection scheme, the simultaneous torque and flux transient can be neglected.

For the case when there is only torque transient, the switching vectors are chosen *a priori* in such a way that they should drive the torque in the desired direction, but allowing deadbeat stator flux-linkage control. If, for example, the stator flux-linkage space vector is in sector 1 shown in Fig. 4.84, which spans the region  $-30^\circ$  to  $30^\circ$  [angle  $\alpha(1)$ ], then the switching vectors  $\bar{u}_2$  and  $\bar{u}_3$  create flux linkages which will increase the original stator flux linkage and will also cause an increase of the electromagnetic torque. Similarly, switching vectors  $\bar{u}_5$ ,  $\bar{u}_6$  result in a decreased stator flux-linkage space vector and in a decreased electromagnetic torque. Thus  $\bar{u}_2$  and  $\bar{u}_3$  (which correspond to switching states 2 and 3) can be used to control the flux linkage to its reference value over the  $T_s$  period, while continuously increasing the torque over the entire interval. Thus it is possible to

construct a switching vector selection table for the transient state, where two switching vectors ( $k$ th and  $(k+1)$ -th vectors) are selected by using the torque error and the sector number  $n=1, 2, \dots, 6$  (where the stator flux linkage is located). This is shown in Table 4.6. The sector where a stator flux-linkage space vector is located can be determined from the position of the stator flux-linkage space vector (see discussion above in Section 4.6.2.2). In Table 4.6,  $k$  and  $k+1$  denote the selected  $k$ th and  $(k+1)$ -th switching states respectively.

Thus by using the selected switching vectors  $\bar{u}_k$ ,  $\bar{u}_{k+1}$ , the stator flux linkage is controlled in deadbeat fashion similarly to that given by eqn (4.6-32); thus

$$\psi_{\text{sref}} = |\bar{\psi}_s| + \Delta|\bar{\psi}_s| = |\bar{\psi}_s(t_n)| + \bar{u}_k t_k + \bar{u}_{k+1} t_{k+1}, \quad (4.6-45)$$

where for duration  $t_k$  the switching vector  $\bar{u}_k$  is applied and for duration  $t_{k+1}$  the switching vector  $\bar{u}_{k+1}$  is applied. In the transient state the zero switching vectors are not used, since it is desired to drive the electromagnetic torque in one direction in the fastest possible way during the switching period. Thus  $t_0=0$ , and it follows from eqn (4.6-44) that

$$T_s = t_k + t_{k+1}. \quad (4.6-46)$$

It should be noted that skipping the zero states while still switching between adjacent states is equivalent to pulse dropping in a conventional sinusoidal PWM. For a given value of  $\psi_{\text{sref}}$ , eqns (4.6-45) and (4.6-46) can then be solved for  $t_k$  and  $t_{k+1}$ . Thus by applying the appropriate switching vectors for the appropriate duration, the stator flux linkage is controlled to its reference value, and the electromagnetic torque is driven continuously to its desired value in the proper direction, with maximum voltage applied to the inverter (due to  $t_0=0$ , the voltage reference is maintained on the boundary of the hexagonal locus; thus the inverter output voltage is maximal).

If the second case is considered, when there is a transient of the stator flux linkage (i.e. the stator flux linkage cannot be driven to its reference value in a single  $T_s$  period), then again the voltage vector selection is made *a priori*. In this case, if for example the stator flux-linkage space vector is in sector 1, then  $\bar{u}_1$  and  $\bar{u}_2$  increase the flux and  $\bar{u}_3$  and  $\bar{u}_4$  decrease the flux, etc. The appropriate switching vector selection table is shown in Table 4.7.

Thus by using the selected switching vectors  $\bar{u}_k$ ,  $\bar{u}_{k+1}$ , the electromagnetic torque is controlled in deadbeat fashion similarly to that given by eqn (4.6-27); thus

$$\Delta t_e = \frac{3P}{2L_s} [\bar{\psi}_s \times (t_k \bar{u}_k + t_{k+1} \bar{u}_{k+1} - T_s \bar{e})]. \quad (4.6-47)$$

**Table 4.6** Switching-voltage vector selection if there is an electromagnetic torque transient

$\text{sgn}(t_e - t_{\text{eref}})$	k						k+1					
	$\alpha(1)$ sect 1	$\alpha(2)$ sect 2	$\alpha(3)$ sect 3	$\alpha(4)$ sect 4	$\alpha(5)$ sect 5	$\alpha(6)$ sect 6	$\alpha(1)$ sect 1	$\alpha(2)$ sect 2	$\alpha(3)$ sect 3	$\alpha(4)$ sect 4	$\alpha(5)$ sect 5	$\alpha(6)$ sect 6
0	$\bar{u}_2$	$\bar{u}_3$	$\bar{u}_4$	$\bar{u}_5$	$\bar{u}_6$	$\bar{u}_1$	$\bar{u}_3$	$\bar{u}_4$	$\bar{u}_5$	$\bar{u}_6$	$\bar{u}_1$	$\bar{u}_2$
1	$\bar{u}_5$	$\bar{u}_6$	$\bar{u}_1$	$\bar{u}_2$	$\bar{u}_3$	$\bar{u}_4$	$\bar{u}_6$	$\bar{u}_1$	$\bar{u}_2$	$\bar{u}_3$	$\bar{u}_4$	$\bar{u}_5$

**Table 4.7** Switching voltage vector selection if there is a stator flux-linkage transient

$\text{sgn}( \bar{\psi}_{\text{sref}}  - \psi_{\text{sref}})$	k						k+1					
	$\alpha(1)$ sect 1	$\alpha(2)$ sect 2	$\alpha(3)$ sect 3	$\alpha(4)$ sect 4	$\alpha(5)$ sect 5	$\alpha(6)$ sect 6	$\alpha(1)$ sect 1	$\alpha(2)$ sect 2	$\alpha(3)$ sect 3	$\alpha(4)$ sect 4	$\alpha(5)$ sect 5	$\alpha(6)$ sect 6
0	$\bar{u}_1$	$\bar{u}_2$	$\bar{u}_3$	$\bar{u}_4$	$\bar{u}_5$	$\bar{u}_6$	$\bar{u}_5$	$\bar{u}_6$	$\bar{u}_1$	$\bar{u}_2$	$\bar{u}_3$	$\bar{u}_4$
1	$\bar{u}_3$	$\bar{u}_4$	$\bar{u}_5$	$\bar{u}_6$	$\bar{u}_1$	$\bar{u}_2$	$\bar{u}_2$	$\bar{u}_3$	$\bar{u}_4$	$\bar{u}_5$	$\bar{u}_6$	$\bar{u}_1$

**Table 4.8** Switching-voltage vector selection if there are both stator flux-linkage and electromagnetic torque transients

$\text{sgn}(t_e - t_{\text{eref}})$	$\text{sgn}( \bar{\psi}_s  - \psi_{\text{sref}})$	$\alpha(1)$ sector 1	$\alpha(2)$ sector 2	$\alpha(3)$ sector 3	$\alpha(4)$ sector 4	$\alpha(5)$ sector 5	$\alpha(6)$ sector 6
		sector 1	sector 2	sector 3	sector 4	sector 5	sector 6
0	0	$\bar{u}_2$	$\bar{u}_3$	$\bar{u}_4$	$\bar{u}_5$	$\bar{u}_6$	$\bar{u}_1$
0	1	$\bar{u}_3$	$\bar{u}_4$	$\bar{u}_5$	$\bar{u}_6$	$\bar{u}_1$	$\bar{u}_2$
1	1	$\bar{u}_5$	$\bar{u}_6$	$\bar{u}_1$	$\bar{u}_2$	$\bar{u}_3$	$\bar{u}_4$
1	0	$\bar{u}_6$	$\bar{u}_1$	$\bar{u}_2$	$\bar{u}_3$	$\bar{u}_4$	$\bar{u}_5$

Equations (4.6-46) and (4.6-47) yield the required  $t_k$  and  $t_{k+1}$ . Thus if the selected switching vector  $\bar{u}_k$  is applied for duration  $t_k$  and  $\bar{u}_{k+1}$  is applied for duration  $t_{k+1}$ , then deadbeat control of the electromagnetic torque is performed, while driving the stator flux-linkage space vector in the desired direction. It should be noted that, as before, the zero switching vectors are not used. Disregarding the zero switching states while still switching between adjacent states is equivalent to pulse-dropping in a conventional sinusoidal PWM.

Finally the third condition is considered: this is the case when there is a transient in both the stator flux linkage and electromagnetic torque. In this case a single switching state is selected for the entire switching period, which drives both the electromagnetic torque and stator flux linkage in the desired directions as quickly as possible. For example, if the stator flux-linkage space vector is in the first sector, and both the flux and the torque have to be increased, then by considering the six switching vectors,  $\bar{u}_2$  has to be selected. If the flux has to be increased but the torque has to be decreased then  $\bar{u}_6$  has to be selected, etc. The switching vectors are given in Table 4.8.

Obviously this agrees with the corresponding parts in Table 4.3 shown in Section 4.6.2.2.

Thus, in general, the algorithm for the switching voltage vector selection is such that first the computational steps (Steps 1–8) given above for the steady-state estimation are performed. However, if in Step 8 it is found that there is no positive solution (for  $t_a$  and  $t_b$ ), e.g.  $t_k + t_{k+1} \leq T_s$  cannot be satisfied, then it is first assumed that there is a transient in the electromagnetic torque reference. Thus Table 4.6 is used for the selection of the appropriate two inverter switching states and then eqns (4.6-45) and (4.6-46) are solved to yield  $t_k$  and  $t_{k+1}$ . If this gives

positive solutions, then  $\bar{u}_k$  and  $\bar{u}_{k+1}$  are applied for the duration of  $t_k$  and  $t_{k+1}$  respectively. However, if a positive solution still does not exist, then it is assumed that a transient in the stator flux linkage is present and therefore eqns (4.6-46) and (4.6-47) are solved. If positive solutions exist then the appropriate switching vectors shown in Table 4.7 are applied for the durations  $t_k$  and  $t_{k+1}$  respectively. However, if a solution does not exist then the switching states shown in Table 4.8 are applied (corresponding switching states and switching times are outputs to the inverter base drives). The predictive algorithm can be implemented by a DSP, but it should be considered that this is a computationally very intensive scheme and at higher switching frequencies very fast computations are required.

It should be noted that, similarly to other types of predictive control schemes, when the present predictive scheme is used, a single  $T_s$ -period steady-state error occurs. This is due to the fact that the estimation of the electromagnetic torque and stator flux linkage is based on inputs from the preceding period. A single-period delay is required to allow time to estimate the switching signals. An ideal deadbeat controller would require the estimations to be performed in zero time. Furthermore, the predictive controller is based only on the electromagnetic torque and stator flux-linkage errors. The combination of this fact with the single-period delay results in a steady-state error of the electromagnetic torque. However, this does not present any problem if a speed controller is also used.

An alternative predictive switching-vector selection technique is now briefly discussed, which is not as computationally intensive as the one described above. It is assumed that there is only a torque transient. Although the alternative technique does not result in deadbeat control of the stator flux linkage, only minimal performance degradation will result. This is achieved by limiting the magnitude of the stator voltage reference to the maximum instantaneous value allowable with space-vector modulation. This is shown in Fig. 4.90.

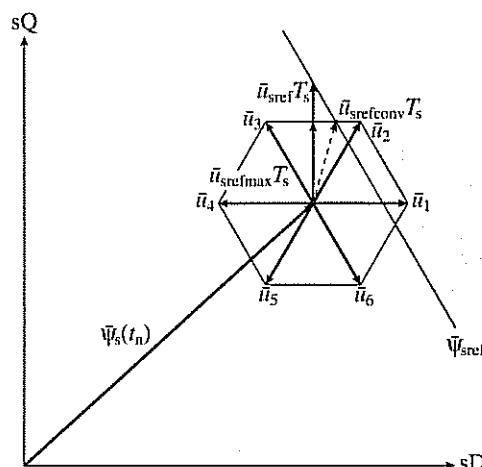


Fig. 4.90. Alternative predictive switching-vector selection.

It is shown in Fig. 4.90 that every time the voltage reference vector ( $\bar{u}_{sref}$ ) resulting from a deadbeat control algorithm is outside the voltage hexagon, the magnitude of the voltage input to the space-vector modulator is limited to the maximum inverter voltage ( $\bar{u}_{srefmax}$ ), which is also shown in Fig. 4.90. The voltage  $\bar{u}_{srefmax}$  has the same angle as the original voltage reference ( $\alpha_{sref}$ ). Thus the magnitude of the voltage reference vector is given as

$$|\bar{u}_{smaxref}| = (1/3)U_d\sqrt{3}/\sin(\alpha_{sref} + \pi/3) \quad (4.6-48)$$

and the angle is unchanged from that computed by using the algorithm given above. In Fig. 4.90 the average value of the stator voltage over one sampling period ( $T_s$ ) computed by the original (not the alternative) predictive scheme is  $\bar{u}_{srefconv}$ ; this is shown by a vector with broken lines. The tip of this vector is at the intersection of the output voltage hexagonal boundary and the reference stator flux linkage. However, when the alternative predictive scheme is used, the average voltage ( $\bar{u}_{srefmax}$ ) over the same period ( $T_s$ ) lies on the voltage boundary at the same angle as  $\bar{u}_{sref}$ . It should be noted that the flux-linkage error increases as the magnitude of  $\bar{u}_{sref}$  increases. It is interesting to note that  $\bar{u}_{sref}$  is leading  $\bar{u}_{srefconv}$  for the transient condition when the electromagnetic torque has to be increased, and it lags  $\bar{u}_{srefconv}$  for the transient condition when the electromagnetic torque has to be decreased. It follows that the torque-producing current is larger with the alternative scheme than with the original predictive scheme. This leads to improved dynamic performance, despite the fact that the improved scheme does not provide deadbeat control of the flux magnitude. This alternative predictive scheme can also be used when overmodulation occurs (i.e. in the transition region between continuous PWM and six-step operation). This operating region is a particular case of the torque/flux transients. Similarly to that discussed above, in the transition region the voltage reference vector  $\bar{u}_{sref}$  lies outside the hexagon boundary. In the limit, as  $\bar{u}_{sref}$  becomes large in magnitude, the inverter voltage  $\bar{u}_{srefmax}$  jumps from one corner of the hexagon to the next, which is equivalent to six-step operation.

#### 4.6.2.10 Speed-sensorless DTC drive implementations

For a speed-sensorless DTC drive it is possible to use any of the techniques described in Section 4.5. Thus the following techniques can be used in a speed-sensorless DTC drive (see Section 4.5.1 for a brief discussion):

1. Open-loop and improved estimators using monitored stator voltages/currents;
2. Estimators using the spatial saturation stator-phase third-harmonic voltage;
3. Estimators using saliency (geometrical, saturation) effects;
4. Model reference adaptive systems (MRAS);
5. Observers (Kalman, Luenberger);
6. Estimators using artificial intelligence (neural network, fuzzy-logic-based systems, fuzzy-neural networks, etc.).

Such techniques have been discussed in detail in Sections 4.5.3.1–4.5.3.6 and thus these will not be repeated here. However, it should be noted that so far only one specific solution using the first technique has been applied for a DTC induction motor drive (in the ABB DTC induction motor drive), but it is expected that the other techniques shown above will also be used in the future. In particular it is expected that estimators using artificial intelligence will play an increased role. Such estimators are also robust to parameter variations.

The speed signal can be required in a DTC induction motor drive for two reasons. One reason is that it can be used for stator flux-linkage estimation, if the stator flux-linkage estimator requires the rotor speed signal (e.g. when a hybrid stator flux-linkage estimator is used, which uses both the stator voltage equation and also the rotor voltage equation, as discussed above in Section 4.6.2.6.3, and the rotor voltage equation contains the rotor speed). The other reason is that a rotor speed signal is required if the drive contains a speed-control loop (in this case the speed controller outputs the torque reference, and the input to the speed controller is the difference between the reference speed and the estimated speed). In many variable-speed drive applications torque control is required, but speed control is not necessary. An example of an application where the electromagnetic torque is controlled without precise speed control is traction drives. In traction applications (diesel-electric locomotives, electrical cars, etc.) the electromagnetic torque is directly controlled, i.e. the electromagnetic torque is the commanded signal, and it is not the result of a speed error signal.

The key to the success of simple open-loop speed estimation schemes is the accurate estimation of the stator (or rotor) flux-linkage components. If the flux linkages are accurately known, then it is possible to estimate the rotor speed by simple means, which utilize the speed of the estimated flux-linkage space vector. It is this technique which is used in the DTC induction motor drive manufactured by ABB, which is the only known industrial DTC drive at present. However, the same technique is also used in some other commercially available drives (vector drives), thus this will now be briefly discussed. In these commercial implementations the stator voltages are not monitored but are reconstructed from the d.c. link voltage and switching states of the inverter (see Section 3.1.3.2.1).

It follows from eqn (4.5-36) that the rotor speed can be expressed as

$$\omega_r = \omega_{mr} - \omega_{sl}, \quad (4.6-49)$$

where  $\omega_{mr}$  is the speed of the rotor flux (relative to the stator)  $\omega_{mr} = d\rho_r/dt$ , and  $\omega_{sl}$  is the angular slip frequency, given by eqns (4.5-34) and (4.5-35), which are now repeated here for convenience:

$$\omega_{sl} = \frac{L_m}{T_r |\bar{\psi}_r|^2} (-\psi_{rq} i_{sD} + \psi_{rd} i_{sQ}) \quad (4.6-50)$$

$$\omega_{sl} = \frac{2t_e R_r}{3P |\bar{\psi}_r|^2}. \quad (4.6-51)$$

Physically,  $\omega_{sl}$  is the speed of the rotor flux-linkage space vector with respect to the rotor. It is possible to obtain an expression for  $\omega_{mr}$  in terms of the rotor

flux-linkage components by expanding the expression for the derivative  $d\rho_r/dt$ . Since the rotor flux-linkage space vector expressed in the stationary reference frame is  $\bar{\psi}'_r = \psi_{rd} + j\psi_{rq} = |\bar{\psi}_r| \exp(j\rho_r)$ , thus  $\rho_r = \tan^{-1}(\psi_{rq}/\psi_{rd})$ , it follows that the derivative can be expanded to give

$$\begin{aligned} \omega_{mr} &= \frac{d\rho_r}{dt} = \frac{d}{dt} [\tan^{-1}(\psi_{rq}/\psi_{rd})] \\ &= \left( \psi_{rd} \frac{d\psi_{rq}}{dt} - \psi_{rq} \frac{d\psi_{rd}}{dt} \right) / (\psi_{rd}^2 + \psi_{rq}^2). \end{aligned} \quad (4.6-52)$$

The numerator of eqn (4.6-52) contains  $|\bar{\psi}_r|^2 = (\psi_{rd}^2 + \psi_{rq}^2)$ . Substitution of eqn (4.6-52) into eqn (4.6-49), and by also considering eqns (4.6-50) or (4.6-51), we obtain

$$\omega_r = \left( \psi_{rd} \frac{d\psi_{rq}}{dt} - \psi_{rq} \frac{d\psi_{rd}}{dt} \right) / |\bar{\psi}_r|^2 - \frac{L_m}{T_r |\bar{\psi}_r|^2} (\psi_{rd} i_{sQ} - \psi_{rq} i_{sD}) \quad (4.6-53)$$

and

$$\omega_r = \left( \psi_{rd} \frac{d\psi_{rq}}{dt} - \psi_{rq} \frac{d\psi_{rd}}{dt} \right) / |\bar{\psi}_r|^2 - \frac{2t_e R_r}{3P |\bar{\psi}_r|^2}. \quad (4.6-54)$$

Such a speed estimator is used in the ABB DTC induction motor drive. A rotor speed estimator based on eqn (4.6-53) or (4.6-54) can then be constructed, which uses the monitored stator currents and the rotor flux components which, however, can be obtained from the stator flux linkages by considering eqns (4.5-16) and (4.5-17):

$$\psi_{rd} = \frac{L_r}{L_m} (\psi_{sD} - L'_s i_{sD}) \quad (4.6-55)$$

$$\psi_{rq} = \frac{L_r}{L_m} (\psi_{sQ} - L'_s i_{sQ}). \quad (4.6-56)$$

In eqns (4.6-55) and (4.6-56) the stator flux linkages can be obtained by using monitored stator currents and monitored or reconstructed stator voltages, as discussed earlier in Section 3.1.3.2. Thus by using the inverter switching functions  $S_A$ ,  $S_B$ ,  $S_C$  (see also Fig. 4.83 in Section 4.6.2.1) the stator-voltage space vector (expressed in the stationary reference frame) can be obtained, by using the switching states and the d.c. link voltage  $U_d$ , as

$$\bar{u}_s = \frac{2}{3} U_d (S_A + aS_B + a^2 S_C) = u_{sD} + ju_{sQ}, \quad (4.6-57)$$

where

$S_A = 1$  when upper switch in phase sA of inverter (S1) is ON and lower switch (S4) is OFF

$S_A = 0$  when upper switch in phase sA of inverter (S1) is OFF and lower switch (S4) is ON

$S_B=1$  when upper switch in phase sB of inverter (S3) is ON and lower switch (S6) is OFF

$S_B=0$  when upper switch in phase sB of inverter (S3) is OFF and lower switch (S6) is ON

$S_C=1$  when upper switch in phase sC of inverter (S5) is ON and lower switch (S2) is OFF

$S_C=0$  when upper switch in phase sC of inverter (S5) is OFF and lower switch (S2) is ON.

It follows from eqn (4.6-57) that

$$u_{sD} = \frac{2}{3}U_d \left( S_A - \frac{S_B}{2} - \frac{S_C}{2} \right) = U_d \left[ S_A - \frac{(S_A + S_B + S_C)}{3} \right] \quad (4.6-58)$$

$$u_{sQ} = U_d \frac{(S_B - S_C)}{\sqrt{3}}. \quad (4.6-59)$$

Thus the  $k$ th sampled value of the estimated stator flux-linkage space vector can be obtained as

$$\bar{\psi}_s(k) = \bar{\psi}_s(k-1) + \frac{2}{3}U_d T_s [S_A(k-1) + aS_B(k-1) + a^2S_C(k-1)] - R_s T_s \bar{i}_s(k-1), \quad (4.6-60)$$

where  $T_s$  is the sampling time (flux control period) and  $\bar{i}_s$  is the stator-current space vector. Resolution of eqn (4.6-60) into its real- and imaginary-axis components gives  $\psi_{sD}$  and  $\psi_{sQ}$ . It is important to note that eqn (4.6-60) is sensitive to voltage errors caused by:

- dead-time effects (e.g. at low speeds, the pulse-widths become very small and the dead time of the inverter switches must be considered);
- the voltage drop in the power electronic devices;
- the fluctuation of the d.c. link voltage (but due to this, the d.c. link voltage must be monitored);
- the variation of the stator resistance (this resistance variation sensitivity is also a feature of the method using the monitored stator voltages).

However, it is possible to have a speed-sensorless DTC drive implementation in which the dead-time effects are also considered (see also Sections 3.1.3.2 and 8.2) and the thermal variation of the stator resistance is also incorporated into the control scheme (e.g. by using a thermal model of the induction machine).

The accuracy of a speed estimator using eqn (4.6-53) or (4.6-54) depends greatly on the machine parameters used, and also on the model used for the estimation of the rotor flux-linkage components. A possible implementation has been shown in Section 4.5.2.1, Fig. 4.53. The speed estimator requires the following machine

parameters:  $R_s$ ,  $L'_s$ ,  $k_r = L_m/L_r$ , and  $L_m/T_r$ . For digital implementation it is possible to use various forms, including the following discrete form:

$$\omega_r(k) = \frac{\psi_{rd}(k-1)\psi_{rq}(k) - \psi_{rq}(k-1)\psi_{rd}(k)}{|\psi_r(k)|^2} - \frac{L_m}{T_r |\psi_r(k)|^2} [-\psi_{rq}(k)i_{sD}(k) + \psi_{rd}(k)i_{sQ}(k)], \quad (4.6-61)$$

where  $|\bar{\psi}_r(k)|^2 = [\psi_{rd}(k-1)]^2 + [\psi_{rq}(k-1)]^2$ . Since this equation contains a modelling error, which results in an error of the estimated rotor speed, in practice a low-pass filter can be used to remove this error.

It is also possible to estimate the rotor speed in another way, which is similar to that described by eqn (4.6-49), but which instead of using the speed of the rotor flux ( $\omega_{mr}$ ) can use the speed of the stator flux  $\omega_{ms}$ . It follows from eqns (4.2-16) and (4.2-23) that in this case the rotor speed can be expressed as

$$\omega_r = \omega_{ms} - \omega'_{sl}, \quad (4.6-62)$$

where

$$\omega'_{sl} = \frac{L_s(i_{sy} + T'_r di_{sy}/dt)}{T_r |\bar{\psi}_s| - L'_s i_{sx}} \quad (4.6-63)$$

is the speed of the stator flux-linkage space vector relative to the rotor (not the speed of the rotor flux relative to the rotor, which has been denoted by  $\omega_{sl}$ ). If the direct- and quadrature-axis stator flux linkages ( $\psi_{sD}, \psi_{sQ}$ ) in the stationary reference frame are known (they are estimated by one of the techniques described in Section 4.6.2.6, which uses the monitored stator voltages and currents or the reconstructed stator voltages and currents), then since  $\bar{\psi}_s = \psi_{sD} + j\psi_{sQ} = |\bar{\psi}_s| \exp(j\rho_s)$ , where  $\rho_s$  is the angle of the stator flux-linkage space vector with respect to the real axis of the stationary reference frame, it follows that

$$\omega_{ms} = \frac{d\rho_s}{dt} = \frac{d}{dt} [\tan^{-1}(\psi_{sQ}/\psi_{sD})]. \quad (4.6-64)$$

By performing the differentiation, this can be put into the following form:

$$\omega_{ms} = \frac{\psi_{sD} d\psi_{sQ}/dt - \psi_{sQ} d\psi_{sD}/dt}{\psi_{sD}^2 + \psi_{sQ}^2}, \quad (4.6-65)$$

where the numerator contains  $|\bar{\psi}_s|^2$ . By using eqns (4.6-15) and (4.6-16), it is possible to express  $\omega_{ms}$  in terms of the stator voltages and stator currents. To obtain a rotor speed estimator, which uses  $\omega_{ms}$  [defined by eqn (4.6-64)], it is possible to proceed in various ways.

It should be noted that eqn (4.6-62) has been directly obtained from the rotor voltage equation of the induction machine, but this expression was expressed in the stator-flux-oriented reference frame (which rotates at the speed of  $\omega_{ms}$ ). Thus in eqn (4.6-63) the stator currents  $i_{sx}$  and  $i_{sy}$  are the stator currents in the

stator-flux-oriented reference frame, and they can be obtained from the stator currents  $i_{sD}$ ,  $i_{sQ}$  (expressed in the stationary reference frame) by considering

$$i_{sx} + j i_{sy} = (i_{sD} + j i_{sQ}) \exp(-j \rho_s) = (i_{sD} + j i_{sQ})(\cos \rho_s - j \sin \rho_s).$$

However,  $\cos \rho_s$  and  $\sin \rho_s$  can be obtained by using  $\cos \rho_s = \psi_{sD}/|\bar{\psi}_s|$  and  $\sin \rho_s = \psi_{sQ}/|\bar{\psi}_s|$ , or  $\rho_s$  can be obtained by using a rectangular-to-polar converter (where the inputs are  $\psi_{sD}$  and  $\psi_{sQ}$  and the outputs are  $|\bar{\psi}_s|$  and  $\rho_s$ ).

It is possible to obtain other solutions as well which use the speed of both the stator and rotor flux-linkage space vectors. For example, such a scheme can be derived by considering that the rotor speed is equal to the sum of the speed of the stator flux-linkage space vector,  $\omega_{ms} = d\rho_s/dt$ , minus the speed difference between the stator and rotor flux-linkage space vectors,  $\omega_d = d\rho/dt$ , minus the speed of the rotor flux-linkage space vector (relative to the rotor),  $\omega_{sr} = d\theta_{sr}/dt$ . Thus it follows from eqn (4.5-44) that

$$\omega_r = \omega_{ms} - \omega_d - \omega_{sr}. \quad (4.6-66)$$

In Section 4.5.3.1 a simple proof of eqn (4.6-66) has been given by considering Fig. 4.55. As stated above,  $\rho_s$  is the angle of the stator flux-linkage space vector with respect to the real axis of the stator reference frame,  $\rho_r$  is the angle of the rotor flux-linkage space vector with respect to the real axis of the stator reference frame, and  $\rho$  is the angle between the stator and rotor flux-linkage space vectors,  $\rho = \rho_s - \rho_r$ . It follows that  $\omega_d = d\rho/dt = d\rho_s/dt - d\rho_r/dt = \omega_{ms} - \omega_{mr}$  is indeed the difference between the speed of the stator flux-linkage space vector and the speed of the rotor flux-linkage space vector. Furthermore,  $\theta_r$  is the rotor angle, and  $\theta_r = \rho_s - \rho - \theta_{sr}$ . Thus  $\omega_r = d\theta_r/dt = d\rho_s/dt - d\rho/dt - d\theta_{sr}/dt = \omega_{ms} - \omega_d - \omega_{sr}$  is obtained, in agreement with eqn (4.6-66). This can be put into the following form (see the derivation of eqn (4.5-45)):

$$\omega_r = \frac{\psi_{sD} d\psi_{sQ}/dt - \psi_{sQ} d\psi_{sD}/dt}{\psi_{sD}^2 + \psi_{sQ}^2} - \frac{d}{dt} [\sin^{-1}(t_e/(c|\bar{\psi}_s||\bar{\psi}_r|))] - (2t_e R_r)/(3P|\bar{\psi}_r|^2), \quad (4.6-67)$$

where it is possible to use different expressions for the electromagnetic torque, e.g.

$$t_e = \frac{3}{2} P(\psi_{sD} i_{sQ} - \psi_{sQ} i_{sD}) \quad (4.6-68)$$

or

$$t_e = \frac{3}{2} P \frac{L_m}{L_r} (\psi_{rd} i_{sQ} - \psi_{rq} i_{sD}). \quad (4.6-69)$$

Equation (4.6-67) can also be used for the estimation of the rotor speed of an induction machine, but this is not simpler than eqns (4.6-53) or (4.6-54).

In summary it should be noted that the speed estimators discussed above depend heavily on the accuracy of the used flux-linkage components. If the stator voltages and currents are used to obtain the flux estimates, then by considering the thermal variations of the stator resistance (e.g. by using a thermal model), and

also by using appropriate saturated inductances (see also Sections 4.6.2.11, 8.2.6), the estimation accuracy can be greatly improved. However, a speed-sensorless high-performance direct-torque-controlled drive using this type of speed estimator will only work successfully at ultra-low speeds (including the zero speed) if the flux estimator is some type of closed-loop observer.

It is expected that in the future universal induction motor drives will emerge which will also incorporate direct torque control. Control techniques Plc (UK) was the first in the world to introduce a universal drive, but at present it does not incorporate direct torque control.

#### 4.6.2.11 The ABB DTC induction motor drive

ABB has introduced in 1995 the first industrial, speed-sensorless DTC induction motor drive in the world. This contains the ACS 600 frequency converter (inverter), which uses power-plate IGBT modules and is shown in Fig. 4.91. The inverter switching directly controls the motor flux linkages and electromagnetic torque.

The ACS 600 product family (ACS 601, 603, 604, 607) suits many applications and operating environments, with a large selection of a.c. voltages (380 V–690 V), power (2.2 kW–630 kW), and enclosure (IP 00, IP 20, IP 21, IP 22, IP 54) ratings, combined with highly flexible communication capabilities. The drive is suitable for 95% of all industrial applications (including pumps, fans, mixers, conveyors, lifts, elevators, cranes, hoists, winders, centrifuges, extruders, etc.).

The ACS 600 can accurately control the rotor speed and electromagnetic torque (and stator flux linkages) without encoder or tachogenerator feedback. The schematic block diagram of the drive is shown in Fig. 4.92. This is similar to that shown in Fig. 4.87 and thus the reader is referred to the many details discussed earlier (in Sections 4.6.1, 4.6.2.1–4.6.2.10) and only some of the main features will be described below. The primary control variables are the electromagnetic torque and stator flux linkage.

In Fig. 4.92 two stator currents are measured together with the d.c. link voltage. The two stator currents can be used to obtain the direct- and quadrature-axis stator currents in the stationary reference frame,  $i_{sD} = i_{sA}$ ,  $i_{sQ} = (i_{sA} + 2i_{sB})/\sqrt{3}$ . By using the measured d.c. link voltage ( $U_d$ ) and the switching signals of the inverter, the stator voltages are reconstructed (see eqn (4.6-57) in Section 4.6.2.10). However, as discussed in Section 4.6.2.10, for an accurate reconstruction of the stator voltages, the interlock delay (dead time, which is programmed in the DSP switching logic to prevent short-circuits of the d.c. link), and voltage drops across the semiconductor switches of the inverter (IGBTs), must also be considered, especially at low rotor speed.

The stator currents together with the stator voltages are inputs to an adaptive induction motor model also shown in Fig. 4.92 (which contains an observer), which estimates in real time (using a DSP) the modulus of the stator flux-linkage space vector,  $|\bar{\psi}_s|$ , its position (with respect to the real-axis of the stationary reference frame),  $\rho_s$ , the electromagnetic torque ( $t_e$ ), and rotor speed ( $\omega_r$ ) in every

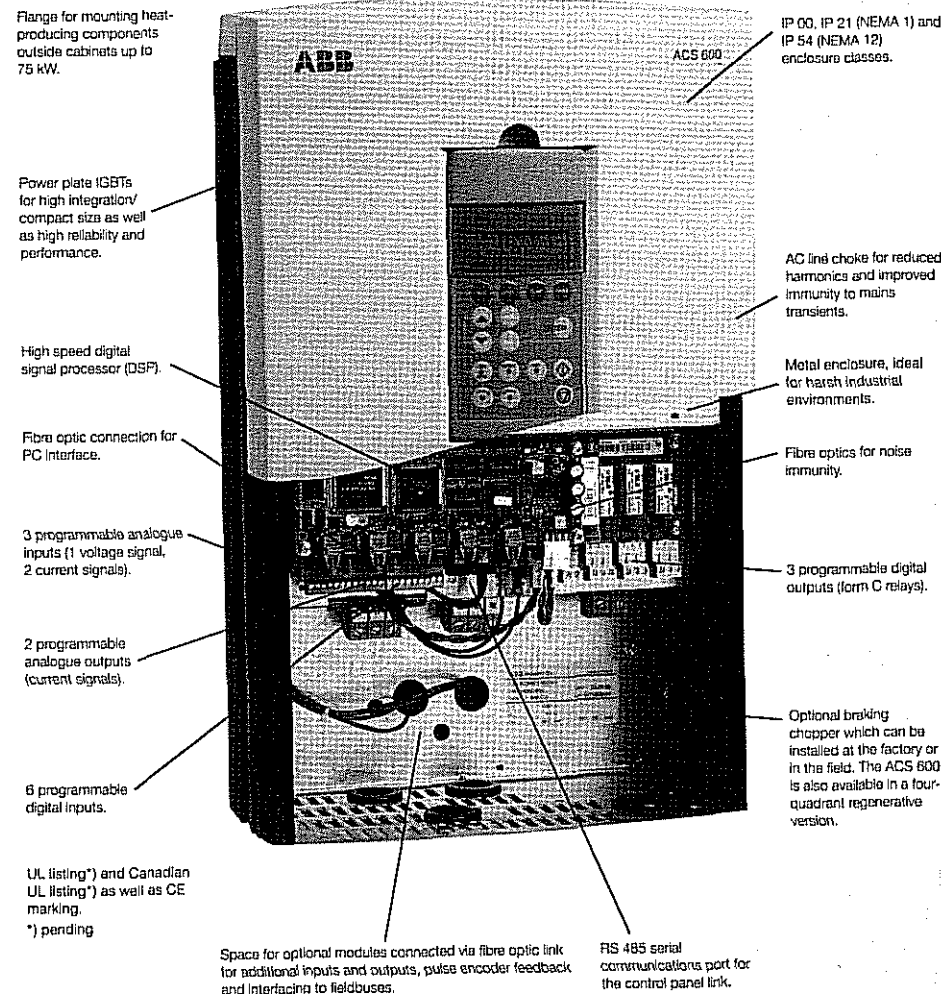


Fig. 4.91. ACS 600 frequency converter (Courtesy of ABB Industry Oy, Helsinki).

25 microseconds. As discussed in Sections 4.6.2.3 and 4.6.2.6, it is very important to consider that the main role of the motor model is to estimate accurately the stator flux-linkage components, since the modulus and position of the stator flux-linkage space vector, the electromagnetic torque, and also the rotor speed are estimated from the stator flux-linkage components. The reader is referred to the previous sections which discuss different techniques of stator flux linkage, electromagnetic torque, and rotor speed estimation. In particular, Sections 4.6.2.3 and 4.6.2.6 discuss the estimation of the stator flux linkages together with the application of various drift compensation techniques. Furthermore, eqns (4.6-11)

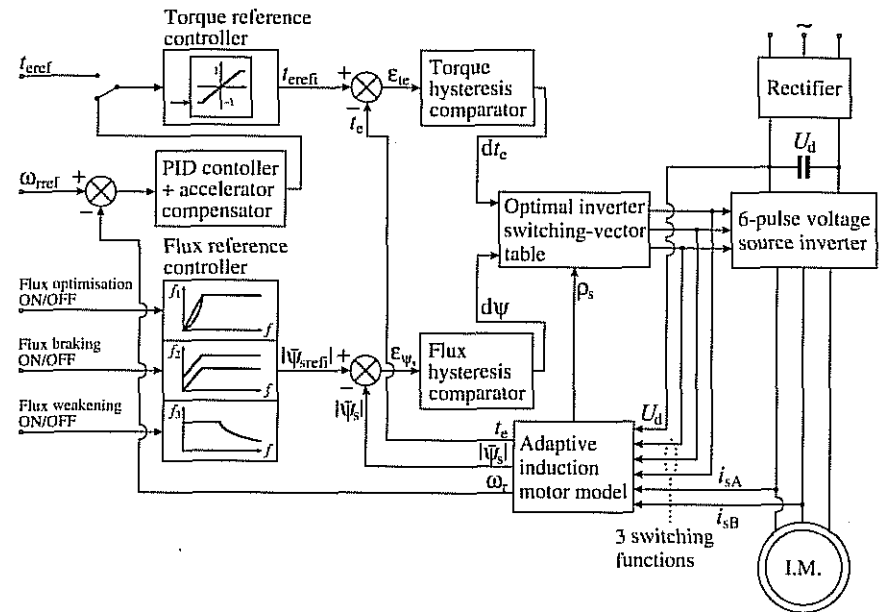


Fig. 4.92. Schematic block diagram of ABB DTC induction motor drive.

and (4.6-54) give the expressions for the electromagnetic torque and rotor speed in terms of flux-linkage components. The rotor flux-linkage components present in eqn (4.6-54) can be obtained from the stator flux linkages by using eqns (4.6-55) and (4.6-56).

To create one possible motor model, the only data which have to be entered by the user into the initialization software of the ABB DTC drive are the nameplate data (e.g. rated motor speed, rated stator current, rated stator voltage, rated power, rated frequency). However, to obtain a more accurate motor model, some of the parameters used in the motor model are initialized during a motor identification run stage (self-commissioning stage, which is also sometimes referred to as the auto-calibration stage). During the start-up of the drive system, the ACS 600 operates the motor for approximately one minute. The control circuitry monitors the response of the induction motor to the applied power and determines various machine parameters (e.g. the stator resistance, stator inductance, magnetizing inductance, saturation coefficients for these two inductances, inertia of the motor, etc.) and enhances the mathematical model of the motor. For example, the stator resistance is required, since in principle, at high speed, the stator flux linkages are obtained by integrating the appropriate stator voltage reduced by the corresponding ohmic drop,  $\psi_{sD} = \int(u_{sD} - R_s i_{sD}) dt$ ,  $\psi_{sQ} = \int(u_{sQ} - R_s i_{sQ}) dt$ . Since the rotor speed is determined by using the speed of the rotor flux-linkage space vector [see eqn (4.6-54)], this also requires the use of various inductance parameters of the induction machine.

There are two identification (ID) run alternatives: the standard ID run, and the reduced ID run. During the standard ID run, the motor is uncoupled from the load. However, the reduced ID run has to be used if the load cannot be disengaged from the induction motor or if stator flux reduction is not allowed. For example, stator flux reduction is not allowed with a braking motor, where the brake is switched on if the motor voltage or flux reduces significantly. To obtain the most accurate motor model and the best possible control performance, the standard ID run has to be selected. If the identification run is not selected, a rapid motor identification is automatically performed (when the START command is issued). During the first start-up procedure, the motor is run at zero speed for several seconds to allow the estimation of the required parameters in the advanced motor model. It should be noted that various techniques of estimating on-line and in real-time the different parameters of an induction motor at standstill have been also discussed in detail in a recent book [Vas 1993], but some aspects are also described in Chapter 8 of the present book.

There are several parameters (e.g. stator resistance) which are continuously updated in the adaptive induction motor model during the operation of the drive. For example, the stator resistance is updated by using a thermal model of the induction motor. In the ABB DTC drive, the temperature of the motor is estimated by assuming that the motor ambient temperature is 30 °C. The motor temperature can be estimated by using two curves: the variation of the motor load with time and the variation of the motor thermal-time with time.

During the motor identification run, the speed controller shown in Fig. 4.92 is automatically tuned. This contains a classical PID controller (and e.g. not a fuzzy controller). However, it is also possible to adjust the PID gains manually. In the auto-tune run mode, the automatic tuning of the PID gains is achieved. This also uses the combined load and machine inertia. With auto-tuning, it is possible to achieve better dynamic performance (faster speed responses) than with manual tuning. According to ABB the static speed controller error is typically between  $\pm 0.1\%$  and  $\pm 0.5\%$  of motor rated speed. Higher speed regulation can only be achieved by using a pulse encoder, and in this case the static speed error is typically in the  $\pm 0.01\%$  range (if an encoder with 1024 pulses/revolution is used). The dynamic speed control error is typically  $\pm 0.4\%$ s at 100% load torque step when an encoder or tachogenerator is not used ('sensorless' drive), and it is typically  $\pm 0.1\%$ s when an incremental pulse encoder is used. However, it should be noted that the dynamic speed error strongly depends on the speed controller tuning.

For many applications, speed control is the most important function of an inverter-fed drive. In a DTC-fed drive, speed control is not a part of the inner inverter control as in traditional inverter-fed drives. In Fig. 4.92 the input to the speed controller is the speed error ( $\omega_{rref} - \omega_r$ ) and on the output of the speed controller, the reference electromagnetic torque is produced. The speed controller consists of a PID controller and also an acceleration compensator. The acceleration compensator (feedforward coupling from the speed reference derivative) is extremely useful for minimizing control deviation during starting, acceleration,

and deceleration. The PID controller can be tuned to be more as a load compensator. The PID controller and acceleration compensator are tuned by an automatic tuning method, which is based on the identification of the mechanical time constant of the drive. By identifying the mechanical time constant in an initial self-tuning stage (see below), or during normal operation, it is possible to tune the PID controller for maximum effectiveness.

In Fig. 4.92 the input to the torque-control loop is either the external torque reference ( $t_{eref}$ ) or the torque reference on the output of the speed controller. The electromagnetic torque reference controller outputs the internal torque reference signal ( $t_{erefi}$ ). Within the electromagnetic torque reference controller, the speed control output is limited by the torque limits and the d.c. bus voltage. In this way the motor torque is prevented from exceeding the pull-out torque and the inverter is protected from overload. The torque limit calculation also uses the maximum inverter current and maximum motor current. In Fig. 4.92, the stator flux-linkage reference controller produces the internal stator flux-linkage modulus reference ( $|\psi_{srefi}|$ ). The ability to control and modify this modulus provides a convenient way to implement the three functions ( $f_1, f_2, f_3$ ) shown in Fig. 4.92, which are flux optimization, flux braking, and field weakening. Flux optimizing provides automatic flux adaptation to load variation, yielding higher efficiency. Flux braking provides the highest possible braking torque without additional hardware. Field weakening enables higher than rated rotor speed. These functions are now briefly discussed.

**Flux optimization** By using the motor model, the optimal magnetizing level (stator flux space-vector modulus) can also be estimated as a function of the load (see also Section 4.6.2.8). In the flux optimization mode, flux optimization reduces the total energy consumption of the motor (thus improves efficiency) and noise level, when the drive operates below nominal load. The total efficiency of the motor and the drive can be improved by 1% to 10%, depending on the operating point (load torque and rotor speed).

**Flux braking** Flux braking is a technique where the mechanical energy of the load is converted into heat inside the motor by increasing the flux. The inverter supplying the motor can provide greater deceleration by raising the level of magnetization in the motor, without any extra hardware. By increasing the stator flux, the energy generated by the motor during braking can be converted into thermal energy. The inverter monitors the status of the motor continuously, and also during flux braking. Thus flux braking can be used for stopping the motor and also for changing from one speed to another speed. It should be noted that the latter is not possible with d.c. (injection) braking, which is a widely used technique (see also the various braking techniques discussed in [Vas 1992]). Some of the other benefits of flux braking compared to d.c. injection braking are as follows:

- The braking action starts immediately after the STOP command is given. With the conventional d.c. (injection) braking, there is typically a 500 ms delay after

the STOP command, before the braking can be started. This delay is essential, since d.c. injection is only possible after the motor flux is sufficiently reduced.

- There is more efficient motor cooling. During flux braking the stator currents increase and with d.c. braking the rotor currents increase. However, the stator cools more efficiently than the rotor.

It is also possible to have effective braking by using resistor braking. However, in this case the inverter must be equipped with extra hardware: a braking chopper and a braking resistor.

**Field weakening** Below base speed, a constant value of the stator flux modulus is used (the stator voltage increases) and above base speed (where the inverter ceiling voltage is reached), this modulus is reduced inversely with the speed (field-weakening). Some aspects of field weakening are also discussed in Section 4.6.2.7.

In Fig. 4.92, the actual values (estimated values) of the electromagnetic torque ( $t_e$ ) and stator space-vector flux-linkage modulus ( $|\bar{\psi}_s|$ ) are compared to their internal reference values (in every 25 microseconds), which are present on the outputs of the electromagnetic torque and stator flux-linkage reference controllers respectively. The resulting errors ( $\epsilon_{te}$ ,  $\epsilon_{\psi_s}$ ) are inputs to the electromagnetic torque and stator flux-linkage comparators respectively, which according to ABB are two-level hysteresis comparators. Depending on the outputs of the two comparators and also on the position of the stator flux-linkage space vector, an optimum switching vector selector, which uses an optimal voltage switching-vector look-up table, determines the optimum inverter switchings. For this purpose a very fast, 40 MHz digital signal processor together with ASIC hardware is used. All the control signals are transmitted via optical links for high-speed data transmission. Thus it can be seen that every switching is determined separately based on the values of the electromagnetic torque and stator flux linkages (modulus and angle of stator flux-linkage space vector), and not in a predetermined pattern as in some other a.c. drives. In the DTC drive there is no need for a separate voltage- and frequency-controlled pulse-width-modulator. Due to the extremely fast torque response (e.g. less than 2 ms), the drive can instantly react to dynamic changes such as sudden load changes, power loss, overvoltage conditions, etc. Since the switching vector selection determines the motor voltages and currents, which in turn influence the electromagnetic torque and stator flux linkages, the control loops are closed.

In the DTC induction motor drive the stator flux-linkage modulus and electromagnetic torque are kept within their respective preset hysteresis bands. The inverter switchings are altered if the values of the actual torque and stator flux linkage differ from their reference values more than that allowed by their respective hysteresis bands. When the rotating stator flux-linkage space vector reaches the upper or lower hysteresis limit, a suitable voltage switching vector is selected, which changes the direction of the stator flux-linkage space vector and thus forces it to be in the required hysteresis band. The physical and other aspects of the selection of the optimal switching table have also been discussed earlier in

Sections 4.6.2.1, 4.6.2.2, and 4.6.2.9. It should be noted that at low frequencies the switching voltage vectors in the tangential direction (e.g. voltage vectors  $\bar{u}_3$ ,  $\bar{u}_6$ , etc.) have a very strong influence on the electromagnetic torque. In the DTC drive there is also the possibility of controlling the switching frequency of the inverter by modifying the hysteresis parameters as a function of the electrical frequency.

In the ABB DTC drive, fast and precise torque control can be achieved without using a speed sensor. For example it is possible to have an electromagnetic torque rise time less than 5 ms with 100% reference electromagnetic torque. By applying a torque reference instead of a speed reference, a specific motor torque can be maintained, and the speed adjusts automatically to maintain the reference torque. By using direct torque control, it is also possible to have maximized starting torque which is controllable and is also smooth.

According to ABB, it is possible to operate the DTC controlled induction motor even at zero speed (not zero stator frequency) and the motor can develop rated torque at this speed, without using any pulse encoder or tachogenerator. This is an important feature for various applications, e.g. elevators, lifts, hoists, extruders, etc. However, if long-term operation at zero-speed is required, a pulse encoder may be required. By activating the so-called motor d.c. hold feature, it is possible to lock the rotor at zero speed. When both the reference and actual (estimated) rotor speed drop below a preset d.c. hold value, the inverter stops the drive and starts to inject d.c. into the motor. When the reference speed rises again above the d.c. hold speed, the normal operation of the inverter is resumed.

Before start-up, the motor is automatically magnetized (by the inverter), and the highest possible breakaway torque (even twice the rated torque) is guaranteed. By adjusting the premagnetizing time, it is possible to fix the motor start with a mechanical brake release. The automatic start feature and d.c. magnetizing cannot be activated at the same time. The automatic start feature outperforms the flying start and ramp start features normally found in other frequency converters. Since the ACS 600 can detect the state of the induction motor rapidly (within a few milliseconds), starting is immediate under all conditions. For example, there is no restarting delay with DTC.

Figure 4.93 shows some experimental results obtained with the speed sensorless ABB DTC induction motor drive using a voltage-source inverter (ACS 600) [Tiiainen 1996]. For the purposes of the experiments, two standard squirrel-cage induction motors were coupled using a torque measurement shaft. The inverters which supply the two motors have a common d.c. link circuit. The first motor did not have an encoder fitted, but the second motor (load motor) was equipped with a tachometer, to enable comparisons to be made between measured and estimated rotor speeds. The induction motor ratings are: 15 kW, 30 A, 380 V, number of poles 4; rated stator frequency 50 Hz, rated rotor speed 1460 r.p.m. The rating of the prototype ACS 600 inverter used is 25 kVA, 400 V.

Figure 4.93(a) shows the measured temporal variation of the electromagnetic torque for a 70% torque reference step at 25 Hz. The electromagnetic torque has been estimated by using the measured stator currents and estimated stator flux linkages [by using  $c(\psi_{sD} i_{sQ} - \psi_{sQ} i_{sD})$ ]. The very fast torque response (less than 2 ms)

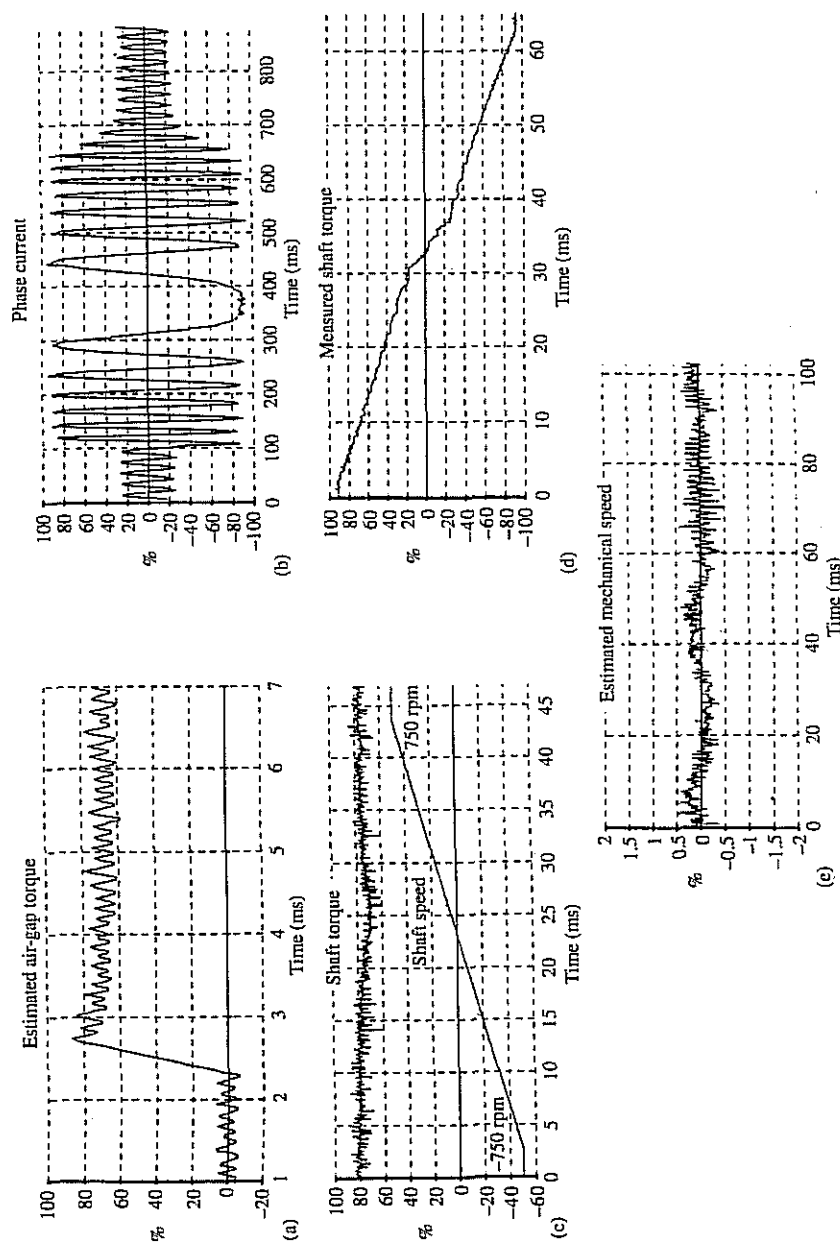


Fig. 4.93. Experimental results for speed-sensorless ABB DTC induction motor drive (Courtesy of ABB Industry Oy, Helsinki). (a) Estimated electromagnetic torque, for 100% reference torque step at 25 Hz; (b) measured stator phase current with constant 20% load; (c) measured shaft torque and measured rotor speed for slow reversal with constant (80%) torque reference; (d) measured shaft torque at zero speed; (e) estimated rotor speed for the case shown in Fig. 4.93(d); the estimation has been performed by using the motor model, which utilizes the speed of the rotor flux linkages to obtain the rotor speed, as discussed in connection with eqn (4.6-54). It should be noted that the accuracy of the rotor-speed estimates has been found to be very satisfactory in the entire speed range.

#### 4.6.3 DTC OF A CSI-FED INDUCTION MACHINE

##### 4.6.3.1 General introduction

In the present section the direct torque control (DTC) of a CSI-fed induction motor drive is discussed briefly. However, for better understanding of the concepts related to direct torque control, the reader is first referred to Section 4.6.2, which discusses in great detail various aspects of the DTC of a VSI-fed induction motor drive. As discussed in Section 4.1.2, in a CSI-fed induction motor drive, a smooth d.c. link current is supplied to the machine-side inverter. The d.c. link current is obtained by using a phase-controlled rectifier and a high-inductance filter. The machine-side inverter contains six force-commutated thyristors (see Fig. 4.17). The d.c. link current is switched through the inverter thyristors to produce the required a.c. currents. Figure 4.18 has also shown the locus of the stator-current space vector (in the stationary reference frame), which corresponds to the six-stepped line currents. It has been shown that during one sixth of a cycle, the stator-current space vector remains in a fixed position (e.g. in the first cycle, it is in position 1 shown in Fig. 4.18, but all the six fixed positions have been shown). The six current vectors corresponding to these fixed positions are the six active (non-zero) switching current vectors used below.

##### 4.6.3.2 Drive scheme

Direct torque control of a CSI-fed induction motor involves the direct control of the rotor flux linkage (or stator flux linkage) and the electromagnetic torque by applying the optimum current switching vectors. Furthermore, in a direct-torque-controlled (DTC) induction motor drive supplied by a current-source inverter, it is possible to control directly the modulus of the rotor flux-linkage space vector  $|\psi_r|$  through the rectifier voltage, and the electromagnetic torque ( $t_e$ ) by the supply frequency of the CSI. For this purpose the appropriate optimal inverter current-switching vectors are produced by using an optimal current switching-vector table. This contains the six possible active current switching vectors ( $\bar{t}_1, \bar{t}_2, \dots, \bar{t}_6$ )

and also the non-active (zero) switching vectors ( $\bar{i}_0$ ). The six active current switching vectors are also shown in Fig. 4.94(a), together with the locus of the stator-current space vector, which is a hexagon. Optimum selection of the switching vectors is made to restrict the electromagnetic torque error within the torque hysteresis band. An input to the optimal current switching table is the discretized torque error ( $dt_e$ ), which is the output of a 3-level hysteresis comparator. A three-level comparator is used, since this corresponds to 0, 1, and -1 torque

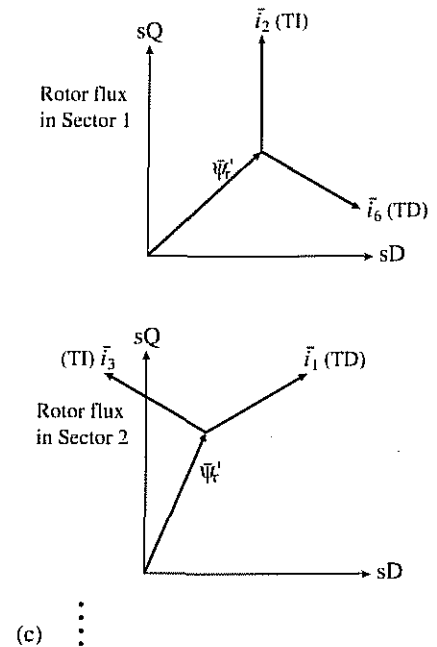
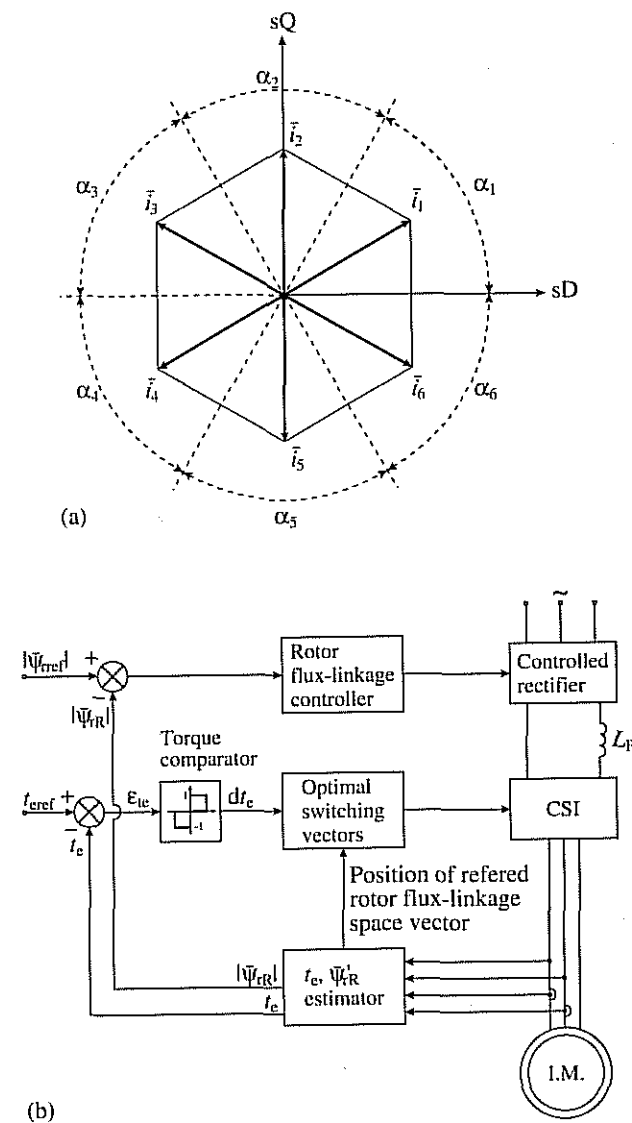


Fig. 4.94. Basic scheme of the DTC CSI-fed induction motor drive and the active current switching vectors. (a) Active current switching vectors; (b) drive scheme; (c) selection of switching vectors; TI: torque increase; TD: torque decrease.

errors. The optimum switching look-up table also requires knowledge of the position of the rotor flux-linkage space vector, since it must be known in which of the six sectors is the rotor flux-linkage space vector. The basic scheme of the DTC CSI-fed induction motor drive is shown in Fig. 4.94(b). The drive scheme contains an electromagnetic torque and rotor flux-linkage estimator.

#### 4.6.3.3 Stator flux-linkage and electromagnetic torque estimation

The electromagnetic torque can be estimated from the terminal quantities by considering eqn (2.1.176), thus

$$t_e = \frac{3}{2} P \frac{L_m}{L_r} \bar{\psi}'_r \times \bar{i}_s = \frac{3}{2} P \frac{L_m}{L_r} (\psi_{rd} i_{sQ} - \psi_{rq} i_{sD}), \quad (4.6-70)$$

where  $P$  is the number of pole pairs,  $\bar{\psi}'_r = \psi_{rd} + j\psi_{rq}$  is the rotor flux-linkage space vector, and  $\bar{i}_s = i_{sD} + j i_{sQ}$  is the stator-current space vector, and both vectors are expressed in the stationary reference frame. The stator currents are monitored and the rotor flux-linkage components can be obtained by considering the stator voltage equation in the stationary reference frame, which gives

$$\frac{d\bar{\psi}'_r}{dt} = \left( u_s - R_s i_s - L'_s \frac{di_s}{dt} \right) \frac{L_r}{L_m}, \quad (4.6-71)$$

where  $L'_s$  is the stator transient inductance. Thus the rotor flux-linkage components are obtained as

$$\psi_{rd} = \frac{L_r}{L_m} \int \left( u_{sD} - R_s i_{sD} - L'_s \frac{di_{sD}}{dt} \right) dt \quad (4.6-72)$$

$$\psi_{rq} = \frac{L_r}{L_m} \int \left( u_{sQ} - R_s i_{sQ} - L'_s \frac{di_{sQ}}{dt} \right) dt. \quad (4.6-73)$$

It can be seen that if eqns (4.6-72) and (4.6-73) are used to estimate the rotor flux-linkage components, then in addition to the stator resistance, the stator transient inductance must also be used together with the inductance ratio  $L_r/L_m$ . However, it is also possible to have an implementation where  $L_r/L_m$  is not required. In this case, instead of estimating the rotor flux linkages, their referred values are estimated. By using eqns (4.5-123) and (4.6-71), it follows that the direct- and quadrature-axis referred rotor flux-linkage components (in the stationary reference frame) can be obtained from  $\bar{\psi}'_{rR} = \int (\bar{u}_s - R_s \bar{i}_s) dt - L'_s \bar{i}_s$  (where for simplicity the subscript R denotes the referred value). Thus

$$\psi_{rdR} = \int (u_{sD} - R_s i_{sD}) dt - L'_s i_{sD} \quad (4.6-74)$$

$$\psi_{rqR} = \int (u_{sQ} - R_s i_{sQ}) dt - L'_s i_{sQ}. \quad (4.6-75)$$

In this case, the electromagnetic torque can be obtained by using eqn (4.5-127); thus

$$t_e = \frac{3}{2} P \bar{\psi}'_{rR} \times \bar{i}_s = \frac{3}{2} P (\psi_{rdR} i_{sQ} - \psi_{rqR} i_{sD}). \quad (4.6-76)$$

Since in the CSI-fed drive, the currents are limited by the forced commutation circuit, saturation of the leakage flux paths can be neglected and thus  $L'_s$  can be assumed to be constant. However, in addition to this open-loop flux estimator it is possible to use more accurate schemes described earlier (e.g. see Sections 3.1.3.2.1 and 4.6.2.6). The angle of the referred rotor flux-linkage space vector (which is the same as the angle of the non-referred rotor flux-linkage space vector) can be estimated by using  $\rho_r = \tan^{-1}(\psi_{rqR}/\psi_{rdR})$ , or  $\rho_r = \cos^{-1}(\psi_{rdR}/|\bar{\psi}_{rR}|)$ , or  $\rho_r = \sin^{-1}(\psi_{rqR}/|\bar{\psi}_{rR}|)$ , where  $|\bar{\psi}_{rR}| = (\psi_{rdR}^2 + \psi_{rqR}^2)^{1/2}$ , but similarly to the case discussed in Section 4.6.2.2, it is possible to avoid the use of trigonometric functions.

In Fig. 4.94(b), the rotor flux-linkage controller acts directly on the rectifier voltage. The physical reason for the presence of this control loop is the fact that the modulus of the rotor flux-linkage space vector can be changed by changing the amplitude of the stator voltage. This also follows from the stator voltage equation [eqn (4.6-71)] given above. However, the stator voltages can be changed by changing the rectifier voltage. On the other hand it can also be shown by simple physical considerations that the electromagnetic torque can be controlled

by changing the stator frequency, but this also follows by considering the rotor voltage equation, eqn (4.1-24), together with  $|\bar{\psi}_r| = L_m |\bar{i}_{mr}|$ . Thus

$$0 = - \frac{L_m}{T_r} \bar{i}_s + \left( \frac{1}{T_r} + p - j\omega_r \right) \bar{\psi}'_r \quad (4.6-77)$$

is obtained, where  $p = j\omega_1$  if it is assumed that the rotor flux linkages are sinusoidal, in which case  $\bar{\psi}'_r = |\bar{\psi}_r| \exp(j\omega_1 t)$  and  $T_r = L_r/R_r$  is the rotor time constant. By considering eqn (4.6-74) and also eqn (4.6-70), it follows that when the position of the stator-current space vector is quickly changed, a quick change in the electromagnetic torque and also in the angular slip frequency ( $\omega_{sl} = \omega_1 - \omega_r$ ) is obtained. This is similar to that in the voltage-source inverter-fed DTC induction motor drive, but in the VSI-fed drive rapid change in the electromagnetic torque is obtained by rapidly changing the appropriate voltage switching vector.

The torque reference can be obtained on the output of a speed controller, which can be PI controller. The input to the speed controller is the difference between the reference speed and the actual speed. It is possible to have a speed-sensorless implementation, where the rotor speed is obtained by using one of the techniques described in Section 4.6.2.10. The hysteresis band of the torque comparator may be increased with rotor speed, since in this case PWM of the currents is avoided at high speeds.

#### 4.6.3.4 Optimal current switching vector selection

It follows from the similarity of the switching states of the current-source inverter and that of the voltage-source inverter that the required optimum inverter current switching-vector selection table must resemble the switching table obtained for the voltage switching vectors in Section 4.6.2.2, but now current vectors replace the voltage vectors. However, as discussed above, for the system with the CSI, the flux error is not an input to the optimum switching table (since the rotor flux is directly controlled through the rectifier voltage, and not through the inverter switching states). Thus it is formally possible to use the first part of the switching table given for the VSI-fed drive, but all the voltages have to be changed to currents. However, for better understanding, the required switching table is also derived below in another way.

The optimal inverter current switching table can be obtained by considering the positions of the rotor flux-linkage space vector in one of the six sectors (e.g. the first sector is in the region spanned by angle  $\alpha_1$  shown in Fig. 4.94(a), the second region spans the angle  $\alpha_2$ , etc.). It can be seen that e.g. if the rotor flux-linkage space vector is in the first sector, then for positive electromagnetic torque the switching current vector  $\bar{i}_2$  has to be applied. This is due to the fact that a stator current vector has to be selected which produces positive electromagnetic torque and is located at an angle less than  $90^\circ$  in the positive direction from the rotor flux-linkage space vector, since the machine behaves like an RL-circuit. However,